JOHANNES
GUTENBERG
UNIVERSITÄT
MAINZ

SILICON-CONTAINING BLOCK COPOLYMERS WITH WELL-DEFINED, BRANCHED ARCHITECTURES

- Synthesis, Characterization and Morphological Studies -

Dissertation zur Erlangung des Grades
“Doktor der Naturwissenschaften”

am Fachbereich Chemie, Pharmazie und Geowissenschaften der
Johannes Gutenberg-Universität Mainz

vorgelegt von

Alejandra Teresa García Marcos

geboren am 15 Oktober 1975 in Avilés/Asturias (Spanien)

Mainz, im April 2006

Die vorliegende Arbeit wurde in der Zeit von

Oktober 2001

bis

Oktober 2005

am Institut für Organische und Makromolekulare Chemie

der Johannes Gutenberg-Universität Mainz

unter der Betreuung von

Herrn Prof. Dr. Holger Frey

angefertigt

Tag der mündlichen Prüfung: 21 Juni 2006

Contents

Preface

This thesis essentially consists of three parts. In the first part a general introduction to block copolymers, miktoarm-star and linear-dendritic copolymers, giving special emphasis on the studies of their solid-state properties, is presented. This is followed by a short description of the motivation of this work.

The second part comprises Chapters 2, 3, 4 and 5. These chapters are essential building blocks for the ensuing structure discussions. Chapter 2 explains how the linear polystyrene-*b*-polybutadiene (PS-*b*-PBD) diblock copolymers, used as templates for the subsequent grafting reactions, are prepared by living anionic polymerization. The characterization data of the different diblock copolymers prepared and their acronyms are provided in Table 2.1. In Chapter 3 synthesis and characterization of different AB_n alkenylsilane and alkenoxysilane monomers, as precursors for the hyperbranched and brush-like polymers, is described. The Appendix of Chapter 3 complements the characterization of the organosilicon monomers. A mechanistic approach to the afterwards employed metal-catalyzed hydrosilylation reaction is presented in Chapter 4. To understand the formation of the side-products, some indispensable knowledge about the different hydrosilylation mechanisms discussed at present is given. Chapter 5 explains in-depth the structural and compositional characterization of hyperbranched and brush-like polycarbosilanes, synthesized by the “one-pot” polymerization approach of the AB_n alkenylsilane monomers. This episode is of significance, as the polycarbosilanes are part of more complex architectures in the next chapters.

The third part is the central theme of this dissertation and encompasses Chapters 6, 7 and 8. The main topic of these chapters is the morphological behavior of unusual AB block copolymer architectures when comparing with that of linear diblock copolymers. A general strategy for the preparation of well-defined linear-hyperbranched systems is developed in Chapter 6. This is based on slow monomer addition of branched AB_2 carbosilane monomers to the linear PS-*b*-PBD block copolymer precursor. In this manner, linear-hyperbranched polycarbosilane diblock copolymers are obtained and the bulk morphology is studied by transmission electron microscopy (TEM), atomic force microscopy (AFM) and temperature-dependent Small-Angle X-ray Scattering (SAXS) measurements. An evaluation of the morphological features of these peculiar systems is given in Chapter 6 and analogous linear brush-like polycarbosilanes are analyzed in Chapter 7. Unusual morphologies are observed for these structures and a qualitative explanation is given to explain the observed results.

Chapter 8 deals with the morphological studies of related linear-hyperbranched and brush-like polyalkoxysilanes. The morphology of the linear-hyperbranched polyalkoxysilanes show interestingly how complications arise when one of the segregating blocks can crystallize. Additionally, the grafting efficiency of the alkenoxysilane and alkylsilane monomers is studied and compared.

CHAPTER 1

GENERAL INTRODUCTION AND MOTIVATION

1.1 BLOCK COPOLYMERS

1.1.1 What are block copolymers?

Block copolymers (BCPs) are fascinating hybrid materials that self-assemble into ordered nanoscocopically structured morphologies.[1] BCPs consist of chemically distinct polymer chains covalently linked to form a single molecule. Owing to their mutual repulsion, dissimilar blocks tend to segregate into different domains, the spatial extent of the domains being limited by the constraint imposed by the chemical connectivity of the blocks. The broad variety of self-organizing structures of BCPs in bulk and in solution is shown in Figure 1.1.

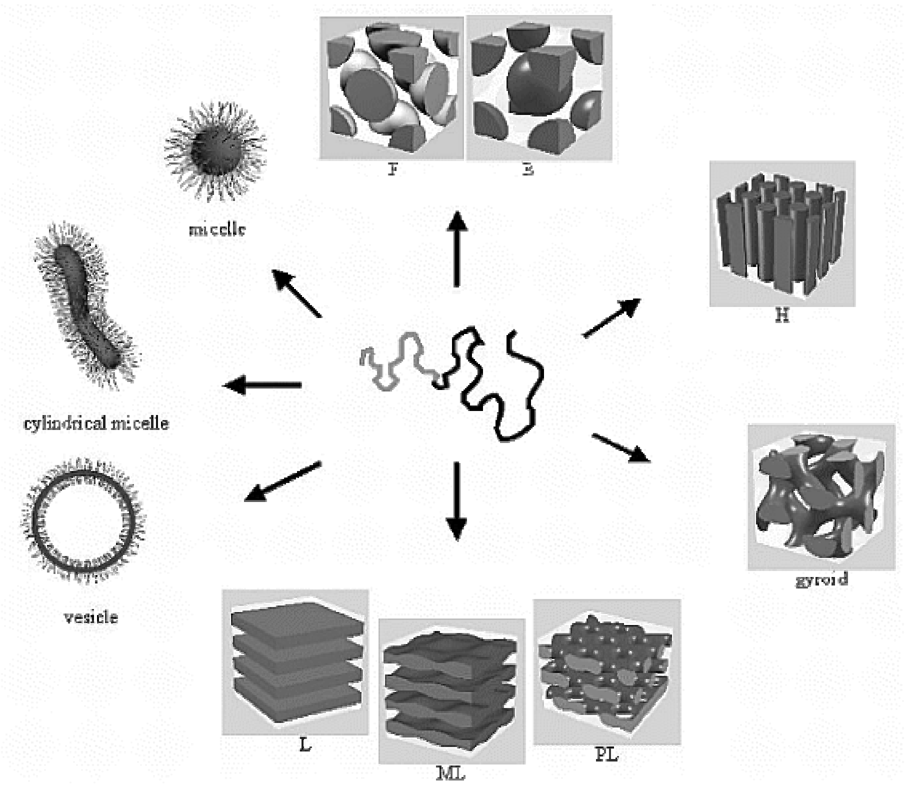

Figure 1.1. Self-organization of BCPs: spherical and cylindrical micelles, vesicles, spheres with face-centered cubic (F) and body-centered cubic (B), hexagonally packed cylinders (H), gyroid, simple lamellae (L), as well as modulated (ML) and perforated (PL) lamellae.

1.1.2 Why are block copolymers interesting? Applications

BCPs have received great attention for the past fifty years, but only within the past decade they have been seriously considered for nanotechnological applications.[2] Their applicability to nanotechnology stems from the scale of the microdomains (tens of nanometers) and the convenient tunability of size, shape and periodicity afforded by changing their molecular parameters. Many potential uses include among others micelles for drug delivery, nanostructured membranes, templates for nanoparticle systems such as metal, ceramic nanodots and wires, photonic crystals and nanopattern masks for fabrication of high-density information storage media. In Figure 1.2 are summarized the various applications. These advanced applications have been proposed on principally the ability of BCPs to form interesting patterns. However, the main challenge of using BCPs resides on control over their microstructures. Until recently the majority of work and principles of self-assembly have focused on linear molecular architectures, due to the lack of synthetic protocols for the preparation of more complex well-defined and near-monodisperse block copolymer structures. But with breakthrough developments in synthetic chemistry, other block copolymer architectures have become available to further explore the benefits of nanostructures in applications.

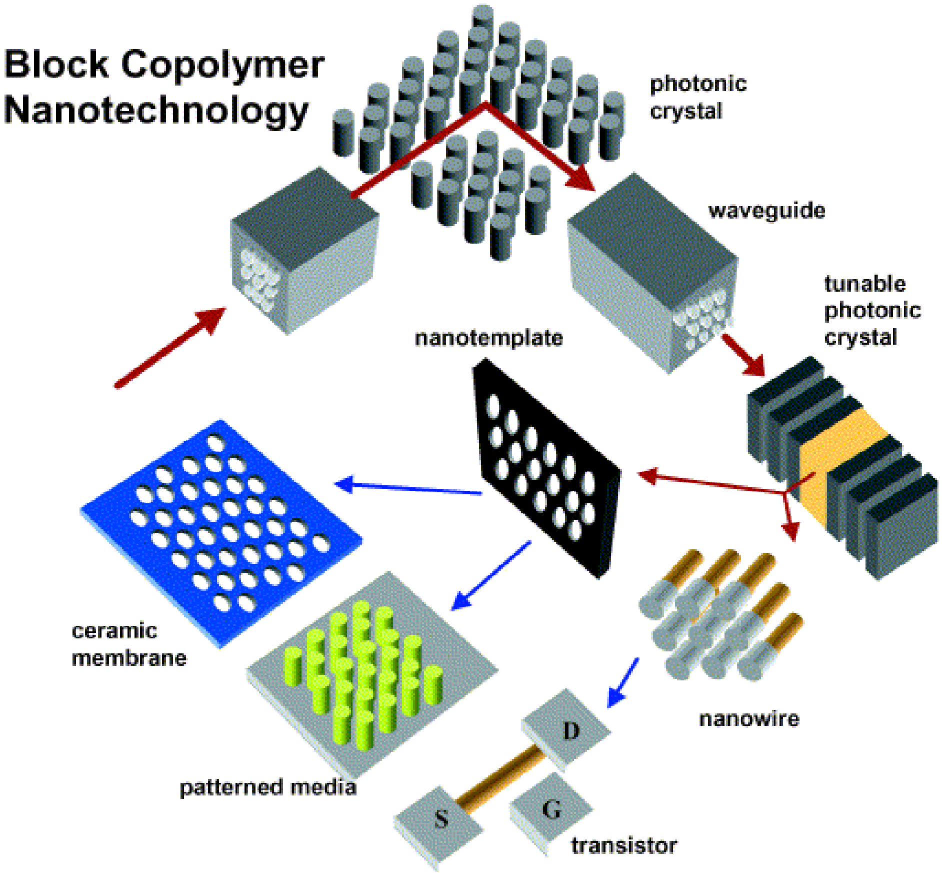

Figure 1.2. Schematic of various applications of BCPs in nanotechnology.

1.1.3 Synthesis of block copolymers. Developments

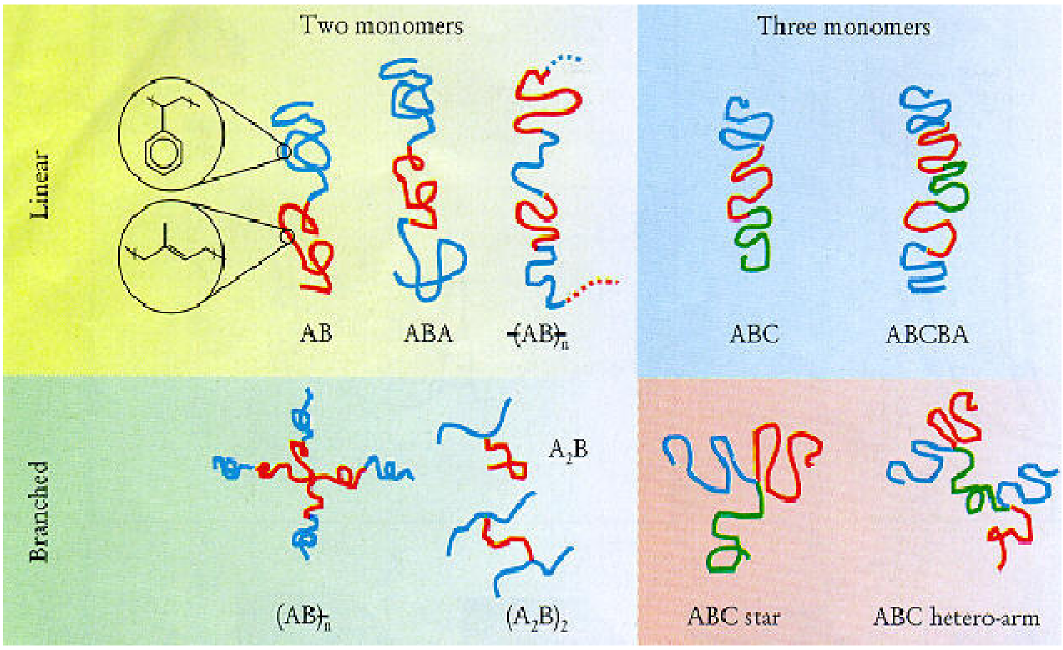

Figure 1.3. Molecular architecture of BCPs (each colour strand represents a polymer block). Architectures are classified by number of monomer types and topology. The upper-left inset shows two representative monomer chemical structures.

Most BCPs used today are prepared by living anionic polymerization (LAP).[3] This has been the method of choice for preparing BCPs of controlled architecture such as those shown in Figure 1.3 through precise sequencing of two, three or even more monomers.[1c] In this process, each copolymer chain is grown from a single reactive site through sequential additions and polymerization of, say, A and then B monomer batches, for a simple A-B diblock. This requires that the growing polymer chains remain alive throughout the polymerization process, that is, they are free of termination or transfer reactions.

The story of living polymers dates back to the mid 1950s when LAP of styrene (S) and styrene/isoprene (S/I) block copolymers was first reported.[4] Not only were the growing chains living, but they were also characterized by a narrow distribution of chain length. This is ensured by the very fast initial creation of anionic active chain ends (initiation) that starts polymerization. Stringent conditions of temperature, purity of the reagents and nature of the polymerization method are necessary to eliminate secondary reactions and control the kinetics of polymerization. Yet, this discovery was rapidly turned into a commercial success with SIS and SBS triblock copolymers.[5] The success of styrene/diene living copolymers soon prompted laboratory-scale research in the anionic synthesis of well-defined block copolymers of other monomers such as methacrylates or acrylates.[6] However, only recently, elegant solutions have been found to overcome technical obstacles such as very low reaction temperatures prohibiting industrial production of these interesting di- or tri- block copolymers.[7] For the first time, these copolymers could thus become available in large quantities. Finally, extension of anionic polymerization to other architectures like star and miktoarm star polymers, graft and α,ω–branched, cyclic and hyperbranched (co)polymers has been proven to be a very powerful tool for the synthesis of well-defined macromolecules with complex architectures.[3]

Post-polymerization chemical modification is one of two general strategies for overcoming the primary limitation of LAP for block copolymers, namely the restriction to a minority of all interesting or otherwise useful monomers. The most widespread example is catalytic hydrogenation of diene blocks,[8] for example, to form polyethylene in the case of 1,4-polybutadiene. Hydrogenation has been further applied in a practical way to PS to form polycyclohexylethylene. Other interesting possibilities include fluorination,[9] transformation to ionic groups and the introduction of photoactive groups or mesogenic moieties. The other strategy, that of using alternative living or controlled polymerization protocols, has also been highly successful. A variety of BCPs have been prepared by cationic, group transfer, metallocen and metathesis routes.[10] However the biggest advance and a dream that motivated synthetic chemists' efforts for over thirty years came true when a few groups were able to achieve an (almost) equally living polymerization in the much more flexible free-radical polymerization. Almost all monomers containing a carbon-carbon double (the broad category of vinyl polymers) undergo radical polymerization, whereas ionic polymerization is restricted to a few of them. Free-radical synthesis is thus by far the most widely spread chain growth polymerization. Yet the extreme and non-selective reactivity of free-radical chain-ends rules out the possibility of living polymerization, transfer and termination reactions being omnipresent. Combined academic and industrial efforts to control this reactivity culminated in the advent of controlled radical polymerization (CRP), with three different mechanisms: nitroxide-mediated CRP,[11] atom-transfer radical polymerization (ATRP)[12] and reversible addition-fragmentation transfer (RAFT).[13] In short, the idea is to artificially introduce and additional, yet reversible, termination reaction of the active chain ends. Thus, by reversible end-capping the growing polymer chains and "putting them to sleep" for long periods of time, the overall instantaneous concentration of free radicals is much lower and chances of irreversible termination grow slimmer. The consequences are twofold. First, chain growth is much slower, in fact slower than initiation, and chain length distributions are narrower. Second, growing chains remain in their end-capped state at the end of polymerization and can be re-activated to add a second type of monomer. These developments enable the preparation of novel BCPs of various architectures from virtually all kinds of vinyl monomers by free-radical mechanisms in common mass, suspension or even emulsion processes.[14] Therefore, one may reasonably anticipate an increasing role for CRP in block copolymer technology.

The block copolymer community is thus witnessing an unprecedented availability of chemical tools to optimize the properties of BCPs through a judicious choice of both monomer type and architecture. The combination of different methods for the hybrid synthesis of distinct monomer sequences is lifting the last obstacles to tunable BCPs. For each method or combination of methods, a delicate compromise has to be established between increased facility and the progressive loss of control over side-reactions it is associated with.

1.1.4 Solid-state phase behavior

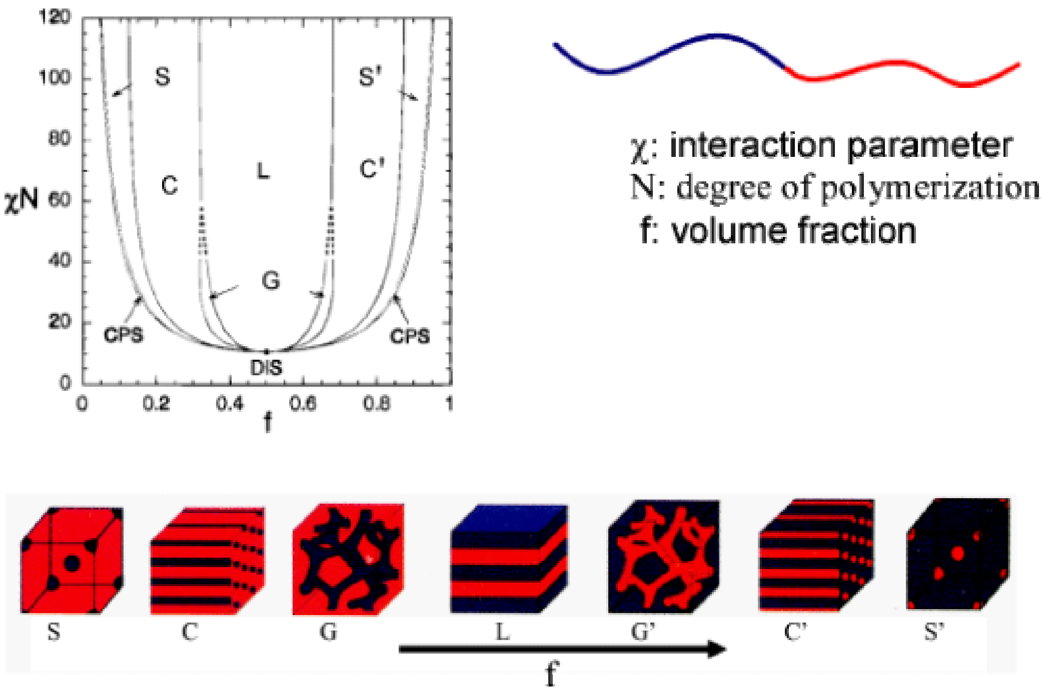

Figure 1.4. Theoretical phase diagram for linear AB diblock copolymers and the different morphologies as predicted by the self-consistent theory. The phase diagram depicts the regions occupied by the different morphologies as a function of the interaction parameter (χ), molecular weight (N) and volume fraction (f). The x-axis shows increasing fraction of the dark blue block, and on the y-axis is plotted the product of χN, which is inversely proportional to temperature; thus at high temperature entropy dominates and the polymer falls into the disordered state. The resulting morphologies are described as spheres (S), cylinders (C), gyroid (G), lamellae (L) and their respective inverse (represented by S′, C′ and G′).

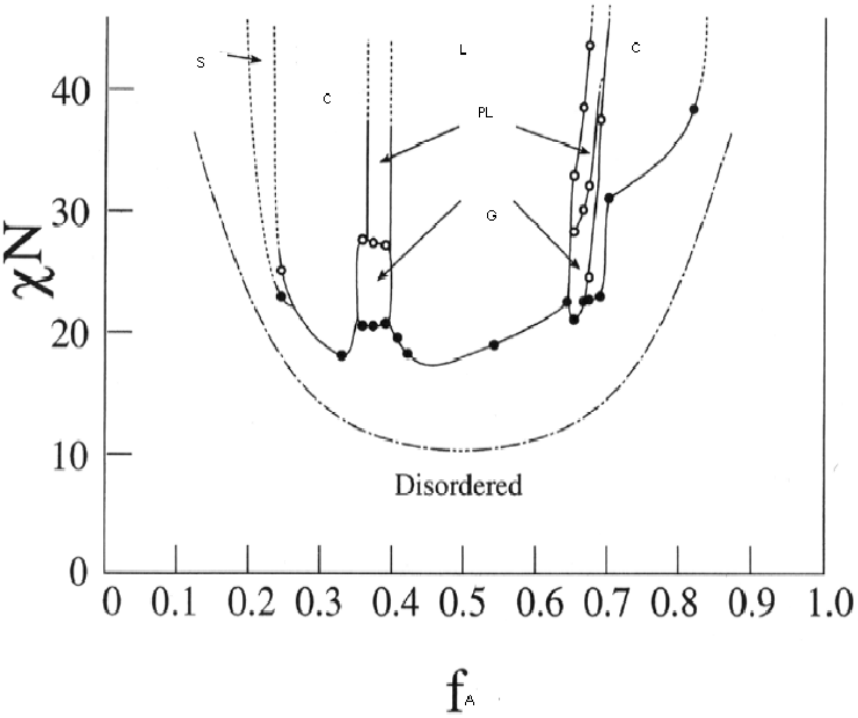

Figure 1.5. Experimental phase diagram for PI-PS diblock copolymers. Open and filled circles represent the order-order (OOT) and order-disorder (ODT) transitions, respectively. The dash-dot curve is the mean field prediction for the ODT.

In recent years, much work has focused on the morphology and phase behavior of BCPs. There are different possibilities for classifying BCPs in the bulk state, which depend on the choice of a particular property such as the number of components, chain topology, or the aggregation state of the blocks. In this section, we will concentrate on amorphous BCPs in the bulk state. Among the amorphous linear BCPs, the morphological behavior of A-*b*-B diblock copolymers has been extensively studied and they can be considered as model systems for more complicated BCPs.[15] Because of the mutual repulsion of dissimilar monomers and the constraint imposed by the connectivity of the A block with the B block, coil-coil diblocks exhibit a wide range of microphase-separated morphologies. The parameters that determine the morphology of an AB diblock copolymer are the Flory-Huggins interaction parameter, χ_{AB}; the total degree of polymerization, $N = N_A + N_B$; and the volume fraction (composition) of the A component, f_A. The parameter χ_{AB} is a measure of the incompatibility between the A and B polymers and is inversely proportional to temperature. In the strong segregation limit (large χN), the morphology formed has been proven to be solely dependent on the relative volume fractions of the constituent blocks. A theoretical phase diagram for estimating the morphology of the different structures in diblock copolymers was first derived in the Mean Field Approximation by Leibler[15d] and later a more complete study encompassing the complete phase behavior was described by Matsen and Bates.[15a,16] Matsen and Schick's calculated phase diagram for AB diblock copolymers is shown in Figure 1.4.[15a,16] Since at high temperatures mixing is favored, a homogeneous melt (disordered phase) is predicted for low values $\chi_{AB}N$. The critical value of $\chi_{AB}N$ for order-disorder transition (ODT) is calculated to be 10.5. At larger values of $\chi_{AB}N$, phase separation occurs and depending on the composition of the BCPs five different, thermodynamically stable morphologies are predicted. If the copolymer is symmetric ($f_A = f_B = 0.5$), phase separation yields a lamellar phase (L). Any asymmetry in composition induces curvature and for slightly asymmetric blocks, a hexagonally packed cylinder phase (C) is found to be stable. At greater compositional asymmetry, a body-centered cubic spherical phase (S) is predicted with the block having lesser fraction forming the core of the spheres. A very narrow region of close-packed spheres (CPS) separates the disordered and S phases at the composition extremes of Figure 1.4. Finally, Matsen and Schick predicted narrow regions of stability of a complex gyroid phase (G) (periodic bicontinuous structure), close to the ODT and between the L and C phases. Polyisoprene-polystyrene (PI-PS) and polybutadiene-polystyrene (PB-PS) diblock copolymers have been the subject of the majority of experimental studies on block copolymer phase behavior. Figure 1.5 shows the experimental phase diagram for PI-PS obtained by Khandpur *et al.*[15b] The overall topology of the experimental diagram is strikingly similar to the theoretical diagram in Figure 1.4, with a few exceptions. Firstly, Figure 1.4 is symmetric about $f_A = 0.5$ while Figure 1.5 does not display this symmetry. The reason for this discrepancy lies in the fact that complete symmetry is assumed in the theoretical model. It is surmised that both monomers have similar shape and size. This assumption is implicit if the monomer Kuhn lengths (l_A and l_B) are taken to be equal. However this assumption does not hold good for most copolymers. Furthermore, some of the asymmetry also results because the S-I interactions are not accurately represented by a single χ_{SI} parameter. Besides the G phase, the experimental diagram contains small regions of a second complex phase, perforated layers (PL). According to Matsen-Schick calculations, the PL phase is not stable in any region of the phase diagram. This discrepancy was resolved by the theory group of Shuyan Qi and Zhen-Gang Wang and the experimental group led by Frank Bates.[17] Based on their independent studies, both groups concluded that the PL phase is indeed not thermodynamically stable, but is rather a long-lived transient structure with epitaxial relation to the C and L phases. A final obvious discrepancy between Figures 1.4 and 1.5 concerns the region of the phase diagram near the ODT. It can be seen that the disordered phase is experimentally found to be stable for much higher values of $\chi_{AB}N$ than those predicted by Matsen and Schick ($\chi_{AB}N = 10.5$). Additionally, the theoretical diagram allows only direct phase transitions between the disordered phase and the spherical (BCC and CPS) ordered phases, while direct transitions to all the five ordered phases is observed experimentally. Experimentally observed phase boundaries do not converge to a single point ($\chi_{AB}N$ = 10.5 and f_A = 1/2) as theoretically predicted, due to composition fluctuations near the weakly first-order ODT curve.

Of late new theoretical and experimental studies of the double gyroid phase (G) in the simplest linear AB diblock copolymers have occupied researchers' attention. This intriguing topology has indeed inspired a diverse array of potential applications ranging from high-performance separation membranes to photonic crystals. However, the practical applicability of G in the AB systems appears limited due to the question of the stability of the phase in the strong-segregation regime. Current calculations by Cochran and Fredrickson[18] demonstrate, in accordance with recent experimental evidence,[19] that G can be stable in the strong segregation regime. Figure 1.6 shows a revised diblock copolymer phase diagram that accounts for the recently G phase boundary calculations.[18] In the diagram, Q^{230} and Q^{229} refer to the double-gyroid phase (G) and body-centered spheres (BCC) respectively. The diagram indicates that Q^{230} survives over a narrow range of compositing deep into the strong segregation regime. It is also noticeable a gradual contraction of the Q^{230} region from χN = 20 to χN = 80, due to the packing frustration caused by the narrowing of the interfacial thickness.

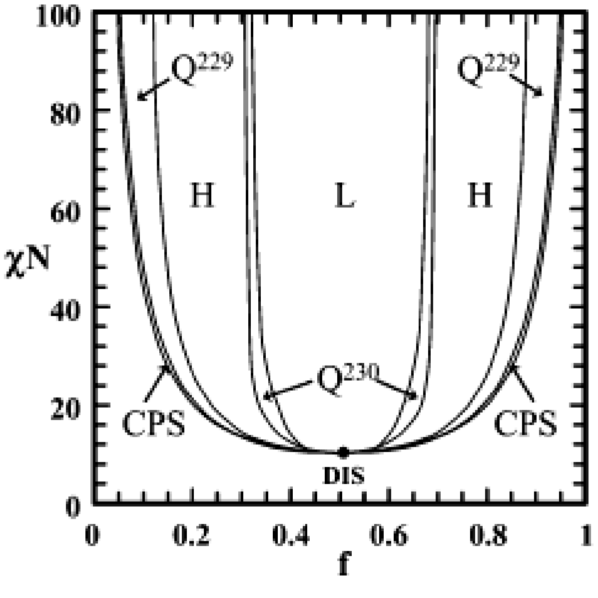

Figure 1.6. Revised diblock copolymer phase diagram, accounting for the new gyroid (Q^{230}) phase boundary calculations. Q^{229} refers to the body-centered spherical phase.

In Figure 1.7 are presented, as a resume, the various “classical” BCP morphologies adopted by AB linear diblock copolymers in function of the volume fraction of the A block.

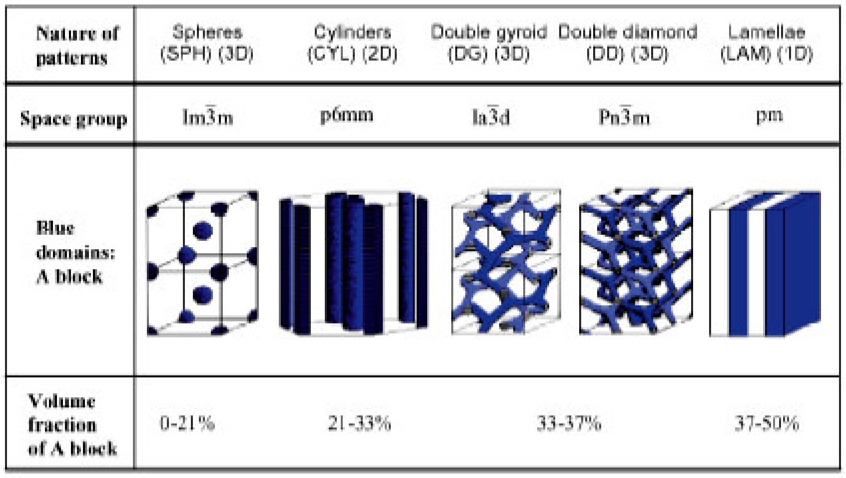

Nature of patterns	Spheres (SPH) (3D)	Cylinders (CYL) (2D)	Double gyroid (DG) (3D)	Double diamond (DD) (3D)	Lamellae (LAM) (1D)
Space group	$Im\bar{3}m$	p6mm	$Ia\bar{3}d$	$Pn\bar{3}m$	pm
Blue domains: A block					
Volume fraction of A block	0-21%	21-33%	33-37%		37-50%

Figure 1.7. Schematic phase diagram showing the various “classical” BCP morphologies adopted by non-crystalline linear AB diblock copolymers. The dark coloured component represents the minority phase and the matrix, majority phase surrounds it.

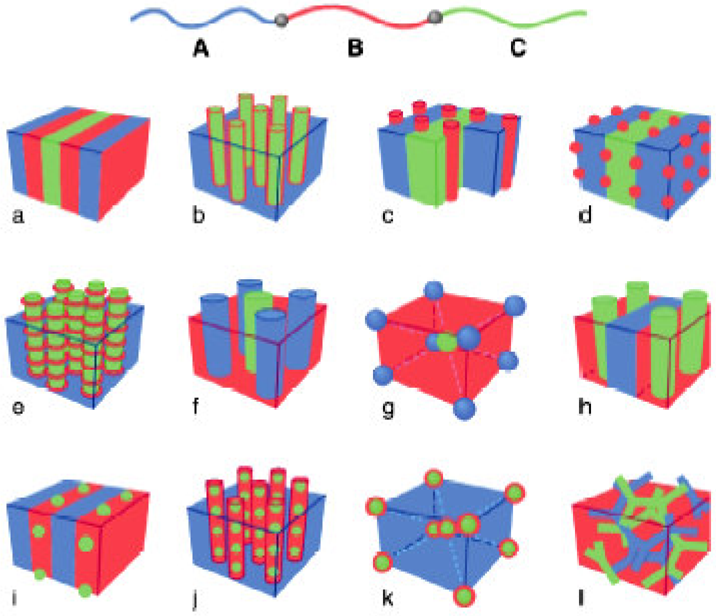

Figure 1.8. Morphologies for linear ABC triblock copolymers. A combination of block sequence (ABC, ACB, BAC), composition and block molecular weights provides an enormous parameter space for the creation of new morphologies. Microdomains are coloured as shown by the copolymer strand at the top, with monomer types, A, B and C confined to regions coloured blue, red and green, respectively.

The quest for generating a larger number of morphologies from BCPs led scientists to study the phase behavior of triblock copolymers.[1f,6c,20] The preparation of such polymers is challenging and the need of imaging three types of domains, due to the presence of two independent composition variables and a changeable block sequence, presents even more difficulties. As a consequence a richer phase diagram results with more complex microphase separated structures, so that this area continues nowadays being explored. To date more than a dozen microphase structures have already been identified in the experiments on ABC systems. Figure 1.8 shows some of the exciting morphologies predicted for triblock copolymers.

1.2 BLOCK COPOLYMER ARCHITECTURE

Manipulation of BCPs microdomain structure through molecular architecture has been demonstrated. Hadjichristidis *et al.* have recently reviewed theoretical and experimental results on the synthesis and bulk and solution properties of well-defined star-block, graft, miktoarm star copolymers and more complex architectures such as umbrella polymers, so a better understanding of the influence of macromolecular architecture on block copolymer properties could be developed.[21] Results can be summarized in that the relationship between the volume fraction of the various block types and the ordered morphology is quite different from that for linear BCPs.

1.2.1 Star-block, miktoarm star and graft copolymers morphology

Star-block copolymers are molecules of the $(AB)_n$ type, in which the arms are identical (Figure 1.3). In 1986 Thomas *et al.* studied the influence of segment molecular weights and star functionality on the morphology of star-branched block copolymers of constant composition having PS-PI arms (30 wt % PS), driven by the lack until then of systematic and concluded studies on the solid state behavior of star-block copolymers.[22] Using selective solvent casting, they found that upon increasing the number (where n ranged from 2 to 18) or molecular weight of the arms of the star (2.3×10^4, 3.3×10^4 and 10×10^4), the morphology results in an ordered, thermodynamically favoured bicontinuos double diamond structure (OBDD). This effect had not been previously seen in linear materials of equivalent compositions, where the equilibrium morphology is that of PS cylinders hexagonally packed in the polydiene matrix. This effect of arm molecular weight on the transition from cylindrical to ordered bicontinuos is by no means well understood. They proposed that OBDD was a more favourable structure that minimized the interfacial area between the two phases, as a consequence of increasing the number of arms on one side. Later, the morphology of a series of 18-arm PS-PI star block copolymers was examined by the same authors as a function of composition.[23] The OBDD structure was observed again at compositions of 30 and 35 wt % of PS as well as 76 wt % of PS, but only when the minority components PS and PI were the outer segments of the diblock arms respectively.

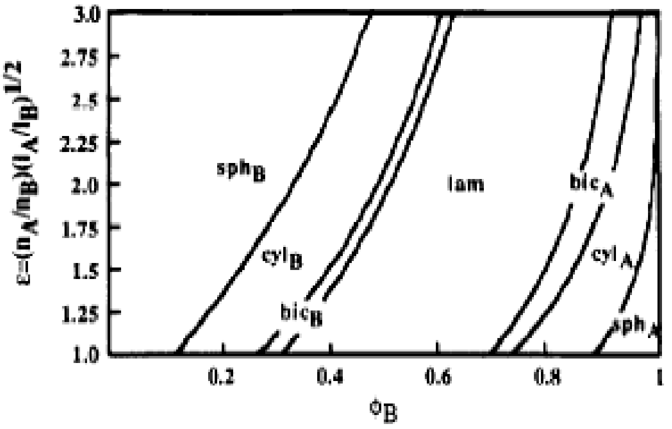

Figure 1.9. Theoretical phase diagram calculated by Milner for miktoarm star BCPs in the SSL with n_A A arms and n_B B arms as a function of the volume fraction of the B monomer (ϕ_B).

The experimental results from the examination of more complex architectures motivated new theoretical studies that would explain and predict the effect of molecular architecture on morphological behavior. In 1994 Milner developed a theoretical approach to predict the morphologies of miktoarm star copolymers (star-shaped molecules of the type A_nB_m with chemically different arms) in the strong-segregation limit (SSL) (Figure 1.10).[24] In his calculation, he grouped the architectural asymmetry, due to the difference in A and B arm numbers, with the conformational asymmetry inherent in the A and B polymer chains together into one asymmetry factor (ε). The degree of asymmetry ε is then defined as: $\varepsilon = (n_A/n_B)(l_A/l_B)^{1/2}$, where n_A and n_B are the number of A and B arms and the differing chain statistics between blocks are represented by $l = V/R^2$, where V and R are the volume and the radius of gyration of each arm in the copolymer. In this way, the morphology of miktoarm polymers at given values of volume fraction (ϕ) and asymmetry parameter (ε) can be determined by the intersection values of the minimized free energy of the different structures, which are associated with the interfacial tension between phases and the stretching of the blocks away from the interface (Figure 1.9). In the asymmetry parameter (ε), different architectures and chain statistics are included. For ε equal to one, the phase diagram illustrates linear AB diblock copolymer behavior. However, as the arm number of one species increases with respect to the other, the phase behavior becomes extremely asymmetric with volume fraction. Although this phase diagram was mostly experimentally unexplored, it was long before the group of Hadjichristidis successfully achieved the synthesis of well-defined miktoarm star BCPs of the type A_nB_m and demonstrated experimentally that the architecture can be an additional variable in controlling the morphology.[25] By using anionic polymerization and controlled cholorosilane coupling chemistry,[3] they synthesized simple S-I graft structures like A_2B stars, A_3B stars, $(AB)_2(BA)_2$ inverse stars and A_3BA_3 bridged stars[26] as model nonlinear BCPs and compared the microphase separation with the corresponding linear BCPs. They found that the asymmetry of the graft architecture for A_2B[27] and A_3B[25b] miktoarm stars shifted the observed morphology at 50 % PS volume fraction to bicontinuous cubic and hexagonally packed cylindrical structures respectively from that which would be formed by diblock analogs with the same composition.

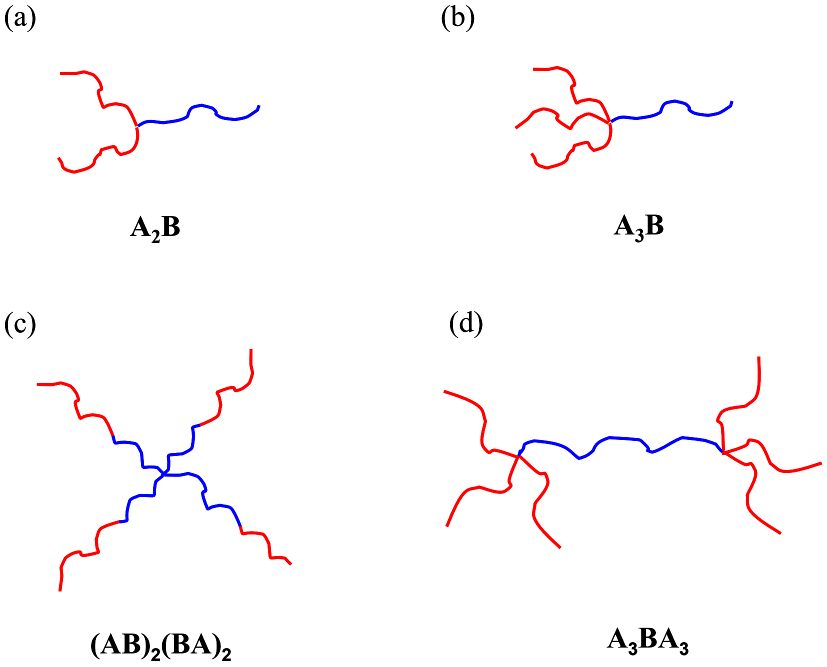

Figure 1.10. Miktoarm star copolymers: (a) 3-miktoarm, (b) 4-mikotarm, (c) inversed 4-miktoarm and (d) bridged miktoarm.

Another important feature of Hadjichristidis' studies is that the spherical morphology for the A_3B structure was no longer observed at high B (PS) volume fractions.[25a] It is clear that the phase diagram in the SSL for diblocks is shifted toward higher volume fractions of the single arm B (PS) and that the amount of this shift depends on n, which is the number of A (PI) chains connected at the star center. The morphologies observed for the A_2B and A_3B miktoarm copolymers are in good agreement with those theoretically predicted by Milner and confirm that macromolecular architecture affects the morphology by moving the classical domain borders. The influence of architecture on the morphology behavior of miktoarm stars can be explained in terms of the local preferred curvature of the A-B interface. The greater the crowding on the A side of the interface, the higher will be the degree of curvature in order to alleviate the enhanced stretching of the A arms due to asymmetry. This degree of curvature dictates the morphology that the system will finally adopt. Thus multiple A arms at a single junction have a preference to remain on the convex side of the interface thereby shifting the order-order transition lines in the morphology diagram to higher B volume fractions. Figure 1.11 shows how a branched A_2B architecture can result in a non-lamellar morphology even in a compositionally symmetric molecule, due to asymmetric interfacial crowding. This architectural asymmetry can be much more effective at shifting phase boundaries between ordered microphases than the weaker conformational asymmetry (monomer size and shape). For example, copolymers with cylindrical or spherical microphases with a relatively large volume fraction of the interior species can be obtained via this approach (Figure 1.11c). As Milner assumed, the number of arms strongly influences the morphology. He predicted that at a constant volume fraction of 40 %, a symmetric diblock where $n_A = n_B = 1$ would form lamellae, while for an "Y" polymer where $n_A = 2$ cylinders would be generated and a spherical phase in the case of a"ψ" polymer. In conclusion, both theory and experiment have demonstrated that the architecture of block copolymers is a controlling factor in morphological behavior.

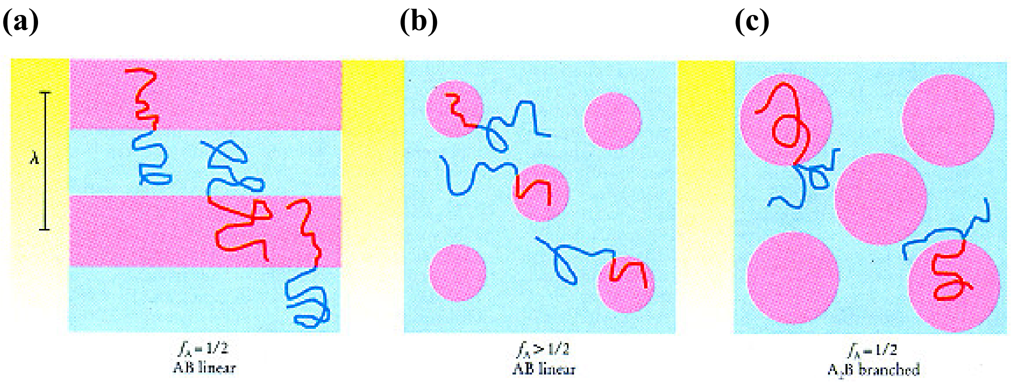

Figure 1.11. Dependence of diblock copolymer morphology on block composition (f) and molecular architecture (linear *vs.* banched).

Milner also predicted a less dramatic effect of architecture in the SSL for star-block copolymers. Star-block copolymers consist of some number of identical diblock copolymer "arms" with the free ends of the A blocks joined at a point. However the effect of the constraints on the free end of the chains can be considered small, so that they would behave roughly as its constituent arms.

Gido and coworkers demonstrated later that not only can the polymer architecture shift the normal diblock morphology phase boundaries but also results in the formation of new morphologies unobtainable with linear diblock structures of the same volume fraction. Their studies focused on the morphological behavior of a series of PI-PS (deuterated) well-defined A_2B simple graft (A = PI and B = PS) or “Y” architecture BCPs by utilizing TEM and SAXS (Figure 1.12a).[28] Their results are in good qualitative agreement with the calculations of Milner in that the observed morphologies occur at a higher PS volume fraction than expected for linear diblock architectures. However, a new morphology appears at high PS (81 %) volume fractions that was neither predicted nor observed in pure linear diblock copolymers. This microphase consists of randomly oriented wormlike micelles (ROW) dispersed in a continuous matrix. Selective solvent casting and prolonged annealing experiments determined the equilibrium nature of this peculiar morphology, allowing the concomitant observation of the transition from the kinetically unstable intermediate structures such as folded-lamellar and folded-lace into the novel thermodynamically favoured ROW.[29] Seemingly the 81 % volume fraction of PS is large enough to force the two PI arms to the concave side of the PS/PI interface in the microphase-separated state thereby inhibiting the formation of a morphology within an ordered lattice.

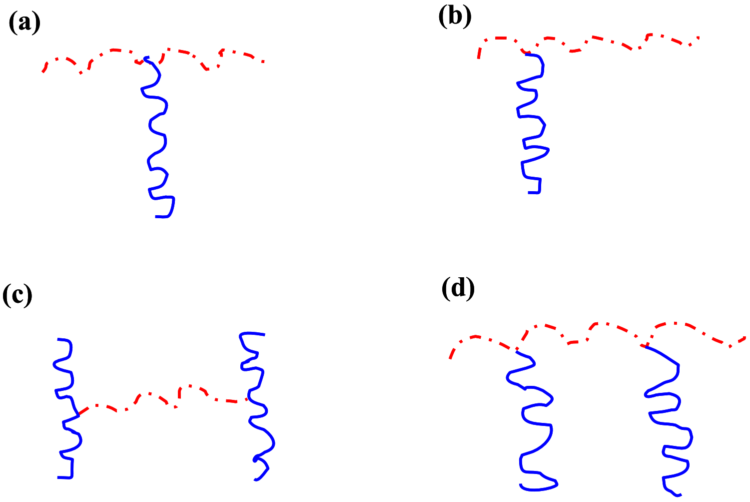

Figure 1.12. Graft copolymer architectures: (a) single graft, (b) asymmetric single graft, (c) H double graft and (d) π double graft.

In 1996 Gido, Hadjichristidis and coworkers synthesized asymmetric simple graft (ASG) block copolymer structures using the same methods developed earlier for miktoarm star copolymers (Figure 1.12b).[30] They studied the morphological behavior of an ASG consisting of two PI blocks of different degrees of polymerization and one deuterated PS block with a fractional location value (τ) of 0.25, which corresponds to the fractional distance along the PI backbone at which the PS graft occurs. By comparing the lattice dimensions with diblock, A_2B and A_3B materials of similar molecular weight and composition, all of which formed lamellar structures, they observed that the lattice dimensions decrease in the order: linear diblocks, ASG, A_2B and A_3B, which is qualitatively consistent with Milner's calculation. In the ASG case, the chain stretching and lateral crowding due to the miktoarm architecture is partially alleviated on account of the different lengths of PI blocks. Although the morphological behavior of the ASG structure cannot be directly predicted by Milner's calculation, because of the applicability of the ε parameter to blocks of the same type with the same molecular weight, they postulated a general relationship between ε and τ: $\varepsilon = f(\tau)(l_A/l_B)^{1/2}$. Therefore, for the ASG structure f(τ) (a function of τ that replaces the ratio of arm numbers in the molecular asymmetry parameter (ε) equation), should be between 1 (value for linear diblocks) and 2 (value for a symmetric simple graft structure). The same authors later described the morphology of a series of double-graft BCPs such as H- or π-shaped (Figure 1.12c and 1.12d).[31] Thus, in order to apply Milner's A_nB_m morphology diagram, they postulated the division of the H (S_2IS_2) or π ((SI)I´(SI)) architecture into two component single grafts by cutting the connecting block in the middle. The morphology of these more complex molecular architectures approximates that of its constituting BCPs. For the π architecture an introduction of a f(τ) function is again necessary for representing the molecular asymmetry as a function of the fractional location of the graft point along the backbone. The resulting morphologies displayed a good agreement with the Milner's morphology diagram, even though some minor discrepancies, especially at higher volume fractions of the graft block, were observed. Further studies by Gido *et al.* on A_5B six-arm miktoarm star BCPs[32] revealed a systematic tendency of the Milner's theory to overestimate the effect of architectural asymmetry on the morphological shift.[33] This overestimation in the theory is attributed to a junction point localization effect which was neglected in Milner's calculation. By comparison with the discrepancies in other studies,[31a,34] they found that the overestimation increases with asymmetry. For three I_5S samples only lamellar and cylindrical morphologies were observed, despite the fact spherical morphologies were predicted by the theory.[33a]This results in a vertical straightening of the order-order transition lines in the Milner's morphology diagram at high ε values, due mainly to the packing constraints in placing a relatively small volume fraction of material in the matrix around the microphase-separated domains. Additionally, unusual chevron tilt grain boundary morphologies were observed in one of the lamella forming materials that were attributed to energy penalties resulting from the bend of the lamellar interface.

Recently Gido, Hadjichristidis and coworkers confirmed experimentally the findings of earlier studies[31b,34a,34c,35] in that the junction point functionality in miktoarm star BCPs has an effect on chain conformation and morphology.[36] This effect had been neglected in the theory of Milner and thus predicted that A_nB_n miktoarm stars[37] of all n values should behave identically to the corresponding AB diblock copolymer with the same A and B arm. Contrary to the theoretical predictions, significant increases in lamellar spacing are found with increasing star functionality (n) in a series of PS-PI star block copolymers with identical PS and PI arms and this can be attributed to molecular crowding near the junction point.[36]

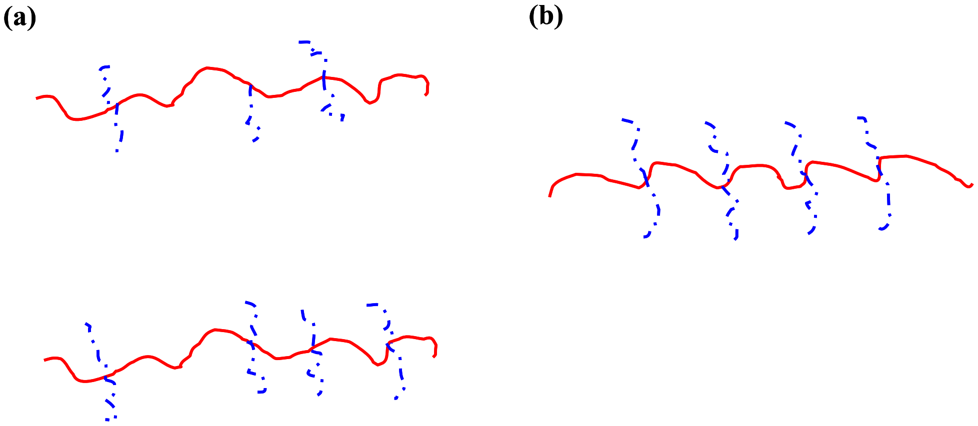

Figure 1.13. Illustrations of (a) random multigraft copolymer architectures with trifunctional and tetrafunctional branch points and (b) regular multigraft copolymer architectures with tetrafunctional branch points.

The morphological behavior of well-defined multiple-graft block copolymers with PBD backbones and PS grafted blocks, with branch points located randomly along the PBD backbone, was also studied.[38] Each branch point was either trifunctional or tetrafunctional (Figure 1.13a). It was observed that the materials formed the domain shapes predicted by the constituting block copolymer hypothesis. However, spherical and cylindrical morphologies lacked the long-range lattice order found in diblocks and other simpler block copolymer molecular architectures, while lamellar morphologies showed some long-range order. The lack of long-range order was attributed to the presence of multiple junction points, limiting the molecular mobility necessary to increase long-range order during solvent casting and thermal annealing and to the architectural dispersity resulting from random graft point locations along the backbone. The role of branch point location along the backbone was later examined by comparing the behavior of multigrafts with regularly located branch points to that of multigrafts with random junction point placement (Figure 1.13).[39] The observation of limited lattice ordering in cylindrical samples in the regular multigraft series indicated that regularity of graft placement improves the ability of multiple-graft copolymers to form long-range order.

1.2.2 Other polymeric complex systems

In other important studies the inherent organizing capacity of diblock copolymers has been tailored for example by introducing liquid crystallinity or by incorporating rod-like moieties within the blocks.[40] Adams and Gronski synthesized liquid crystalline (LC) block-coil BCPs by chemically modifying the diene block of a styrene-diene diblock copolymer so that a cholesterol unit could be attached as a mesogenic side group.[41] The found LC phase was affected by the confinement in the periodically spaced microdomains.[42] Stupp and coworkers have also reported the self-assembly of mushroom-shaped nanostructures built from a miniaturized triblock copolymer of styrene-isoprene and a rodlike oligomer.[43] Thomas *et al.* have presented other examples of novel rod-coil block copolymers that combined poly(hexyl isocyanate) (PHIC) as a rod block and PS as a coil block.[44] The incompatibility of the rod and coil blocks drives the PHIC-*b*-PS solution-cast films to microphase separate into orientationally ordered smectic-like lamellar morphologies such as wavy lamellar (WL), zigzag (ZZ) and arrow headed (AH). The ZZ and AH morphologies were, prior to this point, not addressed for rod-coil structures. Further experimental studies on the phase behavior of rod-coil block copolymers are essential in order to develop a theory that explains its process of self-assembling.

1.3 LINEAR-DENDRITIC BLOCK COPOLYMERS

It is clear that there are many possibilities to manipulate the morphology other than utilizing linear diblock copolymers. Among these are, making linear polymers with three distinct block types,[1f,6c,20] blending linear diblock copolymers,[45] coupling different scale ordering structures,[46] attachment of dendrons to a polymeric core in the so-called "dendronized" polymers[47] and more recently making nonlinear block copolymers.[3,21,48] As shown before, some interesting features have already been discovered on the solid-state behavior of these materials, but there are still probably many more.

The rapid development of dendrimers and hyperbranched polymers − cascade-branched structures that are often summarized as "dendritic" polymers − has greatly enhanced the spectrum of potential building blocks for segmented macromolecular architectures. Dendrimers are perfectly branched and highly symmetrical macromolecules that possess a well-defined number of end groups and an interior area, thus offering numerous interesting possibilities for supramolecular chemistry, such as guess uptake and shell-dependent release.[49] The multiple end groups can be functionalized to tailor solubility, adhesive properties or the diffusion rate into and out of the interior. Additionally, dendrimers have been used as templates for the formation of metal nanoparticles and are intensely studied with respect to biomedical application in diagnostics and therapy.[49,50] Two different synthetic strategies are employed to construct regular dendritic frameworks.[49] The first is the divergent approach, which involves the initial reaction of a monomer unit with a polyfunctional core followed by the iterative repetition of a two-step synthetic procedure that leads to subsequent generations.[51] The second is the "convergent-growth" strategy, where construction is initiated at the periphery of the macromolecule.[52] Although in the divergent approach, structural uniformity is harder to maintain due to the rapid increase of reactive groups at the chain terminus of the growing macromolecule, it is better suited for larger scale syntheses and for the preparation of high-generation dendrimers. However, both synthetic procedures involve multiple steps with intermediate purifications that detract from their widespread use. In contrast, although with an irregular pattern of branching, hyperbranched polymers may be prepared in a single polymerization step using AB_n type polyfunctional monomers.[53] Concluding, dendritic systems play an important role within nonlinear block copolymer structures, not only because of their architectural benefit, but also on account of the possibility to modify their chemistry, so that their role can be examined in polymers of the same architecture.

1.3.1 LINEAR-DENDRIMER BLOCK COPOLYMER STRUCTURES

Within these nonlinear block copolymer systems containing cascade-branched blocks, several groups have focused on block copolymer structures consisting of a linear and a dendrimer block, showing some peculiar properties of such materials.[54] However, the preparation of a perfectly branched dendron block represents a time-consuming multistep synthesis. In addition, the size of the dendrimer block is limited to the respective perfect dendrimer generation. While there are a considerable number of publications regarding the synthesis and solution properties of these linear-dendritic block copolymers (LDBCPs), very little literature exists concerning the solid-state or thin film properties.[55] In this section some examples regarding the synthesis of LDBPCs will be presented. Then a summary on the studied bulk properties of these architectures will follow, as this is a relevant topic for this thesis.

Early works of Newkome on two-directional cascade molecules (arborols) can be considered as an important prelude to the theme of linear-dendrimer hybrid structures.[56] ABA-type structures with a central, apolar alkyl chain and [G2] dendron termini with up to 9 hydroxyl end groups have been described.[57] Figure 1.14 shows an example of a two-directional arborol possessing a rigid oligospirane core.[58] However, in Newkome's structures no polymer segments have been employed. The basic structures of LDBCPs and the general synthetic pathways are presented in Figure 1.15. Generally, the combination of a dendrimer segment ("dendron") with a linear polymer chain to give an hybrid LDBC is possible via three different strategies: (i) coupling of prefabricated dendron and linear polymer chain, (ii) the "chain-first" route and (iii) the "dendron-first" strategy.

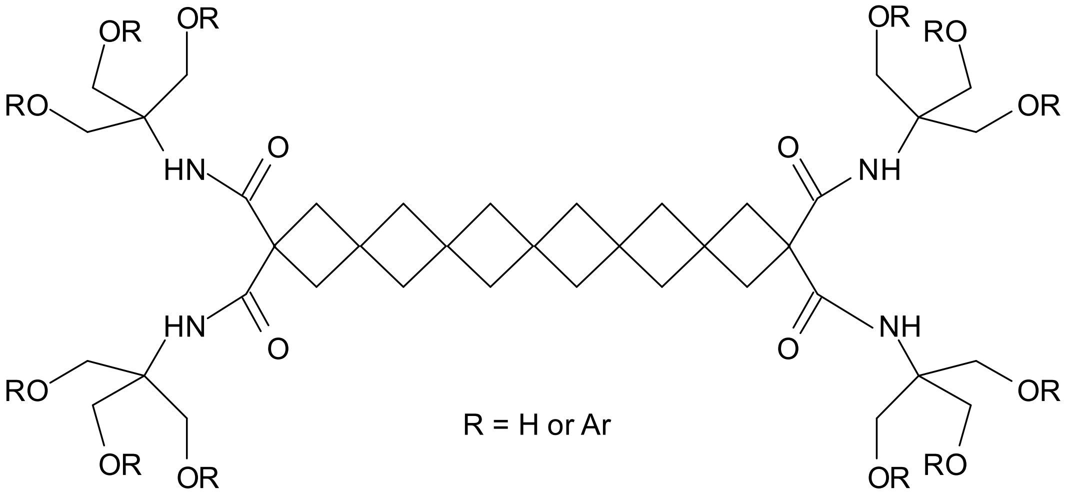

Figure 1.14. Newkome's spirane two-directional arborol structure.

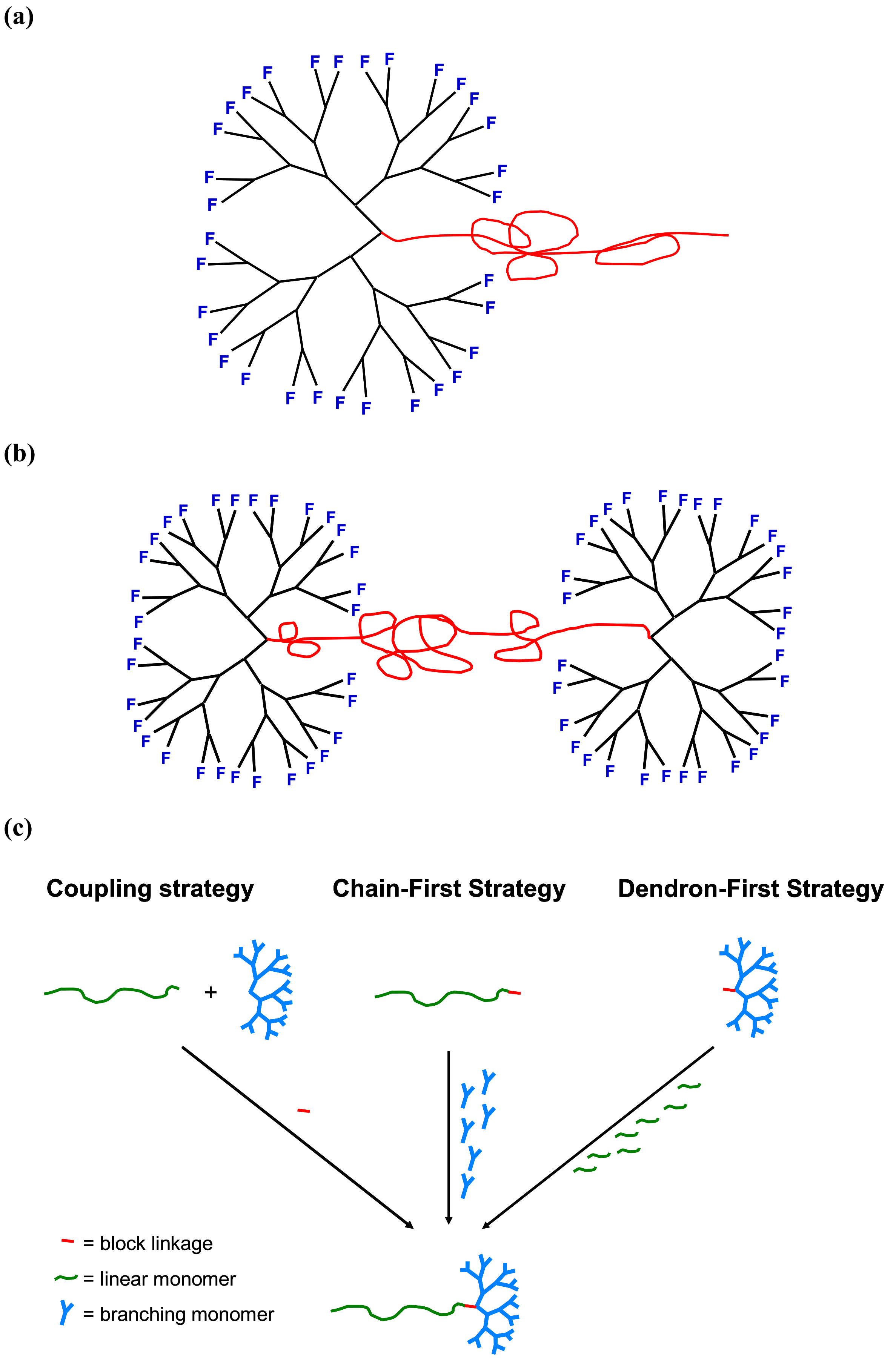

Figure 1.15. (a), (b) Schematic picture of AB and ABA linear-dendrimer structures and (c) general synthetic strategies.

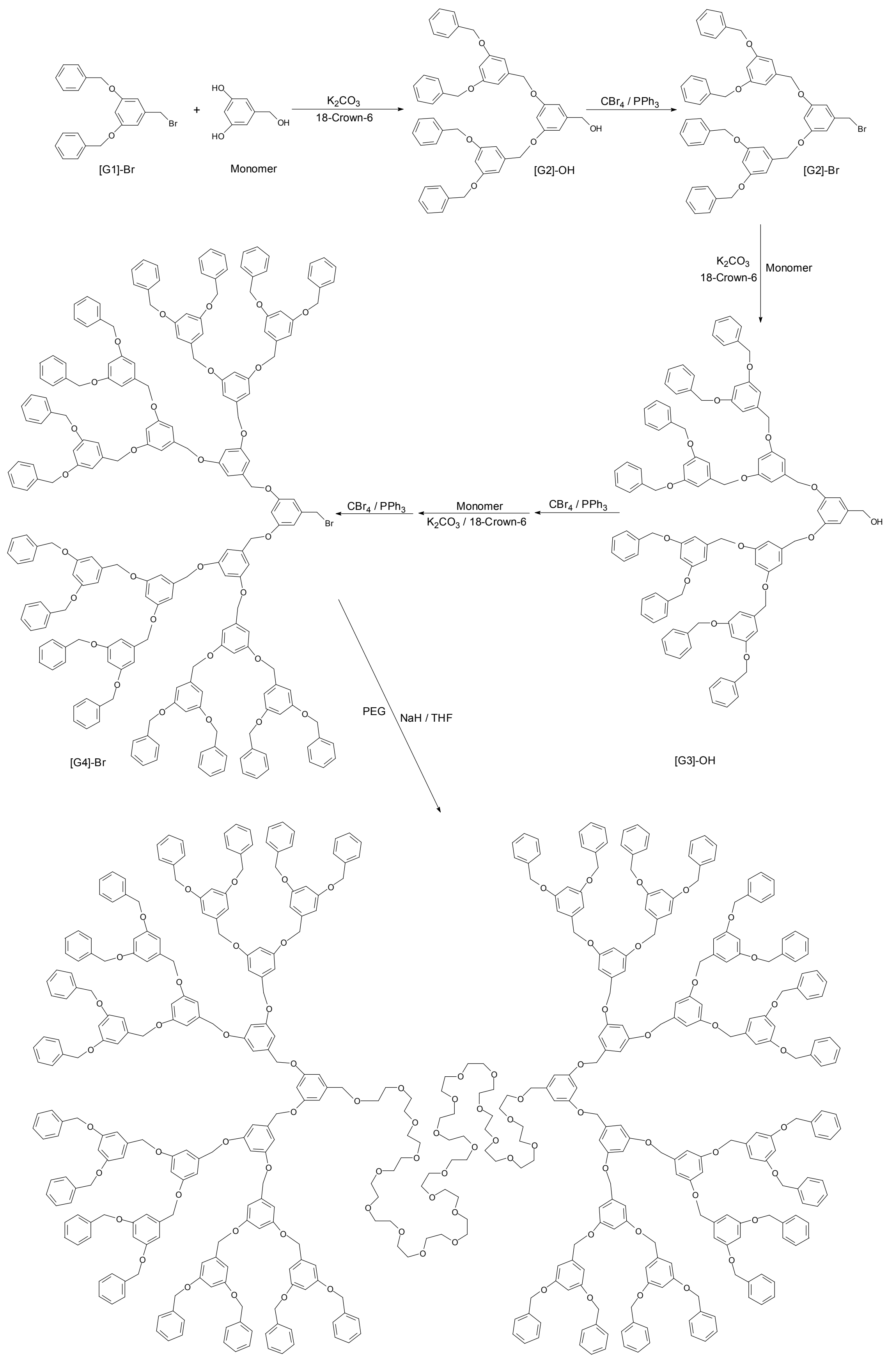

Figure 1.16. Schema of the synthesis of a fourth-generation dendritic bromide [G4]-Br and of the ABA linear-dendritic block copolymer obtained by reaction of PEG with [G4]-Br in the presence of NaH.

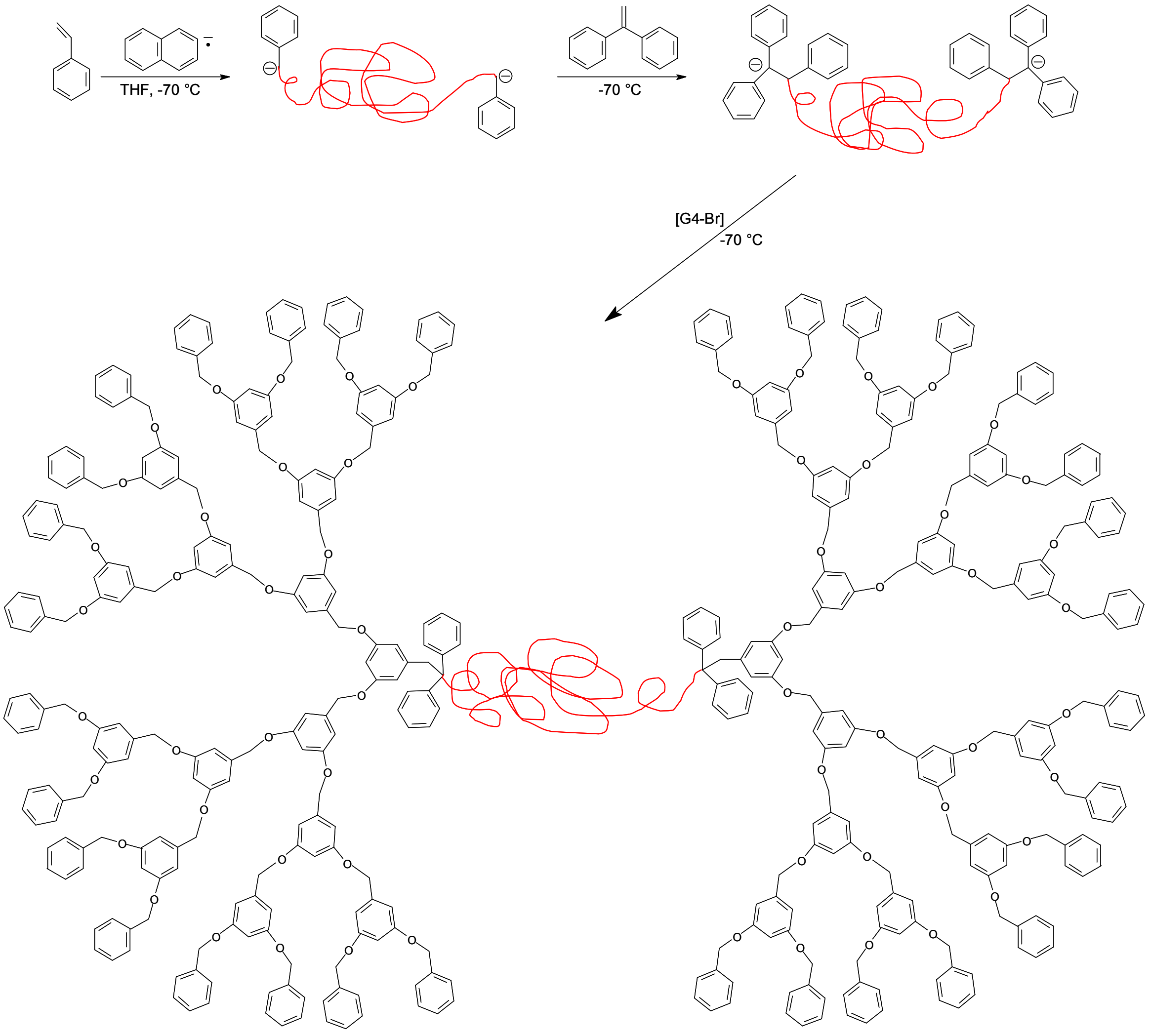

Figure 1.17. Preparation of ABA triblock hybrid with Fréchet-type dendrons as terminal A blocks and PS as the central B block.

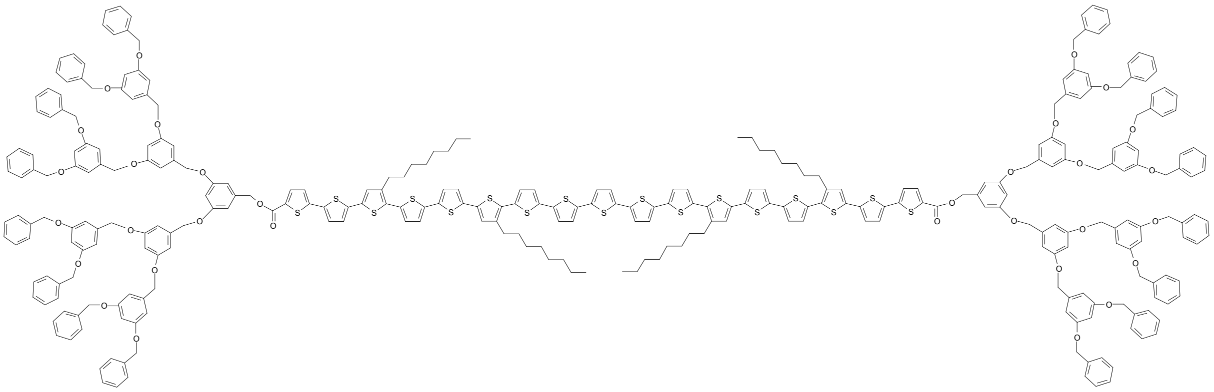

Figure 1.18. Triblock hybrid based on PBE dendron and an oligothiophene core.

Examples of the coupling strategy (Figure 1.15a) include the first LDBCPs prepared by Fréchet and coworkers in 1992,[59] who reported both AB diblock and ABA triblock type structures.[60] They used mono- and difunctional hydroxy-poly(ethylene oxide) (PEO) ($\overline{M}_n$ in the range of 500 to 20,000 g/mol) and convergently prepared poly(benzyl ether) dendrons of generations [G3] and [G4] with 8 and 16 end groups respectively. Coupling of the blocks was achieved via facile Williamson reaction of the deprotonated hydroxyl end groups of PEO with the bromomethyl group at the focal point of the dendrons as shown in Figure 1.16. In a subsequent work, Gitsov and Fréchet prepared in a similar fashion ABA hybrid copolymers consisting of PS and PBE dendrons by endcapping of a "living" bifunctional PS with PBE bromides (Figure 1.17).[60a,61] Anionic polymerization of styrene was initiated with potassium naphtalide to generate bifunctional growth of the reactive PS. To avoid side reactions, the nucleophilicity of the living ends of the PS was decreased by addition of 1,1-diphenyl ethylene (1,1-DPE) prior to reaction with the fourth generation dendritic bromide. This coupling approach has also been employed for the synthesis of unusual ABA block copolymers consisting of lengthy oligothiophenes and PBE dendron termini (Figure 1.18).[62] The main advantage of this fragment coupling method is that the hybrid macromolecule is obtained in a single step from well-defined starting materials.

The alternative chain-first strategy (Figure 1.15b) has been successfully demonstrated by Chapman,[54g] Meijer[54f] and Hammond.[54d] Chapman and coworkers prepared AB block copolymers termed "hydraamphiphiles" consisting of hydrophobic terminal residues (Boc) attached to a poly(l-lysine) dendrimer and a hydrophilic linear PEO chain (Figure 1.19b). Several years later, Park and coworkers extended the synthetic method by introducing poly(l-lysine) dendrimers up to the fourth generation at both ends of the linear PEO to obtain hybrid ABA triblock copolymers.[63] Meijer *et al.* made also use of this approach to prepare low molecular weight PS ($\overline{M}_n$ = 3,000 g/mol) combined with poly(propylene imine) (PPI) dendrimers. Five different generations from PS-*dendr*-NH_2 to PS-*dendr*-$(NH_2)_{32}$ were prepared in good yields. The synthetic path can be followed in Figure 1.19a: the anionically prepared amine-functionalized PS was reacted with acrylonitrile in a double Michael addition, followed by Raney-cobalt catalyzed heterogeneous hydrogenation of the nitriles to amines. Similarly Hammond *et al.* prepared LDBCPs having poly(amido amine) (PAMAM) as the dendrimer block and PEO as the linear block. As shown in Figure 1.20, PAMAM is grown divergently from an amine-modified PEO chain by alternating Michael addition with methylacrylate and subsequent deprotection reaction with ethylenediamine. This process has the advantage of producing hybrids with reactive groups located at the periphery of the dendritic block. However, the presence of the linear block throughout the stepwise divergent synthesis increases somewhat the complexity of the purification procedure.

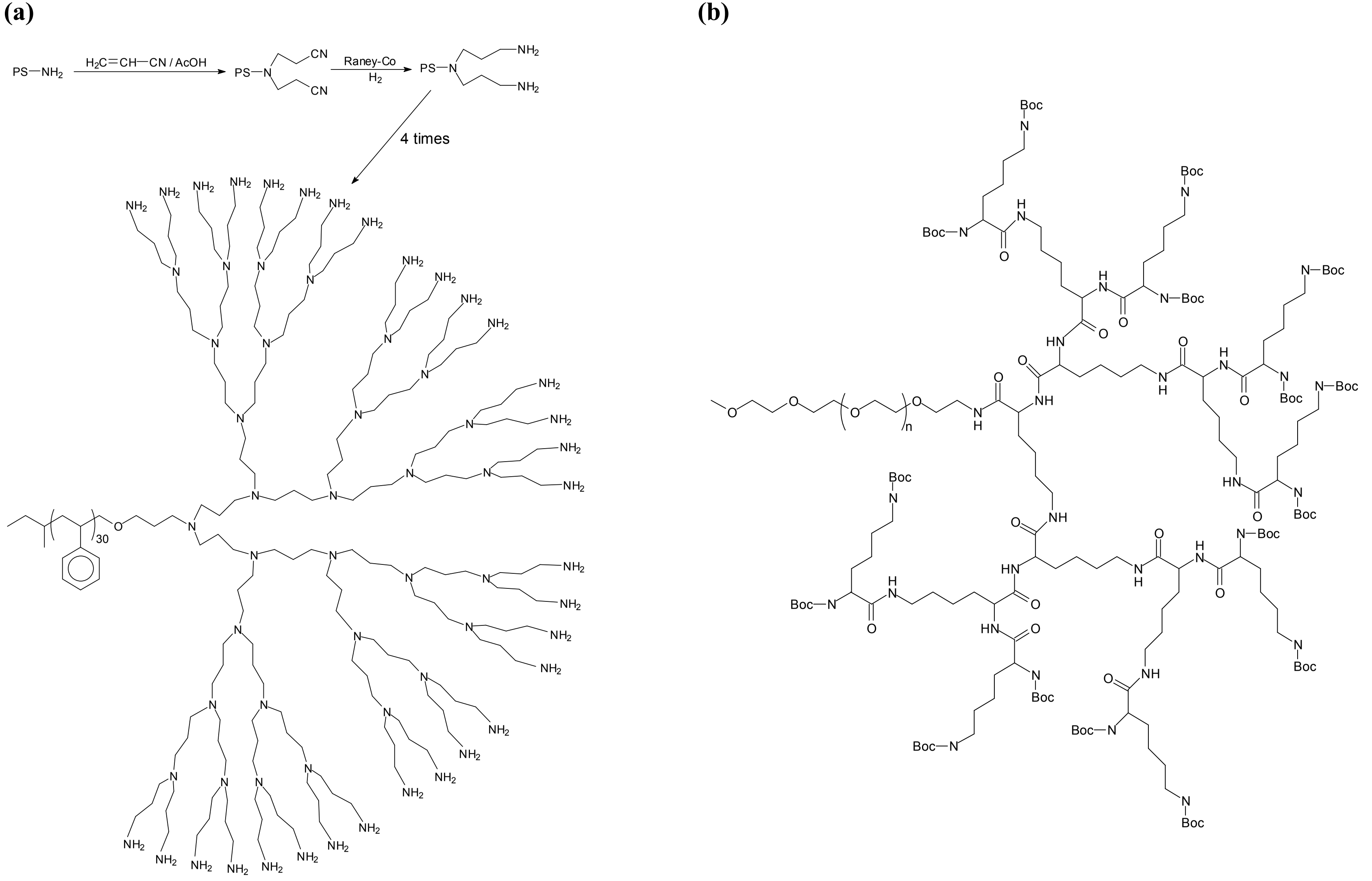

Figure 1.19. (a) Meijer's PS-PPI dendrimer architecture; (b) Chapman's PEO-Boc-poly(L-lysine) hybrid diblock copolymer.

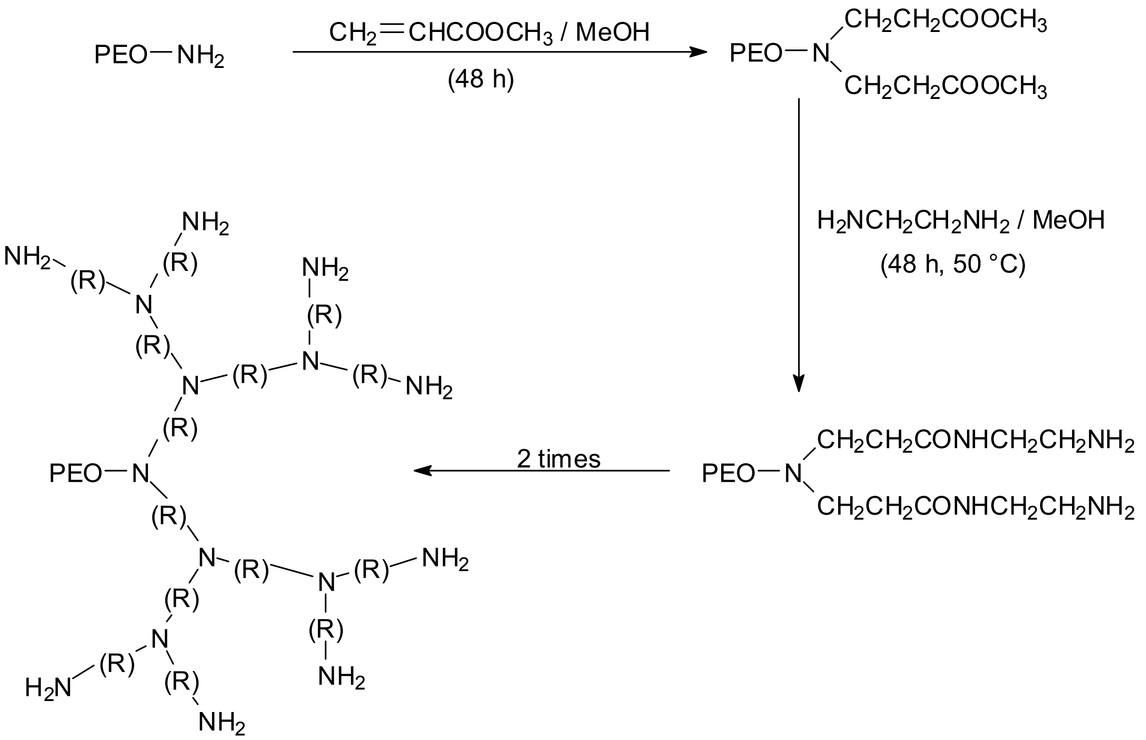

Figure 1.20. Synthesis of PEO-PAMAM diblock copolymer by Hammond *et al.* (R = $CH_2CH_2CONHCH_2CH_2$).

As the coupling synthetic approach has limitations with respect to general applicability and coupling yields, Fréchet's group developed an alternative method (Figure 1.15c) for the preparation of LDBCPs, based on the use of convergently grown dendrimers as macroinitiators for anionic polymerization. Using bases such as potassium naphtalide or diphenylmethylpotassium, the [G4] convergently grown dendritic PBE alcohols were deprotonated to generate alkoxides that initiated the ring-opening polymerization (ROP) of ϵ-caprolactone (ϵ-CL).[54h] This concept of dendrons as macromolecular initiators was extended by Matyjaszewski as well as Hawker and Fréchet for the "living"/controlled free radical polymerization of vinyl monomers.[54e,64] PBE dendrons containing a single, initiating styrene/TEMPO or halide functionality at their focal point were used respectively for the nitroxide mediated and atom transfer radical polymerization (ATRP) of styrene, providing control over molecular weights and polydispersities. Recently, an accelerated route to unusual hybrid block copolymers composed of nanoparticles and linear polymers have been demonstrated by Fréchet and Hawker using controlled radical polymerization.[48b] Particle-coil diblock copolymers were prepared by the synthesiss of poly(*n*-butyl acrylate)-*block*-poly(styrene-*random*-(4-vinylbenzocyclobutene) (pBA-*b*-p(S-*r*-BCB) or pEG-*b*-p(S-*r*-BCB) as linear copolymers, followed by selective intramolecular cross linking of the segments containing pBCB groups (Figure 1.21).

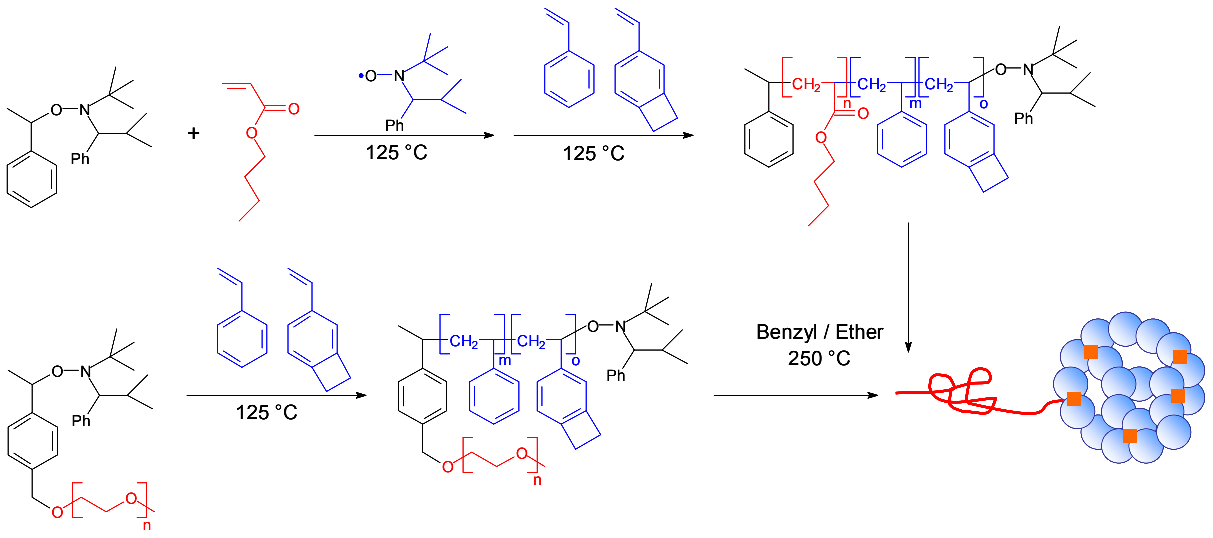

Figure 1.21. Schema for the synthesis of particle-coil copolymers using a combination of controlled/living radical polymerization and poly(4-vinylbenzocyclobutene) (pBCB) intramolecular cross linking processes. The nanoparticle is composed of a crosslinked polystyrenic segment and the lineal coil of poly(*n*-butyl acrylate) (pBA) or poly(ethylene glycol) (pEG).

1.3.1.1 Solid-state properties. Bulk morphologies

LDBCPs are hybrid architectures that may be viewed as the extreme case of miktoarm star copolymers, with the maximum number of branching points in the branched block and thus particularly high crowding at the interface in the segregated structure. Hence these materials are highly intriguing with respect to nanophase segregation and morphology. A comparison to star or miktoarm star BCPs is however not completely rigorous due to the lack of significant chain stretching in dendritic molecules. Up to date only a few papers have been published concerning the solid-state or thin film properties of LDBCPs.[55] In early work, Fréchet *et al.* studied the solid-state behavior of AB and ABA copolymers containing dendritic PBE and linear PEO blocks.[55g] Thermal studies using DSC showed microphase segregation with two thermal transitions being observed when the mass of the PEO block was greater or equal than the benzyl ether dendrimer block, namely a melting transition due to the crystalline PEO phase and a glass transition due to the dendrimer phase. When the dendrimer represented the larger block, phase mixing took place, so no detectable melting point was observed for the PEO block. The influence of the dendritic amorphous block on the crystallization behavior of the linear block was further evaluated using polarized microscopy. The data revealed that the linear blocks were able to crystallize in spherulites, axialites, or dendritic structures depending on the composition of the block and the solvent used.

The first study on the morphologies generated after microphase segregation was reported by the group of Meijer *et al.*, detailing the superstuctures of LDBCPs consisting of PS and carboxylic acid functionalized PPI structures.[55f] These BCPs showed microphase separation in the solid-state as a consequence of the incompatibility between the carboxylic groups and the PS block. The properties of four generations of the PS-*dendr*-$(COOH)_n$ with n = 4, 8, 16 and 32 were studied by Small Angle X-ray Scattering (SAXS), Transmission Electron Microscopy (TEM) and X-ray Diffraction (XRD). The morphological studies revealed that by increasing the dendrimer generation, the structures changed from hexagonally packed cylinders to lamellar while the low-range spatial order decreased in the lattices. By comparing the observed morphologies for the linear-dendritic polymers with the ones expected for linear diblock copolymers, the authors observed that the architecture clearly influences the microdomain structure at a given volume fraction.

Mackay *et al.* have published the most recent results on the bulk behavior studies of LDBCPs without a strong amphiphilic driving force.[55d] The solid-state behavior of linear PS grafted to a sixth-generation dendron of PBE ($\overline{M}_n$ = 13,464 g/mol) was studied by TEM and confirmed by scattering data. An additional entropic factor was suggested to be responsible for the strong phase separation of the materials, caused by the impenetrability of the dendron by the linear chain. Although without a strong effect, they observed that the morphologies deviate from the phase boundaries of the analogous linear-linear diblocks with decreasing linear block fraction. A particularly interesting finding was the formation of a lamellar superstructure already at 29 % volume fraction (31 wt %) of the dendron block. Further studies on the same system but with different relative ratios of block components were performed by Pochan *et al.*, who confirmed a significant molecular architecture effect on the resultant phase-separated morphologies.[55e] A diblock having 51 % weight fraction of the sixth-generation dendrimer exhibited a PS cylindrical phase despite the symmetric volume fraction of the two blocks. Another interesting feature was the observation of a frustrated lamellar-like structure down to a dendrimer weight fraction of 22 %. Excluding a sample with 12 wt % of the dendrimer block, which displayed disordered spherical domains, large grains of regular separated microstructures were obtained.

The bulk phase behavior and microphase segregation of semicrystalline PEO-PAMAM LDBCPs in the solid state was reported by Hammond *et al.*.[55b] In addition, the dendritic end groups were functionalized with stearic acid to make amphiphilic LDBCPs. Observations were made above and below the crystallization melt point of PEO and the results indicated that the crystallinity of the linear PEO can greatly influence the final morphology. The unfunctionalized diblocks exhibited a segregated melt state above the PEO melting point and the PEO experienced confined crystallization below its melting point. At high temperature, a segregated melt state was also exhibited by the stearate functionalized diblocks, while at low temperatures both the stearate and PEO were crystalline and crystallization was strongly confined within the lamellar domains.

1.4 MOTIVATION AND OBJECTIVES OF RESEARCH DESCRIBED IN THIS THESIS

1.4.1 Why linear-hyperbranched diblock copolymers?

LDBCPs show many interesting properties, as they combine the architecture and reactive functionalities of well-defined dendritic macromolecules with the processability and phase separation behavior of linear polymers thus allowing the manipulation of morphology through design making possible the development of new devices within many advanced technology industries.[65] In addition to accessing new morphologies and providing enhanced properties, these "conformational hybrids" can also facilitate the integration of a particular functionality into the non-coil nanodomains. However, a major drawback of the linear-dendrimer architectures is the demanding multistep preparation strategy that represents a clear obstacle for real-world applications. Over the past decade and motivated by the surge of interest in dendrimers, hyperbranched polymers have received considerable attention as a class of very promising material due to their simplicity in synthesis and resemblance of many of the dendrimer's architectural features and properties. Recent progress in this field has been documented by some reviews.[53] Hyperbranched polymers, commonly prepared by a single step-growth polymerization of AB_n monomers, are characterized by a lesser degree of branching and broader molecular weight distributions when compared to dendrimers. In this context, in the middle of the 90's a new synthetic strategy was developed in our group for preparing hyperbranched polymers in a controlled manner. This synthetic technique, designated the slow addition method,[66] is based on the slow addition of AB_2 monomers in high dilution to a given concentration of core molecules B_f. By employing this synthetic pathway, control over molecular weights, polydispersity as well as the degree of branching (DB) has been achieved for various systems, rendering hyperbranched polymers competitors for the tediously prepared dendrimers.[53e]

1.4.2 The two strategies for the preparation of linear-hyperbranched block copolymers

One of the aims of this work is the preparation of novel - linear hyperbranched diblock copolymer systems with narrow polydispersity. Therefore, an important aspect for the preparation of these well-defined architectures is suitable methodology to control the size of the branched block while keeping the polydispersity low. Kricheldorf *et al.* presented in 1998 a first attempt for the preparation of ABA linear-hyperbranched BCPs having a central oligo(ether ketone) B block and hyperbranched polyester A blocks.[67] The silylated 3,5-bis(acetoxy)benzoic acid AB_2 monomer was probed to be useful for a polycondensation with the telechelic acetylated oligo(ether ketone)s only when lowering the reaction temperature to avoid cross linking reactions. Nonetheless, the ideal reaction conditions were not found, *i.e.* no real proof of a fully complete reaction of the linear block was shown and GPC traces revealed a very broad molecular weight distribution. Thus, the suggestion of using terminally functional polymers as a monofunctional polymer core for the preparation of well-defined linear-hyperbranched BCPs was not successful. However, since it is well-known that one of the major problems in the polycondensation of AB_n monomers is the possibility of intramolecular cyclization (*i.e.*, reaction of the focal A group with one of the large number of functional B groups, limiting control of molecular weights), preparation of well-defined linear-hyperbranched BCPs cannot be achieved in this way.

Knauss *et al.* reported in 2001 the first successful synthesis of well-defined linear-hyperbranched block copolymer consisting of a PS hyperbranched block and a PS or PI linear block.[68] The hybrids were made in one-pot by convergent living anionic polymerization. Dendritic PS macroinitiators were synthesized by slowly adding a mixture of a coupling agent (either vinylbenzyl chloride (VBC) or 4-(chlorodimethylsilyl)styrene (CDMSS)) and styrene (1:10 molar ratio) to a solution of living polystyryllithium. The addition was ceased prior to the addition of a stoichiometric amount of coupling agent to retain a living chain end (Figure 1.22). To the living dendritically branched PS was then added either styrene or isoprene to polymerize a linear block from the dendritic PS. A schematic picture of this approach is presented in Figure 1.23a. The Knauss method combines living anionic polymerization with a convergent synthetic approach, and a unique feature of this technique is the persistence presence of a single reactive site at the focal point of the forming macromolecule. Additionally, this method avoids the use of isolated preformed dendritic or linear polymers.

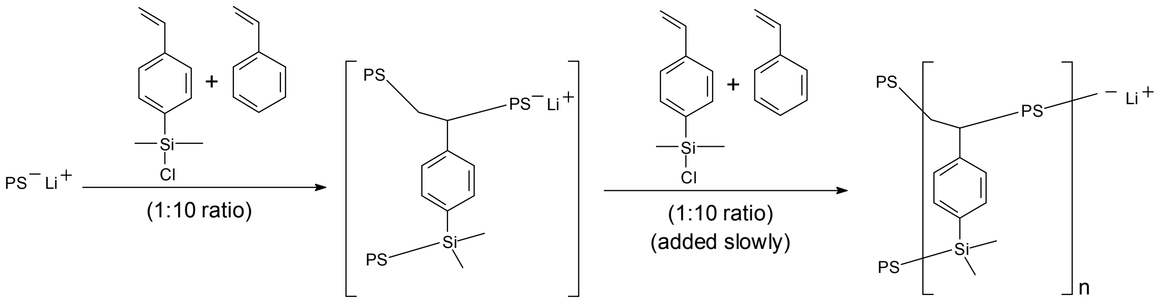

Figure 1.22. Synthesis of a dendritic PS macroinitiator using 4-(chlorodimethylsilyl) styrene and styrene.

In this thesis, an innovative, generally applicable synthetic strategy for the preparation of linear-hyperbranched diblock copolymers with narrow polydispersities is presented. This is based on the grafting of branching monomers onto a linear template structure (Figure 1.23b).[69] If suitable monomers are employed, the "hypergrafting" strategy leads to an unusual class of polymer brushes with dendritic molecular architecture. In order to generate linear-hyperbranched diblock copolymers, a long linear A_n-block is combined with a short polyfunctional B_f-type structure that acts as a core for the ensuing hypergrafting procedure. In a second "pseudo-chain growth" step, suitable designed AB_n monomers are grafted onto the B_f-block. The synthetic approach is realized via slow monomer addition (SMA).[66]

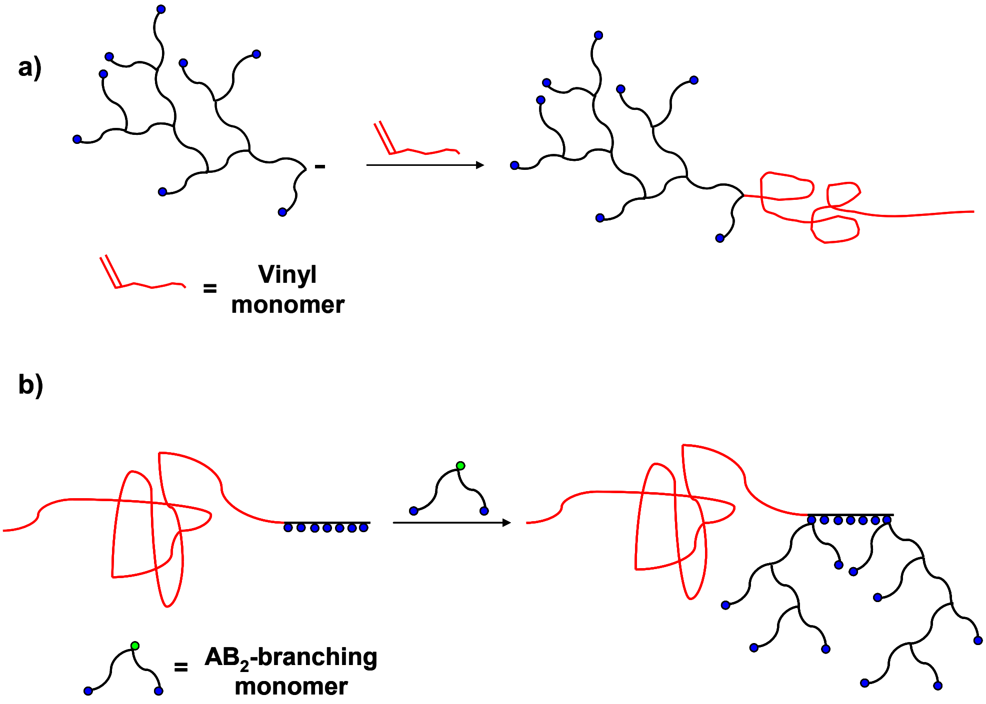

Figure 1.23. Synthetic strategies towards the preparation of linear-hyperbranched BCPs: (a) Knauss strategy, which consists in the use of a dendritic anionic macroinitiator for the linear polymerization of small monomers; (b) Frey strategy, which is based on the grafting of branching monomers onto a linear template structure.

1.4.3 Actual synthesis employed and objectives of research

In the systems presented in this work, polymer analogous chemistry is used to introduce branching monomers to BCPs prepared by anionic polymerization. The advantage of post-polymerization chemistry is that a source polymer with a very precise BCP architecture can be reliably prepared in large quantity and then through modification of one or both of the blocks, a new BCP can be produced. Such a procedure may make it possible to produce BCPs that are impossible to produce directly using living techniques. An additional advantage of the modification approach is that one source block copolymer can be modified in several ways to enable direct comparison between different polymer designs. Polydiene-containing block copolymers are appealing materials for modification because of the reactivity of the double bonds along the polymer chain. Thus polystyrene-*block*-poly(1,2-butadiene) diblock copolymers (PS_x-*b*-PBD_y) have been chosen as linear templates to obtain the different polymer architectures presented in this thesis. To build the hyperbranched structure, AB_n silicon-containing branching monomers have been employed, as silicon chemistry offers a number of reactions with quantitative yields. The schematic approach for obtaining one of the systems presented in this work is shown in Figure 1.24a.

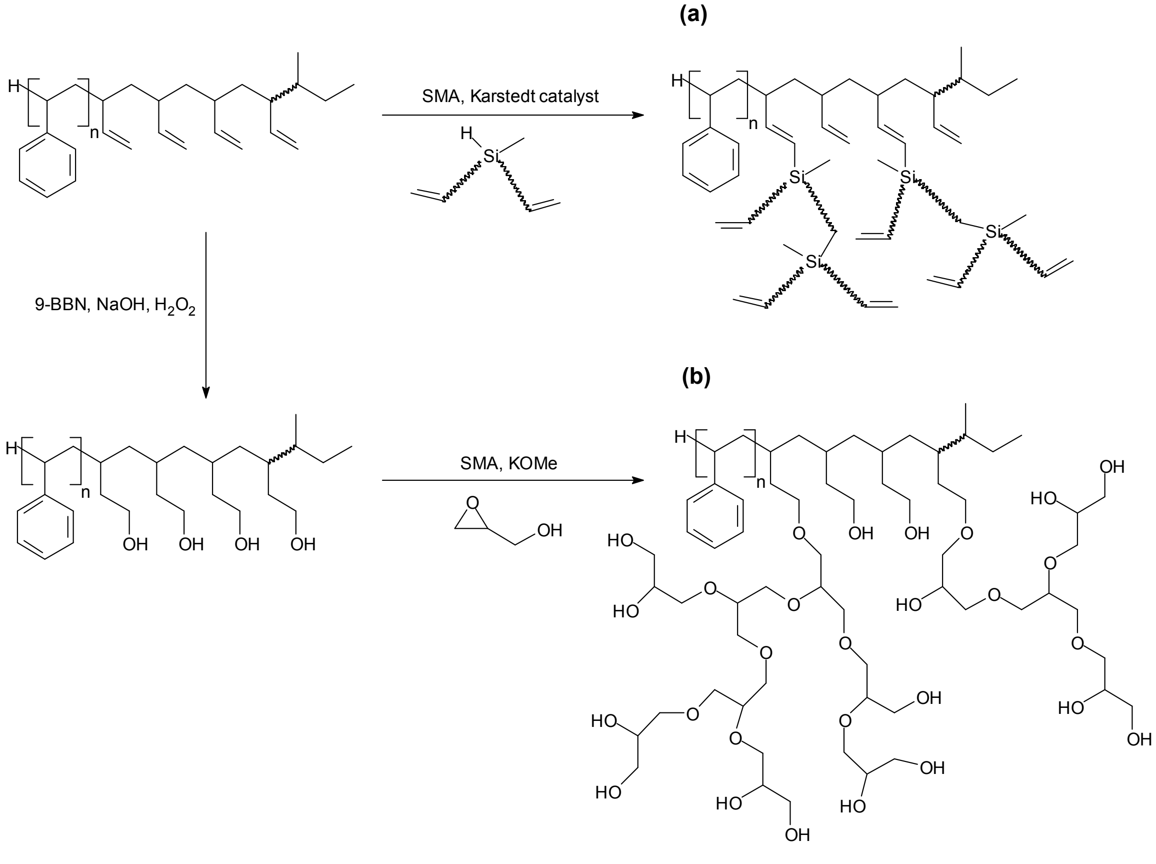

Figure 1.24. Synthesis of linear-hyperbranched BCPs by grafting of branched AB_2 monomers on a short PBD block.

In the next chapters novel silicon-containing BCPs with unusual architectures are presented. Until now, the factors influencing the phase separation of hybrid linear-dendritic systems and the resulting structures are not really well understood, so further studies on the solid-state behavior of these materials are necessary. Therefore, besides establishing a synthetic route, the main objective of this dissertation is to study the role of polymer topology on the physical and chemical properties. It is worth mentioned that in parallel to this work, the general validity of the above mentioned approach has been confirmed by the preparation of amphiphilic linear-hyperbranched BCPs (Figure 1.24b).[70]

1.5 REFERENCES

[1] (a) Ruzette, A.-V.; Leibler, L. *Nature Materials* **2005**, *4*, 19. (a) Lodge, T. P. *Macromol. Chem. Phys.* **2003**, *204*, 265. (b) Bucknall, D. G.; Anderson, H. L. *Science* **2003**, *302*, 1904. (c) Hadjichristidis, N.; Pispas, S.; Floudas, G. *Block Copolymers: Synthetic Strategies, Physical Properties, and Applications*; Wiley-Interscience: New Jersey, 2003. (d) Förster, S.; Plantenberg, T. *Angew. Chem. Int. Ed.* **2002**, *41*, 688. (e) Hamley, I. W. *The Physics of Block Copolymers*; Oxford University Press: Oxford, 1998. (f) Bates, F. S.; Fredickson, G. H. *Physics Today*, **1999**, *32*. (g) Muthukumar, M.; Ober, C. K.; Thomas, E. L. *Science* **1997**, *277*, 1225. (h) Bates, F. S.; Fredickson, G. H. *Annu. Rev. Phys. Chem.* **1990**, *41*, 525.

[2] (a) Hamley, I. W. *Angew. Chem. Int. Ed.* **2003**, *42*, 1692 and references therein. (b) Park, C.; Yoon, J.; Thomas, E. L. *Polymer* **2003**, *44*, 6725 and references therein.

[3] Hadjichristidis, N.; Pitsikalis, M.; Pispas, S.; Iatrou, H. *Chem. Rev.* **2001**, *101*, 3747.

[4] Szwarc, M. *J. Polym. Sci., Part A: Polym. Chem.* **1998**, *36*, 9.

[5] Holden, G.; Milkovich, R. US Patent 3,265,765, 1966.

[6] (a) Jérôme, R.; Teyssié, Ph.: Vuillemin, B.; Zundel, T.; Zune, C. *J. Polym. Sci., Part A: Polym. Chem.* **1999**, *37*, 1. (b) Hong, K.; Uhrig, D.; Mays, J. W. Curr. Opin. Solid State Mater. Sci. **1999**, *4*, 531. (c) Stadler, R.; Auschra, C.; Beckmann, J.; Krappe, U.; Voight-Martin, I.; Leibler, L. *Macromolecules* **1995**, *28*, 3080. (d) Riess, G.; Schlienger, M.; Marti, S. *J. Macrom. Sci. Phys.* **1980**, *2*, 355.

[7] Navarro, C. Marcarian, X.; Vuillemin, B. *Macromol. Symp.* **1998**, *132*, 263.

[8] (a) Adams, J. L.; Quiram, D. J.; Graessley, W. W.; Register, R. A.; Marchand, G. R. *Macromolecules* **1998**, *31*, 201. (b) Gehlsen, M. D.; Bates, F. S. *Macromolecules* **1993**, *26*, 4122.

[9] (a) Wall, L. A., Ed. *Fluoropolymers*; Wiley-Interscience: New York, 1972. (b) Reisinger, J. J.; Hillmyer, M. A. *Prog. Polym. Sci.* **2002**, *27*, 971. (c) Ren, Y.; Lodge, T. P.; Hillmyer, M. A. *J. Am. Chem. Soc.* **1998**, *120*, 6830.

[10] (a) Hillmyer, M. A. *Encyclopedia of Materials: Science and Technolog*y, Elsevier Science: Oxford, 2001. (b) Coates, G. W. *Angew. Chem. Int. Ed.* **2002**, *41*, 2236. (b) Coates, G. W. *Chem. Rev.* **2000**, *100*, 1223. (c) Piotti, M. E. *Curr. Opin. Solid State Mater. Sci.* **1999**, *4*, 539.

[11] (a) Hawker, C. J.; Bosman, A. W.; Harth, E. *Chem. Rev.* **2001**, *101*, 3661. (b) Grimaldi, S.; Finet, J.-P.; Le Moigne, F.; Zeghdaoui, A.; Tordo, P.; Benoit, D.; Fontanille, M.; Gnanou, Y. *Macromolecules* **2000**, *33*, 1141. (c) Listigovers, N. A.; Georges, M. K. Odell, P. G.; Keoshkerian, B. *Macromolecules* **1996**, *29*, 8992. (d) Moad,G.; Rizzardo, E.; Solomon, D. H. *Macromolecules* **1982**, *15*, 909.

[12] (a) Matyjaszewski, K. *Macromol. Symp.* **2001**, *174*, 51. (b) Kato, M.; Kamigaito, M.; Sawamoto, M; Higashimura, T. *Macromolecules* **1995**, *28*, 1721. (c) Wang, J.-S.; Matyjaszewski, K. *J. Am. Chem. Soc.* **1995**, *117*, 5614.

[13] (a) Moad, G.; Mayadunne, R. T. A.; Rizzardo, E.; Skidmore, M.; Thang, S. H. *Macromol. Symp.* **2003**, *192*, 1. (b) Chiefari, J.; Chong, Y. K.; Ercole, F.; Krstina, J.; Jeffery, J.; Le, T. P. T.; Mayadunne, R. T. A.; Meijs, G. F.; Moad, C. L.; Moad, G.; Rizzardo, E.; Thang, S. H. *Macromolecules* **1998**, *31*, 5559.

[14] Nicolas, J.; Charleux, B.; Guerret, O.; Magnet, S. *Macromolecules* **2004**, *37*, 4453.

[15] (a) Matsen, M. W.; Bates, F. S. *Macromolecules* **1996**, *29*, 1091. (b) Khandpur, A. K.; Förster, S.; Bates, F. S.; Hamley, I. W.; Ryan, A. J.; Bras, W.; Almdal, K.; Mortensen, K. *Macromolecules* **1995**, *28*, 8796. (c) Förster, S.; Khandpur, A. K.; Zhao, J.; Bates, F. S.; Hamley, I. W.; Ryan, A. J.; Bras, W. *Macromolecules* **1994**, *27*, 6922. (d) Leibler, L. *Macromolecules* **1980**, *13*, 1602.

[16] (a) Matsen, M. W.; Bates, F. S. *J. Chem. Phys*. **1997**, *106*, 2436. (b) Matsen, M. W.; Schick, M. *Macromolecules* **1994**, *27*, 4014.

[17] (a) Qi, S.; Wang, Z.-G. *Phys. Rev.* **1997**, *E55*, 1682. (b) Hajduk, D. A.; Takenouchi, H.; Hillmyer, M. A.; Bates, F. S.; Vigild, M. E.; Almdal, K. *Macromolecules* **1997**, *30*, 3788.

[18] Cochran, E.; Garcia-Cervera, C. J.; Fredickson G. H. *Macromolecules* **2006**, *39*, 2449.

[19] Davidock, D. A.; Hillmyer, M. A.; Lodge, T. P. *Macromolecules* **2003**, *36*, 4682.

[20] (a) Breiner, U.; Krappe, U.; Thomas, E. L.; Stadler, R. *Macromolecules* **1998**, *31*, 135. (b) Abetz, V.; Stadler, R. *Macromol. Symp.* **1997**, *113*, 19 (c) Krappe, U.; Stadler, R.;

Voigt-Martin, I. *Macromolecules* **1995**, *28*, 4558. (d) Riess, G.; Schlienger, M.; Marti, S. J. *Macromol. Sci. Polym. Phys. Ed.* **1980**, *17*, 355.

[21] Pitsikalis, M.; Pispas, S.; Mays, J. W.; Hadjichristidis, N. *Advances in Polymer Science* **1998**, *135*, 1.

[22] Alward, D. B.; Kinning, D. J.; Thomas, E. L.; Fetters, L. J. *Macromolecules* **1986**, *19*, 215.

[23] Herman, D. S.; Kinning, D. J.; Thomas, E. L.; Fetters, L. J. *Macromolecules* **1987**, *20*, 2940.

[24] (a) Olmsted, P. D.; Milner, S. T. *Macromolecules* **1998**, *31*, 4011. (b) Milner, S. T. *Macromolecules* **1994**, *27*, 2333.

[25] (a) Hadjichristidis, N.; Tselikas, Y.; Iatrou, H.; Efstratiadis, V.; Avgeropoylos, A. *J.M.S.-Pure Appl. Chem.* **1996**, A33(10), 1447. (b) Tselikas, Y.; Iatrou, H.; Hadjichristidis, N.; Liang, K. S.; Mohanty, K.; Lohse, D. J. *J. Chem. Phys.* **1996**, *105*, 2456.

[26] (a) Sioula, S.; Tselikas, Y.; Hadjichristidis, N. *Macromolecules* **1997**, *30*, 1518. (b) Sioula, S.; Tselikas, Y.; Hadjichristidis, N. *Macromol. Symp.* **1997**, *117*, 167. (c) Iatrou, H.; Saikali-Kioulafa, E.; Hadjichristidis, N.; Roovers, J.; Mays, J. W. *J. Polym. Sci., Polym. Phys. Ed.* **1995**, *33*, 1925. (d) Iatrou, H.; Avgeropoulos, A.; Hadjichristidis, N. *Macromolecules* **1994**, *27*, 6232. (e) Iatrou, H.; Hadjichristidis, N. *Macromolecules* **1993**, *26*, 2479. (f) Iatrou, H.; Hadjichristidis, N. *Macromolecules* **1992**, *25*, 4649.

[27] Hadjichristidis, N.; Iatrou, H.; Behal, S. K.; Chludzinski, J. J.; Disko, M.M.; Garner, R.T.; Liang, K. S.; Lohse, D. J.; Milner, S. T. *Macromolecules* **1993**, *26*, 5812.

[28] Pochan, D. J.; Gido, S. P.; Pispas, S.; Mays, J. W.; Ryan, A.J.; Fairclough, J. P. A.; Hamley, I. W.; Terrill, N. J. *Macromolecules* **1996**, *29*, 5091.

[29] Pochan, D.J .; Gido, S. P.; Pispas, S.; Mays, J. W. *Macromolecules* **1996**, *29*, 5099.

[30] Lee, C.; Gido S. P.; Pitsikalis, M.; Mays, J.W.; Tan, N.B.; Trevino, S.F.; Hadjichristidis, N. *Macromolecules* **1997**, *30*, 3732.

[31] (a) Lee, C; Gido, S. P.; Poulos Y.; Hadjichristidis, N.; Tan, N. B.; Trevino, S. F.; Mays, J.W. *Polymer* **1998**, *39*, 4631. (b) Lee, C.; Gido, S. P.; Poulos, Y.; Hadjichristidis, N.; Tan, N. B.; Trevino, S. F.; Mays, J. W. *J. Chem. Phys.* **1997**, *107*, 6460. (c) Gido, S. P.; Lee, C.; Pochan, D. J.; Pispas, S.; Mays, J. W.; Hadjichristidis, N. Macromolecules **1996**, *29*, 7022.

[32] Velis, G.; Hadjichristidis, N. *Macromolecules* **1999**, *32*, 534.

[33] (a) Yang, L.; Hong, S.; Gido, S. P.; Velis, G.; Hadjichristidis, N. *Macromolecules* **2001**, *34*, 9069. (b) Beyer, F. L.; Gido, S. P.; Velis, G.; Hadjichristidis, N.; Tan, N. B. *Macromolecules* **1999**, *32*, 6604.

[34] (a) Grayer, V.; Dormidontova, E. E.; Hadziioannou, G.; Tsitsilianis, C. *Macromolecules* **2000**, *33*, 6330. (b) Matsen, M. W., Gardiner, J. M. *J. Chem. Phys*. **2000**, *113*, 1673. (c) Beyer, F.L.; Gido, S. P.; Uhrig, D.; Mays, J. W.; Beck Tan, N.; Trevino, S. F. *J. Polym. Sci., Part B: Polym. Phys.* **1999**, *37*, 3392.

[35] (a) Buzza, D. M. A.; Fzea, A. H.; Allgaier, J. B.; Young, R. N.; Hawkins, R. J.; Hamley, I. W.; McLeish, T. C. B.; Lodge, T. P. *Macromolecules* **2000**, *33*, 8399. (b) Turner, C.M.; Sheller, N. B.; Foster, M. D.; Lee, B.; Corona-Galvan, S.; Quirk, R. P.; Annis, B.; Lin, J. S. *Macromolecules* **1998**, *31*, 4372.

[36] Zhu, Y.; Gido, S. P.; Moshakou, M.; Iatrou, H.; Hadjichristidis, N.; Park, S.; Chang, T. *Macromolecules* **2003**, *36*, 5719.

[37] Averopoulos, A.; Poulos, Y.; Hadjichristidis, N.; Roovers, J. *Macromolecules* **1996**, *29*, 6076.

[38] Xenidou, M.; Beyer, F. L.; Hadjichristidis, N.; Gido, S. P.; Tan, N. B. *Macromolecules* **1998**, *31*, 7659.

[39] Beyer, F. L.; Gido, S. P.; Büschl, C.; Iatrou, H.; Uhrig, D.; Mays, J. W.; Chang, M. Y.; Garetz, B. A.; Balsara, N. P.; Tan, N. B.; Hadjichristidis, N. *Macromolecules* **2000**, *33*, 2039.

[40] (a) Tu, Y; Wan, X.; Zhang, H.; Fan, X.; Chen, X.; Zhou, Q.-F.; Chau, K. *Macromolecules* **2003**, *36*, 6565. (b) Lee, M.; Cho, B.-K.; Zin, W.-C. *Chem. Rev.* **2001**, *101*, 3869.

[41] Adams, J.; Gronski, W. *Macromol. Rapid Commun.* **1989**, *10*, 553.

[42] Adams, J.; Sänger, J.; Tefehne, Ch.; Gronski, W. *Macromol. Rapid Commun.* **1994**, *15*, 879.

[43] (a) Zubarev, E. R.; Pralle, M. U.; Li, L.; Stupp, S. I. *Science* **1999**, *283*, 523. (b) Stupp, S.I.; LeBonheur, V.; Walker, K.; Li, L. S.; Huggins, K. E.; Keser, M.; Amstutz, A. *Science* **1997**, *276*, 384.

[44] Chen, J. T.; Thomas, E. L.; Ober, C. K.; Mao, G.-p. *Science* **1996**, *273*, 343.

[45] (a) Goldacker, T.; Abetz, V. *Macromol. Rapid Commun.* **2000**, *21*, 16. (b) Goldacker, T.; Abetz, V.; Stadler, R.; Erukhimovich, I.; Leibler, L. *Nature* **1999**, *398*, 137.

[46] Ikkala, O.; ten Brinke, G. *Chem. Commun.* **2004**, 2131.

[47] Zhang, A.; Shu, L.; Bo, Z.; Schlüter, A. D. *Macromol. Chem. Phys.* **2003**, *204*, 328.

[48] (a) Kim, K. T.; Park, C.; Kim, C.; Winnik, M. A.; Manners, I. *Chem. Commun.* **2006**, 1372. (b) Pyun, J.; Tang, C.; Kowalewski, T.; Fréchet, J. M. J.; Hawker, C. J. *Macromolecules* **2005**, *38*, 2674. (c) Messmore, B. W.; Sukerkar, P. A.; Stupp, S. I. *J. Am. Chem. Soc.* **2005**, *127*, 7992. (d) Lecommandoux, S.; Klok, H.-A.; Sayar, M.; Stupp, S. I. *J. Polym. Sci., Part A: Polym. Chem.* **2003**, *41*, 3501. (e) Cho, B.-K.; Jain, A.; Gruner, S. M.; Wiesner, U. *Science* **2004**, *305*, 1598. (f) Roovers, J.; Comanita, B. *Adv. Polym. Sci.* **1999**, *142*, 179.

[49] Fréchet, J. M. J.; Tomalia, D. A. *Dendrimers and Other Dendritic Polymer*s, John Wiley & Sons: New York, 2005.

[50] (a) Aulenta, F.; Hayes, W.; Rannard, S. *Eur. Polym. J.* **2003**, *39*, 1741. (b) Fréchet, J. M. J. *J. Polym. Sci., Part A: Polym. Chem.* **2003**, *41*, 3713. (c) Fischer, M.; Vögtle, F. *Angew. Chem. Int. Ed.* **1999**, *38*, 884. (d) Zeng, F.; Zimmerman, S. C. *Chem. Rev.* **1997**, *97*, 1681.

[51] Tomalia, D. A. *Prog. Polym. Sci.* **2005**, *30*, 294.

[52] Grayson, S. M.; Fréchet, J. M. J. *Chem. Rev.* **2001**, *101*, 3819.

[53] (a) Voit, B. *J. Polym. Sci., Polym. Chem.* **2005**, *43*, 2679. (b) Gao, C.; Yan, D. *Prog. Polym. Sci.* **2004**, *29*, 183. (c) Yates, C. R.; Hayes, W. *Eur. Polym. J.* **2004**, *40*, 1257. (d) Jikei, M.; Kakimoto, M. *Prog. Polym. Sci.* **2001**, *26*, 1233. (e) Sunder, A.; Heinemann, J.; Frey, H. *Chem. Eur. J.* **2000**, *6*, 2499. (f) Kim, Y. H. *Polym. Mater. Sci. Eng.* **1999**, *80*, 61. (g) Feast, W. J.; Cacialli, F.; Daik, R.; Friend, R. H.; Herzog, E.; Heywood, B. R.; Hobson, L.; Megson, J. L.; Snowden, D. *Macromol. Symp.* **1999**, *143*, 81. (h) Hult, A.; Johansson, M.; Malmström, E. *Adv. Polym. Sci.* **1999**, *143*, 1. (i) Turner, S. R. *Polym. Mater. Sci. Eng.* **1995**, *73*, 77.

[54] (a) Gitsov, I. *Linear-Dendritic Block Copolymers. Synthesis and Characterization*; in *Advances in Dendritic Macromolecules*, Newkome G. R.; Elsevier Science, Amsterdam, 2002, Vol. 5, Chapter 2, 45-87. (b) Gitsov, I.; Lambrych, K. L.; Ivanova, P. T.; Lewis, S. *Polym. Mater. Sci. Eng.* **2001**, *84*, 926. (c) Chang, Y.; Kwon, Y. C.; Lee, S. C.; Kim, C. *Macromolecules* **2000**, *33*, 4496. (d) Iyer, J; Fleming, K; Hammond, P. T. *Macromolecules* **1998**, *31*, 8757. (e) Leduc, M.; Hayes, W.; Fréchet, J. M. J. *J. Polym. Sci., Part A: Polym. Chem.* **1998**, *36*, 1. (f) van Hest, J. C. M.; Delnoye, D. A. P.; Baars, M. W. P. L.; van Genderen, M. H. P.; Meijer, E. W. *Science* **1995**, *268*, 1592. (g) Chapman, T. M.; Hillyer, G. L.; Mahan, E. J.; Shaffer, K. A. *J. Am. Chem. Soc.* **1994**, *116*, 11195. (h) Gitsov, I; Ivanova, P. T.; Fréchet, J. M. J. *Macromol. Rapid Commun.* **1994**, *15*, 387. (i) Newkome, G. R.; Baker, G. R.; Arai, S.; Saunders, M. J.; Russo, P.

S.; Theriot, K. J.; Moorefield, C. N.; Rogers, L. E.; Miller, J. E.; Lieux, T. R.; Murray, M. E.; Phillips, B.; Pascal, L. *J. Am. Chem. Soc.* **1990**, *112*, 8458.

[55] (a) Duan, X. X.; Yuan, F.; Wen, X. J.; Yang, M.; He, B.; Wang, W. *Macromol. Chem. Phys.* **2004**, *205*, 1410. (b) Johnson, M. A.; Iyer, J.; Hammond, P. T. *Macromolecules* **2004**, *37*, 2490. (c) Johnson, M. A.; Santini, C. M. B.; Iyer, J.; Satija, S.; Ivkov, R.; Hammond, P. T. *Macromolecules* **2002**, 35, 231-238. (d) Pochan, D. J.; Pakstis, L.; Huang, E.; Hawker, C.; Vestberg, R.; Pople, J. *Macromolecules* **2002**, *35*, 9239. (e) Mackay, M. E.; Hong, Y.; Jeong, M.; Tande, B. M.; Wagner, N. J.; Hong, S.; Gido, S. P.; Vestberg, R.; Hawker, C. J. *Macromolecules* **2002**, *35*, 8391. (f) Román, C.; Fischer, H. R.; Meijer, E. W. *Macromolecules* **1999**, *32*, 5525. (g) Gitsov, J.; Fréchet, J. M. J. *Macromolecules* **1993**, *26*, 6536.

[56] Newkome, G. R.; Yao, Z.; Baker, G. R.; Gupta, V. K. *J. Org. Chem.* **1985**, *50*, 2003.

[57] Newkome, G. R.; Baker, G. R.; Saunders, M. J.; Russo, P. S.; Gupta, V. K.; Yao, Z.; Miller, J. E.; Bouillion, K. *J. Chem. Soc., Chem. Commun.* **1986**, 752.

[58] Newkome, G. R.; Lin, X.; Yaxiong, C.; Escamilla, G. H. *J. Org. Chem.* **1993**, *58*, 3123.

[59] Gitsov, I.; Wooley, K. L.; Fréchet, J. M. J. *Angew. Chem., Int. Ed. Engl.* **1992**, *31*, 1200.

[60] (a) Fréchet, J. M. J.; Gitsov, I. *Macromol. Symp.* **1995**, *98*, 441. (b) Gitsov, I.; Wooley, K. L.; Hawker, C. J.; Ivanova, P. T.; Fréchet, J. M. J. *Macromolecules* **1993**, *26*, 5621.

[61] Gitsov, I.; Fréchet, J. M. J. *Macromolecules* **1994**, *27*, 7309.

[62] (a) Apperloo, J. J.; Janssen, R. A. J.; Malenfant, P. R. L.; Goenendaal, L.; Fréchet, J. M. J. *J. Am. Chem. Soc.* **2000**, *122*, 7042. (b) Malenfant, P. R. L.; Goenendaal, L.; Fréchet, J. M. J. *J. Am. Chem. Soc.* **1998**, *120*, 10990.

[63] Choi, J. S.; Joo, D. K.; Kim, C. H.; Kim, K.; Park, J. S. *J. Am. Chem. Soc.* **2000**, *122*, 474.

[64] (a) Mecerreyes, D.; Dubois, Ph.; Jérôme, R; Hedrick, J. L.; Hawker, C. J. *J. Polym. Sci., Part A: Polym. Chem.* **1999**, *37*, 1923. (b) Leduc, M. R.; Hawker, C. J.; Dao, J.; Fréchet, J. M. J. *J. Am. Chem. Soc.* **1996**, *118*, 11111. (c) Matyjaszewski, K.; Shigemoto, T.; Fréchet, J. M. J.; Leduc, M. R. *Macromolecules* **1996**, *29*, 4167.

[65] Krausch, G.; Magerle, R. *Adv. Mater.* **2002**, *14*, 1579.

[66] (a) Hanselmann, R.; Hölter, D.; Frey, H. *Macromolecules* **1998**, *31*, 3790. (b) Radke, W.; Litvinenko, G.; Müller, A. H. E. *Macromolecules* **1998**, *31*, 239.

[67] Kricheldorf, H. R.; Stukenbrock, T. M. *J. Polym. Sci., Part A: Polym. Chem.* **1998**, *36*, 31.

[68] Al-Muallem, H. A.; Knauss, D. M. *J. Polym. Sci., Part A: Polym. Chem.* **2001**, *39*, 152.

[69] Pusel, T.; Frey, H.; Lee, Y. U.; Jo, W. H. *Polym. Mater. Sci. Eng.* **2001**, *84*, 730.

[70] Barriau, E.; Garcia-Marcos, A.; Kautz, H.; Frey, H. *Macromol. Rapid Commun.* **2005**, *11*, 862.

CHAPTER 2

SYNTHESIS AND CHARACTERIZATION OF POLYSTYRENE-POLYBUTADIENE DIBLOCK COPOLYMERS

2.1 INTRODUCTION

Anionic living polymerization[1] is one of the oldest and most powerful synthetic techniques for the preparation of well-defined polymers. Over the past few years, block copolymers with a plethora of well-defined complex architectures have been prepared by this polymerization mechanism.[2] The ability to form these compositionally uniform macromolecules resides in the absence of termination and chain transfer reactions, under appropriate conditions.[3,4] Block copolymers,[5] normally composed of different linear homopolymer chains joined together by covalent bonds, are fascinating hybrid materials that self-assemble into ordered nanoscopically structured morphologies due to the incompatibility of the different blocks.[6-8] A variety of microdomain structures, like lamellae, hexagonally packed cylinders, gyroids, and body-centered cubic spheres, can be created in bulk depending on the volume fraction of the blocks and their segregating power. Within these systems, polydienes and polydiene-containing block copolymers are appealing materials for modification because the double bond provides a versatile reactive site. In fact, many modification chemistries, such as hydrogenation,[9,10] epoxidation,[11,12] hydrosilylation,[13] sulfonation,[14,15] chorination[16] and fluorination[17-19] have been reported. In this chapter the preparation of amorphous polystyrene-polybutadiene diblock copolymers, as linear core functional materials, is discussed. A series of well-defined polymers, with low PBD content and 100 % atactic 1,2-PBD-microstructure, were synthesized by means of living anionic polymerization and their characterization is presented. A 1,2-arrangement was desired for further functionalization of the double bonds via hydrosilylation, whereas, low PBD contents permit to grow increasingly a hyperbranched or brush-like block by using silicon-containing branched monomers.[20]

2.2 NOMENCLATURE

The diblock copolymers are designated by PS_x-*b*-PBD_y, in which x indicates the degree of polymerization (DP_n) of the PS block and y the DP_n of the 1,2-PBD block. Acronyms are presented in Table 2.1.

2.3 RESULTS AND DISCUSSION

The diblock copolymers used as initiator-templates were synthesized via anionic polymerization using a specially constructed reactor system suitable for working under high vacuum and overpressure. The advantage of such pressure proof reactor systems over other techniques such as Break-seal[21] is that it offers simpler and safer operating conditions during polymerization. Furthermore, polymerization of larger amounts is feasible. An important prerequisite for living anionic polymerization is to completely exclude protic impurities and oxygen on a ppm scale. Control over the purity of the reagents was achieved by a simplified anionic polymerization method as developed by Sänger *et al.*[22] This involved arduous removal of oxygen from the solvents within the reactor set-up and titration of the protic impurities directly within the reaction medium. Conversely, cleaning of the monomer, solvent and the reaction-vessel in separate steps is time-consuming and usually leads to experimental errors.

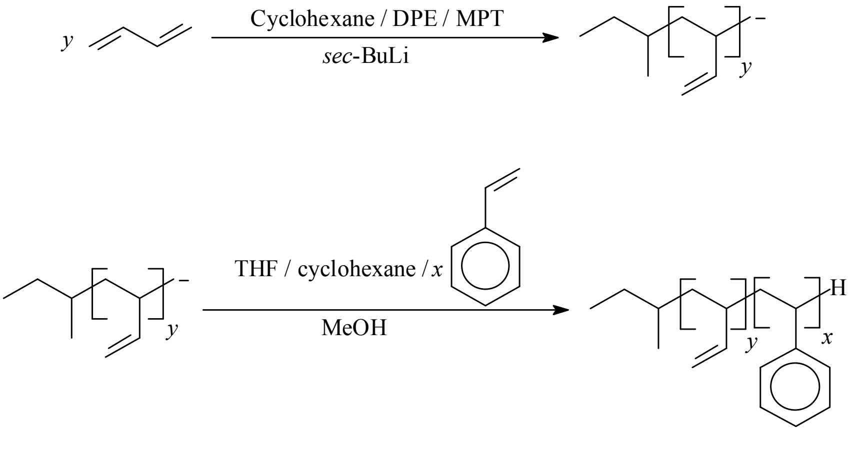

Figure 2.1. Synthesis of PS_x-*b*-PBD_y diblock copolymers by sequential anionic polymerization.

The initial step towards generating the PS_x-*b*-PBD_y diblock copolymers involved the preparation of the PBD block and was followed by the transfer of the styrene monomer solution to the living PBD block (Figure 2.1). Protic impurities were removed from the monomer solution using *sec*-BuLi and 4,5-methylenephenanthrene (MPT), which acts as an indicator. Blocks of the desired degree of polymerization (DP_n) were prepared by varying the monomer:initiator molar concentrations (Equation 2.1).[23,24] The polymerization was initiated with *sec*-BuLi and as the effective concentration of *sec*-BuLi changes rapidly with traces of moisture, the exact activity of the initiator was evaluated immediately by the Gilman procedure prior to use.[25,26] The *sec*-BuLi reacts first with the protic impurities and subsequently with the bridge methylene protons of the MPT (Figure 2.2). The development of a yellow colour, due to the presence of the carbanion, gives the end point of the titration. In addition to indicating the exclusion of protic impurities, MPT is chosen as its anion cannot initiate the polymerization of butadiene or styrene in non-polar reaction media. Moreover, it has no influence on the molecular weight, molecular weight distribution and microstructure of the block copolymers.[22]

$$DP_n = \frac{[Monomer]}{[Initiator]}$$

Equation 2.1. Calculation of the DP_n of polymers in an anionic polymerization procedure.

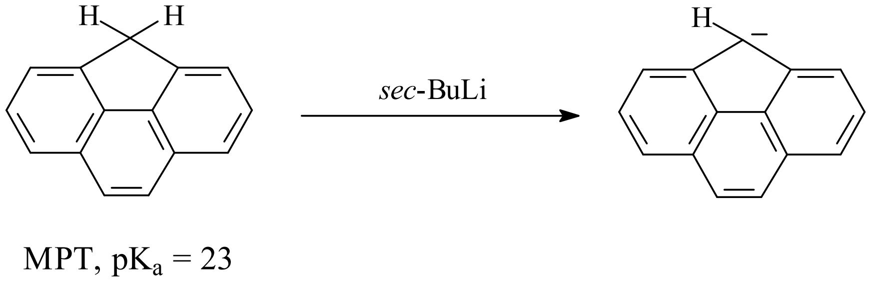

Figure 2.2. Formation of MPT carbanion with *sec*-BuLi.

In principle, 1,3-butadiene can polymerize to give three different microstructures (Figure 2.3). A 1,2-arrangement was accomplished by adding the chelating diamine ligand 1,2-dipiperidinoethane (DPE) in a non-polar solvent.[27] The 1,2-content is dependent on the DPE:initiator molar ratio and the polymerization temperature. A complete 1,2-PBD content was obtained in cyclohexane at 5 °C with a 10 fold DPE:*sec*-BuLi molar excess.[28] The postulated mechanism[27] for the polymerization of 1,3-butadiene to give exclusively a 1,2-PBD structure in a non-polar media in the presence of DPE is shown in Figure 2.4. The first step involves the formation of the chelate complex **I**. Contact with a 1,3-butadiene monomer (**II**) results in the insertion of the butadiene into the C-Li bond to form complex **III**, which is now the active propagating species. Subsequent contact with butadiene monomers results in chain transfer by the processes **II**→**III**.

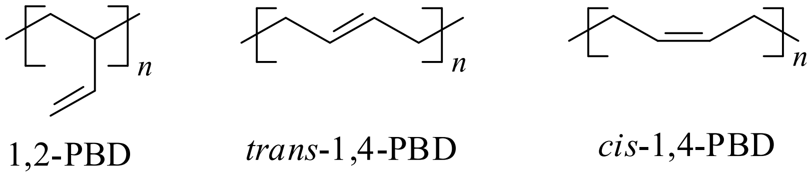

Figure 2.3. Possible arrangements of the monomeric units in PBD.

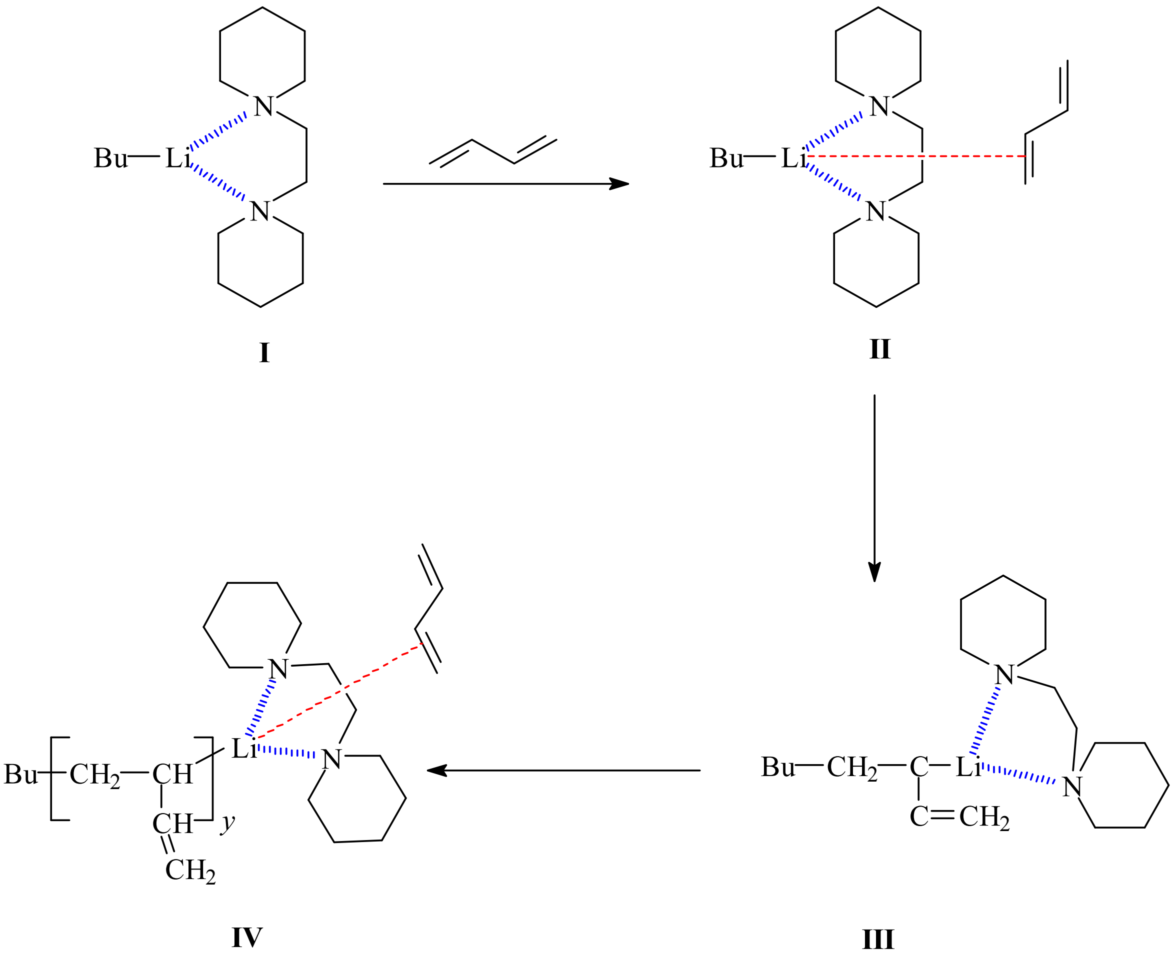

Figure 2.4. Proposed mechanism for the anionic polymerization of 1,3-butadiene in non-polar solvents in the presence of DPE.

Before the polymerization of styrene was started, a PBD sample was taken for controlling the polydispersity and determining the 1,2-content. This is particularly important, as spectroscopic characterization of the PBD structure can be difficult for diblocks having large PS content. The IR and NMR spectral characteristics of isolated PBD samples were in agreement with the exclusive formation of 1,2-PBD. In the IR spectrum of a typical isolated 1,2-PBD block (Figure 2.5), the characteristics peaks due to the vinyl-1,2 deformation at 911 and 996 cm^{-1} were identified, while those due to the *trans*-and *cis*-1,4 deformation at 968 and 729 cm^{-1} respectively were absent.[29,30] The peak at 3074 cm^{-1}, which is characteristic for the stretching of the pendent vinyl double bonds, was also identified.[31,32] This demonstrates initially the *ca.* 100 % 1,2-PBD content.

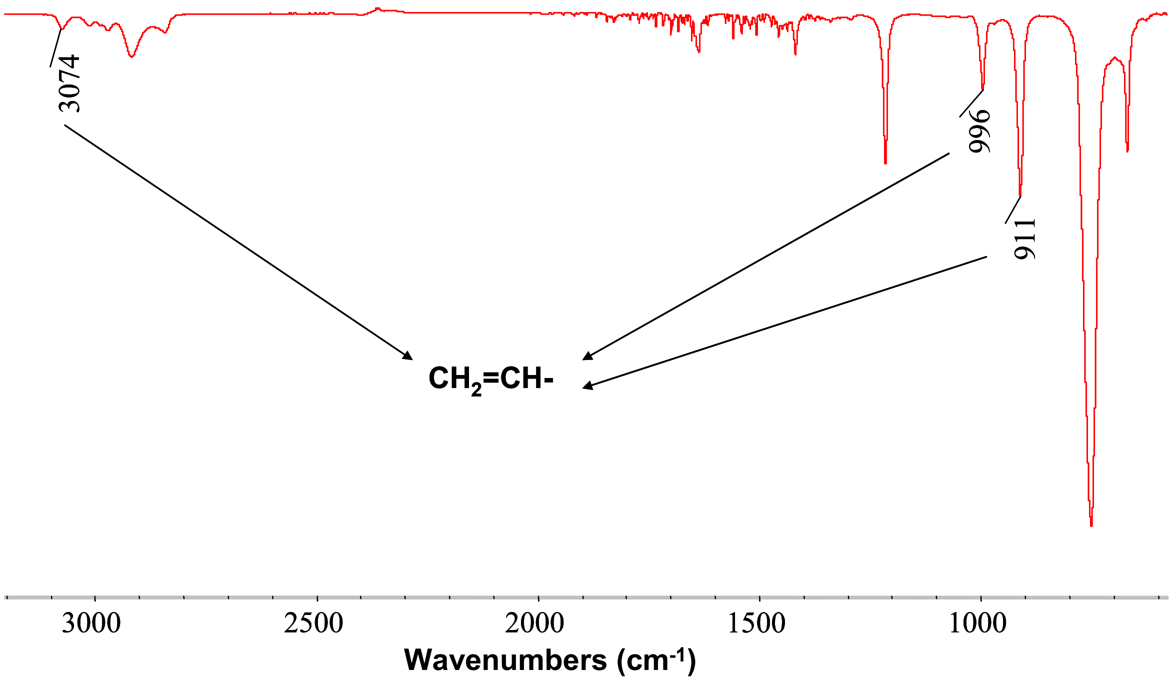

Figure 2.5. IR spectrum of the isolated 1,2-PBD block of the diblock copolymer PS$_{426}$-*b*-PBD$_{40}$.

Further evidence for the isomeric purity of the PBD block was garnered from the ^{1}H NMR spectrum, wherein the percentage of the 1,2 and 1,4-microstructures was evaluated from the integrated areas in the olefinic region (Figure 2.6).[29] The peak at 4.9 ppm (signal “a”), which is the major peak in the olefinic region, corresponds solely to the 1,2-vinylic methylene protons. However the peak at 5.4 ppm (signal “b”) can include the methine protons of the 1,2- and 1,4-microstructure. The peak at 5.8 ppm (signal “c”) is assigned to the methine proton of the terminal vinylic monomer unit. If y is the DP_n of the 1,2-microstructure and y' is the DP_n of the 1,4-microstructure, it follows that the area under the peak "a" is equal to $2y$ and that the area under the peak "b" and "c" is equal to $y+2y'$. For the spectrum depicted in Figure 2.6, we observed relative values of the integrated areas of 2.0 for "a" and 1.07 for "b" and "c". This suggested that the PBD microstructure was almost exclusively 1,2.

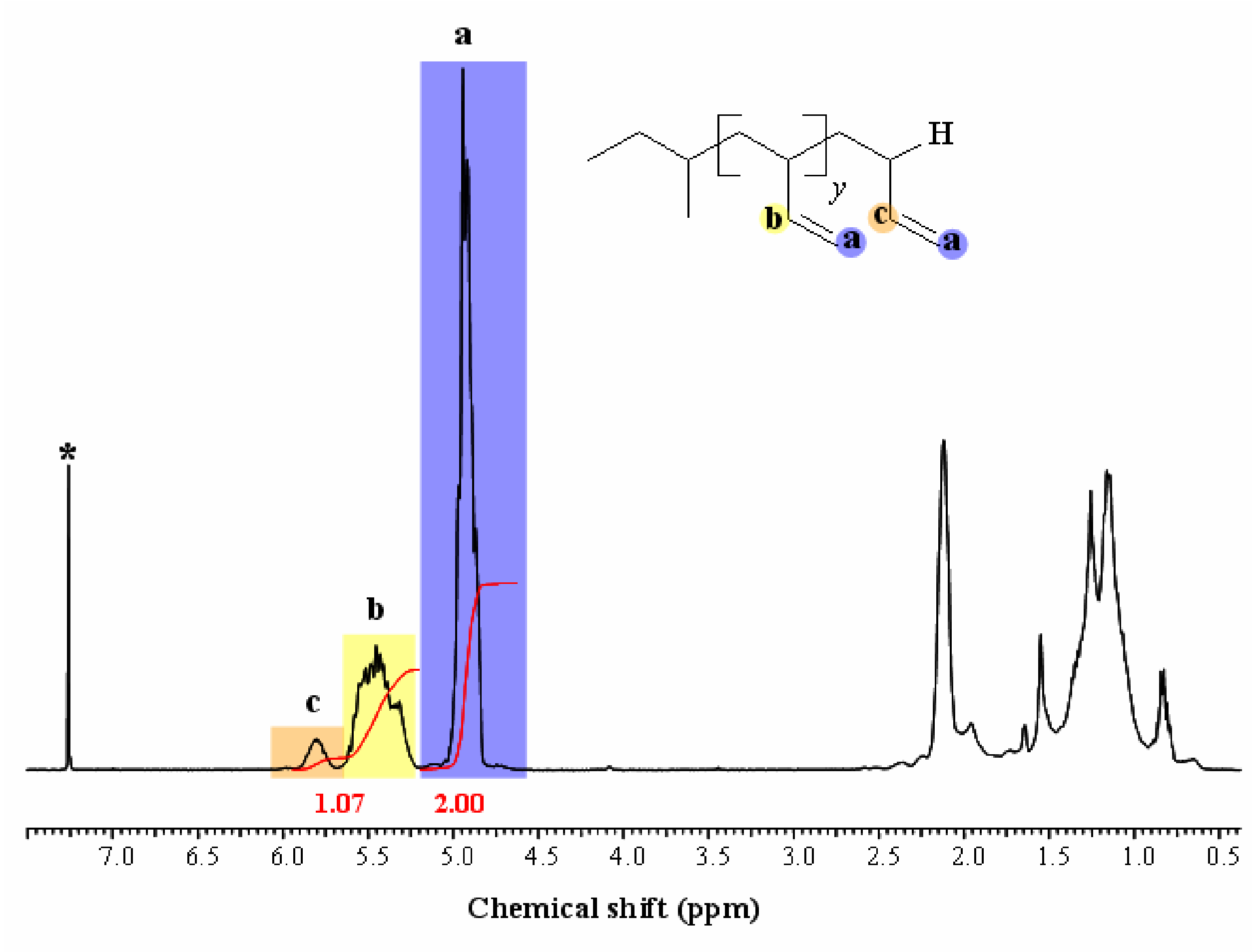

Figure 2.6. ^{1}H NMR spectrum of the isolated 1,2-PBD block of the diblock copolymer PS_{426}-*b*-PBD_{40} in $CDCl_3$ (solvent peak denoted by an asterisk).

Furthermore, in the ^{13}C NMR spectroscopy, the presence of *cis*- and *trans*-1,4-PBD can be identified by the methine carbon signals at 129.2 and 129.7 ppm respectively.[30] However, only the resonances at 114.4 and 143.5, which are assigned to the 1,2-methylene and -methine vinylic carbons respectively, were found in the olefinic region (Figure 2.7). This is consistent with the ^{1}H NMR finding, in that the 1,2-microstructure was exclusive.

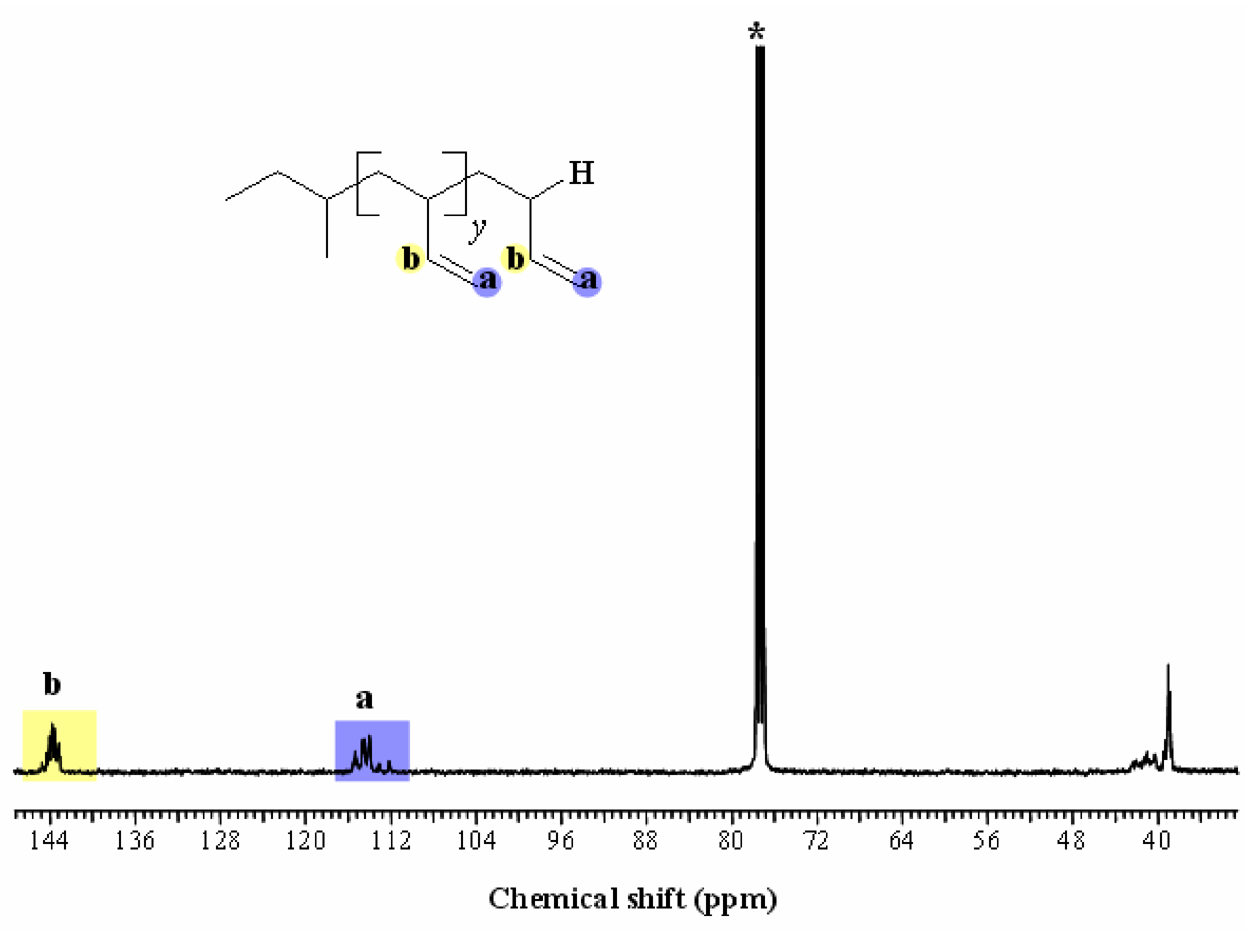

Figure 2.7. ^{13}C NMR spectrum of the isolated 1,2-PBD block of the diblock copolymer PS$_{426}$-*b*-PBD$_{40}$ in CDCl$_3$ (solvent peak denoted by an asterisk).

For the synthesis of the PS block, cyclohexane and THF were used as solvents. The polymerization of styrene without the addition of THF is strongly hindered and hence too slow. The polar THF solvent is necessary to cleave the growing PBD carbanion from the lithium counterion, which forms a complex with the DPE. Addition of 10 % THF was enough to speed up the polymerization. Special care must be taken during the titration of the styrene solution as non-deprotonated MPT has the capacity to terminate the polymerization of some of the PBD anions, while an excess of *sec*-BuLi would start the polymerization of styrene instead of the living PBD anion block. After completion, the polymerization was terminated by adding degassed methanol and the resulting polymers were fully characterized by NMR-spectroscopy, IR, GPC and membrane osmometry (MO).

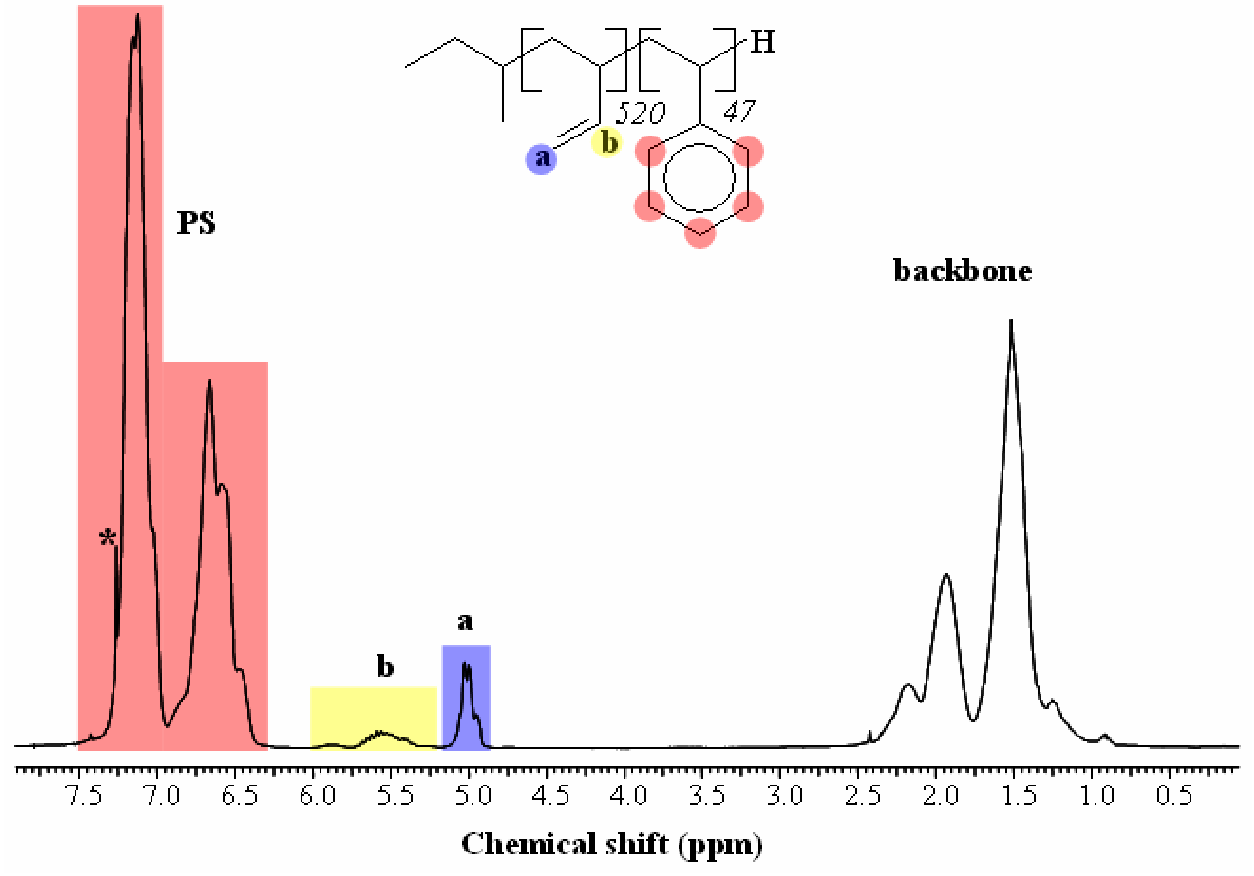

Figure 2.8. ^{1}H NMR spectrum of the diblock copolymer PS_{520}-*b*-PBD_{47} in $CDCl_3$ (solvent peak denoted by an asterisk).

The mol % as well as the weight % (wt %) composition of the diblocks were calculated by ^{1}H NMR spectroscopy by comparing the relative intensities of the proton signals of the PS and the 1,2-PBD block. A representative ^{1}H and ^{13}C NMR spectrum of a diblock copolymer with 4.5 wt % 1,2-PBD is presented respectively in Figures 2.8 and 2.9. In the ^{1}H NMR spectrum of the linear diblock PS_{520}-*b*-PBD_{47} two broad signals at δ = 5.5 ppm (signal “b”) and 5.0 ppm (signal “a”) in the ratio 1:2 can be seen in the olefinic region. These correspond to the methine and methylene protons respectively of the PBD vinyl groups. In the ^{13}C NMR the downfield peak at 145.6 ppm is attributed to the quaternary or *ipso* carbon of the styrene units, while the other aromatic carbon atom signals are in the region 124-130 ppm. The signals at 114.4 ppm (signal “a”) and 143.5 ppm (signal “b”) are assigned to the vinyl methylene and methine carbons of the PBD block respectively.

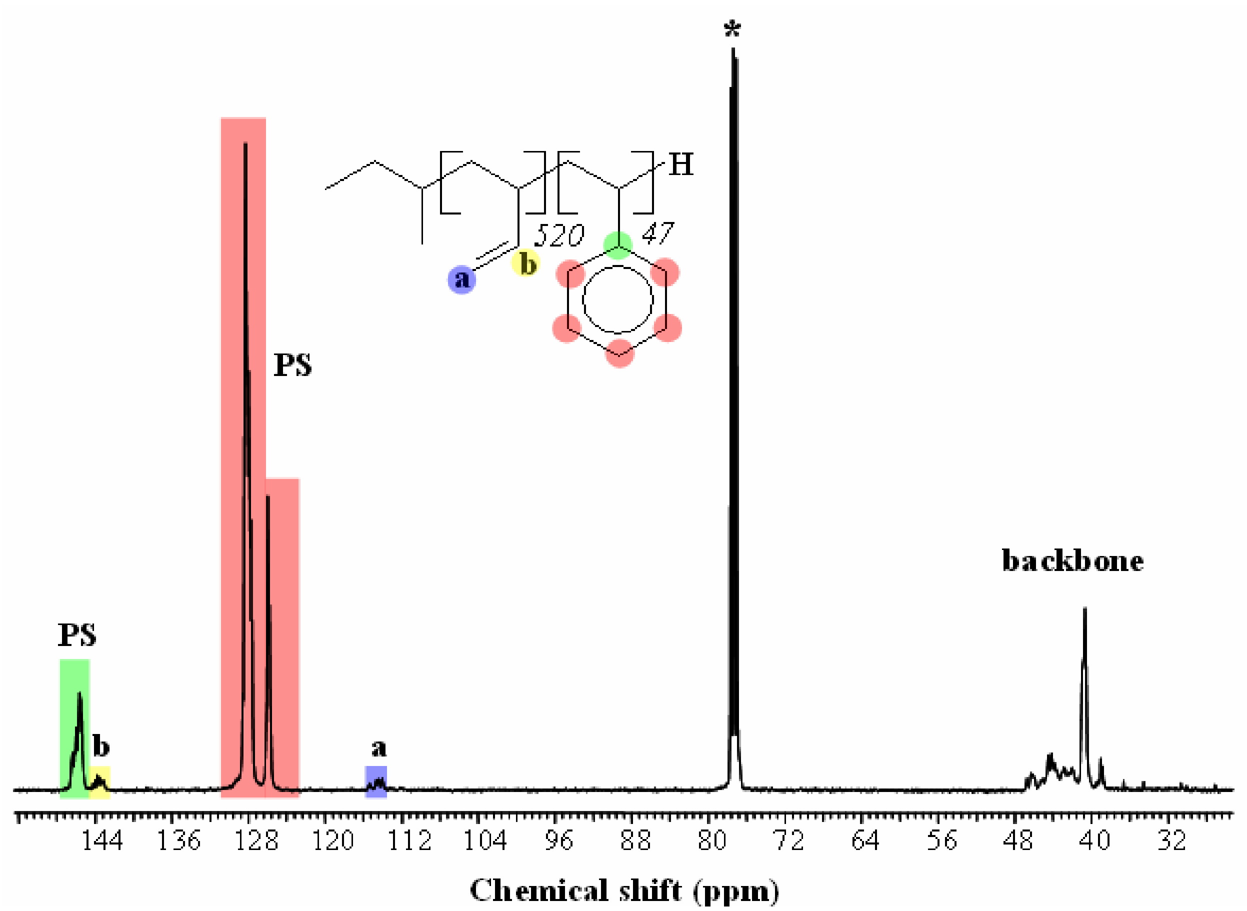

Figure 2.9. ^{13}C NMR spectrum of the diblock copolymer PS$_{520}$-*b*-PBD$_{47}$ in CDCl$_3$ (solvent peak denoted by an asterisk).

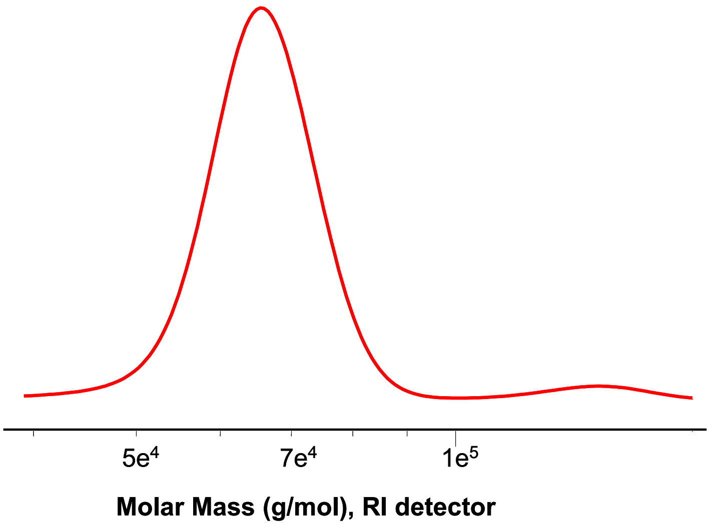

Figure 2.10. GPC chromatogram of PS$_{520}$-*b*-PBD$_{47}$.

GPC was employed for the characterization of the molar mass distributions. As expected, diblock copolymers with narrow distributions were obtained. However, in all cases the GPC chromatograms showed small peaks at higher molecular weights (Figure 2.10). The number-average molecular weight of these peaks is invariably double the molecular weight of the diblocks. An estimation of the dimer content, by integration of both peaks in the GPC chromatogram, gave values between 2 and 5 %. This can be explained by the presence of minute amounts of oxygen, which acts as a di-radical promoting the formation of radical chain ends which can then dimerize.[33] The formation of these dimers could not be avoided, despite the rigorous degassing of the reaction-terminating methanol agent.

Table 2.1. Characterization data and thermal properties for PS$_x$-*b*-PBD$_y$ diblock copolymers.

	^{1}H NMR	**GPC^b**		**MO^c**	**DSC^d**	
Sample^a	wt % 1,2-PBD	M_n (10^3 g/mol)	PDI^e	M_n (10^3 g/mol)	T_g1 (°C)	T_g2 (°C)
PS$_{354}$-*b*-PBD$_{84}$ (**P$_1$**)	11	37.8	1.07	41.4	101.1	-56.7
PS$_{426}$-*b*-PBD$_{40}$ (**P$_2$**)	4.6	40.8	1.03	46.5	88.1	-30.8
PS$_{520}$-*b*-PBD$_{47}$ (**P$_3$**)	4.5	63.8	1.04	56.8	99.7	-48.6
PS$_{580}$-*b*-PBD$_{50}$ (**P$_4$**)	4.3	52.6	1.03	63.1	97.3	-29.3
PS$_{1156}$-*b*-PBD$_{130}$ (**P$_5$**)	5.5	110.0	1.04	127.8	100.1	-18.7

[a] Acronyms in parenthesis. [b] Gel permeation chromatography (GPC) measured in chloroform with PS standard calibration. [c] Membrane osmometry (MO) measured in toluene at 40 °C. [d] Differential Scanning Calorimetry (DSC) measured at a heating rate of 25 °C/min. [e] Polydispersity index $\overline{M}_w/\overline{M}_n$

The characteristics of different diblock copolymers (PS$_x$-*b*-PBD$_y$) are presented in Table 2.1. The DP$_n$ of both blocks was calculated by using the absolute molar masses obtained via MO. The coil dimensions of PS and of PS$_x$-*b*-PBD$_y$ diblock copolymers, even at 5 wt % PBD content, are dissimilar in a given solvent. Therefore, a GPC calibration curve based on PS would not reflect precisely the absolute molecular weight. For this reason, the number-average molecular weights (M_n) obtained by MO, although close to the values obtained by conventional GPC, were considered to be more accurate. Thermal analysis of the amorphous diblock copolymers showed the expected glass transition temperature (T_g) for both blocks. The T_g values are reported in Table 2.1. A representative DSC curve for a diblock copolymer is presented in Figure 2.11. Additionally, the thermostability of the polymers was examined using thermogravimetric analysis (TGA). A representative TGA curve for a diblock copolymer, indicating an onset decomposition temperature of 432 °C is depicted in Figure 2.12.

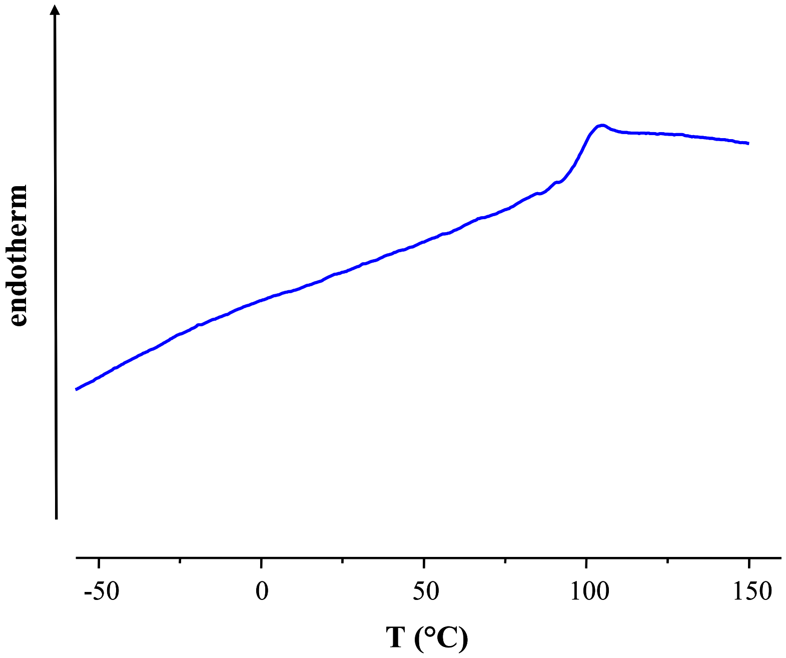

Figure 2.11. DSC curve of $\mathbf{P_4}$, scanning rate 25 °C/min.

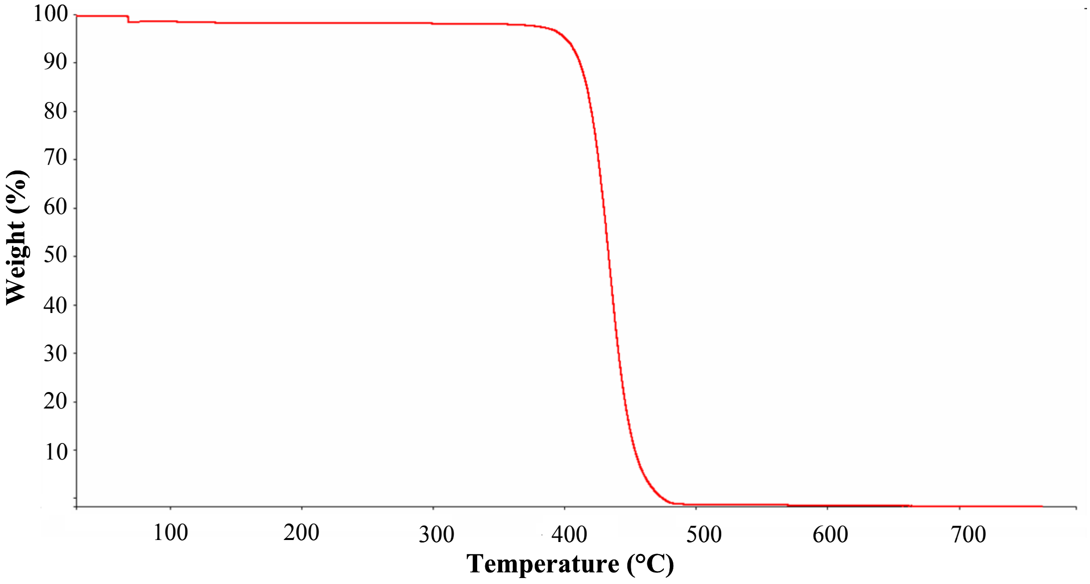

Figure 2.12. TGA curve of $\mathbf{P_2}$ in N_2, heating rate 10 °C/min.

2.4 EXPERIMENTAL

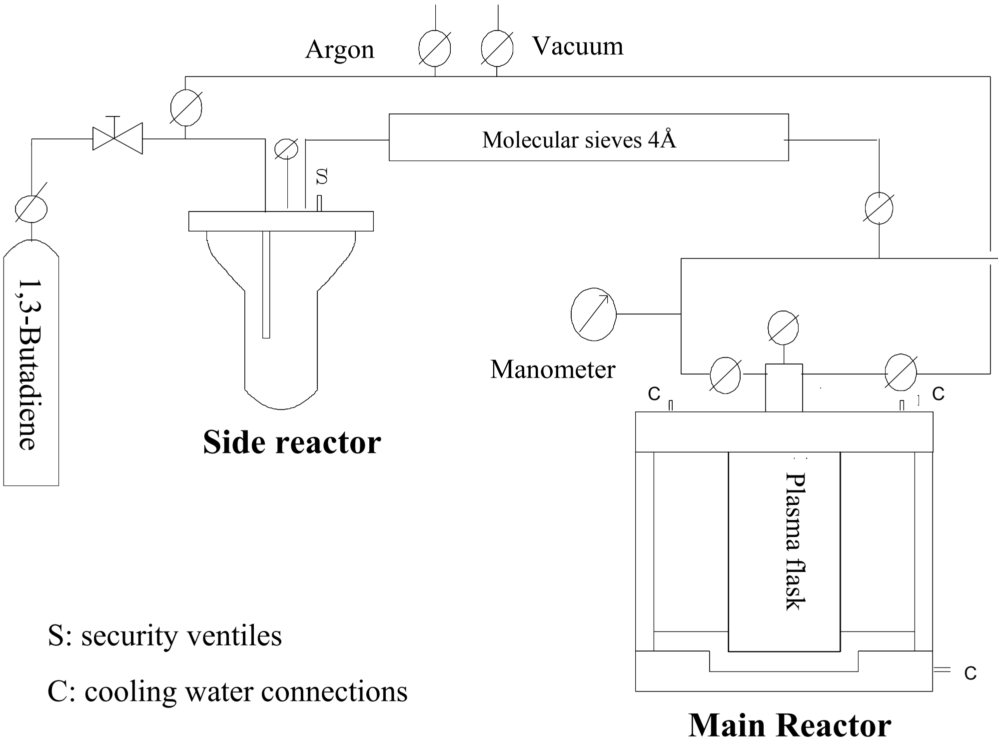

Figure 2.13. Schematic picture of the reactor set-up for the anionic polymerization of PS_x-*b*-PBD_y.

Equipment: A specially constructed reactor set-up with two separate reaction vessels, suitable for working under high vacuum and overpressure, was utilized for the synthesis of the diblock copolymers. This reactor allows the polymerization of both gas and liquid monomers. A schematic picture and a photo are presented in Figures 2.13 and 2.14. All components of the reactor are made from inert materials such as stainless steel, glass, Teflon® or Viton®. The main polymerization reactor consists of a 500 mL plasma flask covered with a polycarbonate shell. There is a valve with a septum at the top of the main and side reactor, where the reagents can be added. A cryostat filled with water or ethanol is connected to the system and allows the main reactor vessel to be operated at lower temperatures. The butadiene is stored as a gas in a 10 L reservoir bottle. Before polymerization, the butadiene is passed through a brass tube filled with molecular sieves into a ballast bottle, which is connected to a digital manometer (with a 5 mbar level of accuracy). The molecular sieves pre-dry the gas and can be regenerated afterwards under high vacuum with an external heat source. For the polymerization, the butadiene is transferred from the ballast bottle into the main polymerization reactor. The quantity introduced is monitored by the drop in pressure in the ballast bottle and can be calculated from a calibrated pressure-difference/quantity relationship (at room temperature, $m_{butadiene}$ (g) = 23.61•ΔP (bar)). The side reactor serves for the preparation of the styrene solution. Both reactors are additionally connected to the THF and cyclohexane stills, so that the solvents can be transferred directly from the drying stills through the stainless steel connections to the reaction vessels under argon overpressure.

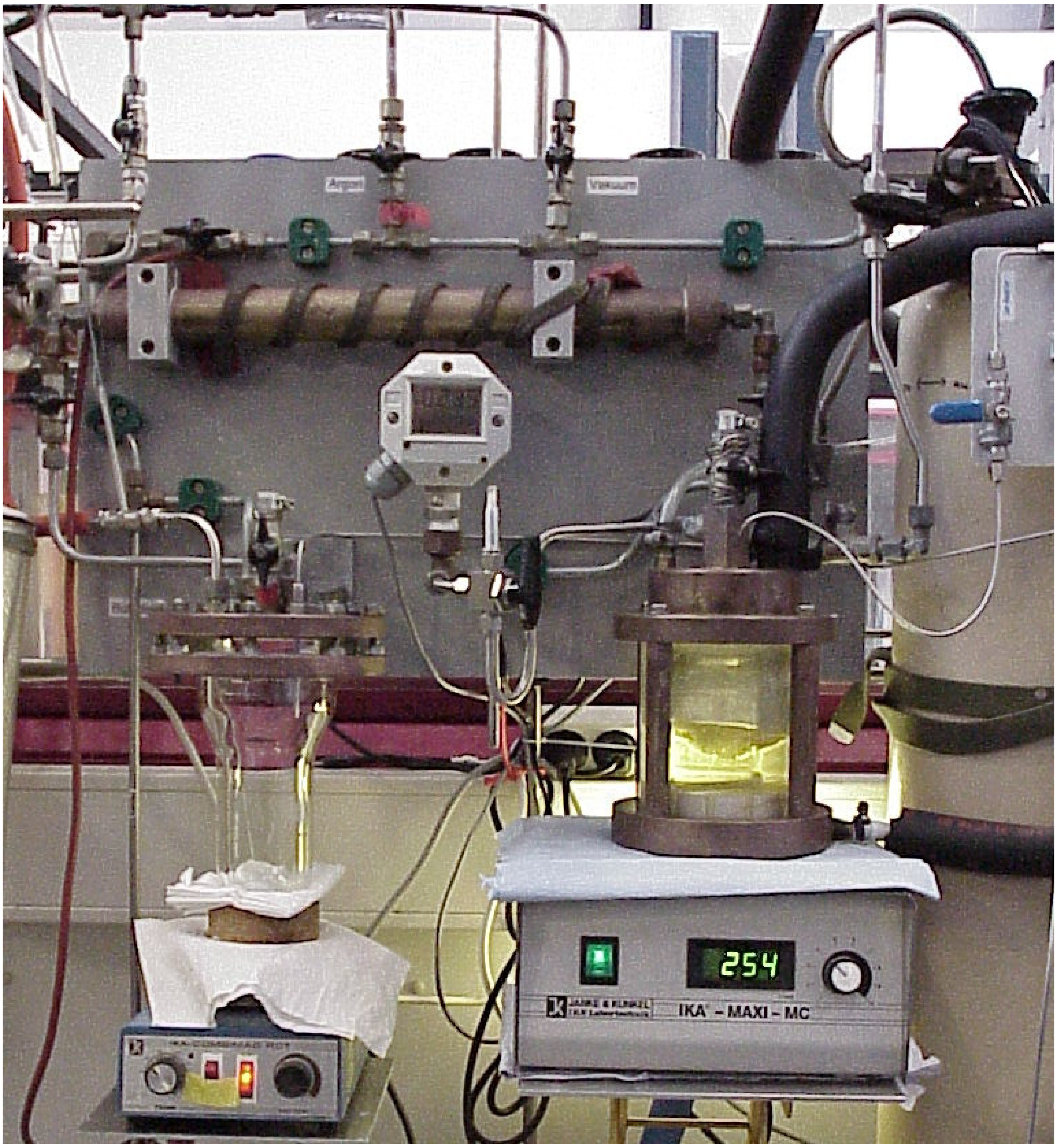

Figure 2.14. Picture of the anionic reactor.

Purification of solvents and materials:

Cyclohexane. *n*-BuLi (30 mL, 1.3 M in hexane) was added to 1.5 L of degassed cyclohexane under argon and the solution was then stirred for circa 2 hours. Styrene (10 mL) was added to check moisture exclusion, which was evidenced by the appearance of a persistent red colour associated with the styrene anion. The solvent was then transferred via canula to the reactor cyclohexane still, which contained sodium, and was refluxed and distilled under argon directly prior to use.

Tetrahydrofuran (THF). *n*-BuLi (50 mL, 1.3 M in hexane) was added to 1.5 L of THF resulting in the appearance of a strong yellow colour. Benzophenone (approx. two spatula amounts) was subsequently added and the solution degassed several times under argon. After the addition of sodium (~ 3 g) to the solution and with vigorous stirring, a deep blue colour developed. Finally, the THF was transferred via canula to the reactor THF still, which contained sodium, and was freshly distilled under argon prior to use.

Butadiene. 1,3-butadiene was pre-dried as a gas under high vacuum for 8 hours in a brass tube integrated into the anionic reactor set-up. The tube contained molecular sieves 4 Å and was heated to approx. 200 °C using an external heat source.

Styrene. Styrene (200 mL, 99 %) was initially stirred over CaH_2 under an argon atmosphere for 1 hour and then distilled under vacuum (23 mbar, $T_{distillation}$ = 51 °C) using a vigreux column. The styrene solution was further purified by treatment with solvent free di-*n*-butylmagnesium (1.0 M in heptane); *i.e* the heptane was removed before adding the styrene. After stirring for 2 hours, the styrene solution was again distilled under vacuum using a vigreux column. Finally the solution was degassed several times under argon by the freeze-thaw method prior to use.

***sec*-Buthyllithium.** *sec*-BuLi (1.3 M in cyclohexane) was used without further purification. However the exact concentration was determined by the Gilman procedure prior to use. In a first step *sec*-BuLi (1 mL) was hydrolyzed with water. The resulting lithium hydroxide solution was then titrated with 0.1 M HCl in the presence of phenolphthalein. In a second step benzyl chloride (2 mL, 99 %) was reacted with *sec*-BuLi (1 mL) in dry THF (40 mL). After 1 hour, water (20 mL) was added and the lithium hydroxide solution titrated with 0.1 M HCl in the presence of phenolphthalein. The Gilman procedure was carried in triplicate and the average value was determined. The concentration was calculated from the difference of the molar quantities of HCl consumed between the first and the second titration.

Others. The indicator 4,5-methylenphenanthrene (MPT) and the ligand complex 1,2-dipiperidinoethane (DPE) were used without further purification. Methanol, which served as the carbanion-terminating agent was degassed several times under argon via the freeze-thaw method.

Synthesis: All diblock copolymers, with a 100 % 1,2-PBD content, were prepared in 20 g scales. The relative quantities of the reagents used depended on the desired molecular weight. The first step was the synthesis of the 1,2-PBD block in cyclohexane. Cyclohexane was introduced into the main reactor, followed by DPE (10 fold excess with respect to the initiator (*sec*-BuLi) molar quantity) and MPT (10 mg MPT/100 mL cyclohexane). The reaction temperature was subsequently set to 5 °C and the required amount of 1,3-butadiene was dissolved in the previously degassed solution. After ~ 30 minutes, small quantities of protic contaminants were titrated with *sec*-BuLi until a pale yellow colour persisted. After the titration, a predetermined volume of *sec*-Buli was added to compensate for the MPT (complete deprotonation) and to initiate the polymerization. After 15 hours 1-2 mL of the PBD solution were taken, precipitated into methanol and dried in vacuo at 40 °C for further analysis. The synthesis of the PS-block was started in a second reaction step (side reactor) by the addition of a previously degassed and titrated styrene solution (5 mg MPT/100 mL cyclohexane) in absolute cyclohexane/THF (10:1) to the living 1,2-PBD block (main polymerization reactor). The total amount of solvent after the addition of the styrene solution should not exceed 400 mL. After a polymerization time of at least 15 hours, the living anionic diblock copolymer was quenched by the injection of 2 mL of degassed methanol. The polymers were precipitated in a 10 fold excess of methanol containing a small quantity of 2,4-di-*tert*-butyl-*p*-cresol (BHT) as a stabilizer and dried in a freeze-drier.

Characterization: Membrane osmometry (MO) and conventional gel permeation chromatography (GPC) using PS standard calibration were used to determine the number-average molecular weights ($\overline{M}_n$) and molecular weight distributions (PDI). The 1,2-PBD content as well as the wt % composition of the blocks was calculated by IR and NMR spectroscopy.

^{1}H NMR (400 MHz, $CDCl_3$): δ (ppm) 0.7-2.6 (polymer backbone), 5.0 (m, -CH=C**H₂**), 5.5 (m, -C**H**=CH₂), 6.35-7.40 (m, C_6H_5); ^{13}C NMR (75 MHz, $CDCl_3$): δ (ppm) 38-48 (polymer backbone), 114.4 (-CH=**C**H₂), 124-130 (C_6H_5), 143.5 (-**C**H=CH₂), 145.6 (C_{ipso}, C_6H_5); IR (characteristic absorption bands): ν (cm^{-1}) 3100 (PBD terminal C=C stretching), 3079, 3055, 3024 (aromatic CH stretching), 2920, 2844 (aliphatic CH stretching), 1639 (PBD C=C stretching), 1601 (aromatic C=C stretching), 1490, 1450 (PS backbone CH bending), 910 (PBD terminal C=C deformation), 753, 693 (aromatic CH deformation and bending).

2.5 REFERENCES

[1] Morton, M. Ed. *Anionic Polymerization: Principles and Practice*; Academic Press: New York, 1983.

[2] Hadjichristidis, N.; Pitsikalis, M.; Pispas, S.; Iatrou, H. *Chem. Rev.* **2001**, *101*, 3747.

[3] Young, R. N.; Quirk, R. P.; Fetters, L. J. *Adv. Polym. Sci.* **1984**, *56*, 1.

[4] Hsieh, H. L.; Quirk, R. P. *Anionic Polymerization: Principles and Practical Applications*: New York, 1996.

[5] Hadjichristidis, N.; Paspas, S.; Floudas, G. *Block Copolymers: Synthetic Strategies, Physical Properties and Application*; John Wiley and Sons, Inc., Hoboken, NJ 2003.

[6] Bates, F. S.; Fredickson, G. H. *Annu. Rev. Phys. Chem.* **1990**, *41*, 525.

[7] Bates, F. S.; Fredickson, G. H. *Physics Today*, **1999**, *32*.

[8] Hamley, I. W. *The Physics of Block Copolymers*; Oxford University Press: Oxford, 1998.

[9] Gehlsen, M. D.; Bates, F. S. *Macromolecules* **1993**, *26*, 4122.

[10] Adams, J. L.; Quiram, D. J.; Graessley, W. W.; Register, R. A.; Marchand, G. R. *Macromolecules* **1998**, *31*, 201.

[11] Wang, S.-M.; Tsiang, R. C.-C. *J. Polym. Sci., Part A: Polym. Chem.* **1996**, *34*, 1483.

[12] Grubbs, R. B.; Broz, M. E.; Dean, J. M.; Bates, F. S. *Macromolecules* **2000**, *33*, 2308.

[13] McGrath, M. P.; Sall, E. D.; Tremont, S. J. *Chem. Rev.* **1995**, *95*, 381.

[14] Weiss, R. A.; Sen, A.; Pottick, L. A.; Willis, C. L.; *Polym. Commun.* **1990**, *31*, 220.

[15] Szczubialka, K.; Ishikawa, K.; Morishima, Y. *Langmuir* **1999**, *15*, 454.

[16] Stone, V. W.; Jonas, A. M.; Legras, R.; Dubois, P.; Jerome, R. *J. Polym. Sci., Part A: Polym. Chem.* **1999**, *37*, 233.

[17] Wall, L. A., Ed. *Fluoropolymers*; Wiley-Interscience: New York, 1972.

[18] Ren, Y.; Lodge, T. P.; Hillmyer, M. A. *J. Am. Chem. Soc.* **1998**, *120*, 6830.

[19] Reisinger, J. J.; Hillmyer, M. A. *Prog. Polym. Sci.* **2002**, *27*, 971.

[20] Oishi, M.; Minakawa, M.; Imae, I.; Kawakami, Y. *Macromolecules* **2002**, *35*, 4938.

[21] Morton, M.; Rembaum, A. A.; Hall, J. L. *J. Polym. Sci., Part A: Polym. Chem.* **1963**, *1*, 461.

[22] Sänger, J.; Tefehne, C.; Lay, R.; Gronski, W. *Polymer Bulletin* **1996**, *36*, 19.

[23] Waack, R.; Rembaum, A.; Coombes, J. D.; Szwarc, M. *J. Am. Chem. Soc.* **1957**, *79*, 2026.

[24] Szwarc, M. *J. Polym. Sci., Part A: Polym. Chem.***1998**, *36*, 9.

[25] Gilman, H.; Haubein, A. H. *J. Am. Chem. Soc.* **1944**, *66*, 1515.

[26] Gilman, H.; Cartledge, F. K. *J. Organomet. Chem.* **1964**, *2*, 447.

[27] Halasa, A. F.; Lohr, D. F.; Hall, J. E.; *J. Polym. Sci., Part A: Polym. Chem.* **1981**, *19*, 1357.

[28] Sänger, J. *Dissertation* **1997**, Freiburg.

[29] Jeyaprakash, J. D.; Samuel, S.; Dhamodharan, R.; Ober, C. K. *J. Polym. Sci., Part A: Polym. Chem.* **2000**, *38*, 1179.

[30] Lacoste, J.; Delor, F.; Pilichowski, J. F.; Singh, R. P.; Prasad, A. V.; Sivaram, S. *J. Appl. Polym. Sci.* **1996**, *59*, 953.

[31] Guo, X.; Farwaha, R.; Rempel, G. L. *Macromolecules* **1990**, *23*, 5047.

[32] Guo, X.; Rempel, G. L. *Macromolecules* **1992**, *25*, 883.

[33] Halasa, A. F.; Mochel, V. D.; Fraenkel, G.; McGrath, J. E. *Anionic Polymerization*: ACS Symposium Series 166, Washington, D. C., 367, 1981.

CHAPTER 3

SYNTHESIS AND CHARACTERIZATION OF AB$_n$ ORGANOSILICON BRANCHED MONOMERS

3.1 INTRODUCTION

Highly branched three dimensional macromolecules, such as dendrimers[1] and hyperbranched polymers,[2] have recently attracted considerable attention due to the wide applicability to novel macromolecular architecture and functional polymers.[3] Both types of macromolecules are prepared from AB$_n$-type monomers, where A and B represent two mutually reactive functional groups and n determines the number of branches per repeat unit.[4] Within these systems, silicon chemistry offers several quantitative reactions (*i.e.* hydrosilylation, Grignard-reactions and controlled condensation of silanols) that are suitable for the preparation of highly flexible dendrimers and hyperbranched organic-inorganic hybrid materials. Among these silicon-containing dendritic polymers,[5] hyperbranched polycarbosilanes,[6] polyalkoxysilanes,[7] polycarbosiloxanes[8] and polysiloxanes[9] have been prepared as interesting functional materials from convenient AB$_2$ and AB$_3$ monomers.

In this chapter the synthesis of different AB$_n$ organosilicon monomers, as precursors for hyperbranched and brush-like polymers, is described. In this way, carbosilane and alkoxysilane monomers, containing Si-H and alkene as A and B reactive functionalities, were prepared by varying the branching multiplicity and the segment length between the branch points respectively.

$$\mathrm{MeCl + Si \xrightarrow[\triangle]{Cu} Me_2SiCl_2 + MeSiCl_3 + Me_3SiCl + MeHSiCl_2 + (Me_4Si) + (SiCl_4)}$$

Figure 3.1. Copper-catalyzed Direct Process favouring the production of Me$_2$SiX$_2$.

The Direct Process,[10] discovered by Rochow[11] and Müller[12] in the early 1940s, is the fundamental industrial process used to create Si-C bonds. At its simplest level, the reaction involves the oxidative addition of alkyl halides to silicon, catalyzed by several different transition metals, to give R_2SiX_2, a variety of related analogues (R_nSiX_{4-n}, $n = 0\text{-}4$) and by-products (Figure 3.1).[13] However, this process is not practical in the laboratory on small scale. A Grignard-type reaction is one of the most convenient methods to construct Si-C bonds (Figure 3.2).[14] Although many metal alkyls will react with halide silanes to make organosilanes, organomagnesium and alkyllithium reagents are most frequently used. Grignard reagents are usually prepared simply by mixing an alkyl halide with magnesium in an ether solvent.

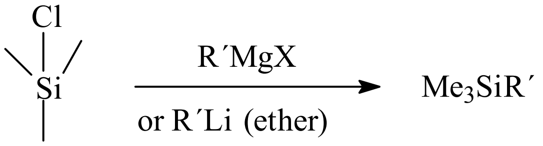

Figure 3.2. Addition of a Grignard reagent to a chorosilane to make organosilanes.

The most common method for the preparation of alkyl silyl ethers involves the reaction of an alcohol with a functionalized silane, usually a chloride, in the presence of a base. Frequently, the excellent silaphilic nucleophile imidazole is used as the base, or as a catalyst in combination with NEt_3 or pyridine, to facilitate silylation (Figure 3.3).[15]

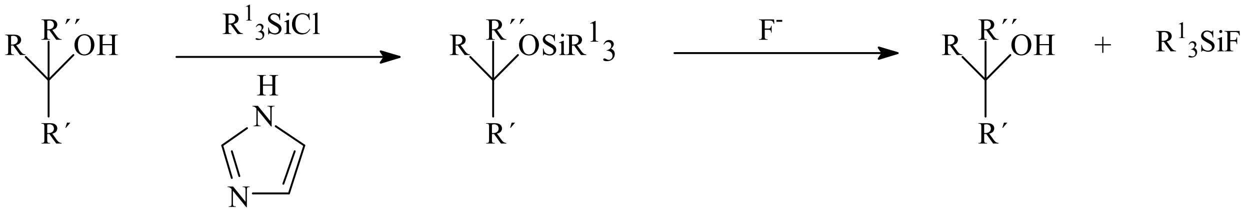

Figure 3.3. Common method for preparing silyl ethers as protecting groups and fluoride catalyzed hydrolysis.

Ligand metathesis is a commonly observed phenomenon with silicon compounds. While carbon-based ligands migrate only with great difficulty, Si-H, Si-SiR_3 and Si-Ph groups are more reactive for redistribution but less than halides and alkoxides.[15] In any case, a strong Lewis acid such as $AlBr_3$ is generally required to promote the reaction. In addition, the Si-C bond length is much longer than the analogous C-C bond length (1.89 *vs.* 1.54 Å), making silicon more accessible than carbon to nucleophilic attack for a given group of substituents. This is also a consequence of silicon having a higher electrophilicity and facility for coordination expansion.

Regarding the stability: carbosilane monomers are very stable compounds due to the dissociation energy of the Si-C bond (306 kJ/mol), which is similar to that of the C-C bond (345 kJ/mol), and the low polarity of the Si-C bond. In contrast, alkoxysilane monomers can undergo hydrolysis under mild acidic (acetic acid, aqueous HCl) or basic ($NaHCO_3$) conditions. In fact, trimethylsilyl ethers are not stable to most types of hydrolysis and hence are commonly used as protecting groups of alcohols in organic synthesis (Figure 3.3).[16] However, Stork and Hudrlik, and Corey and Venkateswarlu, recognized that increasing the steric bulk around silicon would retard nucleophilic attack at silicon, leading to more stable alkoxysilanes or silyl ethers.[17]

3.2 RESULTS AND DISCUSSION

3.2.1 AB*n*-carbosilane type monomers: synthesis and characterization

Branched AB_n-carbosilane type monomers, containing silicon-carbon bonds, were synthesized following a slightly modified strategy as developed by Drohmann *et al.* (Figure 3.4).[18] Due to the higher reactivity of alkyl bromides versus alkyl chlorides with metallic magnesium, the bromide analogues were synthesized from the corresponding alcohols using phosphorus tribromide.[19] The alkene-magnesium bromide Grignard reagent was then generated and further reacted with the corresponding chlorosilane reagent to give the desired carbosilane monomer in a distinctly higher yield than reported for the chloro derivative. Although initially a ten molar excess of magnesium to alkene bromide was employed for the preparation of the Grignard reagent, it was later established that a 4 or 5 molar excess was sufficient for obtaining quantitative yields. In this manner, AB_n linear and branched carbosilane monomers with $n = 1$, 2 and 3 and with different alkenyl chain lengths (allyl and undecenyl) were synthesized. The complete series of monomers synthesized and the abbreviations assigned to them are shown in Figure 3.5.

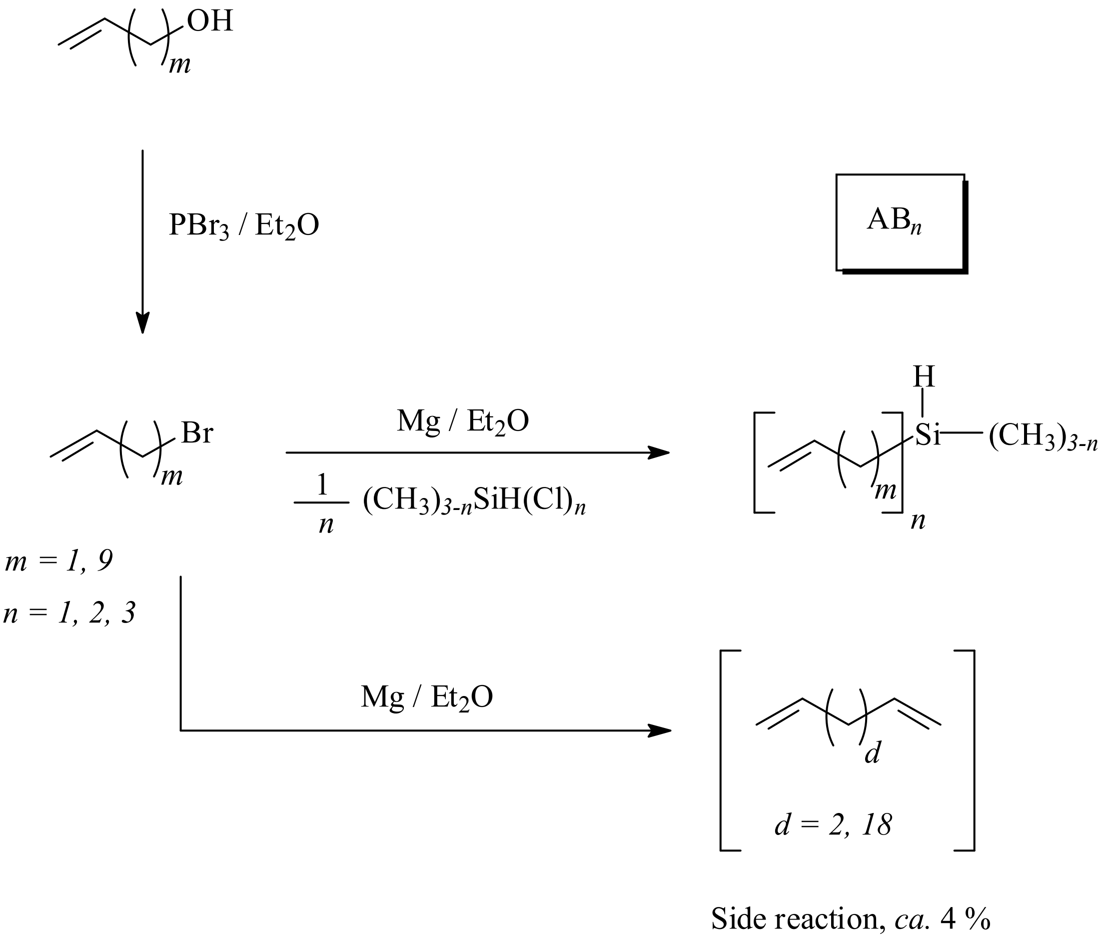

Figure 3.4. Synthetic route for the synthesis of AB$_n$-alkenylsilane type monomers.

In the synthesis of undecenylsilane-type monomers, side products like undec-1-ene and undec-10-en-1-ol were readily separated by fractional distillation. The Wurtz-type homo-coupled dimers were also identified as a side product. For example, the dimer docosa-1,21-diene (*ca.* 4 %) could not be separated from the methyldiundec-10-enylsilane (MDUS) product due to the similar boiling points. However, this contaminant presented no synthetic problems in the ensuing hypergrafting procedure. The chemical shifts of the Wurtz coupling side-product are coincident with the chemical shifts of MDUS in the NMR spectra. The amount of this side-product can be obtained from the ^{1}H NMR spectrum by comparing the relative intensities of the allylic or vinyl protons with the protons of the Si-CH$_3$ group. The yields and boiling points of the monomers are presented in Table 3.1. Their purity was checked by both GC and FD-MS and they were further characterized by NMR, IR and elemental analysis. The ^{1}H and ^{13}C NMR spectra of the samples were consistent with the structures depicted.

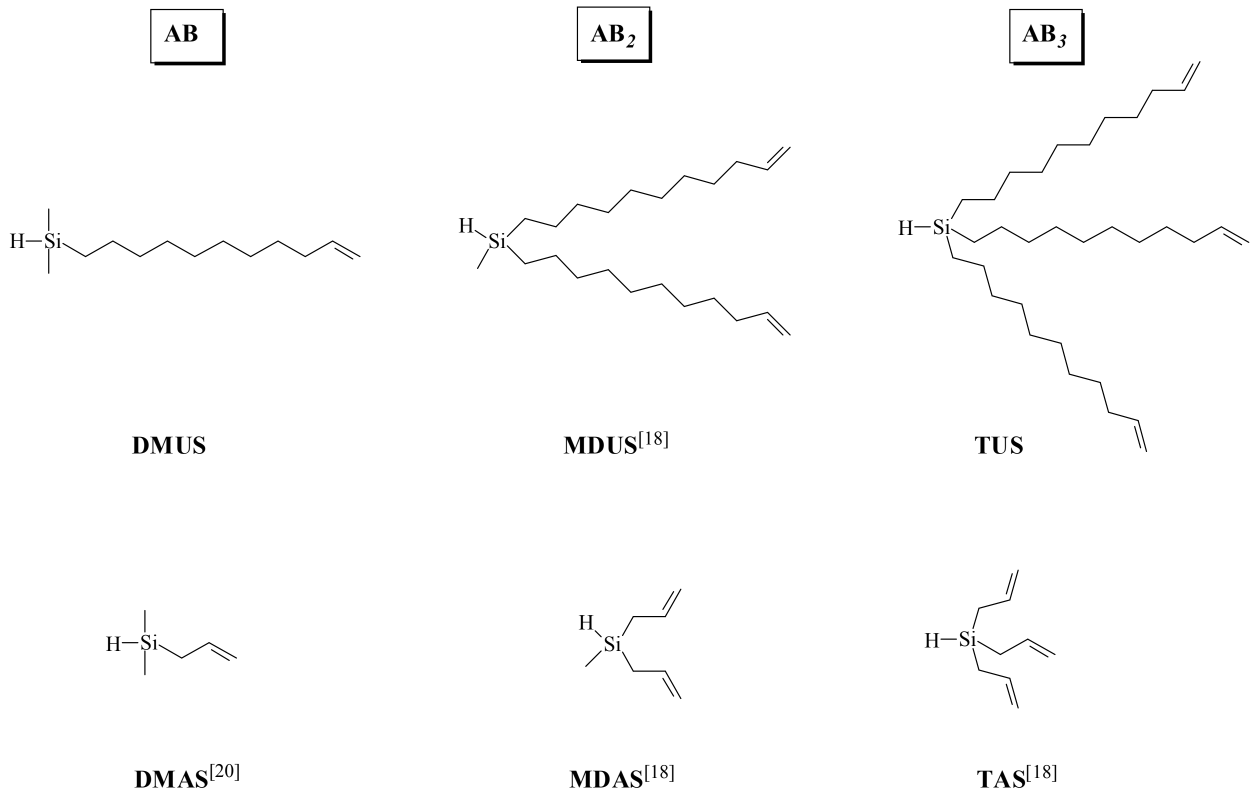

Figure 3.5. Structure of the synthesized AB_n-alkenylsilane type monomers.

Table 3.1. Abbreviations, boiling points (bp) and reaction yields of AB_n- alkenylsilane type monomers.

Monomer	Abbreviation	bp	Yield
methyldiundec-10-enylsilane[a, c]	MDUS	141 °C (0.1 mbar)	83.8 %
dimethyl(undec-10-enyl)silane	DMUS	129 °C (1-2 mbar)	63.5 %
triundec-10-enylsilane	TUS	183 °C (0.05 mbar)	83.2 %
diallyl(methyl)silane[a, c]	MDAS	121 °C	73.8 %
Allyldimethylsilane[b, c]	DMAS	50 °C	19.3 %
Triallylsilane[a]	TAS	57 °C (10 mbar)	81.9 %

[a]Reference [18]. [b]Reference [20]. [c]Contains low fractions of the Wurtz coupled dimers

The preparation of allyldimethylsilane (DMAS) via this procedure, *i.e.* Grignard reaction in diethyl ether, gave the product in a moderate yield of 19 %. This is due to the similar boiling points of diethyl ether and DMAS. It has been documented that replacing diethyl ether by THF leads to better yields.[21]

A general trend was found for the silicon chemical shifts of the different monomers: substituting the methyl groups by alkenyl units resulted in a gradual downfield shift and was greater when the alkenyl chain was longer (Table 3.2). This can be related to the electron density on the silicon atom: the silicon atom is deshielded upon replacing a methyl group by alkenyl substituents and hence the greater the downfield shift. This trend is also found in the shorter allyl substituted silanes. The difference between the silicon chemical shifts of the allyl and undecenyl series can be explained by hyperconjugation.

Table 3.2. ^{29}Si-NMR chemical shifts of AB$_n$- alkenylsilane type monomers.

Monomer	**δ_{Si} (ppm)**
TUS	-6.29
MDUS	-9.7
DMUS	-12.95
TAS	-10.61
MDAS	-12.17
DMAS	-13.98

3.2.2 AB$_n$-alkoxysilane type monomers: synthesis and characterization

Branched AB$_n$-alkoxysilane type monomers, containing silicon-oxygen bonds, were synthesized following the procedure described by Möller *et al.* (Figure 3.6).[7] This consisted of the reaction of the chorosilane reagent with undec-10-en-1-ol or prop-2-en-1-ol. In this way, AB and AB$_2$ monomers having either undecenoxy or alloxy chains were prepared (Figure 3.7). The monomers were again purified by distillation, which removed other condensation products as well as the residual alcohol. The boiling points of these alkoxysilane monomers, along with the reaction yields, are shown in Table 3.3.

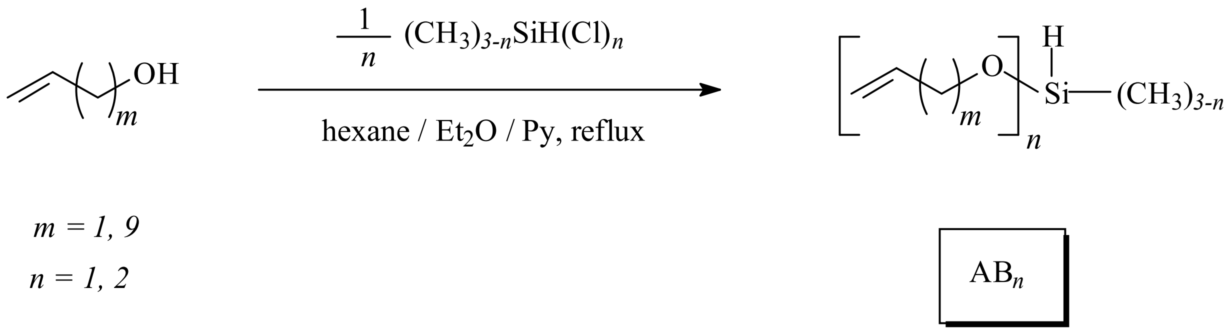

Figure 3.6. Synthetic route for the synthesis of AB$_n$-alkenoxysilane type monomers.

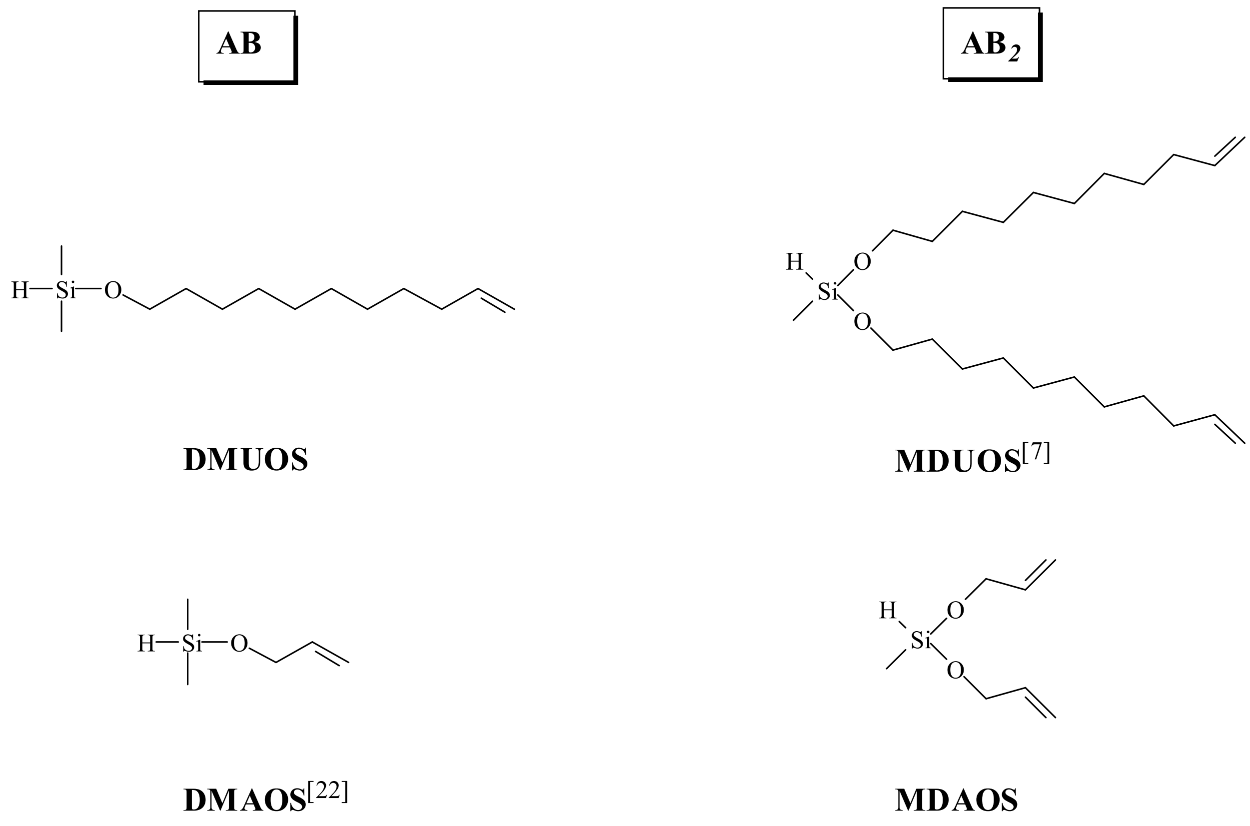

DMUOS **MDUOS**[7]

DMAOS[22] **MDAOS**

Figure 3.7. Structure of the synthesized AB$_n$-alkenoxysilane type monomers.

Table 3.3. Abbreviations, boiling points (bp) and reaction yields of AB$_n$-alkenoxysilane type monomers.

Monomer	Abbreviation	bp	Yield
methylbis(undec-10-enyloxy)silane[a]	MDUOS	152 °C (0.3 mbar)	55 %
dimethyl(undec-10-enyloxy)silane	DMUOS	110 °C (4 mbar)	54.1 %
bis(allyloxy)(methyl)silane	MDAOS	128 °C	48.4 %
Allyloxydimethylsilane[b]	DMAOS	55 °C	11 %

[a]Reference [7]. [b]Reference [22]

Table 3.4. ^{29}Si-NMR chemical shifts of AB$_n$- alkenoxysilane type monomers.

Monomer	δ_{Si} (ppm)
MDUOS	-15.49
DMUOS	5.1
MDAOS	-13.98
DMAOS	6.69

A general trend was also found for the silicon chemical shifts of the alkenoxysilane monomers, which are presented in Table 3.4. It is observed that changing the Si-C by a Si-O bond changes the electronic environment on the silicon atom. Substituting the undecenyl or allyl chain in the AB-alkenylsilane type monomers by an undecenyloxy or allyloxy chain, to give the corresponding AB-alkenoxysilane type monomers respectively, results in an unexpected downfield chemical shift of the ^{29}Si resonance. This “unexpected” effect for heteroatom-substituted silicon compounds was evaluated in the group of Strohmann *et al.* by quantum-chemical calculations.[23] It is obvious, that the electron density at the silicon center, after the introduction of an electron-withdrawing group, cannot alone explain the observed trend. In fact, they demonstrated by localized molecular orbital contributions (LMO), that the combination of very electronegative (*i.e.* alkoxy groups) and electropositive substituents (*i.e.* Li or H in our case) leads to large deshielding contributions in heteroatom-substituted silyllithium compounds. By analogy with these studies, the increased Si-H LMO contribution in the monoalkenoxy silanes, overcompensates the replacement of one Si-C contribution by a less deshielding Si-OR contribution, and an overall greater deshielding than in the corresponding monoalkenyl silanes is observed. However, as seen in Table 3.4, the replacement of a second alkenyl group in the AB_2-alkenylsilane type monomers by an alkenoxy group leads to an overall enhanced shielding. This shielding effect can be explained by an additional contribution of the lone pairs (LP) at the oxygen substituents, which increases with the introduction of a second heteroatomic alkenoxy group.

3.3 EXPERIMENTAL

3.3.1 Materials

Undec-10-en-1-ol, prop-2-en-1-ol, 11-bromoundec-1-ene, 3-bromoprop-1-ene, phosphorus tribromide, magnesium, anhydrous pyridine over molecular sieves and the organochlorosilanes were used as received. The solvents, diethyl ether and *n*-hexane, were dried by refluxing them over sodium/benzophenone and were freshly distilled prior to use. All reactions were carried out under an inert atmosphere of dry argon.

3.3.2 Synthesis of 3-bromoprop-1-ene and 11-bromoundec-1-ene

The synthesis was carried out according to known literature procedures. As an example, the synthesis of 11-bromoundec-1-ene is described.

11-bromoundec-1-ene. A 500 mL two neck flask fitted with a dropping funnel was charged with undec-10-en-1-ol (94 mL, 0.47 mol) in dry diethyl ether (200 mL) under argon. Phosphorus tribromide (18 mL, 0.19 mol) was added slowly to the reaction mixture at 0 °C and in the absence of light. After the addition, the mixture was allowed to stir at 0 °C for one hour and at room temperature overnight. The reaction mixture was poured with stirring into ice water (200 mL). The organic layer was separated and the water phase further extracted with petroleum ether. The organic fractions were combined, washed successively three times with saturated aqueous $NaHCO_3$ and water (100 mL). The organic fractions were then dried over $MgSO_4$, filtered, and the solvent was evaporated. The residue was purified by vacuum distillation.

Yield: 58.2 g (53.1 %) of a colourless, viscous liquid. bp: 78 °C at 1.8 mbar; lit. 149-150°C at 35 mm Hg. Purity: 97 % (GC).

^{1}H NMR (300 MHz, $CDCl_3$): δ (ppm) 1.20-1.50 (12 H, CH_2), 1.85 (m, 2H, -C**H**$_2$-CH_2-Br), 2.02 (m, 2H, -C**H**$_2$-CH=CH_2), 3.40 (t, J = 6.8 Hz, 2H, -C**H**$_2$-Br), 4.95 (m, 2H, -CH=C**H**$_2$), 5.79 (tdd, J = 6.7, 10.2 and 16.9 Hz, 1H, -C**H**=CH_2); ^{13}C NMR (75 MHz, $CDCl_3$): δ (ppm) 28.50 (-**C**H$_2$-CH_2-CH_2-Br), 29.08 (-**C**H$_2$-CH_2-CH_2-CH_2-Br), 29.23 (-**C**H$_2$-CH_2-CH=CH_2), 29.41 (-**C**H$_2$-CH_2-CH_2-CH=CH_2), 29.70 (Br-CH_2-CH_2-CH_2-CH_2-**C**H$_2$-**C**H$_2$-CH_2-CH_2-CH_2-CH=CH_2), 33.17 (-**C**H$_2$-CH_2-Br), 34.12 (-**C**H$_2$-Br), 34.28 (-**C**H$_2$-CH=CH_2), 114.46 (-CH=**C**H$_2$), 139.46 (-**C**H=CH_2).

3.3.3 Synthesis of AB$_n$-alkenylsilane type monomers; n = 1, 2, 3

Methyldiundec-10-enylsilane (MDUS). In a 1 L three neck flask equipped with a mechanical stirrer, reflux condenser and dropping funnel, was added magnesium (109.40 g, 4.5 mol) and iodine (few granules) in dry diethyl ether (400 mL) under argon. A solution of 11-bromoundec-1-ene (100 mL, 0.45 mol) in dry diethyl ether (80 mL) was added slowly at room temperature. The initiation of the Grignard reaction was indicated by a modest reflux accompanied with the development of a grey coloured solution. After the addition, the reaction mixture was allowed to react for a further 3 hours at room temperature. The Grignard solution was then transferred via canula to a 1 L three-neck flask also equipped with a reflux condenser and a dropping funnel. A solution of dichloro(methyl)silane (15.5 mL, 0.15 mol) in dry diethyl ether (45 mL) was added dropwise. A white salt precipitate of MgBrCl was formed. Finally the reaction mixture was refluxed overnight under argon. After the reaction mixture was cooled to room temperature, a saturated aqueous solution of NH_4Cl (100 mL) was added carefully followed by the addition of water (160 mL). The organic and the water phase were separated and the water phase further extracted with diethyl ether. The combined organic fractions were washed several times with a saturated aqueous $NaHCO_3$ solution and water. The organic phase was then dried with $MgSO_4$, filtered and the solvent was evaporated. 82 g of a slightly yellow viscous liquid was obtained. This was carefully fractionated under vacuum.

Yield: 44.1 g (83.8 %) of a colourless, viscous liquid. bp: 141 °C at 0.1 mbar.

^{1}H NMR (300 MHz, $CDCl_3$): δ (ppm) 0.05 (d, *J* = 3.7 Hz, 3 H, Si-CH_3), 0.59 (m, 4H, Si-CH_2), 1.2-1.5 (m, 28 H, -CH_2-), 2.05 (m, 4H, -C**H**$_2$-CH=CH_2), 3.77 (m, 1H, Si-H), 4.96 (m, 4H, -CH=C**H**$_2$), 5.80 (tdd, *J* = 6.7, 10.2 and 16.9 Hz, 2H, -C**H**=CH_2); ^{13}C NMR (75 MHz, $CDCl_3$): δ (ppm) -5.87 (Si-CH_3), 13.14 (Si-CH_2), 24.89 (Si-CH_2-**C**H_2), 29.34 (-CH_2-), 29.54 (-CH_2), 29.74 (-CH_2), 29.91 (-CH_2-), 33.67 (-CH_2-), 34.20 (-**C**H_2-CH=CH_2), 114.45 (-CH=**C**H_2), 139.46 (-**C**H=CH_2); ^{29}Si NMR (80 MHz, $CDCl_3$): δ (ppm) -9.7; IR (characteristic absorption bands): ν (cm^{-1}) 2101 (stretching Si-H mode), 1639 (stretching C=C mode), 1248 (stretching Si-CH_3 mode); GC: 96 % purity; FD-MS: 152.4 (3.62), 306.6 (27.39), 350.6 (100); Elemental Analysis: C, 78.11 %; H, 12.80 % (calculated for $C_{23}H_{46}Si$: C, 78.77 %; H, 13.22 %).

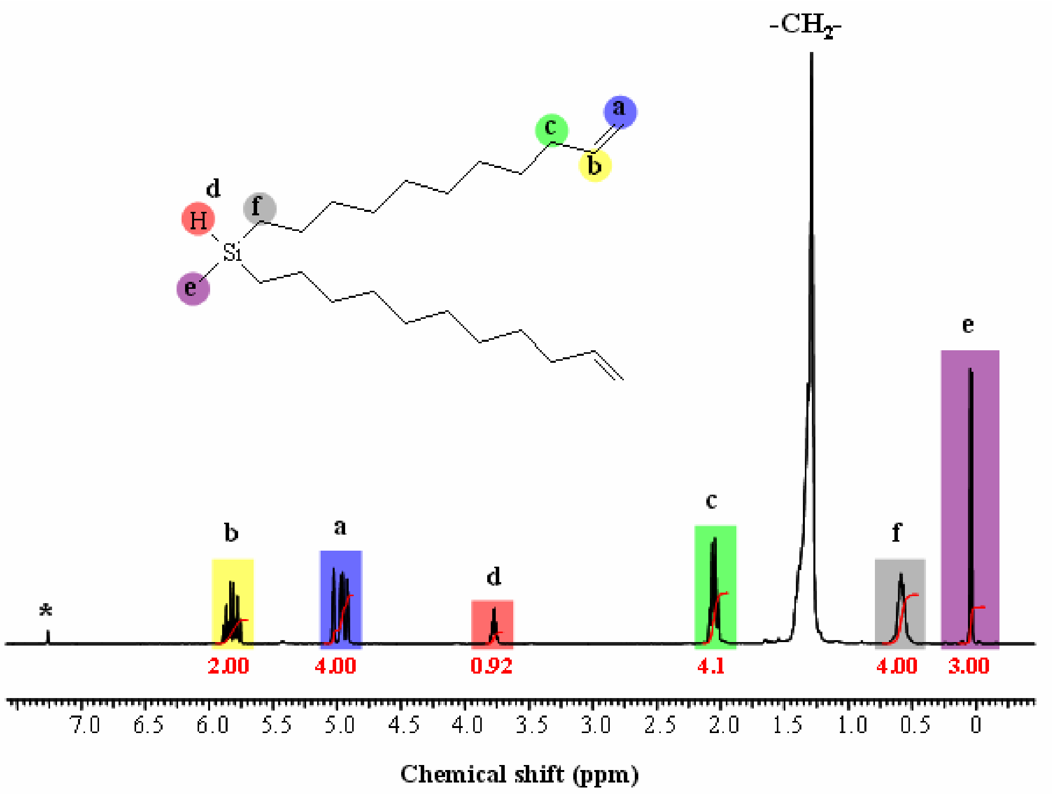

Figure 3.8. ^{1}H NMR spectrum of MDUS in $CDCl_3$ (solvent peak denoted by an asterisk).

Dimethyl(undec-10-enyl)silane (DMUS) was prepared analogously to MDUS from magnesium (109.40 g, 4.5 mol), 11-bromoundec-1-ene (100 mL, 0.45 mol) and chlorodimethylsilane (33.3 mL, 0.3 mol) in dry diethyl ether. Yield: 40.5 g (63.5 %) of a colourless, viscous liquid. bp: 129 °C at 1-2 mbar.

^{1}H NMR (300 MHz, CDCl$_3$): δ (ppm) 0.05 (d, J = 3.7 Hz, 6 H, Si-CH$_3$), 0.59 (m, 2H, Si-CH$_2$), 1.2-1.5 (m, 14 H, -CH$_2$-), 2.05 (m, 4H, -$\mathbf{CH_2}$-CH=CH$_2$), 3.85 (m, 1H, Si-H), 4.96 (m, 2H, -CH=$\mathbf{CH_2}$), 5.82 (tdd, J = 6.7, 10.2 and 16.9 Hz, 1H, -$\mathbf{CH}$=CH$_2$); ^{13}C NMR (75 MHz, CDCl$_3$): δ (ppm) -4.07 (Si-CH$_3$), 14.55 (Si-CH$_2$), 24.75 (Si-CH$_2$-$\mathbf{CH_2}$), 29.33 (-CH$_2$-), 29.54 (-CH$_2$), 29.75 (-CH$_2$), 29.91 (-CH$_2$-), 33.59 (-CH$_2$-), 34.21 (-$\mathbf{CH_2}$-CH=CH$_2$), 114.44 (-CH=$\mathbf{CH_2}$), 139.58 (-$\mathbf{CH}$=CH$_2$); ^{29}Si NMR (80 MHz, CDCl$_3$): δ (ppm) -12.95; IR (characteristic absorption bands): ν (cm^{-1}) 2110 (stretching Si-H mode), 1640 (stretching C=C mode), 1251 (stretching Si-CH$_3$ mode), 833 (bending CH$_3$-Si-CH$_3$ mode); GC: 100 % purity; FI-MS: 212.3 (100); Elemental Analysis: C, 72.85 %; H, 12.46 % (calculated for C$_{13}$H$_{28}$Si: C, 73.50 %; H, 13.28 %).

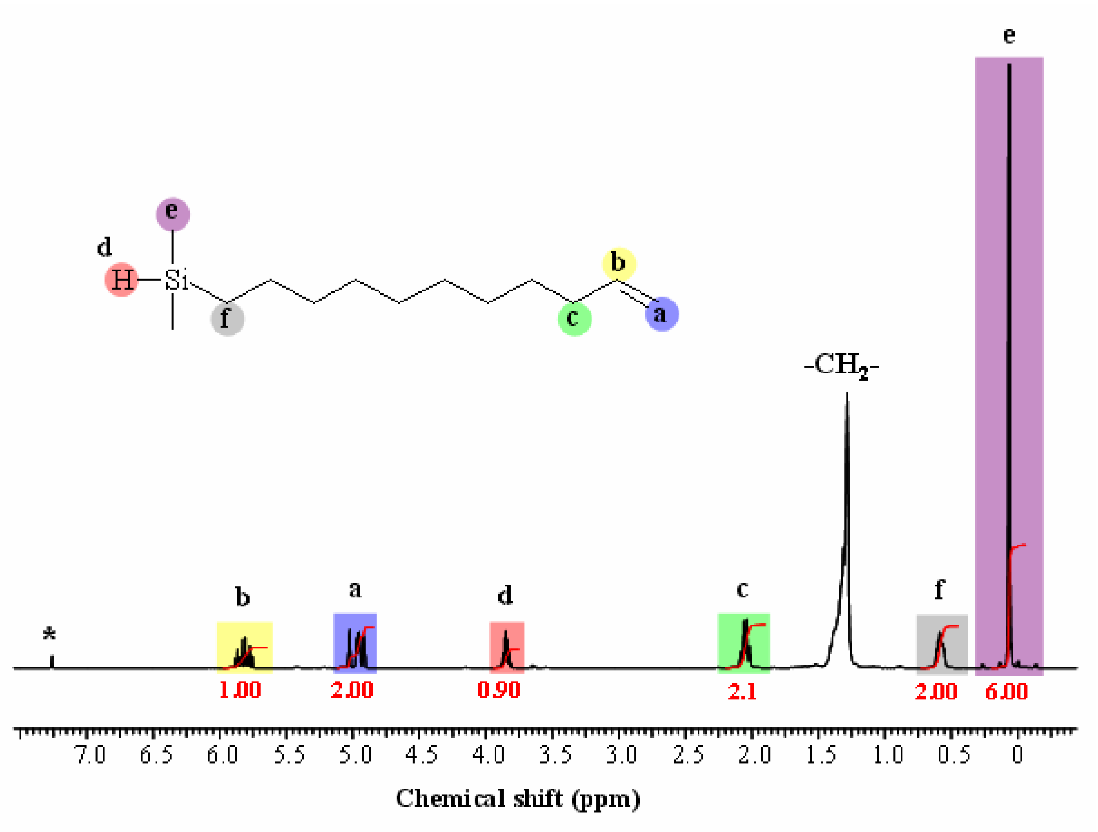

Figure 3.9. ^{1}H NMR spectrum of DMUS in CDCl$_3$ (solvent peak denoted by an asterisk).

Triundec-10-enylsilane (TUS) was prepared analogously to MDUS from magnesium (109.40 g, 4.5 mol), 11-bromoundec-1-ene (100 mL, 0.45 mol) and trichorosilane (10 mL, 0.1 mol) in dry diethyl ether. Yield: 40.7 g (83.2 %) of a colourless, viscous liquid. bp: 183 °C at 0.05 mbar.

^{1}H NMR (400 MHz, $CDCl_3$): δ (ppm) 0.57 (m, 6H, Si-CH_2), 1.15-1.5 (m, 42 H, -CH_2-), 2.04 (m, 6H, -$\mathbf{CH_2}$-CH=CH_2), 3.67 (m, 1H, Si-H), 4.96 (m, 6H, -CH=C$\mathbf{H_2}$), 5.81 (tdd, *J* = 6.7, 10.2 and 16.9 Hz, 3H, -C**H**=CH_2); ^{13}C NMR (100 MHz, $CDCl_3$): δ (ppm) 11.71 (Si-CH_2), 25.06 (Si-CH_2-$\mathbf{CH_2}$), 29.33 (-CH_2-), 29.54 (-CH_2), 29.70 (-CH_2), 29.91 (-CH_2-), 33.74 (-CH_2-), 34.20 (-$\mathbf{CH_2}$-CH=CH_2), 114.44 (-CH=$\mathbf{CH_2}$), 139.56 (-**C**H=CH_2); ^{29}Si NMR (80 MHz, $CDCl_3$): δ (ppm) -6.29; IR (characteristic absorption bands): ν (cm^{-1}) 2095 (stretching Si-H mode), 1641 (stretching C=C mode); FD-MS: 488.5 (100); Elemental Analysis: C, 81.27 %; H, 13.17 % (calculated for $C_{33}H_{64}Si$: C, 81.06 %; H, 13.19 %).

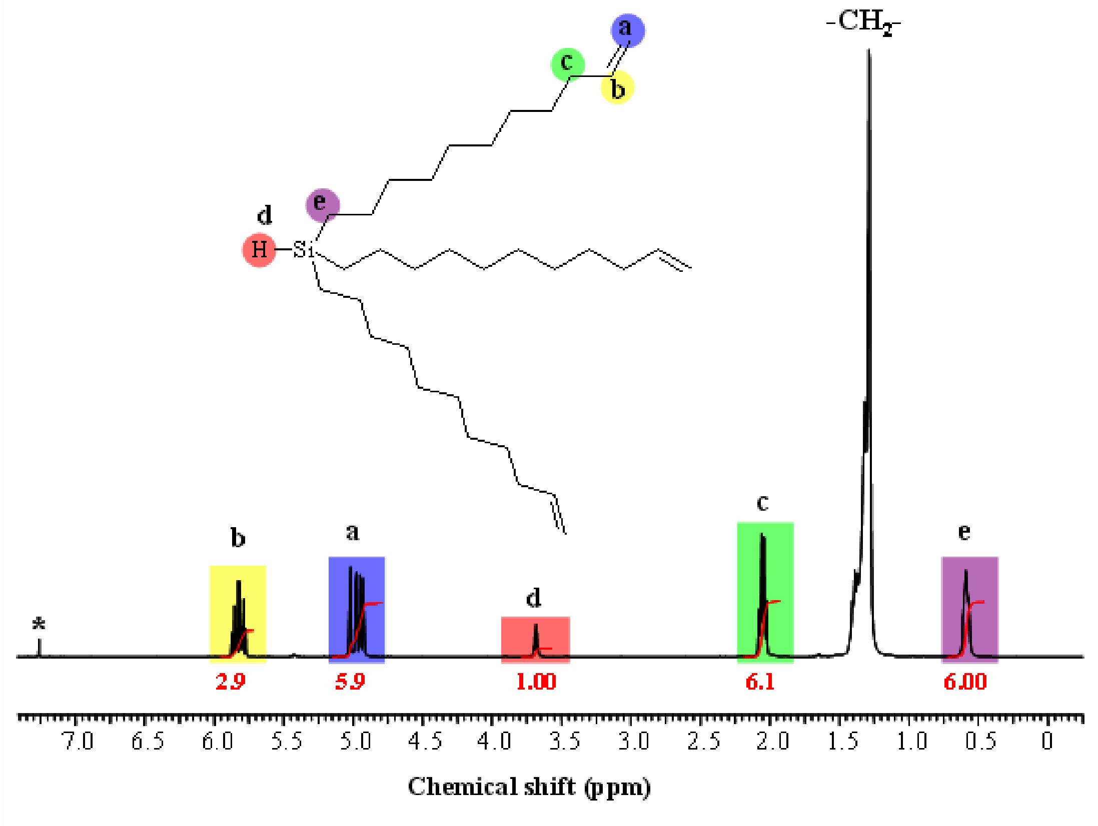

Figure 3.10. ^{1}H NMR spectrum of TUS in $CDCl_3$ (solvent peak denoted by an asterisk).

Diallyl(methyl)silane (MDAS) was prepared analogously to MDUS from magnesium (139 g, 5.7 mol), 3-bromoprop-1-ene (50 mL, 0.57 mol) and dichloro(methyl)silane (19.7 mL, 0.19 mol) in dry diethyl ether. Yield: 17.7 g (73.8 %) of a colourless, viscous liquid. bp: 121 °C.

^{1}H NMR (300 MHz, $CDCl_3$): δ (ppm) 0.08 (d, *J* = 3.7 Hz, 3 H, Si-CH_3), 1.63 (m, 4H, -**C**$\mathbf{H}_2$-CH=CH_2), 3.81 (m, 1H, Si-H), 4.90 (m, 4H, -CH=**C**$\mathbf{H}_2$), 5.81 (tdd, *J* = 6.7, 10.2 and 16.9 Hz, 2H, -C**H**=CH_2); ^{13}C NMR (100 MHz, $CDCl_3$): δ (ppm) -6.84 (Si-CH_3), 20.19 (-**C**H_2-CH=CH_2), 114.00 (-CH=**C**H_2), 134.71 (-**C**H=CH_2); ^{29}Si NMR (80 MHz, $CDCl_3$): δ (ppm) -12.17; IR (characteristic absorption bands): ν (cm^{-1}) 2113 (stretching Si-H mode), 1629 (stretching C=C mode), 1251 (stretching Si-CH_3 mode); FI-MS: 85.1 (4.15), 126.2 (100); Elemental Analysis: C, 66.74 %; H, 11.05 % (calculated for $C_7H_{14}Si$: C, 66.58 %; H, 11.18 %).

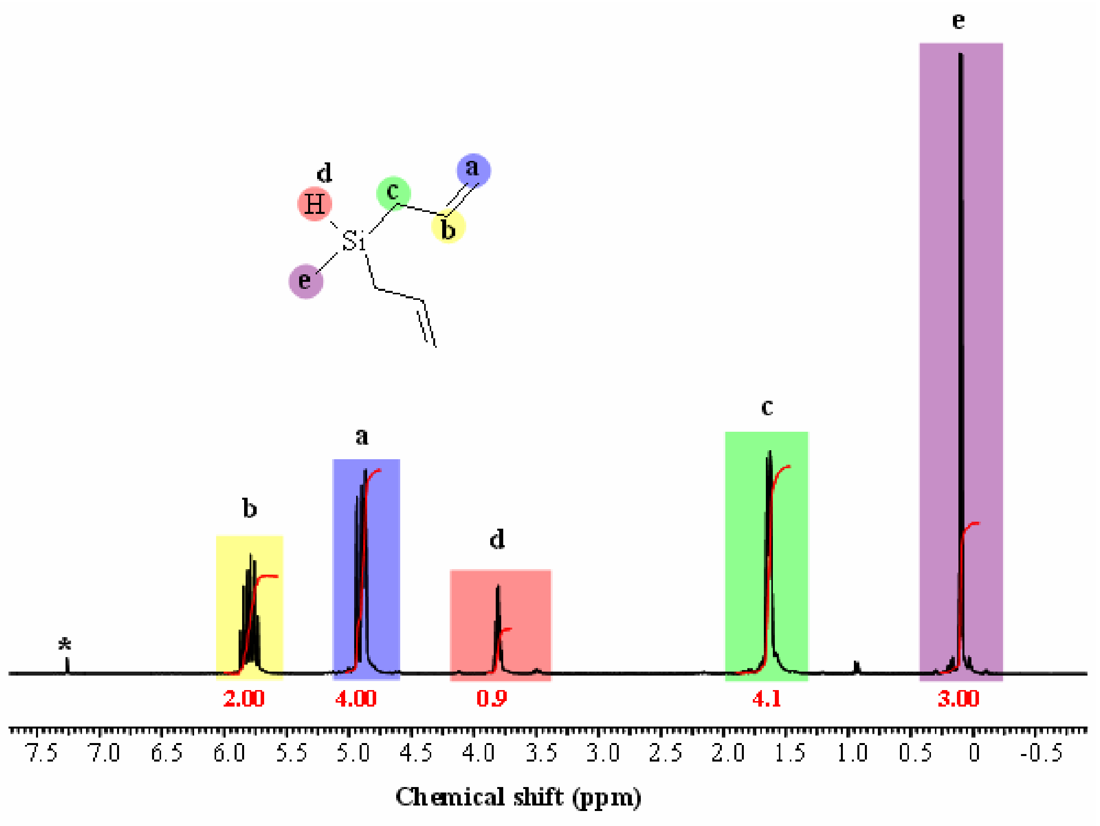

Figure 3.11. ^{1}H NMR spectrum of MDAS in $CDCl_3$ (solvent peak denoted by an asterisk).

Allyldimethylsilane (DMAS) was prepared analogously to MDUS from magnesium (134 g, 5.5 mol), 3-bromoprop-1-ene (83 mL, 0.95 mol) and chlorodimethylsilane (65 mL, 0.6 mol) in dry diethyl ether. Yield: 11.6 g (19.3 %) of a colourless, viscous liquid. bp: 50 °C.

^{1}H NMR (400 MHz, $CDCl_3$): δ (ppm) 0.10 (d, *J* = 3.7 Hz, 6 H, Si-CH_3), 1.61 (m, 2H, -**C**$\mathbf{H}_2$-CH=CH_2), 3.89 (m, 1H, Si-H), 4.88 (m, 2H, -CH=**C**$\mathbf{H}_2$), 5.81 (m, 1H, -C**H**=CH_2); ^{13}C NMR (100 MHz, $CDCl_3$): δ (ppm) -4.61 (Si-CH_3), 22.20 (-**C**H_2-CH=CH_2), 113.59 (-CH=**C**H_2), 135.05 (-**C**H=CH_2); ^{29}Si NMR (80 MHz, $CDCl_3$): δ (ppm) -13.98; IR (characteristic absorption bands): ν (cm^{-1}) 2115 (stretching Si-H mode), 1632 (stretching C=C mode), 1252 (stretching Si-CH_3 mode), 838 (bending CH_3-Si-CH_3 mode); FI-MS: 100.2 (100); Elemental Analysis: C, 62.14 %; H, 12.17 % (calculated for C_5H_{12} Si: C, 59.91 %; H, 12.06 %).

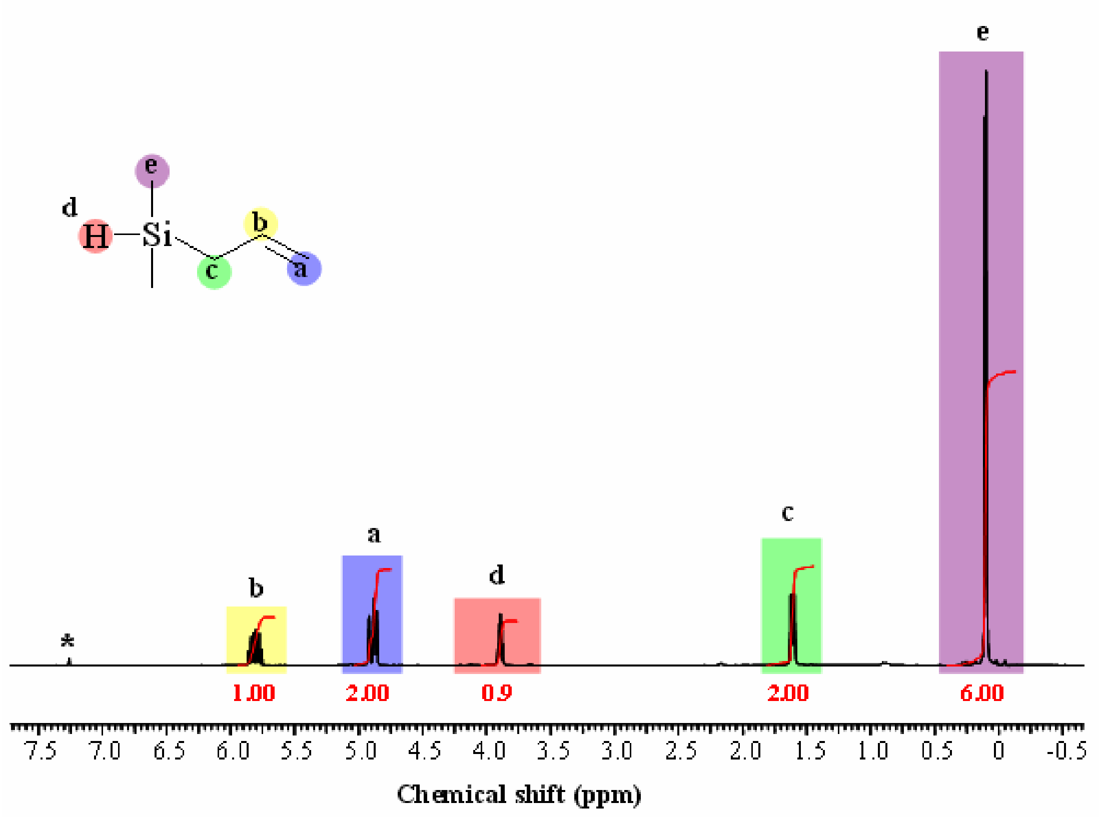

Figure 3.12. ^1H NMR spectrum of DMAS in $CDCl_3$ (solvent peak denoted by an asterisk).

Triallylsilane (TAS) was prepared analogously to MDUS from magnesium (134 g, 11.5 mol), 3-bromoprop-1-ene (100 mL, 1.15 mol) and trichorosilane (25 mL, 0.25 mol) in dry diethyl ether. Yield: 31.2 g (81.9 %) of a colourless, viscous liquid. bp: 57 °C at 10 mbar.

^1H NMR (300 MHz, $CDCl_3$): δ (ppm) 1.67 (m, 6H, -C**H**$_2$-CH=CH$_2$), 3.76 (m, 1H, Si-H), 4.95 (m, 6H, -CH=C**H**$_2$), 5.81 (tdd, *J* = 8.0, 10.1 and 17.0 Hz, 3H, -C**H**=CH$_2$); ^{13}C NMR (100 MHz, $CDCl_3$): δ (ppm) 18.26 (-**C**H$_2$-CH=CH$_2$), 114.42 (-CH=**C**H$_2$), 134.43 (-**C**H=CH$_2$); ^{29}Si NMR (80 MHz, $CDCl_3$): δ (ppm) -10.61; IR (characteristic absorption bands): ν (cm^{-1}) 2115 (stretching Si-H mode), 1628 (stretching C=C mode); FD-MS: 152.1 (100); Elemental Analysis: C, 70.31 %; 11.30 % (calculated for $C_9H_{16}Si$: C, 70.97 %; H, 10.59 %).

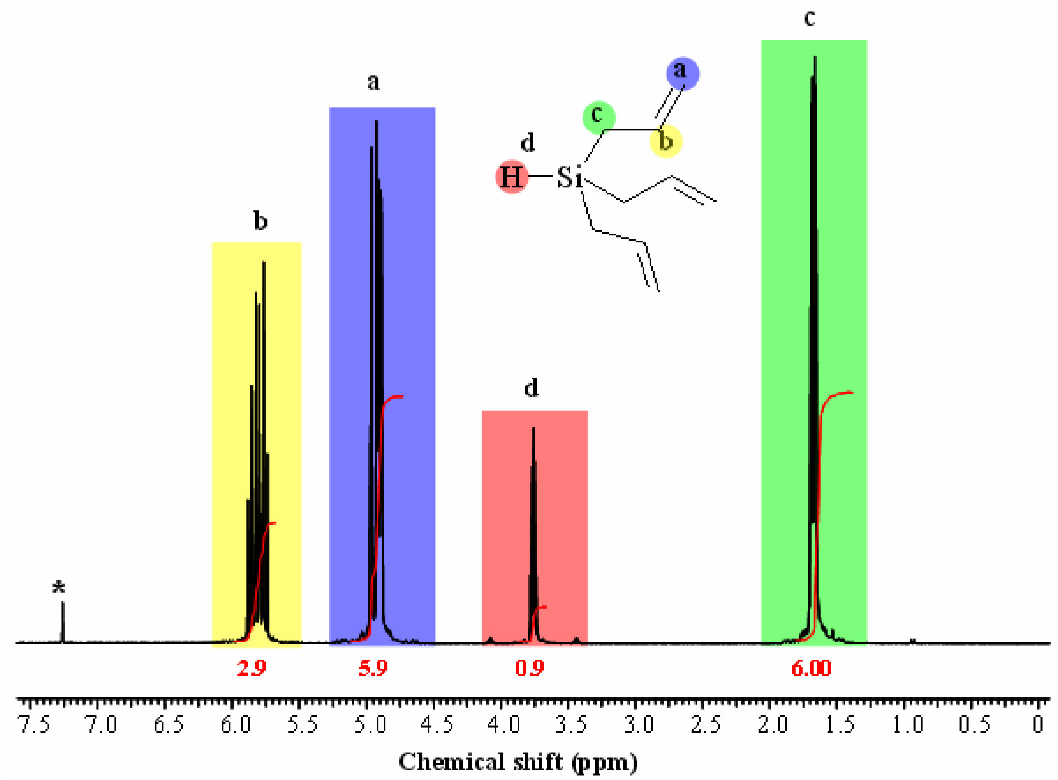

Figure 3.13. ^{1}H NMR spectrum of TAS in $CDCl_3$ (solvent peak denoted by an asterisk).

3.3.4 Synthesis of AB_n-alkenoxysilane type monomers; $n = 1, 2$

Methylbis(undec-10-enyloxy)silane (MDUOS). In a 1L three-neck flask under argon fitted with a dropping funnel was placed undec-10-en-1-ol (60.1 mL, 0.30 mol) in a 1:1 mixture of dry diethyl ether (150 mL) and hexane (150 mL) containing pyridine (24.2 mL, 0.30 mol). A solution of dichloro(methyl)silane (15.4 mL, 0.15 mol) in dry hexane (50 mL) was then added slowly at room temperature. After the addition was completed, the reaction was stirred under reflux for another 2 hours. Finally the pyridinium hydrochloride precipitate formed was removed by filtration under argon and the product isolated by vacuum distillation, after removal of the solvent. Yield: 31.61 g (55 %) of a colourless, viscous liquid. bp: 152 °C at 0.3 mbar.

^{1}H NMR (300 MHz, $CDCl_3$): δ (ppm) 0.18 (d, J = 1.8 Hz, 3 H, Si-CH_3), 1.15-1.45 (m, 24 H, -CH_2-), 1.56 (m, 4H, -O-CH_2-$\mathbf{CH_2}$-), 2.03 (m, 4H, -$\mathbf{CH_2}$-CH=CH_2), 3.71 (t, J = 6.6 Hz, 4H, -O-CH_2-), 4.56 (q, J = 1.6 Hz, 1H, Si-H), 4.94 (m, 4H, -CH=$\mathbf{CH_2}$), 5.79 (tdd, J = 6.7, 10.1 and 16.9 Hz, 2H, -**CH**=CH_2); ^{13}C NMR (75 MHz, $CDCl_3$): δ (ppm) -2.85 (Si-CH_3), 26.09 (-CH_2-), 29.28 (-CH_2-), 29.46 (-CH_2-), 29.72 (-CH_2), 29.79 (-CH_2), 29.91 (-CH_2-), 32.83 (-CH_2-), 34.15 (-CH_2-), 63.95 (-O-CH_2-), 114.44 (-CH=$\mathbf{C}H_2$), 139.50 (-**C**H=CH_2); ^{29}Si NMR (80

MHz, $CDCl_3$): δ (ppm) -15.49; IR (characteristic absorption bands): ν (cm^{-1}) 2157 (stretching Si-H mode), 1642 (stretching C=C mode), 1256 (stretching Si-CH_3 mode), 1089 (stretching Si-O-CH_2- mode); FD-MS: 383 (100); Elemental Analysis: C, 71.53 %; H, 11.80 % (calculated for $C_{23}H_{46}O_2Si$: C, 72.18 %; H, 12.12 %).

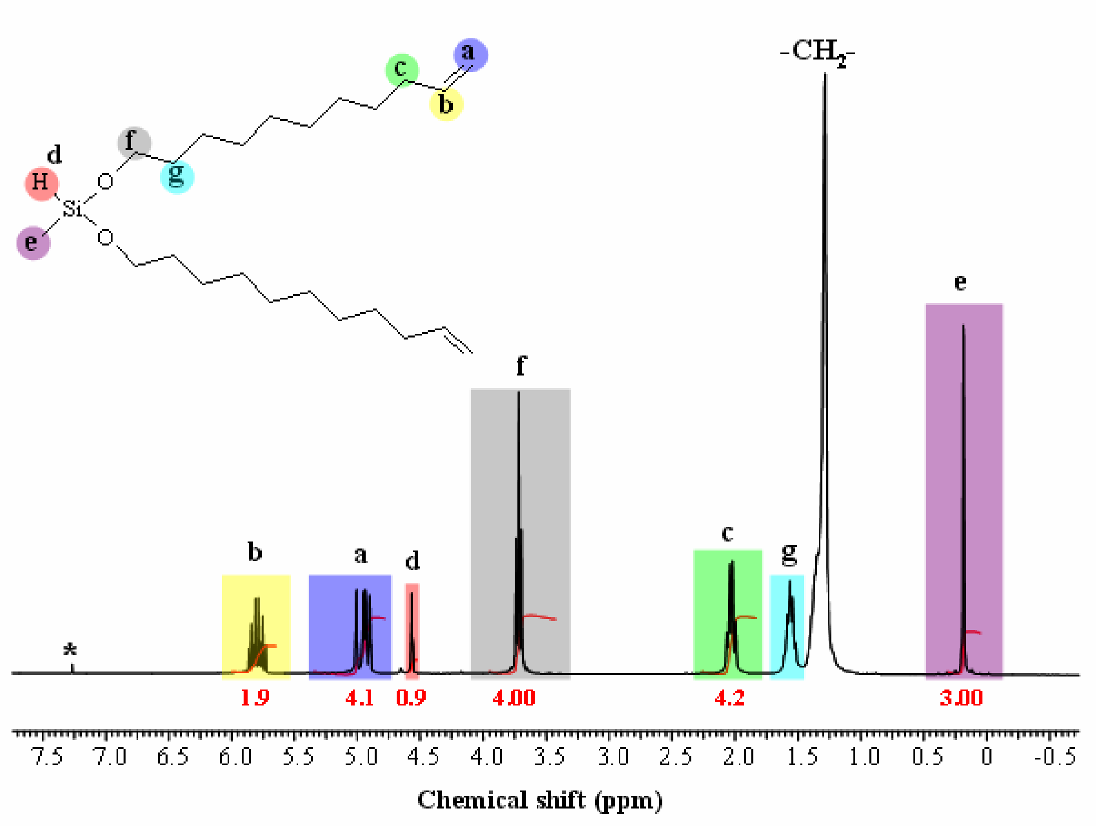

Figure 3.14. ^1H NMR spectrum of MDUOS in $CDCl_3$ (solvent peak denoted by an asterisk).

Dimethyl(undec-10-enyloxy)silane (DMUOS) was prepared analogously to MDUOS from undec-10-en-1-ol (80 mL, 0.40 mol) and pyridine (32 mL, 0.40 mol) in dry diethyl ether (200 mL)/hexane (200 mL) and chlorodimethylsilane (44 mL, 0.40 mol) in dry hexane (100 mL). Yield: 49.4 g (54.1 %) of a colourless, viscous liquid. bp: 110 °C at 4 mbar.

^1H NMR (300 MHz, $CDCl_3$): δ (ppm) 0.19 (d, J = 2.8 Hz, 6 H, Si-CH_3) , 1.15-1.45 (m, 12 H, -CH_2-), 1.53 (m, 2H, -O-CH_2-C**H**$_2$-), 2.03 (m, 2H, -C**H**$_2$-CH=CH_2), 3.61 (m, 2H, -O-CH_2-), 4.61 (m, 1H, Si-H), 4.94 (m, 2H, -CH=C**H**$_2$), 5.80 (tdd, J = 6.7, 10.2 and 16.9 Hz, 1H, -C**H**=CH_2); ^{13}C NMR (100 MHz, $CDCl_3$): δ (ppm) -1.24 (Si-CH_3), 26.11 (-CH_2-), 29.27 (-CH_2-), 29.45 (-CH_2-), 29.72 (-CH_2), 29.76 (-CH_2), 29.90 (-CH_2-), 32.82 (-CH_2-), 34.13 (-CH_2-), 64.57 (-O-CH_2), 114.43 (-CH=**C**H_2), 139.46 (-**C**H=CH_2); ^{29}Si NMR (80 MHz, $CDCl_3$): δ (ppm) 5.1; IR (characteristic absorption bands): ν (cm^{-1}) 2109 (stretching Si-H mode), 1638 (stretching C=C mode), 1249 (stretching Si-CH_3 mode), 1091 (stretching Si-O-CH_2-), 832 (bending CH_3-Si-CH_3 mode); FD-MS: 227.4 (100); Elemental Analysis: C, 67.6 %; H, 11.52 % (calculated for $C_{13}H_{28}OSi$: C, 68.35 %; H, 12.35 %).

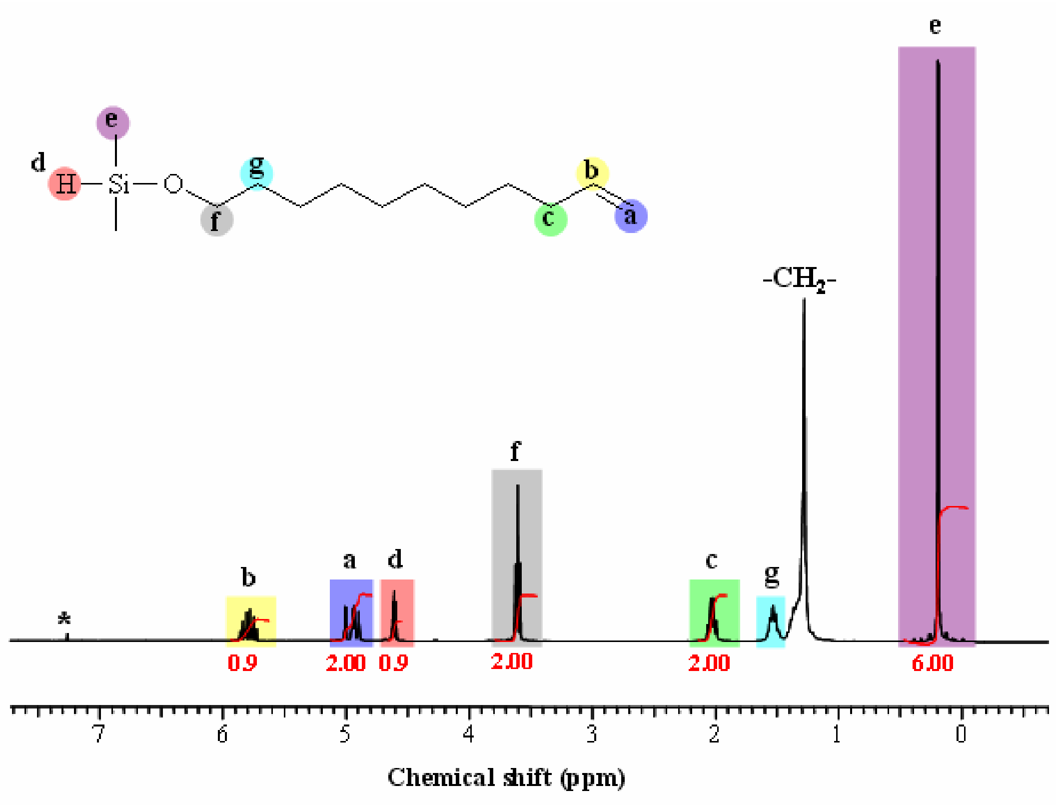

Figure 3.15. ^{1}H NMR spectrum of DMUOS in $CDCl_3$ (solvent peak denoted by an asterisk).

Bis(allyloxy)(methyl)silane (MDAOS) was prepared analogously to MDUOS from prop-2-en-1-ol (48 mL, 0.7 mol) and pyridine (56.5 mL, 0.7 mol) in dry diethyl ether (200 mL)/hexane (200 mL) and dichloro(methyl)silane (36 mL, 0.35 mol) in dry hexane (100 mL). Yield: 26.8 g (48.4 %) of a colourless, viscous liquid. bp: 128 °C.

^{1}H NMR (300 MHz, $CDCl_3$): δ (ppm) 0.23 (d, J = 1.7 Hz, 3 H, Si-CH_3), 4.27 (td, J = 1.6 and 4.9 Hz, 4H, O-CH_2-), 4.62 (q, J = 1.6 Hz, 1H, Si-H), 5.11 (ddd, J = 1.5, 3.1 and 10.4 Hz, 2H, -CH=$\mathbf{CH_2}$), 5.27 (ddd, J = 1.7, 3.5 and 17.1 Hz, 2H, -CH=$\mathbf{CH_2}$), 5.93 (tdd, J = 4.9, 10.1 and 17.1 Hz, 2H, -**CH**=CH_2); ^{13}C NMR (100 MHz, $CDCl_3$): δ (ppm) -3.19 (Si-CH_3), 64.40 (-O-CH_2-), 114.93(-CH=$\mathbf{C}H_2$), 136.34 (-**C**H=CH_2); ^{29}Si NMR (80 MHz, $CDCl_3$): δ (ppm) -13.98; IR (characteristic absorption bands): ν (cm^{-1}) 2160 (stretching Si-H mode), 1646 (stretching C=C mode), 1257 (stretching Si-CH_3 mode), 1069 (stretching Si-O-CH_2- mode); FD-MS: 159.2 (100); Elemental Analysis: C, 51.33 %; H, 8.11 % (calculated for $C_7H_{14}O_2Si$: C, 53.12 %; H, 8.92 %).

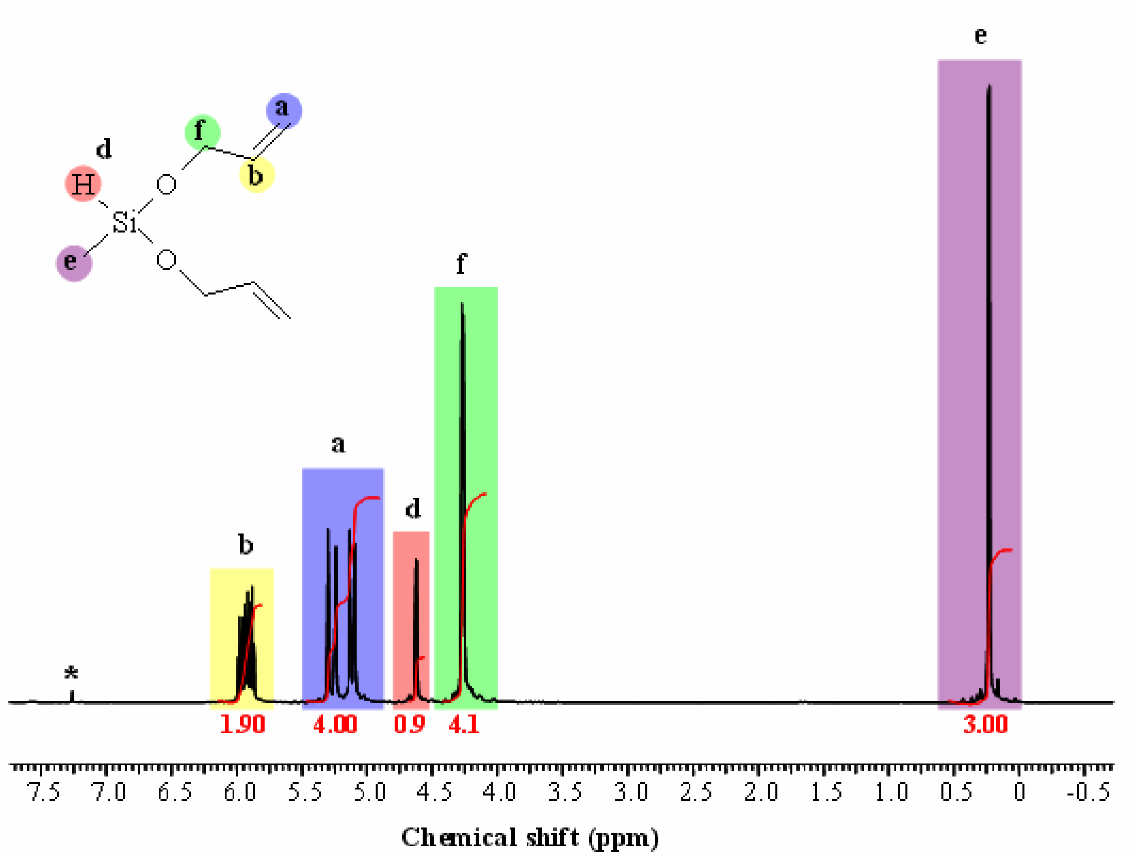

Figure 3.16. ^{1}H NMR spectrum of MDAOS in $CDCl_3$ (solvent peak denoted by an asterisk).

Allyloxydimethylsilane (DMAOS) was prepared analogously to MDUOS from prop-2-en-1-ol (29 mL, 0.42 mol) and pyridine (34 mL, 0.42 mol) in dry diethyl ether (150 mL)/hexane (150 mL) and chlorodimethylsilane (47 mL, 0.42 mol) in dry hexane (100 mL). Yield: 5.3 g (11 %) of a colourless, viscous liquid. bp: 55 °C. Note: the product contained 4 % of *n*-hexane that could not be separated by distillation due to the similar boiling points.

^{1}H NMR (300 MHz, $CDCl_3$): δ (ppm) 0.22 (d, $J = 2.8$ Hz, 6 H, Si-CH_3), 4.17 (m, 2H, O-CH_2-), 4.64 (m, 1 H, Si-H), 5.10 (m, 1H, -CH=C**H**$_2$), 5.25 (m, 1H, -CH=C**H**$_2$), 5.92 (tdd, $J = 4.9$, 10.1 and 17.1 Hz, 1H, -C**H**=CH_2); ^{13}C NMR (100 MHz, $CDCl_3$): δ (ppm) -1.27 (Si-CH_3), 65.41 (O-CH_2-), 115.12 (-CH=**C**H$_2$), 137.0 (-**C**H=CH_2); ^{29}Si NMR (80 MHz, $CDCl_3$): δ (ppm) 6.69; IR (characteristic absorption bands): ν (cm^{-1}) 2110 (stretching Si-H mode), 1645 (stretching C=C mode), 1250 (stretching Si-CH_3 mode), 1077 (stretching Si-O-CH_2- mode), 833 (bending CH_3-Si-CH_3 mode); FI-MS: 116.1 (100); Elemental Analysis: C, 52.85 %; H, 9.48 % (calculated for $C_5H_{12}OSi$: C, 51.67 %; H, 10.41 %).

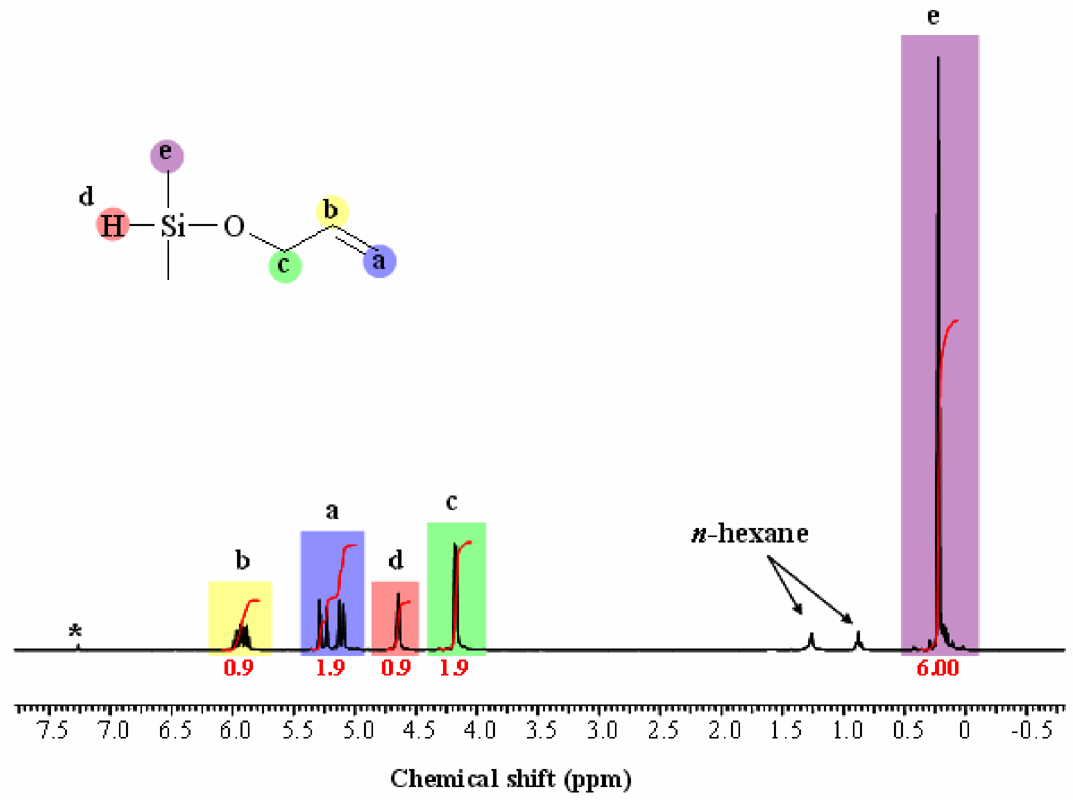

Figure 3.17. ^{1}H NMR spectrum of DMAOS in $CDCl_3$ (solvent peak denoted by an asterisk).

3.4 REFERENCES

[1] (a) Bosman, A. W.; Janssen, H. M.; Meijer, E. W.; *Chem. Rev.* **1999**, *99*, 1665. (b) Newkome, G.; He, E.; Moorefield, C. N. *Chem. Rev.* **1999**, *99*, 1689. (c) Fisher, M.; Vögtle, F. *Angew. Chem. Int. Ed.* **1999**, *38*, 885. (d) Fréchet, J. M. J.; Hawker, C. J.; Gitsov, I.; Leon, J. W. *J. Macromol. Sci., Pure Appl. Chem. A* **1996**, *33*, 1399. (e) Tomalia, D. A.; Durst, H. D. *Top. Curr. Chem.* **1993**, *165*, 193.

[2] (a) Voit, B. *J. Polym. Sci., Polym. Chem.* **2005**, *43*, 2679. (b) Gao, C.; Yan, D. *Prog. Polym. Sci.* **2004**, *29*, 183. (c) Jikei, M.; Kakimoto, M. *Prog. Polym. Sci.* **2001**, *26*, 1233. (d) Sunder, A.; Heinemann, J.; Frey, H. *Chem. Eur. J.* **2000**, *6*, 2499. (e) Kim, Y. H. *Polym. Mater. Sci. Eng.* **1999**, *80*, 61. (f) Feast, W. J.; Cacialli, F.; Daik, R.; Friend, R. H.; Herzog, E.; Heywood, B. R.; Hobson, L.; Megson, J. L.; Snowden, D. *Macromol. Symp.* **1999**, *143*, 81. (g) Hult, A.; Johansson, M.; Malmström, E. *Adv. Polym. Sci.* **1999**, *143*, 1. (h) Turner, S. R. *Polym. Mater. Sci. Eng.* **1995**, *73*, 77.

[3] (a) Kleij, A. W.; Gossage, R. A.; Jastrzebski, J. T. B. H.; Boersama, J.; van Koten, G. *Angew. Chem. Int. Ed.* **2000**, *39*, 176. (b) Percec, V.; Ahn, C.-H.; Ungar, G., Yeardley, D. J. P.; Möller, M.; Sheiko, S. S. *Nature* **1998**, *391*, 161. (c) Jansen, J. F. G. A.; de Brabander van der Berg, E. M. M.; Meijer, E. W. *Science* **1994**, *266*, 1226. (d) Fréchet, J. M. J. *Science* **1994**, *263*, 1710.

[4] Kim, Y. H.; Webster, O. W. *Macromolecules* **1996**, *29*, 8583.

[5] (a) Lang, H.; Lühmann, B. *Adv. Mater.* **2001**, *13*, 1523. (b) Frey, H.; Schlenk, C. *Topics in Current Chemistry* **2000**, 210, 69. (c) Majoral, J.-P.; Carminade, A.-M. *Chem. Rev.* **1999**, *99*, 845. (d) Frey, H.; Schlenk, H. *Monatshefte für Chemie* **1999**, *130*, 3. (e) Uchida, H.; Kabe, Y.; Yoshino, K.; Kawamata, A.; Tsumuraya, T.; Masamune, S. *J. Am. Chem. Soc.* **1990**, *112*, 7077.

[6] (a) Xiao, Y.; Wong, R. A.; Son, D. Y. *Macromolecules* **2000**, *33*, 7232. (b) Schlenk, C.; Kleij, A. W.; Frey, H.; van Koten, G. *Angew. Chem. Int. Ed.* **2000**, *39*, 3445. (c) Lach, C.; Frey, H. *Macromolecules* **1998**, *31*, 2381. (d) Whitmarsh, C. K.; Interrante, L. V. *Organometallics* **1991**, *10*, 1336.

[7] (a) Muzafarov, A. M.; Rebrov, E. A.; Gorbacevich, O. B.; Golly, M.; Gankema, H.; Möller, M. *Macromol. Symp.* **1996**, *102*, 35. (b) Muzafarov, A. M.; Golly, M.; Möller, M. *Macromolecules* **1995**, *28*, 8444.

[8] (a) Oishi, M.; Minakawa, M.; Imae, I.; Kawakami, Y. *Macromolecules* **2002**, *35*, 4938. (b) Miravet, J. F.; Fréchet, J. M. J. *Macromolecules* **1998**, *31*, 3461. (c) Rubinsztajn, S.; Stein, J. *J. Inorg. Organomet. Polym.* **1995**, *5*, 43. (d) Rubinsztajn, S. *J. Inorg. Organomet. Polym.* **1994**, *4*, 61. (e) Mathias, L. J.; Carothers, T. W. *J. Am. Chem. Soc.* **1991**, *113*, 4043.

[9] (a) Paulasaari, J. K.; Weber, W. P. *Macromolecules* **2000,** *33*, 2005. (b) Paulasaari, J. K.; Weber, W. P. *Macromol. Chem. Phys.* **2000**, *201*, 1585.

[10] (a) Zuckerman, J. *J. Adv. Inorg. Chem. Radiochem.* **1964**, *6*, 383. (b) Voorhoeve, R. J. H. *Organosilanes, Precursors to Silicones*; Elsevier: Amsterdam 1967.

[11] (a) Rochow, E. G. *J. Am. Chem. Soc.* **1945**, *67*, 693. (b) Rochow, E. G. U.S. Patent No. 2,380,995 (to General Electric), 1941.

[12] Müller, R. German Patent No. C57411, 1942.

[13] Rappoport, Z.; Apeloig, Y. *The Chemistry of Organic Silicon Compounds*; Wiley: Chichester, U. K., 1998, Vol.2, Chap. 26, p. 1581.

[14] Kipping, F. S. *Proc. Chem. Soc.* **1904**, *20*, 15.

[15] Brook, M. A. *Silicon in Organic, Organometallic and Polymer Chemistry*; Wiley: Canada, 2000.

[16] (a) Kocienski, P. J. *Protecting Groups*; Theime: Stuttgart, 1994. (b) Greene, T. W. *Protective Groups in Organic Synthesis*; Wiley: New York, 1981.

[17] (a) Stork, G.; Hudrlik, P. F. *J. Am. Chem. Soc.* **1968**, *90*, 4462. (b) Corey, E. J.; Venkateswarlu, A. *J. Am. Chem. Soc.* **1972**, *94*, 6190.

[18] Drohmann, C.; Möller, M.; Gorbatsevich, O. B.; Muzafarov, A. M. *J. Polym. Sci., Part A: Polym. Chem.* **2000**, *38*, 741.

[19] Diaper, D. G. M. *Can. J. Chem.* **1961**, *39*, 1723.

[20] Curry, J. W.; Harrison, G. W. *J. Org. Chem.* **1958**, *23*, 1219.

[21] Zhun, V. I.; Tsvetkov, A. L.; Sheludyakov, V. D.; Lavygin, I. A.; Leitan, O. V.; Chalbysheva, N. V.; Bochkarev, V. N.; Slyusarenko, T. F. *Zhurnal Obshchei Khimii* **1988**, *58*, 1599.

[22] (a) Mironov *et al. J. Gen. Chem.* **1969**, *39*, 937. (b) Mironov *et al. J. Gen. Chem.* **1971**, *41*, 2497.

[23] Auer, D.; Kaupp, M.; Strohmann, C. *Organometallics* **2004**, *23*, 3647.

CHAPTER 4

MECHANISTIC APPROACH: THE HYDROSILYLATION REACTION

4.1 INTRODUCTION

Macromolecular substitution is a synthetic approach that involves the functionalization of a preformed polymer backbone containing reactive groups with an appropriate reagent (Figure 4.1).[1] As polymer properties are often heavily influenced by the identity of their pendant groups, it is plausible to achieve different families of novel polymers from the same polymer backbone by simply modifying the side chains.[2] By using this methodology, a variety of different materials with desirable physical properties and functional groups, which are otherwise inaccessible, can be synthesized from only one antecedent. However, the challenge resides on the preparation of modified monodisperse polymers with controlled architectures. This may be achieved by utilizing parent polymers prepared by living polymerization methods.

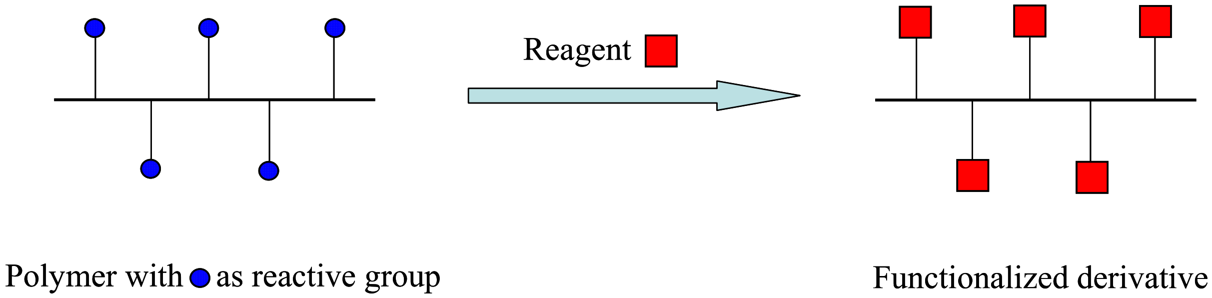

Figure 4.1. Macromolecular substitution of a reactive polymer backbone.

Unsaturated polymers, especially diene polymers, are ideal polymers for chemical modification because of the reactivity of the double bonds along the polymer chain.[3] Catalytic hydrosilylation of unsaturated polymers is the second most important silicon-carbon bond forming reaction after the Rochow process[4] and is of paramount importance for the silicon industry.[5] Hydrosilylation describes the addition reaction of Si-H, which is relatively weak (378 kJ/mol in Me_3SiH), across a π-bond (Figure 4.2). Normally, the bond is a C=C or C≡C bond, although the reduction of carbonyl groups by hydrosilanes is also known. In the literature, the incorporation of various silicon segments into homo- and block copolymers via the hydrosilylation reaction has been reported.[6] In this study, we describe analogous hydrosilylation reactions on the pendant double bonds of PBD in PS-*b*-PBD diblock copolymers in order to introduce silicon-containing monomers. Although hydrosilylation reactions were formerly performed under free-radical conditions[7] (*i.e.* with ultraviolet light or organic peroxides as initiators), metal-assisted hydrosilylation is presently more popular and has been found to be more efficient.[8] Therefore, an overview on metal-catalyzed hydrosilylation, proposed mechanisms and possible side reactions is presented, emphasizing the type of hydrosilylation used for the synthesis of the branched polymers in this thesis. The mechanistic discussion is of crucial importance for the subsequent understanding of the side-products formed.

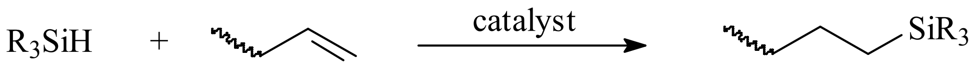

Figure 4.2. The hydrosilylation reaction.

4.2 METAL-ASSISTED HYDROSILYLATION MECHANISMS

Hydrosilylation of an unsaturated bond with a transition metal catalyst has in the last years attracted considerable attention.[9] Two possibilities exist for the addition of a silane R_3SiH to a substituted alkene: namely, Markovnikov or anti-Markovnikov addition mechanism, which results in the formation of branched (α-adduct) and/or linear (β-adduct) products, respectively (Figure 4.3). It has been shown that the amount of each depends on the catalyst and the nature of the substituents on both the alkene and the silane, but generally the β-adduct tends to predominate.[8,10]

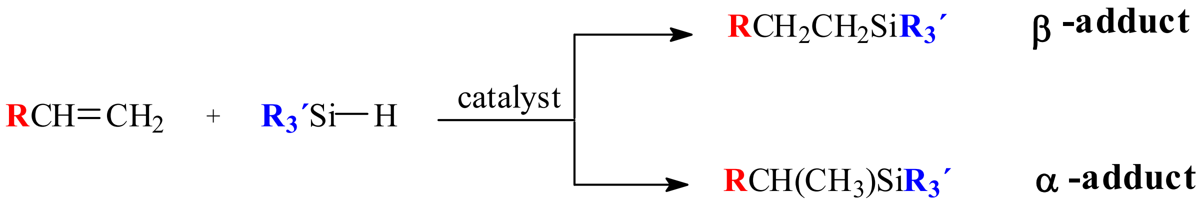

Figure 4.3. Possible adducts in the hydrosilylation reaction.

All nine group VIII transition metals display some catalytic activity in hydrosilylation reactions, with platinum being the most active and therefore the most widely used.[8] Platinum complexes, such as the Speier catalyst (H_2PtCl_6-^{i}PrOH)[11] or the Karstedt catalyst[12] are most commonly employed. Although the reaction requires only ppm quantities of the platinum-containing species, it is plagued by numerous undesired side-reactions, such as isomerization of the terminal alkene, hydrogenation of the C=C double bond and coloration of the reaction medium due to the formation of platinum colloids. This has encouraged researches to search for modified platinum complexes in order to minimize the formation of these unwanted by-products. Markó *et al.* have recently described a new class of *N*-heterocyclic carbine platinum(0) complexes, which efficiently catalyze the hydrosilylation of alkenes, producing low amounts of isomerized olefins and no detectable formation of colloids.[13]

The relative rate of addition to olefins for Pt-catalyzed reactions follows the trend: R_3SiH > R_2SiH_2> $RSiH_3$. Dialkylsilanes (R_2SiH_2) and monoalkylsilanes ($RSiH_3$) can “poison” platinum catalysis by forming chelates, which are more difficult to remove than monohydrides. This results in the observed slower reactions rates for di- and tri-hydrides.[14]

4.2.1 Chalk-Harrod mechanism

The most commonly accepted mechanism for platinum-catalyzed hydrosilylation has been postulated by Chalk and Harrod and was initially postulated for the Speier catalyst (H_2PtCl_6-^{i}PrOH).[15] The classical[15] and modified[16] Chalk-Harrod mechanisms are illustrated in Figure 4.4. The classical mechanism follows the route depicted with blue arrows, while the modified mechanism follows the red route. The first step involves the oxidative addition of the silane monomer to the platinum-alkene complex **I** and subsequent formation of the platinum-alkene silyl hydride complex **II**. These steps are common to both mechanisms. This is followed by alkene insertion into either the [Pt]-hydride (classical Chalk-Harrod) or [Pt]-silyl bond (modified Chalk-Harrod) of complex **II** to give the resulting complexes **III** and **IV** respectively. Finally the complexes **III** and **IV** undergo Si-C or C-H reductive elimination, respectively to form **V** and in this way complete the catalytic cycle. It is not easy to determine through which mechanism the hydrosilylation occurs. If the Si-C reductive elimination requires higher activation energy than the alkene insertion into the [Pt]-Si bond, then the modified Chalk-Harrod mechanism is more favorable than the classical one. This is difficult to determine experimentally and therefore theoretical studies have been carried out: *i.e.* the platinum(0)-catalyzed hydrosilylation of ethylene was proposed to occur via the Chalk-

Harrod mechanism since the ethylene insertion into the Pt-SiR_3 bond seemed to need a much higher activation barrier.[17] Other variants of the Chalk-Harrod mechanism have been proposed for hydrosilylation when using other metal complexes (cobalt, iridium and iron).[18]

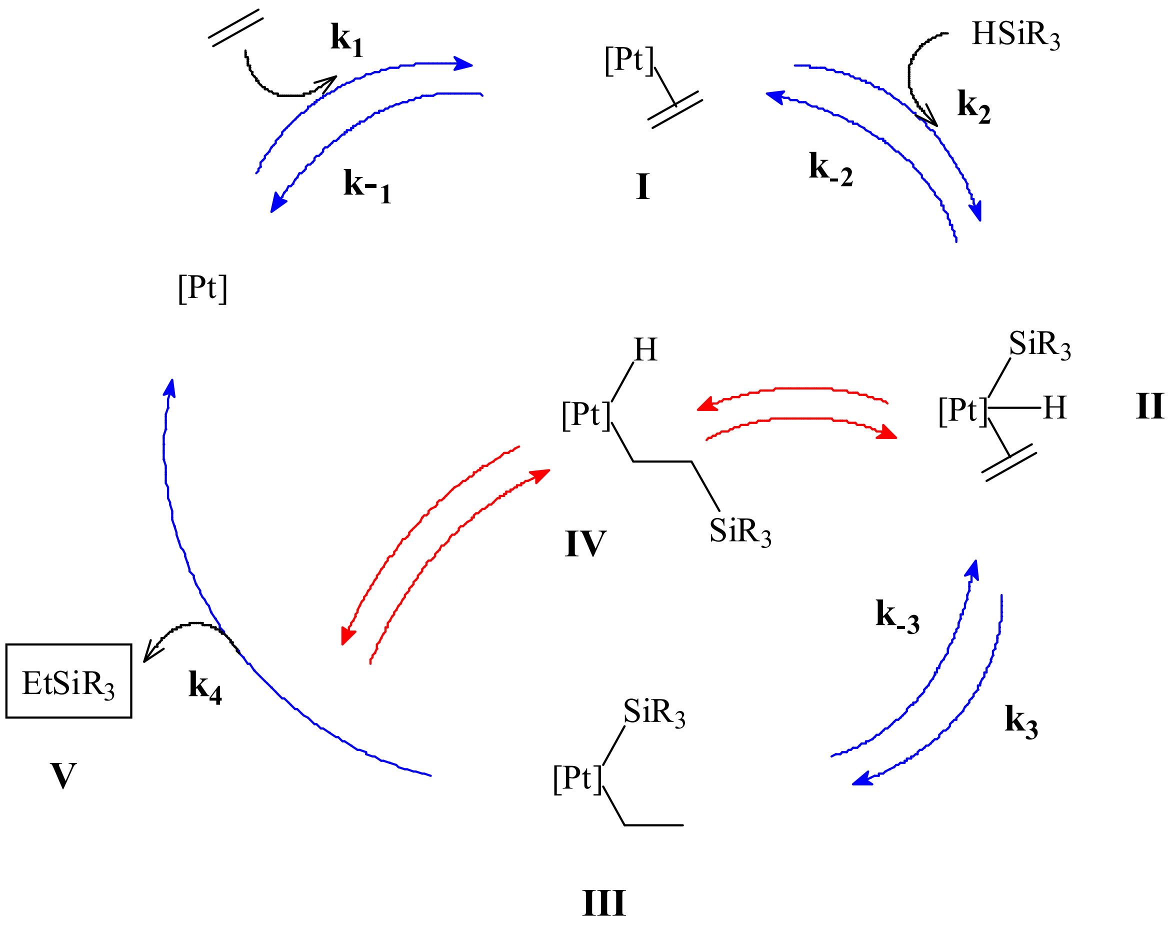

Figure 4.4. Classical (blue cycle) and modified Chalk-Harrod (red cycle) mechanisms for the hydrosilylation of olefins.

The Chalk-Harrod mechanism is generally accepted although the intermediate platinum complexes **I** and **II** depicted in Figure 4.4 have not been observed with highly active catalysts, like Pt(0) species. Moreover some experimental observations (such as the formation of an initial yellow color which turns brown with time, the existence of an induction period of variable length and the requirement for oxygen in certain hydrosilylation reactions), that accompany platinum-catalyzed hydrosilylation reactions are not readily accountable by the Chalk-Harrod mechanism.

4.2.2 Lewis mechanism based on colloidal platinum species

In the middle of the 1980s, Lewis and co-workers proposed an alternative mechanism for hydrosilylation based on the formation of colloidal platinum when using Pt(0) species and accounted for the above mentioned observations.[19] Platinum bis(divinyltetramethyldisiloxane), commonly referred to as the Karstedt catalyst,[12] is a Pt(0)-tetraolefin complex that is typically employed by industry. Its structure, analogous to that of Pt(COD)$_2$,[20] was determined crystallographically by the Lappert group and is depicted in Figure 4.5.[21] However, Lewis concluded that this mechanism was applicable also for the Speier catalyst, wherein the induction period was related to the reduction process. Nonetheless, it is likely that the Chalk-Harrod mechanism is operative for authentic homogeneous hydrosilylation catalysts such as (Ph$_3$P)$_4$Pt.

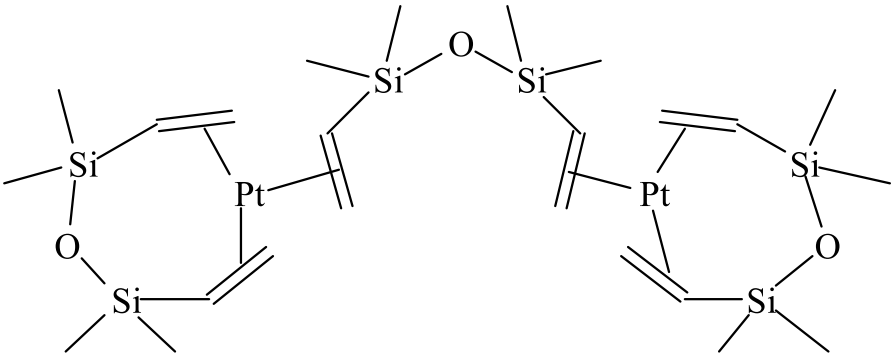

Figure 4.5. Structure of the Karstedt catalyst.

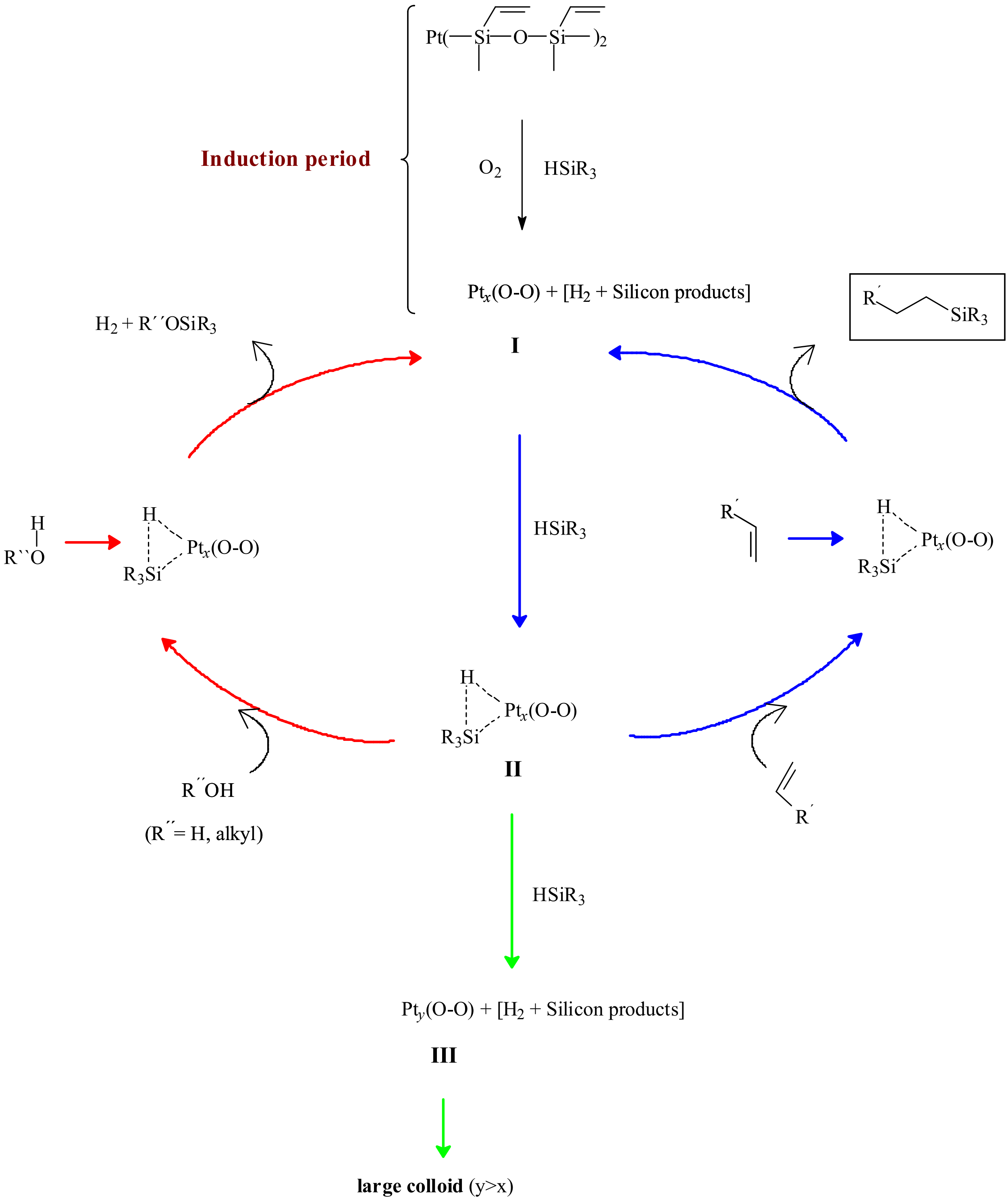

Figure 4.6. Lewis hydrosilylation mechanism based on Pt-colloids as the active species.

Direct evidence for colloid formation was presented and the colloids were proposed as the active catalytic intermediate species in the reaction. In addition, the colloids showed higher activity than the compounds from which they were derived. The main difference between both mechanisms, beyond the induction period, is that in the Lewis mechanism, the reaction of the silane with platinum occurs first and is subsequently followed by the attack of the olefin as depicted in Figure 4.6. During the induction period, the Karstedt catalyst reacts with the silane to give H_2, silicon products and the platinum colloid active species (complex **I**). The colloid formation has been identified as being responsible for the yellow color of the reaction medium. Moreover, the bonding of dioxygen as a co-catalyst (oxygen is not consumed in the reaction) further stabilizes the colloidal species. The catalytic cycle, denoted by the blue arrows in Figure 4.6, involves oxidative addition of the silane to the platinum-colloid (complex **II**) and is followed by nucleophilic attack by the olefin, generating the hydrosilylation product and regenerating the platinum-colloid active catalyst **I**. Possible competitive side reactions are illustrated as well in Figure 4.6 by using red and green arrows. The nucleophilic attack by trace amounts of water or alcohols on the platinum-silane intermediate complex **II** (red route) is a side reaction that can also regenerate the active complex **I** by producing H_2 and alkoxysilanes. Hydrogen can also be produced by the attack of another silane molecule to form complex **III** (green route). This side reaction deactivates the hydrosilylation catalyst and generates products containing Si-Si bonds.

Although some evidence was found for the precoordination of the olefin to the colloid prior to the reaction at the silicon center, an important aspect of the “metal colloid” mechanism is that it readily explains the experimental data regarding the effects of the silane substituents on the efficiency of the hydrosilylation reaction. It has been found that electron withdrawing substituents on the silane and electron donating groups on the olefin accelerate the rate of addition.[19] These facts can be understood if the intermediate complex **II** and the olefin are considered as an electrophile and a nucleophile respectively (*i.e.* the rate of addition of $(EtO)_3SiH$ to olefins proceeds at a higher rate than the addition of Et_3SiH while, the addition of Et_3SiH to $Me_3SiCH=CH_2$ occurs at a faster rate than to $Cl_3SiCH=CH_2$).

The role of oxygen is thus to make **II** more electrophilic and therefore more susceptible to nucleophilic attack by the olefin. In addition the oxygen may prevent irreversible colloid agglomeration. Further support for the “metal colloid” mechanism and the proposed electrophilic intermediate **II** came from the study of the rearrangement of allyltrimethylsilane in the presence of platinum catalyst and triethylsilane (Figure 4.7).[19] In addition to the predicted hydrosilylation product two other minor products were also identified. The formation of these side products can be rationalized on the basis of the formation of complex **II** and subsequent rearrangements to form $Et_3SiCH_2CH_2{=}CH_2$ and Me_3SiH. The observed minor products come from SiH additions of Me_3SiH to the starting material $Me_3SiCH_2CH_2{=}CH_2$ and $Et_3SiCH_2CH_2{=}CH_2$ plus the starting Et_3SiH.

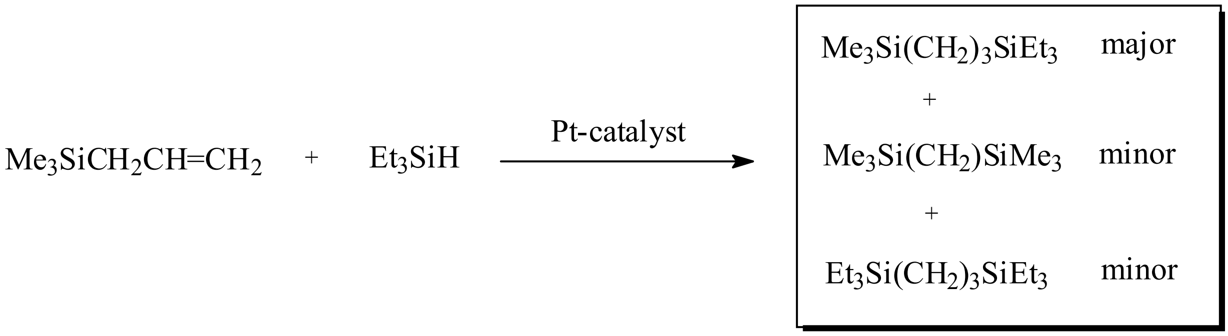

Figure 4.7. Hydrosilylation reaction accompanied with the formation of rearrangement products.

4.2.3 Lewis mechanism based on monomeric platinum

The proposal that colloids act as intermediates in the hydrosilylation reaction was based mainly on microscopy studies of evaporated solutions from reactions after completion.[22] In 1999 Lewis *et al.* proposed another reaction mechanism based on a series of experiments to determine the active catalytic species generated in situ during hydrosilylation using the Karstedt catalyst.[23] Their conclusions were established using SAXS measurements with neutrons of frozen, catalytically active mixtures. Contrary to their previous reports suggesting the formation of a colloidal based catalyst, they found that monomeric platinum compounds were in fact the most active catalytic species, whereas multinuclear platinum species were merely end products. In other words, analyses of samples that were catalytically active did not contain Pt-Pt bonds. They suggested that, during the induction period, the Karstedt catalyst undergoes a series of ligand exchange (dissociation of the bridging olefin) and hydrosilylation processes, to give rise to the active catalytic species: the mononuclear two-coordinate platinum complex **I** (Figure 4.8). Moreover a shorter induction period was observed with Pt(0) catalysts compared with other higher oxidation state platinum catalysts, because they do not need to undergo reduction prior to ligand exchange or hydrosilylation.

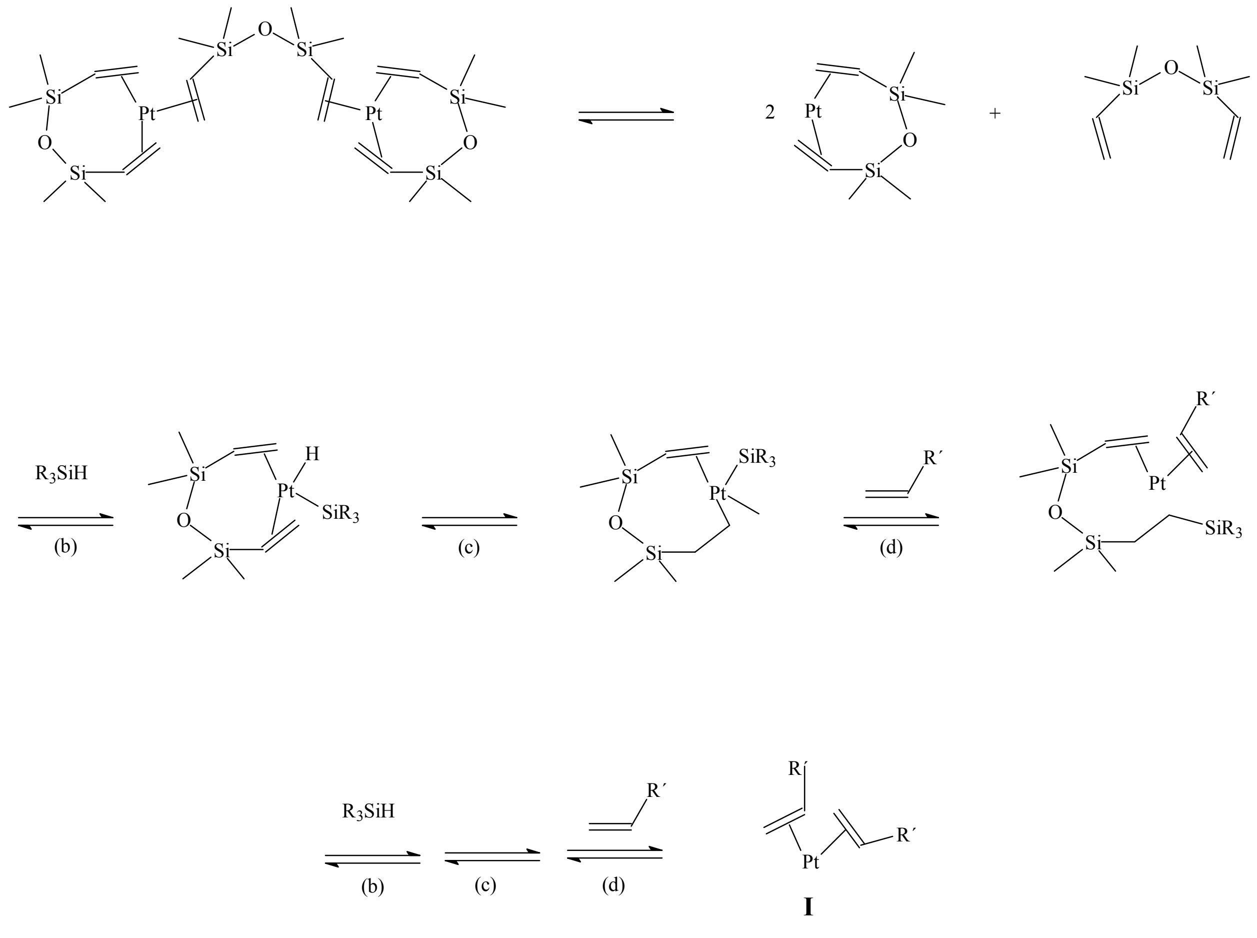

Figure 4.8. Induction period for the hydrosilylation reaction using the Karstedt catalyst.

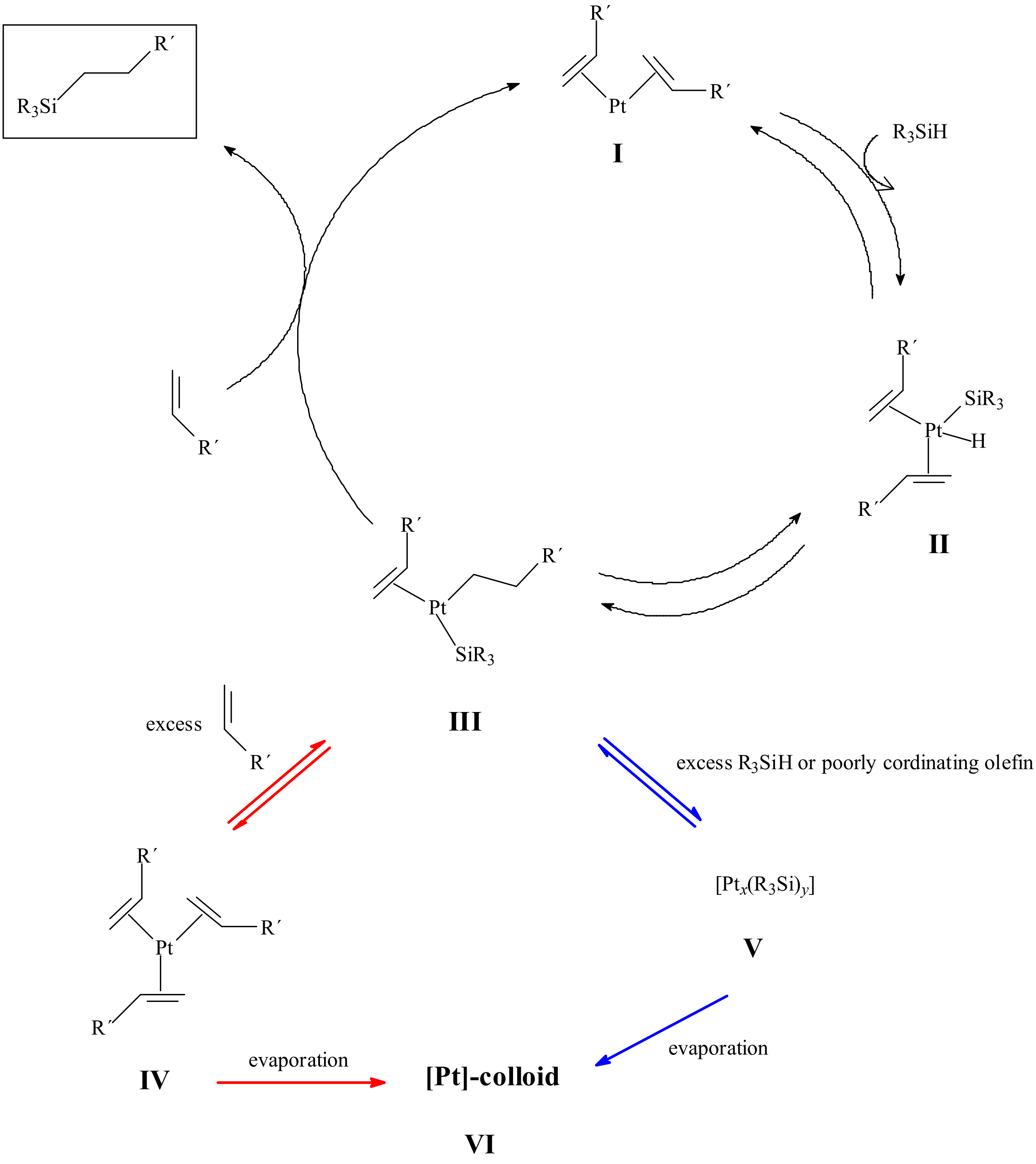

Figure 4.9. Lewis hydrosilylation mechanism based on monomeric platinum as the active species.

In fact the overall catalytic cycle as developed by Lewis *et al.* incorporates aspects of both the Chalk-Harrod and the "metal colloid" mechanism and is summarized in Figure 4.9. The mechanism begins with the oxidative addition of the silane to the mononuclear, two-coordinate platinum complex to give a Pt(II) complex (**II**) and is followed by the migratory insertion of the olefin into the Pt-H bond. The platinum alkyl silyl complex thus formed then (complex **III**) undergoes reductive elimination to give the Si-C bond product and this step is most likely to be the rate-determining step. Colloids were observed experimentally as end products but not during catalysis. The platinum end products were shown to be dependent on the stoichiometry of the reagents: at excess olefin concentrations, the platinum end product contains only Pt-C bonds (complex **IV**) while at high hydrosilane concentrations, the platinum end product is multinuclear and also contains Pt-Si bonds (complex **V**). Both end products can however interconvert by the addition of the reagent which is deficient. The evaporation of solutions with high hydrosilane-to-olefin ratios and with high olefin concentrations showed the presence of colloidal species (**VI**). An explanation of the "oxygen" effect was verified by reacting 1-hexene with hexylsilane in the presence of the Karstedt catalyst under both aerobic and anaerobic conditions (Figure 4.10).[23] In the absence of air, no reaction was observed after 30 minutes. However, the reaction occurred after 30 minutes in the presence of air. This indicated that, with poorly coordinating olefinic substrates, oxygen was necessary for hydrosilylation to occur. While Pt-Pt and Pt-Si species were observed after the reaction performed under the exclusion of air, only Pt-Si monomeric species were identified after the reaction performed in air. These results suggested that the role of oxygen is to prevent the formation of the inactive multinuclear platinum species.

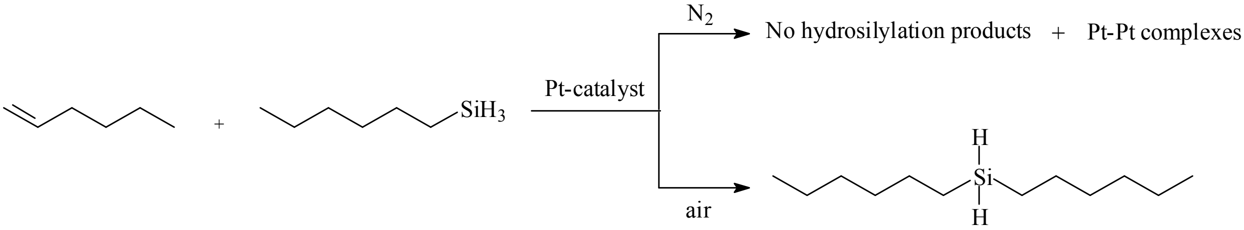

Figure 4.10. Hydrosilylation reaction under aerobic and anaerobic conditions.

In further experiments, electronic and steric effects were evaluated using different reactants in the hydrosilylation reactions. As reported previously,[14,19,24] electron-donating groups on the olefin and electron-withdrawing groups on the hydrosilane were found to increase the hydrosilylation rate. In addition, it was found that strongly coordinating olefins decreased the rate of conversion. Concomitantly, steric effects were shown to be extremely important in the hydrosilylation reaction. For a series of silicon hydride compounds, the order of reactivity was found to be contrary to expected, based on the electrophilicity of the silicon compound, as presented in Figure 4.11.[23,24] The kinetics of the hydrosilylation were also investigated and it was found that a stoichiometric excess of hydrosilane increased the rate of addition. This led to the conclusion that there is a positive dependence of the rate on hydrosilane concentration and an inverse dependence on olefin concentration.[23]

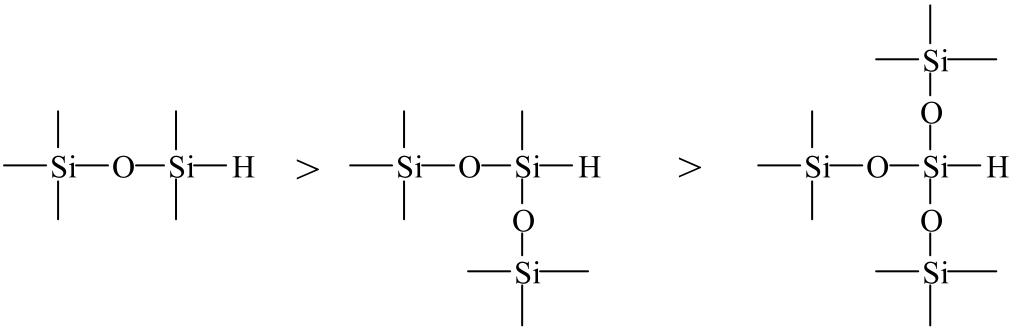

Figure 4.11. Order of reactivity of silicon hydride compounds in a hydrosilylation reaction.

4.3 COMPETING SIDE REACTIONS DURING HYDROSILYLATION AND THEIR MECHANISMS

The hydrosilylation reaction works best for activated silanes containing electron withdrawing groups such as halogens or alkoxys and electron-rich alkenes. With less active monoalkyl-, dialkyl-, trialkylsilanes and 1-alkenes, the reaction affords only low yields of products and is accompanied by side reactions and catalyst deactivation.[25]

4.3.1 Alkene rearrangements

Metal-mediated rearrangements of alkenes are well-known and necessitate Pt-H activation processes. A description of the most common mechanistically interesting rearrangements is therefore presented.

4.3.1.1 Alkene isomerization

The migration of the terminal double bonds, generating internal double bonds, is frequently identified as being a problematic side reaction in the hydrosilylation of 1-alkenes with an unsubstituted β-position (such as 1-hexene).[14,15,26] The occurrence of isomerization during hydrosilylation can be explained if two different modes are considered for the addition of the silicon hydride fragments to the double bond (Figure 4.4):[23]

(i) The rates at which the hydride fragment and the silicon fragment attack the olefin are comparable, resulting in a concerted addition of the silane to the olefin. In this case $k_4 > k_{-3}$ and no isomerization is to be expected.

(ii) The rate at which the silicon fragment attacks the olefin is much slower than the rate of hydride attack, and the life-time of the hydride-olefin complex is long enough for a reversible alkyl-olefin equilibrium to lead to isomerization of the olefin. In this case $k_{-3} > k_4$ and isomerization can occur.

Isomerization can be understood if a platinum-hydrogen bond is involved during the process.[26b] Two mechanisms are most commonly proposed: the first, depicted in Figure 4.12, proceeds via alkyl intermediates and the second, depicted in Figure 4.13 involves the formation of η^3-allyls.[27] Each step in the cycle is reversible, so that the substrates and products are in equilibrium, and therefore the thermodynamic ratio of alkenes is formed. The open box symbol in Figures 4.12 and 4.13 represents a two electron vacant site or a potential site in the form of a labile ligand. The lability of the ligands in the Karstedt catalyst allows for the generation of vacant coordination sites for alkene coordination and oxidative addition processes.

In the proposed mechanism presented in Figure 4.12, a [Pt]-H bond and a vacant site are required. However, there is no direct evidence for the source of the hydride ion. The hydride ion could be generated from the oxidative addition of the silane monomer to the platinum complex or from the hydrogen generated during the induction period according to the Lewis “colloid” mechanism as depicted in Figure 4.6. The alkene coordinates to the platinum and undergoes insertion to give a primary or secondary alkyl. β-elimination of the primary alkyl can only give back the former 1-olefin, while β-elimination of the secondary alkyl gives the 2-olefin. The initial *cis*:*trans* ratio of the 2-olefins formed depends on the catalyst, but the *cis* isomer is sometimes favored. However the final ratio depends only on the thermodynamics, and the *trans* isomer is preferred.

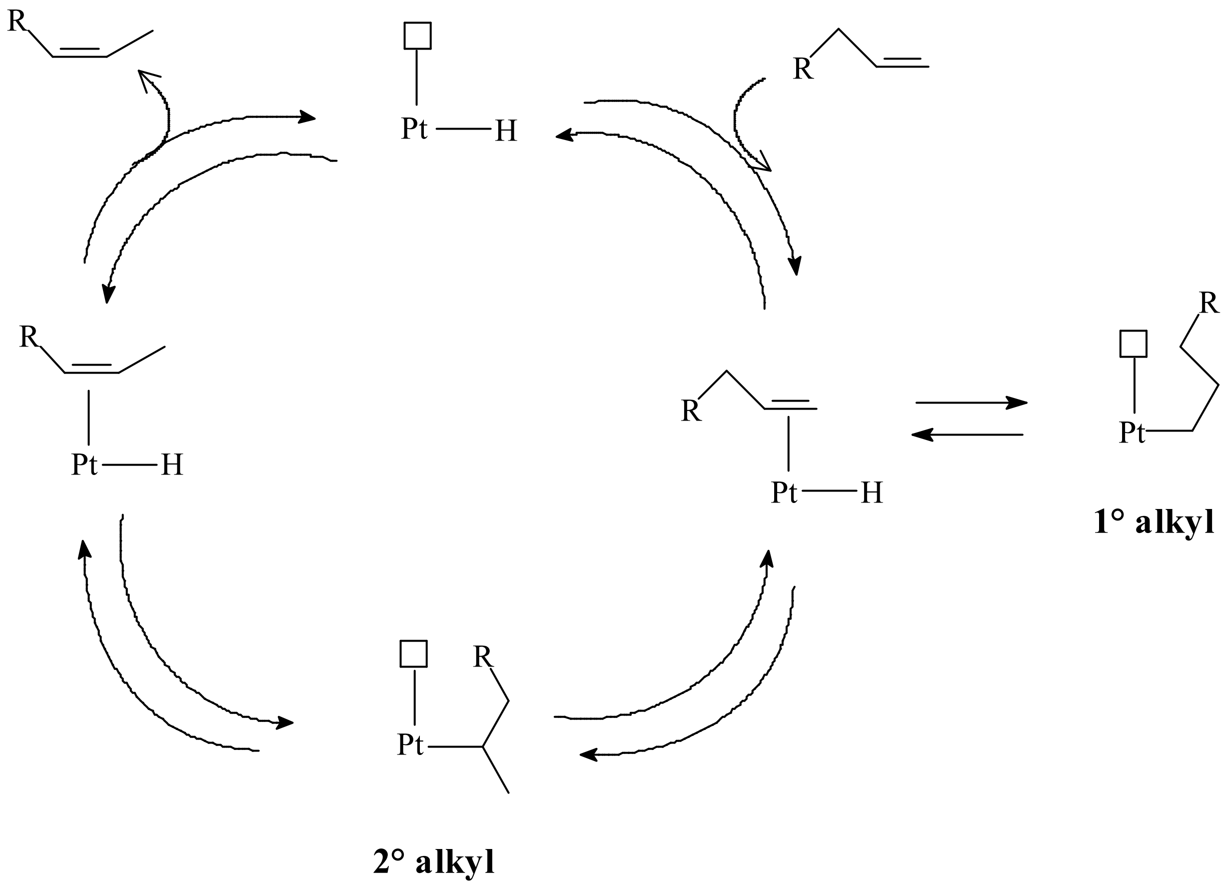

Figure 4.12. Hydride mechanism of alkene isomerization.

In the second possibility (Figure 4.13), the platinum complex with a two vacant site forms an olefin-complex. This is followed by abstraction of the allylic hydrogen to form a η^3-allyl platinum hydride complex, in which rearrangement of the double bond can take place. Reductive elimination gives the 1-olefin if the proton returns to the same site it left, while the isomerized 2-olefin is formed if the proton goes to the opposite end of the allyl group. The difference between the two routes is that the alkyl mechanism involves a 1,2 hydrogen shift, while the allyl mechanism a 1,3 shift.

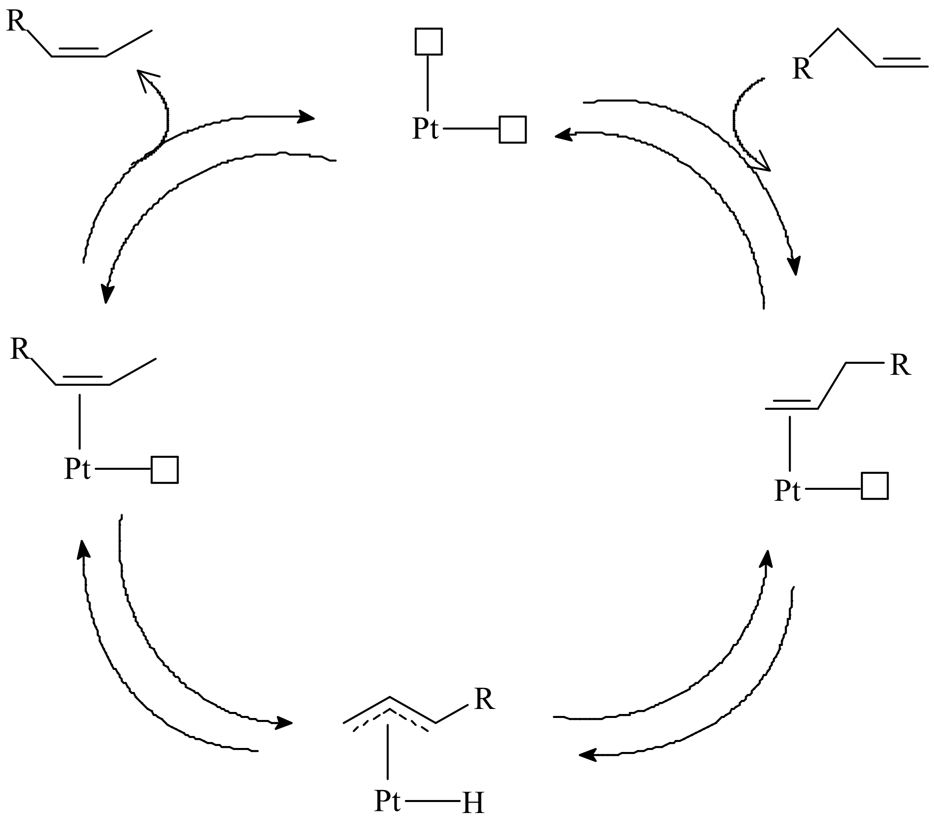

Figure 4.13. Allyl mechanism of alkene isomerization.

This type of olefin rearrangement often occurs when less active hydrosilanes such as trialkenylsilanes are employed in the hydrosilylation reaction.[23] The use of less active monomers for the hydrosilylation (in the absence of oxygen) might favor the formation of multinuclear platinum species as depicted in Figure 4.9. The internal olefins produced do not typically undergo hydrosilylation. Lewis *et al.* analyzed the reaction mixtures in cases where isomerization occurred and found multinuclear platinum species with Pt-Pt and Pt-Si bonds.[23] These multinuclear platinum species persisted after isomerization and were found not to catalyze the hydrosilylation of internal olefins. In these cases the rate constants "k_3" and "k_4" depicted in the Chalk-Harrod mechanism in Figure 4.4 are not very large compared to the rate of deactivation of the catalyst. This results in lower conversion and simultaneous olefin bond isomerization. This type of situation has been observed previously from the reaction of 1-hexene with triethyl-,tribenzyl-, and triphenylsilane, where the poor yield of addition products was due to the thermal deactivation of the catalyst.[15b,25]

4.3.1.2 Alkene hydrogenation

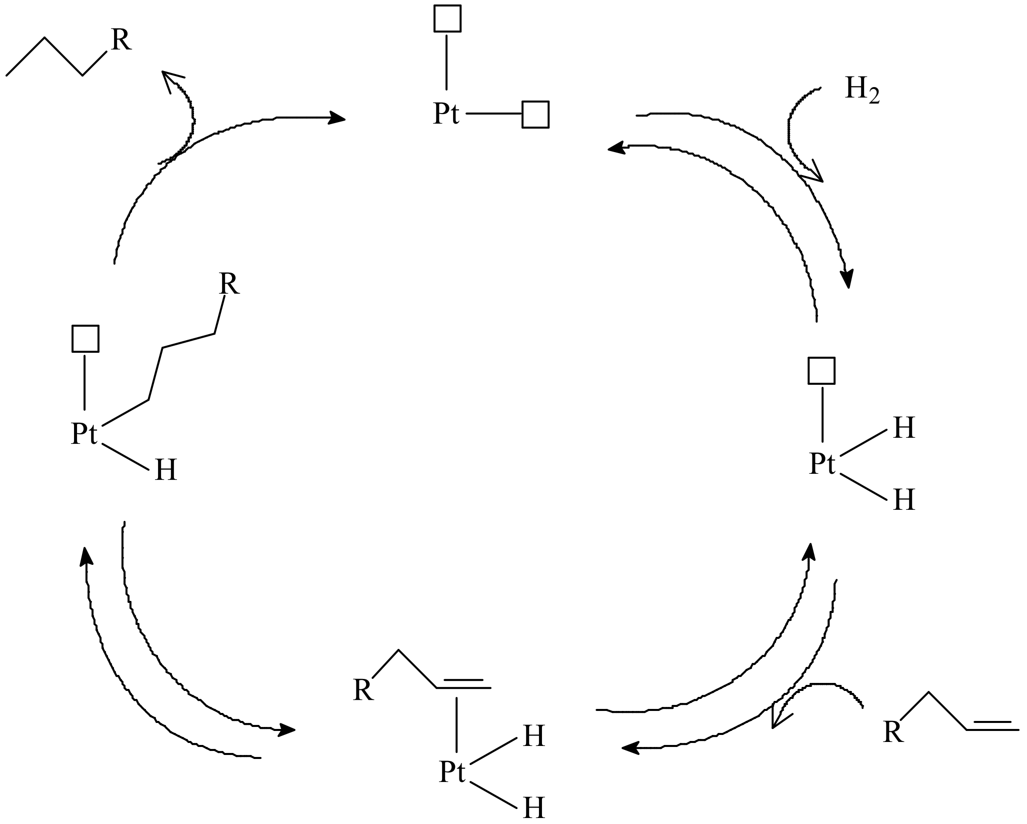

Figure 4.14. Hydrogenation of alkenes by a Pt catalyst. Open box represents a two electron site or a labile ligand.

Other side reactions, besides double bond isomerization, can take place during the hydrosilylation process. For example, it has been reported that the addition of *n*-hexylsilane to 1-octene in the presence of platinum catalysts, gave *n*-octane as a minor side product.[25] Hydrogenated vinyl groups may result from the reduction of the double bonds in the presence of the platinum catalyst. According to the "colloid" mechanism,[19] hydrogen is evolved during the induction period and additionally during the course of other side reactions as depicted in the reaction mechanism in Figure 4.6. As the hydrogen produced during colloid formation can cause bulk metal precipitation, it is feasible that the vinyl double bonds act as hydrogen acceptors thereby minimizing the deactivation of the catalyst. In fact, in the reaction of $RhCl_3$ with $Me_2(EtO)SiH$ cyclohexene was added as a hydrogen acceptor in order to minimize the formation of bulk rhodium metal and consequently obtain a higher yield of the rhodium colloid.[22a] In this case cyclohexene was quantitatively converted to cyclohexane. In the reaction of trialkylsilanes (R_3SiH) (*i.e.* methyldioctylsilane and triethylsilane) with 1-alkenes catalyzed by chloroplatinic acid, higher yields were reported when the reaction was frequently activated with air or a larger Pt/R_3SiH ratio (*ca.* 10^{-3}mol/mol) was used.[25] Concomitantly, it is evident that the use of a high catalyst concentration will increase the amount of hydrogen evolved.[28]

Mechanistically, hydrogenation can happen by the oxidative addition of hydrogen to generate a metal dihidride (Figure 4.14).[27] The resulting intermediate alkyl, after the coordination of the alkene and insertion into one Pt-H bond, is irreversibly trapped by reductive elimination with the second hydride to give an alkane and regenerate the catalyst.

4.3.1.3 Alkene dimerization

If metal complexes are able to coordinate to more than one alkene, the possibility of alkene coupling arises (Figure 4.15), as is the case for the Karstedt catalyst. Two mechanisms which involve β-M-H elimination as the key step can account for such catalytic alkene dimerizations as shown in Figures 4.16 and 4.17.[29] If another vacant coordination site is available after elimination, further alkene coordination leading to oligomerization or polymerization may occur.

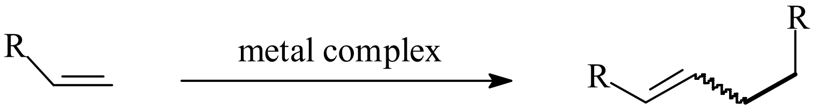

Figure 4.15. Dimerization of alkene in the presence of a metal complex.

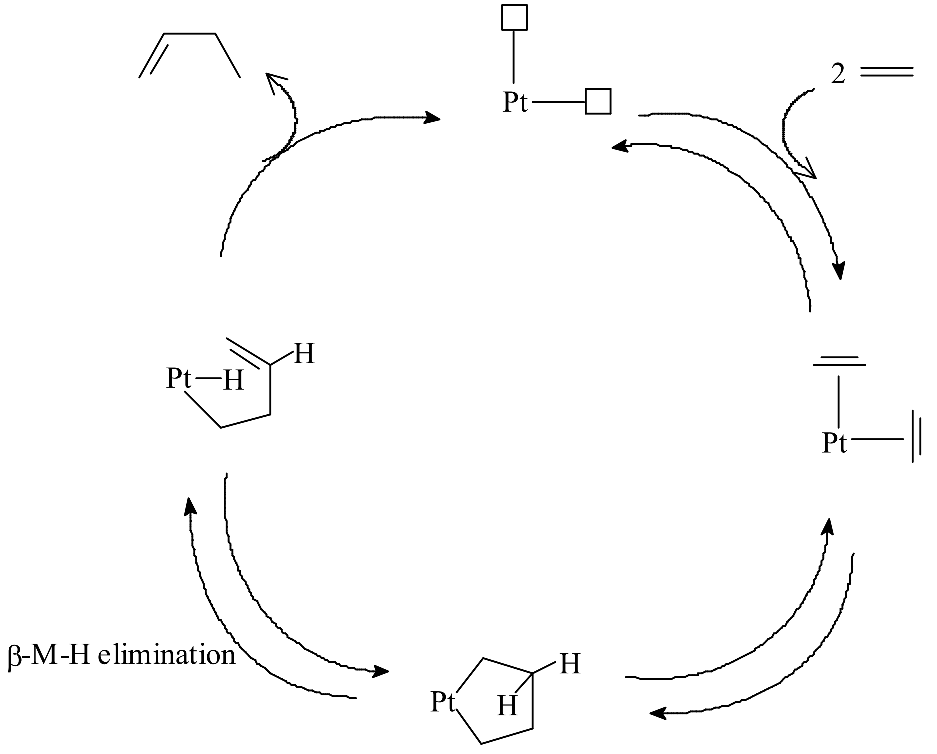

Figure 4.16. Proposed mechanism for catalytic alkene dimerization via coordination of two alkenes.

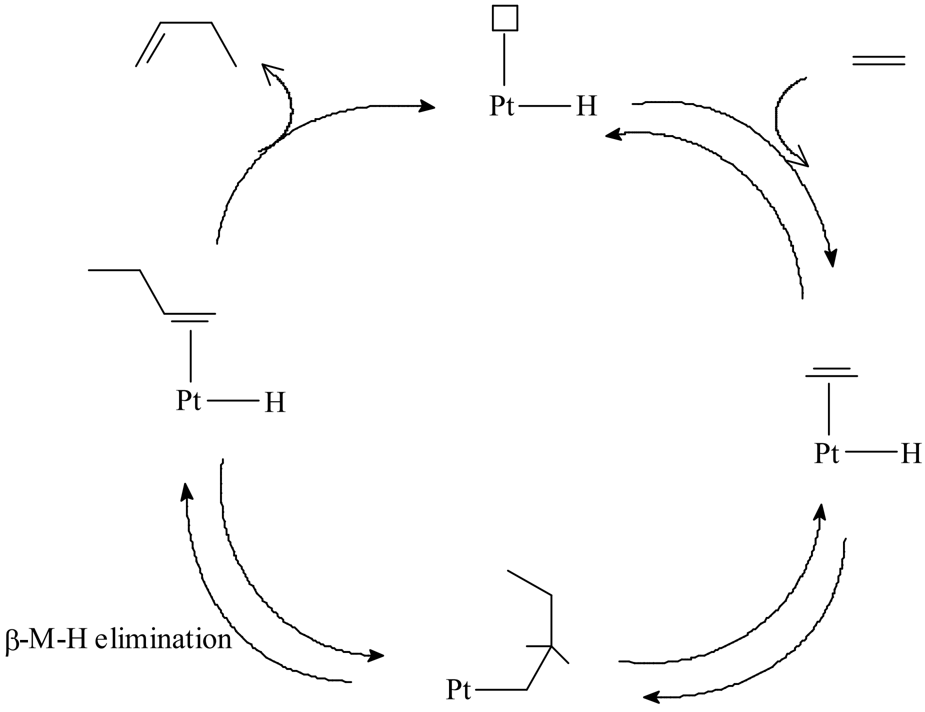

Figure 4.17. Proposed mechanism for catalytic alkene dimerization via a Pt-H complex.

4.3.2 Rearrangements reactions involving silicon

Rearrangements at silicon may be roughly grouped into two categories: ionic and neutral. Within the neutral rearrangements, processes involving radicals and carbenes together with sigmatropic (orbital controlled) and dyotropic (two groups migrate simultaneously) rearragements are the most important ones.[30]

4.3.2.1 Dyotropic rearrangements

There are several examples in the literature of dyotropic rearragements, from the hydrosilylation reaction in the presence of a platinum catalyst:

Stober *et al.* observed that bis(trimethylsiloxy)methylsilane (BTS) exchanged methyl and trimethylsiloxy groups when added to 2-hexene and hexachloroplatinic acid under mild conditions (T<138 °C).[31] This reaction was reproducible and resulted in a mixture of pentamethyldisiloxane (PMDS) and tris(trimethylsiloxy)silane (TTS) (Figure 4.18). They found that the TTS could not be attached to 2-hexene, presumably because of steric hindrance. A similar rearrangement was presumed by Ober *et al.* to be the cause of the lower attachment yield obtained when a molar ratio of BTS:vinyl group of 1:1 was employed in the reaction of BTS with PS-*b*-PBD diblock copolymers in the presence of the Karstedt catalyst.[6d] This was explained because some of the BTS was converted to the non-reactive TTS.

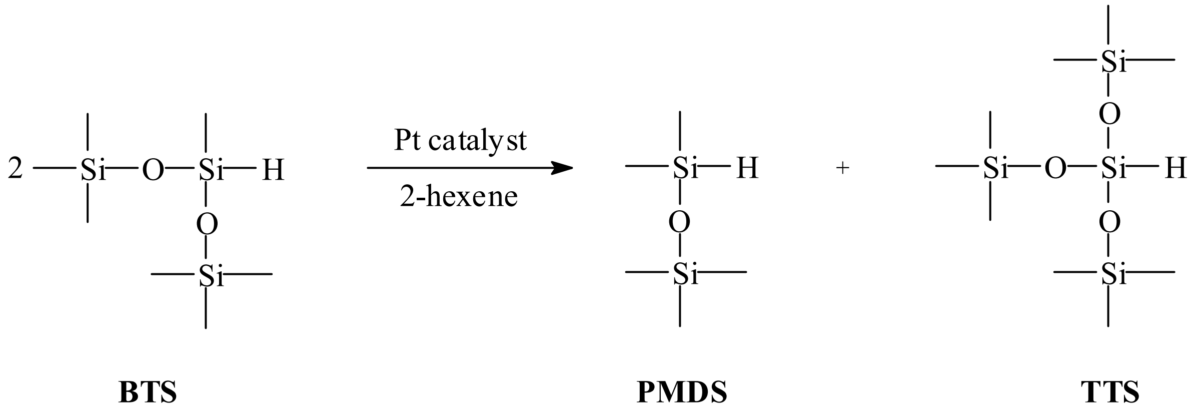

Figure 4.18. Rearragement reaction of BTS when added to 2-hexene in the presence of H_2PtCl_6.

Moreover, Möller *et al.* found that the polyaddition reaction of methylbis(undec-10-enyloxy)silane to a hyperbranched polymer in bulk in the presence of a platinum catalyst lead to gelation.[32] This gelation was explained by the rearrangement reaction depicted in Figure 4.19, which yielded monomers of the type B_3 and A_2B.

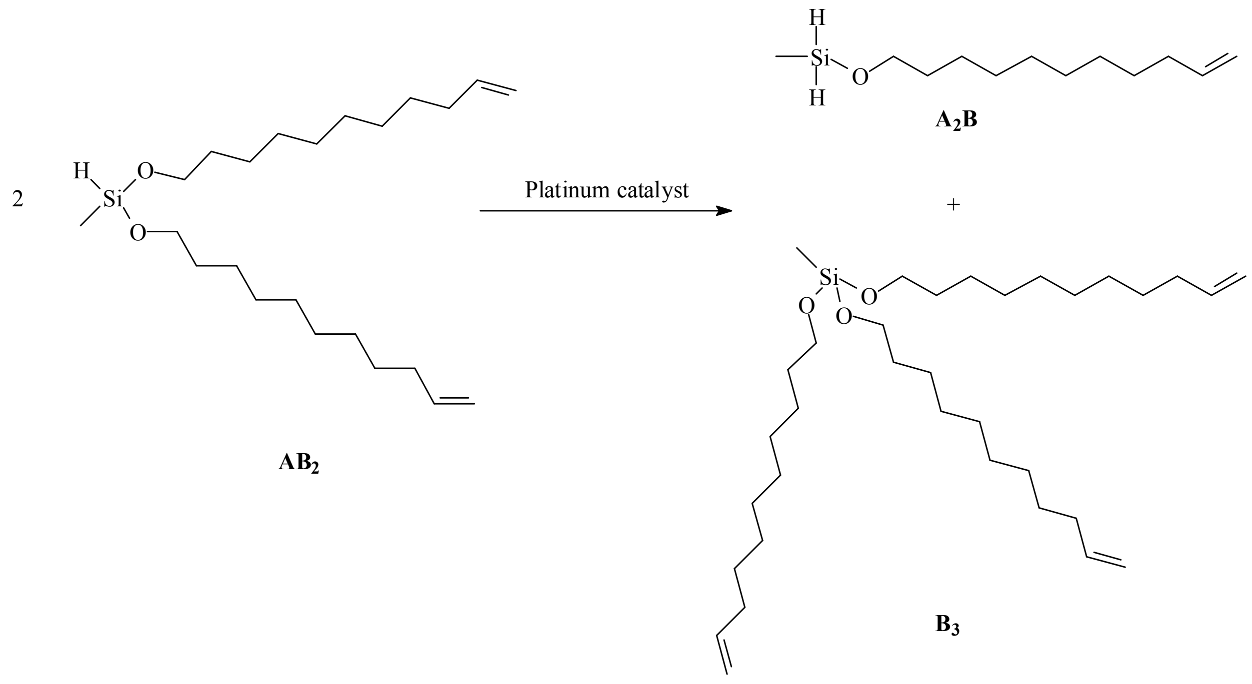

Figure 4.19. Rearragement of methylbis(undec-10-enyloxy)silane in bulk in the presence of a platinum catalyst.

4.4 REFERENCES

[1] (a) Allcock, H. R.; Lampe, F. W. *Contemporary Polymer Chemistry*; Prentice Hall: Englewood Cliffs, NJ, 1981. (b) Mark, J. E.; Allcock, H. R.; West, R. *Inorganic Polymers*; Prentice Hall: Englewood Cliffs, NJ, 1992.

[2] (a) Carraher, C. E.; Tsuda, M. *Modification of Polymers*; American Chemical Society: Washington, DC, 1980; Vol. 121. (b) Carraher, C. E.; Moore, J. A. *Modification of Polymers*; Plenum Press: New York, 1983; Vol. 21.

[3] Schulz, D. N.; Turner, S. R.; Golub, M. A.; *Rubber Chem. Technol.* **1982**, *55*, 809.

[4] Rochow, E. G. *J. Am. Chem. Soc.* **1945**, *67*, 963.

[5] Marciniec, B.; Gulinski, J.; Urbaniac, W.; Kornetka, Z. W. *Comprehensive Handbook on Hydrosilylation*; Pergamon: Oxford, UK, 1992.

[6] (a) Baum, K; Baum, J. C.; Ho, T. *J. Am. Chem. Soc.* **1998**, *10*, 2993. (b) Hadjichristidis, N.; Xenidou, M. *Macromolecules* **1998**, *31*, 5690. (c) Hempenius, M. A.; Michelberger, W.; Möller, M. *Macromolecules* **1997**, *30*, 5602. (d) Gabor, A. H.; Lehner, E. A.; Mao, G.; Schneggenburger, L. A.; Ober, C. K. *Chem. Mater.* **1994**, *6*, 927. (e) Guo, X.; Rempel, G. L. *Macromolecules* **1992**, *25*, 883. (f) Guo, X.; Farwaha, R.; Rempel, G. L. *Macromolecules* **1990**, *23*, 5047. (g) Cameron, G. G., Qureshi, M. Y. *Makromol. Chem., Rapid Commun.* **1981**, *2*, 287.

[7] (a) Kopping, B.; Chatgilialoglu, C.; Zehnder, M.; Giese, B. *J. Org. Chem.* **1992**, *57*, 3994. (b) Chatgilialoglu, C. *Acc. Chem. Res.* **1992**, *25*, 188. (c) Sommer, L. H.; Pietrusza, E. W.; Whitmore, F. C. *J. Am. Chem. Soc.* **1947**, *69*, 188.

[8] Speier, J. L. *Adv. Organomet. Chem* **1979**, *17*, 407.

[9] Ojima, I. *The Chemistry of Organic Silicon Compounds*; Patai, S.; Rappoport, Z.; Wiley: New York, 1989; 1479-1526.

[10] (a) Lestel, L.; Cheradame, H.; Boileau, S. *Polymer* **1990**, *31*, 1154. (b) Lapp, A.; Xiongwei, H.; Herz, J. *Makromol. Chem.* **1988**, *189*, 1061. (c) Brown-Wesley, K. *Organometallics* **1987**, *6*, 1590.

[11] Speier, J. L.; Webster, J. A.; Barnes, G. H. *J. Am. Chem. Soc.* **1956**, *79*, 974.

[12] (a) Ashby, B. A.; Modic, F. J. US Patent 4,288,345, 1981. (b) Karstedt, B. D. (General Electric) US Patent 3,715,334, 1973.

[13] Buisine, O.; Guillaume, B.-G.; Brière, J.-F.; Stérin, S.; Mignani, G.; Branlard, P.; Tinant, B.; Declercq, J.-P.; Markó, I. *Chem. Commun.* **2005**, *30*, 3856.

[14] Uriarte, R. J.; Lewis, L. N. *Organometallics* **1990**, *9*, 621.

[15] (a) Harrod, J. F.; Chalk, A. J. *Organic Synthesis via Metal Carbonyls*; Wender, I.; Pino, P.; John-Wiley: New York, 1977; 673. (b) Harrod, J. F.; Chalk, A. J. *J. Am. Chem. Soc.* **1965**, *87*, 16.

[16] (a) Randolph, C. L., Wrighton, M. S. *J. Am. Chem. Soc.* **1986**, *108*, 3366. (b) Reichel, C. L.; Wrighton, M. S. *Inorg. Chem.* **1980**, *19*, 3858. (c) Schroeder, M. A.; Wrighton, M. S.; *J. Organomet. Chem.* **1977**, *128*, 345.

[17] (a) Sakaki, S.; Mizoe, N.; Musashi, Y.; Sugimoto, M. *THEOCHEM* **1999**, *461-462*, 533. (b)Sakaki, S.; Mizoe, N.; Sugimoto, M. *Organometallics* **1998**, *17*, 2510.

[18] (a) Brunner, H. *Angew. Chem., Int. Ed. Engl.* **2004**, *43*, 2749. (a) Duckett, S.; Perutz, R. H. *Organometallics* **1992**, *11*, 90.

[19] Lewis, L. N. *J. Am. Chem. Soc.* **1990**, *112*, 5998.

[20] Chandra, G.; Lo, P. Y. *Organometallics* **1987**, *6*, 191.

[21] Hitchcock, P. B.; Lappert, M. F.; Warhurst, N. J. W. *Angew. Chem., Int. Ed. Engl.* **1991**, *30*, 438.

[22] (a) Lewis, L. N.; Lewis, N. *Chemistry Mater.* **1989**, *1*, 106. (b) Lewis, L. N.; Lewis, N. *J. Am. Chem. Soc*. **1986**, *108*, 7228.

[23] Stein, J.; Lewis, L. N.; Gao, Y.; Scott, R. A. *J. Am. Chem. Soc.* **1999**, *121*, 3693.

[24] Stein, J.; Lewis, L. N.; Smith, K. A.; Lettko, K. X. *J. Inorg. Organomet. Polym.* **1991**, *1*, 325.

[25] Onopchenko, A.; Sabourin, E. T. *J. Org. Chem.* **1987**, *52*, 4118.

[26] (a) Haszeldine, R. N.; Parish, R. V.; Taylor, R. J. *J. Chem. Soc. A.* **1974**, 2311. (b) Chalk, A. J.; Harrod, J. F. *J. Am. Chem. Soc.* **1964**, *86*, 1776.

[27] Crabtree, R. H. *The Organometallic Chemistry of the Transition Metals*; John Wiley & Sons: New York, 1948.

[28] Britcher, L; Kehoe, D. C; Matisons, J. G.; Swincer, A. G. *Macromolecules* **1995**, *28*, 3110.

[29] Hill, A. F. *Organotransition Metal Chemistry*; Royal Society of Chemistry: Cambridge, UK, 2002.

[30] Brook, M. A. *Silicon in Organic, Organometallic and Polymer Chemistry*; Wiley: Canada, 2000.

[31] Stober, M. R.; Musolf, M. C.; Speier, J. L. *J. Org. Chem.* **1965**, *30*, 1651.

[32] Muzafarov, A. M.; Golly, M.; Möller, M. *Macromolecules* **1995**, *28*, 8444.

CHAPTER 5

SYNTHESIS AND CHARACTERIZATION OF HYPERBRANCHED AND BRUSH-LIKE POLYALKENYLSILANES

5.1 INTRODUCTION

In comparison with linear polymers with similar molecular weights, hyperbranched polymers[1] exhibit unique properties such as low viscosities, due to the lack of chain entanglement, favorable solubilities and better reactivities.[2] These polymers can be prepared in a one-step procedure by polymerization of AB_2 or AB_3 monomers and possess a certain polydispersity and randomly branched structure, as expected from the statistics of an AB_n polymerization. Via this method, hyperbranched polymers possess lower degrees of branching (DB) and broader molecular weight distributions (MWDs) than the monodisperse dendrimers. Their behaviour is intermediate between dendrimers and linear polymers. Nonetheless, hyperbranched polymers are strong competitors to dendrimers, particularly in applications where molecular perfection is not a necessary prerequisite. In fact, the polycondensation or step-growth polymerization synthetic approach of AB_n monomers has shown to reduce costs and environmental pollution and is very attractive for both laboratory and commercial applications.[3] If side reactions are excluded, the AB_n stoichoimetry does not permit gelation, unless an unlikely 100 % intermolecular reaction of A groups is achieved.[4] At full monomer conversion, the growth can be terminated either by increasing steric screening on A or B or, depending on the chain flexibility, by ring formation through the intramolecular reaction of A with B in the same macromolecule (Figure 5.1).[4] Accordingly, intramolecular cyclization leads to complications in the synthesis of hyperbranched polymers from AB_n monomers, limiting their molecular weight.[5]

Organosilicon dendritic polymers are inorganic-organic hybrid polymers that are beginning to attract considerable interest for materials applications. Hyperbranched[6] and dendritic[7] silicon based materials have been prepared and these highly processable polymers have already shown promise as preceramic polymer precursors,[6l,8] degradable template molecules,[6h-i] high-temperature elastomer precursors[9] and modifiers of composite polymers.[10]

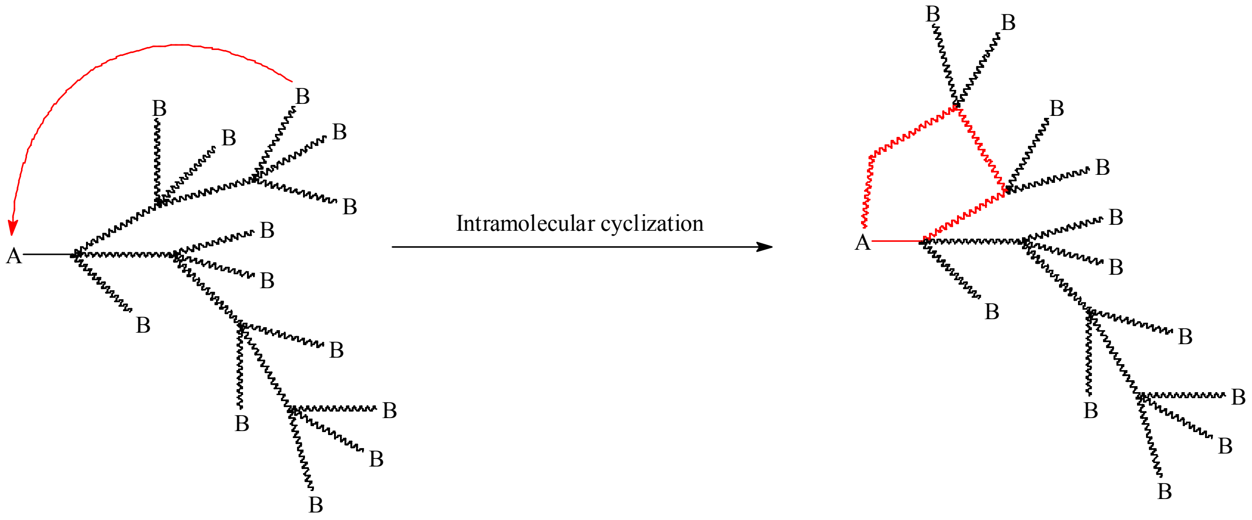

Figure 5.1. Formation of a five-membered ring as a consequence of the intramolecular cyclization side reaction between the A and B groups in the one-pot polymerization of a branched AB_3 monomer.

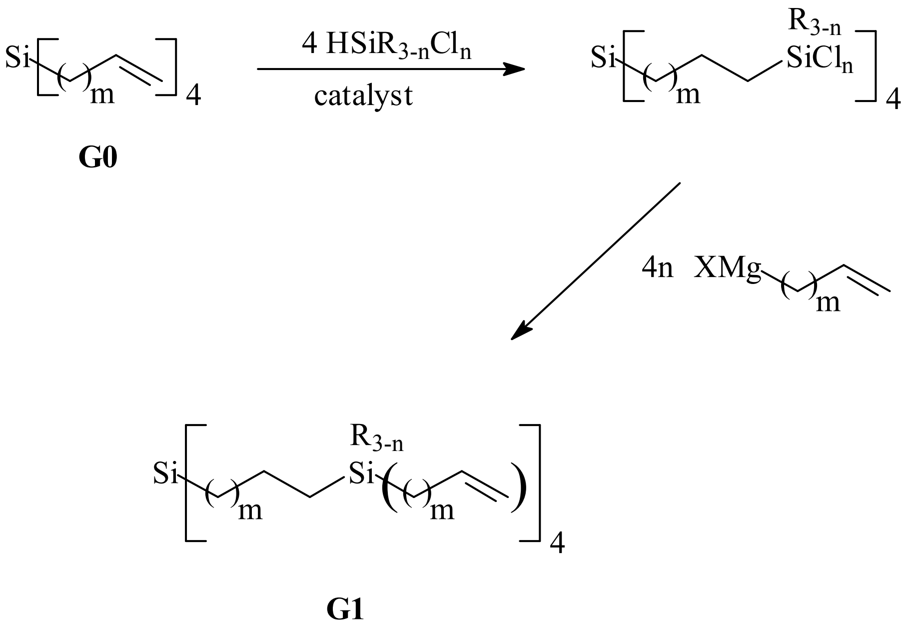

R = Me; **X** = Cl, Br; **m** = 0, 1; **n** = 2, 3

Figure 5.2. Divergent synthesis of a typical carbosilane dendrimer (G = dendrimer generation).

Schlenk *et al.* have summarized recent developments in the field of carbosilane dendrimers.[7b,7d] Their synthesis via the divergent approach has been reported by several authors and the construction is mainly based on repeating sequences of alternating hydrosilylations with chlorosilanes and ω-alkenylations with Grignard reagents (Figure 5.2). This synthetic route offers high flexibility and versatility: the hydrosilylation reagent, the ω-alkenylation reagent and the core molecule can be varied without drastic changes in the reaction conditions. Furthermore, due to their spherical topology, large number of end groups and chemical stability, carbosilane dendrimers have been used as core molecules for star shaped polymers with an unusually large number of arms ("multiarm star polymers"; *i.e.* by treating carbosilane dendrimers with Si-Cl bonds with monodisperse poly(butadienyl)lithium).[7b] One major drawback of these systems is nevertheless the low amount of material obtained owing to the tedious multi-step synthetic procedure.

The majority of hyperbranched carbosilane polymers have been prepared via hydrosilylation reactions based on random "one-pot" polymerization of AB_n monomers, although this procedure allows no control over the molecular weight and MWD.[7b] Muzafarov *et al.* and Lach *et al.* reported on the synthesis of hyperbranched poly(triallylsilanes)[10,11] and characterization of their branched structure was described by the latter authors via ^{29}Si NMR spectroscopy.[11] Furthermore, enhancement of the DB of poly(triallylsilane) was achieved postsynthetically by hydrosilylating an oxazoline-poly(triallylsilane) with $HSiCl_3$ followed by reaction with allylmagnesium bromide in order to transform all the triallysilane branch points into dendritic units.[6f,12] Drohmann *et al.* reported later on the synthesis of hyperbranched polycarbosilanes by polyaddition of AB_2 monomers (methyldivinylsilane (MDVS), methyldiallylsilane (MDAS) and methyldiundecenylsilane (MDUS)) and AB_3 monomers (triallylsilane (TAS)) via hydrosilylation in the presence of a platinum catalyst.[13] A study of the molecular weight of the resulting polyaddition products and its dependence on the reaction conditions (various catalysts, reactions in solvent *vs.* in bulk) and monomer structure was provided. Control over the molecular weight of the polycarbosilanes by subsequent addition of monomer was only achieved for the polymer emanating from MDUS AB_2 monomer. This was justified in terms of the lower probability of rearrangements and cross linking reactions as well as of the increased flexibility of the undecenyl *vs.* the allyl and vinyl chain, which should decrease the sterical hindrance in the interaction with the catalyst. However, according to work by Fréchet *et al.*[14] and Frey *et al.*,[15] the non-increase of the molecular weight in the case of MDAS and MDVS after subsequent addition of further monomer is probably due to "cyclization" consuming Si-H functionalities, while growth of the polymer in the case of MDUS is likely due to kinetically disfavored "cyclization" of the larger monomer. There are in fact investigations that show lower kinetics of formation for eight and bigger-membered rings than for the smaller rings.[16] This can be ascribed to the lower probability of existing molecules in the right orientation to form a ring. Hyperbranched polycarbosilanes have also been prepared utilizing nucleophilic substitution reactions: Interrante *et al.* reported on the preparation of a highly branched hydridopolycarbosilane $[SiH_2CH_2]_n$ by Grignard coupling of (chloromethyl)trichlorosilane, followed by reduction with lithium aluminium hydride.[6l,8a] This hydridopolycarbosilane showed potential interest as a precursor to silicon carbide ceramics.[8b-c] This Grignard coupling approach was also utilized by Yao and Son for the synthesis of hyperbranched polycarbosilane oligomers containing both alkene and silyl hydrid groups as well as for hyperbranched poly(silylthiophenes).[3,17] The first aromatic hyperbranched polycarbosilane was obtained by Son and Yoon via polyaddition of 1-dimethylsilyl-4-trivinylsilylbenzene.[6b]

It is noteworthy that highly branched poly(silylenevinylene)s have been synthesized via polymerization of methyldiethynylsilane AB_2 monomers containing terminal triple-bond moieties .[18] The advantage is that ethynyl groups can react with each other readily with heating or irradiation, and thus catalysts are not required and side-products are avoided. Terminal ethynyl groups can also be further functionalized.

In this chapter, hyperbranched polycarbosilanes from dialkenylsilane (AB_2) and trialkenylsilane (AB_3) monomers have been synthesized via the “one-pot” synthetic procedure. The length of the alkenyl spacer was varied by choosing a long and a short undecenyl and allyl chain, respectively. Analogously, linear or brush-like polycarbosilanes have been prepared from monoalkenylsilane (AB) monomers possessing a long undecenyl chain. Thus platinum-catalyzed hydrosilylation (Karstedt catalyst) has been used as the polyaddition reaction of MDUS, MDAS (AB_2 monomers); TUS, TAS (AB_3 monomers) and DMUS (AB monomer). The Pt(0) complex has been reported to yield soluble products for a large range of reaction temperatures and catalyst concentrations, when compared to H_2PtCl_6.[13] Although the polymerization from MDUS, MDAS and TAS has been described before,[13] poor structural analysis of these polymers has been reported. Therefore, it is the purpose of this chapter to provide a complete structural characterization of the hyperbranched and brush-like polymers that were obtained under different polymerization conditions (different reaction times, solvents and concentrations). The in-depth discussion concerning the structure of the polycarbosilanes is of significance as they will be part of more complex architectures in the next chapters.

5.2 RESULTS AND DISCUSSION

5.2.1 Polymerization

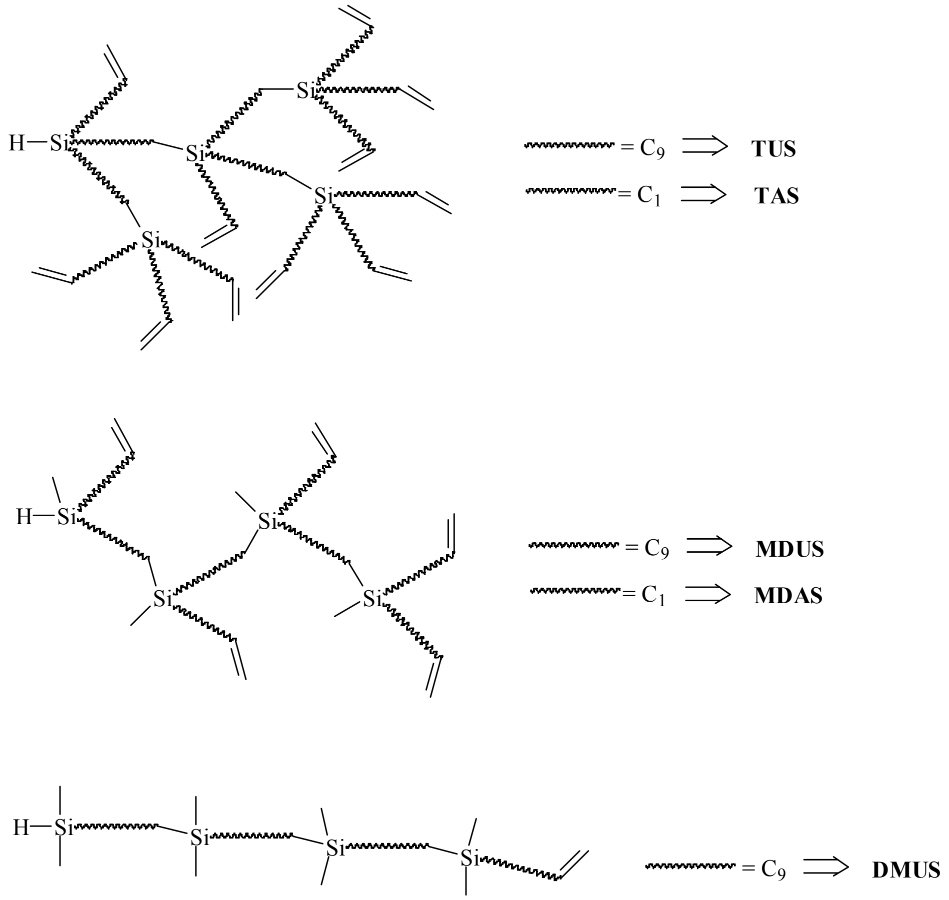

Figure 5.3. Hyperbranched and brush-like polyalkenylsilanes obtained from the step-growth polymerization of AB_3, AB_2 and AB monomers.

The hydrosilylation polymerization of the monomers MDUS, MDAS, TUS, TAS and DMUS was accomplished via the "one-pot" procedure in solution or in bulk at r.t. in the presence of the Karstedt catalyst. In this way, hyperbranched and brush-like polymers carrying terminal double bonds were obtained. The Karstedt catalyst[19] was chosen for the polymerization as it afforded the best results (*i.e.* when comparing to H_2PtCl_6 or $RhCl(PPh_3)_3$). The polymers were isolated as viscous yellow, honey-like liquids by precipitation into methanol and were very soluble in common organic solvents like diethyl ether, toluene and chloroform. A schematic representation of the final polymers obtained from the AB_3, AB_2 and AB alkenylsilane monomers is presented in Figure 5.3.

The relative molecular weight of the hyperbranched and brush-like polymers was determined by GPC analysis with PS standards for calibration. In all cases, the GPC traces (see for example Figure 5.4) show the presence of multiple resolved peaks with elution volumes corresponding to low molecular weight compounds, which are assigned to oligomeric species. Since spectroscopic analysis of these polymers revealed in general no Si-H peaks, these low-molecular weight GPC peaks likely correspond to the product obtained by intramolecular cyclization of the monomer and/or to oligomers involving cyclized species. It is however difficult to assess the exact extent to which this cylization process is taking place in the different systems. Table 5.1 provides a summary of the typical molecular weight distributions obtained in the polymerization of the various monomers together with the polydispersities (PDI). All PDI are measured for the crude products without removal of the oligomers. Nevertheless, the observed PDI values for the hyperbranched structures are lower to what would be expected from theory ($\overline{M}_w / \overline{M}_n = 4 - 10$).

Table 5.1. Characterization of polyalkenylsilanes prepared via the “one-pot” procedure[a]

		GPC[b]	
Polymer	**Monomer**	**M_w (g/mol)**	**PDI**[c]
PMDUS	AB_2	13,600	3.3
PDMUS	AB	7,800	2.5
PTUS	AB_3	5,800	3.9
PMDAS	AB_2	7,800	4.6
PTAS	AB_3	7,100	2.5

[a]Synthesis of polyalkenylsilanes was performed in pentane at r.t. with the Karstedt catalyst for 24 hrs. [b]Gel permeation chromatography (GPC) measured in chloroform at 30 °C with PS standard calibration. [c]Polydispersity index measured by GPC in chloroform at 30 °C

Limited molecular weights were achieved for the hyperbranched and brush-like alkenylsilane polymers. This can be explained by several factors that influence the growth of the polymers. The MWD is likely to be affected by intramolecular cyclization of monomers and oligomers, by steric crowding within the structure and also by the presumably lower reactivity of the functional groups in the hyperbranched polymers caused by steric crowding. For the DMUS AB monomer, in which a linear polymer structure is obtained, less crowding of the double bond functionalities is expected. Although comparing different polymer structures, lower values of $\overline{M}_w$ were obtained for PDMUS (linear) than for PMDUS (hyperbranched). This suggests that crowding within the polymer structure is not the only factor that can explain the limitation in the molecular weights achieved. It is evident that competing side reactions take place during the metal-catalyzed-hydrosilylation process (*i.e.* alkene isomerization and hydrogenation). An overview of these side reactions is presented in Chapter 4. These side reactions decrease the amount of reactive species, limiting the molecular weight of the polymers. Isomerization results in non-reactive inner double bonds, while hydrogenation leads to vinyl-depleted structures. It is also noticeable that higher PDI were obtained for hyperbranched PMDAS with the shorter allyl chain. This might be related to cross linking reactions as already observed by Drohmann *et al.*.[13] Although gelation can be excluded in principle from the polycondensation of AB_n monomers, it can be interpreted in view of monomer rearrangements reactions that seem more facile for AB_2 monomers possessing a shorter alkenyl chain (Chapter 4, section 4.3.2). Within the series of undecenylsilane polymers, lower PDI were attained for the linear PDMUS than for the hyperbranched PMDUS and PTUS respectively. This is clearly related to the lower probability of the DMUS AB monomer of building "cyclized" species than the analogous AB_2 and AB_3 monomers, due to the lower ratio of B:A species. Higher branching degrees of the AB_n monomer increase then the probability for the end groups to have the right orientation to build a "cycle".

5.2.2 Kinetic studies

Relative variations in the MWDs of the polycarbosilanes obtained from MDUS, DMUS, TUS and MDAS after different polymerization times were analyzed by GPC (Figures 5.4-5.7). All the polymerization reactions were carried out in toluene or pentane at r.t. in the presence of the Karstedt catalyst. The GPC traces of the polycarbosilanes show commonly low and high MW impurities and the MWDs are in general relatively broad. In particular, for the hyperbranched PMDUS, an oligomer peak with a retention volume essentially identical to that of the monomer (m) is seen (Figure 5.4). The following peaks can be respectively assigned to the dimmeric (d), tetrameric (t), pentameric (p) and hexameric (h) species. It can also be observed, that the high molecular weight shoulder in PMDUS, PDMUS, PTUS and PMDAS becomes more evident with increasing reaction times. This high molecular weight shoulder is consistent with the occurrence of rearrangements reactions that lead to cross linking and is more evident in PMDAS, corroborating that rearrangements reactions are more facile to occur when utilizing the AB_2 monomer with a short allyl chain (Figure 5.7). The presence of oligomers and/or "cyclized" species is particularly more noticeable in PTUS, resulting in a multimodal distribution and larger PDI values (Figure 5.6). This is due to the higher probability of an AB_3 monomer and/or the corresponding oligomers to form "cyclic" species that cannot be attached to the growing polymer branched structure. The fraction of oligomeric species is slightly reduced for all the polycarbosilanes within time. However, they still remain present in considerable amounts, indicating the presence of oligomeric "cycles" within the polymer structures.

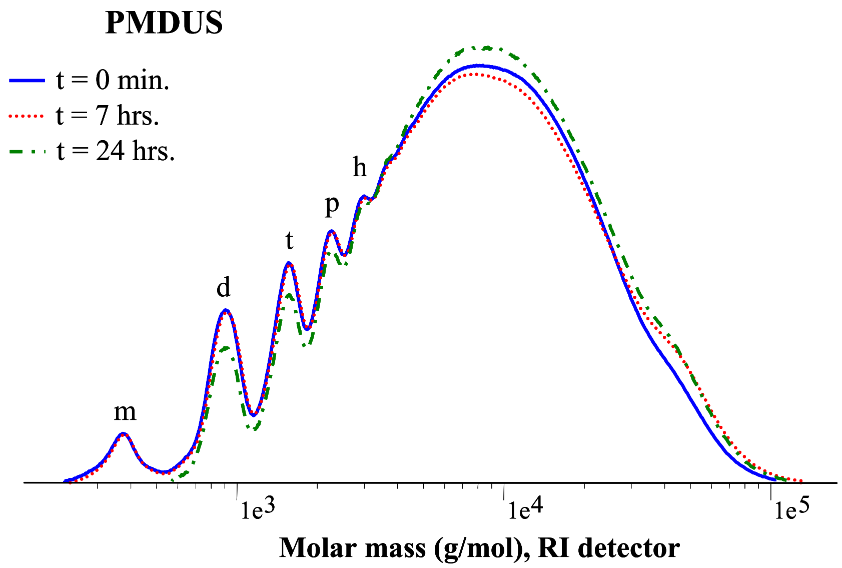

Figure 5.4. GPC traces of *hb*-PMDUS at different polymerization times (toluene, r.t., Karstedt).

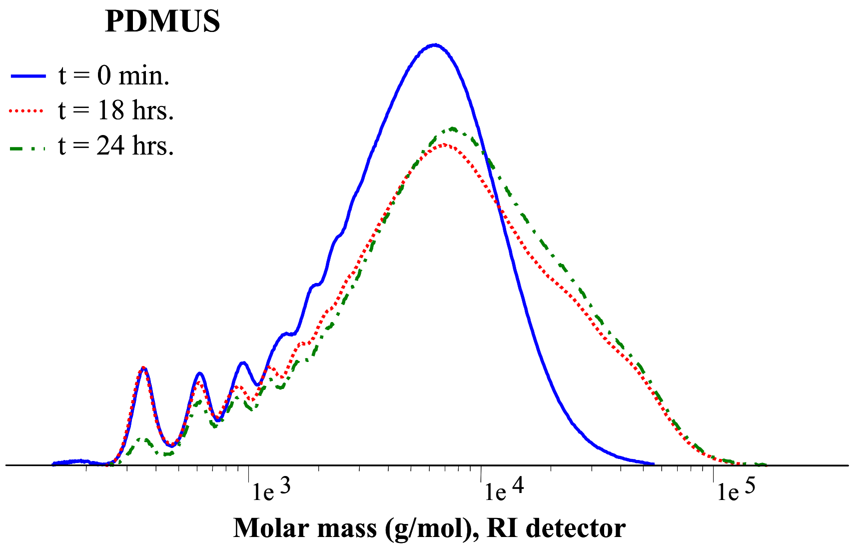

Figure 5.5. GPC traces of linear PDMUS at different polymerization times (toluene, r.t., Karstedt).

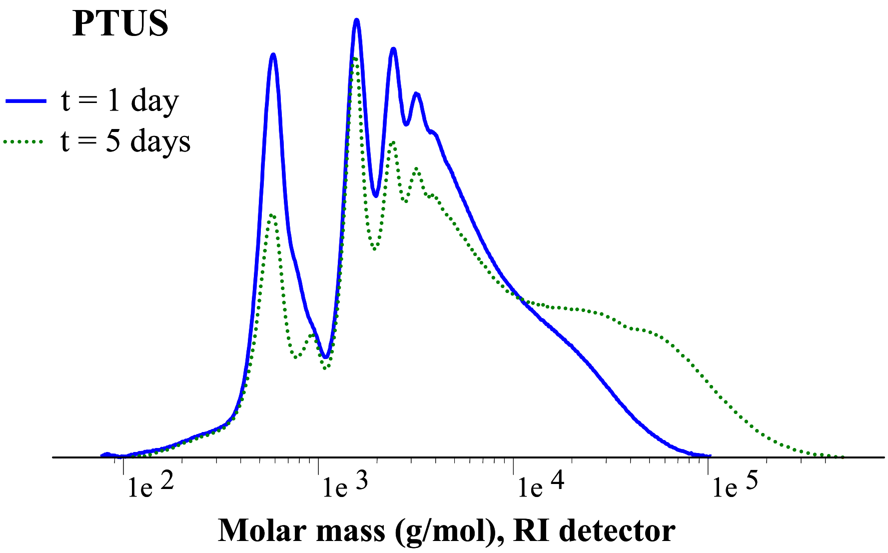

Figure 5.6. GPC traces of *hb*-PTUS at different polymerization times (pentane, r.t., Karstedt).

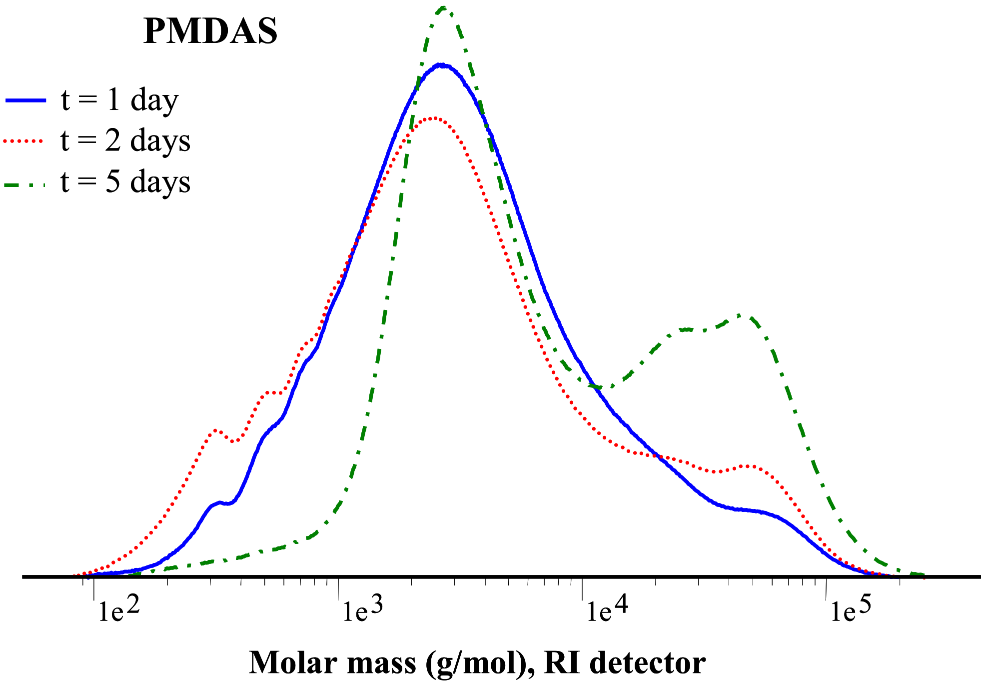

Figure 5.7. GPC traces of *hb*-PMDAS at different polymerization times (pentane, r.t., Karstedt).

5.2.3 Effect of monomer concentration

The molecular weights of the polycarbosilanes were also dependent on the starting concentration of the monomer solutions. Figures 5.8 and 5.9 show the GPC traces of *hb*-PMDUS and linear PDMUS at two different monomer concentrations in toluene and in bulk respectively, after 24 hours of polymerization in the presence of the Karstedt catalyst. The GPC curves show that dilution of the monomer solutions results in lower molecular weights. This was already predicted by Drohmann *et al.* and Lach *et al.*.[13,20] In the case of *hb*-PMDUS, a more concentrated solution results in a polymer with lower PDI (Figure 5.8). However, when the catalyst is added to the bulk monomer (in an attempt to keep the concentration of reactive functionalities as high as possible and therefore minimize undesired intramolecular side reactions), a bimodal distribution with a tailing to higher molecular weights is obtained. In contrast, the polymerization of MDUS AB monomer in bulk gives a monomodal distribution with higher molecular weights and lower amount of "cyclic" species (Figure 5.9).

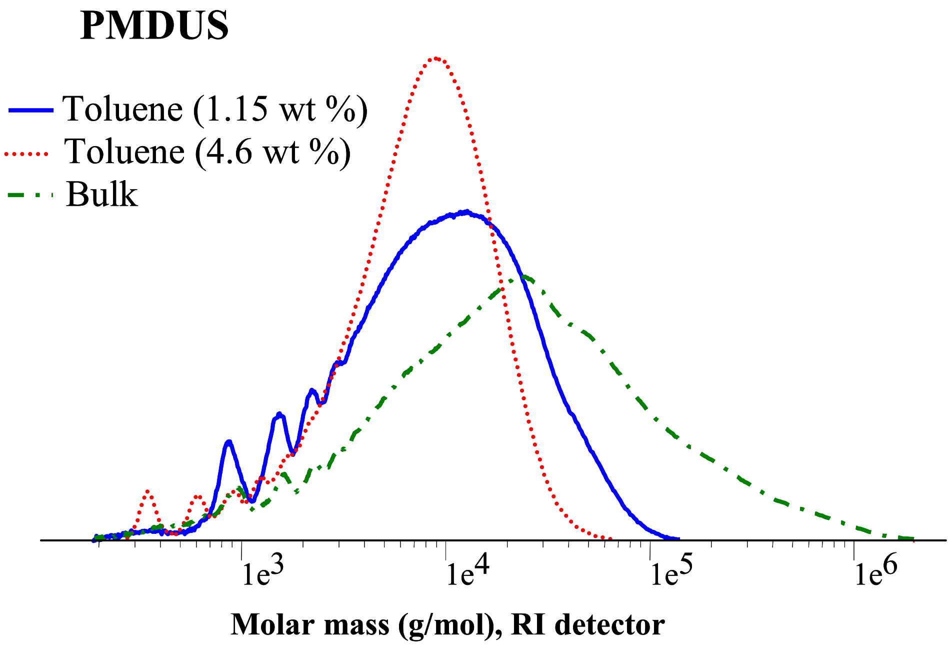

Figure 5.8. GPC traces of *hb*-PMDUS at different monomer concentrations and in bulk (r.t., Karstedt).

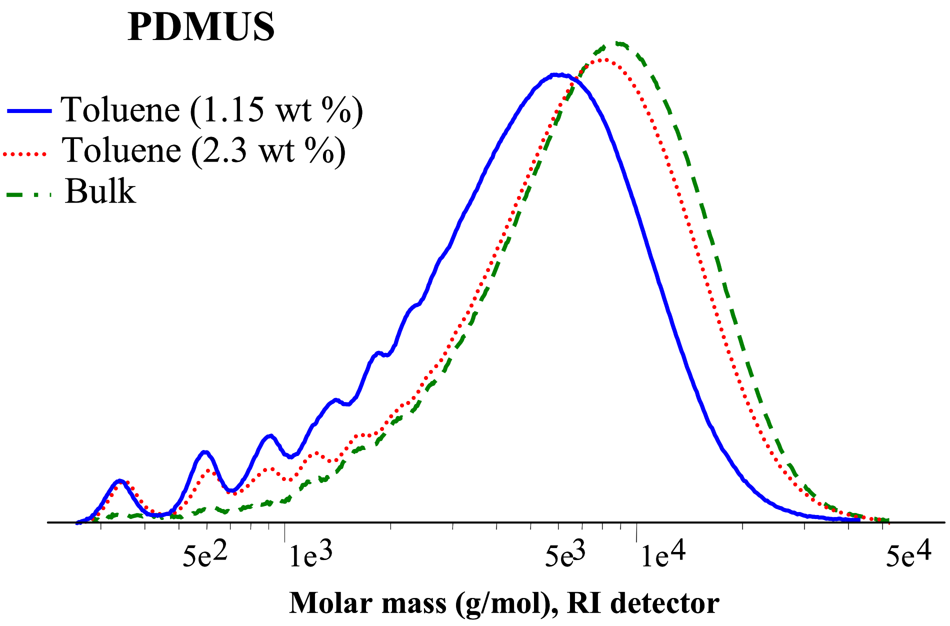

Figure 5.9. GPC traces of linear PDMUS at different solvent concentrations and in bulk (r.t., Karstedt).

5.2.4 Chemical structure and composition

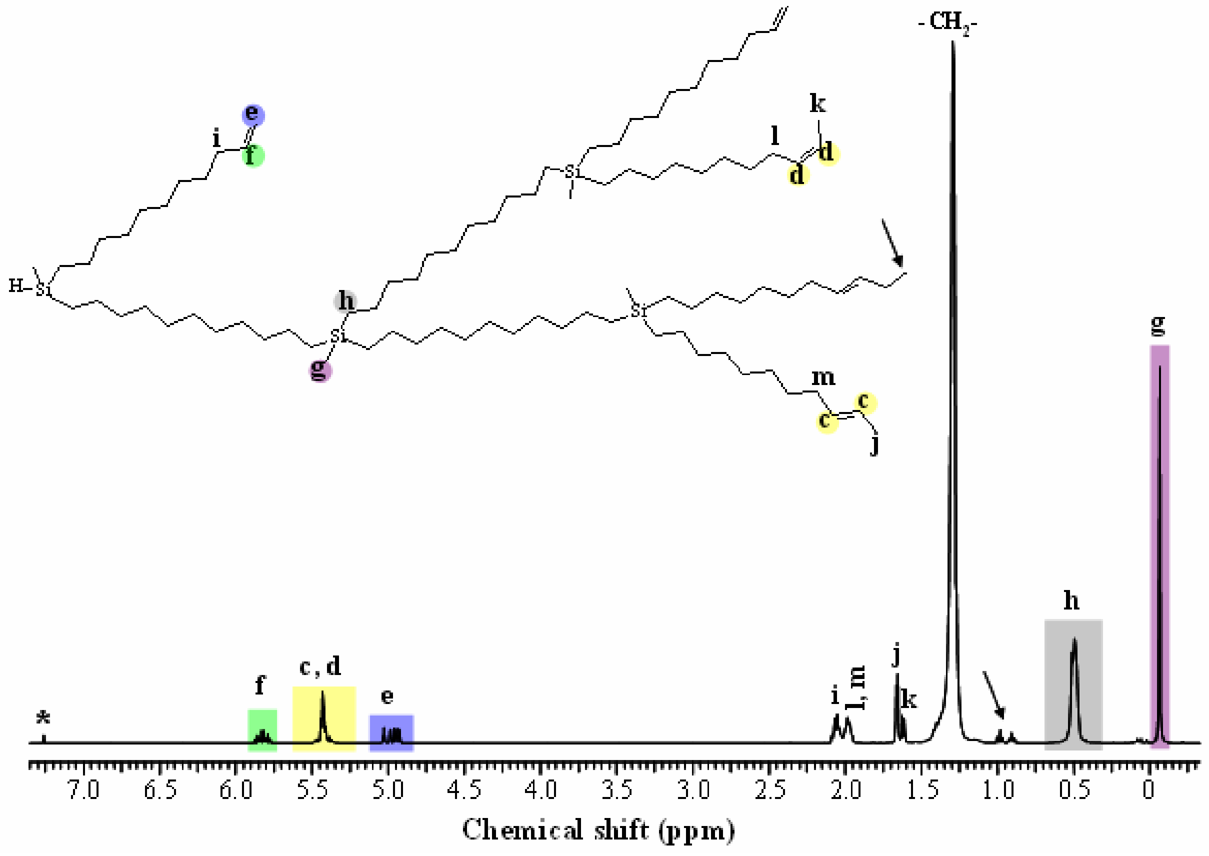

Figure 5.10. ^{1}H NMR of *hb*-PMDUS in CDCl$_3$ (solvent peak denoted by an asterisk).

The structure of the alkenylsilane polymers was elucidated via NMR and was found to be very solvent-dependent. Partial alkene isomerization took place when using toluene or pentane as solvents, while isomerization of the double bonds was complete when employing diethyl ether. Complete assignment of the resonances observed in the ^1H and ^{13}C NMR spectra was possible using 2D COSY and HETCOR NMR experiments. Two-dimensional proton-proton chemical shift correlation spectroscopy (COSY) provides a map of all coupling networks between protons in a molecule in a single experiment, and is an example of homonuclear correlation spectroscopy. The COSY experiment can be modified so as to provide evidence of coupling between protons and heteronuclei, so-called heteronuclear chemical shift correlation spectroscopy (hetero-COSY). We are interested in correlating carbon nuclei with their directly attached protons (HETCOR). In this manner, assignments obtained from the analysis of the proton spectra may then be transferred directly onto the carbon spectrum. Alternatively, the extra dispersion gained by spreading the proton spectrum along the ^{13}C dimension of the 2D-spectrum, may assist in the interpretation of the proton spectrum itself.

The ^1H NMR spectrum of *hb*-PMDUS, after polymerization in pentane using the Karstedt catalyst, is shown in Figure 5.10. The ^1H NMR of the corresponding alkenylsilane AB_2 monomer (MDUS) is presented in Chapter 3 (Figure 3.8). The ^1H NMR after polymerization shows a new sharp peak in the alkenyl region at 5.4 ppm, which corresponds to the isomerized methylene protons labeled “c” and “d”. “c” and “d” represent the olefinic protons from a *trans*- and *cis*-isomerization in the 2-position respectively. The methylene and methine protons of the terminal double bonds appear at 4.9 and 5.8 ppm respectively (signals “e” and “f”). This assignment can be verified by examining the ^1H-^1H COSY spectrum of PMDUS, where the sharp multiplet at 5.4 ppm exhibits no coupling with the other olefinic protons (Figure 5.11). In the region between 3.5 and 4.0 pmm no Si-H groups left were detected after termination of the reaction, suggesting the presence of “cyclized” monomer and/or “cyclized” oligomeric species. The broad peak centered at 1.3 ppm is due to the interior -CH_2- protons of the alkyl chain. Evidence on the β-addition regiospecificity of the hydrosilylation reaction is provided by the appearance of only one signal corresponding to the Si-CH_3 and Si-CH_2 groups at -0.07 and 0.5 ppm respectively (signals “g” and “h”). The other features of the ^1H NMR spectrum agree well with the depicted polymer structure in Figure 5.10 and were assigned with the assistance of the ^1H-^1H COSY spectrum presented in Figure 5.12. The peak at 2.05 ppm labeled “i” presents only coupling with the terminal double bonds and therefore is ascribed to the allylic protons of the terminal vinyl units. The new small broad peak next to “i” (signals “l” and “m”) is assigned respectively to the allylic protons of *cis*- and *trans*-isomerized double bonds, as it shows only coupling with “c” and “d”. The new peaks in the polymer at 1.65 and 1.62 ppm (signals “j” and “k”), showing exclusive coupling with the isomerized double bonds, correspond respectively to the methyl protons resulting from a *trans*- and *cis*-isomerization in the 2-position. The stereospecificity of the chemical shift assignment (*cis*- and *trans*-) for the isomerized allylic protons “l “ and “m” and for the methyl groups of the isomerized double bonds “j” and “k” will be explained later with the help of 2D HETCOR experiments.

The degree of isomerization of *hb*-PMDUS can be estimated from the integration ratio of the resonances in the olefinic region and is estimated between 45-65 % and this can be reduced to *ca.* 33 % when the reaction is performed in bulk at r.t.. Polymerization at elevated temperature raises the amount of isomerized species (*i.e.* from 33 to 43 % in bulk at 70 °C). This differs from the findings of Drohmann *et al.*,[13] who encountered only 3 % isomerization of the terminal olefinic groups to inner double bonds. However, no verification through NMR characterization or spectra was provided. Theoretically the polyaddition reaction of AB_2 monomers leads to hyperbranched macromolecules with one terminal Si-H group and DP_n+1 alkenyl groups respectively. However, the comparison in the ^{1}H NMR spectrum of the relative intensities of the $Si\text{-}CH_3$ groups with the olefinic protons suggests that other side reactions besides isomerization are taking place. It is suspected that alkene hydrogenation occurs as the number of double bonds does not increase as expected. This side reaction was also not encountered by Drohmann *et al.*. The resulting DP_n for *hb*-PMDUS cannot be calculated from the ^{1}H NMR spectrum due to the absence of a core molecule for the hyperbranched material.

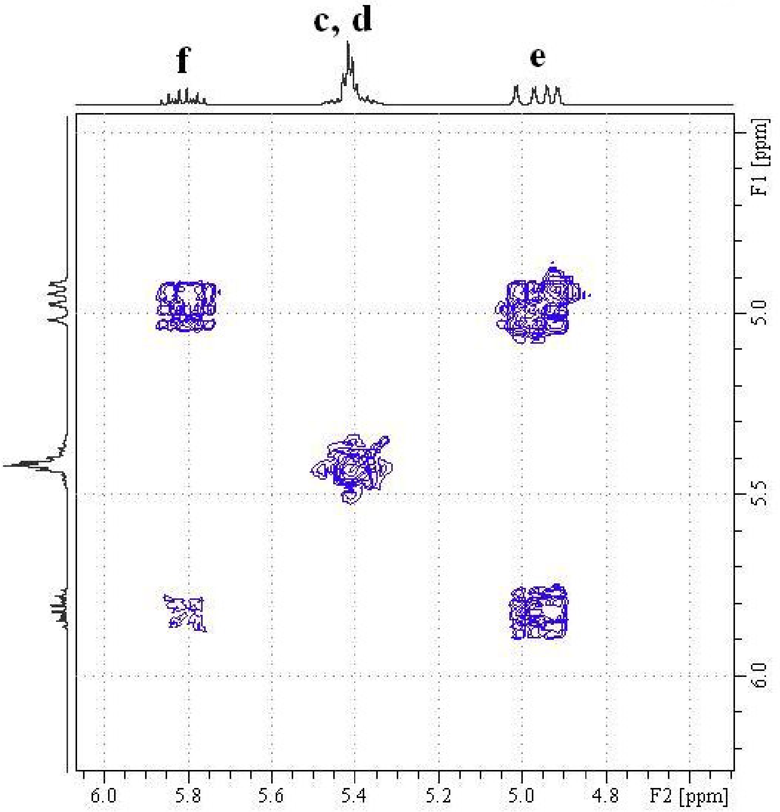

Figure 5.11. ^{1}H-^{1}H COSY spectrum of *hb*-PMDUS.

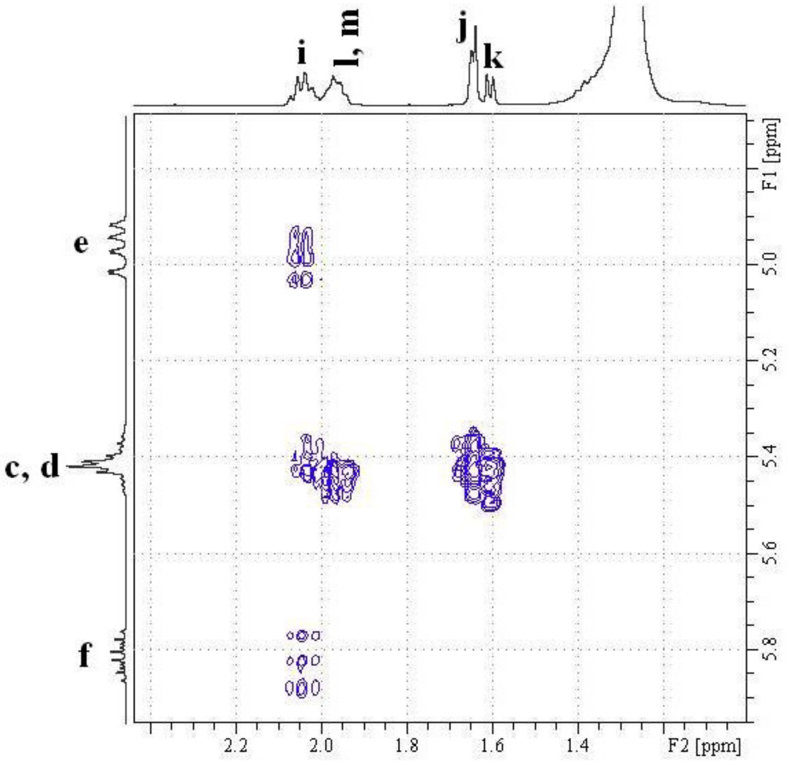

Figure 5.12. ^{1}H-^{1}H COSY spectrum of *hb*-PMDUS.

PMDUS was also investigated by ^{13}C NMR. The ^{13}C NMR DEPT spectrum of *hb*-PMDUS is presented in Figure 5.13. In Figure 5.13 are also included enlargements of the ^{13}C downfield and highfield regions that were recorded with a higher number of scans. ^{13}C NMR of the corresponding AB$_2$ monomer (MDUS) is presented in the Appendix of Chapter 3 (Figure A3.1). In the polymer, there are four new signals in the alkenyl region labeled "c$_1$", "c$_2$" and "d$_1$", "d$_2$". These positive signals are clearly associated with the methine carbons arising from an isomerization of the vinyl groups in the 2-position. The more intense signals "c$_1$" and "c$_2$" at 124.8 and 132.9 ppm probably correspond to the thermodynamically favored *trans*-2-isomer, while "d$_1$" and "d$_2$" at 123.9 and 131.2 ppm to the *cis*-2-isomer. Enlarging of the alkenyl region reveals the presence of other small carbon signals (denoted by asterisks), suggesting other types of isomerization along the alkyl chain. The methylene and methine carbon signals corresponding to the terminal double bonds (signals "e" and "f") appear at chemical shifts analogous to the corresponding monomer. The assignment of these signals was verified by examining the ^{1}H-^{13}C long range HETCOR spectrum (Figure 5.14). The carbon signals "e" and "f" are coupled with the allylic protons "i" of the terminal vinyl groups. The 2-isomerized carbon signals "c$_1$" and "c$_2$" and "d$_1$" and "d$_2$" exhibit coupling with the allylic protons from the isomerized double bonds "m" and "l" respectively. Additionally, "c$_1$" and "c$_2$" are coupled with "j", which now can be accurately assigned to the methyl protons arising from a *trans*-2-isomerization. Analogously, "d$_1$" and "d$_2$" are coupled with "k", which is likewise assigned to the methyl protons arising from a *cis*-2-isomerization. The ^{1}H NMR upfield region of PMDUS displays small peaks (designed by an arrow) that couple with one of the small carbon signals arising from other than 2-olefinic isomers (Figure 5.14). Therefore, the small proton peak at 1.0 ppm can be assigned to methyl groups resulting from isomerization in other positions along the chain. Analysis of the ^{13}C NMR upfield region reveals the Si-CH$_3$, Si-CH$_2$ and Si-CH$_2$-CH$_2$ characteristic resonances denoted by "g", "h" and "n". Enlargement of the region containing the Si-CH$_3$ peak "g" shows the close presence of another tiny peak that can probably be assigned to the Si-CH$_3$ peak from an α-addition product. However and in accordance with the ^{1}H NMR, the β-addition products are preferentially formed.

The new carbon signals "j" and "k" in the upfield region are coupled in the ^{1}H-^{13}C long range HETCOR spectrum with the isomerized protons "c" and "d" (Figure 5.15). These carbon signals are additionally coupled with the proton signals "j" and "k" that were previously assigned to the methyl groups of *trans*- and *cis*-2-isomers (Figure 5.16). Thus the more intense carbon signal “j” can be assigned to the methyl groups resulting from a *trans*-2-isomerization, while “k” to the methyl groups from a *cis*-2-isomerization.

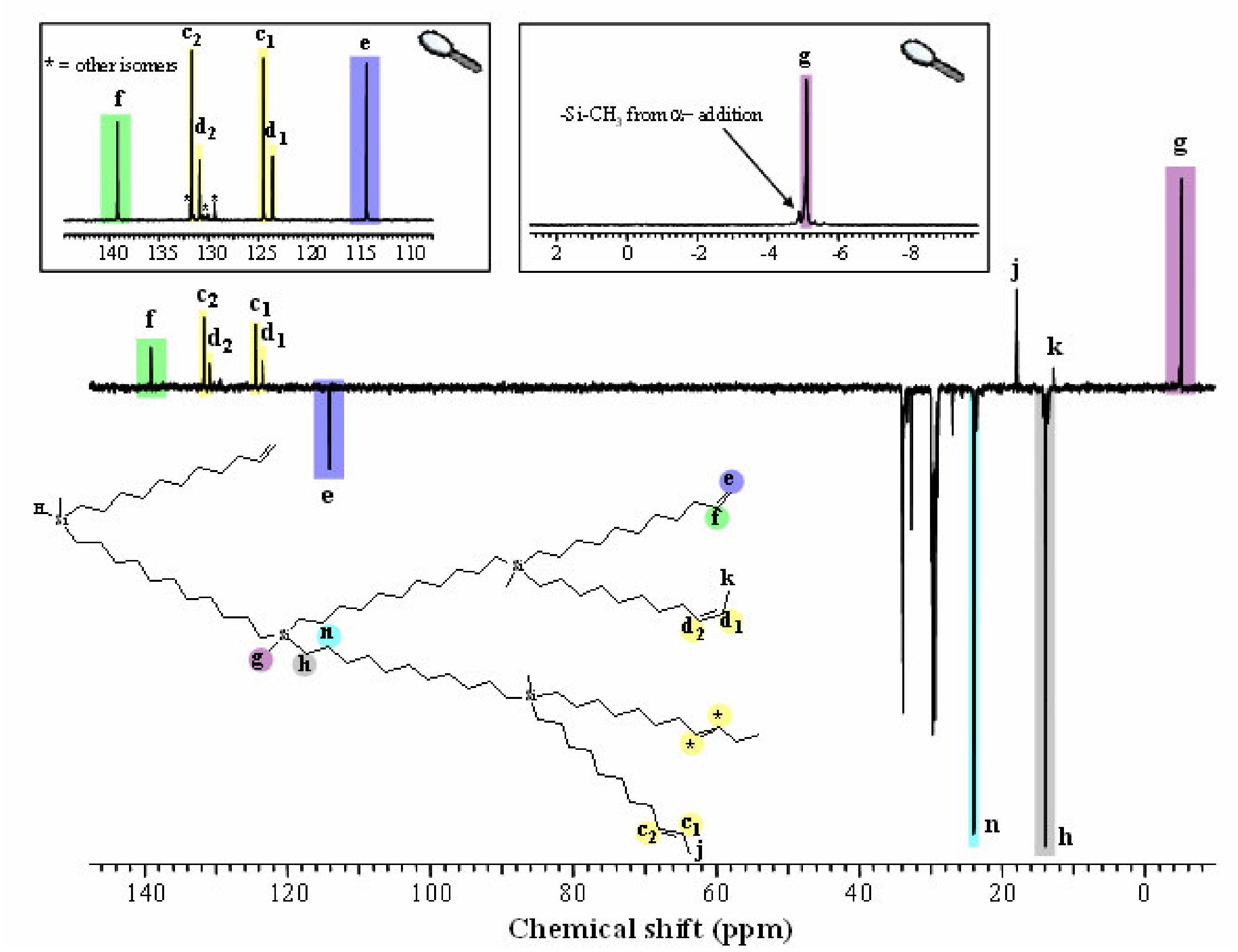

Figure 5.13. ^{13}C NMR DEPT of *hb*-PMDUS in $CDCl_3$.

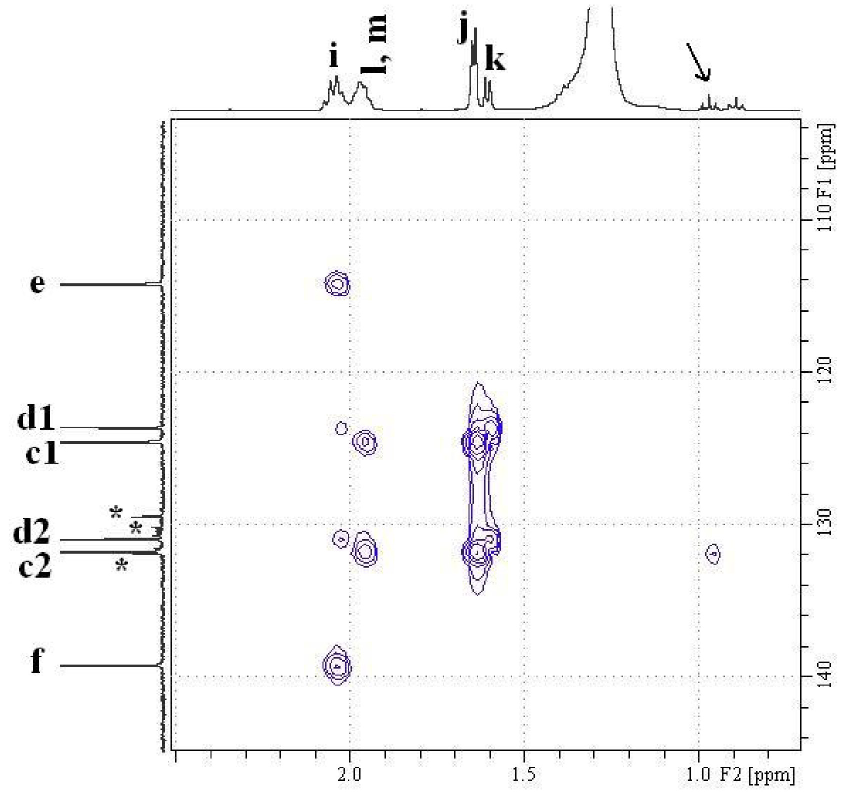

Figure 5.14. ^{1}H-^{13}C long range HETCOR spectrum of *hb*-PMDUS.

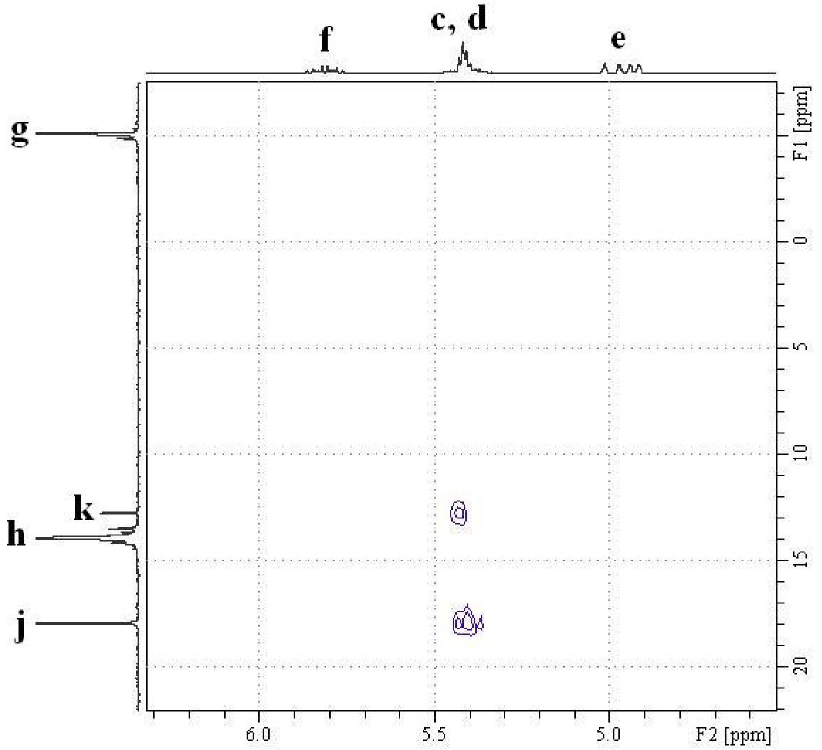

Figure 5.15. ^{1}H-^{13}C long range HETCOR spectrum of *hb*-PMDUS.

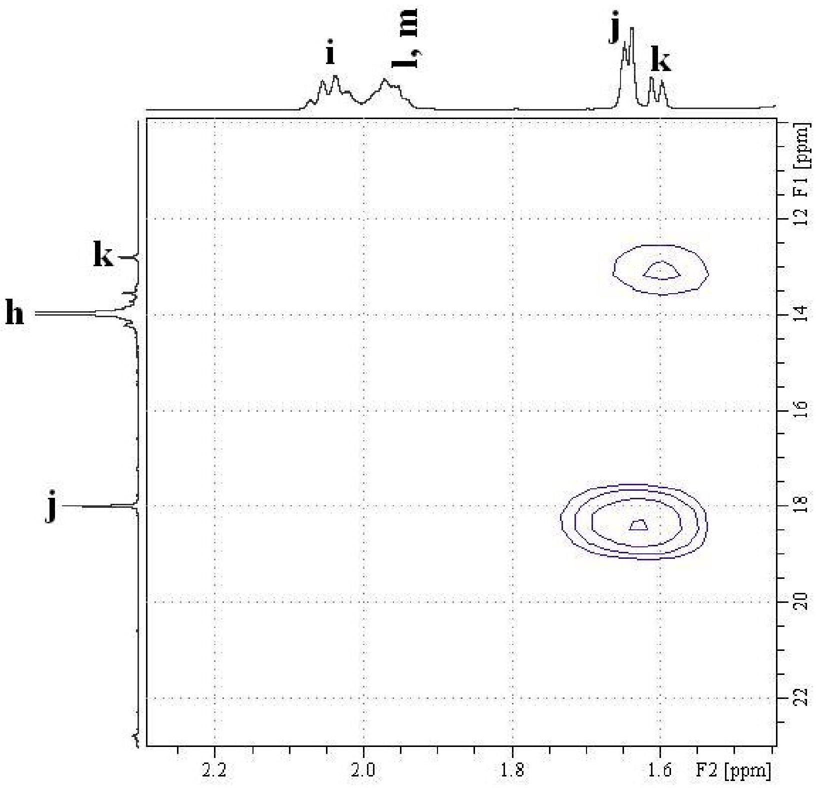

Figure 5.16. ^{1}H-^{13}C HETCOR spectrum of *hb*-PMDUS.

The ^{1}H NMR spectrum of *hb*-PMDUS, resulting from a polymerization in diethyl ether in the presence of the Karstedt catalyst, is presented in Figure 5.17. In comparison with the previous ^{1}H NMR, the presence of only one signal at 5.4 ppm in the olefinic region is noticeable. This indicates complete isomerization of the terminal double bonds by using diethyl ether as solvent. Additional evidence for this fact is the absence of the signal at *ca.* 2.05 ppm corresponding to the allylic protons of non-isomerized double bonds. The signals "i" and "i′" at 0.96 and 0.88 ppm respectively were already evident in the ^{1}H NMR of the non-completely isomerized polymer structure. However, these peaks are now more discernible and assigned, as previously, to the methyl protons arising from other than 2-olefinic isomers. The ^{1}H-^{1}H long range COSY spectrum shows the coupling of both signals "i" and "i′" with the protons of the isomerized double bonds (Figure 5.18).

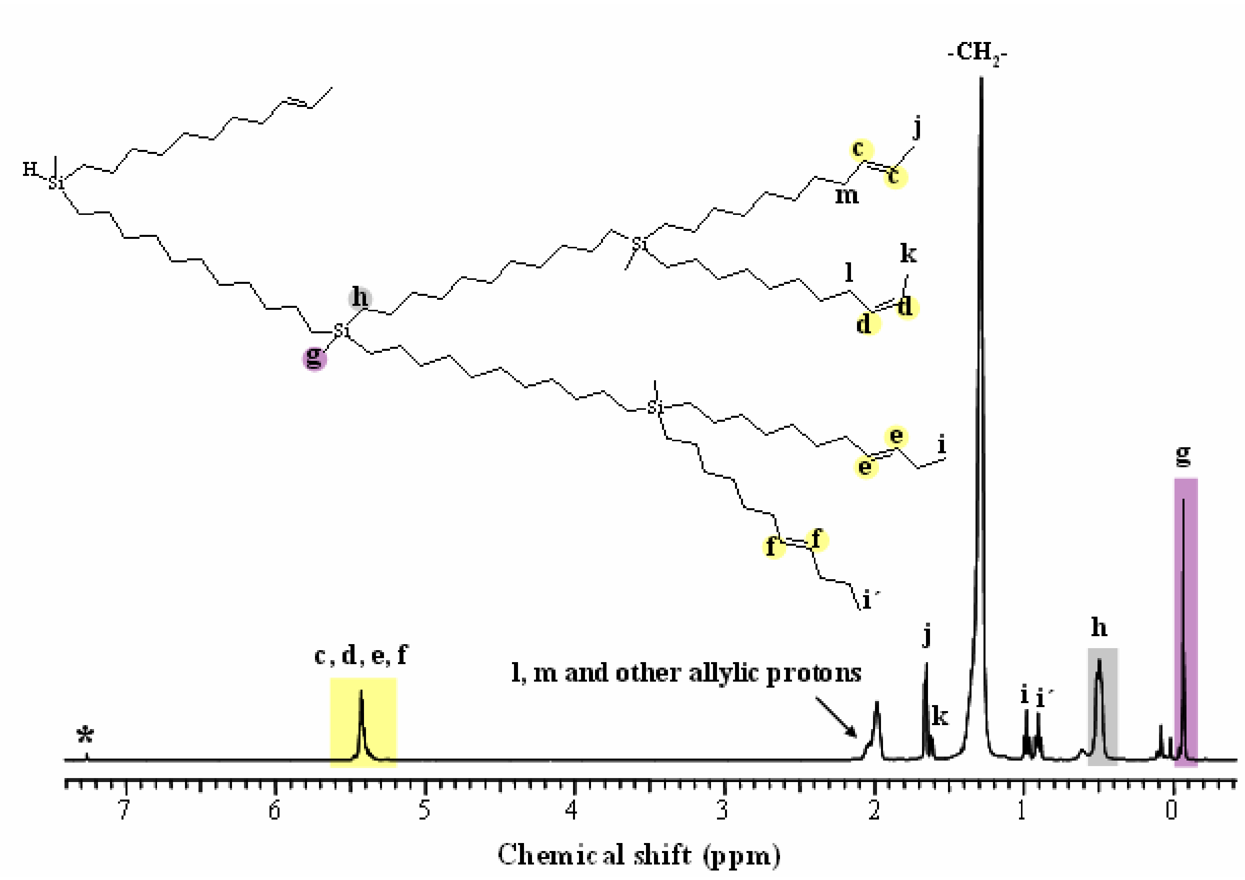

Figure 5.17. ^{1}H NMR of *hb*-PMDUS, obtained using diethyl ether as solvent, in CDCl$_3$.

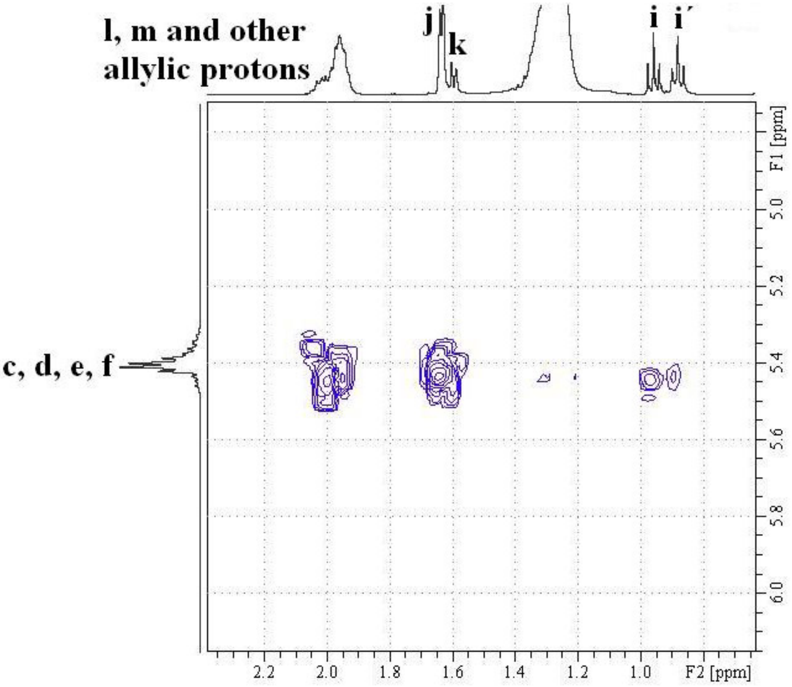

Figure 5.18. ^{1}H-^{1}H long range COSY spectrum of *hb*-PMDUS, obtained using diethyl ether as solvent.

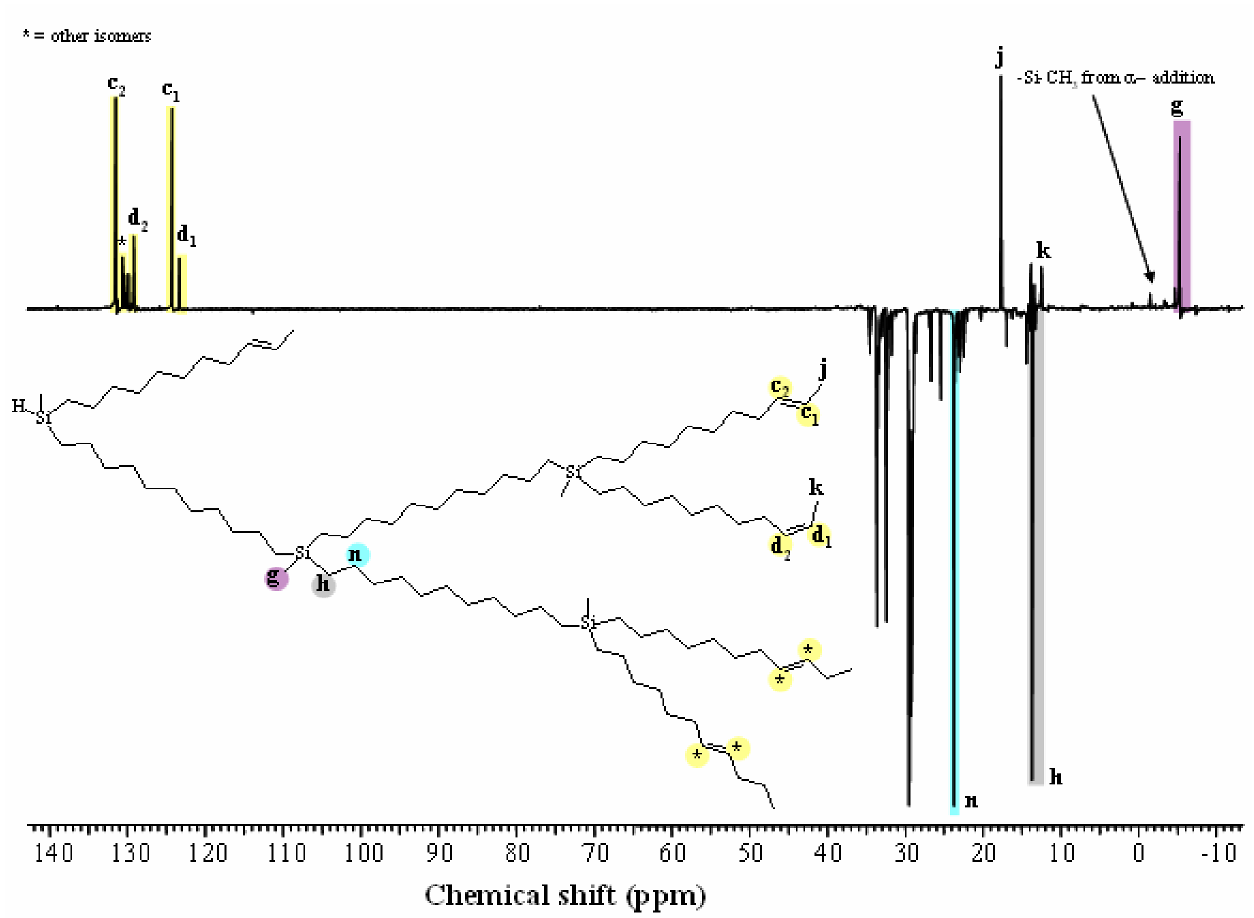

Figure 5.19. ^{13}C NMR DEPT of *hb*-PMDUS, obtained using diethyl ether as solvent, in $CDCl_3$.

The corresponding ^{13}C NMR DEPT spectrum is shown in Figure 5.19. The carbon resonances at 139.5 and 114.5 ppm are absent, agreeing with the analysis from the ^{1}H NMR in that isomerization of the double bonds is complete. The positive signals “c_1”, “c_2” and “d_1” and “d_2” correspond respectively to the methine carbons resulting from an isomerization of the double bonds in the 2-position (*trans*-2 and *cis*-2 isomers with a high *trans*:*cis* ratio). Coupling of these methine carbons with the corresponding allylic and methyl protons can be seen in the ^{1}H-^{13}C long range HETCOR spectrum (Figure 5.20). In the vicinity of the *trans*-2 and *cis*-2 methine carbons are other small carbon signals (denoted by an asterisk), which were previously noticeable in smaller ratios and correspond to methine carbons from other olefin isomers. One of this methine carbons shows coupling with “i”, which was assigned to the methyl protons from other isomers along the chain. In the upfield region the positive signals “j” and “k”, assigned to the methyl carbons generated by isomerization in the 2-position, are now more intense as expected from a complete isomerization. In this case, they are additionally surrounded by other small carbon signals that are coupled with the proton signals "i" and "i´" and therefore assigned to the methyl protons generated by isomerization in other positions along the alkyl chain (Figure 5.21).

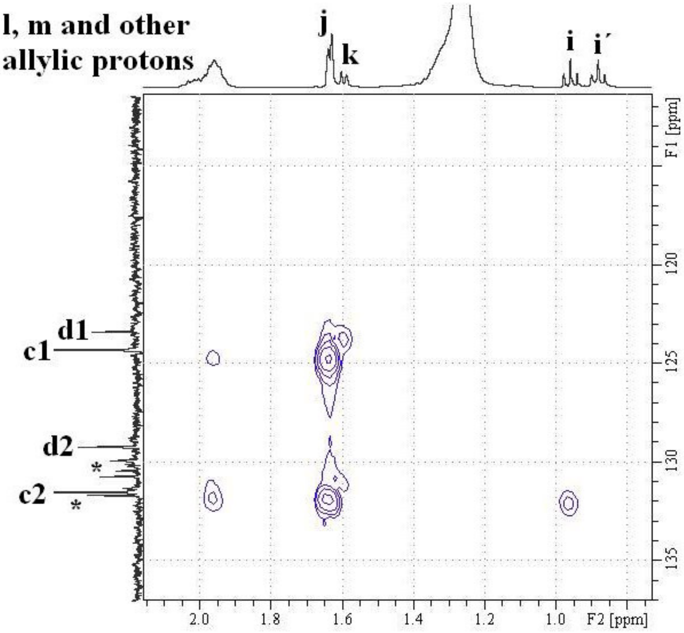

Figure 5.20. ^{1}H-^{13}C long range HETCOR spectrum of *hb*-PMDUS, obtained using diethyl ether as solvent.

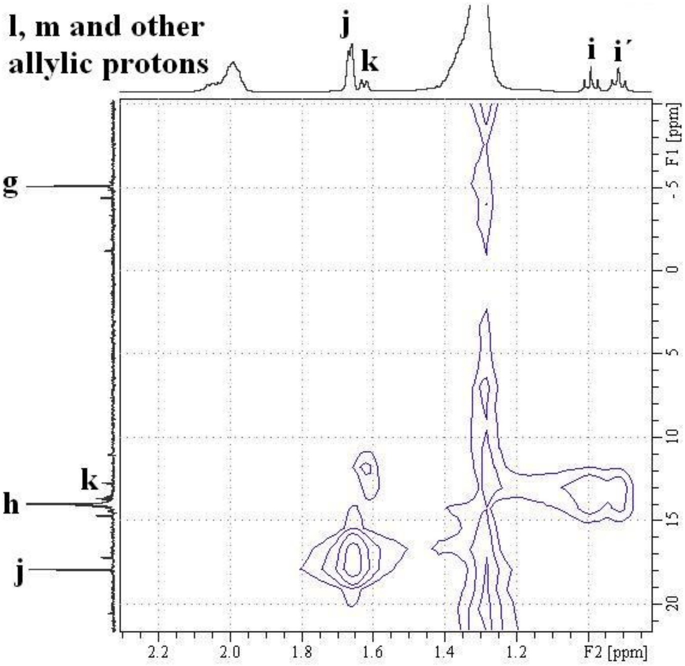

Figure 5.21. ^{1}H-^{13}C HETCOR spectrum of *hb*-PMDUS, obtained using diethyl ether as solvent.

The hydrosilylation reaction yielded a very small fraction of α-addition products as indicated by the ^{1}H and ^{13}C NMR spectra, which show the presence of other small peaks near the Si-CH$_3$ proton and carbon peak "g".

The ^{1}H and ^{13}C NMR spectra of PDMUS brush-like polymer are analogous to the PMDUS hyperbranched structure. Nonetheless, in the case of PDMUS the polyaddition of AB (DMUS) monomers yields polymers with one terminal Si-H (if no "cyclization" has taken place) and one sole alkenyl group. Therefore, the DP$_n$ and $\overline{M}_n$ of the resulting polymer can be calculated by comparing the relative intensitities of the Si-CH$_3$ and olefinic groups in the ^{1}H NMR spectrum. Only isomerized double bonds were discernible in the ^{1}H and ^{13}C NMR spectra of linear PDMUS, regardless of the solvent used for polymerization. Furthermore, alkene hydrogenation could have taken place, but this is difficult to assure as the number of end groups of linear PDMUS is small compared to *hb*-PMDUS. A tiny multiplet at 3.6 ppm was also distinguished , which is most probably due to Si-H groups. This demonstrates the lower probability for the AB monomers to "cyclize", in agreement with the GPC results.

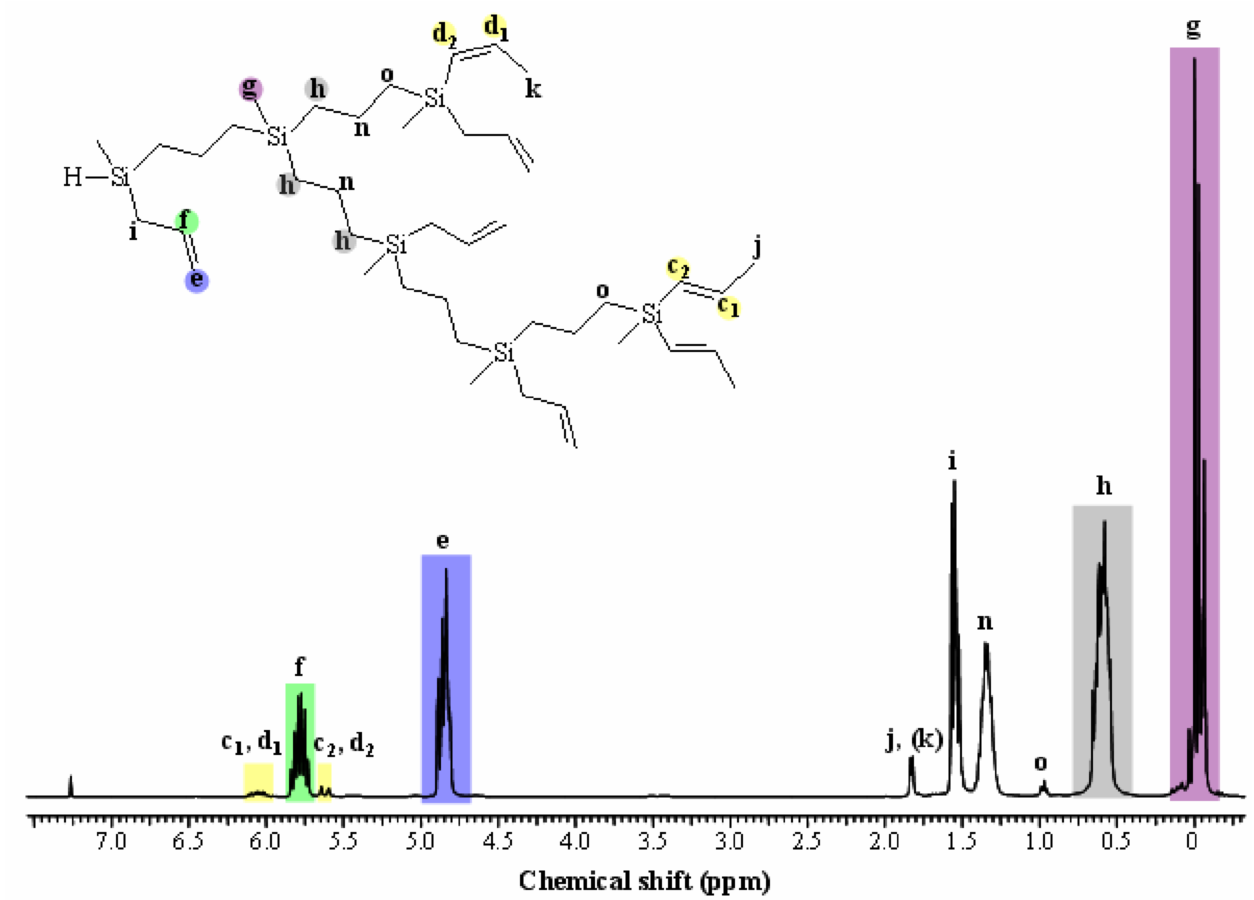

Figure 5.22. ^{1}H NMR of *hb*-PMDAS in CDCl$_3$.

The ^{1}H NMR spectrum of *hb*-PMDAS, resulting from polymerization in pentane with the Karstedt catalyst, is presented in Figure 5.22. For comparison, the ^{1}H NMR of the corresponding monomer (MDAS) is presented in Chapter 3 (Figure 3.11). Alike MDAS, the methylene and methine protons of the allylic double bonds appear as multiplets at 4.8 (signal “e”) and 5.8 (signal “f’) ppm. However, in PMDAS there are other small signals in the olefinic region that can be assigned to the isomerized *trans*-2 (signals “c_1” and “c_2”) and *cis*-2 (signals “d_1” and “d_2”) methine protons. This is verified by examining the ^{1}H-^{1}H COSY spectrum of *hb*-PMDAS (Figure 5.23). The small signals of the isomerized protons are not coupled with the proton signals of the terminal double bonds. The relative integration of the isomerized to terminal olefinic protons indicate that isomerization occurs for about 2.5 % of the double bonds. There is no evidence for the Si-H peak in the region between 3-4 ppm, indicating the presence of “cyclized” monomer and/or “cyclized” oligomers. In the upfield region, the Si-CH_3 signal “g” is now separated in several peaks, reflecting that the silicon atoms to which the CH_3 groups are attached have different substituents. At least four types of Si-CH_3 signals are distinguishable and these correspond to the dendritic (D), linear (L), terminal (T) and terminal isomerized ($T_{\text{isomerized}}$) units. The proton signal “i” at 1.5 ppm corresponds as in the monomer to the allylic protons. This is furthermore demonstrated by the exclusive coupling of “i” with the protons of the terminal double bonds “e” and “f’ (Figure 5.24). The new signal “h” at 0.6 ppm is attributed to the Si-CH_2 protons of D, L and T units, while the new small peak “o” at 0.97 ppm corresponds to the Si-CH_2 protons of T units possessing isomerized double bonds ($T_{\text{isomerized}}$). The methyl groups as a result of the *trans*-2 and *cis*-2 isomerization (signals “j” and “k”) give a small peak at 1.8 ppm and couple correspondingly with the isomerized protons “c_1”, “c_2” and “d_1” and “d_2” (Figure 5.24). The CH_2 protons resulting from the hydrosilylation of an allyl branch are designed as “n” and appear at 1.3 ppm.

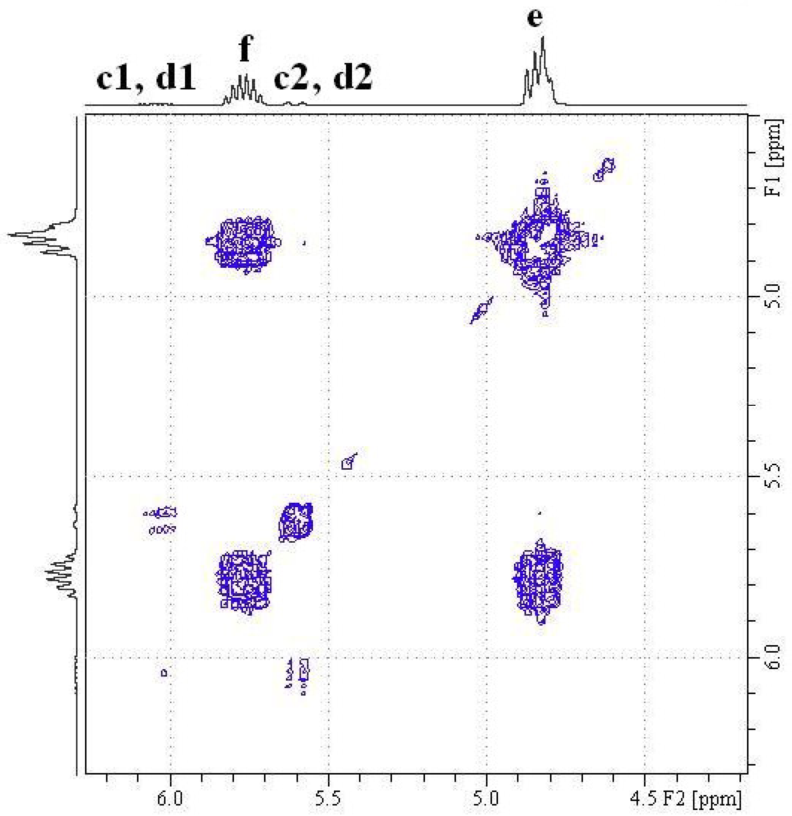

Figure 5.23. ^{1}H-^{1}H COSY spectrum of *hb*-PMDAS.

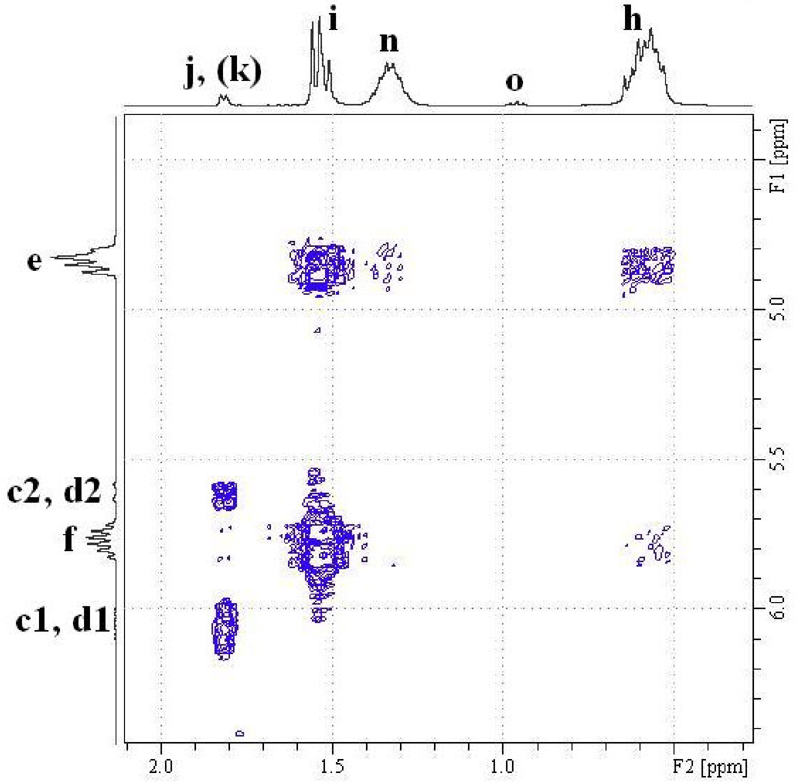

Figure 5.24. ^{1}H-^{1}H long range COSY spectrum of *hb*-PMDAS.

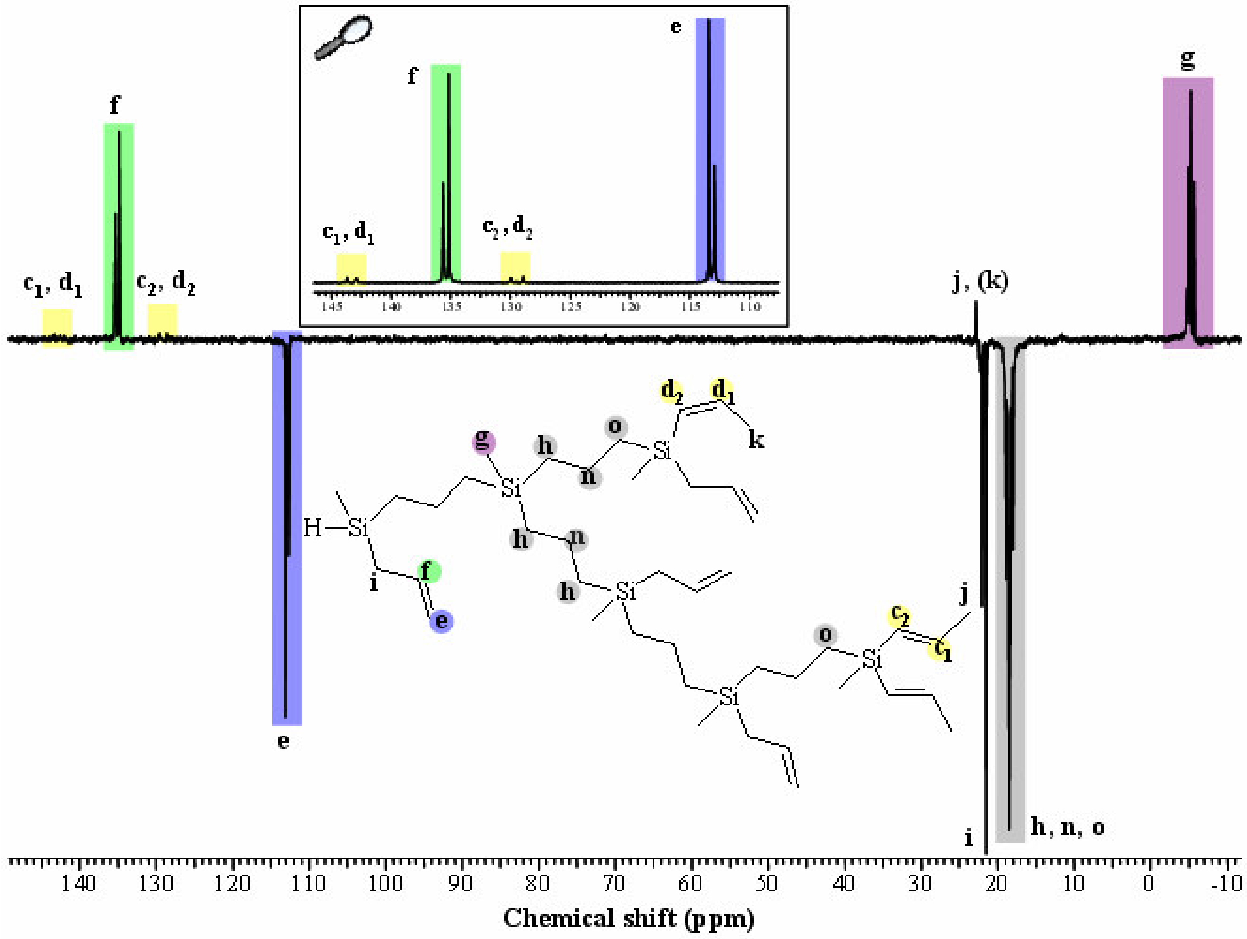

Figure 5.25. ^{13}C NMR DEPT of *hb*-PMDAS in $CDCl_3$.

The ^{13}C NMR DEPT of *hb*-PMDAS is shown in Figure 5.25. The ^{13}C NMR spectrum of MDAS is presented in the Appendix of Chapter 3 (Figure A3.13). In comparison with MDAS monomer, the negative methylene "e" and positive methine "f" carbon double bond signals in the polymer are now split respectively into two different signals. The more intense carbon signals of "e" and "f" correspond to the olefinic terminal carbons of the silicon L units, while the less intense to the ones of the silicon T units. This will be explained later by quantitative ^{29}Si NMR. Enlargement of the olefinic region allows the perception of the methine carbon peaks of the isomerized double bonds. The methine carbon signals of the *trans*-2-isomer ("c_1" and "c_2") appear at 143.6 and 129.9 ppm, whereas the *cis*-2-isomer signals "d_1" and "d_2" at 142.9 and 128.9 ppm respectively. The carbon chemical shift of the $Si-CH_3$ group (signal "g") is split after polymerization into five detectable peaks, demonstrating the branching nature of the polymer. The more intense three peaks possibly correspond to L, T and D units respectively and the two smaller peaks to $T_{\text{isomerized}}$ units possessing one or two isomerized double bonds, respectively. This agrees with the ^{1}H NMR results, where 4 signals for the protons of the Si-CH_3 group were at least observed. The absence of a fifth signal in the ^{1}H NMR spectrum could be related to the lower number of scans performed in the experiment. Additionally, there are new positive signals labeled “j” and “k”, which due to the coupling with the isomerized protons, are assigned to the methyl groups resulting from the *trans*-2 and *cis*-2 isomerization (Figure 5.26). The ^{1}H-^{13}C HETCOR spectrum in Figure 5.27 shows the coupling of the isomerized methine carbon signal with the methyl protons “j” and “k” of the resulting isomerization, verifying the assignment of these signals in the ^{1}H NMR spectrum. Likewise, the “e” and “f” carbon signals show coupling with the previously assigned methylene allylic protons labeled “i”. The CH_2 groups of the short polymer alkyl chain (“h”, “n” and “o”) give a negative multiplet at 18.3 ppm. This carbon multiplet peak shows, excluding the tiny signal “o”, coupling with the corresponding protons “h and “n” (Figure 5.28).

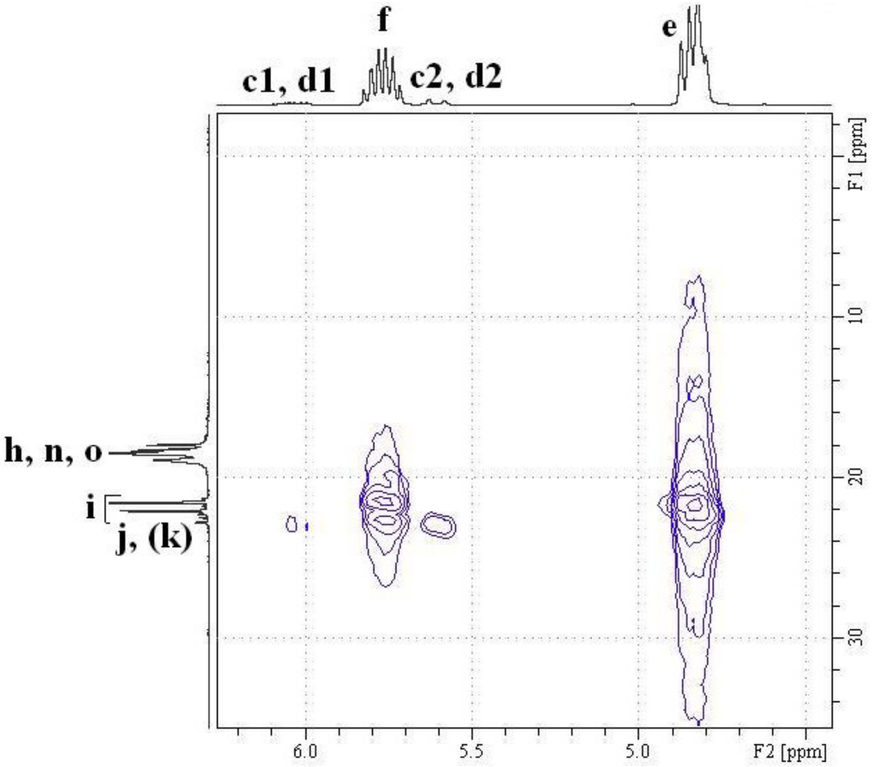

Figure 5.26. ^{1}H-^{13}C long range HETCOR spectrum of *hb*-PMDAS.

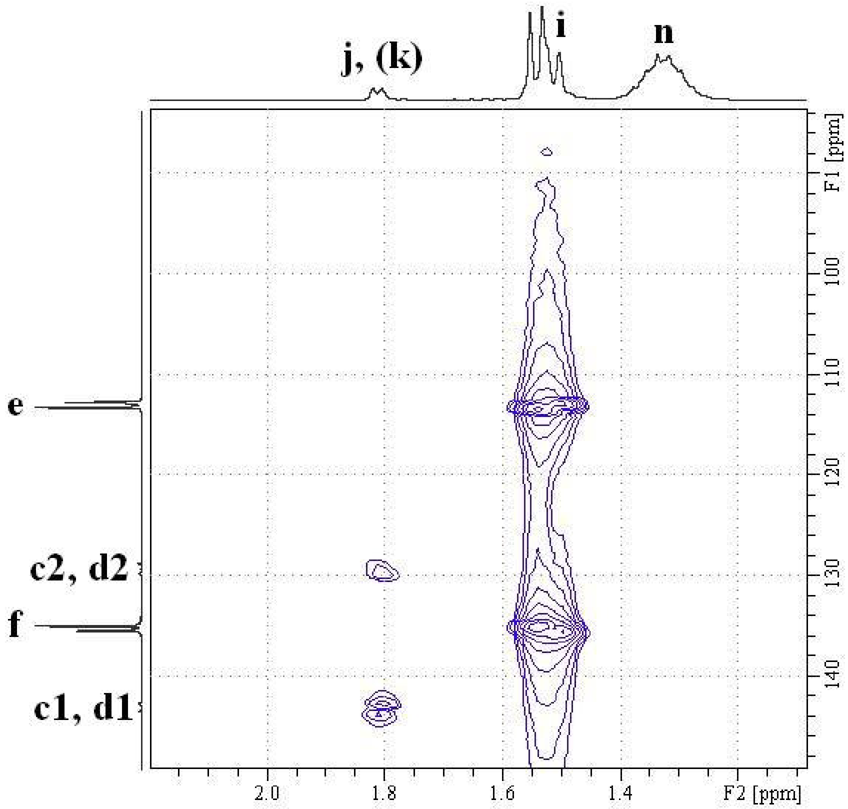

Figure 5.27. ^{1}H-^{13}C long range HETCOR spectrum of *hb*-PMDAS.

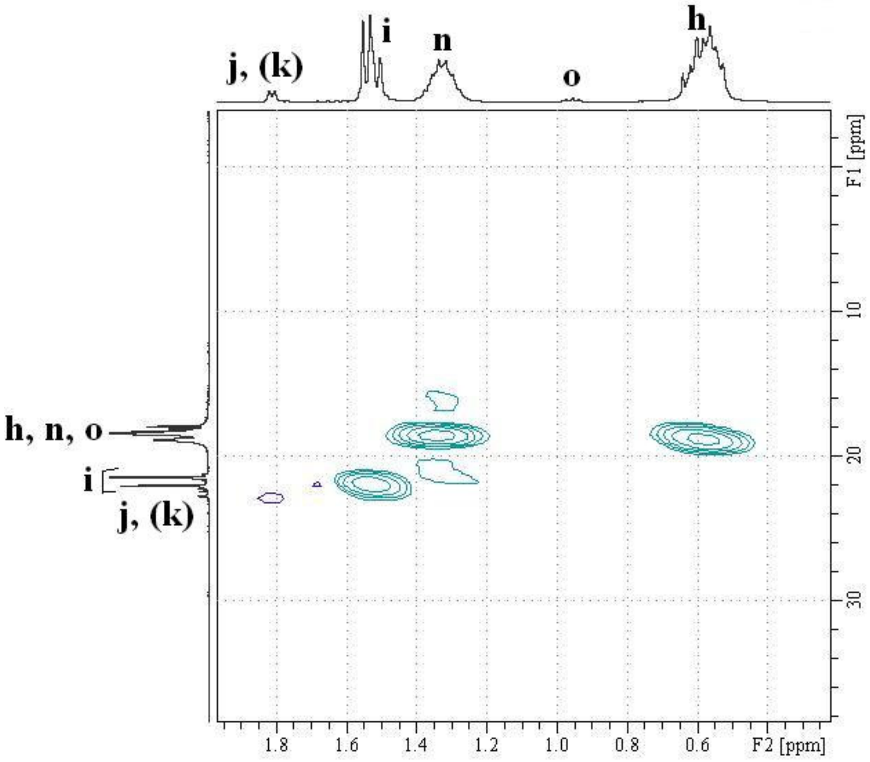

Figure 5.28. ^{1}H-^{13}C HETCOR spectrum of *hb*-PMDAS.

Polymerization of MDAS in diethyl ether at r.t. in the presence of the Karstedt catalyst gives a slightly higher percentage of isomerized double bonds (6 % *vs.* 2.5 %). The higher isomerization in diethyl ether is moreover enhanced to *ca.* 10 % when the reaction is performed at 70 °C. This is confirmed not only by the relative integration ratio of the isomerized to the terminal olefinic protons, but also by the presence of the signals "j", "k" and "o" with relative higher integration values in the ^{1}H NMR spectrum.

Analysis of the ^{1}H and ^{13}C NMR spectra of *hb*-PTUS and *hb*-PTAS give analogous chemical shifts and tendencies as those obtained for *hb*-PMDUS and *hb*-PMDAS. The only difference is the absence of the Si-CH$_3$ groups arising from the AB$_3$ branching structure.

5.2.5 Degree of branching

The DB is one of the key parameters for the characterization of hyperbranched polymers.[12,21] The branched nature of PMDAS and PTAS was confirmed by ^{1}H and ^{13}C NMR spectra. However, additional information about the branching structures of the polycarbosilanes can be obtained by quantitative ^{29}Si NMR analysis. No information on the shape of the polymers can be given for *hb*-PMDUS and *hb*-PTUS because the long undecenyl chain does not permit to distinguish the different silicon environments. In other words, only one signal was obtained in the ^{29}Si NMR of these polymers. In contrast, the different branch units in *hb*-PMDAS and *hb*-PTAS bearing allyl substituents can be discerned.

The ^{29}Si NMR of *hb*-PMDAS shows five groups of peaks, which can be assigned from left to right to the D, L and T silicon units and reflect the branching structure of the polymer (Figure 5.29). The T silicon units are divided into three signals: a more intense peak (T$_0$) and two smaller peaks (T$_1$ and T$_2$), depending if the T groups possess none (T$_0$), one (T$_1$) or two (T$_2$) isomerized double bonds. There is additionally a small peak to the right of the L silicon units, which can be tentatively assigned to the L units having isomerization of the double bond. The ^{29}Si NMR shifts of *hb*-PMDAS are presented in Table 5.2. Furthermore, the areas of the peaks allow an estimation of the relative amount of D, L and T units and these are presented in Table 5.3. It is noticeable that the relative amount of L is somehow higher than T. If we assume equal reactivities of all B groups and complete conversion of all monomers we can calculate a theoretical DB and the relative amount of individual units according to the equations derived by Hölter and Frey (Equations 5.1 and 5.2).[21a] Using the equation derived in the literature (Equation 5.1) and according to the ^{29}Si NMR a DB value of 0.63 is obtained for *hb*-PMDAS and this is slightly higher than the theoretical value of 0.50 (Table 5.3). This discrepancy is due to the higher integration of L:T monomer units and might possibly be due to an error in the ^{29}Si NMR peak integration values, resulting from baseline noise in the spectrum, which can be rather large.

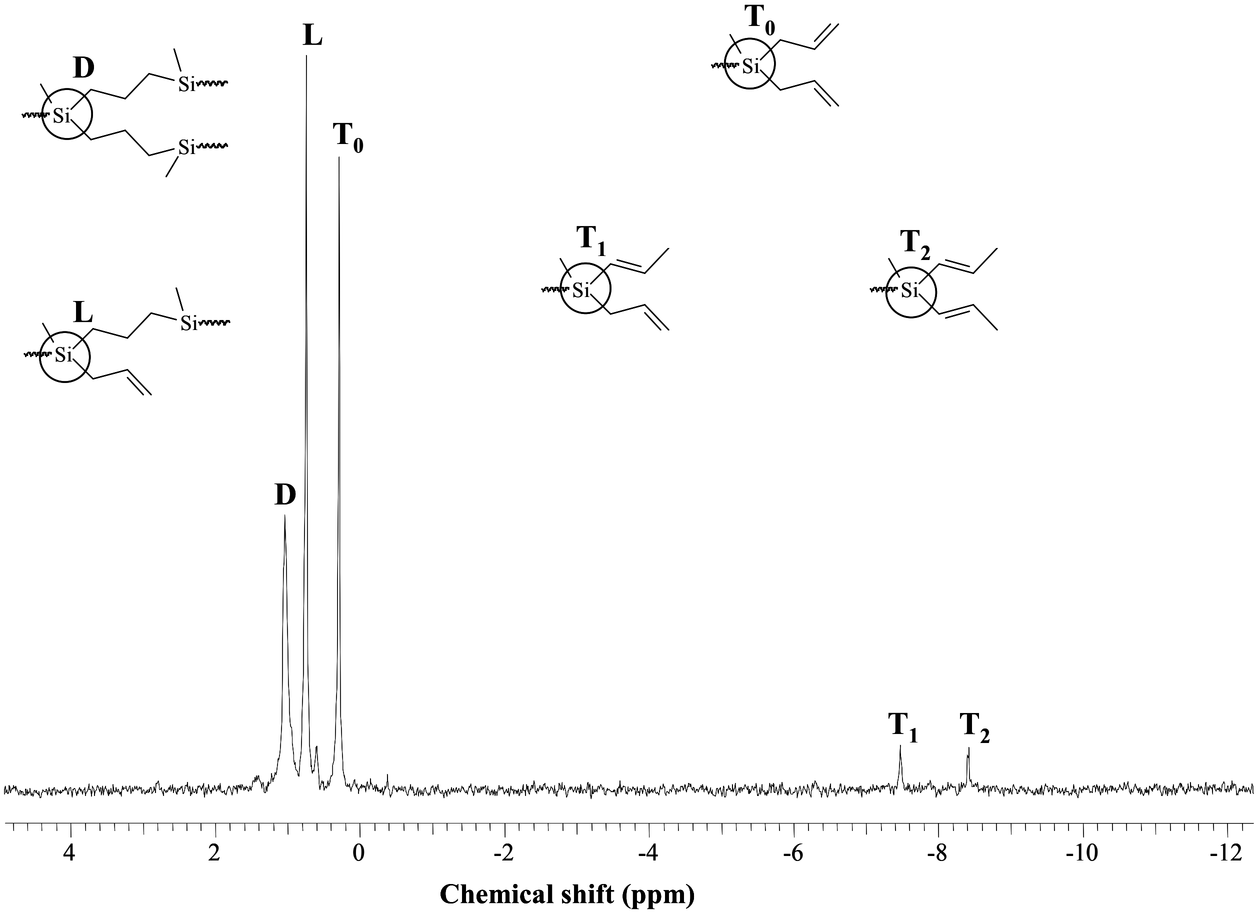

Figure 5.29. ^{29}Si NMR of *hb*-PMDAS in CDCl$_3$ and possible silicon atom environments within the polymer.

Table 5.2. ^{29}Si NMR shifts of *hb*-PMDAS and *hb*-PTAS structures.

	^{29}Si chemical shifts						
Compound	**Si^{D}**	**Si^{sD}**	**Si^{L}**	**Si^{T0}**	**Si^{T1}**	**Si^{T2}**	**Si^{T3}**
hb-PMDAS	1.04	---	0.75	0.29	-7.47	-8.42	---
hb-PTAS	0.49	0.15	-0.4	-1.05	-7.73	-8.8	-10.01

Table 5.3. Relative amounts of the different branching monomer units and calculated DB for *hb*-PMDAS and *hb*-PTAS structures.

	Relative abundances								
Compound	**D**	**sD**	**L**	**T**^{a}	**T$_0$**	**T$_1$**	**T$_2$**	**T$_3$**	**DB**
hb-PMDAS	32	---	37	31	26	2.5	2.5	---	0.63^b
hb-PTAS	8	17	28	47	34	2.8	5.4	4.8	0.57^c

^{a}T = $T_0+T_1+T_2+T_3$. ^{b}Theoretical value: 0.50. ^{c}Theoretical value: 0.44

$$DB = \frac{2D}{2D+L}$$

Equation 5.1. DB for AB*2* systems as derived by Hölter and Frey.

$$DB = \frac{2D+sD}{\frac{2}{3}(3D+2sD+L)}$$

Equation 5.2. DB in AB*3*-type hyperbranched polymers as derived by Hölter and Frey.

The ^{29}Si NMR of PTAS shows seven peaks. These are assigned as presented in Figure 5.30. PTAS possess a branched AB*3* structure and therefore two more additional peaks are expected, when comparing to PMDAS. One additional peak (sD) is observed when two of the three branches have reacted and the other one when complete isomerization of the double bonds in a T unit (T_3) have occurred. The small peak to the right of the sD units might be due to sD units with isomerized double bonds. The ^{29}Si NMR shifts of *hb*-PTAS and the relative abundances of D, sD, L and T units are presented respectively in Tables 5.2 and 5.3. From the spectral integration a DB value of 0.57 was calculated, which is close to the theoretically expected value of 0.44 (Equation 5.2).[21a] This deviation is due to the unexpected higher ratio of T:L silicon atoms and might only be explained in terms of the errors within the experimental integration values. Lach *et al.* reported before on the quantitative ^{29}Si NMR spectrum (from 4.5 to -4.5 ppm) of a random AB*3* PTAS. Nevertheless, the signals T_1, T_2 and T_3 from isomerized terminal monomer units were not identified.

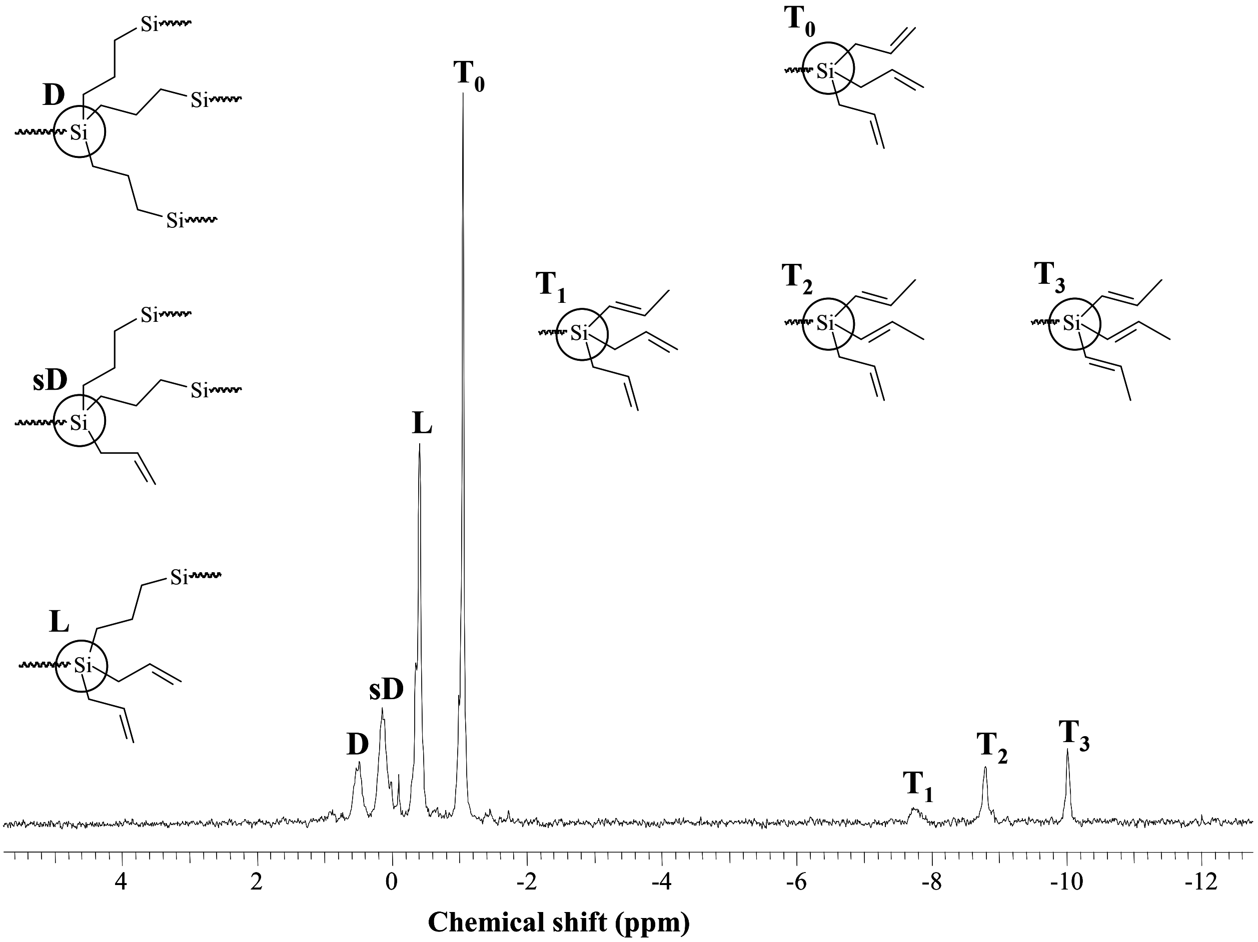

Figure 5.30. ^{29}Si NMR of *hb*-PTAS in $CDCl_3$ and possible silicon atom environments in the polymer.

5.2.6 Thermal properties

Thermal characterization of the polycarbosilanes was performed by DSC. The DSC thermograms are shown in Figure 5.31. All the polymers exhibit a low T_g, reflecting the conformational freedom of the carbosilane scaffold and despite the presence of different branching patterns, the T_gs are similar. In dendritic and hyperbranched polymers, the number of branches (a factor that tends to increase the T_g) and the number of end groups (a factor that tends to diminish T_g) grow in parallel and therefore no significant dependence of T_g values on molecular weights is expected.[22]

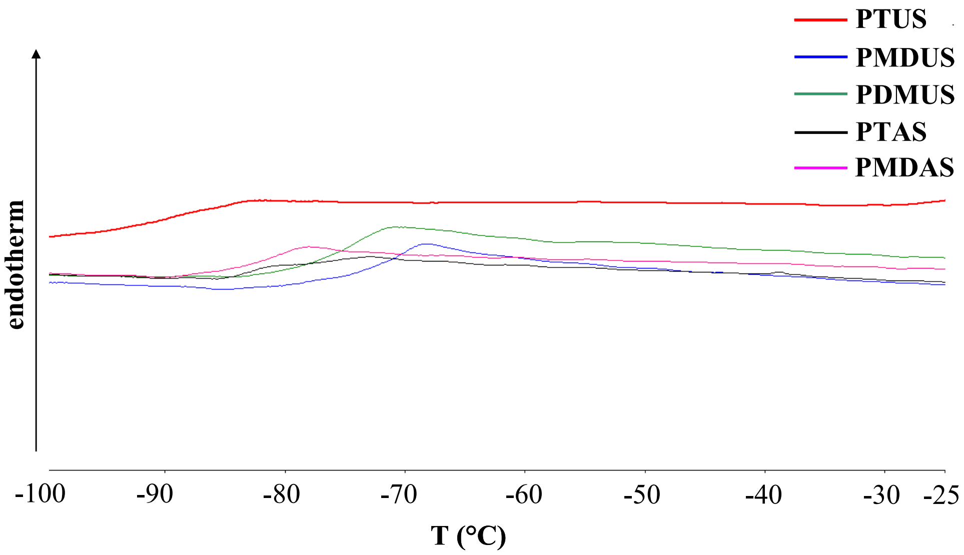

Figure 5.31. Glass transition temperature (T_g) of the polyalkenylsilanes, scanning rate 10 °C/min.

5.3 CONCLUSIONS

Several known alkenylsilane monomers like MDUS, MDAS and TAS and some new structures as DMUS and TUS were used for the synthesis of hyperbranched and brush-like polycarbosilanes. A "one-pot" synthesis approach by polyhydrosilylation of the AB_n polyfunctional monomers (fast and cheap) in the presence of the Karstedt catalyst was employed. The polymers were analyzed by GPC and showed, as expected, relatively broad polydispersities (PDI in the range of 2.5 to 5) and limited molecular weights. All materials were contaminated with low-molecular weight components. However, samples were not fractionated in order to identify the different oligomeric species. It is supposed that intramolecular cyclization between Si-H and terminal double bonds led to different cyclic species as no Si-H bonds left were in general identified in the ^{1}H NMR spectra of the resulting polymers. Thus, the limited growth of the polymers can be explained by the tendency of the different oligomeric species to form cyclic species. Additionally, side-reactions like isomerization and hydrogenation of the terminal double bonds occurred (as confirmed by NMR analysis), diminishing therefore the number of reactive functionalities. Raising the reaction temperature increased the fraction of isomerized species and isomerization was significant when using MDUS with the longer undecenyl chain. In fact, analysis of *hb*-PMDUS showed that *ca.* 45-65 % of the double bonds were isomerized. High molecular weight impurities were also noticeable, particularly when using MDAS AB_2 monomer. These impurities grew with increasing reaction times and could only be explained by rearrangement reactions, which seemed more prevalent when using the AB_2 monomer having the shorter allyl chain. Table 5.4 shows a summary of the structural characteristics found for the synthesized polyalkenylsilanes.

Table 5.4. Structural characterization of the synthesized polyalkenylsilanes.

			^{1}H NMR	**^{29}Si NMR**
Monomer	**Polymer**	**Structure**	**Isomerization (%)[a]**	**DB**
MDUS	PMDUS	hyperbranched	45-65	---
DMUS	PDMUS	linear	100	---
TUS	PTUS	hyperbranched	100	---
MDAS	PMDAS	hyperbranched	2.5	0.63
TAS	PTAS	hyperbranched	10	0.57

[a] Polymerizations were performed in toluene at r.t. with the Karstedt catalyst. In general, lower degrees of isomerization were obtained for more concentrated solutions, whereas temperature increased the number of isomerized species.

In general and agreeing with previous results, dilution of the monomer led to lower molecular weights. It is obvious that dilute concentrations enhance the probability of cyclization. Moreover, the greater the branching multiplicity, the higher will be the probability of cyclization.

Structural characterization of the polycarbosilanes was performed by NMR spectroscopy and 2D NMR experiments permitted unequivocal assignment of all spectral resonances. The choice of solvent demonstrated to have an influence on the structure of the polymer. This was more pronounced when utilizing *hb*-MDUS: a partially isomerized hyperbranched structure was obtained when using either pentane or toluene as solvent, while a completely isomerized structure was attained when employing diethyl ether.

The branched nature of the polycarbosilanes was confirmed in the case of *hb*-PMDAS and *hb*-PTAS by ^{1}H, ^{13}C and quantitative ^{29}Si NMR spectra. The DBs were calculated by making use of the integration values of the different signals in the ^{29}Si NMR spectrum and these showed to be within the reasonable limits of the theoretical calculated values. The different terminal isomerized branching units were also identified by ^{29}Si NMR analysis.

5.4 EXPERIMENTAL

Synthesis of PMDUS. 0.006 mmol of Karstedt catalyst (61 µL of the Pt solution) were added under argon to a solution of MDUS (1 g, 2.85 mmol) in toluene (10 ml), and the system was stirred at r.t. for 24 hours. The resulting polymer was isolated by precipitation in methanol to give **PMDUS** (0.75 g, $\overline{M}_w$ = 13,000 g/mol, PDI = 3.7, T_g = -74 °C).

^{1}H NMR (400 MHz, $CDCl_3$): δ (ppm) -0.07 ($Si-CH_3$), 0.5 ($Si-CH_2$), 1.1-1.5 (polymer backbone), 1.62 (m, $-CH_2-CH=CH-C\mathbf{H}_3$, *cis*), 1.65 (m, $-CH_2-CH=CH-C\mathbf{H}_3$, *trans*), 1.98 (m, $-C\mathbf{H}_2-CH=CH-CH_3$, *cis* and *trans*), 2.05 (m, $-C\mathbf{H}_2-CH=CH_2$), 4.9 (m, $-CH=C\mathbf{H}_2$), 5.3-5.5 (m, $-C\mathbf{H}=C\mathbf{H}-$), 5.8 (m, $-C\mathbf{H}=CH_2$); ^{13}C NMR (100 MHz, $CDCl_3$): δ (ppm) -4.73 ($Si-CH_3$), 13.11 ($\mathbf{C}H_3-CH=CH-$, *cis*), 14.28 ($Si-CH_2$), 18.30 ($\mathbf{C}H_3-CH=CH-$, *trans*), 23.90, 24.33 ($Si-CH_2-\mathbf{C}H_2-$), 26, 27.25, 29.37, 29.58, 29.66, 29.75, 29.81, 29.97, 30.09, 30.21, 33.02, 33.57, 34.21, 34.26, 114.5 ($\mathbf{C}H_2=CH-$), 123.9 ($CH_3-\mathbf{C}H=CH-$, *cis*), 124.8 ($CH_3-\mathbf{C}H=CH-$, *trans*), 131.2 ($CH_3-CH=\mathbf{C}H-$, *cis*), 132.9 ($CH_3-CH=\mathbf{C}H-$, *trans*), 139.5 ($\mathbf{C}H_2=CH-$).

Note. Identical reaction conditions were employed for the synthesis of PMDUS using diethyl ether as solvent:

^{1}H NMR (400 MHz, $CDCl_3$): δ (ppm) -0.09 ($Si-CH_3$), 0.5 ($Si-CH_2$), 0.88 (m, $-CH=CH-CH_2-CH_2-C\mathbf{H}_3$), 0.96 (m, $-CH=CH-CH_2-C\mathbf{H}_3$), 1.1-1.4 (polymer backbone), 1.60 (m, $-CH_2-CH=CH-C\mathbf{H}_3$, *cis*), 1.63 (m, $-CH_2-CH=CH-C\mathbf{H}_3$, *trans*), 1.96 (m, $-C\mathbf{H}_2-CH=CH-CH_3$, *cis* and *trans*), 5.3-5.5 (m, $-C\mathbf{H}=C\mathbf{H}-$); ^{13}C NMR (100 MHz, $CDCl_3$): δ (ppm) -4.74 ($Si-CH_3$), 13.10 ($\mathbf{C}H_3-CH=CH-$, *cis*), 14.27 ($Si-CH_2$), 18.28 ($\mathbf{C}H_3-CH=CH-$, *trans*), 23.09, 23.51, 24.30 ($Si-CH_2-\mathbf{C}H_2-$), 26, 27.24, 29.24, 29.53, 29.65, 29.71, 29.80, 29.89, 30.04, 30.08, 30.20, 32.33, 32.97, 33.02, 34.0, 34.2, 35.1, 123.9 ($CH_3-\mathbf{C}H=CH-$, *cis*), 124.8 ($CH_3-\mathbf{C}H=CH-$, *trans*), 129.7 ($CH_3-CH=\mathbf{C}H-$, *cis*), 130.4, 131.2, 131.8, 131.9, 132.1 ($CH_3-CH=\mathbf{C}H-$, *trans*), 132.2.

Synthesis of PDMUS. 0.005 mmol of Karstedt catalyst (51 µL of the Pt solution) were added under argon to a solution of DMUS (1 g, 4.7 mmol) in toluene (10 ml), and the system was stirred at r.t. for 24 hours. The resulting polymer was isolated by precipitation in methanol to give **PDMUS** (0.73 g, $\overline{M}_w$ = 6,100 g/mol, PDI = 2.04, T_g = -76.2 °C).

^{1}H NMR (400 MHz, $CDCl_3$): δ (ppm) -0.06 ($Si-CH_3$), 0.49 ($Si-CH_2$), 0.89 (m, $-CH=CH-CH_2-CH_2-C\mathbf{H}_3$), 0.97 (m, $-CH=CH-CH_2-C\mathbf{H}_3$), 1.1-1.4 (polymer backbone), 1.61 (m, $-CH_2-$

CH=CH-C**H**$_3$, *cis*), 1.65 (m, -CH$_2$-CH=CH-C**H**$_3$, *trans*), 1.98 (m, -C**H**$_2$-CH=CH-CH$_3$, *cis* and *trans*), 3.6 (m, Si-H), 5.3-5.5 (m, -C**H**=C**H**-); ^{13}C NMR (100 MHz, CDCl$_3$): δ (ppm) -2.96 (Si-CH$_3$), 13.95 (**C**H$_3$-CH=CH-, *cis*), 15.69 (Si-CH$_2$), 18.34 (**C**H$_3$-CH=CH-, *trans*), 23.10, 23.50, 23.83, 24.29 (Si-CH$_2$-**C**H$_2$-), 29.23, 29.39, 29.52, 29.62, 29.79, 30.02, 30.20, 33.84, 33.94, 34.1, 35.1, 123.9 (CH$_3$-**C**H=CH-, *cis*), 124.8 (CH$_3$-**C**H=CH-, *trans*), 129.7 (CH$_3$-CH=**C**H-, *cis*), 130.4, 131.05, 131.3, 132.1 (CH$_3$-CH=**C**H-, *trans*), 132.2.

Synthesis of PTUS. 0.006 mmol of Karstedt catalyst (67 µL of the Pt solution) were added under argon to a solution of TUS (1 g, 2.05 mmol) in toluene (10 ml), and the system was stirred at r.t. for 24 hours. The resulting polymer was isolated by precipitation in methanol to give **PTUS** (0.73 g, $\overline{M}_w$ = 8,300 g/mol, PDI = 3.8, T_g = -90.1 °C).

^{1}H NMR (400 MHz, CDCl$_3$): δ (ppm) 0.49 (Si-CH$_2$), 0.88 (m, -CH=CH-CH$_2$-CH$_2$-C**H**$_3$), 0.96 (m, -CH=CH-CH$_2$-C**H**$_3$), 1.1-1.5 (polymer backbone), 1.61 (m, -CH$_2$-CH=CH-C**H**$_3$, *cis*), 1.64 (m, -CH$_2$-CH=CH-C**H**$_3$, *trans*), 1.96 (m, -C**H**$_2$-CH=CH-CH$_3$, *cis* and *trans*), 5.3-5.5 (m, -C**H**=C**H**-).

Synthesis of PMDAS. 0.0158 mmol of Karstedt catalyst (171 µL of the Pt solution) were added under argon to a solution of MDAS (1 g, 7.9 mmol) in toluene (10 ml), and the system was stirred at r.t. for 24 hours. The resulting polymer was isolated by precipitation in methanol to give **PMDAS** (0.56 g, $\overline{M}_w$ = 10,600 g/mol, PDI = 3.2, T_g = -82.8 °C).

^{1}H NMR (400 MHz, CDCl$_3$): δ (ppm) -0.03 (m, Si-CH$_3$, D, L, T and $T_{isomerized}$), 0.6 (Si-CH$_2$, D, L and T), 0.97 (Si-CH$_2$, $T_{isomerized}$), 1.34 (m, Si-CH$_2$-C**H**$_2$-CH$_2$-Si), 1.55 (m, -C**H**$_2$-CH=CH$_2$), 1.8 (m, -CH=CH-C**H**$_3$), 4.85 (m, -CH=C**H**$_2$), 5.62 (m, -C**H**=CH-CH$_3$, *cis* and *trans*), 5.78 (m, -C**H**=CH$_2$), 6.06 (m, -CH=C**H**-CH$_3$, *cis* and *trans*); ^{13}C NMR (100 MHz, CDCl$_3$): δ (ppm) -5.36 (Si-CH$_3$), -4.96 (Si-CH$_3$), -4.83 (Si-CH$_3$), -4.63 (Si-CH$_3$), -4.46 (Si-CH$_3$), 18.62, 18.75, 18.86, 19.16, 19.24, 21.61, 21.84 (-**C**H$_2$-CH=CH$_2$), 22.07, 22.38, 22.60, 22.80, 23.10 (-CH=CH-**C**H$_3$), 112.96 (**C**H$_2$=CH-, T), 113.40 (**C**H$_2$=CH-, L), 128.96 (CH$_3$-CH=**C**H-, *cis*), 129.95 (CH$_3$-CH=**C**H-, *trans*), 135.14 (CH$_2$=**C**H-, L), 135.64 (CH$_2$=**C**H-, T), 142.90 (CH$_3$-**C**H=CH-, *cis*), 143.69 (CH$_3$-**C**H=CH-, *trans*); ^{29}Si NMR (80 MHz, CDCl$_3$): δ (ppm) 1.04 (Si, D), 0.75 (Si, L), 0.29 (Si, T), -7.47 (Si, $T_{isomerized}$, one isomerized double bond), -8.42 (Si, $T_{isomerized}$, two isomerized double bonds).

Synthesis of PTAS. 0.0198 mmol of Karstedt catalyst (213 μL of the Pt solution) were added under argon to a solution of TAS (1 g, 6.6 mmol) in toluene (10 ml), and the system was stirred at r.t. for 24 hours. The resulting polymer was isolated by precipitation in methanol to give **PTAS** (0.5 g, $\overline{M}_w$ = 7,100 g/mol, PDI = 4.6, T_g = -81.8 °C).

^{1}H NMR (400 MHz, $CDCl_3$): δ (ppm) 0.6 (Si-CH_2, D, L and T), 0.97 (Si-CH_2, $T_{isomerized}$), 1.35 (m, Si-CH_2-C**H**$_2$-CH_2-Si), 1.57 (m, -C**H**$_2$-CH=CH_2), 1.8 (m, -CH=CH-C**H**$_3$), 4.85 (m, -CH=C**H**$_2$), 5.58 (m, -C**H**=CH-CH_3, *cis* and *trans*), 5.78 (m, -C**H**=CH_2), 6.08 (m, -CH=C**H**-CH_3, *cis* and *trans*); ^{29}Si NMR (80 MHz, $CDCl_3$): δ (ppm) 0.49 (Si, D), 0.15 (Si, sD), -0.4 (Si, L), -1.05 (Si, T), -7.73 (Si, $T_{isomerized}$, two isomerized double bonds), -8.8 (Si, $T_{isomerized}$, two isomerized double bonds), -10.01 (Si, $T_{isomerized}$, three isomerized double bonds).

5.5 REFERENCES

[1] (a) Voit, B. *J. Polym. Sci., Polym. Chem.* **2005**, *43*, 2679. (b) Gao, C.; Yan, D. *Prog. Polym. Sci.* **2004**, *29*, 183. (c) Jikei, M.; Kakimoto, M. *Prog. Polym. Sci.* **2001**, *26*, 1233. (d) Sunder, A.; Heinemann, J.; Frey, H. *Chem. Eur. J.* **2000**, *6*, 2499. (e) Kim, Y. H. *Polym. Mater. Sci. Eng.* **1999**, *80*, 61. (f) Feast, W. J.; Cacialli, F.; Daik, R.; Friend, R. H.; Herzog, E.; Heywood, B. R.; Hobson, L.; Megson, J. L.; Snowden, D. *Macromol. Symp.* **1999**, *143*, 81. (g) Hult, A.; Johansson, M.; Malmström, E. *Adv. Polym. Sci.* **1999**, *143*, 1. (h) Turner, S. R. *Polym. Mater. Sci. Eng.* **1995**, *73*, 77.

[2] (a) Wei, H. Y.; Shi, W. F.; Yuan, H. Y.; Chen, Y. L. *J. Appl. Polym. Sci.* **2001**, *80*, 51. (b) Wooley, K. L.; Fréchet, J. M. J.; Hawker, C. J. *Polymer* **1994**, *53*, 4489. (c) Hult, A.; Malmström, E.; Johansson, M.; Sörensen, K.; Swed. Patent SE468771 1993 (U. S. Patent 5,418,301. (d) Hawker, C. J.; Lee, R.; Fréchet, J. M. J. *J. Am. Chem. Soc.* **1991**, *113*, 4583.

[3] Yao, J. Z.; Son, D. Y. *J. Polym. Sci., Part A: Polym. Chem.* **1999**, *37*, 3778.

[4] Flory, P. J. *J. Am. Chem. Soc.* **1952**, *74*, 2718.

[5] (a) Gong, C.; Miravet, J.; Fréchet, J. M. J. *J. Polym. Sci., Part A: Polym. Chem.* **1999**, *37*, 3193. (b) Dušek, K.; Šomvársky, J.; Smrčkova, M.; Simonsick, W. J.; Wilczek, Jr., L. *Polym. Bull.* **1999**, *42*, 489. (c) Cameron, C.; Fawcett, A. H.; Hetherington, C. R.; Mee, R. A. W.; McBride, F. V. *J. Chem. Phys.* **1998**, *108*, 8235.

[6] (a) Oishi, M.; Minakawa, M.; Imae, I.; Kawakami, Y. *Macromolecules* **2002**, *35*, 4938. (b) Xiao, Y.; Wong, R. A.; Son, D. Y. *Macromolecules* **2000**, *33*, 7232. (c) Schlenk, C.; Kleij, A. W.; Frey, H.; van Koten, G. *Angew. Chem. Int. Ed.* **2000**, *39*, 3445. (d) Paulasaari, J. K.; Weber, W. P. *Macromolecules* **2000,** *33*, 2005. (e) Paulasaari, J. K.;

Weber, W. P. *Macromol. Chem. Phys.* **2000**, *201*, 1585. (f) Lach, C.; Frey, H. *Macromolecules* **1998**, *31*, 2381. (g) Miravet, J. F.; Fréchet, J. M. J. *Macromolecules* **1998**, *31*, 3461. (h) Muzafarov, A. M.; Rebrov, E. A.; Gorbacevich, O. B.; Golly, M.; Gankema, H.; Möller, M. *Macromol. Symp.* **1996**, *102*, 35. (i) Muzafarov, A. M.; Golly, M.; Möller, M. *Macromolecules* **1995**, *28*, 8444. (j) Rubinsztajn, S.; Stein, J. *J. Inorg. Organomet. Polym.* **1995**, *5*, 43. (k) Rubinsztajn, S. *J. Inorg. Organomet. Polym.* **1994**, *4*, 61. (l) Whitmarsh, C. K.; Interrante, L. V. *Organometallics* **1991**, *10*, 1336. (m) Mathias, L. J.; Carothers, T. W. *J. Am. Chem. Soc.* **1991**, *113*, 4043.

[7] (a) Lang, H.; Lühmann, B. *Adv. Mater.* **2001**, *13*, 1523. (b) Frey, H.; Schlenk, C. *Topics in Current Chemistry* **2000**, 210, 69. (c) Majoral, J.-P.; Carminade, A.-M. *Chem. Rev.* **1999**, *99*, 845. (d) Frey, H.; Schlenk, H. *Monatshefte für Chemie* **1999**, *130*, 3. (e) Uchida, H.; Kabe, Y.; Yoshino, K.; Kawamata, A.; Tsumuraya, T.; Masamune, S. *J. Am. Chem. Soc.* **1990**, *112*, 7077.

[8] (a) Interrante, L. V.; Rushkin, I.; Shen, Q. *Appl. Organomet. Chem.* **1998**, *12*, 695. (b) Interrante, L. V.; Whitmarsch, W.; Sherwood, W. Ceram. Trans. **1995**, *58*, 111.(c) Whitmarsch, C. K.; Interrante, L. V. U. S. Patent 5,153,295 1992.

[9] Yoon, K.; Son, D. Y. *Macromolecules* **1999**, *32*, 5210.

[10] Muzafarov, A. M.; Gorbacevich, O. B.; Rebrov, E. A.; Ignat'eva, G. M.; Chenskaya, T. B.; Myakushev, V. D.; Bulkin, A. F.; Papkov, V. S. *Polym. Sci.* **1993**, *35*, 1575.

[11] Lach, C.; Müller, P.; Frey, H.; Mülhaupt, R. *Macromol. Rapid Commun.* **1997**, *18*, 253.

[12] Hölter, D.; Frey, H. *Acta Polym.* **1997**, *48*, 298.

[13] (a) Drohmann, C.; Möller, M.; Gorbatsevich, O. B.; Muzafarov, A. M. *J. Polym. Sci., Part A: Polym. Chem.* **2000**, *38*, 741. (b) Drohmann, C.; Gorbatsevich, O. B.; Muzafarov, A. M.; Möller, M. *Polym. Prep.* **1998**, *39*, 471.

[14] Gong, C. G.; Miravet, J.; Fréchet, J. M. J. *J. Polym. Sci., Part A: Polym. Chem.* **1999**, *37*, 3193.

[15] Burgath, A.; Sunder, A.; Frey, H. *Macromol. Chem. Phys.* **2000**, *201*, 782.

[16] Illuminati, G.; Mandolini, L. *Acc. Chem. Res.* **1981**, *14*, 95.

[17] Yao, J; Son, D. Y. *Organometallics* **1999**, *18*, 1736.

[18] Xiao, Y.; Wong, R. A.; Son, D. Y. *Macromolecules* **2000**, 33, 7232.

[19] (a) Ashby, B. A.; Modic, F. J. US Patent 4,288,345, 1981. (b) Karstedt, B. D. (General Electric) US Patent 3,715,334, 1973.

[20] C. Schlenk, Dissertation, Institut für Makromolekulare Chemie, Albert-Ludwigs-Universität, Freiburg 2001.

[21] (a) Hölter, D.; Burgath, A.; Frey, H. Acta Polym. **1997**, *48*, 30. (b) Hawker, C. J.; Lee, R.; Fréchet, J. M. J. *J. Am. Chem. Soc.* **1991**, *113*, 4583.

[22] Stutz, H. *J. Polym. Sci., Part B: Polym. Phys. B* **1995**, *33*, 333.

CHAPTER 6

LINEAR-HYPERBRANCHED DIBLOCK COPOLYMERS CONSISTING OF POLYSTYRENE AND DENDRITIC POLYCARBOSILANE BLOCK*

6.1 INTRODUCTION

In recent years, with the development of controlled synthetic techniques,[1] interest has increased in complex copolymer architectures of well-defined structures, to acquire a better understanding of the relation between chemical structure and morphology of block copolymers.[2] Within these new systems, nonlinear miktoarm star block copolymers[2f] have been synthesized by the group of Hadjichristidis to investigate the influence of chain architecture on polymer properties.[3] Comparison of these systems with linear block copolymers has revealed that the macromolecular architecture not only strongly affects the morphology of the domain borders but can also introduce new morphologies.[4] More recently, block copolymers containing cascade-branched blocks, particularly AB-diblock structures consisting of a linear and a dendrimer-block, have been studied by several groups and were found to exhibit unusual solution, solid-state and interfacial properties that were distinctively different from their linear counterparts.[5] However, the preparation of a perfectly branched dendron-block represents a time-consuming multi-step synthesis. In addition, the size of the dendrimer block is limited to the respective generations. While there are a considerable number of publications devoted to the preparation and characterization of these linear-dendritic architectures,[5a] very little literature exits concerning solid-state or thin film properties.[6]

In this chapter we describe an innovative, general strategy for the preparation of well-defined diblock copolymers combining a hyperbranched and a linear block (Figure 6.1). In this manner, linear-hyperbranched polycarbosilane diblock copolymers have been prepared via the hypergrafting reaction of methyldiundec-10-enylsilane (MDUS), as a branched AB_2 monomer, from the polybutadiene core (PBD) of the anionically synthesized polystyrene-*block*-poly(1,2-butadiene) diblock copolymers (PS_x-*b*-PBD_y). The MDUS monomer with its long alkyl chain was initially chosen because it is plausible that the long alkyl chain would reduce the likelihood of cyclization reactions.[7] The slow monomer addition (SMA) synthetic

---

*this chapter has been published in: (a) *Polymer Preprints* **2003**, *44*, 534. (b) *Macromolecules* **2006**, *39*, 971.

approach[8] has been employed for the preparation of the linear-hyperbranched materials, since it permits control of the size of the hyperbranched block. In addition, the SMA is compared with one-pot procedures, regarding the grafting efficiency. Finally, complete characterization and solid-state morphological studies of the resulting linear-hyperbranched diblock copolymer systems are presented and discussed.

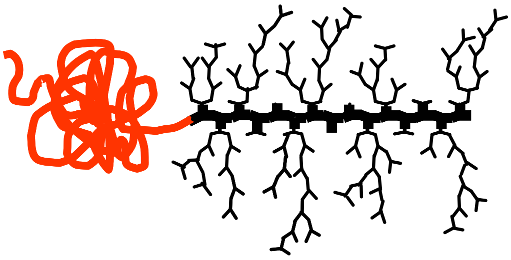

Figure 6.1. Schematic picture of the linear-hyperbranched architecture.

6.2 NOMENCLATURE

Linear-hyperbranched diblock copolymers are denoted by PS_x-*b*-[PBD_y-*hb*-$PCSi_z$], in which *x* indicates the degree of polymerization (DP_n) of the PS block, *y* the DP_n of the 1,2-PBD block and *z* indicates DP_n of the polycarbosilane block (PCSi). The hyperbranched block is represented by [PBD_y-*hb*-$PCSi_z$], wherein the short 1,2-PBD block is regarded as being part of the final PCSi block. However, for ease of presentation all of the polymers presented will be given an acronym. For example the polymer PS_{520}-*b*-[PBD_{47}-*hb*-$PCSi_{46}$] is abbreviated **P_3LH_{25}**. **P_3** refers to the linear block PS_{520}-*b*-PBD_{47} and **LH_{25}** denotes a linear-hyperbranched diblock copolymer with a weight percentage fraction of 25 for the PCSi block (including the short PBD-backbone). For details on the composition of the linear diblock copolymers, see Chapter 2 (Table 2.1).

6.3 RESULTS AND DISCUSSION

6.3.1 Synthetic strategy and compositional characterization

The hyperbranched block was prepared via the SMA strategy in order to achieve "pseudo chain growth" kinetics.[8] In this procedure, a dilute solution of MDUS monomer was slowly added (12-36 hours) to a concentrated solution of the PS_x-*b*-PBD_y diblock copolymer in decaline in the presence of the Karstedt catalyst (Figure 6.2).[9] The choice of monomer solvent was driven by the necessity that the diblock reaction mixture concentration should remain constant and so a low boiling point monomer solvent, *i.e.* pentane, was required. The reaction was performed at 70 °C, which resulted in the constant removal of the monomer solvent. The amount of silane monomer used depended on the desired molecular weight of the hyperbranched block. The nomenclature and abbreviations of the linear-hyperbranched diblock copolymers obtained are given in Table 6.1.

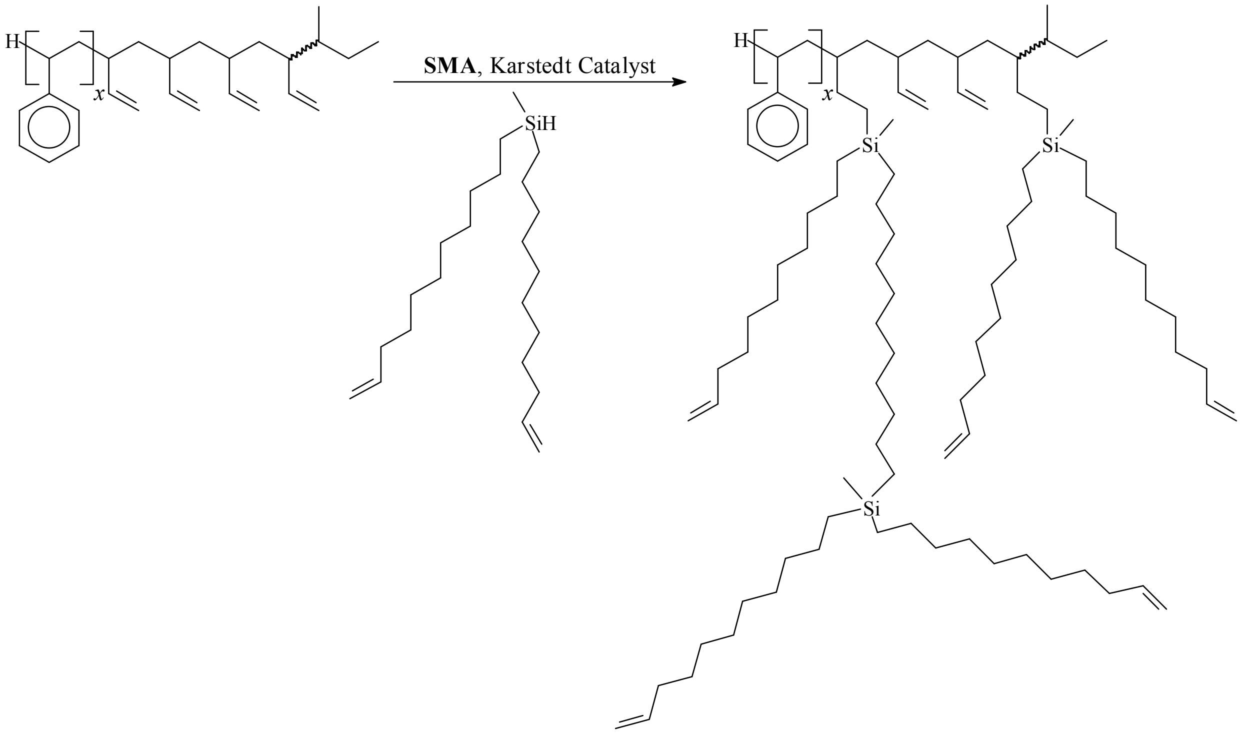

Figure 6.2. Synthesis of linear-hyperbranched diblock copolymers by grafting of branched AB_2 MDUS monomers from a short PBD-block of PS_x-*b*-PBD_y (The PBD block has an atactic configuration, although for simplicity the vinyl groups have been only depicted on one side).

Table 6.1. Designation of the AB Linear-Hyperbranched Block Copolymers.

Sample	**Acronym**[a]
PS$_{520}$-*b*-[PBD$_{47}$-*hb*-PCSi$_{46}$]	**P$_3$LH$_{25}$**
PS$_{520}$-*b*-[PBD$_{47}$-*hb*-PCSi$_{61}$]	**P$_3$LH$_{30}$**
PS$_{520}$-*b*-[PBD$_{47}$-*hb*-PCSi$_{76}$]	**P$_3$LH$_{35}$**
PS$_{520}$-*b*-[PBD$_{47}$-*hb*-PCSi$_{85}$]	**P$_3$LH$_{37}$**
PS$_{520}$-*b*-[PBD$_{47}$-*hb*-PCSi$_{142}$]	**P$_3$LH$_{49}$**

[a] For example, in **P$_3$LH$_{25}$**: **P$_3$** refers to the linear block PS$_{520}$-*b*-PBD$_{47}$ and **LH$_{25}$** denotes the corresponding linear-hyperbranched diblock copolymer with a weight fraction of 25 % for the PCSi block (including the short PBD-backbone)

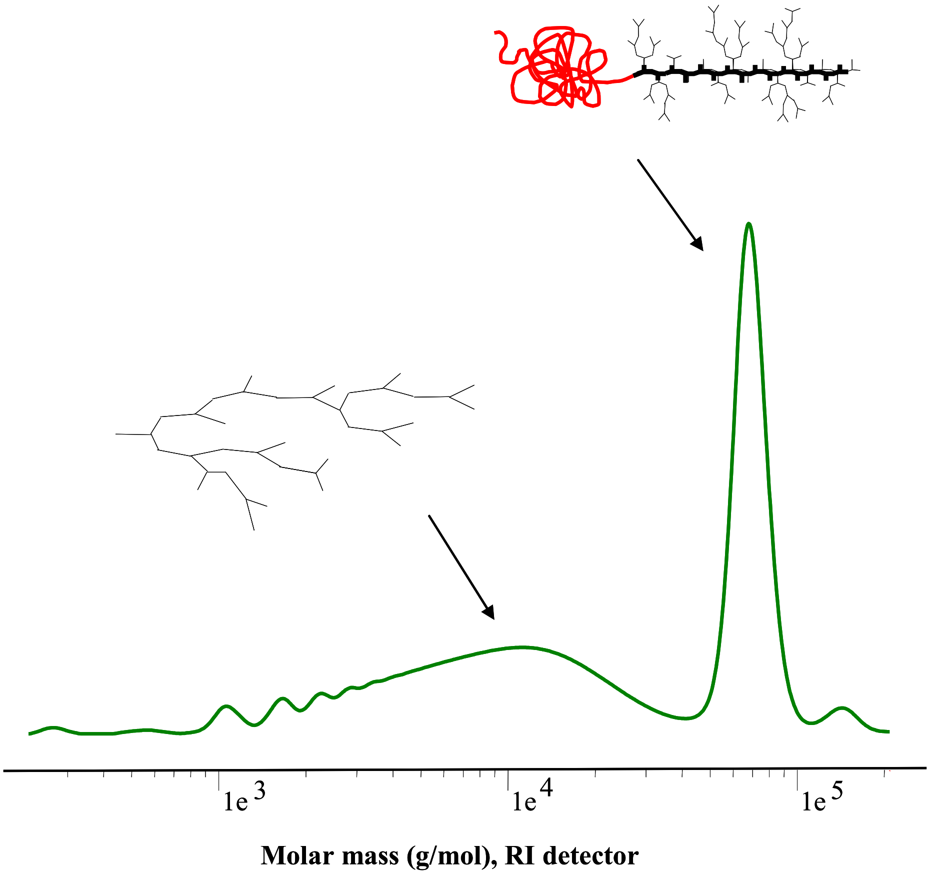

Figure 6.3. GPC chromatogram of the crude reaction product of **P$_3$LH$_{35}$**.

GPC analysis of the crude reaction product showed a bimodal molecular weight distribution (Figure 6.3). The broad low molecular weight-mode ($\overline{M}_w/\overline{M}_n \sim 3.0$) corresponds to AB_2 monomers polymerized via a step-growth mechanism to build up low molecular weight hyperbranched polycarbosilanes, which can eventually cyclize and therefore cannot be attached to the growing branched diblock structure. However, utilizing the solubility characteristics of the large PS-block, these non-attached hyperbranched polycarbosilane homopolymers were completely separated from the desired hypergrafted diblock copolymers by fractionating precipitation in diethyl ether/methanol.

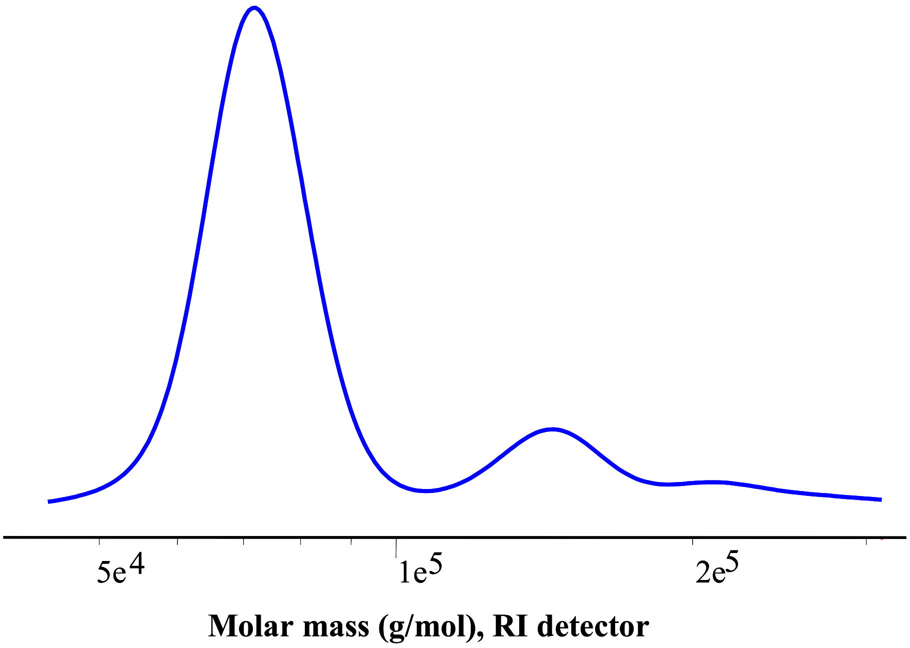

Figure 6.4. GPC chromatogram of $\mathbf{P_3LH_{37}}$ after fractionating precipitation.

For some polymers the GPC chromatograms (Figure 6.4) showed low amounts of a higher molecular weight tail, in addition to the diblock dimer peak (Chapter 2, Figure 2.10). This higher molecular weight peaks were included in the calculation of the molecular weights and thus the polydispersities for the resulting PS_x-*b*-[PBD_y-*hb*-$PCSi_z$] diblocks were slightly larger in comparison to the starting linear diblocks. It is thought that the high concentration of the linear diblock in the reaction medium (7.6 % polymer concentration) may cause a certain amount of “cross linking” of the modified PS_x-*b*-PBD_y diblock copolymers as a consequence of the close proximity of the polymer chains. This small fraction of a supposed undesired gelation can be explained by a dyotropic rearrangement reaction of the AB_2 monomer in the presence of the Karstedt catalyst.[10] This type of rearrangement has been reported for methylbis(undec-10-enyloxy)silane (Chapter 4, Figure 4.19).[11] Likewise, the migration of methyl and undecenyl groups could give monomers of the type B_3 (non-reactive) and A_2B (potential cross linker). Another possible explanation might be thermally induced rearrangement[10a] leading to the formation of radicals in the alkyl chains, which can branch in an intermolecular fashion.

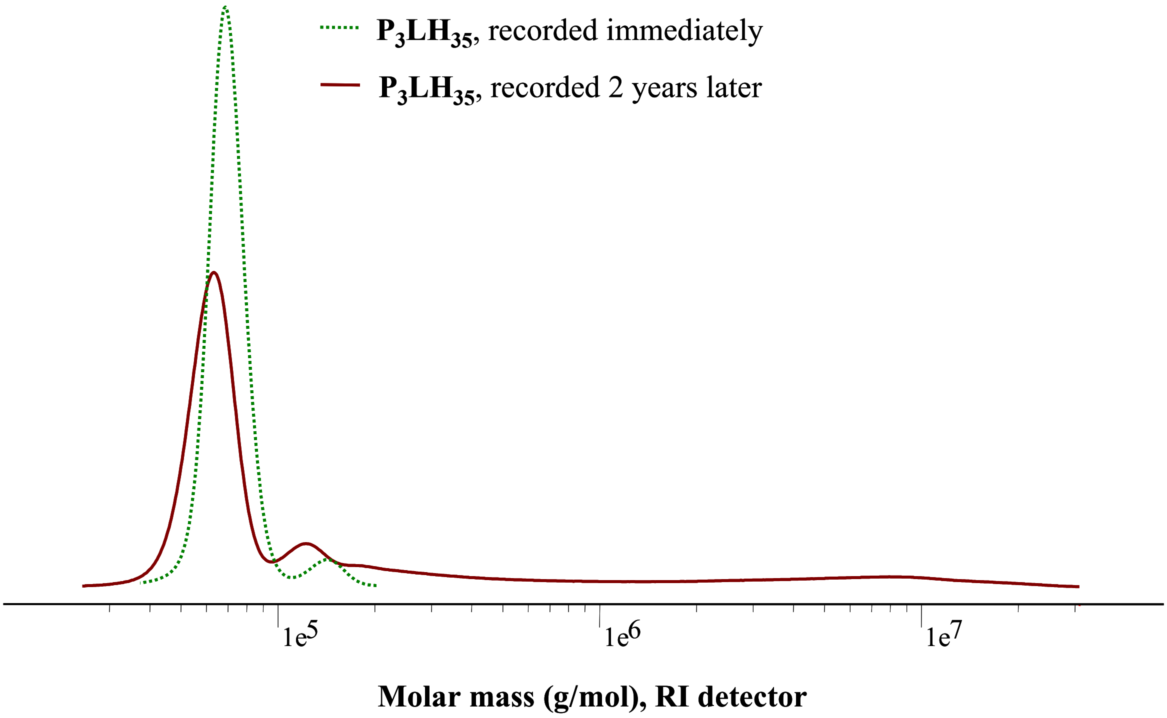

Figure 6.5. GPC plots of $\mathbf{P_3LH_{35}}$ recorded immediately and two years after fractionating precipitation in diethyl ether/methanol.

Moreover, this higher molecular weight tail was not always present in the GPC chromatograms of the freshly precipitated polymers. Repeating the GPC measurements on these polymers, which were stored at room temperature as solids, sometimes gave a noticeable increase in this higher molecular weight shoulder. For example, the GPC chromatograms of freshly prepared $\mathbf{P_3LH_{35}}$ and of a two year old sample, indicating the changing stability with time, are presented in Figure 6.5. There was also a noticeable yellowing of the polymers during storage at room temperature. It is suspected that these polymers are not totally catalyst free and may contain trace amounts of “platinum”, which remains coordinated to the unreacted vinyl groups. It is plausible that this catalyst can cause alkene dimerization with time, resulting in a type of cross linking effect. An in-depth discussion on this type of catalytic alkene dimerization is presented in Chapter 4 (Section

4.3.1.3). Furthermore Ober *et al.* noted that their hydrosiloxane SB modified polymers also showed degradation when stored as solids and they recommended that this type of polymers should be stored as solutions.[10b]

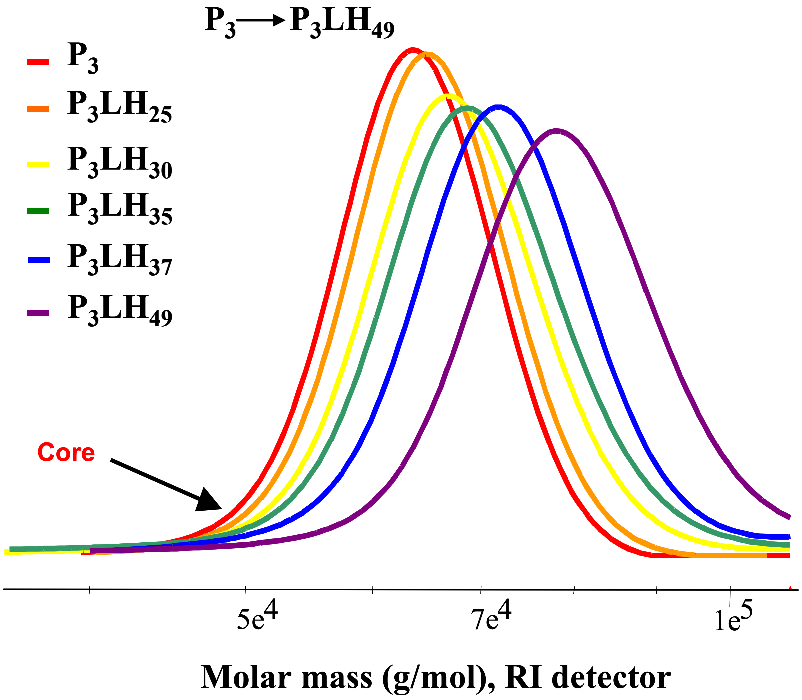

Figure 6.6. GPC diagrams of the linear core (**P_3**, $\overline{M}_n$ = 63,800 g/mol) and of the resulting linear-hyperbranched block copolymers with increasing amount of MDUS monomer added.

Although the SMA does not proceed in an ideal manner, the molecular weight of the resulting linear-hyperbranched polycarbosilane block copolymers increases linearly with the amount of AB_2 monomer added. Hence, very narrow molecular weight distributions were obtained ($\overline{M}_w/\overline{M}_n$ = 1.04-1.25) and the characteristics of a controlled polymerization appear to be fulfilled. This is illustrated in Figure 6.6, which shows the superimposition of the molecular weight distributions of a linear core with five linear-hyperbranched polycarbosilanes, which were obtained with increasing monomer:core mol ratios. Nonetheless, the merit of carrying out the SMA as opposed to one-pot reaction can be appreciated by comparing the GPC chromatograms of the resulting polymers before fractionation (Figure 6.7).

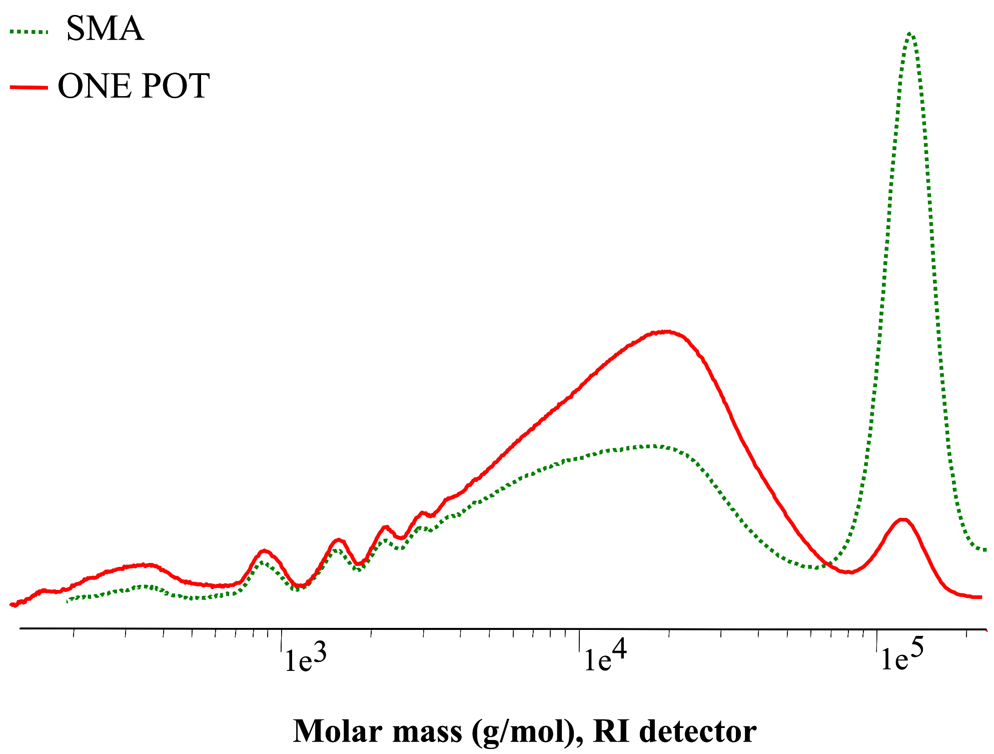

Figure 6.7. Comparison of the GPC chromatograms of a hypergrafting reaction, using MDUS AB_2-type monomer, carried out in one-pot versus SMA mode for the sample $\mathbf{P_5}$ ($\overline{M}_n$ = 127,800 g/mol).

We propose that the formation of the hyperbranched homopolymer, formally representing a new (B_2–type) core molecule, is a consequence of the increased monomer concentration in the reaction mixture during the hypergrafting process, which results in competition between the chain-growth and the step-growth mechanisms. There are several contributing factors that could explain this: (i) due to sterics effects, the large PS block of our PS_x-*b*-PBD_y block copolymer retards the polymer-analogue hydrosilylation reaction, when compared to pure PBD;[12] (ii) isomerization of the carbosilane double bonds during the reaction generates non-reactive internal double bonds of the linear-hyperbranched PS-*b*-polycarbosilanes;[13] (iii) the reactivity of the MDUS monomer can be considered to be relatively low due to the absence of electron-withdrawing groups which are known to expedite the formation of the intermediate Si-Pt complex in the hydrosilylation mechanism;[10a,14] (iv) the induction period for the Karstedt catalyst might be slowed as a consequence of the low silane/C=C concentration ratio at the beginning of the reaction; [13a,15] (v) attachment of the catalytic species to the more flexible, non bulky double bonds of the carbosilanes may be favoured. Anyone or a combination of the above would retard the coupling reaction between the core and the AB_2 monomer.

6.3.2 Chemical structural characterization

The linear-*b*-hyperbranched diblock copolymers, obtained after fractionating precipitation, were characterized by ^{1}H, ^{13}C and ^{29}Si NMR and by IR spectroscopy. An examination of the ^{1}H and ^{13}C NMR spectra reveals that competitive isomerization of the terminal double bonds occurred during the hydrosilylation reaction. A comprehensive discussion on the mechanisms of alkene isomerization, which may occur during metal-assisted hydrosilylation, is presented in Chapter 4 (Section 4.3.1.1). The choice of monomer solvent appeared to have an influence on the hyperbranched structure of the diblock copolymers. For example olefin isomerization was observed when either pentane or diethyl ether was used. However, only partial isomerization occurred when using pentane, while when diethyl ether was employed the degree of isomerization was complete. These results are in agreement with the investigations performed on hyperbranched polycarbosilanes (Chapter 5).

The ^{1}H NMR spectrum of a linear-*b*-hyperbranched diblock copolymer, obtained from the reaction of MDUS with $\mathbf{P_3}$ using pentane as the monomer solvent, is shown in Figure 6.8. For comparison, the ^{1}H NMR of the linear precursor diblock $\mathbf{P_3}$ is presented in Chapter 2 (Figure 2.8). After hypergrafting, the ^{1}H NMR exhibits three signals in the olefinic region. Firstly, a relatively sharp new signal at $\delta = 5.9$ ppm is identified, which is assigned to the methine protons of the pendant vinyl groups of the carbosilane units and is denoted by “f”. Additionally, a further signal at $\delta = 5.0$ ppm is now ascribed to the methylene protons of the pendant vinyl groups of the carbosilane units (signal “e”) and the methylene protons of the unreacted polybutadiene vinyl groups (signal “a”). Finally, the methine protons of the unreacted butadiene units (signal “b”) again give rise to a very broad signal between 5.7 and 5.3 ppm with an additional sharp peak at $\delta = 5.5$ ppm. Examining the ^{1}H-^{1}H COSY spectrum (Figure 6.9) reveals that the sharp signal at $\delta = 5.5$ ppm exhibits no coupling within the olefinic region. A similar effect was found in the ^{1}H correlation spectrum of the analogous hyperbranched polycarbosilanes (Chapter 5, Figure 5.11) and therefore we assign this signal to the isomerized protons of the carbosilane groups labeled “c” and “d”. Other characteristic signals of the attached carbosilane units in the ^{1}H NMR are: the protons of the Si-CH_3 (signal “g”) at 0 ppm and the Si-CH_2 groups at 0.55 ppm (signal “h”) in the ratio 3:6. The signals at 2.1 ppm and 1.7 ppm correspond respectively to the allylic protons of the terminal carbosilane vinyl units (signal “i”) and to the protons of the methyl groups resulting from isomerized vinyl units in the 2-position (signal “j” and “k). The broad peak between 1.8 and 2.05 ppm includes the signals denoted by “l” and “m”, which correspond to the allylic CH_2 protons of the isomerized double bonds. The signal assignment was achieved by analyzing the ^{1}H-^{1}H

COSY spectrum (Figure 6.10) and the clear similarities between the NMR spectra of the linear-hyperbranched polycarbosilanes and the analogous hyperbranched polymers (Chapter 5, Figure 5.12) corroborated these assignments.

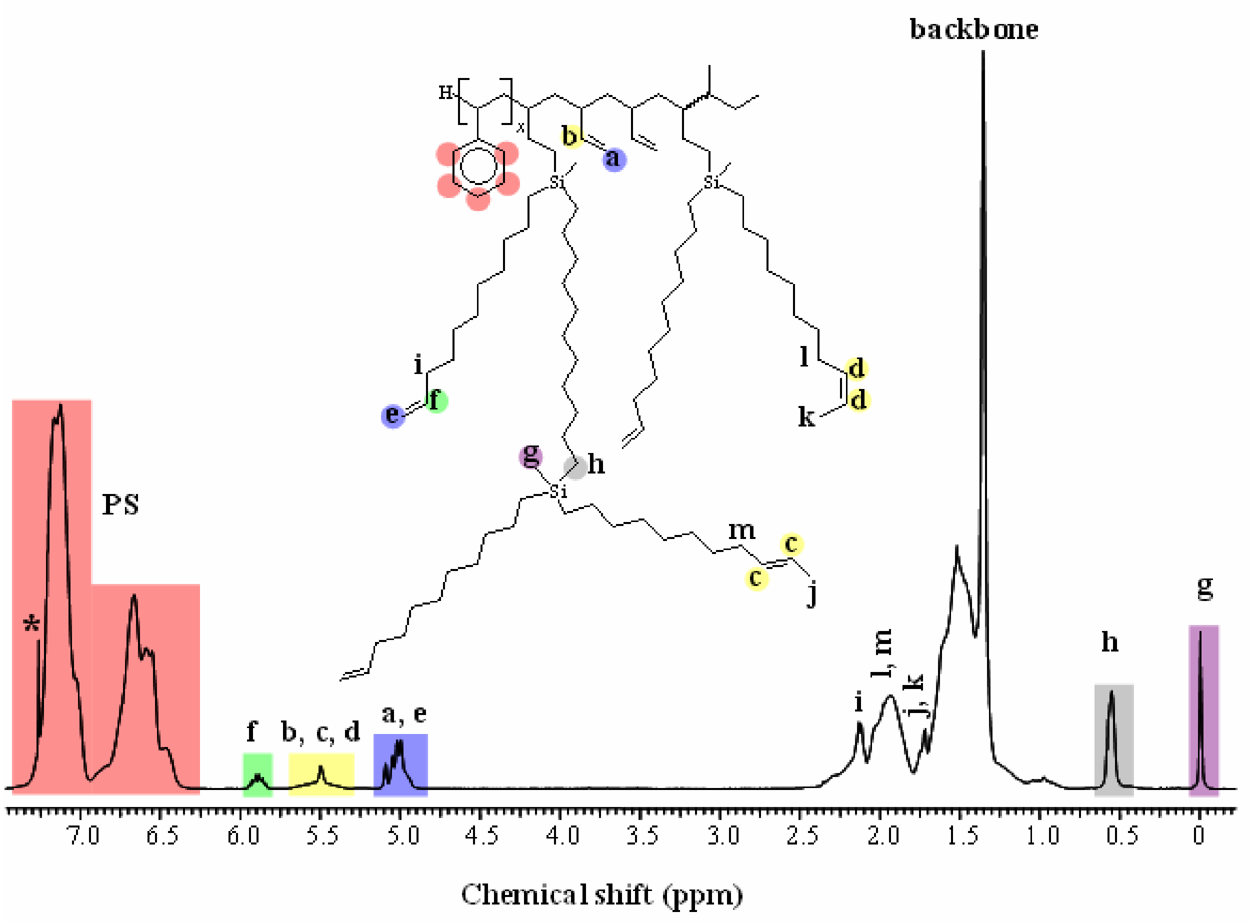

Figure 6.8. ^{1}H NMR spectrum of **P_3LH_{35}** in $CDCl_3$ (solvent peak denoted by an asterisk).

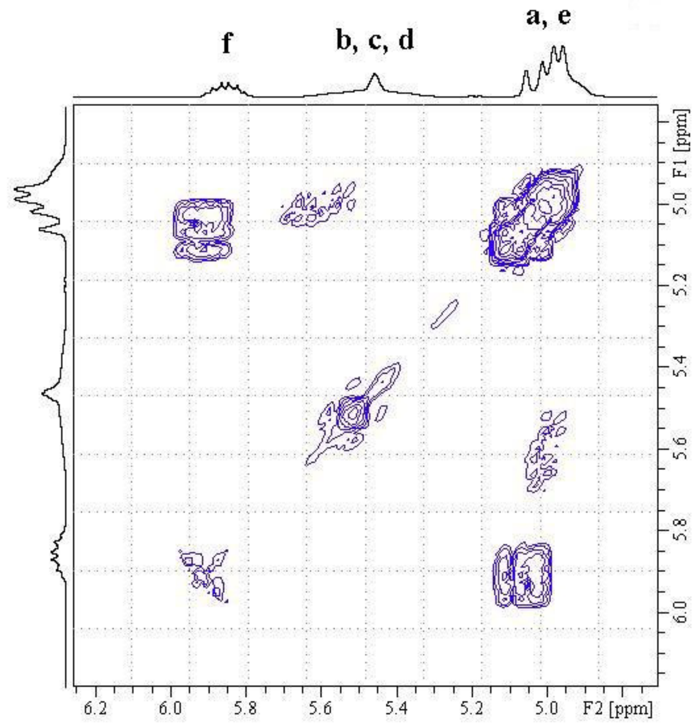

Figure 6.9. ^{1}H-^{1}H COSY spectrum of $\mathbf{P_3LH_{35}}$.

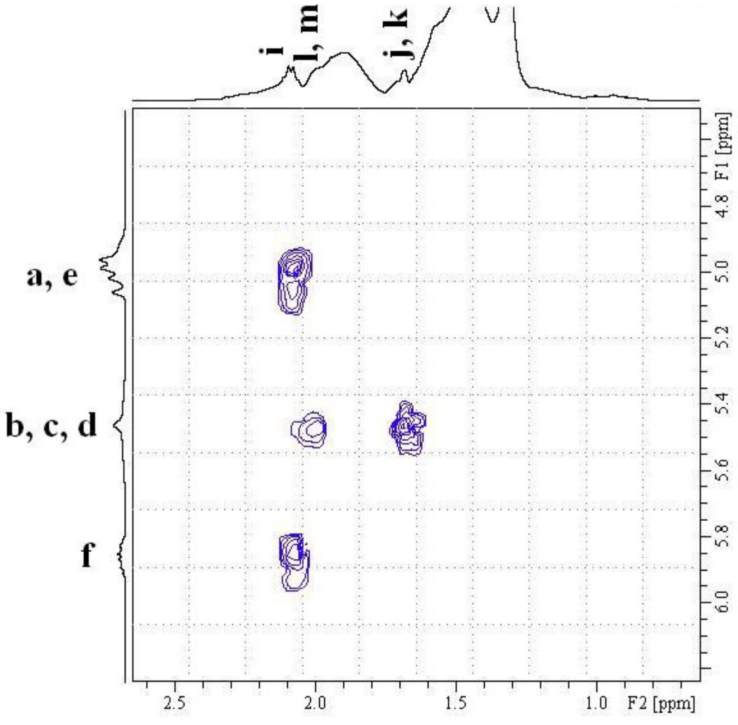

Figure 6.10. ^{1}H-^{1}H COSY spectrum of $\mathbf{P_3LH_{35}}$.

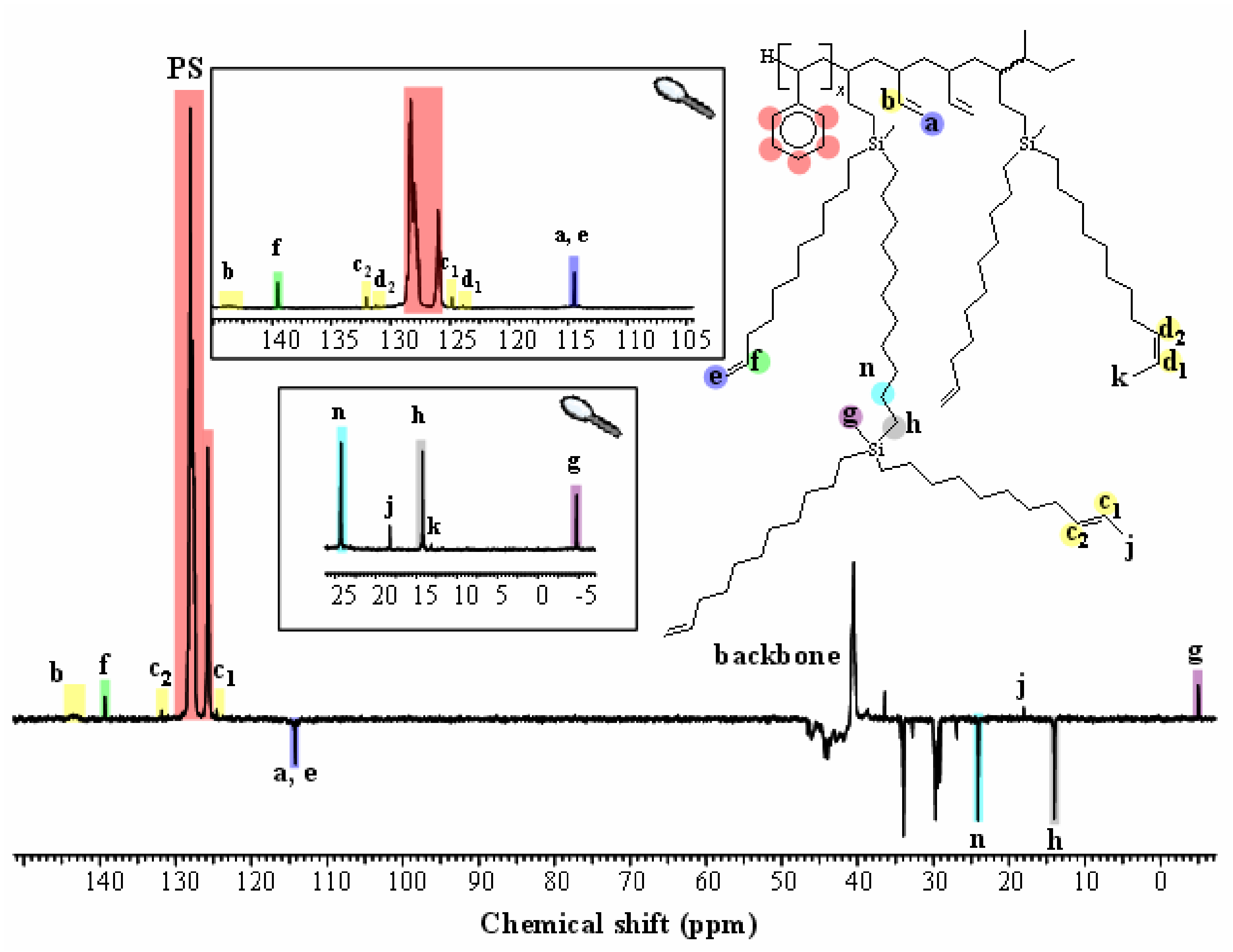

Figure 6.11. ^{13}C NMR DEPT spectrum of **P_3LH_{35}** in $CDCl_3$.

The corresponding ^{13}C NMR DEPT spectrum is depicted in Figure 6.11. It displays positive signals for the CH and CH_3 groups and negative or inverted signals for the CH_2 groups. The insets in Figure 6.11 are expansions of the aromatic and alkyl regions of the ^{13}C NMR spectrum, which was recorded with a higher number of scans. For comparison with the ^{13}C NMR of the linear diblock **P_3** before modification, see Chapter 2 (Figure 2.9). There is an increase in the intensity of the resonance at 114.4, which now corresponds to the methylene carbons of the terminal C=C bonds of the carbosilane groups (signal "e") in addition to the unreacted methylene carbons of the vinyl polybutadiene groups (signal "a"). The new signal at 139.5 ppm is assigned to the methine carbons of the terminal double bonds of the carbosilane groups (signal "f"). The methine carbons of the unreacted vinyl polybutadiene groups remain in the same position as in the spectrum of the precursor linear diblock copolymer **P_3** (signal "b", δ = 143.5 ppm), although with diminished intensity. The new signals at 124.8, 132.0 and 123.9, 131.2 ppm (signals "c_1", "c_2" and "d_1", "d_2" respectively) are clearly due to the methine carbons associated with the isomerization of the carbosilane double bonds. The olefinic methine carbon signals “c_1” and “c_2” are present in a higher ratio compared to the signals “d_1” and “d_2”. This is in agreement with the studies on the corresponding hyperbranched systems. Thus, by analogy, it can be concluded that a mixture of *trans*-2 and *cis*-2 isomers is formed, with the more intenses signals “c_1” and “c_2” most probably belonging to the thermodynamically favored *trans*-2-isomer. Examining the ^{1}H-^{13}C HETCOR spectrum (Figure 6.12) illustrates as expected, that the carbons of the terminal C=C bonds of the carbosilanes (signals “e” and “f”) are coupled with the signal at $\delta = 2.1$ ppm, which was assigned to the corresponding allylic protons (signal “i”). Furthermore the carbons of the isomerized double bonds (“c_1”, “c_2” and “d_1”, “d_2”) are coupled with the signal at 1.7 ppm (signals “j” and “k”), which was attributed to the protons of the methyl groups of the isomerized double bonds in the 2-position. This is supported by analysis on the analogous hyperbranched polycarbosilanes (Chapter 5, Figure 5.14). Other characteristic signals in the ^{13}C NMR high field region are: the resonances at -4.7, 14.2 and 24.3 ppm, which are assigned to the carbons of the Si-CH_3 (signal “g”), Si-CH_2 (signal “h”) and Si-CH_2-**CH_2** (signal “n”) groups respectively of the carbosilane branches. The small signals at 13.1 (signal “k”) and 18.3 ppm (signal “j”) are ascribed to the methyl protons of the 2-isomerized double bonds (Chapter 5, Figures 5.15 and 5.16).

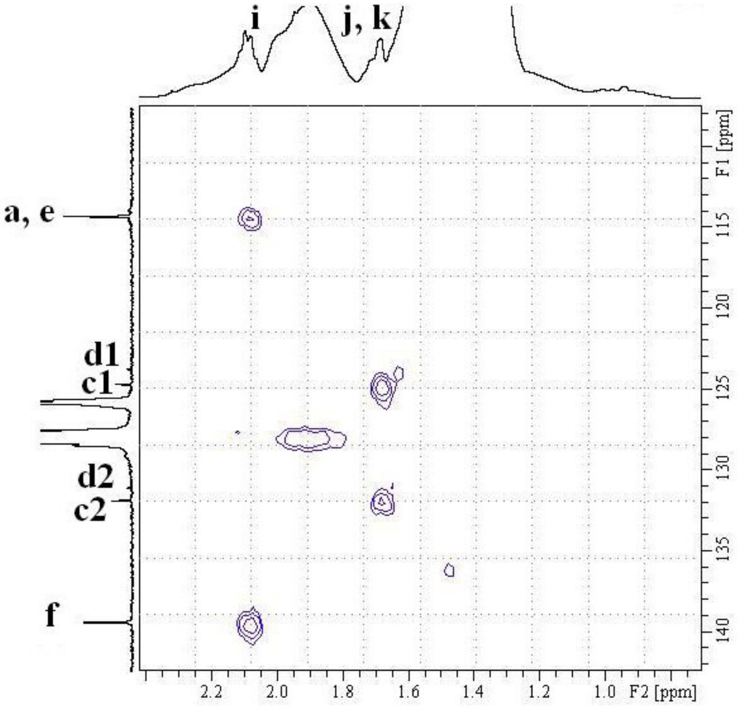

Figure 6.12. ^{1}H-^{13}C long range HETCOR spectrum of **P_3LH_{35}**.

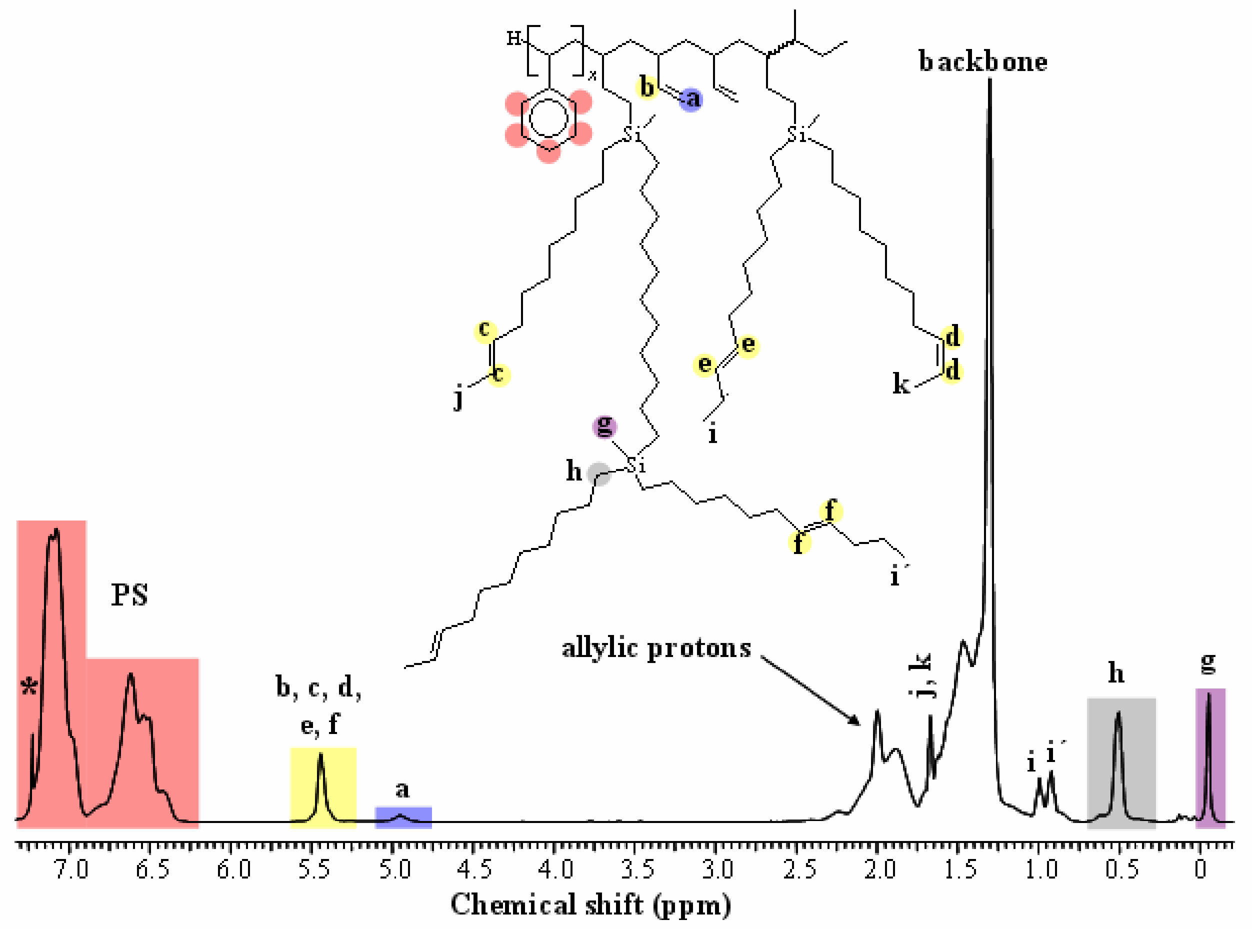

Figure 6.13. ^{1}H NMR spectrum of $\mathbf{P_3LH_{37}}$, obtained using diethyl ether as the monomer solvent, in $CDCl_3$ (solvent peak denoted by an asterisk).

The ^{1}H NMR spectrum of a linear-*b*-hyperbranched diblock copolymer obtained from the reaction of MDUS with $\mathbf{P_3}$ using diethyl ether as the monomer solvent is presented in Figure 6.13. In contrast to the ^{1}H NMR spectrum of the polymer resulting from the hypergrafting reaction in decaline/pentane (Figure 6.8), only 2 signals are observed in the olefinic region. The signal at $\delta = 5.90$ ppm, which was previously ascribed exclusively to the methine protons of the pendent vinyl groups of the carbosilane branches, is absent. This indicates complete migration of the double bonds when using diethyl ether as the monomer solvent. As before, the signal centered at 5.50 ppm is assigned, to the methine protons of the isomerized double bonds of the carbosilanes (signals “c”, “d”, “e” and “f”) as well as to the methine protons of the non-hydrosilylated 1,2-butadiene units (signal “b”). As there is complete migration of the terminal double bonds, the signal at 5.0 ppm (signal “a”), which is relatively weak, is attributed exclusively to the methylene protons of the non-hydrosilylated 1,2-butadiene units. The signal at 1.7 ppm is more intense when compared with $\mathbf{P_3LH_{35}}$ and again corresponds to the protons of the CH_3 groups coming from a 2-isomerization (signals “j” and “k”). Moreover, there are a further two new small signals at 0.9 and 1.0 ppm (signals “i” and “i´”). These are assigned to the protons of CH_3 groups arising from further isomerization along the alkyl chain. This is supported by comparing the ^{1}H-^{1}H COSY spectrum of **P_3LH_{37}** with the analogous hyperbranched polycarbosilanes (Chapter 5, Figure 5.18).

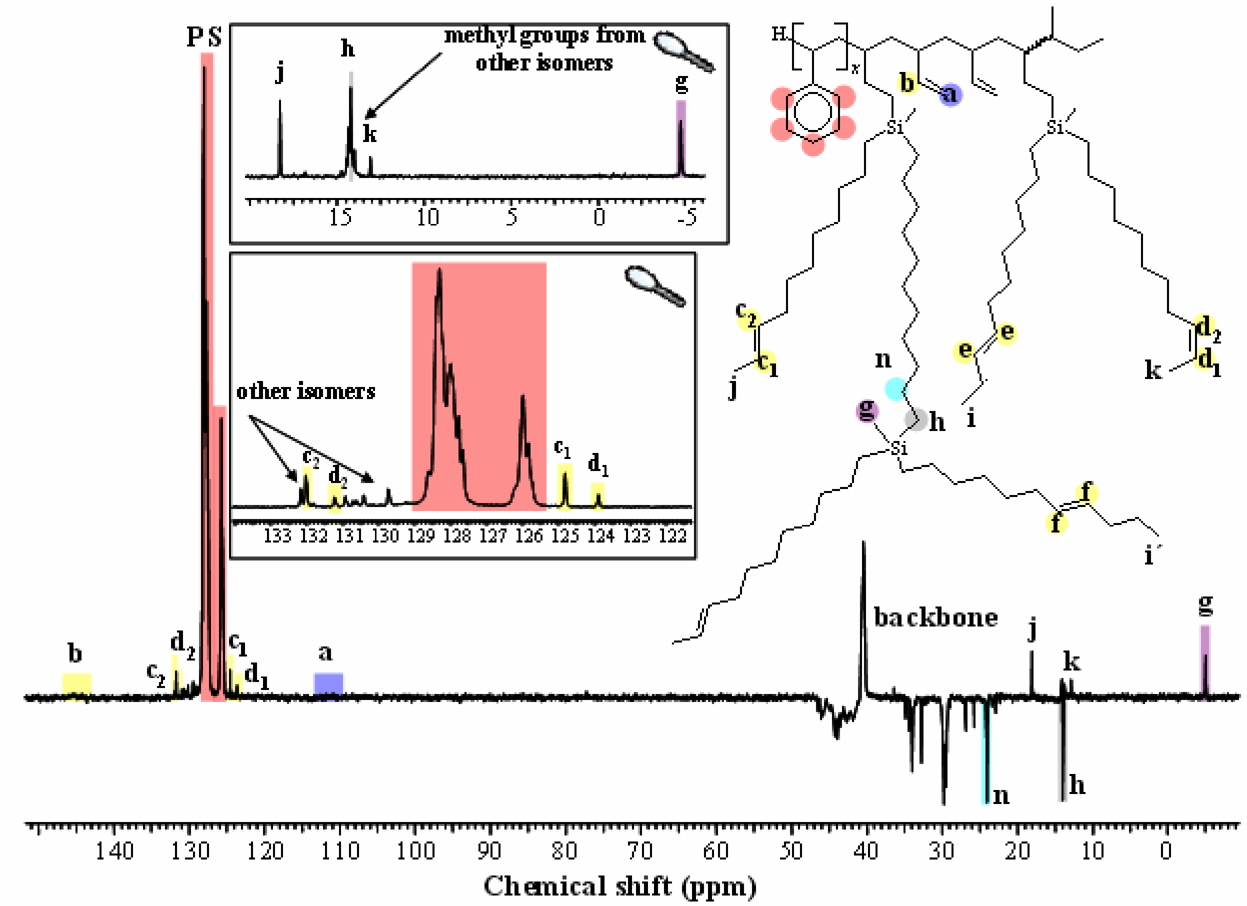

Figure 6.14. ^{13}C NMR DEPT spectrum of **P_3LH_{37}**, obtained using diethyl ether as the monomer solvent, in $CDCl_3$.

The corresponding ^{13}C NMR DEPT spectrum, with magnifications of the upfield and downfield region, is depicted in Figure 6.14. Firstly the resonances at 114.4 and at 139.5 ppm associated with the methine and methylene carbons of the terminal C=C bonds of the carbosilane branches are absent, which agrees with the conclusions made from the ^{1}H NMR spectrum in that isomerization is complete. Additionally, all the carbons signals in the olefinic region display positive signals, evidencing the absence of vinyl methylene carbons. The signals at 124.8, 132.0 and 123.9, 131.2 ppm (designated as “c_1”, “c_2” and “d_1”, “d_2” respectively) are, as in the previous case, assigned to the carbosilane methine carbons from isomerized double bonds in the 2-position (*cis*-2 and *trans*-2 isomer with a high *trans*:*cis* ratio). However, the presence of several other small peaks in the olefinic region suggests, in accordance with the ^{1}H NMR spectral evidence, that additional isomerization has occurred along the chain with varying degrees of stereospecifity (*i.e.* 3- and 4-isomer and/or others).

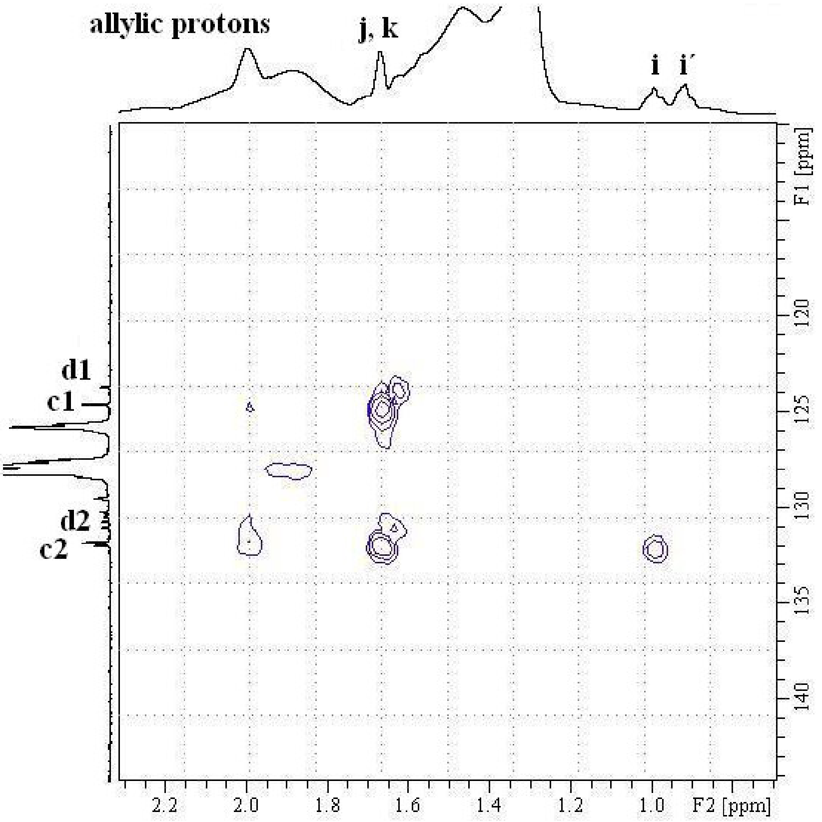

Figure 6.15. ^{1}H-^{13}C long range HETCOR spectrum of $\mathbf{P_3LH_{37}}$, obtained using diethyl ether as the monomer solvent.

In the HETCOR spectrum (Figure 6.15), the methine carbons of the *trans*- and *cis*-2-isomer (signals "c_1", "c_2" and "d_1", "d_2") are coupled, with the protons of the methyl groups and the allylic protons from the isomerization of the double bond to the 2-position. Furthermore, the other weaker methine carbon signals also show coupling with the new proton signals in the high-field region (signals "i" and "i′") and are tentatively assigned to the protons of the methyl groups resulting from isomerization beyond the 2-position. For justification and clarification, we refer to the HETCOR spectrum of the analogous hyperbranched polymers (Chapter 5, Figure 5.20). Furthermore, other small positive signals can be seen in the vicinity of the signals "j" and "k" in the ^{13}C NMR DEPT spectrum and these are assigned to the CH_3 carbons generated by isomerization in other positions along the alkyl chain (Chapter 5, Figure 5.21). The carbon signals "g", "h" and "n" of the attached carbosilane units were identified as in the previous case.

The use of polar solvents like diethyl ether appeared to favor complete isomerization. This could be explained by the ability of diethyl ether to coordinate to the platinum. This coordination might favor the formation of the π–allyl platinum hydride complex, which leads to rearrangement of the olefin (Chapter 4, Figure 4.13).

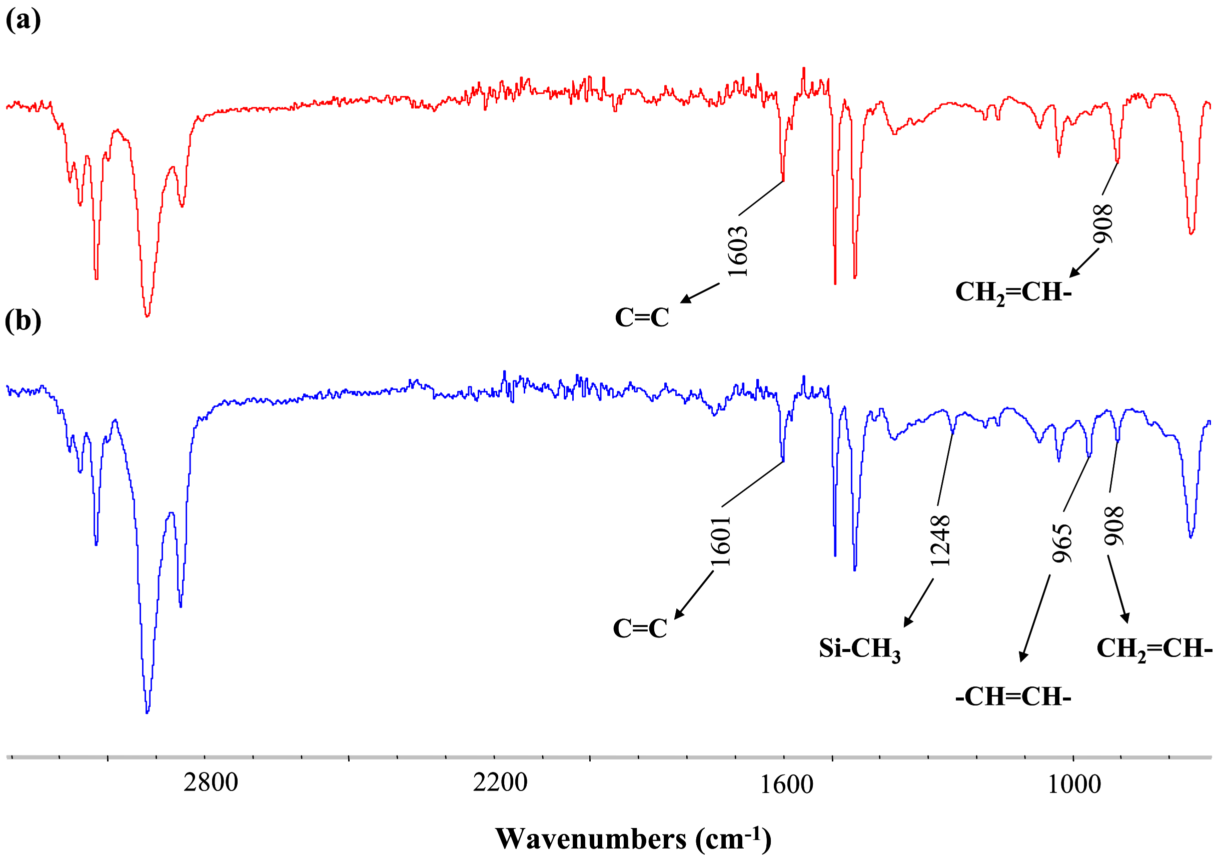

Figure 6.16. IR spectra of (a) **P_3** and (b) **P_3LH_{37}**.

IR analysis of the linear core **P_3** and of the linear-hyperbranched sample **P_3LH_{37}** confirms the incorporation of the polycarbosilane branches into the PBD core (Figure 6.16). The intensity of the peak at 908 cm^{-1}, initially associated with the vinyl 1,2-PBD deformation, diminishes after hypergrafting. This is due to a combination of the grafting of some of the PBD sites and to the isomerization of the introduced polycarbosilane terminal vinyl groups into internal double bonds, which is confirmed by the appearance of the band at 965 cm^{-1} (characteristic of an internal double bond deformation). Furthermore, the peak at 1248 cm^{-1} for **P_3LH_{37}** is attributed to the stretching mode of the newly introduced Si-CH$_3$ structure.

The yields of the linear-hyperbranched polymers isolated after removal of the low molecular weight side-products were in the range of 25-57 %. The materials obtained exhibited good solubility in a wide range of common organic solvents like THF, diethyl ether, chloroform, chlorbenzene and toluene. However, they were poorly soluble in non-polar solvents like pentane and insoluble in polar solvents like water, methanol, DMSO and DMF.

Some general trends, regarding the microstructure of these systems, can be summarized as follows:

(1) From the ^{1}H NMR data complete hydrosilylation on the pendant vinyl groups of the PBD was not achieved, regardless of the monomer solvent. It is plausible that the reduced conversion of the functional groups on the polymer backbone may result from steric effects that limit access to the reactive vinylic sites.

In the ^{1}H NMR spectra, the peaks associated with the phenyl groups of the styrene block (PS) can be used as an internal reference when comparing the vinyl signals of the linear PS$_x$-*b*-PBD$_y$ (Chapter 2, Figure 2.8) and the linear-hyperbranched PS$_x$-*b*-[PBD$_y$-*hb*-PCSi$_z$] (Figure 6.8 and 6.13) diblock copolymers. For the sample **P$_3$LH$_{35}$** (Figure 6.8), it was found that *ca.* 65.5 % of the total 1,2-PBD-vinyl groups remained unreacted according to Equation 6.1. For the completely isomerized **P$_3$LH$_{37}$** diblock copolymer, the amount of remaining 1,2-PBD vinyl groups can be estimated from the ^{1}H NMR spectrum (Figure 6.13) using the simplified Equation 6.2 and is calculated as *ca.* 25 %.

$$\%\quad remaining\quad PBD\quad active\quad sites = \frac{(a,e)_{\mathrm{PS_x\text{-}b\text{-}[PBD_y\text{-}hb\text{-}PCSi_z]}} - (f_{\mathrm{PS_x\text{-}b\text{-}[PBD_y\text{-}hb\text{-}PCSi_z]}} \times 2)}{a_{\mathrm{PS_x\text{-}b\text{-}PBD_y}}} \times 100$$

Equation 6.1. Evaluation of the remaining 1,2-PBD-vinyl groups after hypergrafting for a partially isomerized sample.

$$\%\quad remaining\quad PBD\quad active\quad sites = \frac{a_{\mathrm{PS_x\text{-}b\text{-}[PBD_y\text{-}hb\text{-}PCSi_z]}}}{a_{\mathrm{PS_x\text{-}b\text{-}PBD_y}}} \times 100$$

Equation 6.2. Evaluation of the remaining 1,2-PBD-vinyl groups after hypergrafting for a completely isomerized sample.

(2) In the ^{1}H and ^{13}C NMR spectra only one downfield signal associated with the Si-CH_3 group was visible, which is consistent with the exclusive formation of the Anti-Markovnikov addition product and also demonstrates that the internal double bonds, formed by double bond isomerization, remained unreactive. Therefore the addition of the dialkenylsilanes was chemically selective and occurred only at the less crowded end (Anti-Markovnikov) of the terminal double bonds (Figure 6.17). The formation of non-reactive internal isomers is a conversion limiting process for the hypergrafting reaction. This high regioselectivity can be explained by either the presence of multinuclear platinum species that does not catalyze the hydrosilylation of internal olefins or by the fact that the hydrosilylation of internal olefins is slow compared to the rate of the deactivation of the catalyst (Chapter 4, Section 4.3.1.1).[13a,13d,16] Additionally, the hydrosilylation of internal olefins might be slower due to the fact that the [Pt]-internal olefin complex **I** (Figure 6.18) is likely to be more sterically hindered.[17]

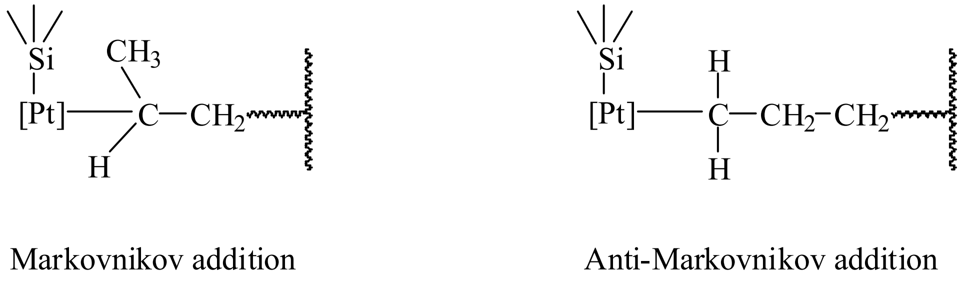

Figure 6.17. Possible modes of addition on the terminal C=C bonds.

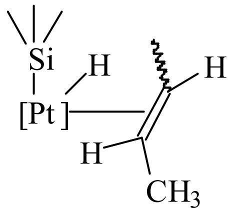

I

Figure 6.18. Sterically hindered alkenylplatinum intermediate complex formed with internal olefins.

(3) The extent of isomerization can be estimated from the ^{1}H NMR spectra by making use of the integration values of the signals in the olefinic region (Equation 6.3). The ^{1}H NMR of **P_3LH_{35}** (Figure 6.8) shows that *ca.* 25.5 % of the total double bonds were isomerized.

$$\text{Integration for one proton of isomerized double bonds} = \frac{\left[(b,c,d) - \left(\frac{(a,e) - f \times 2}{2}\right)\right]_{\mathrm{PS_x\text{-}b\text{-}[PBD_y\text{-}hb\text{-}PCSi_z]}}}{2} = is$$

$$\%\ \text{isomerized double bonds} = \frac{is}{(is + f)_{\mathrm{PS_x\text{-}b\text{-}[PBD_y\text{-}hb\text{-}PCSi_z]}}} \times 100$$

Equation 6.3. Formula to calculate the extent of isomerization of terminal carbosilane C=C bonds of PS_x-*b*-[PBD_y-*hb*-$PCSi_z$].

(4) There is a substantial change in the silicon chemical shift of the MDUS monomer and the signal from the corresponding linear-hyperbranched polymers, which reflects the charge in the electronic environment of the silicon atom after hypergrafting (Table 6.2). However, the presence of only one resonance in the ^{29}Si NMR spectrum (Figure 6.19) negates the possibility to determine the degree of branching. In other words, the long C_{11} alkyl chains do not permit to distinguish the different possible type of silicon units (*i.e.* branched, linear and terminal) that would give us information regarding the "branching density" of the structure.

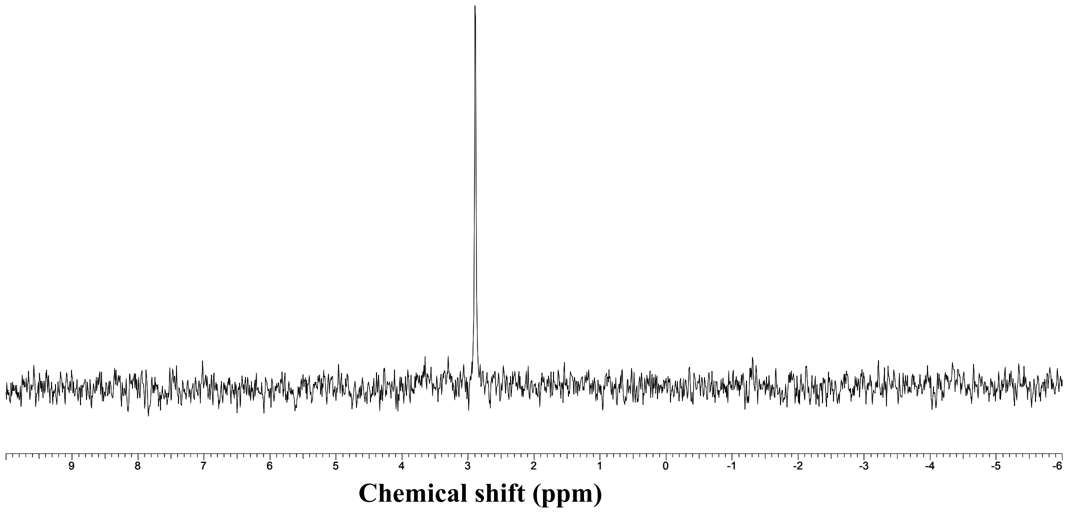

Figure 6.19. ^{29}Si NMR spectrum of $\mathbf{P_3LH_{35}}$.

Table 6.2. ^{29}Si NMR chemical shifts.

Compound	**δ_{Si} (ppm)**
MDUS	-9.7
$\mathbf{P_3LH_{35}}$	2.9

(5) In theory the addition of each AB_2 monomer should increase the total number of available functionalities of the core by one.[8a] However the number of potentially active vinyl end groups did not increase as expected. It is suspected that this is due to competing side reactions, such as hydrogenation, which take place during the hydrosilylation process. Hydrogenated vinyl groups may result from the reduction of the double bonds in the presence of the platinum catalyst.[16] An insight into alkene hydrogenation in the presence of a metal complex is provided in Chapter 4 (Section 4.3.1.2).

Changing the molecular weight of the linear diblock copolymer, from 56,800 g/mol (**P_3**) to 127,800 g/mol (**P_5**), but keeping the same weight percent of the blocks (*ca.* 5 wt % PBD), resulted in less efficient grafting of the MDUS AB_2 monomer onto the core when using identical monomer:core mol ratios. This suggests that with the higher molecular weight polymers, the reaction is more difficult due to the shear bulk of the polymer material relative to the monomer/catalyst/catalytic species.

6.3.3 Solid state behavior

Table 6.3. Characterization data and thermal properties for the linear (**P_3**) and the respective linear-hyperbranched diblock copolymers.

	GPC^a		MO^b		DSC^c	
Sample	M_n (10^3 g/mol)	PDI^d	M_n (10^3 g/mol)	wt % PS	T_g1 (°C)	T_g2 (°C)
P_3	63.8	1.04	56.8	95.5	99.7	-48.6
P_3LH_{25}	65.2	1.06	72.8	75	88.2	-24.7
P_3LH_{30}	67.8	1.04	78.0	70	93.4	-42.2
P_3LH_{35}	69.6	1.05	83.4	65	87.0	-31.0
P_3LH_{37}	80.7	1.25	86.7	63	96.0	-61.1
P_3LH_{49}	86.0	1.13	106.4	51	101.7	-68.6

^{a}Gel permeation chromatography (GPC) measured in chloroform at 30 °C with PS standard calibration. ^{b}Membrane osmometry (MO) measured in toluene at 40 °C. ^{c}Differential Scanning Calorimetry (DSC) measured at a heating rate of 25 °C/min. ^{d}Polydispersity index $\overline{M}_w/\overline{M}_n$ measured by GPC in chloroform at 30 °C

The characterization data for the linear core diblock copolymer **P_3** (PS_{520}-*b*-PBD_{47}) containing 4.5 wt % of PBD and for the resulting linear-hyperbranched polycarbosilane structures are summarized in Table 6.3. In the linear-hyperbranched structures the short PBD block becomes part of the final polycarbosilane block and is also treated as such in all ensuing considerations. This is justified by the fact that the PBD-core in the final linear-hyperbranched architectures is indistinguishable from the grafted carbosilane units. It is well known that branched polymers have smaller hydrodynamic radii compared to the corresponding linear polymers of similar molecular weight.[18] Therefore, as expected, the molecular weights of the hyperbranched block copolymer structures, as determined by conventional GPC (PS standards), are underestimated. Consequently, the wt % of the linear PS and the hyperbranched [PBD-*hb*-PCSi] blocks was calculated for each sample from membrane osmometry (MO) measurements.

The thermal behavior of the polymers was studied by Differential Scanning Calorimetry (DSC). The amorphous linear-hyperbranched polycarbosilanes exhibit two glass transition temperatures (T_g), which indicates microphase segregation in the bulk state. The T_g values for the diblock copolymers are reported in Table 6.3. The polycarbosilane blocks possess low T_g values as a consequence of a high degree of chain flexibility. A representative DSC curve for a linear-hyperbranched sample is depicted in Figure 6.20. Additionally, the thermal stability of the linear-hyperbranched materials, as determined by thermogravimetric analysis (TGA), indicated that the modified polymers are as stable as their linear precursors. Figure 6.21 shows a TGA curve for the sample **P_3LH_{37}**, indicating decomposition at temperatures above 436 °C.

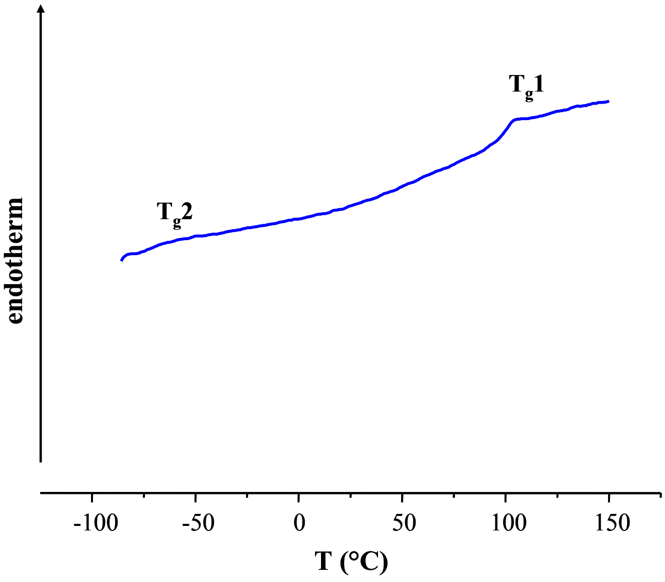

Figure 6.20. DSC curve of **P_3LH_{37}**, scanning rate 25 °C/min.

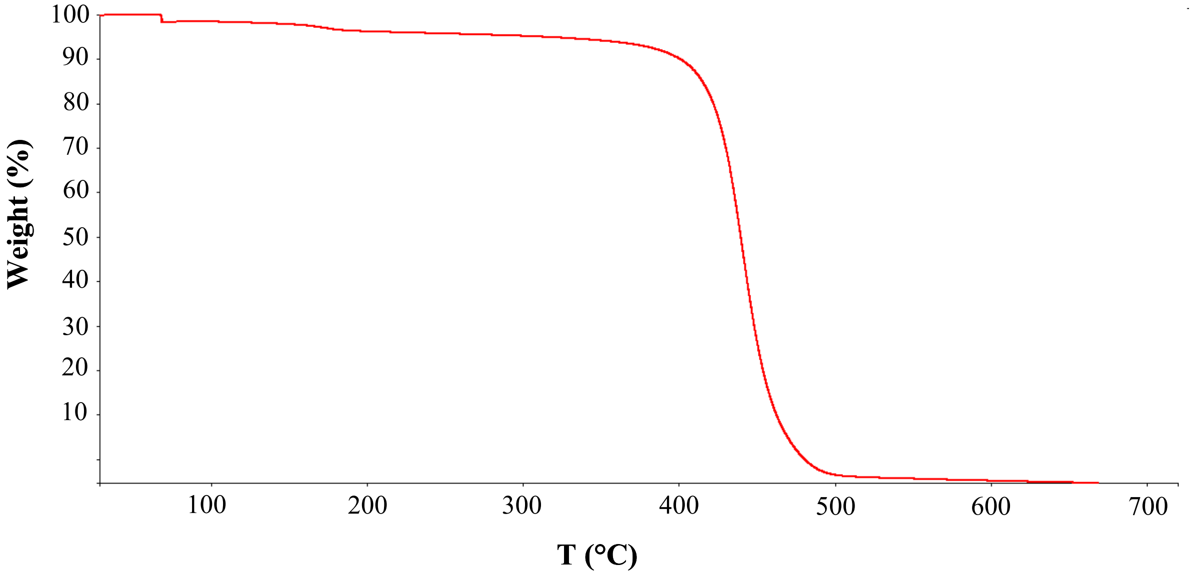

Figure 6.21. TGA curve of **P_3LH_{37}** in N_2, heating rate 10 °C/min, exemplifying the thermal stability of the linear-hyperbranched diblock copolymers.

Characterization of the resulting bulk morphologies was accomplished by Transmission Electron Microscopy (TEM), Atomic Force Microscopy (AFM) and temperature-dependent Small Angle X-ray Scattering (SAXS) measurements. The combination of these methods was sufficient to confirm the structures. The SAXS patterns were obtained from compression-molded samples, while the AFM and TEM images were taken from both compression-molded and solution-cast films using toluene or THF, as non-preferential solvents. However, the observed morphologies were in general largely independent of the sample pre-treatment, the only difference being that the solution cast films displayed a higher degree of order than the melt-processed samples. Generally, the contrast in the TEM images, unless otherwise specified, is based solely on the differences in electron density between silicon and carbon, in other words, no additional staining has been applied. In the TEM unstained images, the bright areas correspond to the PS (linear block) and the dark areas to the polycarbosilanes (hyperbranched block). In the TEM images of samples that have been stained with OsO_4 to enhance contrast under the electron beam, the polycarbosilane domains appear dark. Contrast in the AFM phase images is based on hard and soft material: PS (hard), polycarbosilane (soft). In the AFM images presented the hard domains are bright, while the soft domains are dark.

A TEM micrograph of sample **P_3LH_{25}** containing 25 wt % of the hyperbranched block (HB) is shown in Figure 6.22a. In the case of a linear diblock copolymer with similar wt % fractions, formation of cylinders at the strong segregation limit (SSL) is expected.[19] Nevertheless, the micrograph shows rather irregular [PBD-*hb*-PCSi] domains dispersed in the PS matrix with no discernible lattice. Additionally, the corresponding SAXS patterns recorded up to 200 °C do not fit exactly to a hexagonally packed cylindrical morphology (Figure 6.22b). The scattering has an intense but broad scattering peak at the scattering vector (s^*) with only a weak second order broad peak, resembling patterns from nearest neighbor correlated arrangements of domains without a specific shape. The broad peak shapes and the presence of only low order Bragg reflections, becoming more diffuse with increasing annealing temperature, suggests that this sample may not be within the strongly phase-segregated regime.[20]

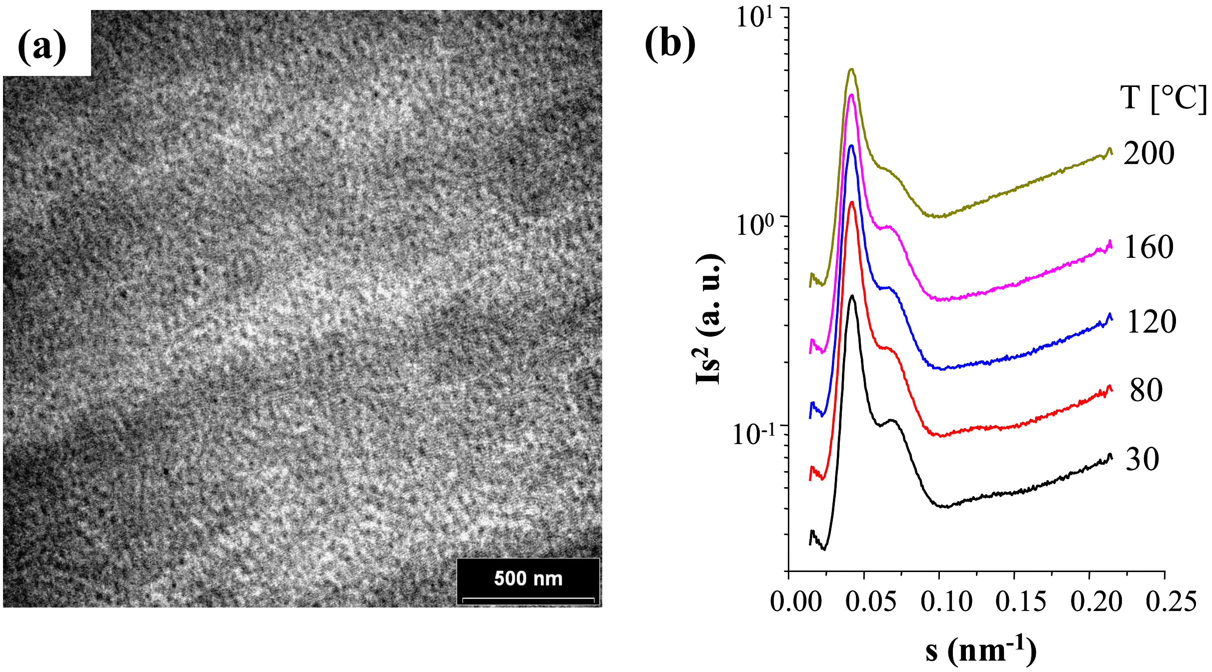

Figure 6.22. (a) Unstained TEM (solution-cast film in toluene, scale marker is 500 nm) and (b) SAXS diffraction pattern (compression-molded sample) of **P_3LH_{25}**.

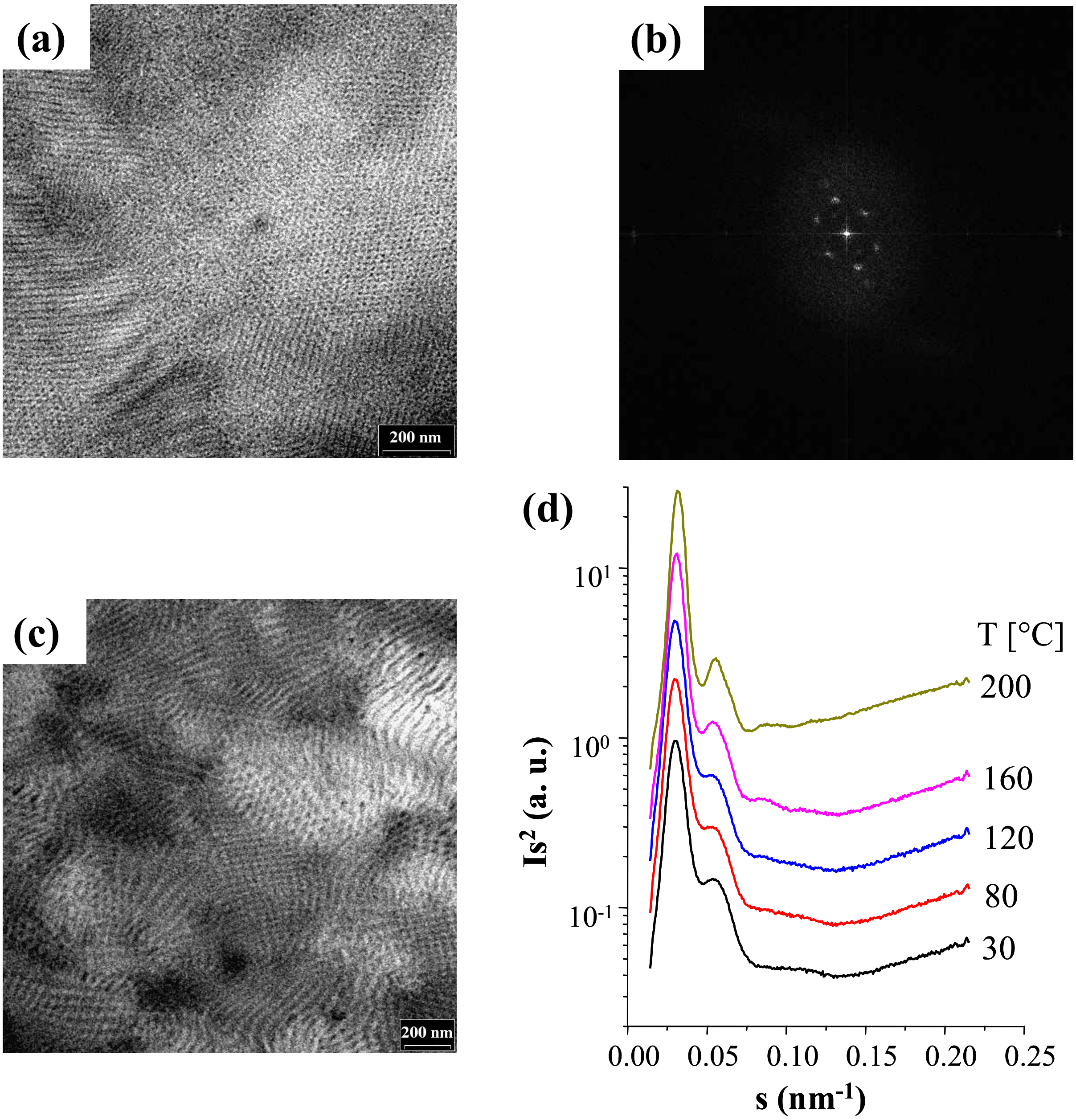

Figure 6.23. (a) Unstained TEM (solution-cast film in toluene, scale marker is 200 nm) and (b) FFT of **P_3LH_{30}**; (c) Unstained TEM (solution-cast film in toluene, scale marker is 200 nm) and (d) SAXS diffraction pattern (compression-molded sample) of **P_3LH_{35}**.

Samples **P_3LH_{30}** and **P_3LH_{35}** with 30 and 35 wt % HB respectively show a cylindrical morphology (Figure 6.23). The TEM for the sample **P_3LH_{30}** (Figure 6.23a) demonstrates hexagonally packed cylinders with long-range order as evidenced by the fast Fourier transformation (FFT) of the TEM micrograph (Figure 6.23b). It is a reasonable conclusion that soft cylinders (in this case PCSi) in a hard matrix (PS) are easier to align than the reverse structure. In the TEM pictures of both samples (Figures 6.23a and 6.23c), grains which are imaged parallel and perpendicular to the rods are distinguished. Excellent long-range order of the hexagonal phase could be induced by external forces such as temperature gradients, electric and magnetic field poling, mechanical shear and surface interactions.[21] The overall regular ordered packing of the HB domains is consistent with the X-ray diffraction patterns. The SAXS for **P_3LH_{35}** is illustrated in Figure 6.23d. The intensity distribution exhibit three reflections at s^*, $s^*\surd 3$ and $s^*\surd 7$, which corresponds to cylinders packed in hexagonal arrays with a domain periodicity (D) of 39 nm. There should be also a reflection at $s^*\surd 4$ but this is coincident with a minimum in the form factor of the cylinders and is systematically absent. **P_3LH_{30}** showed a similar series of scattering vectors with a D of 35 nm. Annealing the sample above the T_g of PS (200 °C), causes the intensity of the third Bragg peak to become sharper and reflects the increased order and more uniform phase separation upon heat treatment.

A clear lamellar phase was found for the sample **P_3LH_{37}**, which contains 37 wt % of the HB component (Figure 6.24). This morphology is also expected in the SSL for linear diblock copolymers with similar composition. However, in the TEM picture in Figure 6.24a it is clearly seen that the lamellae are ordered in different grains. A magnification of the lamellae is shown in the TEM image in Figure 6.24b. The sample exhibits well-developed order and as a result SAXS reflections up to the fifth order are detected. The corresponding SAXS pattern and the related intensity distribution, which comprises a series of Debye-Scherrer rings in the position ratio 1:2:3:4:5, is presented in Figure 6.24d. A lamellar long period of 42 nm was determined. The individual block lamellar thicknesses can be readily calculated from the corresponding wt % fractions. The lamellar surface texture, with a long-period in agreement with the X-ray structural data, is shown in the AFM phase image of the sample (Figure 6.24c).

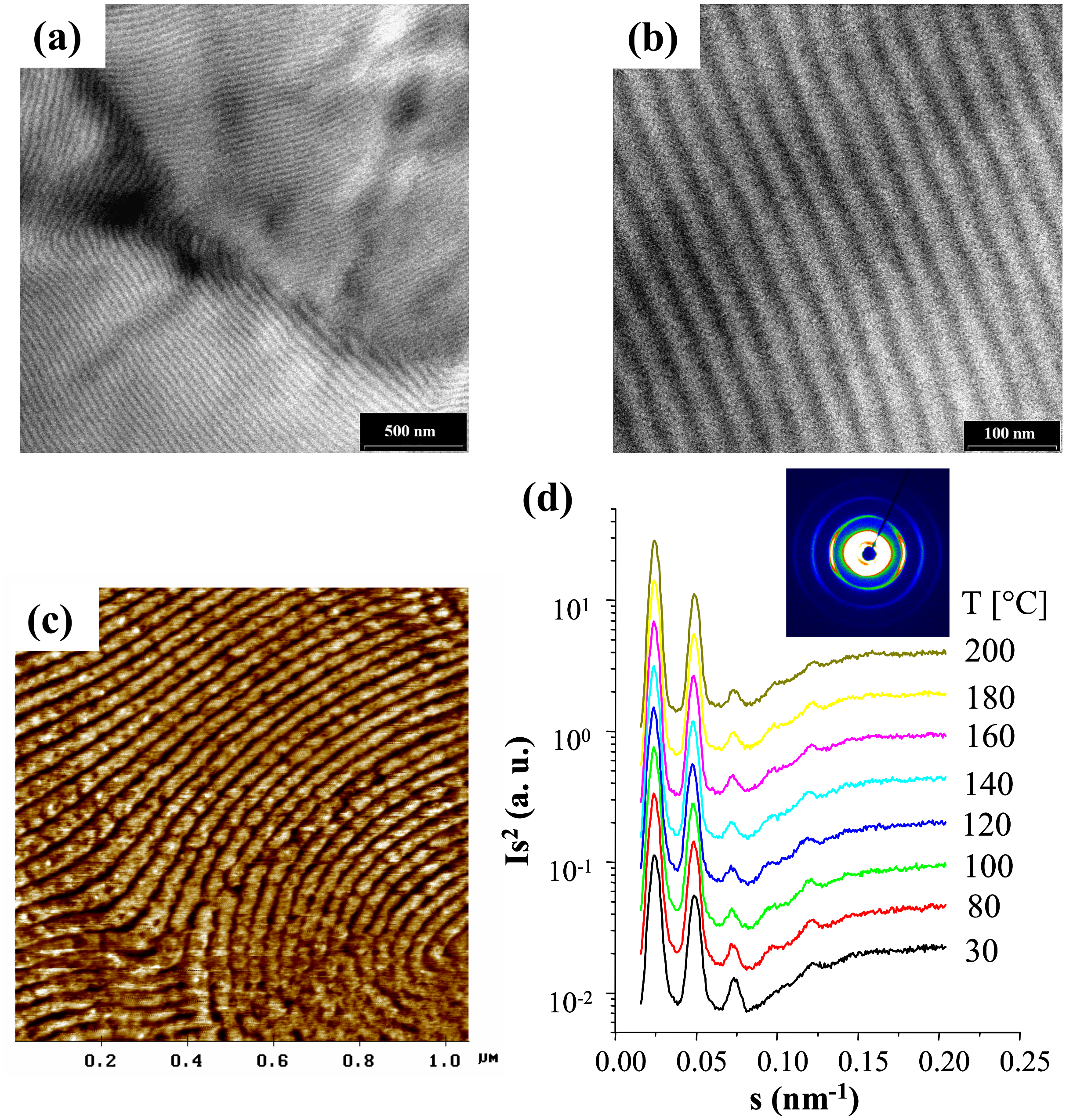

Figure 6.24. (a) and (b) Unstained TEMs (solution-cast film in toluene, scale markers are 500 and 100 nm respectively), (c) AFM phase image and (d) one and two-dimensional SAXS pattern (compression-molded sample) of **P_3LH_{37}** illustrating long-range lamellar order.

Except for the first linear-hyperbranched sample **P_3LH_{25}**, we assume that these systems are within the SSL because no order-disorder transition was observed prior to heating in the SAXS experiments. Often samples require annealing periods of several days; however these samples showed high order after only half an hour of annealing above the T_g of PS, indicating a rapid ordering process. The fact that the materials displayed in general long-range periodicity is indicative of well-defined monodisperse samples.[20,22] Microstructures detected in the studied samples were maintained in the melt up to temperatures far above the glass transition temperature of PS (up to 200 °C). Additionally, long-range order appeared to improve upon heating the sample. This indicates well-stabilized structures characteristic of the strong segregation range. We presume that a large entropic factor must contribute to the conformational asymmetry existing between the dendritic and the linear blocks (as also noted by Pochan *et al.* and Mackay *et al.*), making the blocks less compatible.[6d,6e] Most probably a limited penetrability of the HB blocks by linear PS chains is responsible for this entropic contribution and constitutes a strong component to the driving force for the microphase separation.

The linear-hyperbranched **P_3LH_{49}** sample with 49 wt % of the HB component displayed the most unusual morphological behavior (Figures 6.25 and 6.26). "Hexagonally" packed PS cylinders in a [PBD-*hb*-PCSi] matrix can be observed for the compression-molded sample as demonstrated by TEM (Figures 6.25a and 6.25c) and AFM images (Figures 6.25b, 6.25d, 6.25e and 6.25f). The SAXS intensity distributions display the reflections typical of a cylindrical morphology at relative scattering values of $1:\sqrt{3}:\sqrt{13}$ with D of 50.4 nm up to 120 °C (Figure 6.26c). However above this temperature the morphology pattern unexpectedly changes to a lamellar-like structure, characterized by peaks spaced at reciprocal space position ratios of 1:2:3:4, with a lamellar period of 40.5 nm. The morphology change observed upon heating was reproducible, but not reversible. In other words, when the samples were cooled down slowly the lamellar morphology remained. As the relaxation of a non-equilibrium structure is in principle an irreversible process, it can be supposed that the cylindrical structure detected initially can only be formed during sample deformation but when annealed it transforms to a lamellar morphology, which is characteristic for an equilibrium state with this molecular composition.

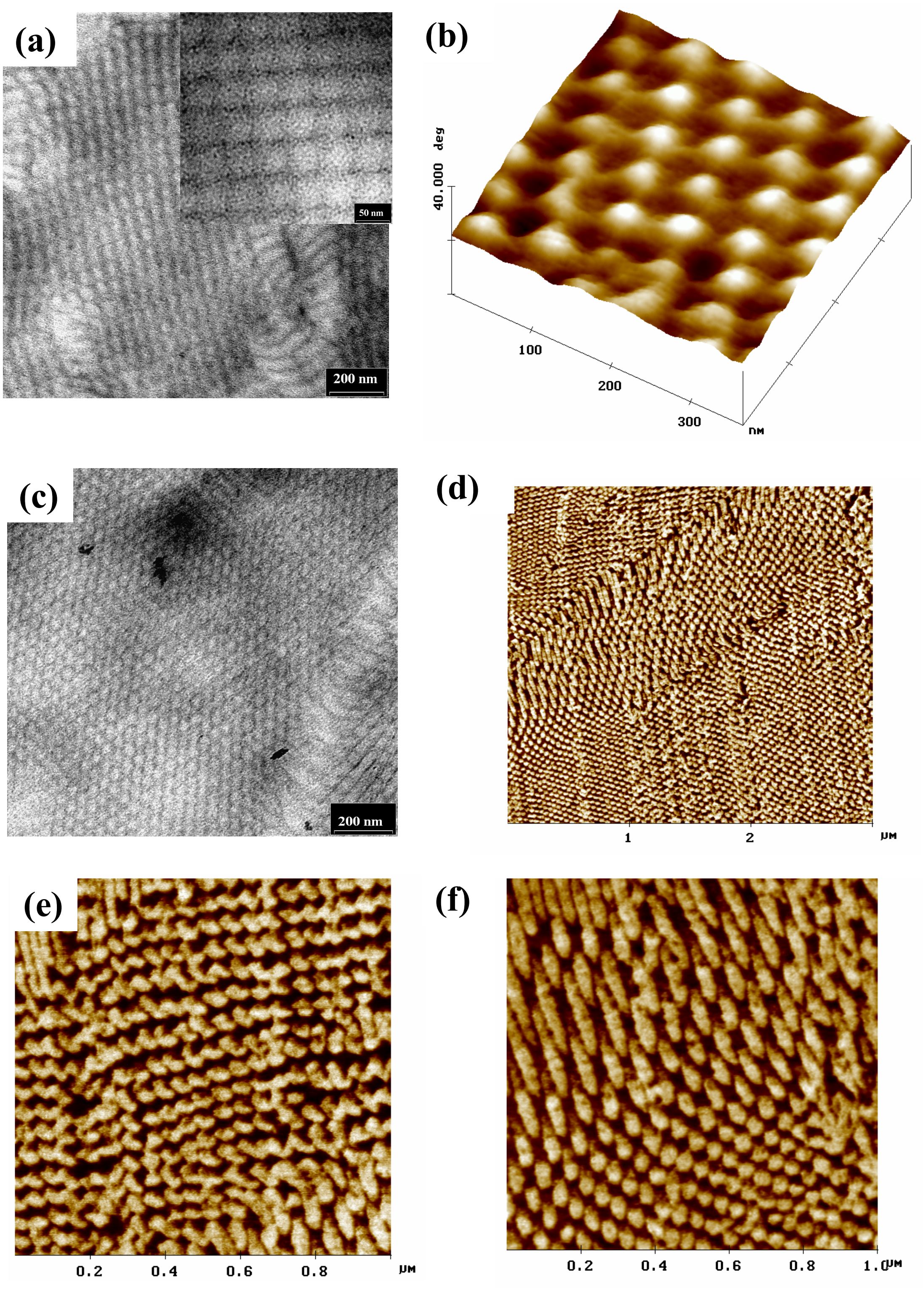

Figure 6.25. (a) and (c) Unstained TEMs (compression-molded sample, scale markers are 200 nm and 50 nm for the inset of Figure a), (b) 3D visualization of an AFM phase image, (d), (e) and (f) AFM phase images of **P_3LH_{49}**.

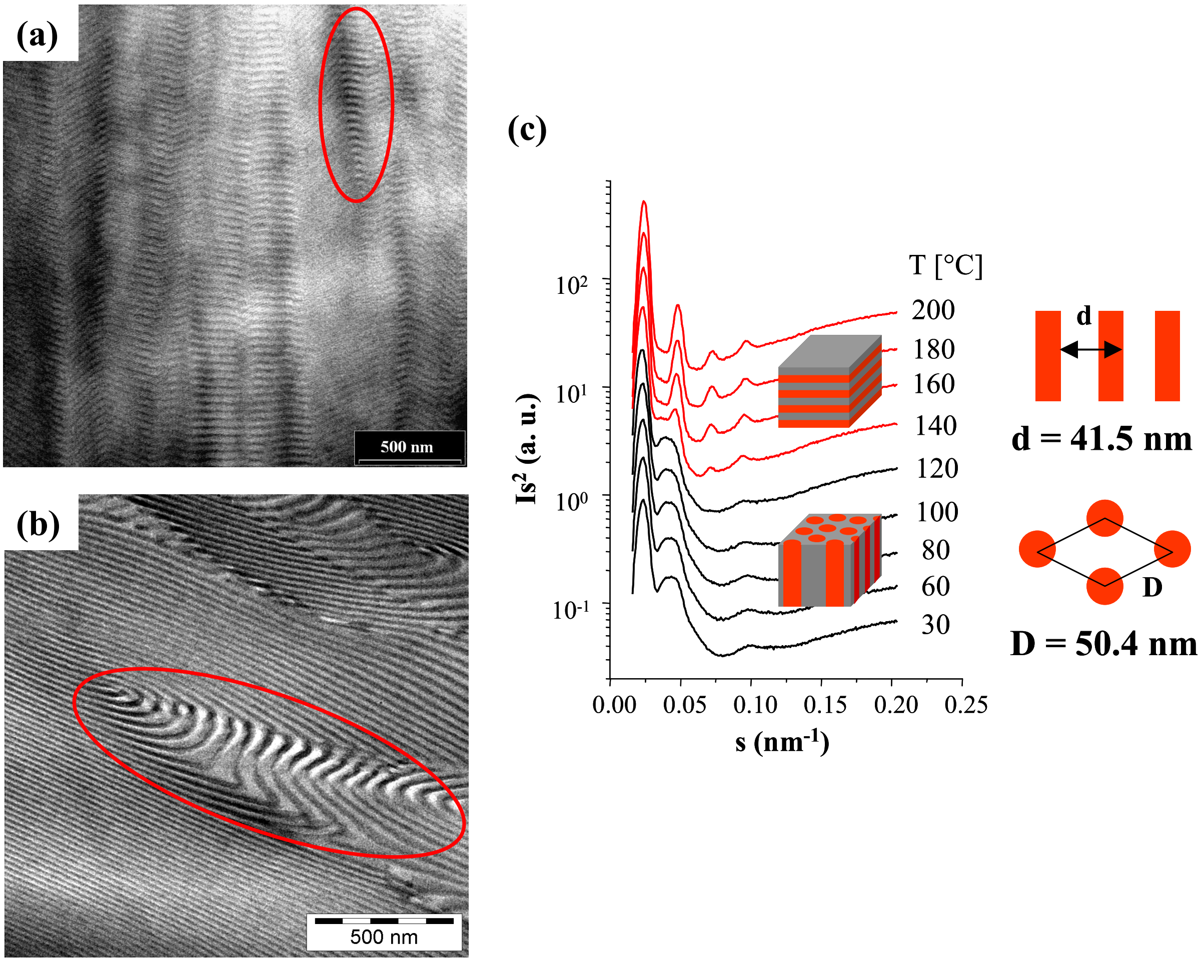

Figure 6.26. (a) Unstained TEM (solution-cast film in toluene, scale marker is 500 nm), (b) TEM image selectively stained with OsO_4 (solution-cast film in THF) and (c) temperature-dependent one dimensional SAXS pattern (compression-molded sample) of **P_3LH_{49}**.

The lamellar phase can also be recognized in the TEM pictures from the solution-cast sample in toluene and THF (Figures 6.26a and 6.26b), which agrees with the SAXS patterns obtained from samples held above the T_g of PS for long periods of time. Examining closely the TEM and AFM pictures of the compression-molded sample in Figure 6.25 reveals that the PS cylinder shape is not classical. This is especially noticeable in the TEM picture in Figure 6.25a and in the AFM images in Figures 6.25b and 6.25e. In these pictures, the PS cylinders appear to be interconnected and consequently deformed. In some way, this is similar in appearance to an hexagonally perforated layer morphology (HPL), which might result from instabilities of the lamellar morphology.[23] Although this cannot be confirmed by the scattering signature of the sample, it is supposed that the thermally induced irreversible morphological transition from cylindrical to lamellar microdomains happens through coalescence of undulating cylinders as represented pictorially in Figure 6.27. In this schematic picture, undulations develop (Figure 6.27, **I**) before the cylinders approach each other and coalescence forming channels (Figure 6.27, **II**). Finally the cylinders are transformed to lamellae (Figure 6.27, **IV**) by growth of the channel in the direction along the axes of the cylinders (Figure 6.27, **III**).

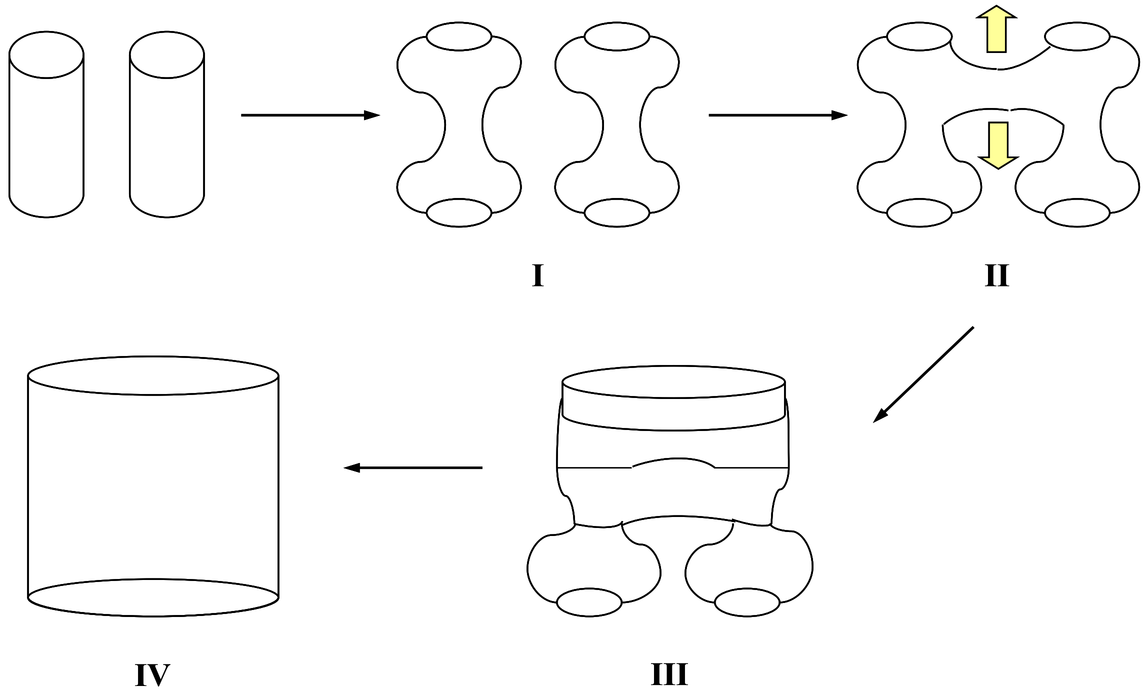

Figure 6.27. Scheme for the morphological transition from cylinders to lamellae through coalescence of the cylinders.

Dissolution of the cylinders was not observed prior to formation of the lamellar structure as observed in the T-dependent SAXS measurements (Figure 6.26c). The transition path via the disordered state might be considerably large due to the mixing of strongly linear and HB chains. Similar undulating interfaces have been reported by Sakurai *et al.*.[24] However, in our case there is a peak shift in the SAXS profile throughout the morphological transition. This implies that the transition could be induced by collisions of the cylinders with their translational movements, which is likely to happen at high temperatures and in solution. Additionally, the lamellar sample obtained from the solution-cast film in THF (Figure 6.26b) shows an unusual chevron tilt grain boundary morphology. In specific regions, the lamellar layers retain their continuity while bending cooperatively in a narrowly defined boundary region. Although the chevrons are not broken, some lamellae terminate at the boundary in rows of semi-cylindrical end caps. These observed phase boundaries, although less prominent, are also present in the TEM micrograph from the sample prepared from a solution-cast film in toluene (Figure 6.26a). A schematic picture of the observed chevron tilt boundaries is presented in Figure 6.28a. We postulate that the appearance of the chevron tilt grain boundaries in this sample results from the asymmetry inherent in the linear-hyperbranched molecular architecture. As shown in Figure 6.28b, the chevron boundary involves equal degrees of interfacial curvature both toward and away from the HB side of the interface. Because of crowding inherent in packing the HB block on the same side of the interface, it would be more energetically favored to replace the structure with a broken or discontinuous structure, for which the HB block would reside on the convex side of the interfacial curvatures (Figure 6.28c). Although some of the tilt angles (θ) of the observed chevrons in Figure 6.26b are relative high, a transition from the continuous to the discontinuous chevron structure was not observed. It is assumed that the energy penalty of locating the HB block on the concave side of the interface is not high enough to allow the formation of PS cylinders with the hyperbranched block on the convex side of the interface as an equilibrium morphology.

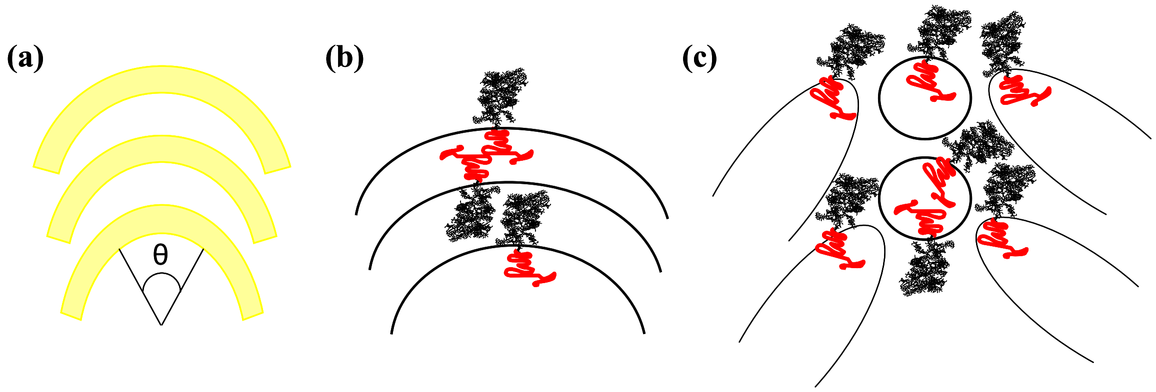

Chevron

Broken chevron with cylinders

Figure 6.28. (a) Schematic picture of the observed chevron tilt boundaries; (b) Illustration of chevron tilt boundaries observed for the linear-hyperbranched sample $\mathbf{P_3LH_{49}}$; (c) Illustration of broken or discontinuous chevron tilt boundaries.

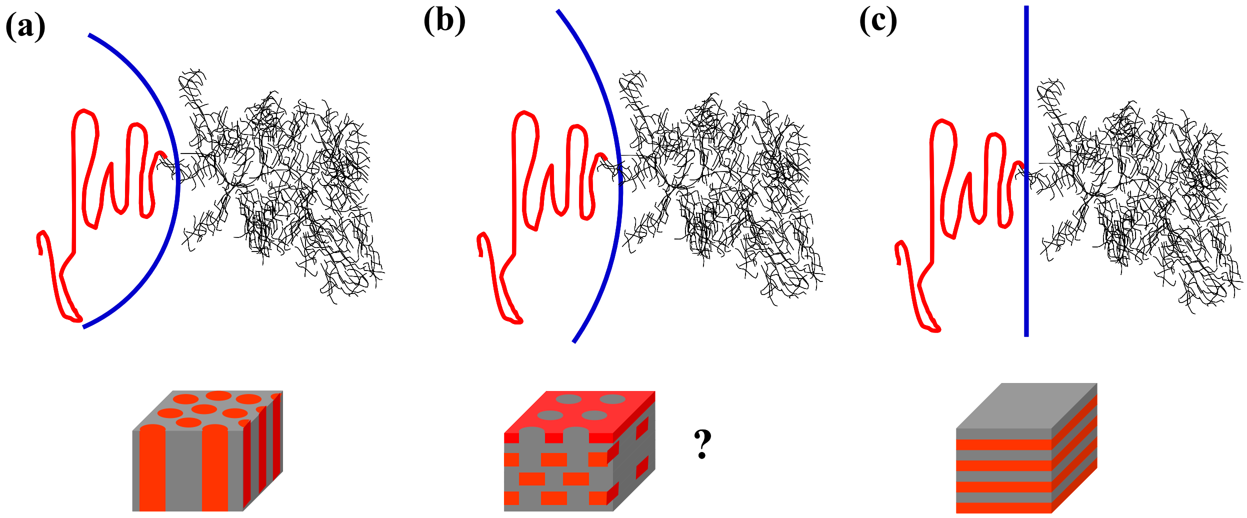

Figure 6.29. Proposed change of the interfacial curvature in the morphological transition of **P_3LH_{49}** (b represents an HPL morphology).

Taking into account the studies of miktoarm star block copolymers,[3] one could speculate that because of the strong architectural asymmetry between the linear and HB blocks, even at the comparable weight fractions of both components, a local preferential curvature of the PS-*b*-[PBD-*hb*-PCSi] interface can be formed. In such a case, patterns other than lamellar morphologies could be formed in contrast to linear diblock copolymers of comparable composition for which a lamellar morphology is expected.[25] Determination of the complete phase diagram for the studied system would, however, require samples well distributed over the composition scale. Based on these results, we can surmise that the interface is forced to curve towards the PS system only under deformation. This is probably due to an overcrowding of the hyperbranched blocks, forcing PS domains to assume cylindrical forms. Such a structure becomes unstable at high temperatures and in solution where the higher chain mobility allows an irreversible relaxation to the equilibrium morphology. Hence the initially formed cylindrical conformation is relaxed to lamellae above the T_g of PS and in solution. As deformed cylinders and chevron tilt grain boundary lamellae were observed in the AFM and TEM pictures, it is believed that the original curved interface decreases in a transition process until it becomes nearly flat (Figure 6.29). The energy barrier for this order-order transition via the postulated coalescence of the cylinders would be small because it only involves local disruption of the interface. Moreover, the coherence of the lamellar equilibrium structure formed becomes higher with prolonged annealing times as was observed in the SAXS pattern in Figure 6.26c.

6.3.4 Analytical microscopy

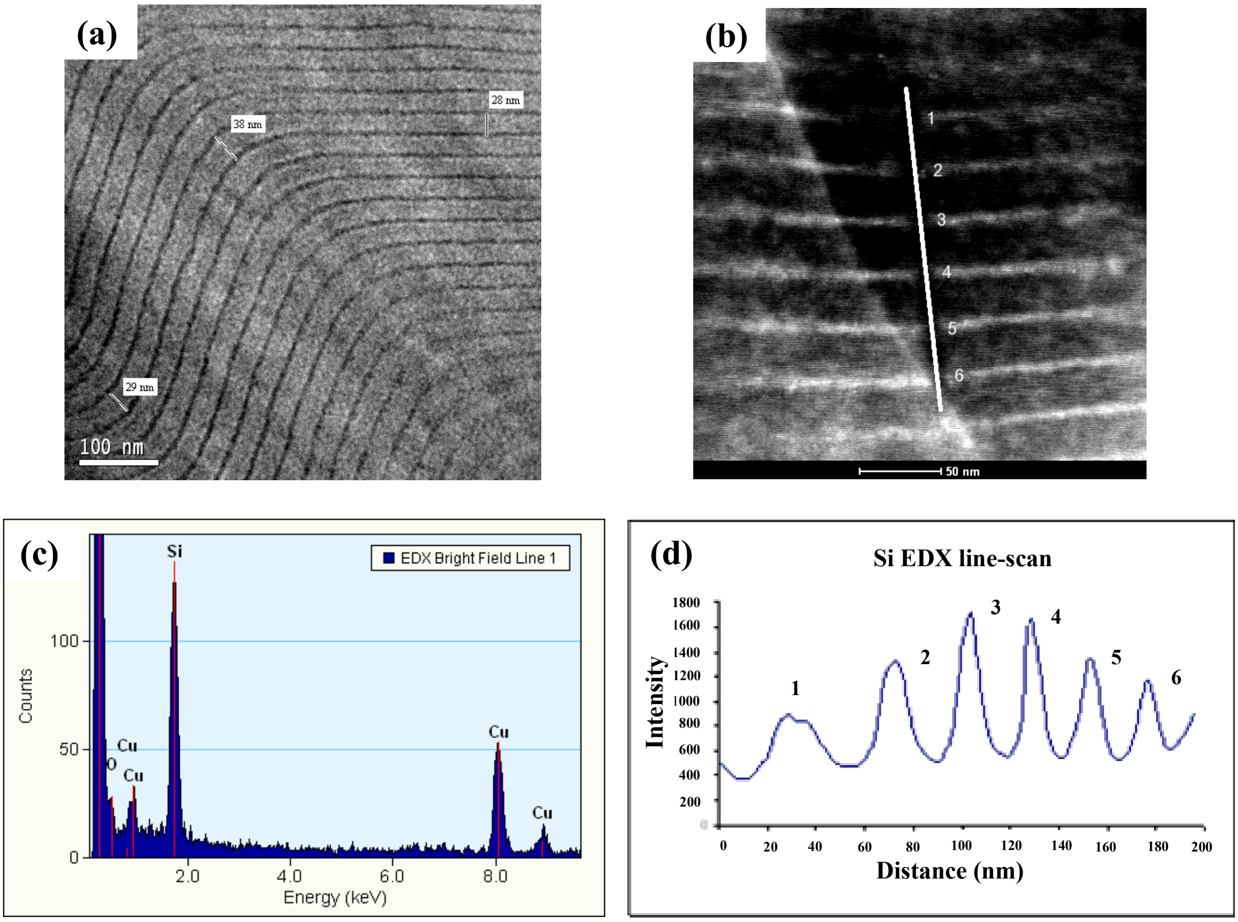

Figure 6.30. (a) TEM micrograph (scale bar is 100 nm), (b) STEM image (scale bar is 50 nm), (c) EDX spectrum obtained for line 1 performed over a Quantifoil hole and (d) Plot showing the variation in concentration of silicon within the specified layers of $\mathbf{P_3LH_{37}}$.

Transmission electron microscopy (TEM) and elemental analysis were carried out for $\mathbf{P_3LH_{37}}$ using an ultramicrotomy cut of approx. 40 nm deposited on a Quantifoil Cu grid. The unstained TEM micrograph depicted in Figure 6.30a, shows a lamellar structure originating from compositional fluctuations of a silicon containing layer (dark line). The layer thickness changes slightly along the curved contours in the range of 25-40 nm. Scanning Transmission Electron microscopy (STEM) offers, compared to TEM, unique imaging modes and enhanced microanalysis capabilities.[26] Energy-dispersive X-ray analysis (EDX) can be used in conjunction with STEM to display the spatial distribution of different elements at the nanometer scale in a thin sample. A STEM micrograph, together with EDX spectrum and elemental line scan for $\mathbf{P_3LH_{37}}$ are presented in Figures 6.30b-d. In the STEM image derived with a high angular annular dark field detector (HAADF) only scattered electrons are used for imaging (dark field image), resulting in the inverse contrast compared to TEM. The STEM image of **P_3LH_{37}** also shows a lamellar structure with a distance range of approx. 20-40 nm. EDX line scans (Figure 6.30d) reveal the variation in concentration of silicon for the hyperbranched polycarbosilane layers selected in the STEM image, confirming that silicon is contained in the bright lines. The full-width at half-maximum (FWHM) of the layers 3-6 in the STEM image is 8 nm. The doubling visible for layer 1 is likely an artifact. As electron irradiation causes heating of the material, the further the point of measurement from the edge of the Quantifoil hole the lower the amount of heat that can be transported and therefore the stronger the bending will be with respect to the movement of the free standing material. An interesting aspect of this kind of analysis would be to determine the silicon distribution in lamellar forming linear-hyperbranched polycarbosilanes.

6.4 CONCLUSIONS

In summary, an innovative strategy for the preparation of well-defined linear-hyperbranched diblock copolymers has been developed. The strategy is based on a classical AB diblock copolymer with a short, functional B-block. Subsequently, the functional B-block is used for the grafting of branched AB_2-type monomers. Slow addition of these monomers permitted control of the molecular weight of the HB block, while keeping the apparent polydispersity of the materials low (almost always $\overline{M}_w/\overline{M}_n < 1.1$). The linear-hyperbranched materials, consisting of PS and polycarbosilane blocks, do possess neither a strong amphiphilic force nor a crystallizable block that would hinder the solid-state or bulk morphological studies. It has been demonstrated – for the first time – that linear-hyperbranched polymers are capable of forming highly ordered nanophase-segregated morphologies, despite additional isomerism of the branched block in addition to the polydispersity regarding molecular weight. In addition, manipulation of the composition of the branched block in these novel materials allowed morphological control analogous to that in linear diblock copolymers. Despite the structural asymmetry between the blocks, microphase-separated states similar to those observed for linear diblock copolymers were detected. Phase segregation persists above the T_g of PS up to the decomposition temperature of the materials, and even at elevated temperatures highly ordered, phase-segregated structures were observed, indicative of the very strong segregation.

The branched structure appeared to represent a topological contribution to the incompatibility and the resulting order, *i.e.*, cylindrical structures were observed for the sample **P_3LH_{49}** with 49 wt % of the hyperbranched component. However, after annealing an irreversible transformation to the expected lamellar structure took place. Thus, the cylindrical morphology is likely to represent a kinetically controlled or metastable state and does not represent an equilibrium morphology.

Further studies over a wider range of compositions would be necessary in order to construct a precise phase diagram for such copolymers. This would allow a comprehensive comparison of the structure-morphology relationship of these intriguing copolymers with established polymer architectures.

6.5 EXPERIMENTAL

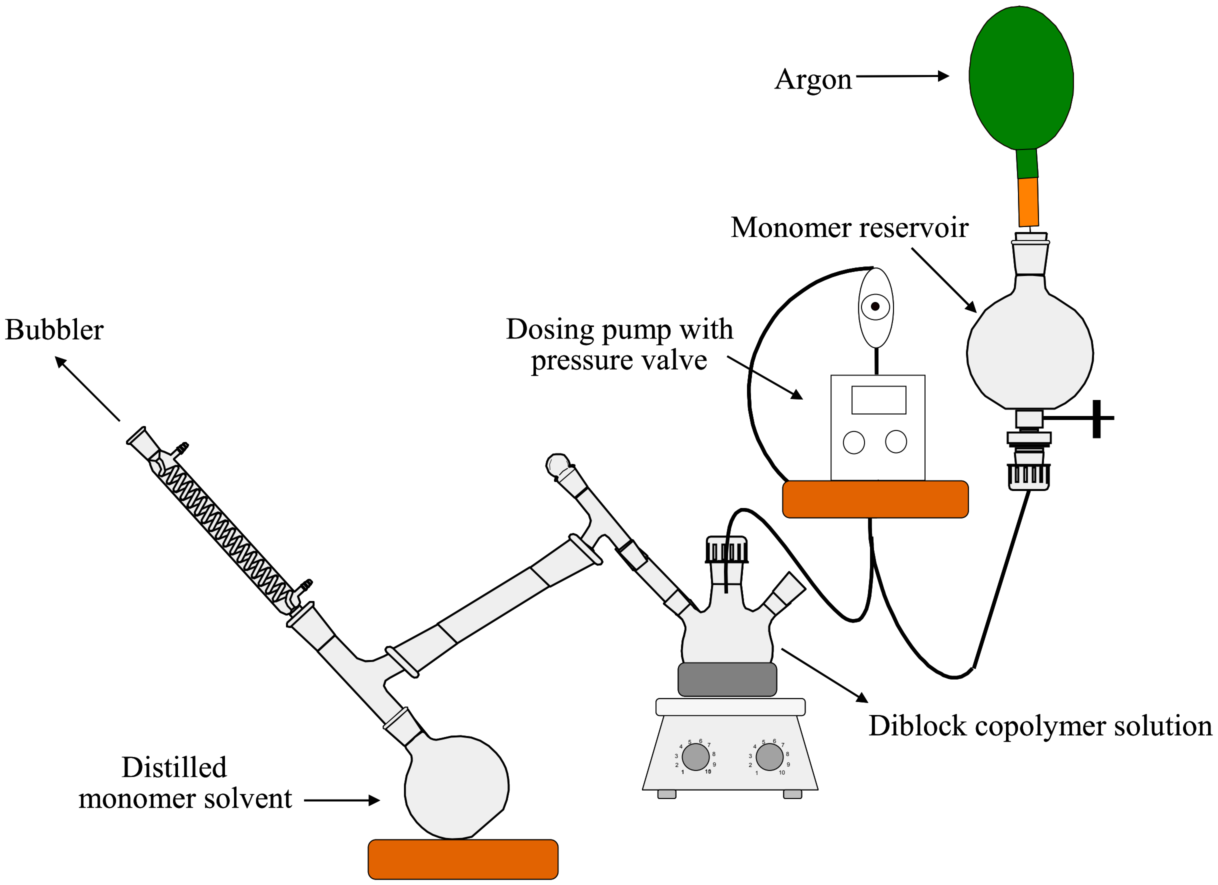

Figure 6.31. Schematic build-up of the apparatus employed for the polymer-analogous hydrosilylation reaction in the SMA mode.

Materials. **P_3** and **P_5** diblock copolymers were prepared in 20 g scales via a *Sänger et al.* simplified procedure of anionic polymerization as described in Chapter 2. Methyldiundec-10-enylsilane (MDUS) was synthesized according to described literature procedures and the details for the synthesis are given in Chapter 3. For the hypergrafting reaction, anhydrous *cis,trans*-decahydronaphtalene was used as received and diethyl ether and *n*-pentane distilled over sodium before use. Platinum-1,3-divinyltetramethyldisiloxane complex in xylene (2.1-2.4 % platinum, Karstedt catalyst) was used as the hydrosilylation catalyst.

Equipment. The polymerization via the SMA procedure was carried out in a specially designed apparatus as depicted in Figure 6.31.

Synthesis of P_3LH_{35}. The polymer-analogous hydrosilylation reaction was carried out under argon atmosphere. MDUS (1.75 g, 5 mmol) was dissolved in pentane (350 ml) and slowly added via a dosing pump to a solution of the diblock copolymer **P_3** (1g, 0.83 mmol PBD) in *cis,trans*- decahydronaphtalene (15 mL) at 70 ºC containing 0.01 mmol of Karstedt catalyst (115 µL of the Pt solution). Pentane was removed by distillation during the slow addition of the monomer. The polymer **P_3LH_{35}** was purified by fractionating precipitation. This was achieved by diluting the decaline reaction mixture with diethyl ether (*ca.* 150 mL), followed by the drop wise addition of methanol until the polymer precipitated. The supernatant fluid was decanted and the precipitate was washed several times with methanol and dried in vacuo at 40 °C. For the synthesis of analogous linear-hyperbranched diblock copolymers, the quantity of monomer added was gradually increased, so that the molar quantity of the monomer was at least equal to the molar quantity of the 1,2-PBD core. A polymer with a number-average molecular weight ($\overline{M}_n$) of 83,400 g/mol and with a polydispersity index (PDI) of 1.05 was obtained as determined by MO and GPC measurements respectively. The analogous one pot reaction was carried out by adding the neat monomer directly to a solution of the diblock copolymer in decaline and heating at 70 °C for 24 hours.

^{1}H NMR (400 MHz, $CDCl_3$): δ (ppm) 0 ($Si\text{-}CH_3$), 0.55 ($\text{-}Si\text{-}CH_2$), 1.1-1.65 (polymer backbone), 1.7 (m, $C\mathbf{H}_3\text{-}CH{=}CH\text{-}$), 1.8-2.05 (m, $\text{-}C\mathbf{H}_2\text{-}CH{=}CH\text{-}CH_3$ and polymer backbone), 2.1 (m, $\text{-}C\mathbf{H}\text{-}CH{=}CH_2$), 5.0 (m, $\text{-}CH{=}C\mathbf{H}_2$, PBD, PCSi), 5.3-5.7 (m, $\text{-}C\mathbf{H}{=}C\mathbf{H}\text{-}$, PCSi; $C\mathbf{H}{=}CH_2$, PBD), 5.9 (m, $\text{-}C\mathbf{H}{=}CH_2$, PCSi), 6.3-7.4 (m, C_6H_5); ^{13}C NMR (100 MHz, $CDCl_3$): δ (ppm) -4.7 ($Si\text{-}CH_3$), 13.1 ($\mathbf{C}H_3\text{-}CH{=}CH\text{-}$, *cis*), 14.2 ($Si\text{-}CH_2$), 18.3 ($\mathbf{C}H_3\text{-}CH{=}CH\text{-}$, *trans*), 24.3 ($Si\text{-}CH_2\text{-}\mathbf{C}H_2$), 27, 29-30.5, 33, 34.2, 34.6, 36.6, 39-47 (polymer backbone), 114.4 ($\mathbf{C}H_2{=}CH\text{-}$, PBD, PCSi), 123.9 ($CH_3\text{-}\mathbf{C}H{=}CH\text{-}$, *cis*), 124.8 ($CH_3\text{-}\mathbf{C}H{=}CH\text{-}$, *trans*), 126.0 ($C_6H_5$), 128.3 ($C_6H_5$), 131.2 ($CH_3\text{-}CH{=}\mathbf{C}H\text{-}$, *cis*), 132 ($CH_3\text{-}CH{=}\mathbf{C}H\text{-}$, *trans*), 139.5 ($\mathbf{C}H_2{=}CH\text{-}$, PCSi), 143.5 ($CH_2{=}\mathbf{C}H\text{-}$, PBD), 145.4 ($C_6H_5$, C_{ipso}); ^{29}Si NMR (80 MHz, $CDCl_3$): δ (ppm) 2.9; IR (characteristic absorption bands): γ(cm^{-1}) 1601 (stretching C=C mode), 1248 (stretching Si-CH_3 mode), 965 (internal PCSi C=C deformation), 907 (terminal PBD and PCSi C=C deformation).

6.6 REFERENCES

[1] Hadjichristidis, N.; Pitsikalis, M.; Pispas, S.; Iatrou, H. *Chem. Rev.* **2001**, *101*, 3747.

[2] (a) Lee, M.; Cho, B.-K.; Zin, W.-C. *Chem. Rev.* **2001**, *101*, 3869. (b) Zubarev, E. R., Pralle, M. U.; Li, L.; Stupp, S. I. *Science* **1999**, *283*, 523. (c) Jenekhe, S. A.; Chen, X. L. *Science* **1999**, *283*, 372. (d) Osuji, C.; Zhang, Y.; Mao, G.; Ober, C. K.; Thomas, E. L. *Macromolecules* **1999**, *32*, 7703. (e) Poser, S.; Fischer, H.; Arnold, M. *Prog. Polym. Sci.* **1998**, *23*, 1337. (f) Pitsikalis, M; Pispas, S.; Mays, J. W.; Hadjichristidis, N. *Adv. Polym. Sci.* **1998**, *135*, 1. (g) Muthukumar, M.; Ober, C. K.; Thomas, E. L. *Science* **1997**, *277*, 1225. (h) Stupp, S. I.; LeBonheur, V.; Walker, K.; Li, L. S.; Huggins, K. E.; Keser, M.; Amstutz, A. *Science* **1997**, *276*, 384. (i) Adams, J.; Gronski, W. *Macromol. Rapid Commun.* **1989**, *10*, 553.

[3] (a) Yang, L.; Hong, S.; Gido, S. P.; Velis, G.; Hadjichristidis, N. *Macromolecules* **2001**, *34*, 9069. (b) Beyer, F. L.; Gido, S. P.; Velis, G.; Hadjichristidis, N.; Tan, N. B. *Macromolecules* **1999**, *32*, 6604. (c) Hadjichristidis, N.; Tselikas, Y.; Iatrou, H.; Efstratiadis, V.; Avgeropoylos, A. *J. Macromol. Sci., Pure Appl. Chem.* **1996**, *A33*, 1447. (d) Tselikas, Y.; Iatrou, H.; Hadjichristidis, N.; Liang, K. S.; Mohanty, K.; Lohse, D. J. *J. Chem. Phys.* **1996**, *105*, 2456.

[4] (a) Pochan, D. J.; Gido, S. P.; Pispas, S.; Mays, J. W. *Macromolecules* **1996**, *29*, 5099. (b) Pochan, D, J.; Gido, S. P.; Pispas, S.; Mays, J. W.; Ryan, A. J.; Fairclough, J. P. A.; Hamley, I. W.; Terrill, N. J. *Macromolecules* **1996**, *29*, 5091.

[5] (a) Pyun, J.; Tang, C.; Kowalewski, T.; Fréchet, J. M. J.; Hawker, C. J. *Macromolecules* **2005**, *38*, 2674. (b) Zubarev, E. R.; Stupp, S. I. *J. Am. Chem. Soc.* **2002**, *124*, 5762. (c) Zubarev, E. R.; Pralle, M. U.; Sone, E. D.; Stupp, S. I. *J. Am. Chem. Soc.* **2001**, *123*, 4105. (d) Gitsov, I. *Linear-Dendritic Block Copolymers. Synthesis and Characterization*; in *Advances in Dendritic Macromolecules*, Newkome G. R.; Elsevier Science, Amsterdam, 2002, Vol. 5, Chapter 2, 45-87. (e) Gitsov, I.; Lambrych, K. L.; Ivanova, P. T.; Lewis, S. *Polym. Mater. Sci. Eng.* **2001**, *84*, 926. (f) Chang, Y.; Kwon, Y. C.; Lee, S. C.; Kim, C. *Macromolecules* **2000**, *33*, 4496. (g) Iyer, J; Fleming, K; Hammond, P. T. *Macromolecules* **1998**, *31*, 8757. (h) Leduc, M.; Hayes, W.; Fréchet, J. M. J. *J. Polym. Sci., Part A: Polym. Chem.* **1998**, *36*, 1. (i) van Hest, J. C. M.; Delnoye, D. A. P.; Baars, M. W. P. L.; van Genderen, M. H. P.; Meijer, E. W. *Science* **1995**, *268*, 1592. (j) Chapman, T. M.; Hillyer, G. L.; Mahan, E. J.; Shaffer, K. A. *J. Am. Chem.*

Soc. **1994**, *116*, 11195. (k) Gitsov, I; Ivanova, P. T.; Fréchet, J. M. J. *Macromol. Rapid Commun.* **1994**, *15*, 387. (l) Newkome, G. R.; Baker, G. R.; Arai, S.; Saunders, M. J.; Russo, P. S.; Theriot, K. J.; Moorefield, C. N.; Rogers, L. E.; Miller, J. E.; Lieux, T. R.; Murray, M. E.; Phillips, B.; Pascal, L. *J. Am. Chem. Soc.* **1990**, *112*, 8458.

[6] (a) Duan, X. X.; Yuan, F.; Wen, X. J.; Yang, M.; He, B.; Wang, W. *Macromol. Chem. Phys.* **2004**, *205*, 1410. (b) Johnson, M. A.; Iyer, J.; Hammond, P. T. *Macromolecules* **2004**, *37*, 2490. (c) Johnson, M. A.; Santini, C. M. B.; Iyer, J.; Satija, S.; Ivkov, R.; Hammond, P. T. *Macromolecules* **2002**, 35, 231-238. (d) Pochan, D. J.; Pakstis, L.; Huang, E.; Hawker, C.; Vestberg, R.; Pople, J. *Macromolecules* **2002**, *35*, 9239. (e) Mackay, M. E.; Hong, Y.; Jeong, M.; Tande, B. M.; Wagner, N. J.; Hong, S.; Gido, S. P.; Vestberg, R.; Hawker, C. J. *Macromolecules* **2002**, *35*, 8391. (f) Román, C.; Fischer, H. R.; Meijer, E. W. *Macromolecules* **1999**, *32*, 5525. (g) Gitsov, J.; Fréchet, J. M. J. *Macromolecules* **1993**, *26*, 6536.

[7] Drohmann, C.; Möller, M.; Gorbatsevich, O. B.; Muzafarov, A. M. *J. Polym. Sci., Part A: Polym. Chem.* **2000**, *38*, 741.

[8] (a) Hanselmann, R.; Hölter, D.; Frey, H. *Macromolecules* **1998**, *31*, 3790. (b) Radke, W.; Litvinenko, G.; Müller, A. H. E. *Macromolecules* **1998**, *31*, 239.

[9] (a) Ashby, B. A.; Modic, F. J. US Patent 4,288,345, 1981. (b) Karstedt, B. D. (General Electric) US Patent 3,715,334, 1973.

[10] (a) Brook, M. A. *Silicon in Organic, Organometallic and Polymer Chemistry*; Wiley: Canada, 2000. (b) Gabor, A. H.; Lehner, E. A.; Mao, G.; Schneggenburger, L. A.; Ober, C. K. *Chem. Mater.* **1994**, *6*, 927. (c) Stober, M. R.; Musolf, M. C.; Speier, J. L. *J. Org. Chem.* **1965**, *30*, 1651.

[11] Muzafarov, A. M.; Golly, M.; Möller, M. *Macromolecules* **1995**, *28*, 8444.

[12] Guo, X.; Rempel, G. L. *Macromolecules* **1992**, *25*, 883.

[13] (a) Stein, J.; Lewis, L. N.; Gao, Y.; Scott, R. A. *J. Am. Chem. Soc.* **1999**, *121*, 3693. (b) Uriarte, R. J.; Lewis, L. N. *Organometallics* **1990**, *9*, 621. (c) Haszeldine, R. N.; Parish, R. V.; Taylor, R. J. *J. Chem. Soc. A.* **1974**, 2311. (d) Harrod, J. F.; Chalk, A. J. *J. Am. Chem. Soc.* **1965**, *87*, 16. (e) Chalk, A. J.; Harrod, J. F. *J. Am. Chem. Soc.* **1964**, *86*, 1776. (f) Harrod, J. F.; Chalk, A. J. *Organic Synthesis via Metal Carbonyls*; Wender, I.; Pino, P.; John-Wiley: New York, 1977; p 673.

[14] (a) Lewis, L. N. *J. Am. Chem. Soc.* **1990**, *112*, 5998.

[15] Hazzika-Laskar, J.; Hélary, G.; Sauvet, G. *Makromol. Chem., Macromol. Symp.* **1991**, *47*, 383.

[16] Onopchenko, A.; Sabourin, E. T. *J. Org. Chem.* **1987**, *52*, 4118.

[17] Guo, X; Farwaha, R.; Rempel, G. L. *Macromolecules* **1990**, *23*, 5047.

[18] (a) Rabek, J. F. *Experimental Methods in Polymer Chemistry*; John Wiley & Sons: New York, 1980, p. 438. (b) Billingham, N. C. *Molar Mass Measurement in Polymer Science*; Kogan Press Ltd.: 1977, p 220.

[19] (a) Bates, F. S. *Science* **1991**, *251*, 898. (b) Leibler, L. *Macromolecules* **1980**, *13*, 1602. (c) Fredrickson, G. H.; Helfand, E. *J. Chem. Phys.* **1987**, *87*, 697.

[20] Hamley, I. W. *The Physics of Block Copolymers*; Oxford University Press: New York, 1998.

[21] (a) Kim, S. O.; Solak, H. H.; Stoykovich, M. P.; Ferrier, N. J.; de Pablo, J. J.; Nealey, P. F. *Nature* **2003**, *424*, 411. (b) Segalman, R. A.; Yokoyama, H.; Kramer, E. J. *Adv. Mater.* **2001**, *13*, 1152. (c) Maring, D.; Wiesner, U. *Macromolecules* **1997**, *30*, 660. (d) Morkved, T. L.; Lu, M.; Urbas, A. M.; Jaeger, H. M.; Mansky, P.; Russell, T. P. *Science* **1996**, *273*, 931.

[22] Bucknall, D. G.; Anderson, H. L. *Science* **2003**, *302*, 1904.

[23] (a) Laradji, M.; Shi, A.-C.; Desai, R. C.; Noolandi, J. *Phys. Rev. Lett.* **1997**, *78*, 2577. (b) Qi, S.; Wang, Z.-G. *Phys. Rev. E* **1997**, *55*, 1682. (c) Qi, S.; Wang, Z.-G. *Phys. Rev. Lett.* **1996**, *76*, 1679. (d) Shi, A.-C.; Noolandi, J.; Desai, R. C. *Macromolecules* **1996**, *29*, 6487.

[24] Sakurai, S.; Momii, T.; Taie, K.; Shibayama, M.; Nomura, S. *Macromolecules* **1993**, *26*, 485.

[25] (a) Bates, F. S.; Fredrickson, G. H. *Phys. Today* **1999**, *52*, 32. (b) Abetz, V.; Stadler, R.; *Macromol. Symp.* **1997**, *113*, 19.

[26] http://www.inpress.co.uk/microscope.html

CHAPTER 7

LINEAR BRUSH-LIKE DIBLOCK COPOLYMERS CONSISTING OF POLYSTYRENE AND POLYCARBOSILANE BLOCK

7.1 INTRODUCTION

Highly branched polymers (*i.e.* star and cascade-branched) are of academic and industrial interest because of their peculiar mechanical and melt properties.[1] Recently there has been an increasing interest in densely grafted or “brush” copolymer architectures.[2] In order to better understand the structure property relationship of these macromolecules, a series of well-defined polymers varying the nature of side chains, their chain length, architecture, composition as well as the structure of the polymer backbone is needed. Within these polymer brushes, comb polymers are cascade-branched polymers in which linear side-groups are attached to a linear backbone and can be considered as the first series of hyperbranched polymers – zero generation according to dendrimer nomenclature.[3] If the backbone is relatively short, comb-like polymers may adopt star-like conformations wherein the side chains are able to wrap around the flexible backbone without too much repulsion between side chains.[4] However, when the main chain is much longer than the side chains, elongation becomes preferable and the comb-like polymers adopt the shape of cylindrical brushes. This conformation has lead to them being described as “molecular bottle-brushes”.[5] The observed stiffening of the normally flexible main chain originates from the steric repulsion of the densely grafted side chains. A similar phenomenon to the induced rigidity of the backbones of these comb polymers has been experimentally observed for “poly(dendrons)”, which are polymers comprised of a linear backbone with regularly branched side-groups (“dendrons”) attached.[6]

In the literature, there are three synthetic routes for the preparation of brush-like polymers utilizing anionic, cationic or controlled radical polymerization mechanisms: “grafting through”[5d-e] (polymerization of macromonomers), “grafting onto”[2g] (attachment of prepolymerized side chains to the backbone) and “grafting from”[2f,d] (grafting side chains from the backbone). Each procedure exhibits certain advantages and disadvantages as described elsewhere.[7]

It is well-established that the morphology and properties of block copolymer materials are dictated by the composition, molar mass and architecture of the copolymer segments. However, of these structural aspects, architecture is the most poorly studied, yet it has the potential to be an extremely powerful tool for controlling material properties. Hybrid materials composed of dendritic and linear segments are an interesting class of block copolymers[8] that have shown unusual solid-state morphologies and remain relatively unexplored.[9] To date, bulk morphological studies on linear (coil)-comb (brush-like) block copolymer architectures have not been performed and therefore it remains a challenge to create well-controlled linear-comb structures to enable studies on the structure-property relationship.

This chapter deals with the grafting reaction of dimethyl(undec-10-enyl)silane (DMUS) from the polybutadiene core (PBD) of different polystyrene-*block*-poly(1,2-butadiene) diblock copolymers (PS_x-*b*-PBD_y), which were synthesized by means of anionic polymerization. The DMUS AB-type monomer is analogous in its structure to the previously employed MDUS AB_2 branching monomer. In this manner linear-comb diblock copolymers with a linearly-grafted block unit are obtained. A schematic representation of the molecular architecture described in this chapter is depicted in Figure 7.1. As before, the slow monomer addition (SMA) synthetic approach was employed for the preparation of well-defined linear-comb materials.[10] The grafting efficiency is evaluated relative to the one-pot strategy and is compared with the analogous AB_2 monomer. These novel materials, like those examined in the previous chapter, illustrate the effect of the conformational asymmetry between the linear polymer chain and the brush-like block on the overall block copolymer morphology. Therefore, complete characterization and bulk morphological studies through TEM and scattering results are provided.

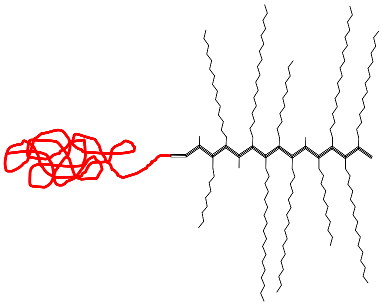

Figure 7.1. Schematic representation of the linear brush-like molecular architecture.

7.2 NOMENCLATURE

Linear brush-like diblock copolymers are denoted by PS_x-*b*-[PBD_y-*brush*-$PCSi_z$], in which *z* indicates the DP_n of the polycarbosilane block (PCSi). The brush-like block is designated by [PBD_y-*brush*-$PCSi_z$], wherein the short 1,2-PBD block is regarded as being part of the final PCSi block. However, for ease of presentation all of the polymers presented will be given an acronym. For example the polymer PS_{354}-*b*-[PBD_{84}-*brush*-$PCSi_{78}$] is abbreviated **P_1LB_{36}**. **P_1** refers to the linear block PS_{354}-*b*-PBD_{84} and **LB_{36}** denotes a linear brush-like polymer with a weight fraction of 36 % for the polycarbosilane block (including the short PBD-backbone). For details on the composition of the linear polymers, see Chapter 2 (Table 2.1).

7.3 RESULTS AND DISCUSSION

7.3.1 Synthetic strategy and compositional characterization

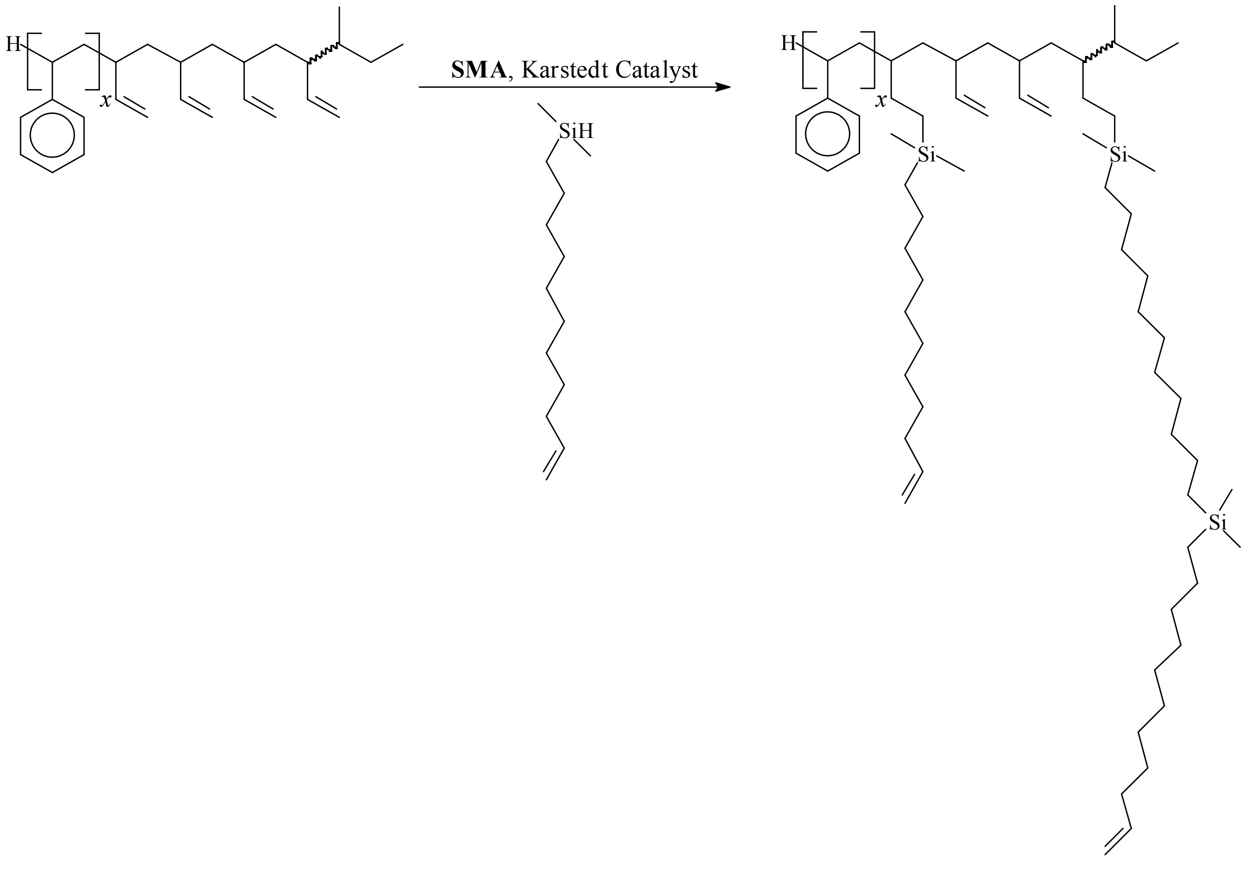

Figure 7.2. Synthesis of linear-comb diblock copolymers by grafting of linear AB DMUS monomers from a short PBD-block of PS_x-*b*-PBD_y (The PBD block has an atactic configuration, although for simplicity the vinyl groups are depicted on one side).

DMUS was grafted by hydrosilylation from the PBD-core of different PS$_x$-*b*-PBD$_y$ diblock copolymers ($\overline{M}_n$ = 41,400-127,800; wt % PBD = 4.5-11) using the Karstedt catalyst (Figure 7.2).[11] In this manner, linear brush-like diblock copolymers were obtained analogues to the linear-hyperbranched polymers described in Chapter 6. The comb block was prepared in a controlled manner via the SMA synthetic strategy. The reaction conditions employed were the same as for the linear-hyperbranched systems (pentane and decaline as the monomer and core solvents, respectively, and grafting reaction temperature of 70 °C) and the size of the brush-like block was controlled by the monomer:core ratio. The complete series of linear-comb diblock copolymers prepared including their nomenclature and abbreviations are presented in Table 7.1.

Table 7.1. Designation of the AB Linear Brush-like Block Copolymers.

Sample	Acronym
PS$_{520}$-*b*-[PBD$_{47}$-*brush*-PCSi$_{104}$]	**P$_3$LB$_{31}$**
PS$_{520}$-*b*-[PBD$_{47}$-*brush*-PCSi$_{159}$]	**P$_3$LB$_{40}$**
PS$_{520}$-*b*-[PBD$_{47}$-*brush*-PCSi$_{177}$]	**P$_3$LB$_{42}$**
PS$_{520}$-*b*-[PBD$_{47}$-*brush*-PCSi$_{195}$]	**P$_3$LB$_{45}$**
PS$_{354}$-*b*-[PBD$_{84}$-*brush*-PCSi$_{78}$]	**P$_1$LB$_{36}$**
PS$_{354}$-*b*-[PBD$_{84}$-*brush*-PCSi$_{110}$]	**P$_1$LB$_{43}$**
PS$_{354}$-*b*-[PBD$_{84}$-*brush*-PCSi$_{198}$]	**P$_1$LB$_{56}$**
PS$_{1156}$-*b*-[PBD$_{130}$-*brush*-PCSi$_{218}$]	**P$_5$LB$_{28}$**
PS$_{1156}$-*b*-[PBD$_{130}$-*brush*-PCSi$_{285}$]	**P$_5$LB$_{34}$**
PS$_{1156}$-*b*-[PBD$_{130}$-*brush*-PCSi$_{491}$]	**P$_5$LB$_{46}$**

[a]For example, in **P$_1$LB$_{36}$**: **P$_1$** refers to the linear block PS$_{354}$-*b*-PBD$_{84}$ and **LB$_{36}$** denotes the corresponding linear brush-like diblock copolymer with a weight fraction of 36 % for the PCSi block (including the short PBD-backbone).

As with the grafting reaction between the AB$_2$ monomer and the linear core, a fraction of the AB monomer was not attached to the polyfunctional core. The AB monomer can not only attach to the PBD-core via a chain-growth mechanism, which is the desired outcome, but also, the monomer can build brush-like polycarbosilanes, which may eventually cyclize or “loose” functionality negating the possibility to connect to the linear core. A representative GPC chromatogram of the crude reaction mixture reveals a broad low molecular weight peak with a polydispersity of ~ 3.0 (Figure 7.3a). However, as for the linear-hyperbranched structures, complete separation of these non-attached structures was achieved by fractionating precipitation in diethyl ether/methanol. This is confirmed by obtaining a GPC chromatogram of the polymer after fractionation (Figure 7.3b).

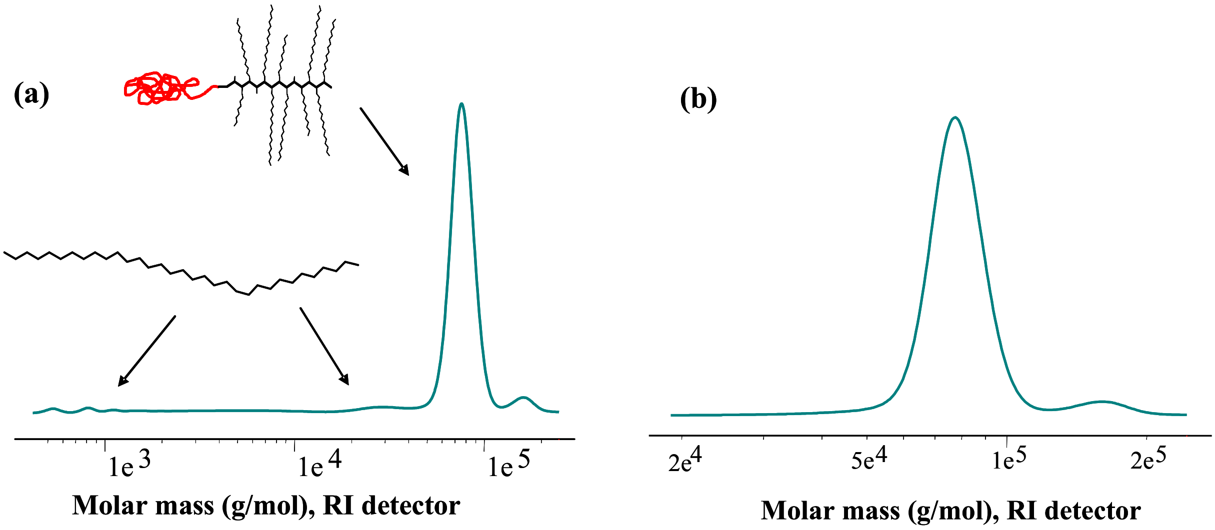

***Figure** 7.3.* GPC chromatograms of (a) $\mathbf{P_3LB_{40}}$ crude reaction product and (b) $\mathbf{P_3LB_{40}}$ fractionated sample.

The GPC chromatograms of some polymers (Figure 7.4) showed low amounts of a higher molecular weight tail, in addition to the diblock dimer peak and these were included in the molecular characterization of the linear-brush materials. These peaks were also observed in the case of the linear-hyperbranched diblocks described in Chapter 6 and possible explanations for the presence of this high molecular weight tail are discussed therein. These higher molecular weight peaks generally increased with time and we speculate that traces of catalyst, which remain after the workup, enable cross linking of the double bonds. This changing stability can be clearly seen in the GPC plots of freshly precipitated $\mathbf{P_1LB_{43}}$ and of a two year old sample (Figure 7.5).

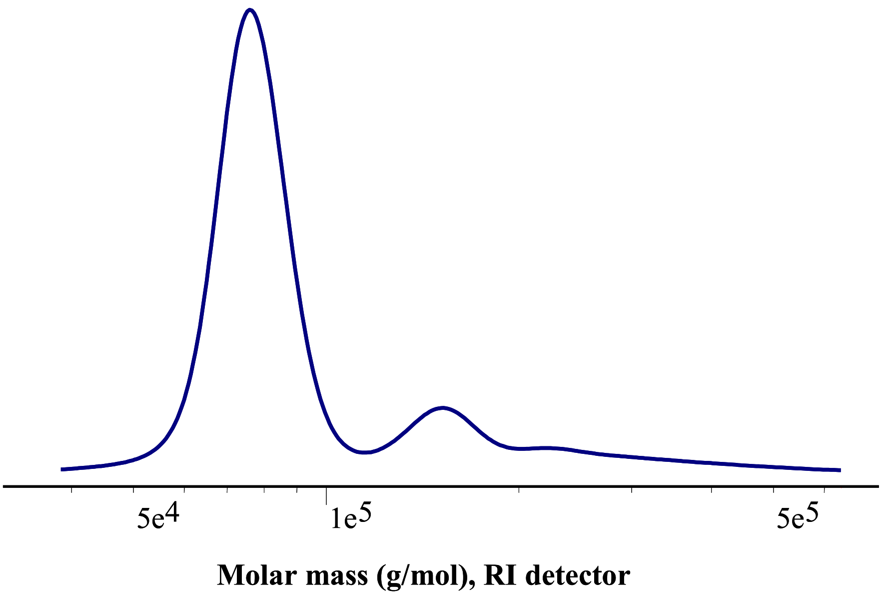

Figure 7.4. GPC chromatogram of **P_3LB_{42}** after fractionating precipitation.

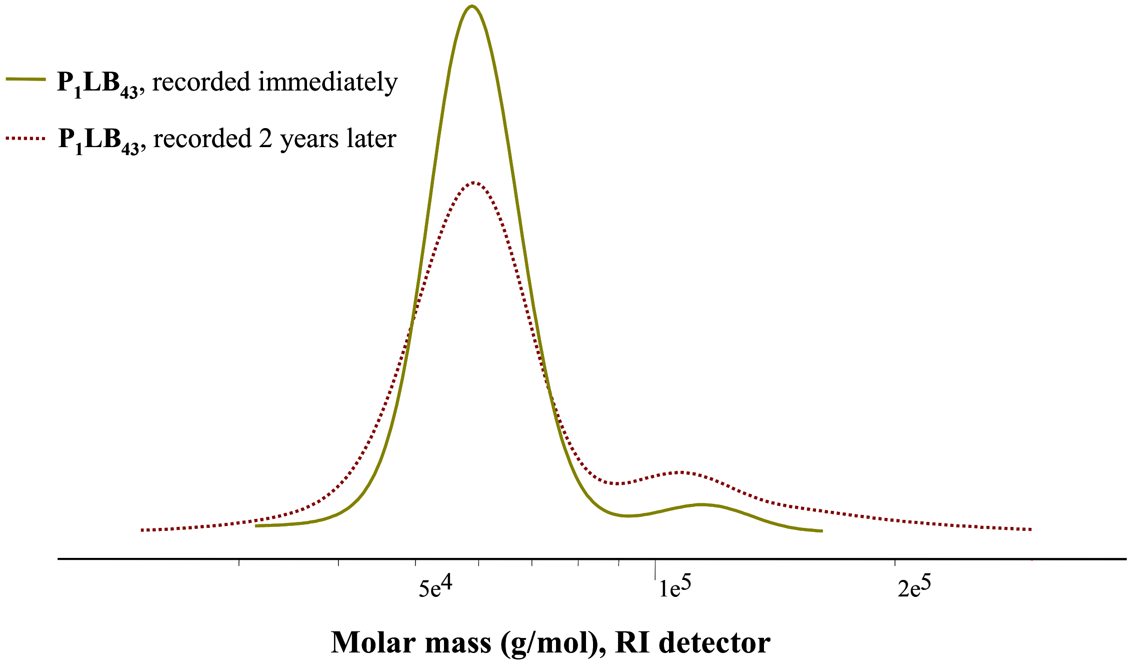

Figure 7.5. GPC plots of **P_1LB_{43}** recorded immediately and two years after fractionating precipitation in diethyl ether/methanol.

The amount of the linear (potentially “cyclic”) homopolymers obtained in the grafting reaction using the AB monomer was lower than in the reaction of the analogous AB_2 monomer under the same monomer:core ratio. This can be seen by comparing the relative intensities of the two modes in the GPC elutogramms for the crude reaction products of both the AB_2 and the AB grafting reactions (Figure 7.6). In the GPC diagram, the main peak corresponding to the linear-brush architecture (depicted in blue), is clearly displaced to higher molecular weights. Hence, it is evident that the reaction with the AB_2 monomer is not as effective as the reaction with the AB monomer. This might be related to the lower probability of “cyclization” of the AB versus the AB_2 monomer, due to the presence of just one end group. In Chapter 6 a general insight into the factors that might contribute to the formation of homopolymers during the SMA procedure was proposed. It can be concluded that an additional factor contributing to the decreased coupling between the AB_2 monomer and the linear core is the steric hindrance inherent in the branching monomer structure.

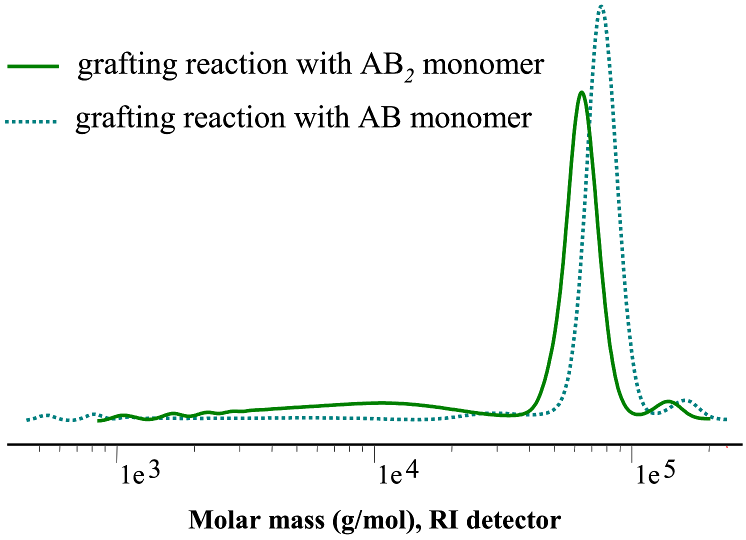

Figure 7.6. Overlay of the GPC chromatograms of the crude reaction products obtained in a grafting reaction of MDUS (AB_2) and DMUS (AB) monomers from $\mathbf{P_3}$ using the same molar excess of monomer.

In the SMA procedure, the molecular weight of the resulting linear-brush polycarbosilanes, increased linearly with the amount of AB monomer added, despite the fact that the monomer did not react exclusively with the growing brush structure. This is demonstrated in Figure 7.7, which shows a linear core and a series of linear brush-like polycarbosilanes. The polydispersity values of the linear brush-like polymers remains relatively low ($\overline{M}_w/\overline{M}_n$ = 1.04-1.50). As in the case of the linear-hyperbranched systems, controlled growth of the macromolecules was achieved and furthermore, as ascertained from the GPC chromatogram in Figure 7.8, the reactions in the SMA mode lead to the formation of less "cyclic homopolymers" than the reactions performed in one-pot.

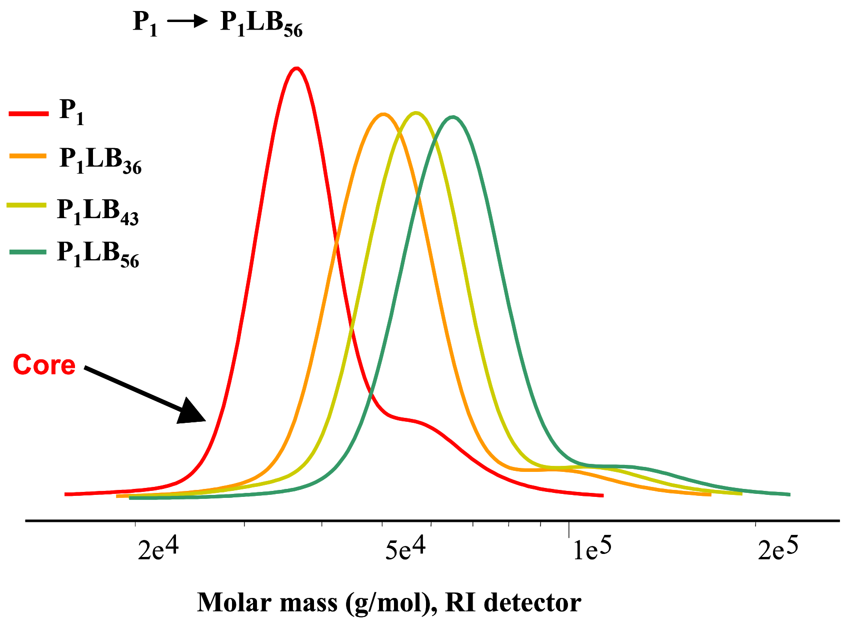

Figure 7.7. GPC diagrams of the linear core (**P₁**, $\overline{M}_n$ = 37,800 g/mol) and of the resulting linear brush-like block copolymers with increasing amount of DMUS monomer added.

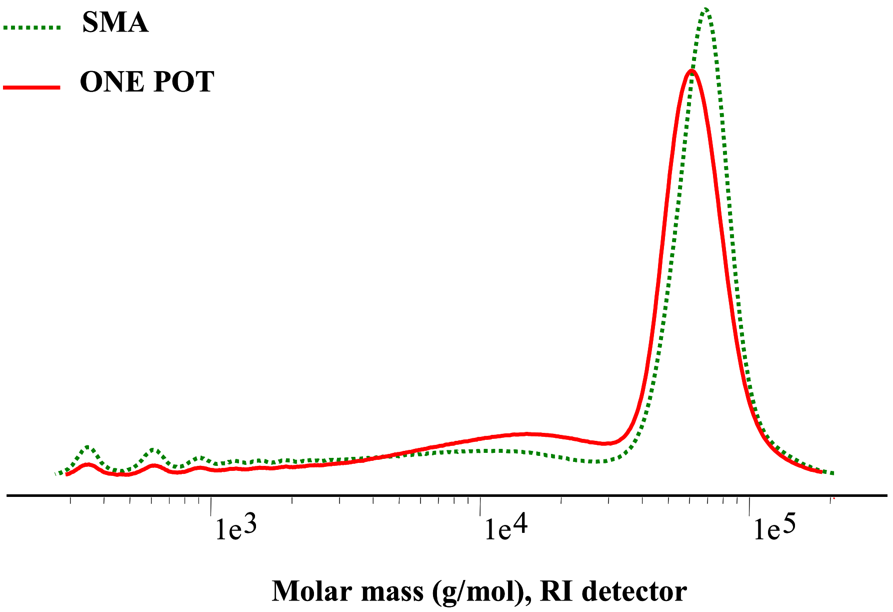

Figure 7.8. Comparison of the GPC chromatograms of a grafting reaction, using DMUS AB-type monomer, carried out in one-pot versus SMA mode for the linear core **P_2** ($\overline{M}_n$ = 40,800 g/mol).

7.3.2 Chemical structural characterization

The linear brush-like diblock copolymers obtained after fractionating precipitation were characterized by ^{1}H, ^{13}C and ^{29}Si NMR and by IR spectroscopy. The typical yields of the isolated linear brush-like polymers were in the range of 33-60 %. They displayed good solubility in a wide range of common organic solvents like THF, diethyl ether, chloroform, chlorobenzene and toluene. However, they exhibited poor solubility in non-polar solvents like pentane and were totally insoluble in polar solvents like water, methanol, DMSO and DMF, as expected.

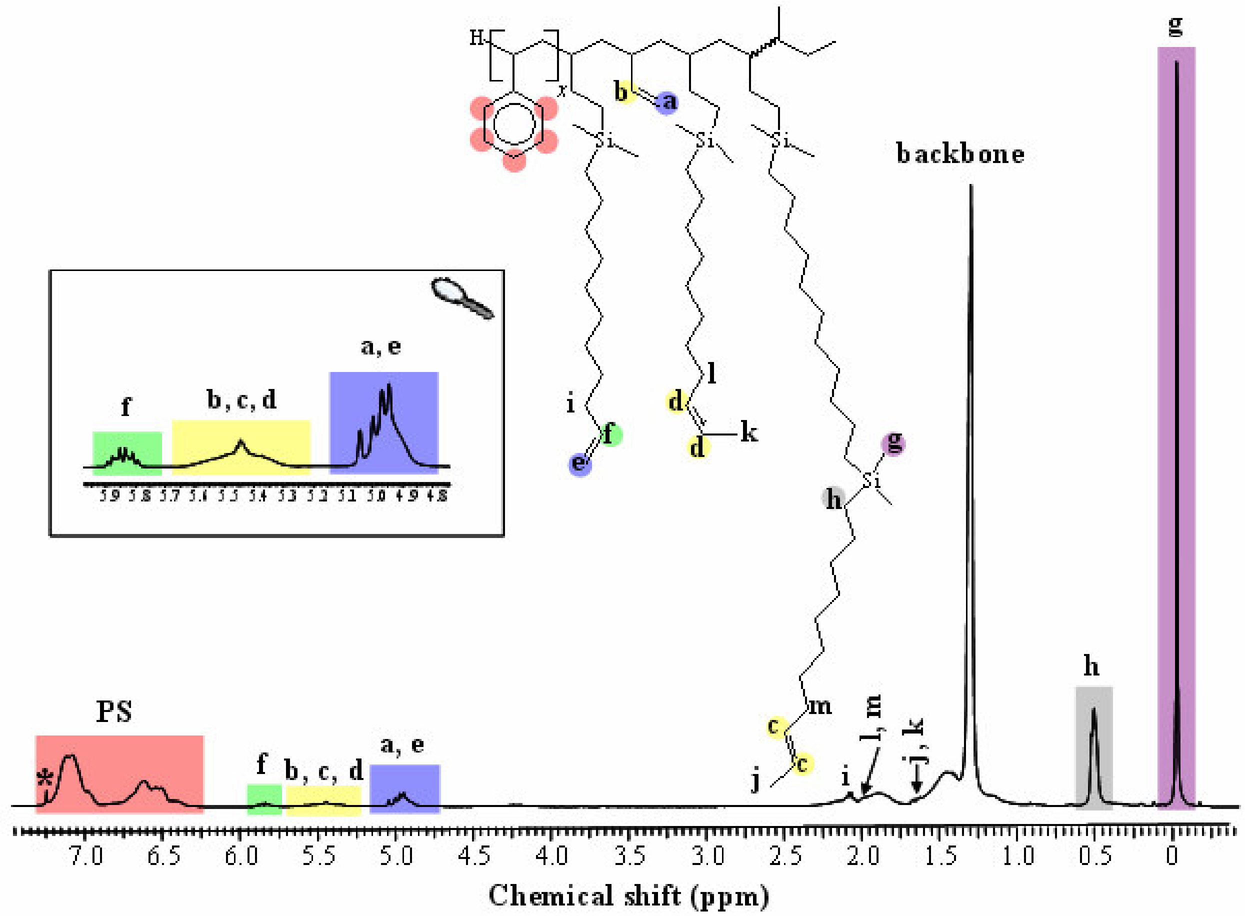

Figure 7.9. ^{1}H NMR spectrum of **P_1LB_{43}** in $CDCl_3$ (solvent peak denoted by an asterisk).

The ^{1}H NMR spectrum of a linear-*b*-brush diblock copolymer is shown in Figure 7.9. As expected, isomerization of the terminal double bonds occurred during the hydrosilylation reaction, resulting in three signals in the vinylic region of the ^{1}H NMR. For the linear-hyperbranched structures (Chapter 6), complete isomerization of the terminal double bonds occurred, when using diethyl ether as the monomer solvent. This was also the case for the linear brush-like diblock copolymers, as it can be seen from the ^{1}H NMR spectrum of a sample obtained from the reaction of DMUS with **P$_3$** using diethyl ether as the monomer solvent (Figure 7.10). The NMR signals were assigned by analogy with the linear-hyperbranched structures (Chapter 6, section 6.3.2).

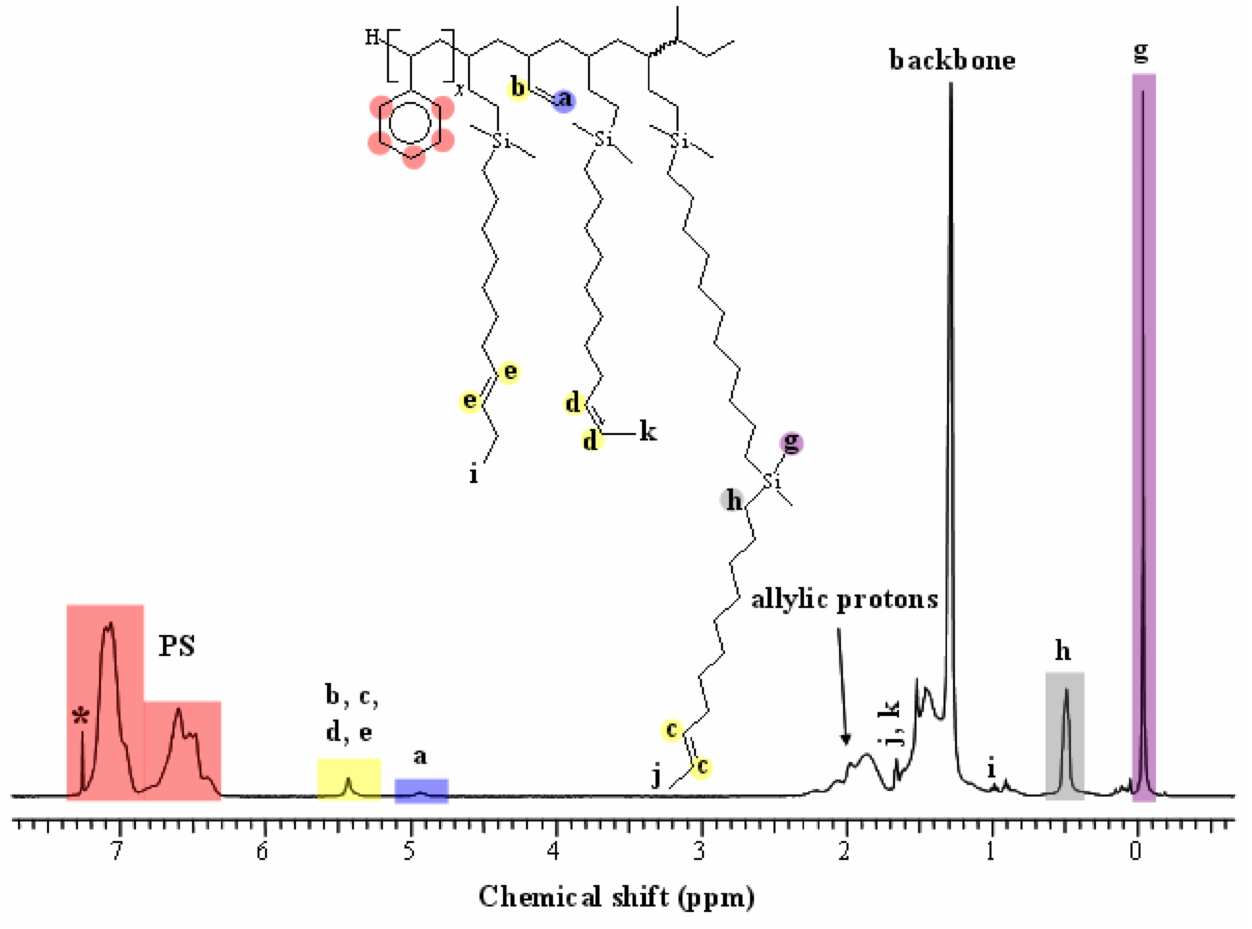

Figure 7.10. ^{1}H NMR spectrum of **P$_3$LB$_{42}$**, obtained by using diethyl ether as the monomer solvent, in CDCl$_3$ (solvent peak denoted by an asterisk).

The general trends regarding the microstructure of these linear-brush systems are similar to those found for the linear-hyperbranched polymers and they can be briefly summarized as follows:

(1) Some of the pendant vinyl groups of the PBD core remained unreacted and it is possible to estimate by ^{1}H NMR the number of grafted functionalities per PBD backbone. For these calculations, the equations 6.1 and 6.2 presented in Chapter 6 can also be used for the linear brush-like diblock copolymers. The percentages of the PBD-grafted sites for the different polymers synthesized are presented in Table 7.2. It is important to remark that this is a semi-quantitative analysis due to the high molecular weight of the polymers and the relatively small

number of sites. Therefore the values for the linear-brushes obtained from the parent polymer **P_5** with the highest molecular weight are not presented, as these are unreliable. The number of hydrosilylated sites varied between 30 and 45 %. For the samples that were synthesized using diethyl ether as the monomer solvent, the percentages were higher possibly due to the better solvation and therefore flexibility of the PBD sites in a more polar solvent (diethyl ether *vs.* pentane).

Table 7.2. Percentage of hydrosilylated PBD sites for the AB Linear Brush-like Block Copolymers.

Linear-Brush samples	PBD grafted sites
P_3LB_{31}	31.2 %
P_3LB_{40}	39.3 %
P_3LB_{42}[a]	93.7 %
P_3LB_{45}[a]	54.4 %
P_1LB_{36}	36.6 %
P_1LB_{43}	44.8 %
P_1LB_{56}	41.2 %

[a] Polymers synthesized using diethyl ether as the monomer solvent

(2) Grafting of the silane AB-type monomers gave the Anti-Markovnikov addition products and as before, the internal double bonds formed remained unreactive. This is consistent with the structural results obtained for the linear-hyperbranched polymers. Equation 6.3 presented in Chapter 6 can also be used to estimate the percentage of isomerized double bonds for the linear brush-like systems and in the case of these systems displayed circa 19-26 % isomerization.

(3) As expected, only one signal was observed in the ^{29}Si NMR spectrum (Figure 7.11), giving no possibility to differentiate between linear and terminal units. After reacting, the proton in the DMUS monomer is replaced by an alkyl chain to give the resulting brush architecture and this results in a considerable downfield shift of the silicon signal (Table 7.3). This downfield shift is analogous to that observed for the linear-hyperbranched systems.

Table 7.3. ^{29}Si NMR chemical shifts.

Compound	δ_{Si} (ppm)
DMUS	-12.95
P_3LB_{40}	2.4

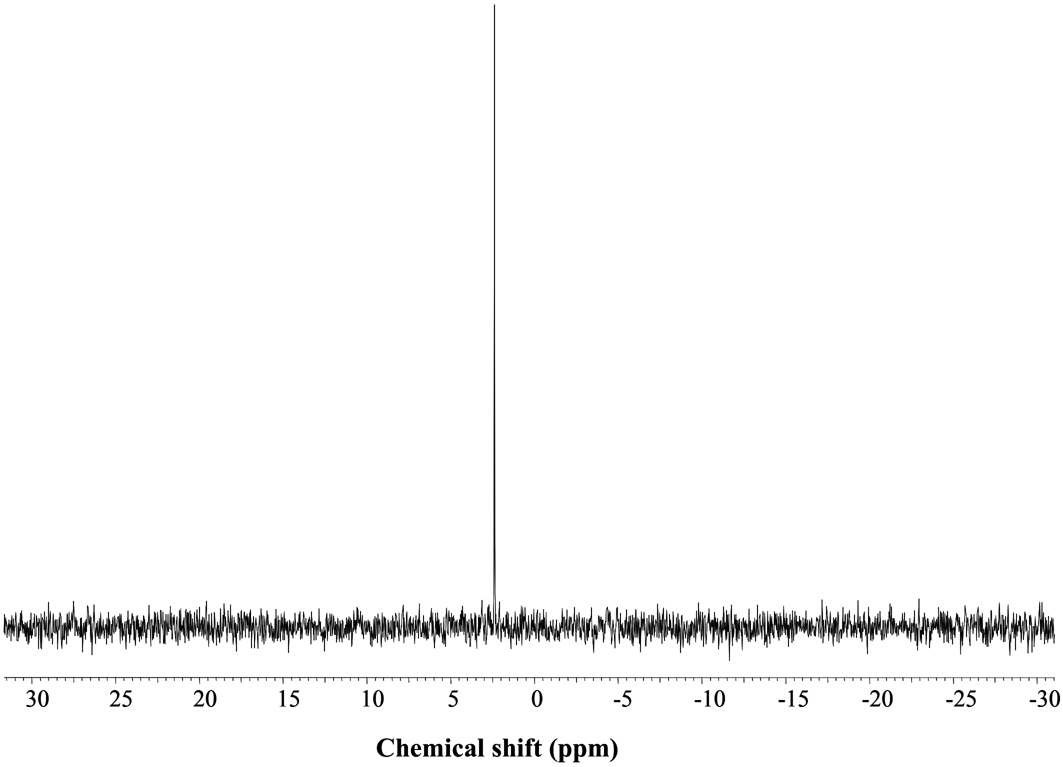

Figure 7.11. ^{29}Si NMR spectrum of **P_3LB_{40}** in $CDCl_3$.

(4) Ideally, the number of double bonds should remain constant after performing the grafting reaction with the AB monomer. However analysis of the NMR spectra confirmed that the number of vinyl group signals decreased, as a result of competing side reactions. The reasons for this are presented in Chapter 6 and concern mainly alkene hydrogenation side reactions.

(5) The stability of the polymers deteriorated at ambient temperature and in the presence of light with time. This was evidenced by a decrease in the integration values for the vinyl signals in the ^{1}H NMR spectrum and is in agreement with the GPC studies indicating that a type of cross linking takes place due to the presence of catalyst residues.

The IR spectra of a linear diblock copolymer and of the corresponding grafted linear brush-like polymer are presented in Figure 7.12 and confirm the grafting of DMUS from the PBD core. In Figure 7.12b the new absorbances at 1248 cm^{-1} and 832 cm^{-1} are due to the stretching and bending modes of Si-CH_3 and CH_3-Si-CH_3 respectively.

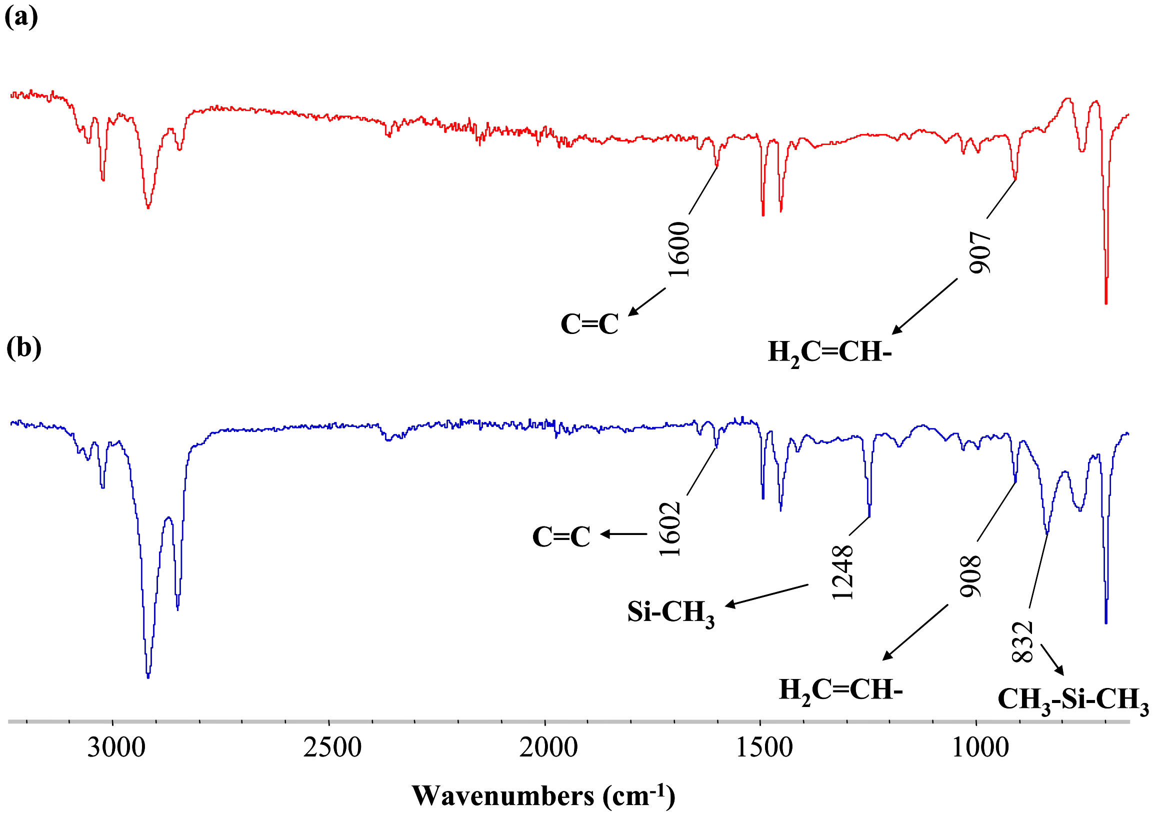

Figure 7.12. IR spectra of (a) $\mathbf{P_1}$ (b) $\mathbf{P_1LB_{43}}$.

Grafting reactions were performed on three different linear cores, namely $\mathbf{P_3}$, $\mathbf{P_1}$ and $\mathbf{P_5}$, having molecular weights of 56,800 (4.5 wt % PBD), 41,400 (11 wt % PBD) and 127,800 g/mol (5.5 wt % PBD), respectively. Better efficiencies were obtained for the linear polymer with lower molecular weight ($\mathbf{P_1}$), when using the same monomer:core mol ratios as in the case of AB_2 hypergrafting reactions.

7.3.3 Solid state behavior

Table 7.4. Characterization data, thermal properties and bulk morphology for the linear cores (PS_x-*b*-PBD_y) and the respective linear brush-like diblock copolymers.

	GPC[a]		**MO**[b]		**DSC**[c]		**TEM/SAXS**
Sample	M_n (10^3 g/mol)	PDI[d]	M_n (10^3 g/mol)	wt % PS	T_g1 (°C)	T_g2 (°C)	Morphology
P_3	63.8	1.04	56.8	95.5	99.7	-48.6	---
P_3LB_{31}	69.7	1.04	78.8	69	93.1	-43.1	Gyroid
P_3LB_{40}	78.4	1.05	90.6	60	101	-50.5	Lamellae
P_3LB_{42}	85.6	1.26	94.3	58	103.3	-59.5	Lamellae
P_3LB_{45}	79.3	1.26	98.2	55	92.7	-37.3	Lamellae
P_1	37.8	1.07	41.4	89	101	-56.7	---
P_1LB_{36}	51.8	1.06	57.9	64	94.8	-51.2	Lamellae
P_1LB_{43}	59.2	1.06	64.7	57	105.6	-59.3	Ellipsoidal
P_1LB_{56}	66.0	1.08	83.5	44	84	-57.8	Ellipsoidal
P_5	110.0	1.04	127.8	94.5	100.1	-18.7	---
P_5LB_{28}	128.0	1.26	167.2	72	105.3	-60.4	Lamellae
P_5LB_{34}	146.0	1.32	181.3	66	107.3	-62.1	Lamellae
P_5LB_{46}	183.0	1.50	225.1	54	108.6	-58.1	Cylindrical

[a] Gel permeation chromatography (GPC) measured in chloroform at 30 °C with PS standard calibration. [b] Membrane osmometry (MO) measured in toluene at 40 °C. [c] Differential Scanning Calorimetry (DSC) measured at a heating rate of 25 °C/min. [d] Polydispersity index $\overline{M}_w/\overline{M}_n$ measured by GPC in chloroform at 30 °C

GPC data analysis using refractive index detection does not yield accurate molecular weight data due to the high density of branches. Molecular weights obtained via membrane osmometry (MO) measurements were therefore used to calculate the wt % of the linear PS and the comb [PBD-*brush*-PCSi] blocks for each sample. The characterization data of the linear core diblock copolymers $\mathbf{P_3}$, $\mathbf{P_1}$ and $\mathbf{P_5}$ containing 4.5, 11 and 5.5 wt % of PBD respectively and of the resulting linear brush-like polycarbosilane structures, are presented in Table 7.4. In these structures the short PBD block becomes part of the final PCSi and is also treated as such in all ensuing considerations. This is justified by the fact that the PBD-core in the final polymer architectures is indistinguishable from the linearly grafted carbosilane unit, as verified by DSC measurements.

The thermal properties of both the precursor and modified polymers were determined by Differential Scanning Calorimetry (DSC) and Thermogravimetric Analysis (TGA). The presence of two glass transition temperatures (T_g) is already evidence of microphase separation in the bulk state (Figure 7.13). The T_g values for the obtained diblock copolymers are reported in Table 7.4. As anticipated, the comb PCSi block has low T_g values in the range of -37 to -62 °C, while the PS block exhibits a T_g in the range 95-109 °C. The thermal stability of the linear brush-like polycarbosilanes is comparable to that of the linear PS_x-*b*-PBD_y cores and the linear-hyperbranched modified polymers (Figure 7.14). Although the onset of weight loss for $\mathbf{P_5LB_{46}}$ is slightly higher than for the linear-hyperbranched structures (451 °C *vs.* 436 °C), this might be due to the higher molecular weight of $\mathbf{P_5LB_{46}}$.

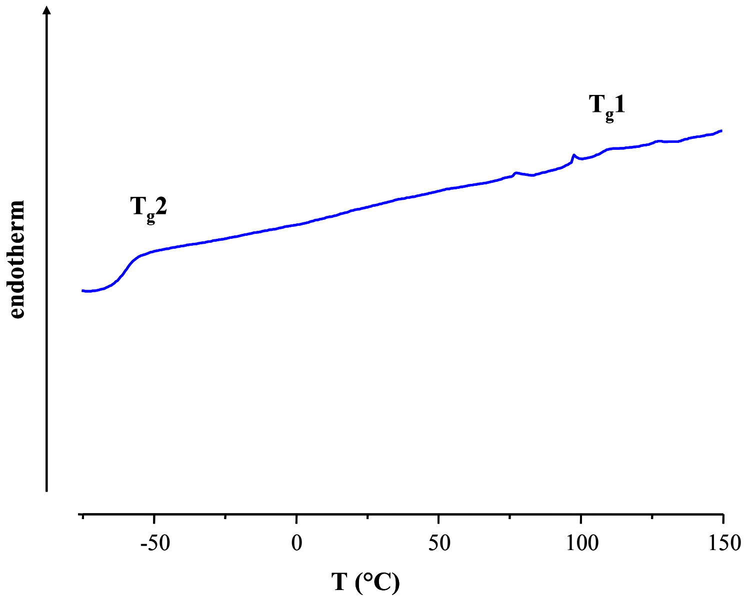

Figure 7.13. DSC curve of $\mathbf{P_1LB_{43}}$, scanning rate 25 °C/min.

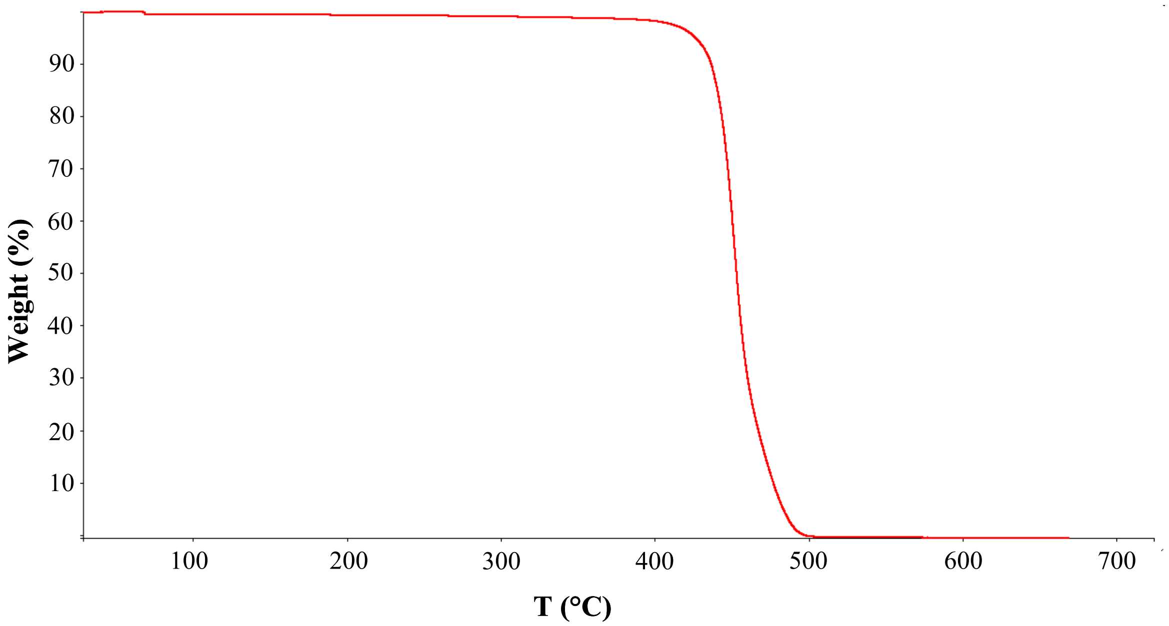

Figure 7.14. TGA curve of **P_5LB_{46}** in N_2, heating rate 10 °C/min, exemplifying the thermal stability of the linear brush-like diblock copolymers.

Characterization of the resulting bulk morphologies was accomplished by Transmission Electron Microscopy (TEM), Atomic Force Microscopy (AFM) and temperature-dependent Small Angle X-ray Scattering (SAXS) measurements. The SAXS patterns were obtained from compression-molded samples, while the AFM and TEM images were taken from both compression-molded samples and solution-cast films using toluene or THF as non-preferential solvents. However, the observed morphologies were in general largely independent of the sample pre-treatment, the only difference being that the solution cast films displayed a higher degree of order than the melt-processed samples. Generally, the contrast in the TEM images, unless otherwise specified, is based solely on differences in the electron density between silicon and carbon, in other words, no additional staining has been applied. In the unstained TEM images, the bright areas correspond to the PS (linear block) and the dark areas to the PCSi (brush-like block). The PCSi domains appear dark in the TEM images taken from samples that have been stained with OsO_4 to enhance contrast under the electron beam. Contrast in the AFM phase images is based on hard and soft material: PS (hard), PCSi (soft). In the AFM images presented the hard domains are bright, while the soft domains are dark.

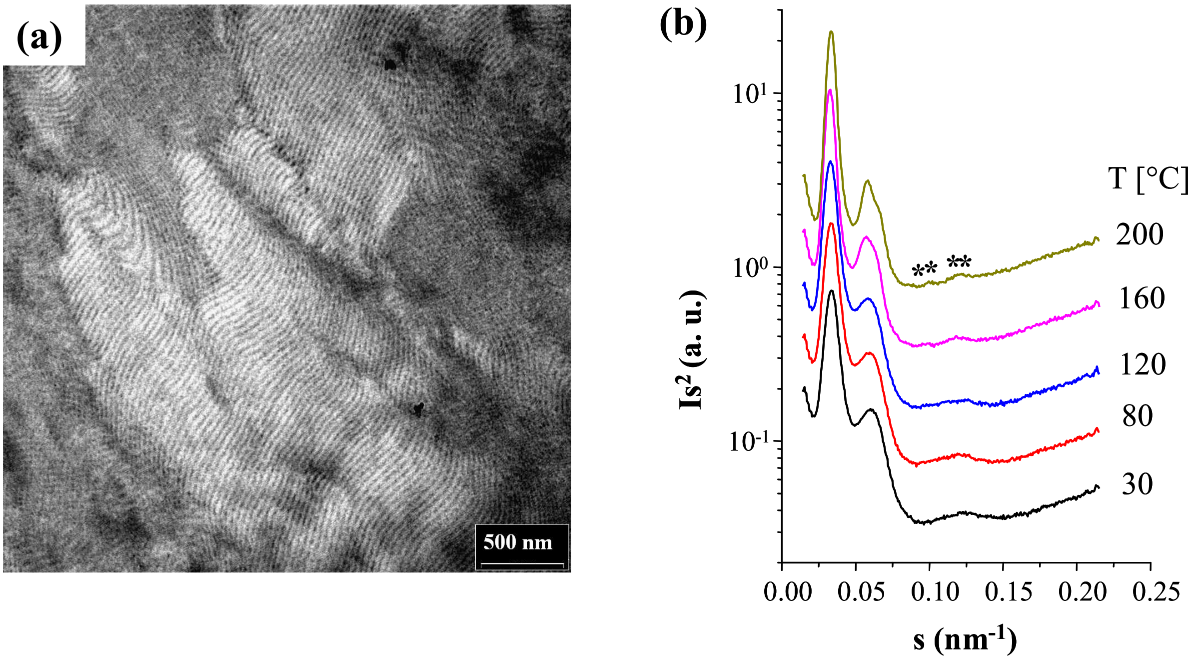

Figure 7.15. (a) Unstained TEM (compression-molded sample) and (b) SAXS diffraction pattern (compression-molded sample) of $\mathbf{P_3LB_{31}}$.

A total of ten linear brush-like polycarbosilane samples with a brush block weight content between 28 and 56 % have been prepared and studied. A summary of the morphological behavior exhibited by these samples is presented in Table 7.4. Four samples, with a PCSi brush block weight content ranging between 31 and 45 %, were prepared from the linear copolymer $\mathbf{P_3}$ (PS_{520}-*b*-PBD_{47}). A TEM micrograph of the compression-molded sample $\mathbf{P_3LB_{31}}$ containing 31 wt % of the brush PCSi block is presented in Figure 7.15a. It is not possible to unambiguously ascertain from this image whether a lamellar or a cylindrical morphology has been formed and perhaps this sample is at a phase boundary. The corresponding SAXS pattern is presented in Figure 7.15b and shows reflections consistent with cylinders, *i.e.*, ratio spacings of 1, √3, √4 and √12, with a repeat spacing of approx. 36 nm. However, in the SAXS profile at 200 °C some new relatively broad and weak peaks (denoted by an asterisk) at ratio spacings of √10, √11 and √15, √16 are observed, which are tentatively assigned to a gyroid morphology.[12] The presence of only low order peaks in the X-ray pattern again leads to ambiguities in the phase identification. It is possible that the equilibrium structure of $\mathbf{P_3LB_{31}}$ simply has not been achieved due to the relatively short annealing times (*ca.* 30 minutes above the T_g of PS) before performing the TEM and SAXS measurements.

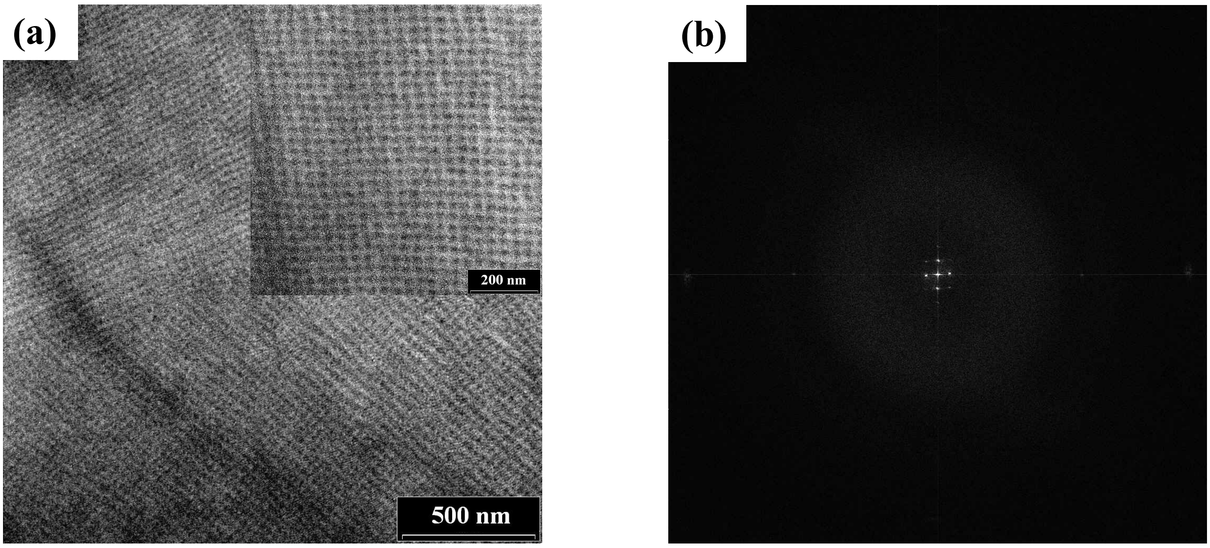

Figure 7.16. (a) Unstained TEM with inset magnification (solution-cast film in toluene, scale marker is 200 nm for the inset figure), showing 4-fold symmetry corresponding to the [100] projection of a cubic structure and (b) FFT image of **P$_3$LB$_{31}$**.

In order to improve the long-range order in the sample and to determine the equilibrium microphase, films of **P$_3$LB$_{31}$** were cast from toluene and THF (as non-preferential solvents) and examined by TEM after annealing for 30 minutes at *ca.* 120 °C. The resulting unstained TEM micrograph of **P$_3$LB$_{31}$** cast from toluene is presented in Figure 7.16a and shows a high degree of long-range order. Such a TEM image is inconsistent with the formation of PCSi cylinders in an hexagonal arrangement or with various packing formations of spheres. Interestingly, the PCSi domains seem to be ordered in a square lattice. The symmetry of the TEM images was determined by a two-dimensional fast Fourier transform (FFT), showing four strong reflections with approx. 4-fold symmetry about the origin (Figure 7.16b). The observation of a square lattice image could be as a result of two orthogonal orientations of cylinders as depicted in Figure 7.17. However, as described in the literature the presence of these 4-fold projections means that a cubic phase is more likely.[12b-c,13,15e] Therefore the TEM images in Figure 7.16a can be indexed as the [100] projection of a cubic structure.

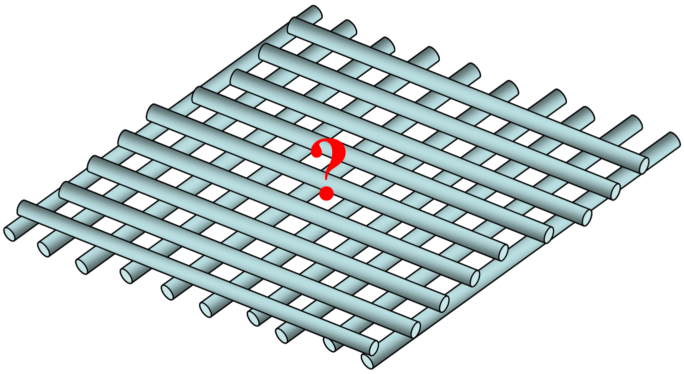

Figure 7.17. Schematic picture of two layers of cylindrical domains at a grain boundary.

To confirm this finding, a film of **P_3LB_{31}** cast from THF, annealed for *ca.* 30 minutes and subsequently stained with OsO_4, was prepared and examined by TEM. The observed microdomain structures are presented in Figures 7.18 and 7.19 wherein, the brush-PCSi domains are selectively stained with the OsO_4 and appear dark. The electron micrograph in Figure 7.18a shows mixed regions with apparently different morphologies. Cylindrical PCSi domains in a PS matrix are clearly observed via enlargement of the circled region "A" (Figure 7.18b). Magnification of the region denoted by "B" shows again a hexagonally packed cylindrical morphology (Figure 7.18c) with additional regions displaying a kind of a transition state from cylinders to lamellae as schematically represented in Figure 7.20.[14] Region circled "C" (Figure 7.18d) probably corresponds to superimposed cylinders as the size of the stacks normal to the interface is small. However, a lamellar structure, as a result of the mentioned transition, was not observed in this sample. In the area denoted by the circled region "D" a network of connected cylinders with hexagonal symmetry is identified and presented in Figures 7.19a-c. This network structure resembles a bicontinuous morphology of interpenetrating PS and PCSi domains analogous to those for the known ordered bicontinuous double-diamond (OBDD) and gyroid (G) morphologies.[12,13,15] Figures 7.19a and 7.19b show micrographs exhibiting similarity with the [111] projection of a cubic structure possessing a 3 fold-symmetry, resembling the known "wagon wheel" images that are typical for a bicontinuous structure.[12b-c,15b,15d-e] For such a weight percentage of PCSi, a "wagon-wheel" type of morphology with a PCSi cubic lattice within a PS matrix would be expected. However, the images 7.19a-b seem to show that the PS block forms the cubic networks.[13a] Figure 7.19c shows a micrograph, which could correspond according to the literature, to a [001] projection of a cubic structure.[13b]

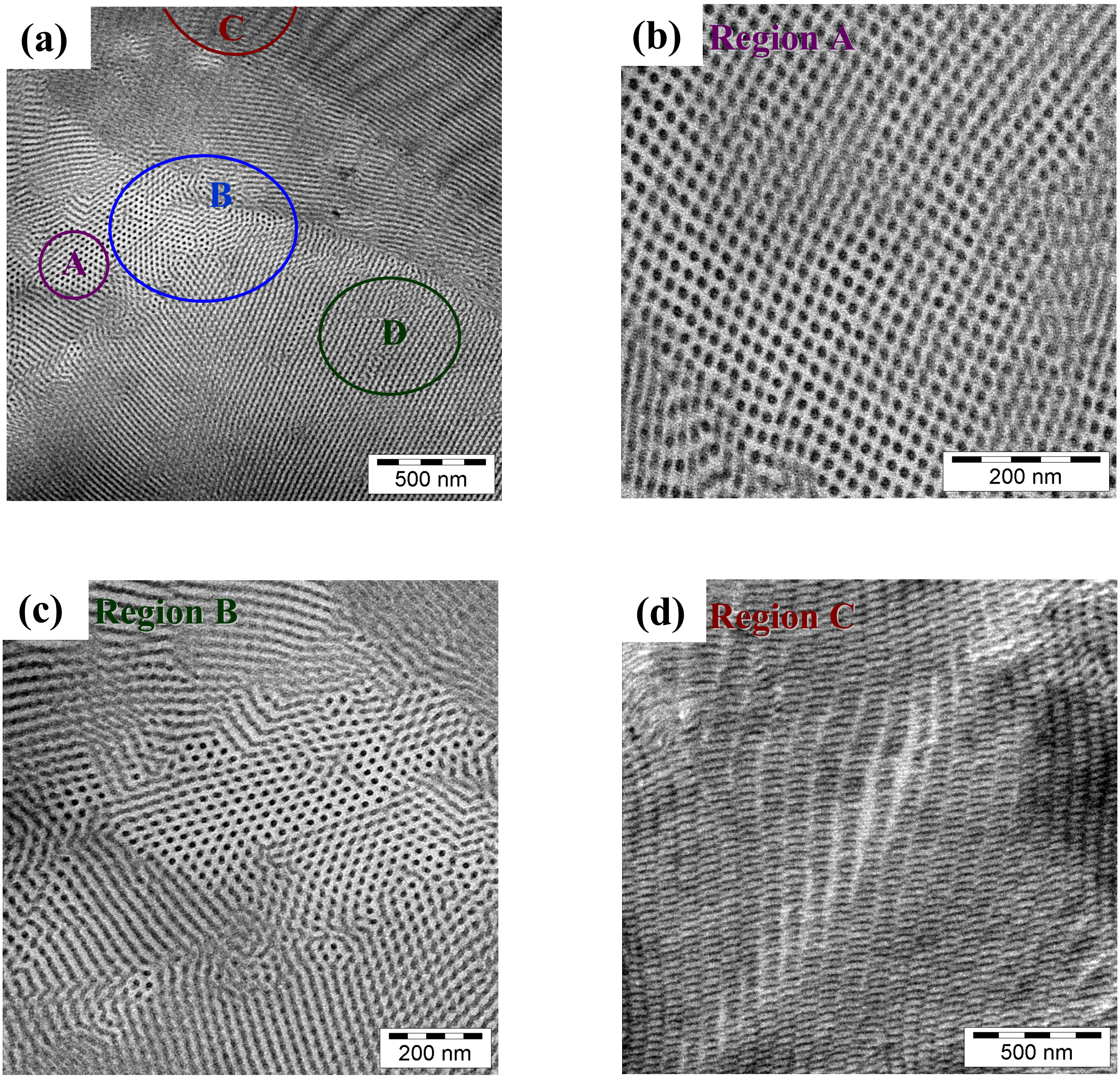

Figure 7.18. (a), (b), (c) and (d) TEMs selectively stained with OsO_4 (solution-cast film in THF) of $\mathbf{P_3LB_{31}}$.

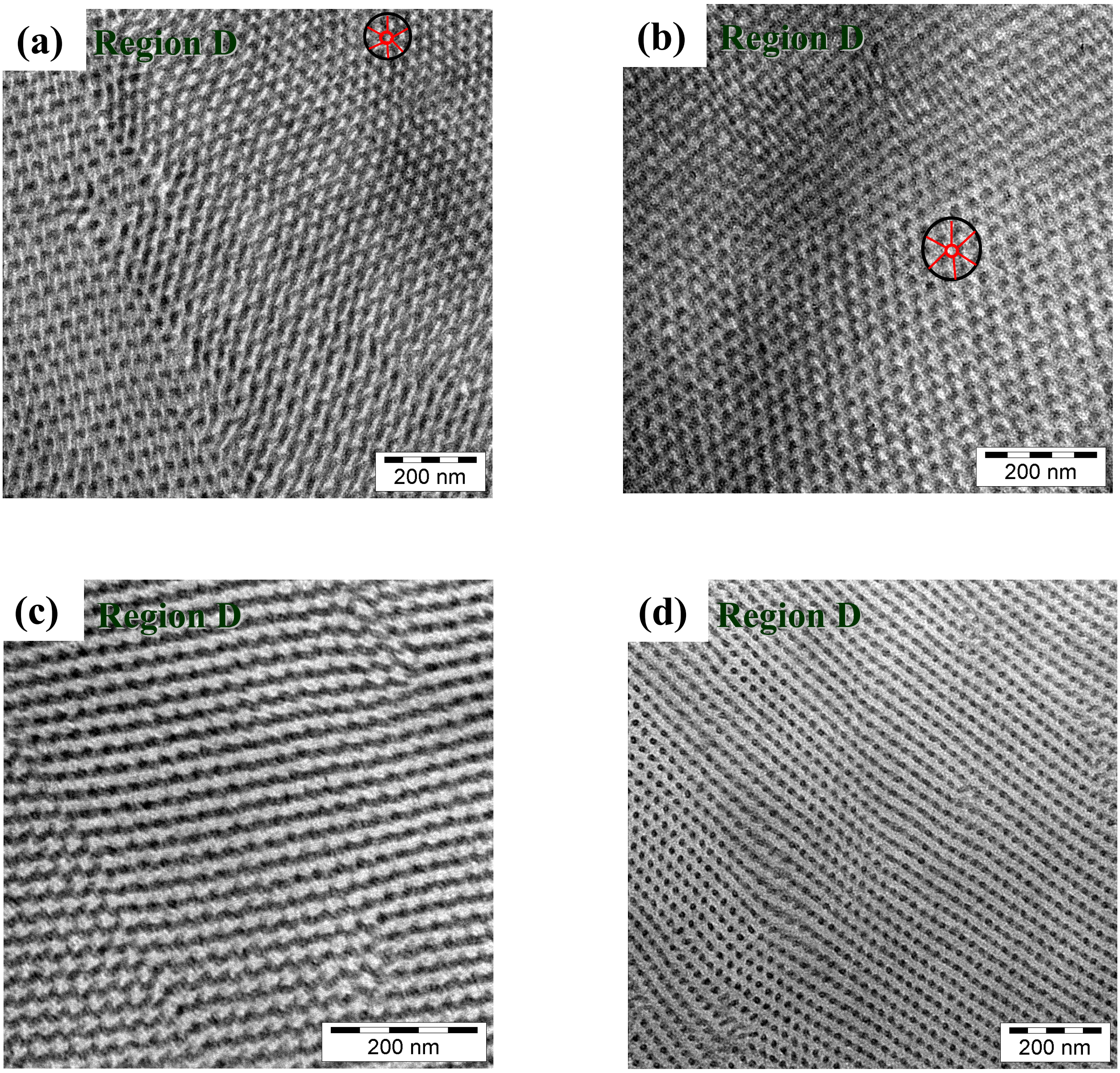

Figure 7.19. TEMs selectively stained with OsO_4 (solution-cast film in THF) of $\mathbf{P_3LB_{31}}$ showing: (a) and (b) 3-fold symmetry corresponding to the [111] projection of a cubic structure, (c) [001] projection of a cubic structure, (d) HPL morphology.

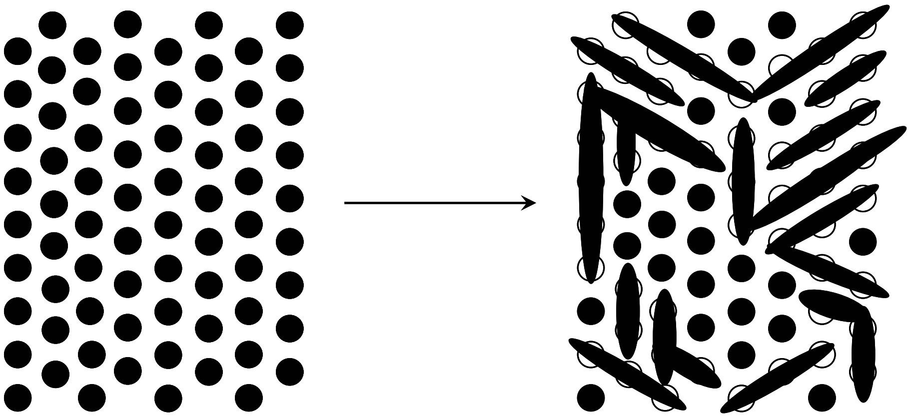

Figure 7.20. Two dimensional projections for a transition state from cylinders to lamellae.

The observed coexistence of cylindrical domains and a bicontinuous structure in the THF cast film from sample $\mathbf{P_3LB_{31}}$, could occur as a result of solvent evaporation leading to a non-equilibrium effect. Alternatively the short annealing periods above the T_g of PS may not allow for a clean transition between the cylindrical morphology and the bicontinuous microstructure. In fact, the effect of the duration of the annealing on the morphology was not tested for this sample. An interconnected lamellar morphology[16] or lamellar catenoid (LC) morphology,[15d,17] has been found in block copolymers and in blends of diblock copolymers with homopolymers respectively, as a consequence of the short annealing times. This hexagonally perforated lamellar (HPL) morphology showing layers of PCSi penetrated by catenoid-like channels of PS was also detected for $\mathbf{P_3LB_{31}}$ and is depicted in Figure 7.19d. The HPL is a metastable phase (long-lived non-equilibrium structure) that has been observed in several systems as an intermediate when accessing the gyroid state from either the cylindrical or the lamellar morphology. [15a-b,12c,18] It is obvious that obtaining the equilibrium microdomain structure for a block copolymer in the bulk is not an easy task.[19] The occurrence of both 3-fold (observed in the THF cast film) and 4-fold (observed in the toluene cast film) axes of symmetry in the TEM images of $\mathbf{P_3LB_{31}}$ indicate the presence of a cubic lattice. It has been reported that slow kinetics in the transition from HPL (also observed for $\mathbf{P_3LB_{31}}$) to G are to be expected in highly entangled systems[18d] and might explain the incomplete conversion of the non-equilibrium cylindrical and HPL structures to the bicontinuous morphology, as observed in the TEM pictures of $\mathbf{P_3LB_{31}}$ cast from THF (Figures 7.18 and 7.19). On this account it can be concluded that a cubic bicontinuous structure is more than likely the equilibrium morphology for $\mathbf{P_3LB_{31}}$. Attempts to ascertain whether the lattice is OBDD or G by TEM or SAXS are inconclusive.

In truth the projected TEM images from the G and the OBDD architecture are nearly indistinguishable, as the similarities are numerous. In the OBDD, the channels in a particular network are tetrahedrally connected while in the G, the channels join as triads and the two networks are enantiomorphic (mirror images of one another). In our case, it is not clear from the TEM pictures if the structural unit for the PCSi block is a tetrapod or a tripod. This may be due to the fact that the morphological unit is smaller than the thickness of the ultrathin sections used for the electron microscopic analyses. It is also possible that the morphology of **P_3LB_{31}** is related to the "strut structure" found by Gido *et al.* in H-shaped double graft copolymers as well as for block copolymer blends.[21] This morphology is defined as a bicontinuous structure, which is not well-ordered in a lattice. In any case, the observed bicontinuous cubic structure for **P_3LB_{31}** can be considered a "non-classical" but not unique morphology as it has been found in block copolymer blends,[15d] star block copolymers,[13b,20] a three-component pentablock copolymer[22] and a graft polymer.[23] Although the bicontinuous double gyroid phase is predicted to be found at low to intermediate segregation values[12b] for compositions ranging from 27 to 33 %, it has been observed in polystyrene-*b*-polyisoprene (PS-*b*-PI) systems in the strong segregation[13a,24] over a reasonable broad range of composition. **P_3LB_{31}** is within the composition range wherein the bicontinuous structure is expected to occur. Alward *et al.* reported that the bicontinuous structure in AB_n stars with a constant composition becomes more favorable with respect to a hexagonal phase as the number of arms or the arm molecular weight increases.[20b] Therefore, the bicontinuous structure should be favored for our linear brush-like architecture, as this can be regarded as a miktoarm star structure with multiple arms.

In synopsis a "non-classical" bicontinuous cubic structure was found for **P_3LB_{31}**. This is located between the lamellar and cylindrical morphologies on one side of the phase diagram. The morphology found was additionally linked with a perforated lamellar type transient. However, it is uncertain if the composition at which this transition occurs depends on the overall molecular weight of the linear brush-like diblock, as samples proceeding from a different linear core were not explored.

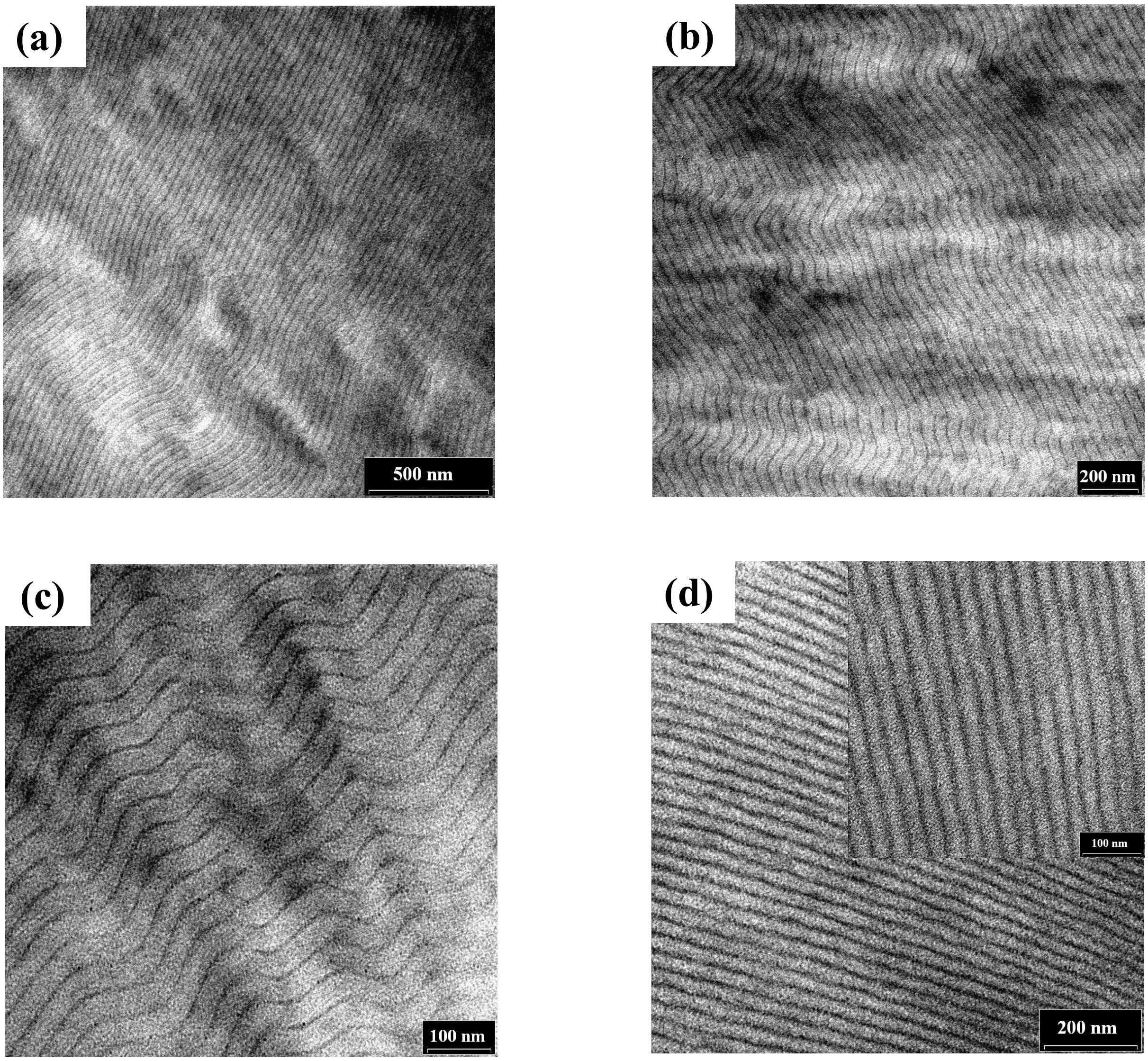

Figure 7.21. (a), (b) and (c) Unstained TEMs (compression-molded sample) and (d) unstained TEM (solution-cast film in toluene, scale marker is 100 nm for the inset figure) of **P$_3$LB$_{40}$**.

Samples **P$_3$LB$_{40}$**, **P$_3$LB$_{42}$** and **P$_3$LB$_{45}$**, with 40, 42 and 45 % weight fractions of the PCSi brush block respectively, showed well-ordered lamellar morphologies (Figures 7.21-7.24). A linear diblock copolymer with similar weight fractions would also be expected to display a lamellar morphology. Representative unstained TEM micrographs for the lamellar phase of **P$_3$LB$_{40}$** are presented in Figure 7.21 and were confirmed by AFM and SAXS analysis (Figure 7.22). The scattering at high temperatures shows six clear diffraction peaks at reciprocal space position ratios of 1:2:3:4:5:6, indicating a well-developed lamellar morphology. From the SAXS data, a lamellar long period of 41 nm was found for **P$_3$LB$_{40}$**.

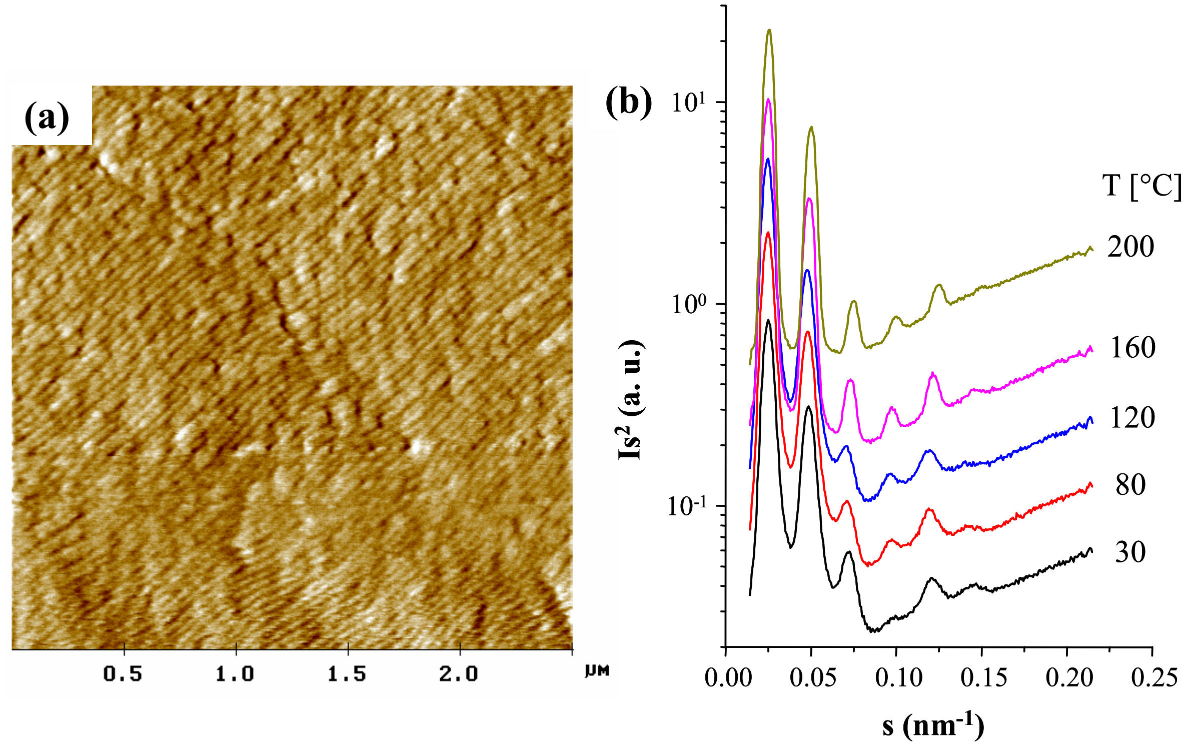

Figure 7.22. (a) AFM tapping mode phase image and (b) SAXS powder pattern (compression-molded sample) of $\mathbf{P_3LB_{40}}$.

An unstained TEM and two AFM phase images for the lamellar morphology of $\mathbf{P_3LB_{42}}$ are presented in Figure 7.23. The AFM phase image in Figure 7.23b shows a lamellar disruption. In the corresponding SAXS profile (Figure 7.23d), a lamellar diffraction signature with reflections in the ratio 1:2:4:5 and a repeat spacing of 41 nm are obtained. The absence of the third and sixth scattering signals have been noted in systems wherein the volume composition of one component is between 30 and 40 %,[25] which is in close agreement with the PCSi weight fraction calculated for the polymer $\mathbf{P_3LB_{42}}$.

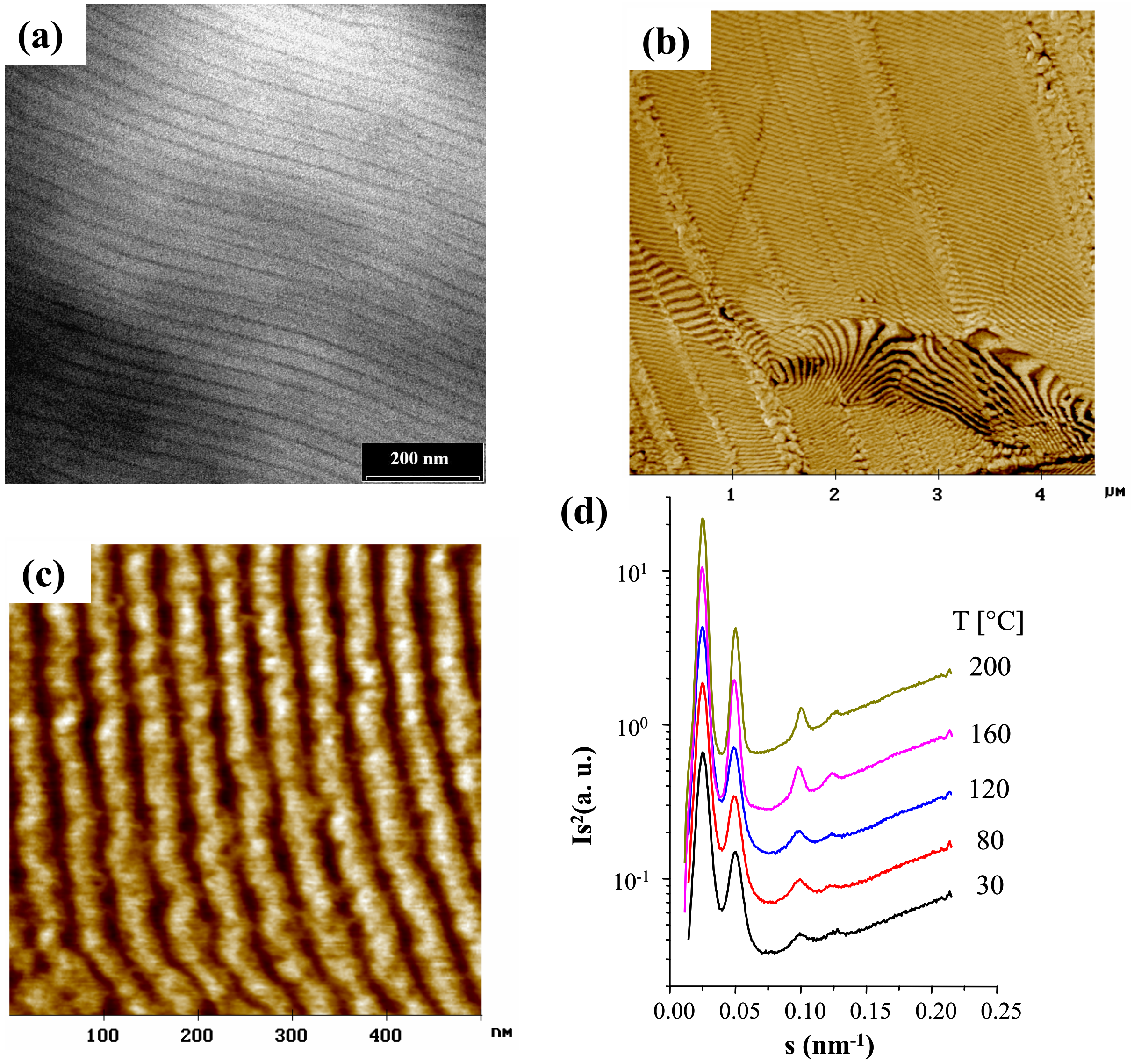

Figure 7.23. (a) Unstained TEM (solution-cast film in toluene), (b) and (c) AFM tapping mode phase images and (d) one-dimensional scattering profile (compression-molded sample) of $\mathbf{P_3LB_{42}}$.

Representative TEM and AFM pictures illustrating the lamellar morphology of $\mathbf{P_3LB_{45}}$ are depicted in Figure 7.24. In the unstained TEM in Figure 7.24b, a nice "whale" effect of the lamellae is observed. The SAXS pattern for $\mathbf{P_3LB_{45}}$ is typical of a lamellar structure with a domain periodicity of 38 nm, similar to the ones obtained for $\mathbf{P_3LB_{40}}$ and $\mathbf{P_3LB_{42}}$.

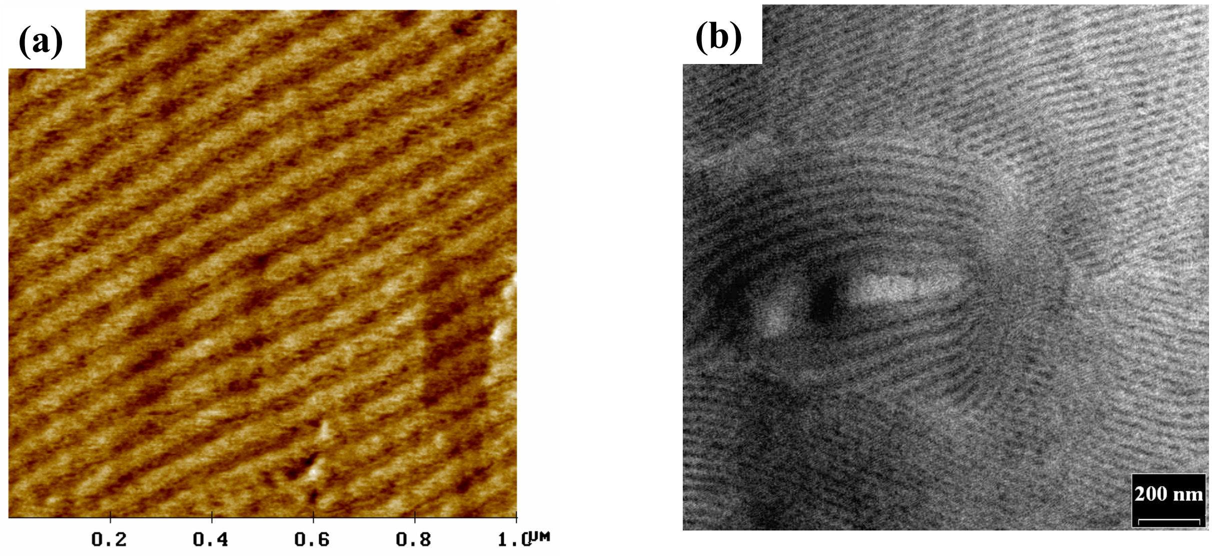

Figure 7.24. (a) AFM tapping mode phase image and (b) unstained TEM (compression-molded sample) of **P_3LB_{45}**.

Three linear brush-like diblock copolymers, with a PCSi brush block weight fraction between 36 and 56 %, were obtained from the linear copolymer **P_1** (PS_{354}-*b*-PBD_{84}). An unstained TEM image of **P_1LB_{36}** having a 36 wt % fraction of PCSi is presented in Figure 7.25a. From this micrograph it is difficult to determine if a lamellar or a cylindrical morphology is the domain structure and it is likely that the sample is not an equilibrium morphology. In order to determine the equilibrium morphology, a film of **P_1LB_{36}** was prepared by casting from toluene. A clear lamellar morphology was subsequently obtained with excellent long-range order (Figures 7.25b-c). The corresponding SAXS diffraction pattern with the two-dimensional diffraction image (Figure 7.25d) displays strong reflections up to the fourth order at high temperatures and indicates a lamellar morphology with a repeat distance of 31 nm. Thermal treatment of the sample results in augmented order as evidenced by an increase in the intensity of the Bragg reflections. Hence, it can be concluded that the lamellar morphology is the equilibrium morphology for **P_1LB_{36}**. This concurs with the general trend that a lamellar morphology is common for linear diblock copolymers with a volume fraction of 50 % (± 10 %) with low and high volume fractions of 36 and 72 % respectively.[26] However, it is obvious that we are close to the phase boundary between cylinders and lamellae as demonstrated by the TEM obtained from the compression-molded sample (Figure 7.25a) and the SAXS data at low temperatures (Figure 7.25d).

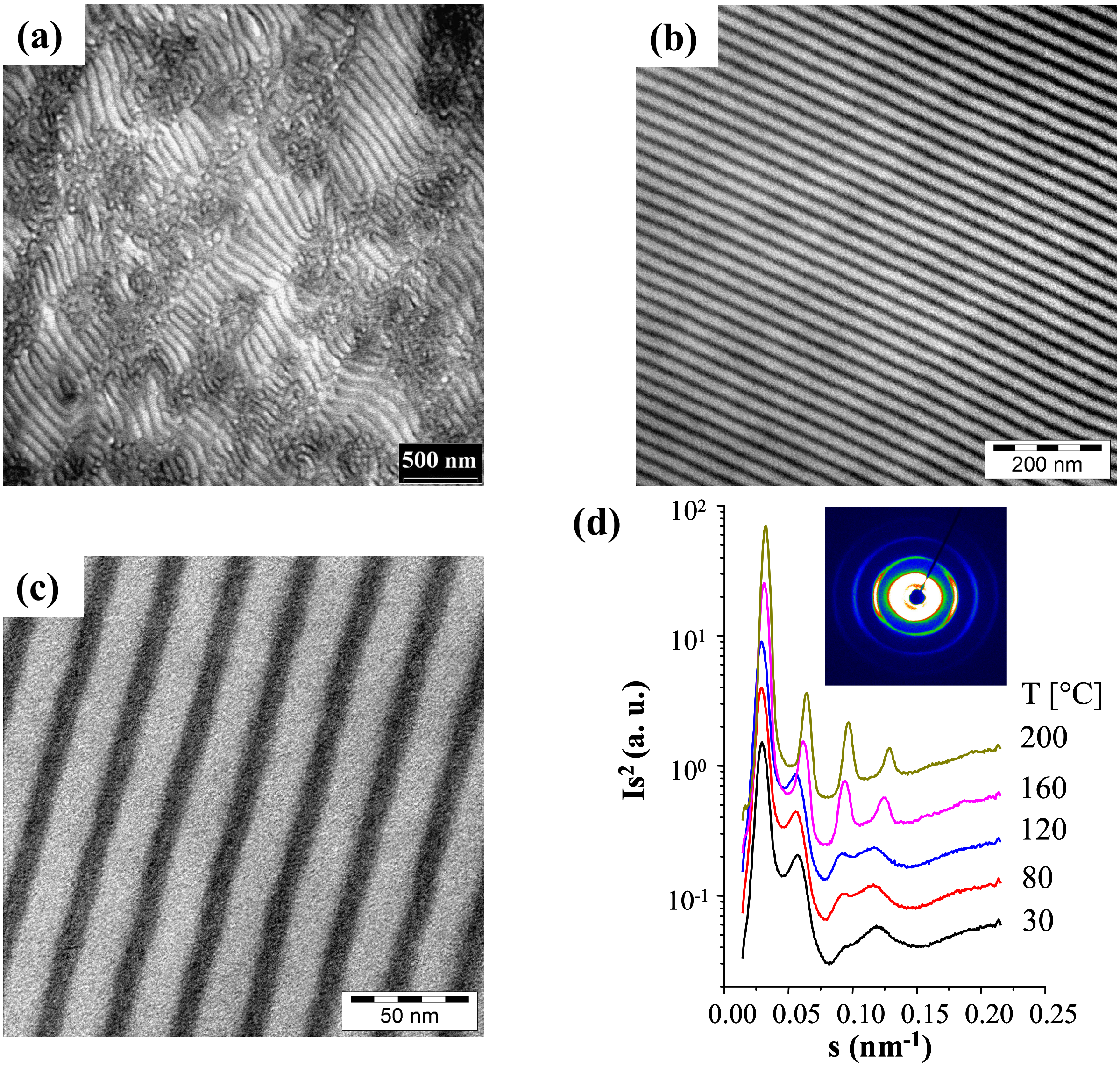

Figure 7.25. (a) Unstained TEM (compression-molded sample), (b) and (c) TEMs selectively stained with OsO_4 (solution-cast film in toluene) and (d) 2D- and 1D-SAXS diffraction pattern (compression-molded sample) of $\mathbf{P_1LB_{36}}$.

The morphologies of $\mathbf{P_1LB_{43}}$ and $\mathbf{P_1LB_{56}}$, possessing 43 and 56 wt % respectively for the PCSi block, display the most interesting effects of the linear brush-like architecture. While a linear diblock with 43 or 56 wt % for one of the blocks would be expected to exhibit a lamellar-like structure, the linear brush-like diblocks $\mathbf{P_1LB_{43}}$ and $\mathbf{P_1LB_{56}}$ display extremely well ordered cylindrical morphologies.

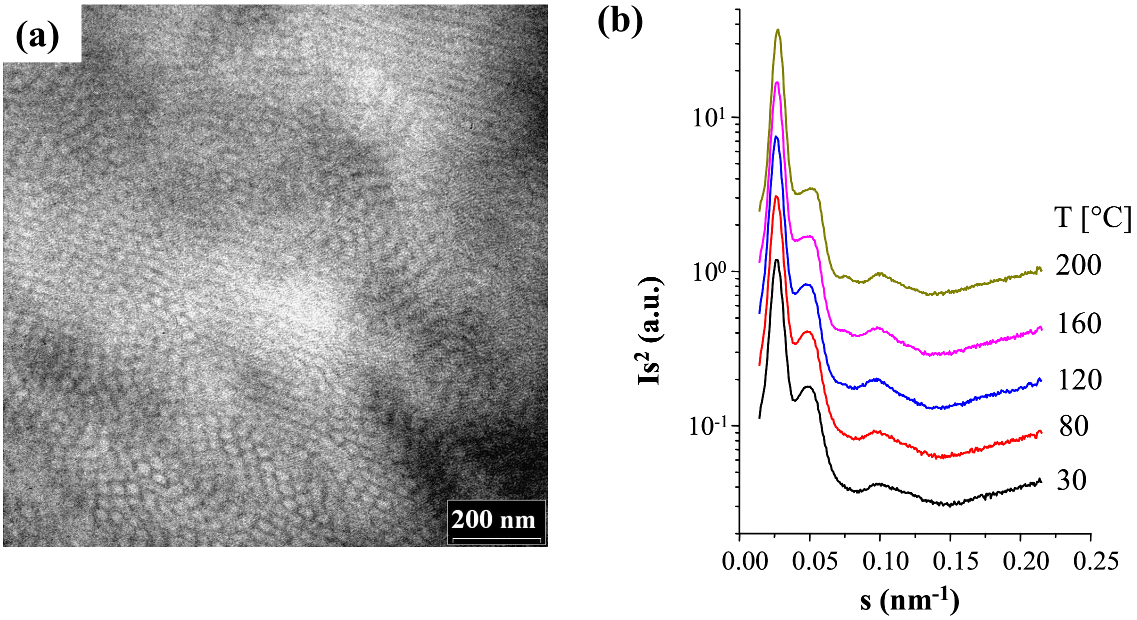

Figure 7.26. (a) Unstained TEM (compression-molded sample, scale marker is 200 nm) and (b) SAXS diffraction pattern (compression-molded sample) of $\mathbf{P_1LB_{43}}$.

An unstained TEM of $\mathbf{P_1LB_{43}}$, showing hexagonally packed PS cylinders in a PCSi matrix, is presented in Figure 7.26a. The corresponding SAXS pattern (Figure 7.26b) shows peaks with relative positions of 1, √3 and √4, √7 and √9 and √12, indicating hexagonally packed cylinders with a D spacing of 43 nm. Representative TEM micrographs of $\mathbf{P_1LB_{43}}$ cast from toluene and selectively stained with OsO_4 (PS domains are light), show remarkable hexagonally packed PS “cylinders” with a tremendously long-range order (Figure 7.27). It is clear that the solution-casting of the samples produces more long-range ordered grains of the “cylindrical” morphology. The curious TEM image presented in Figure 7.27b shows projections both parallel and perpendicular to the PS “cylinders”. The TEM images in Figures 7.27c and 7.27d reveal that the shape of the PS domains is ellipsoidal and hence we designate these PS domains as ellipsoids. The TEM micrographs show a sort of triple shading pattern with [PS] as white domains, [PCSi] as dark domains and a supposed silicon poor [PBD-PCSi] as grey domains surrounding the PS ellipsoids.

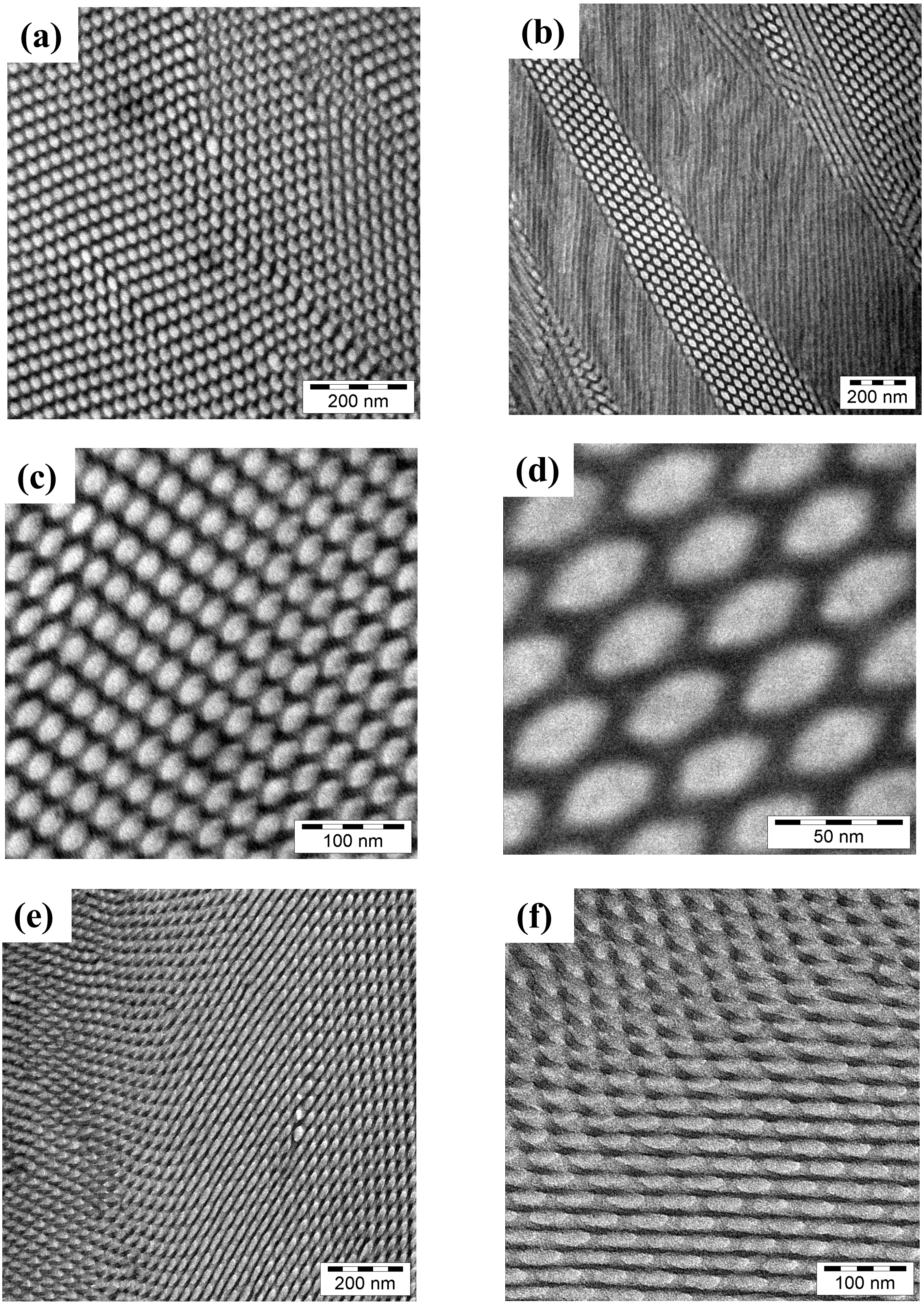

***Figure** 7.27.* (a), (b), (c) and (d) TEMs selectively stained with OsO_4 (solution-cast film in toluene) of $\mathbf{P_1LB_{43}}$.

Representative TEM micrographs of **P$_1$LB$_{56}$** cast from toluene and selectively stained with OsO$_4$ (PS domains are light) are presented in Figure 7.28. Again an extremely well-ordered ellipsoidal morphology is observed. However for **P$_1$LB$_{43}$**, the size of the hexagonally arranged elliptical PS domains is much narrower (Figure 7.28d). The SAXS profile (not represented) for **P$_1$LB$_{56}$** was similar to that obtained for **P$_1$LB$_{43}$** with a D of 38 nm. An unusual three-phase system can be clearly seen in the TEM picture shown in Figure 7.28c, wherein the PS ellipsoids are separated from the PCSi matrix by a lighter shell.

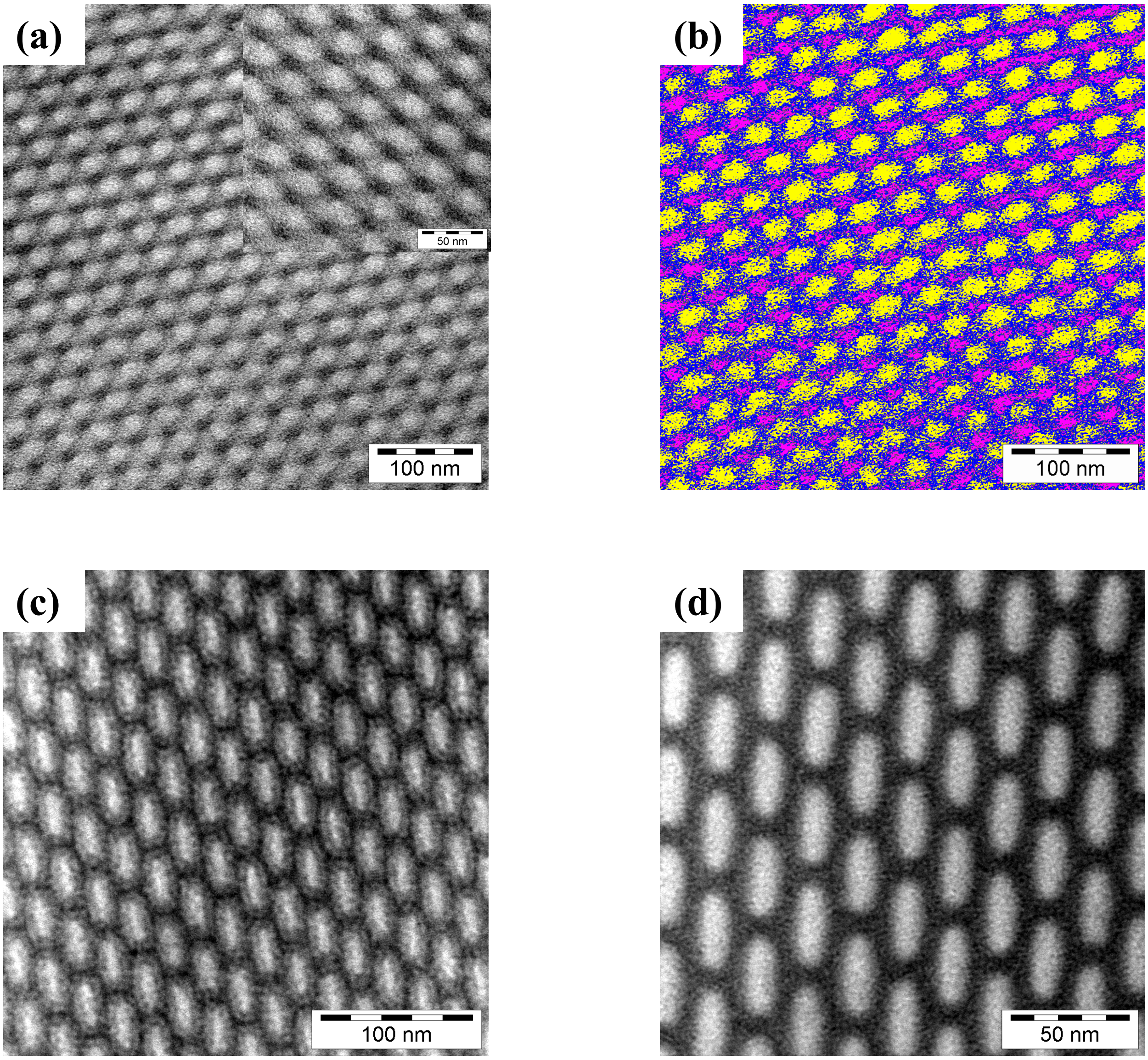

Figure 7.28. (a), (c), (d) TEMs selectively stained with OsO$_4$ (solution-cast film in toluene) and (b) color visualization of the grey scale image of **P$_1$LB$_{56}$**.

There are two possible interpretations that could explain the presence of these PS rhomboid or ellipsoid type cylinders in the samples **P_1LB_{43}** and **P_1LB_{56}**. One would be simply as a consequence of the sample preparation procedure. The ultra-thin TEM sections are not always cut perpendicular to the cylinder direction, which would give the PS cross sections an elliptical appearance (Figure 7.29). Moreover, these samples are cut at *ca.* -120 °C, and although the T_gs for both samples are well above this temperature, there can be a certain degree of mobility during the slicing process. The heat generated through frictional forces during cutting, could be sufficient to allow a certain mobility of at least one of the phases at the surface. For example, in the TEM images of sample **P_1LB_{43}** in Figures 7.27d-e, the full gamut of cubic, rhomboid, ellipsoid and cylindrical PS domains can be discerned. However, the uniformity of the PS ellipsoids for **P_1LB_{56}** observed in Figure 7.28d is remarkable and one would not expect such a pattern to arise from sample preparation procedures. Although the reason for the preferential formation of these ellipsoidal forms is unclear, an explanation could reside in the space-filling requirements of the PCSi brush block. The PS domains deform into ellipsoids in order to minimize the stretching of the PCSi chains away from the interface and fill space efficiently. Therefore, the driving force for the formation of these new exciting ellipsoidal morphologies might indeed be the packing frustration caused by the PCSi brush block.

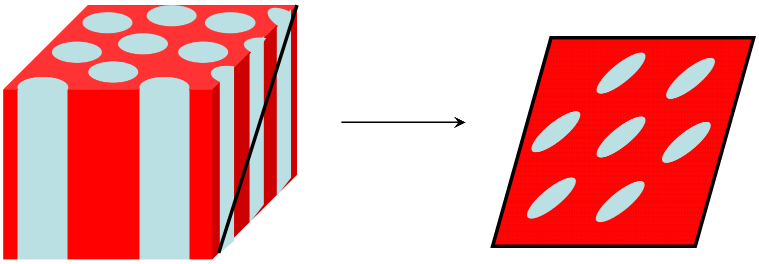

Figure 7.29. Sample section cut of a cylindrical morphology, which may result in ellipsoidal domains.

Another intriguing feature is the presence of a triple shading pattern in samples **P_1LB_{43}** and **P_1LB_{56}** (Figures 7.27c-d and 7.28c). For the linear-brush-like diblock copolymers samples **P_1LB_{43}** and **P_1LB_{56}**, there is patently a factor, most probably compatibility based that results in the formation of an interface between the non-covalently linked segments of PS and PCSi. This produces a morphology that in a way resembles a core-shell pattern. That is, an ellipsoidal structure based on a [PS] core surrounded by a silicon poor [PBD-PCSi] thin layer which is then hexagonally arranged in a [PCSi] matrix. Similar core-shell structures have been observed for more complex ABC block copolymers,[27] although it has been also experimentally observed for a diblock copolymer of PS and poly(1,3-cyclohexadiene) (PHCD)[28] and theoretically predicted for blends of diblock copolymers.[29] Therefore these materials are perhaps more related to “triblocks”, although from a thermal properties point of view, they are more akin to diblock copolymers, that is only two T_gs have been observed (Figure 7.13). This is the basis for regarding the short PBD block and the PCSi block as a unit. However, from a microscopic point of view, the formation of these interesting structures may occur in order to minimize the alleged unfavorable interactions between [PS]-[PCSi] blocks by forming a third silicon poor [PBD-PCSi] interfacial layer. An additional factor contributing to the interface formation could be the higher content of the PBD block in the linear core $\mathbf{P_1}$ (11 wt %).

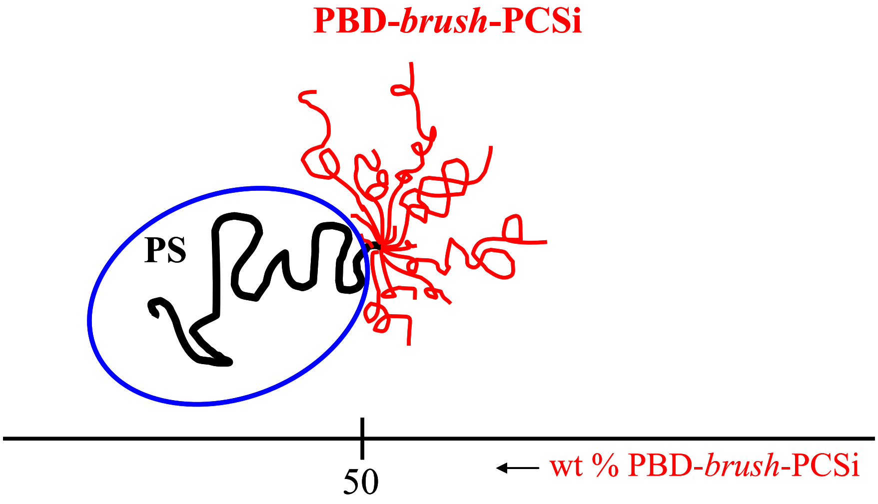

Figure 7.30. Curved interface for a linear brush-like architecture at PS weight fractions of 44 to 57 %.

Clearly, the extremely well-ordered microphase-separated morphologies exhibited by $\mathbf{P_1LB_{43}}$ and $\mathbf{P_1LB_{56}}$ are dependent on the architecture of these exotic linear brush-like diblock copolymers as hexagonally packed ellipsoidal morphologies and not the expected lamellar structures were present for nearly similar block compositions. It is suspected that architectural packing constraints of the brush domains prevent the formation of a planar interface between the two blocks. In other words, due to the overcrowding of the alkyl chains in the brush block the interface is curved towards the PS block, forcing the PS chains to assume an ellipsoidal morphology (Figure 7.30). In this way uniform segmental packing is achieved without a significant loss of conformational entropy. Although stiff PS cylinders in a soft PCSi matrix are harder to align than the reverse structure, the samples exhibited excellent ordering of the elliptical PS domains in hexagonal arrays, especially considering that no special efforts, such as shearing, were employed to induce alignment. In the literature, a tremendous degree of long-range order of cylindrical micelles has been reported even without sharing for linear diblock copolymers when the stiffer chain is in the cylinder corona.[30] In our case, the well developed order could be due to the fact that both samples do not posses extremely high molecular weights. Furthermore, the effects of architecture on the degree of long-range order of cylindrical morphologies have been reported by Hadjichristidis and Gido in I_2S and I_3S miktoarm star copolymers.[31] When the two PI blocks were on the outside of the cylinders, the structures had remarkable long-range order even without special sample preparation compared to the case when the single PS block was on the outside of the cylinders. This observation can be translated to the samples **P_1LB_{43}** and **P_1LB_{56}**, where the grafted PCSi blocks are also located on the outside of the cylinders.

Concluding, samples **P_1LB_{43}** and **P_1LB_{56}** having nearly similar weight fractions for both blocks exhibited exceptionally well-ordered ellipsoidal morphologies instead of the expected lamellar structures due to the overcrowding of the PCSi brush block, which forces the interface towards the PS side. **P_3LB_{42}** and **P_3LB_{45}** are derived from the linear copolymer **P_3**, which posses an intermediate molecular weight between **P_1** and **P_5** and both samples displayed a lamellae morphology as it would be expected. This is understandable if there is a dependence of the morphology on the total molecular weight of the linear brush-like diblock copolymer in addition to the composition and architecture. Sharp transitions between morphologies with varying composition of blocks and independence of morphology from molecular weight were theoretically predicted by Helfand in the SSL.[32] In contrast Leibler predicted that the morphology of block copolymers depends on both composition and molecular weight[33] and our observations coincide with the latter theory. Furthermore, **P_1LB_{43}** and **P_1LB_{56}** exhibited untypical core-shell ellipsoidal structures, consisting of PS ellipsoids surrounded by a shell of PBD and electron-poor silicon domains with the electron-rich PCSi domains as the matrix. It might be thermodynamically favorable for the PBD block, which has a higher DP_n in these blocks, to minimize its curvature along the interface by forming ellipsoidal shells. The appearance of such core-shell morphologies may occur as a means to reduce the contacts between the PS and the PCSi blocks.

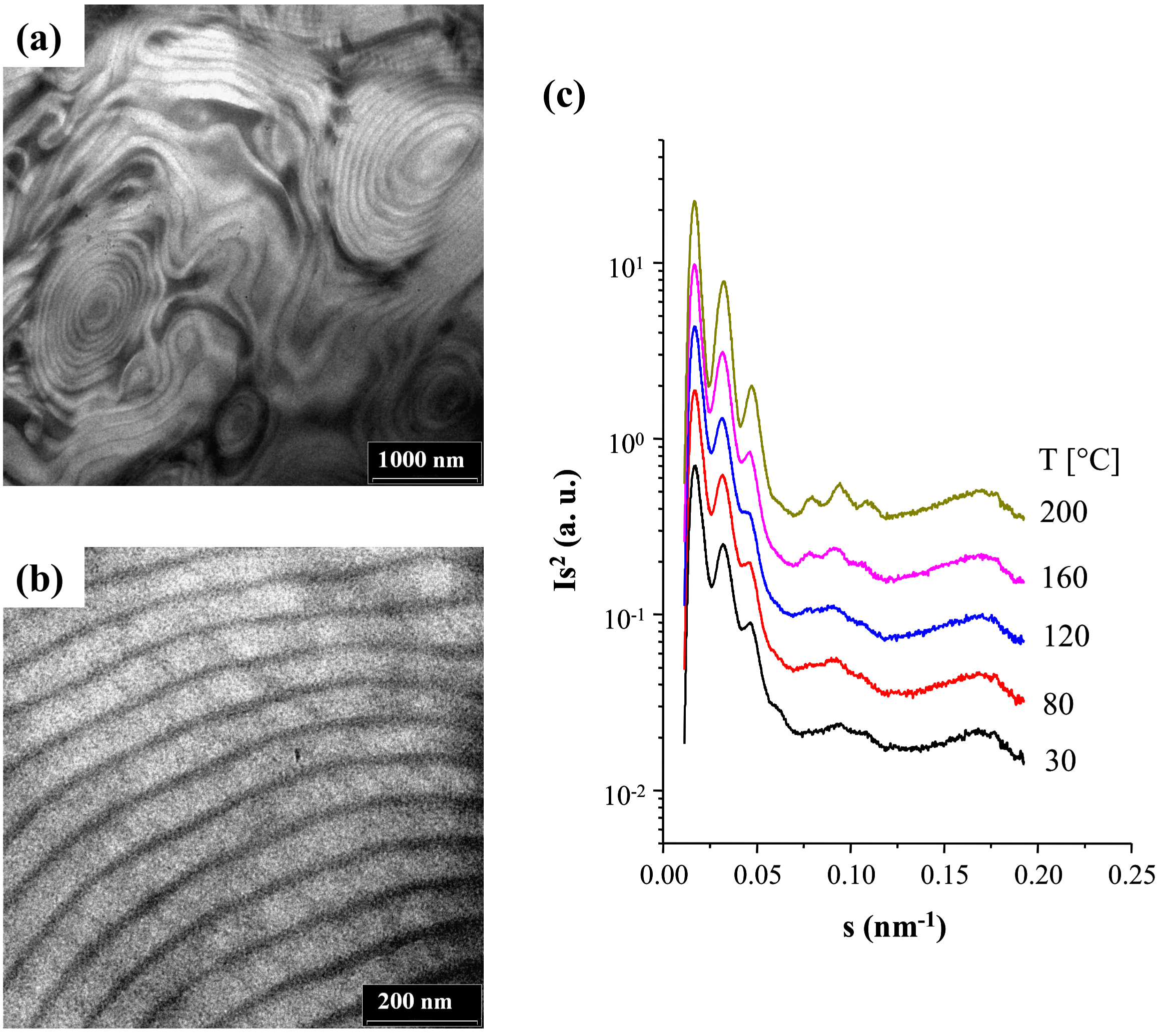

Figure 7.31. (a), (b) Unstained TEMs (compression-molded sample) and (c) SAXS diffraction pattern (compression-molded sample) of $\mathbf{P_5LB_{28}}$.

Three samples with 28 to 46 wt % of the PCSi brush block were prepared from the linear core $\mathbf{P_5}$ (PS$_{1156}$-*b*-PBD$_{130}$). In all three samples a significant molecular architecture effect on the resultant morphologies is apparent relative to what is observed in linear diblock copolymers of similar weight characteristics. $\mathbf{P_5LB_{28}}$ exhibits a lamellar-like morphology as revealed from the unstained TEM micrographs and the SAXS (Figure 7.31). However for a diblock of similar weight percent (28 %) a cylindrical morphology is expected The brush architecture seems to affect the phase boundary for the lamellar morphology and hence is found at a lower than expected weight fraction. This might be a useful consequence, as it may allow a polymer to be assembled into a lamellar morphology when it is by far the major component. Such characteristics in block copolymers are rare but not unique. For example, lamellar morphologies were found at lower weight fractions in linear-dendritic systems, with perfect dendrimer block, like PS-poly(propylenimine) (PS-PPI) studied by Román *et al.* and

PS-poly(benzylether) (PS-PBE) investigated by Pochan *et al.* and Mackay *et al.*[9c-e] Also a structure of alternating PS and PI lamella was also observed in an H-shaped double graft copolymer for a sample with 27 % volume fraction for the PS block.[21a] Figure 7.31a illustrates how the lamellae are organized in onion-like structures. It can be observed how the lamellar morphology is composed of irregular concentric rings with several layers. Similar onion-like architectures have also been found in bulk block copolymer blends, in block copolymer solutions and in small molecule surfactant systems.[31] The formation of this multi-lamellar onion-like structure is probably related to size limitations that prevent the formation of large flat lamellae. The interface PS-[*brush-like* PCSi] becomes flatter due to the more voluminous shape of the brush-like block, resulting in a more stretched conformation of the PS chains and consequently these are not able to pack in a well-defined pattern. Although for **P$_5$LB$_{28}$** a flat interfacial curvature is preferred, it is believed that the overwhelming PS fraction component forces the lamellae to form a curved structure. Figure 7.31b shows an enlargement of a projection parallel to the layers of the onion-like structure. The corresponding SAXS intensity profile at high temperatures shows five clear diffraction peaks at relative positions of 1:2:3:4:5 that are typical of a lamellar structure (Figure 7.31c). It is clear that the rate of ordering increases with increasing annealing temperature. An interlamellar spacing of 64 nm was calculated from the SAXS measurements. Neglecting effects from morphology, the domain periodicity for **P$_5$LB$_{28}$** is higher than in the previous samples, which is consistent with the norm that the domain periodicity scales with the total molecular weight of the block copolymer.

A lamellar-like morphology was also observed for **P$_5$LB$_{34}$**, which has 34 wt % of the brush PCSi block. However, linear blocks of the same relative weight fraction would reside on the lamellar/perforated or lamellar/bicontinuous/cylindrical phase boundaries depending on differences in chain flexibility and/or molecular weight.[34] A representative unstained TEM micrograph and the SAXS pattern of the lamellar-like structure are presented in Figure 7.32. The TEM micrograph in Figure 7.32a shows a lamellar morphology with fingerprint domains resulting from a hydrodynamic instability or from dense nucleation of the lamellar order. The SAXS pattern indicates a lamellar structure with a periodicity equal to 65.5 nm (Figure 7.32b). The reflection peaks have relative positions of 1:2:3:4:6 and upon heating the sample the order is augmented as evidenced by the increase in intensity of the higher order Bragg reflections.

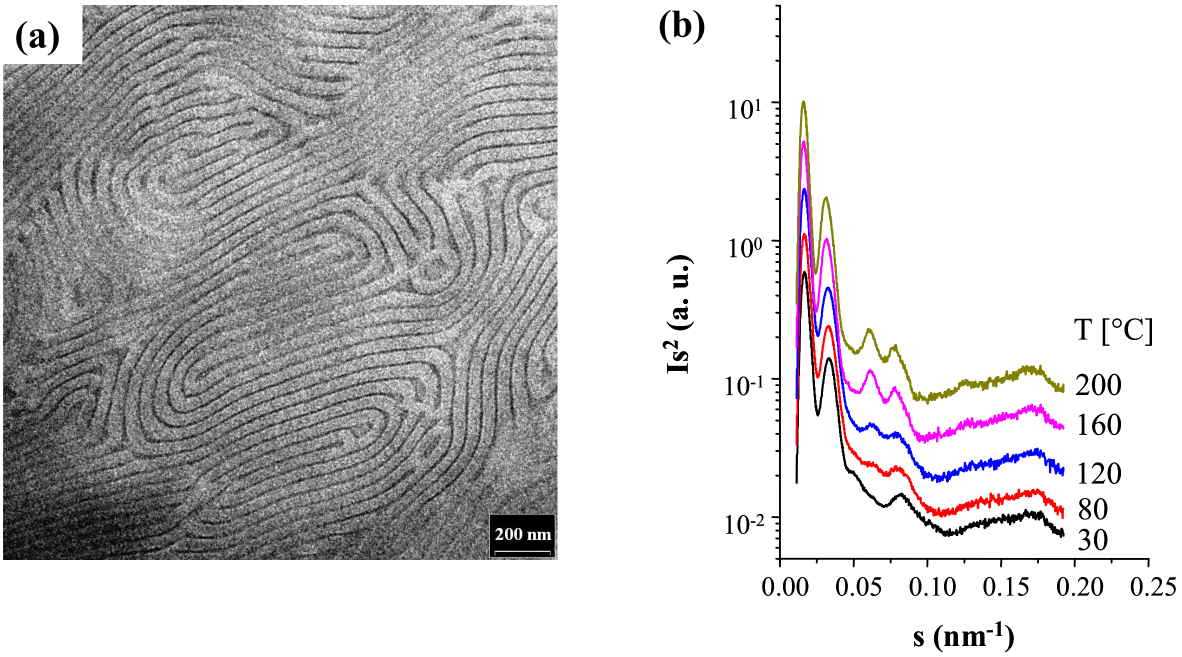

Figure 7.32. (a) Unstained TEM (compression-molded sample) and (b) SAXS diffraction pattern (compression-molded sample) of **P$_5$LB$_{34}$**.

The morphology of **P$_5$LB$_{46}$** is presented in Figure 7.33 and appears as dispersed PS cylinders in a PCSi matrix. This cylindrical phase is unusual due to the symmetric weight fractions of both blocks. Moreover, there is a lack of preferential grain orientation and the sample does not appear to be ordered in a lattice. The lack of higher order reflections in the SAXS pattern at lower temperatures is consistent with the lack of long-range order observed in the TEM and AFM images. However, upon annealing thee scattering intensities continuously increased and a series of Bragg peaks in the ratios of 1, $\sqrt{3}$, $\sqrt{4}$, $\sqrt{7}$ and $\sqrt{9}$ becomes discernible, which are consistent with hexagonally packed cylindrical domain structures with an inter-cylinder spacing of 78 nm. It is obvious that the regularity of the microdomain structures decreases with increasing M_n, probably due to the time necessary for the molecular rearrangement during annealing. This observation suggests that the long-range order in **P$_5$LB$_{46}$** is frustrated, presumably due to the molecular weight of the copolymer. Longer annealing periods would probably be necessary to obtain TEM and AFM images exhibiting well-developed order. Random morphologies without long-range order have been found in linear-dendritic systems when the dendritic macromolecule was the major component. For example Román *et al.* and Mackay *et al.* found less perfect morphologies at 58 and 67 % volume fraction respectively of the dendron block compared to linear diblock copolymers.[9d-e] The disordered cylindrical morphology observed in the AFM phase images in Figure 7.33 is in some way similar to the disordered "wormlike micelle" morphology found by Gido *et al.* for a I_2S graft block copolymer having 81 % volume fraction of the styrene block.[35] They hypothesized that packing frustrations of the two PI chains inhibited the formation of a morphology with an ordered lattice. These wormlike cylindrical domains were also found in graft copolymers with multiple branch points. The decreased molecular mobility in the multi-junction materials being the cause of the lost of long-range order.[36] In our case, the high molecular weight of **P$_5$LB$_{46}$** ($\overline{M}_n$ = 225,100 g /mol) as well as the brush-like architecture probably combine to limit the mobility necessary to achieve a perfect lattice structure.

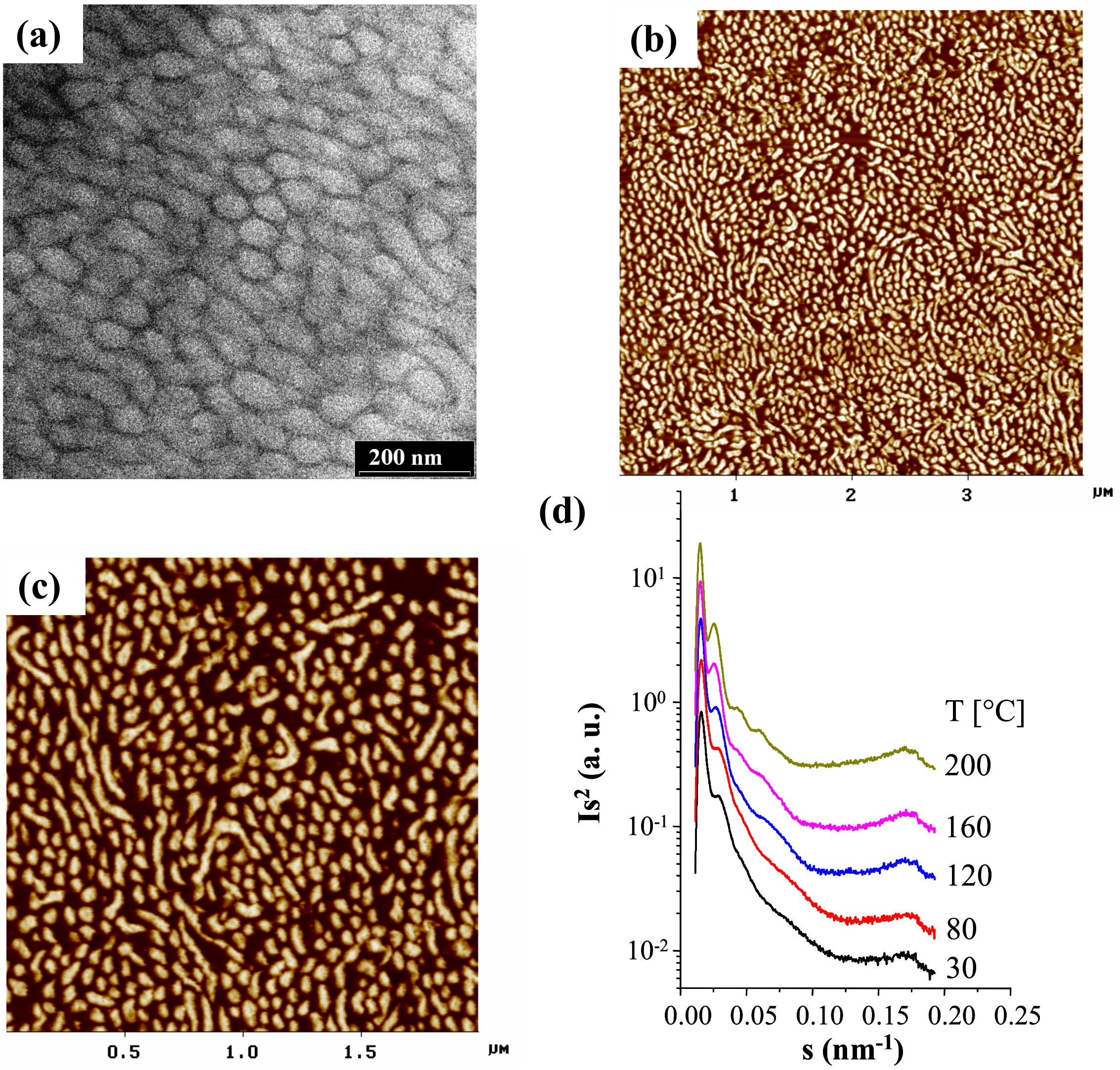

Figure 7.33. a) Unstained TEM (compression-molded sample), (b) and (c) AFM tapping mode phase images and (d) SAXS diffraction pattern (compression-molded sample) of **P$_5$LB$_{46}$**.

In summary, all samples derived from $\mathbf{P_5}$ showed a significant shift of the morphology phase boundaries to significantly higher weight fractions of the linear PS block so that the brush-like block can reside on a convex or flat interface.

7.4 CONCLUSIONS

The innovative strategy employed for the preparation of the linear-hyperbranched polycarbosilanes, presented in Chapter 6, was also applicable for the synthesis of the analogous linear brush-like polycarbosilanes. However, better grafting efficiencies were obtained for the linear brush-like systems, probably due to the less bulky nature as well as the lower cyclization probability of the AB (DMUS) monomer compared to the branched AB_2 (MDUS) monomer. The linear brush-like diblock copolymers were able to microphase separate into a variety of morphologies in spite of the presence of some heterogeneity (even with narrowly distributed samples) and the added isomerism of the brush block. In general, well-ordered morphologies were observed despite the non-uniform length of the brushes on the core. Further examination of the bulk morphologies suggests that a large configurational asymmetry leads to a state of frustration for certain weight percentage fractions of the PCSi brush block, producing in this way a richer variety of ordered phases than would be expected for a linear AB diblock copolymer:

In the examined range of weight fractions for the brush-like block, it has been observed that the architecture of the block copolymers is a controlling factor in the morphological behavior. In these systems, lamellar morphologies for low brush PCSi weight fractions and cylindrical morphologies for nearly symmetric compositions have been found. This finding has been confirmed in the linear brush-like architectures for several samples, while in the linear-hyperbranched polycarbosilanes only one sample seemed to show an unexpected morphology. This limitation is related to the lower reactivity of the branched AB_2 monomer versus the AB monomer. However a dependence of morphology, not totally related to the molecular weights of the linear brush-like diblock copolymers was also observed. The morphological shifts in the phase diagram for higher PCSi weight fractions were not discernable in all range of molecular weights.

Additionally and on the basis of the TEM images and the SAXS data the linear brush-like diblock copolymers appear to be strongly segregated. Overall, the classical phase boundaries were found to be shifted to higher PS weight percentage fractions. A curved interface is believed to relieve the overcrowding of the brush PCSi-PS junctions at the block interface.

Interestingly, new morphologies consisting of well-ordered hexagonally packed ellipsoids were also found, indicating the dramatic effect that macromolecular architecture can have on the morphology of diblock copolymers. Therefore, by utilizing the linear brush-like architecture, one is able to produce phase behavior unobtainable with linear diblock copolymers at the same volume fractions.

7.5 EXPERIMENTAL

Materials. $\mathbf{P_3}$, $\mathbf{P_1}$ and $\mathbf{P_5}$ diblock copolymers were prepared in 20 g scales via a simplified procedure of the anionic polymerization described by Sänger *et al.* A detailed description of the set-up is given in Chapter 2. DMUS was synthesized according to described literature procedures and the details for the synthesis are given in Chapter 3. For the polymer-analogous hydrosilylation grafting reaction, anhydrous *cis,trans*-decahydronaphtalene was used as received, diethyl ether and *n*-pentane were distilled over sodium before use and platinum-1,3-divinyltetramethyldisiloxane complex in xylene (2.1-2.4 % platinum, Karstedt catalyst) was used as the hydrosilylation catalyst.

Equipment. The polymerization via the SMA procedure was carried out in a specially designed apparatus as depicted in Chapter 6 (Figure 6.31).

Synthesis of $\mathbf{P_5LB_{28}}$. The monomer DMUS (0.86 g, 4 mmol) was dissolved in pentane (350 ml) and slowly added via a dosing pump to a solution of the diblock copolymer $\mathbf{P_5}$ (0.5 g, 0.51 mmol PBD) in *cis,trans*- decahydronaphtalene (7.5 mL) under a stream of argon containing 0.004 mmol of Karstedt catalyst (45 µL of the Pt solution). The reaction mixture was stirred at 70 °C to enable the constant removal of the pentane during the slow addition of the monomer. After addition of the monomer solution, the mixture was cooled down to room temperature and an aliquot taken for GPC analysis of the crude reaction product. The polymer $\mathbf{P_5LB_{28}}$ was purified by fractionating precipitation. This was achieved by diluting the decaline reaction mixture with diethyl ether (*ca.* 150 mL), followed by the drop wise addition of methanol until the polymer precipitated. The supernatant fluid was decanted and the isolated polymer was washed several times with methanol and dried in vacuo at 40 °C. For the synthesis of the analogous linear brush-like diblock copolymers, the quantity of monomer added was gradually increased, so that the molar quantity of the monomer was at least equal to the molar quantity of the 1,2-PBD core. A polymer (0.53 g, 41 %) with a number-average molecular weight ($\overline{M}_n$) of 167,200 g/mol and with a polydispersity index (PDI) of 1.26 was obtained as determined by MO and GPC measurements respectively. The analogous one pot reaction was carried out by adding the neat monomer directly to a solution of the diblock copolymer in decaline and heating at 70 °C for 24 hours.

^{1}H NMR (400 MHz, $CDCl_3$): δ (ppm) -0.03 (Si-CH_3), 0.49 (-Si-CH_2), 1.05-1.6 (polymer backbone), 1.7 (m, C**H**$_3$-CH=CH-), 1.8-2.05 (m, -C**H**$_2$-CH=CH-CH_3 and polymer backbone), 2.2 (m, -C**H**$_2$-CH=CH_2), 4.9 (m, -CH=C**H**$_2$, PBD, PCSi), 5.3-5.7 (m, -C**H**=C**H**-, PCSi; -C**H**=CH_2, PBD), 5.9 (m, -C**H**=CH_2, PCSi), 6.3-7.4 (m, C_6H_5); ^{13}C NMR (100 MHz, $CDCl_3$): δ (ppm) -2.97 (Si-CH_3), 13.1 (**C**H$_3$-CH=CH-, *cis*), 15.7 (Si-CH_2), 18.3 (**C**H$_3$-CH=CH-, *trans*), 24.3 (Si-CH_2-**C**H$_2$), 29.3, 29.5, 29.8, 29.9, 30, 34.1, 34.2, 39-47 (polymer backbone), 114.4 (**C**H$_2$=CH-, PBD, PCSi), 123.9 (CH_3-**C**H=CH-, *cis*), 124.8 (CH_3-**C**H=CH-, *trans*), 126.0 (C_6H_5), 128.3 (C_6H_5), 131.2 (CH_3-CH=**C**H-, *cis*), 132 (CH_3-CH=**C**H-, *trans*), 139.5 (**C**H$_2$=CH-, PCSi), 144.2 (CH_2=**C**H-, PBD), 145.6 (C_6H_5, C_{ipso}); ^{29}Si NMR (80 MHz, $CDCl_3$): δ (ppm) 2.4; IR (characteristic absorption bands): γ(cm^{-1}) 1602 (stretching C=C mode), 1248 (stretching Si-CH_3 mode), 907 (terminal PBD and PCSi C=C deformation), 832 (bending CH_3-Si-CH_3 mode).

7.6 REFERENCES

[1] (a) Lohse, D. J.; Milner, S. T.; Fetters, L. J.; Xenidou, M.; Hadjichristidis, N.; Mendelson, R. A.; Garcia-Franco, C. A.; Lyon, M. K. *Macromolecules* **2002**, *35*, 3066. (b) Daniels, D. R.; McLeish, T. C. B.; Crosby, B. J.; Young, R. N.; Ferryhough, C. M. *Macromolecules* **2001**, *34*, 7025. (c) Pakula, T.; Vlassopoulos, D.; Fytas, G.; Roovers, J. *Macromolecules* **1998**, *31*, 8931. (d) Mathias, L. J.; Reichert, V. R.; Carothers, T. W.; Bozen, R. M. *Polym. Prep.* **1993**, *34*, 77.

[2] (a) Neiser, M. W.; Muth, S.; Kolb, U.; Harris, J. R.; Okuda, J.; Schmidt, M. *Angew. Chem., Int. Ed. Engl.* **2004**, *43*, 3192. (b) Mori, H.; Müller, A. H. E. *Prog. Polym. Sci.* **2003**, *28*, 1403. (c) Neugebauer, D.; Zhang, Y.; Pakula, T.; Matyjaszewski, K. *Polymer* **2003**, 44, 6863. (d) Zhang, M.; Breiner, T.; Mori, H.; Müller, A. H. E. *Polymer* **2003**, *44*, 1449. (e) Börner, H.; Duran, D.; Matyjaszewski, K.; da Silva, M.; Sheiko, S. S. *Macromolecules* **2002**, *35*, 3387. (f) Börner, H. G.; Beers, K.; Matyjaszewski, K.; Sheiko, S. S.; Möller, M. *Macromolecules* **2001**, *34*, 4375. (g) Deffieux, A.; Schappacher, M. *Macromolecules* **2000**, *33*, 7371.

[3] (a) Gauthier, M.; Möller, M. *Macromolecules* **1991**, *24*, 4548. (b) Tomalia, D. A.; Naylor, R.; Goddard, W. III. *Angew. Chem., Int. Ed. Engl.* **1990**, *29*, 138.

[4] (a) Lesné, T.; Heroguez, V.; Gnanou, Y.; Duplessix, R. *Colloid Polym. Sci.* **2001**, *279*, 190. (b) Ito, K.; Kawaguchi, S. *Adv. Polym. Sci.* **1999**, *142*, 129.

[5] (a) You, Y.; Hong, C.; Wang, W.; Wang, P.; Lu, W.; Pan, C. *Macromolecules* **2004**, *37*, 7140. (b) Djalali, R.; Li, S.-Y.; Schmidt, M. *Macromolecules* **2002**, *35*, 4282. (c) Lecommandoux, S.; Chécot, F.; Borsali, R.; Schappacher, M.; Deffieux, A.; Brûlet, A.; Cotton, J. P. *Macromolecules* **2002**, *35*, 8878. (c) Lecommandoux, S.; Chécot, F.; Borsali, R.; Schappacher, M.; Deffieux, A.; Brûlet, A.; Cotton, J. P. *Macromolecules* **2002**, *35*, 8878. (d) Gerle, M.; Fischer, K.; Roos, S.; Müller, A. H. E.; Schmidt, M.; Sheiko,S. S.; Prokhorova, S.; Möller, M. *Macromolecules* **1999**, *32*, 2629. (e) Wintermantel, M.; Gerle, M.; Fischer, K.; Schmidt, M.; Wataoka, I.; Urakawa, H.; Kajiwara, K.; Tsukahara, Y. *Macromolecules* **1996**, *29*, 978. (f) Tsukahara, Y.; Tsutsumi, K; Yamashita, Y.; Shimada, S. *Macromolecules* **1990**, *23*, 5201.

[6] (a) Zhang, A.; Shu, L.; Bo, Z.; Schlüter, A. D. *Macromol. Chem. Phys.* **2003**, *204*, 328. (b) Schlüter, A. D.; Rabe, J. P. *Angew. Chem., Int. Ed. Engl.* **2000**, *112*, 860. (c) Schlüter, A. D.; Rabe, J. P. *Angew. Chem., Int. Ed. Engl.* **2000**, *39*, 864.

[7] Neiser, M. W.; Okuda, J.; Schmidt, M. *Macromolecules* **2003**, *36*, 5437.

[8] (a) Pyun, J.; Tang, C.; Kowalewski, T.; Fréchet, J. M. J.; Hawker, C. J. *Macromolecules* **2005**, *38*, 2674. (b) Zubarev, E. R.; Stupp, S. I. *J. Am. Chem. Soc.* **2002**, *124*, 5762. (c) Gitsov, I. *Linear-Dendritic Block Copolymers. Synthesis and Characterization*; in *Advances in Dendritic Macromolecules*, Newkome G. R.; Elsevier Science, Amsterdam, 2002, Vol. 5, Chapter 2, 45-87. (d) Zubarev, E. R.; Pralle, M. U.; Sone, E. D.; Stupp, S. I. *J. Am. Chem. Soc.* **2001**, *123*, 4105. (e) Gitsov, I.; Lambrych, K. L.; Ivanova, P. T.; Lewis, S. *Polym. Mater. Sci. Eng.* **2001**, *84*, 926. (f) Chang, Y.; Kwon, Y. C.; Lee, S. C.; Kim, C. *Macromolecules* **2000**, *33*, 4496. (g) Iyer, J; Fleming, K; Hammond, P. T. *Macromolecules* **1998**, *31*, 8757. (h) Leduc, M.; Hayes, W.; Fréchet, J. M. J. *J. Polym. Sci., Part A: Polym. Chem.* **1998**, *36*, 1. (i) van Hest, J. C. M.; Delnoye, D. A. P.; Baars, M. W. P. L.; van Genderen, M. H. P.; Meijer, E. W. *Science* **1995**, *268*, 1592. (j) Chapman, T. M.; Hillyer, G. L.; Mahan, E. J.; Shaffer, K. A. *J. Am. Chem. Soc.* **1994**, *116*, 11195. (k) Gitsov, I; Ivanova, P. T.; Fréchet, J. M. J. *Macromol. Rapid Commun.* **1994**, *15*, 387. (l) Newkome, G. R.; Baker, G. R.; Arai, S.; Saunders, M. J.; Russo, P. S.; Theriot, K. J.; Moorefield, C. N.; Rogers, L. E.; Miller, J. E.; Lieux, T. R.; Murray, M. E.; Phillips, B.; Pascal, L. *J. Am. Chem. Soc.* **1990**, *112*, 8458.

[9] (a) Duan, X. X.; Yuan, F.; Wen, X. J.; Yang, M.; He, B.; Wang, W. *Macromol. Chem. Phys.* **2004**, *205*, 1410. (b) Johnson, M. A.; Iyer, J.; Hammond, P. T. *Macromolecules* **2004**, *37*, 2490. (c) Pochan, D. J.; Pakstis, L.; Huang, E.; Hawker, C.; Vestberg, R.;

Pople, J. *Macromolecules* **2002**, *35*, 9239. (d) Mackay, M. E.; Hong, Y.; Jeong, M.; Tande, B. M.; Wagner, N. J.; Hong, S.; Gido, S. P.; Vestberg, R.; Hawker, C. J. *Macromolecules* **2002**, *35*, 8391. (e) Román, C.; Fischer, H. R.; Meijer, E. W. *Macromolecules* **1999**, *32*, 5525. (f) Gitsov, J.; Fréchet, J. M. J. *Macromolecules* **1993**, *26*, 6536.

[10] (a) Hanselmann, R.; Hölter, D.; Frey, H. *Macromolecules* **1998**, *31*, 3790. (b) Radke, W.; Litvinenko, G.; Müller, A. H. E. *Macromolecules* **1998**, *31*, 239.

[11] (a) Ashby, B. A.; Modic, F. J. US Patent 4,288,345, 1981. (b) Karstedt, B. D. (General Electric) US Patent 3,715,334, 1973.

[12] (a) Davidock, D. A.; Hillmeyer, M. A.; Lodge, T. P. *Macromolecules* **2003**, *36*, 4682. (b) Hajduk, D. A.; Harper, P. E.; Gruner, S. M.; Honeker, C. C.; Kim, G.; Thomas, E. L.; Fetters, L. J. *Macromolecules* **1994**, *27*, 4063. (c) Förster, S.; Khandpur, A. K.; Zhao, J.; Bates, F. S.; Hamley, I. W.; Ryan, A. J.; Bras, W. *Macromolecules* **1994**, *27*, 6922.

[13] (a) Hasegawa, H.; Tanaka, H.; Yamasaki, K.; Hashimoto, T. *Macromolecules* **1987**, *20*, 1651. (b) Thomas, E. L.; Alward, D. B.; Kinning, D. J.; Martin, D. C.; Handlin, D. L.; Fetters, L. J. *Macromolecules* **1986**, *19*, 2197.

[14] Sakurai, S.; Momii, T.; Taie, K.; Shibayama, M.; Nomura, S.; Hashimoto, T. *Macromolecules* **1993**, *26*, 485.

[15] (a) Vigild, M. E.; Almdal, K.; Mortensen, K.; Hamley, I. W.; Fairclough, J. P. A.; Ryan, A. J. *Macromolecules* **1998**, *31*, 5702. (b) Khandpur, A. K.; Förster, S.; Bates, F. S.; Hamley, I. W.; Ryan, A. J.; Bras, W.; Almdal, K.; Mortensen, K. *Macromolecules* **1995**, *28*, 8796. (c) Winey, K. I.; Gobran, D. A.; Xu, Z.; Fetters, L. J.; Thomas, E. L. *Macromolecules* **1994**, *27*, 2392. (d) Spontak, R. J.; Smith, S. D.; Ashraf, A. *Macromolecules* **1993**, *26*, 956. (d) Kinning, D. J.; Thomas, E. L.; Ottino, J. M. *Macromolecules* **1987**, *20*, 1129. (e) Herman, D. S.; Kinning, D. J.; Thomas, E. L.; Fetters, J. L. *Macromolecules* **1987**, *20*, 2940.

[16] (a) Hamley, I. W.; Koppi, K. A.; Rosedale, J. H.; Bates, F. S.; Almdal, K.; Mortensen, K. *Macromolecules* **1993**, *26*, 5959. (b) Thomas, E. L.; Anderson, D. M.; Henkee, C. S.; Hoffman, D. *Nature* **1988**, *334*, 598.

[17] (a) Disko, M. M.; Liang, K. S.; Behal, S. K.; Roe, R.-J.; Jeon, K. J. *Macromolecules* **1993**, *26*, 2983.

[18] (a) Wang, C.-Y.; Lodge, T. P. *Macromolecules* **2002**, *35*, 6997. (b) Hamley, I. W.; Fairclough, J. P. A.; Ryan, A. J.; Mai, S. M.; Booth, C. *Phys. Chem. Chem. Phys.* **1999**, *1*, 2097. (c) Hajduk, D. A.; Ho, R. M.; Hillmyer, M. A.; Bates, F. S.; Almdal, K. *J.*

Phys. Chem. B **1998**, *102*, 1356. (d) Hajduk, D. A.; Takenouchi, H.; Millmyer, M. A.; Bates, F. S.; Vigild, M. E.; Almdal, K. *Macromolecules* **1997**, *30*, 3788. (e) Zhao, J.; Majumdar, B.; Schukz, M. F.; Bates, F. S.; Almdal, K.; Mortensen, K.; Hajduk, D. A.; Gruner, S. M. *Macromolecules* **1996**, *29*, 1204.

[19] (a) Shibayama, M; Hashimoto, T.; Kawai, H. *Macromolecules* **1983**, *16*, 1434. (b) Todo, A.; Uno, H.; Miyoshi, K., Hashimoto, T.; Kawai, H. *Polym. Eng. Sci.* **1977**, *17*, 587. (c) Hashimoto, T.; Fujimura, M.; Kawai, H. *Macromolecules* **1980**, *13*, 1660.

[20] (a) Kinning, D. J.; Thomas, E. L.; Alward, D. B.; Fetters, L. J.; Handlin, D. L., Jr. *Macromolecules* **1986**, *19*, 1288. (b) Alward, D. B.; Kinning, D. J.; Thomas, E. L.; Fetters, L. J. *Macromolecules* **1986**, *19*, 215. (c) Aggarwal, S. L. *Polymer* **1976**, *17*, 938.

[21] (a) Lee, C.; Gido, S. P.; Poulos, Y.; Hadjichristidis, N.; Beck Tan, N.; Trevino, S. F.; Mays, J. W. *J. Chem. Phys.* **1997**, *107*, 6460. (b) Hashimoto, T.; Koizumi, H.; Hasegawa, T.; Izumitani, T.; Hyde, S T. *Macromolecules* **1992**, *25*, 1433. (c) Schwier, C. E.; Argon, A. S.; Cohen, R. E. *Polymer* **1985**, *26*, 1985.

[22] Hasegawa, H.; Sumitomo, T.; Hashimoto, T. *Polym. Prepr. Jpn.* **1983**, *32*, 1695.

[23] Hasegawa, H.; Hashimoto, T.; Hyde, S. T. *Polymer* **1996**, *37*, 3825.

[24] (a) Urbas, A. M.; Maldovan, M.; DeRege, P.; Thomas, E. L. *Adv. Mater.* **2002**, *14*, 1850. (b) Lodge, T. P.; Pan, C.; Jin, X.; Liu, Z.; Zhao, J.; Maurer, W. W.; Bates, F. S. *J. Polym. Sci., Polym. Phys. Ed.* **1995**, *33*, 2289. (c) Hajduk, D. A.; Harper, P. E.; Gruner, S. M.; Honeker, C. C.; Thomas, E. L.; Fetters, L. J. *Macromolecules* **1995**, *28*, 2570.

[25] Shibayama, M.; Hashimoto, T. *Macromolecules* **1986**, *19*, 740.

[26] Gido, S. P.; Wang, Z.-G. *Macromolecules* **1997**, *30*, 6771.

[27] (a) Gido, S. P.; Schwark, D. W.; Thomas, E. L.; do Carmo Gonçalves, M. *Macromolecules* **1993**, *26*, 2636. (b) Mogi, Y.; Nomura, M.; Kotsuji, H.; Ohnishi, K.; Matsushita, Y.; Noda, I. *Macromolecules* **1994**, *27*, 6755. (c) Breiner, U.; Krappe, U.; Abetz, V.; Stadler, R. *Macromol. Chem. Phys.* **1997**, *198*, 1051.

[28] David, J. L.; Gido, S. P.; Hong, K.; Zhou, J.; Mays, J. W.: Tan, N. B. *Macromolecules* **1999**, *32*, 3216.

[29] Birshtein, T. M.; Lyatskaya, Y. V.; Zhulina, E. B. *Polymer* **1992**, *33*, 2750.

[30] Pochan, D. J.; Gido, S. P.; Zhou, J.; Mays, J. W.; Whitmore M.; Ryan, A. J. *J. Polym. Sci., Part B. Polym. Phys.* **1997**, *35*, 2629.

[31] (a) Burke, S.; Shen, H.; Eisenberg, A. *Macromol. Symp.* **2001**, *175*, 273. (b) Shen, H.; Eisenberg, A. *Angew. Chem. Int. Ed.* **2000**, *39*, 3310. (c) Talingting, M. R.; Munk, P.; Webber, S. E.; Tuzar, Z. *Macromolecules* **1999**, *32*, 1593. (d) Zipfel, J.; Lindner, P.;

Tsianou, M.; Alexandridis, P.; Richtering, W. *Langmuir* **1999**, *15*, 2599. (e) Ding, J.; Liu, G. *Macromolecules* **1999**, *32*, 8413. (f) Gauffre, F.; Roux, D. *Langmuir* **1999**, *15*, 3738. (g) Regev, O.; Guillemet, F. *Langmuir* **1999**, *15*, 4357. (h) Bergmeier, M.; Gradzielski, H.; Hoffmann, H.; Mortensen, K. *J. Phys. Chem. B.* **1999**, *103*, 1605. (i) Danino, D.; Talmon, Y.; Zana, R. *J. Colloid Interface Sci.* **1997**, *185*, 84. (j) Prochazka, K.; Martin, T. J.; Webber, S. E.; Munk, P. *Macromolecules* **1996**, *29*, 6526. (k) Sein, A.; Engberts, J. B. F. N. *Langmuir* **1993**, *9*, 1714. (l) Kinning, D. J.; Winey, K. I.; Thomas, E. L. *Macromolecules* **1988**, *21*, 3502.

[32] Helfand, E.; Wassermann, Z. R. *In Developments in Block Copolymers*; Goodman, I.; Ed.; Applied Science: Essex, U.K., 1984.

[33] Leibler, L. *Macromolecules* **1980**, *13*, 1602.

[34] (a) Matsen, M. W.; Bates, F. S. *J. Polym. Sci., Part B. Polym. Phys.* **1997**, *35*, 945. (b) Bates, F. S.; Fredickson, G. H. *Annu. Rev. Phys. Chem.* **1990**, *41*, 525.

[35] (a) Pochan, D.; Gido, S. P.; Pispas, S.; Mays, J. W.; Ryan, A. J.; Fairclough, J. P. A.; Hamley, I. W.; Terrill, N. J. *Macromolecules* **1996**, *29*, 5091. (b) Pochan, D.; Gido, S. P.; Pispas, S.; Mays, J. W. *Macromolecules* **1996**, 29, 5099.

[36] Beyer, F. L.; Gido, S. P.; Büschl, C.; Iatrou, H.; Uhrig, D.; Mays, J. W.; Chang, M. Y.; Garetz, B. A.; Balsara, N. P.; Tan, N. B.; Hadjichristidis, N. *Macromolecules* **2000**, *33*, 2039.

CHAPTER 8

LINEAR-HYPERBRANCHED AND BRUSH-LIKE DIBLOCK COPOLYMERS CONSISTING OF POLYSTYRENE AND POLYALKOXYSILANE BLOCK

8.1 INTRODUCTION

The study of hyperbranched siloxy-type polymers is an especially appealing target if one considers the wide-spread use of linear polysiloxanes.[1] Siloxane materials have low temperature flexibility, high thermal stability, biocompatibility, significant gas permeability, hydrophobicity and oxidative resistance.[2] In particular, the synthesis of hyperbranched siloxy-type polymers with terminal silicon hydride groups or vinyl groups is an attractive goal as a result of the possibility of end-group chemical modification. A few dendritic polysiloxanes and silicon-containing dendrimers, obtained either by convergent or divergent multi-step syntheses, have been reported.[3] In addition, hyperbranched polysiloxysilanes and polyalkoxysilanes have been prepared by polyhydrosilylation of AB_2 and AB_3 monomers containing SiH and alkene functionalities.[4]

In the past decades hybrid block copolymers consisting of dendritic and linear blocks have been successfully synthesized.[5] However, the study of microdomain structures of dendritic-linear block copolymers in the solid state is very limited.[6] Among others, Gitsov *et al.* have studied the solid state properties of a series of di- and triblock copolymers consisting of the first- to fourth- generation monodendrons of poly(benzyl ether) (PBE) and linear poly(ethylene glycol) (PEG).[6f,7] At low molecular weights of the PEG block these copolymers showed a single glass transition temperature, indicating the formation of a homogeneous phase. However, for samples with higher molecular weight of the PEG block, a melting point was observed, demonstrating crystallization of the PEG block as confirmed by X-ray diffraction. Spherulites, axialites and dendritic structures have been observed in the cast film samples, depending on the composition of the copolymers and the solvent used.[6f] Nonetheless, a detailed study on the crystalline morphology of such block copolymer architectures is lacking. Moreover, phase separation studies on such diblock copolymer systems are influenced by the crystallization of the linear PEG block.

In this chapter AB_2 and AB undecenoxysilane type monomers,[4i,4k] analogous to the undecenylsilane monomers previously utilized,[8] are employed for the grafting reaction from PS_x-*b*-PBD_y diblock copolymers in order to obtain a linear-hyperbranched and brush-like architecture respectively. It has earlier been reported that electron-withdrawing groups on the hydrosilane accelerate the hydrosilylation rate.[9] Thus, one of the objectives is to investigate the effect of electron-withdrawing substituents on the silane on the hydrosilylation grafting efficiency. It is obvious that a better grafting efficiency could enhance the growth of the hyperbranched or brush-like block from the PBD core and consequently allow facile access to architectures where the branched block is the major block.

On this basis the preparation and characterization of novel linear-hyperbranched and brush-like polyalkoxysilanes is described. The general method based on the Slow Monomer Addition (SMA) procedure has been again used to construct the hyperbranched and brush-like topologies.[10] Control over the macromolecular structure via SMA is compared with the faster one-pot synthetic procedures. Finally, the thermal and solid-state properties of the modified linear PS_x-*b*-PBD_y cores are studied and presented. DSC and WAXS measurements confirm the crystallization of the polyalkoxysilane hyperbranched blocks. Microdomain formation in semicrystalline block copolymers can result either from incompatibility of the two blocks or by crystallization of one of the blocks. Furthermore, experimental work on semicrystalline block copolymers has demonstrated that the final morphology is often path-dependent.[11] Thus, different microdomain structures can be obtained if microphase separation precedes crystallization or vice versa.[12] Consequently, the interplay between crystallization of the polyalkoxysilane hyperbranched block and the microphase separaration of the block copolymer in the linear-hyperbranched systems results in extremely different morphologies that are discussed.

8.2 NOMENCLATURE

Linear-hyperbranched and brush-like diblock copolymers are denoted by PS_x-*b*-[PBD_y-*hb*-$PCSiO_z$] and PS_x-*b*-[PBD_y-*brush*-$PCSiO_z$] respectively, in which *z* indicates the DP_n of the polyalkoxysilane block (PCSiO). The hyperbranched and brush-like block are designated by [PBD_y-*hb*-$PCSiO_z$] and [PBD_y-*brush*-$PCSiO_z$] respectively, wherein the short 1,2-PBD block is regarded as being part of the final PCSiO block. However, for ease of presentation all of the polymers presented will be given an acronym. For example, the polymer PS_{426}-*b*-[PBD_{40}-*hb*-$PCSiO_{30}$] is abbreviated $\mathbf{P_2LHO_{23}}$. $\mathbf{P_2}$ refers to the linear block PS_{426}-*b*-PBD_{40} and $\mathbf{LHO_{23}}$ denotes a linear-hyperbranched polymer with a weight fraction of 23 % for the polyalkoxysilane block (including the short PBD-backbone). For details on the composition of the linear polymers, see Chapter 2 (Table 2.1).

8.3 RESULTS AND DISCUSSION

8.3.1 Synthetic strategy and compositional characterization

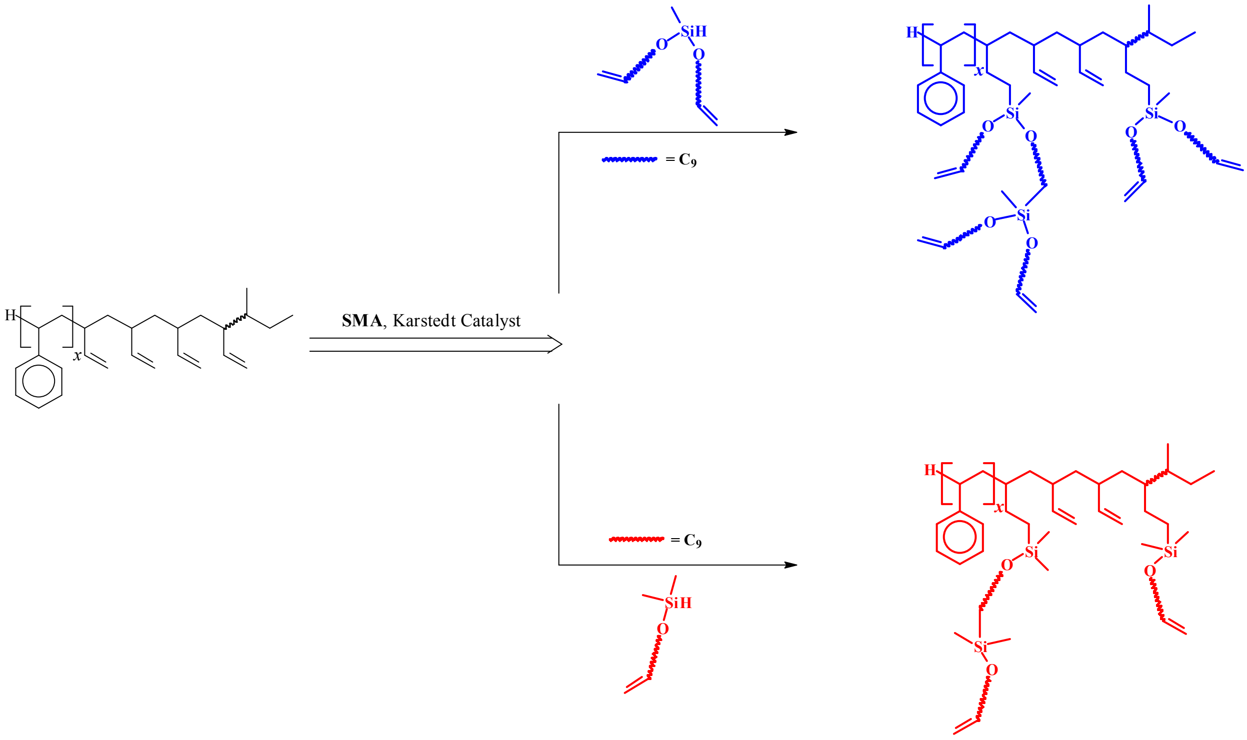

Figure 8.1. Synthesis of linear-hyperbranched and linear brush-like polyalkoxysilanes by grafting of branching AB_2 (MDUOS) and linear AB (DMUOS) alkoxysilane monomers respectively, from a short PBD-block of PS_x-*b*-PBD_y (The PBD block has an atactic configuration, although for simplicity the vinyl groups are depicted on one side).

It has been experimentally determined that the hydrosilylation reaction is faster with hydrosilanes bearing electron-withdrawing groups.[9] It is thought that this polarization stabilizes the intermediate Si-Pt complex, reducing the activation energy for its formation.[13] Therefore, in order to investigate the grafting efficiencies between the silicon-containing monomers and the PBD-core in the linear PS_x-*b*-PBD_y diblock copolymers, AB_2 and AB monomers containing alkoxysilane groups[4i,4k] have been employed for the synthesis of the complex linear-hyperbranched and brush-like polymer architectures.

Pt-catalyzed hydrosilylation (Karstedt catalyst)[14] between MDUOS[4i,4k] (AB_2) and DMUOS (AB) and a series of PS_x-*b*-PBD_y diblock copolymers have been used to prepare the linear-hyperbranched and brush-like polyalkoxysilane modified materials respectively (Figure 8.1). SMA has been again employed as the controlling synthetic strategy.[10] The nomenclature and abbreviations of the diblock copolymers obtained upon modification are presented in Table 8.1.

Table 8.1. Designation of the AB Linear-Hyperbranched and Linear Brush-like Polyalkoxysilane Block Copolymers.

Sample	Acronym[a]
PS_{426}-*b*-[PBD_{40}-*hb*-$PCSiO_{30}$]	$\mathbf{P_2LHO_{23}}$
PS_{426}-*b*-[PBD_{40}-*hb*-$PCSiO_{123}$]	$\mathbf{P_2LHO_{53}}$
PS_{426}-*b*-[PBD_{40}-*hb*-$PCSiO_{202}$]	$\mathbf{P_2LHO_{64}}$
PS_{426}-*b*-[PBD_{40}-*hb*-$PCSiO_{219}$]	$\mathbf{P_2LHO_{66}}$
PS_{426}-*b*-[PBD_{40}-*hb*-$PCSiO_{362}$]	$\mathbf{P_2LHO_{76}}$
PS_{580}-*b*-[PBD_{50}-*brush*-$PCSiO_{40}$]	$\mathbf{P_4LBO_{17}}$
PS_{580}-*b*-[PBD_{50}-*brush*-$PCSiO_{63}$]	$\mathbf{P_4LBO_{22}}$
PS_{580}-*b*-[PBD_{50}-*brush*-$PCSiO_{119}$]	$\mathbf{P_4LBO_{33}}$
PS_{580}-*b*-[PBD_{50}-*brush*-$PCSiO_{136}$]	$\mathbf{P_4LBO_{36}}$
PS_{580}-*b*-[PBD_{50}-*brush*-$PCSiO_{144}$]	$\mathbf{P_4LBO_{37}}$

[a] For example, in $\mathbf{P_2LHO_{23}}$: $\mathbf{P_2}$ refers to the linear block PS_{426}-*b*-PBD_{40} and $\mathbf{LHO_{23}}$ denotes the corresponding linear-hyperbranched polyalkoxysilane diblock copolymer with a weight fraction of 23 % for the PCSiO block (including the short PBD-backbone)

As in the case of grafting reactions with alkylsilane monomers, the GPC chromatograms (Figure 8.2a) show a broad peak at higher retention volumes (lower molecular weights) next to the main peak. This smaller broad peak corresponds to alkoxysilane monomers that have polymerized via a step-growth mechanism and were not attached to the PBD-core, whereas the main peak corresponds to the grafted diblock copolymers. However, by fractionated precipitation in diethyl ether/methanol, it was possible to completely remove the homopolymers as demonstrated by GPC analyses (Figure 8.2b). Control over the structure of the linear-hyperbranched and brush-like polymers is achieved via SMA by the amount of monomer added. This can be clearly seen from the ^1H NMR spectra of a series of linear-hyperbranched polyalkoxysilanes that were obtained by increasing the amount of MDUOS (AB_2) monomer added (Figure 8.3). The increase growing of the hyperbranched structure can be seen by comparing the relative intensities of the protons of the styrene units with the protons corresponding to the alkoxysilane groups.

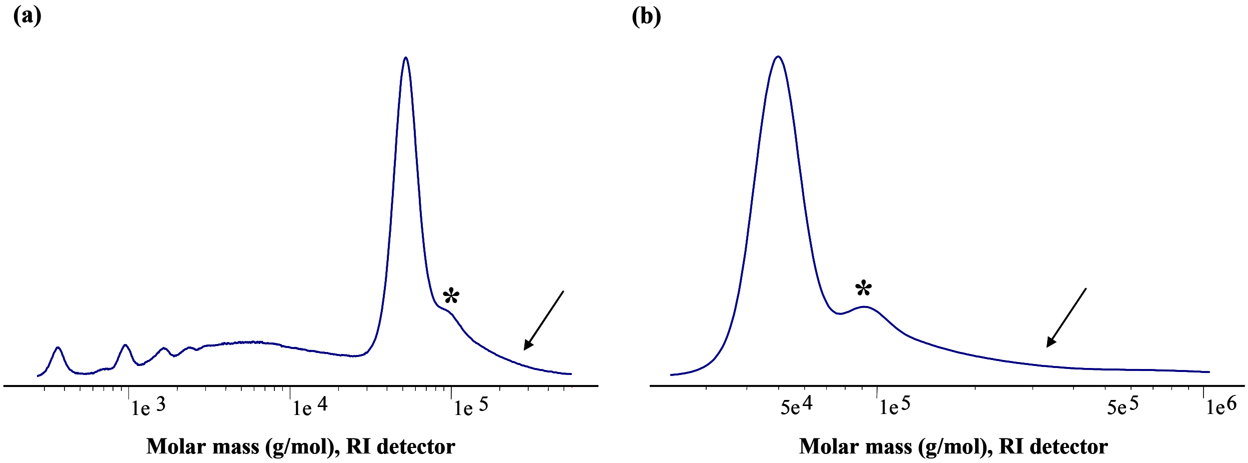

Figure 8.2. Representative GPC chromatograms of the linear-hyperbranched polyalkoxysilanes: (a) **P_2LHO_{53}** crude reaction product and (b) **P_2LHO_{53}** fractionated sample (the asterisk and the arrow represent the linear diblock copolymer dimer and supposable cross linked polymer, respectively).

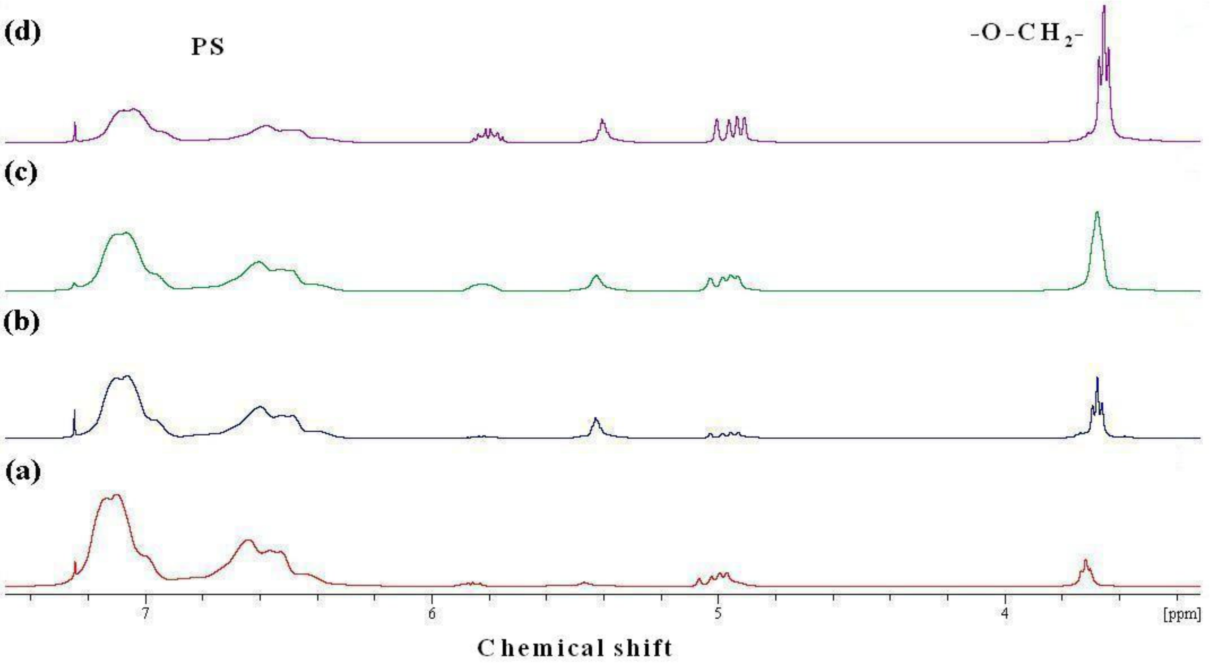

Figure 8.3. ^1H NMR of a series of linear-hyperbranched polyalkoxysilanes with increasing amount of MDUOS (AB_2) monomer added: (a) **P_2LHO_{23}**, (b) **P_2LHO_{53}**, (c) **P_2LHO_{64}** and (d) **P_2LHO_{76}**.

Table 8.2. Equivalents of monomer:PBD vinyl group employed to prepare the linear-hyperbranched and brush-like polyalkoxysilanes and the corresponding calculated grafting efficiencies.

Sample	**Equivalents monomer:PBD vinyl group**[a]	**Grafting efficiency**[b] **(%)**
P_2LHO_{23}	5	15
P_2LHO_{53}	10	31
P_2LHO_{64}	14	36
P_2LHO_{76}	25	36
P_4LBO_{17}	5	16
P_4LBO_{22}	7	18
P_4LBO_{33}	10	24
P_4LBO_{36}	20	14
P_4LBO_{37}	30	9.5

[a]Experimental values. [b]Calculations based on the absolute molecular weights of the samples obtained by membrane osmometry (MO)

The equivalents of monomer per PBD vinyl group added to obtain the linear-hyperbranched and brush-like samples along with calculated grafting efficiencies are presented in Table 8.2. The grafting efficiencies are evaluated making use of the absolute molecular weights of the samples obtained from membrane osmometry (MO) measurements. It can be seen from the table that the grafting efficiencies for the linear-hyperbranched samples increase with the amount of monomer added. However, a plateau at 36 % is reached at a monomer:PBD vinyl group molar excess of 14. A less pronounced increase in the grafting efficiencies with increasing amount of monomer added was found for the linear brush-like samples. Additionally, the grafting efficiency starts to decrease significantly with large molar excess of DMUOS (AB) monomer. This is indeed, as it will be explained later, a first indication of the unexpected lower reactivity of the DMUOS (AB) alkoxysilane monomer. Grafting efficiencies for the linear-hyperbranched and brush-like polycarbosilanes, which were presented in previous chapters, reached a maximum at 25 and 35-50 % respectively. However, the grafting efficiencies from the PS_x-*b*-PBD_y linear cores with the different silane monomers employed cannot be strictly compared. The polymers were prepared from distinct linear cores and the molecular weight of the parent polymer has also an influence on the resulting grafting efficiency, most probably due to shielding effects by the coil of the PS block.

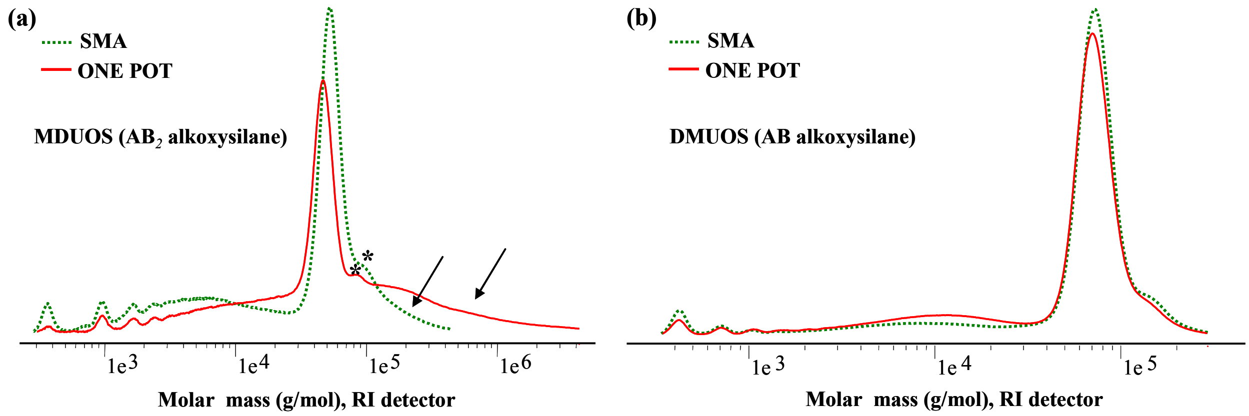

Figure 8.4. Comparison of the crude GPC chromatograms of a grafting reaction carried out in one-pot versus SMA mode from (a) **P$_2$** with MDUOS (AB$_2$) monomer and (b) **P$_4$** with DMUOS (AB) monomer (the asterisk and the arrow represent the linear diblock copolymer dimer and supposable cross linked polymer, respectively).

Comparison of the GPC traces from the crude reaction products of the linear-hyperbranched and brush-like obtained via the SMA strategy and the one-pot polymerization procedures respectively are presented in Figure 8.4. In both architectures, the SMA procedure led to less homopolymers than the one-pot synthesis. The effect is more pronounced when using the more sterically hindered branching MDUOS (AB$_2$) monomer. This is as well related to the higher probability of “cyclization” of the AB$_2$ versus the AB monomer.

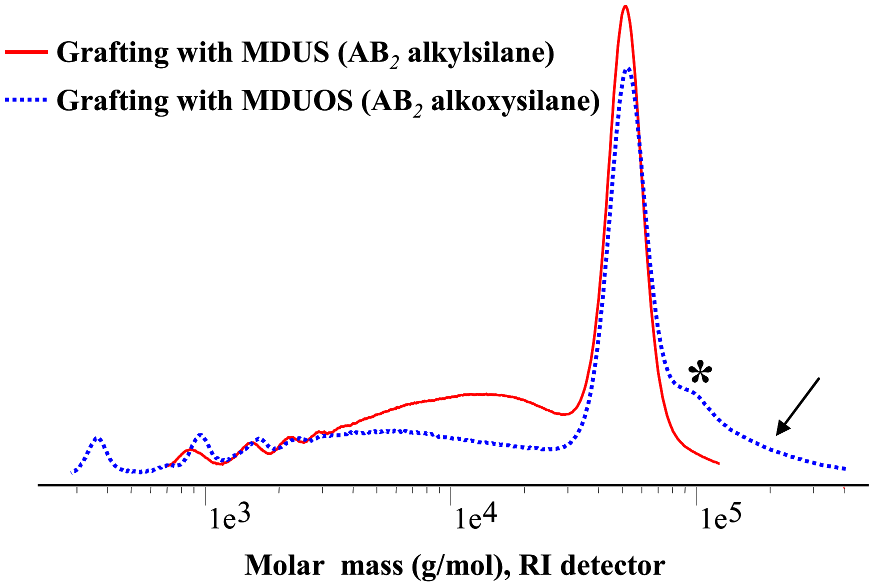

Figure 8.5. Comparison of the GPC curves of the crude reaction products of a SMA hypergrafting reaction from **P$_2$** with MDUS and MDUOS AB$_2$ monomers using the same

molar excess of monomer (the asterisk and the arrow represent the linear diblock copolymer dimer and supposable cross linked polymer, respectively).

The SMA hypergrafting reaction of MDUS (alkylsilane) and MDUOS (alkoxysilane) AB_2 monomers from the linear core $\mathbf{P_2}$ were compared when using the same monomer:core mol ratio (Figure 8.5). It is obvious that the MDUOS monomer gives lower formation of homopolymers and also the molecular weight peak maximum of the "cycles" is clearly displaced to lower molecular weights (*ca.* 5,000 g/mol). Although the grafting efficiency of MDUOS versus MDUS is clearly improved, this is not as good as expected in view of the electronic effects. The lower grafting efficiency when using MDUOS can be explained by a rearrangement reaction first reported by Stober *et al.*[15] This rearrangement reaction is presented in Chapter 4 (Section 4.3.2.1). We believe that a similar rearrangement occurs with MDUOS, thereby reducing the amount of monomer available for grafting and/or rendering the terminal groups of already grafted monomer unavailable for further reaction. The MDUOS rearrangement reaction, which was already predicted by Möller *et al.*,[4k] generates A_2B and B_3 type monomers (Chapter 4, Figure 4.19). An A_2B type monomer, methyl(undec-10-enyloxy)silane, is also produced and represents a potential cross linker. This could explain the higher molecular weight tail (denoted by an arrow) evident in the GPC chromatograms (Figures 8.2, 8.4a and 8.5) of the linear-hyperbranched polyalkoxysilanes (in addition to the peak proceeding from the linear diblock copolymer dimer formed during the end-capping reaction and denoted by an asterisk in the GPC chromatograms). Nevertheless, these higher molecular weight tails are not always immediately evident in the GPC chromatogram of a freshly precipitated polymer prepared from MDUS (AB_2) branching alkylsilane monomer (Figure 8.5, red solid curve). It is known that silicone redistribution reactions normally involve exchange of Si-O bonds, while carbon-based ligands on silicon migrate only with great difficulty.[13]

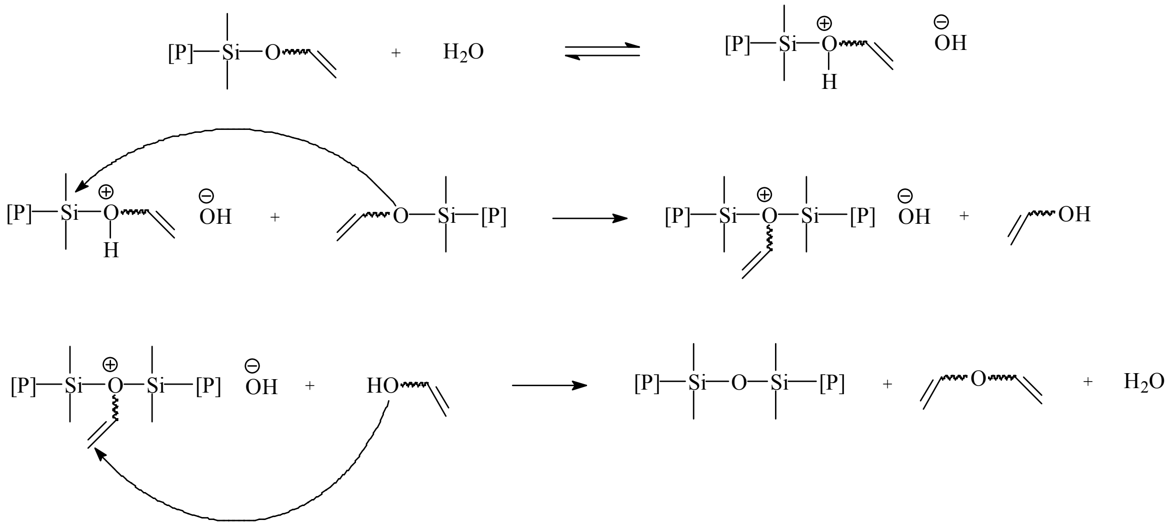

Figure 8.6. Possible cross linking side reaction for the polyalkoxysilane-modified diblock copolymers in the presence of water ([P] represents the polymer backbone).

The more pronounced higher molecular weight peaks for the polyalkoxysilane *vs.* the polycarbosilane architectures can also be explained if, during precipitation, small traces of water are present. Small traces of water can readily catalyze the condensation of alkoxysilyl groups as shown in Figure 8.6, causing coupling of the polymer.[16] The polymers were not precipitated using anhydrous diethyl ether/methanol. Usually, the higher molecular weight peaks in the linear-hyperbranched polycarbosilanes appeared with time as a consequence of storage. This observation was related to the presence of residual catalyst even after precipitation, which can cause a slow coupling process to occur within the polymers after their isolation. This explanation is also valid for the linear-hyperbranched polyalkoxysilanes, wherein higher molecular peaks present after precipitation became larger with time. Moreover, the polyalkoxysilane materials were stored under ambient conditions in the presence of moisture and this could also justify the increase of the coupled polymer peak with time.

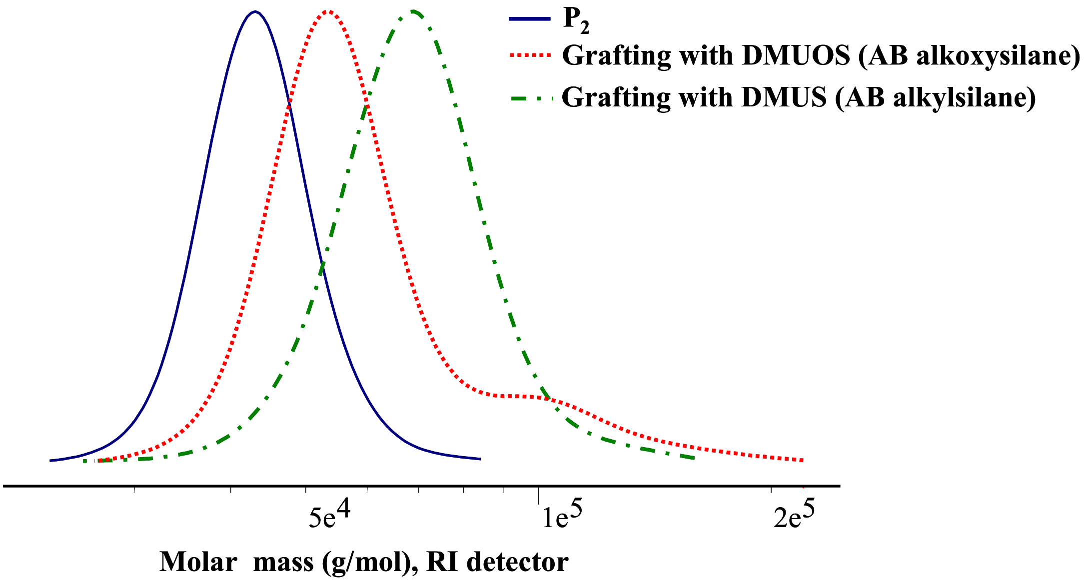

Figure 8.7. GPC chromatogram superimposition of the linear core **P$_2$** and of the resulting linear-brush-like polymers from a SMA grafting reaction with DMUOS and DMUS AB monomers, using the same molar excess of monomer.

Unexpectedly, DMUOS (alkoxysilane) bearing an electron-withdrawing alkoxy group on the silicon gave lower grafting efficiencies than the DMUS (alkylsilane) AB monomer. This can be seen from the superimposition of the GPC traces of a linear core and of the resulting linear brush-like architectures having DMUOS and DMUS as the building monomer units respectively (Figure 8.7). The relative molecular weight of the brush-like polycarbosilane architecture is clearly higher under the same monomer:core molar ratio. This is surprising in view of the favorable electronic effects of the DMUOS monomer for the hydrosilylation reaction. However, there are two possible explanations that can help to understand this finding. The first one might be related to the stability of the alkoxysilanes. It is known that alkylsilyl ethers are neither stable to most types of hydrolysis nor to the harsh conditions that frequently accompany organic chemistry (acid, base, strong nucleophiles, transition metal catalysts, reduction, oxidation, etc.).[13] Nonetheless, the more the bulk of organic groups on silicon, the more difficult is nucleophilic substitution at silicon under acidic or basic conditions.[17] Based on this principle, the silicon in the DMUOS (alkoxysilane) AB monomer, possessing only one undecenoxysilane chain, would be more susceptible to nucleophilic attack than the silicon in the MDUOS (alkoxysilane) AB$_2$ monomer. Thus, a lower stability of the AB undecenoxysilane upon hydrolysis might explain its lower reactivity *vs.* the AB undecenylsilane monomer despite the favorable electronic effects. The second explanation might be related to the substantially different silicon chemical shifts found for the

DMUS alkylsilane and DMUOS alkoxysilane AB monomers. A relative reactivity trend of the hydrosilanes used for the hydrosilylation grafting reaction from PS_x-*b*-PBD_y diblock copolymers, as experimentally found, is proposed in Figure 8.8. This is presented together with the corresponding silicon chemical shifts. It can be observed that the greater the downfield shifts at the silicon atom, the less reactive are the monomers. DMUOS alkoxysilane AB monomer shows the greatest silicon downfield shift of all of the employed monomers, which would explain its remarkably lower reactivity.

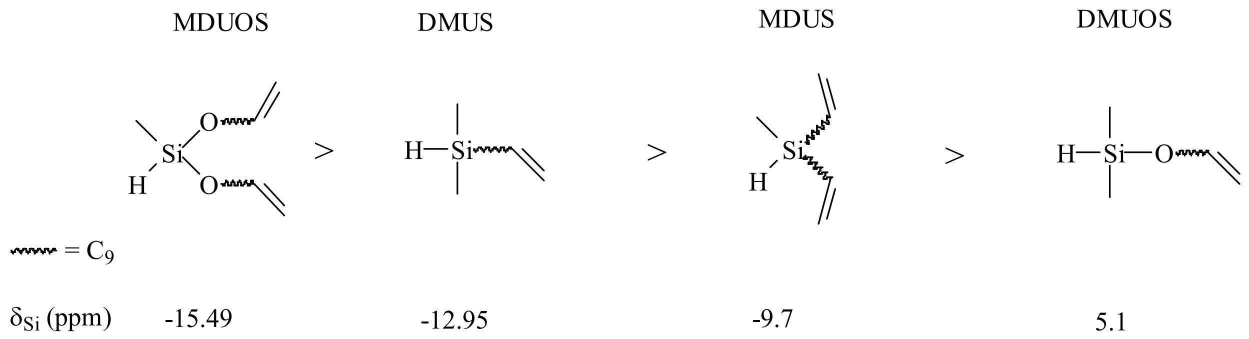

Figure 8.8. Proposed relative reactivity of the hydrosilanes employed in the hydrosilylation grafting reaction from PS_x-*b*-PBD_y diblock copolymers together with the corresponding silicon chemical shifts.

8.3.2 Chemical structural characterization

The modified diblock copolymers were characterized by ^{1}H, ^{13}C, ^{29}Si NMR and by IR spectroscopy. The ^{1}H NMR spectra of the linear-hyperbranched and brush-like polyalkoxysilanes show several new peaks with respect to the linear core, which are assigned as shown in Figures 8.9 and 8.10 and are consistent with the proposed structure. The new peaks at 0.12 or 0.15 ppm (denoted by “g”) and 0.63 or 0.66 ppm (denoted by “h”) correspond to the Si-CH_3 and Si-CH_2 groups of the hyperbranched or brush-like architecture respectively. These resonances are shifted slightly downfield with respect to the ones for the hyperbranched and brush-like polycarbosilanes, as a result of the alkoxy functionalization on silicon. The peaks of the Si-O-CH_2 moiety (denoted by “p”) appear at about 3.7 ppm. NMR integration values of the Si-CH_3, Si-CH_2 and Si-O-CH_2 peaks give the expected 3:2:4 and 3:1:1 ratio for the linear-hyperbranched and linear brush-like architecture respectively. The rest of the NMR chemical shift values are comparable to those found for the linear-hyperbranched and brush-like polycarbosilanes (See Chapters 6 and 7).

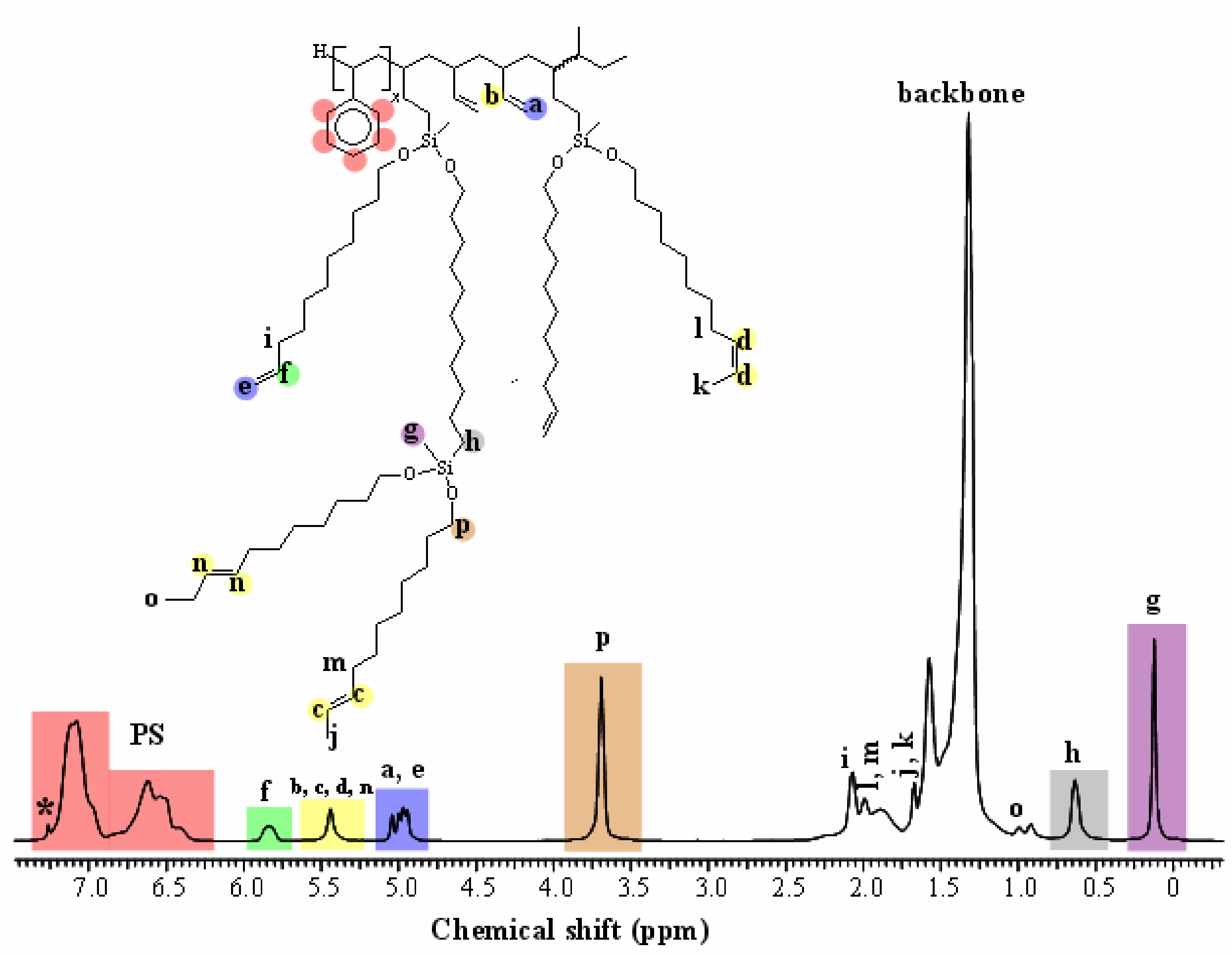

Figure 8.9. ^{1}H NMR spectrum of $\mathbf{P_2LHO_{64}}$ in $CDCl_3$ (solvent peak denoted by an asterisk).

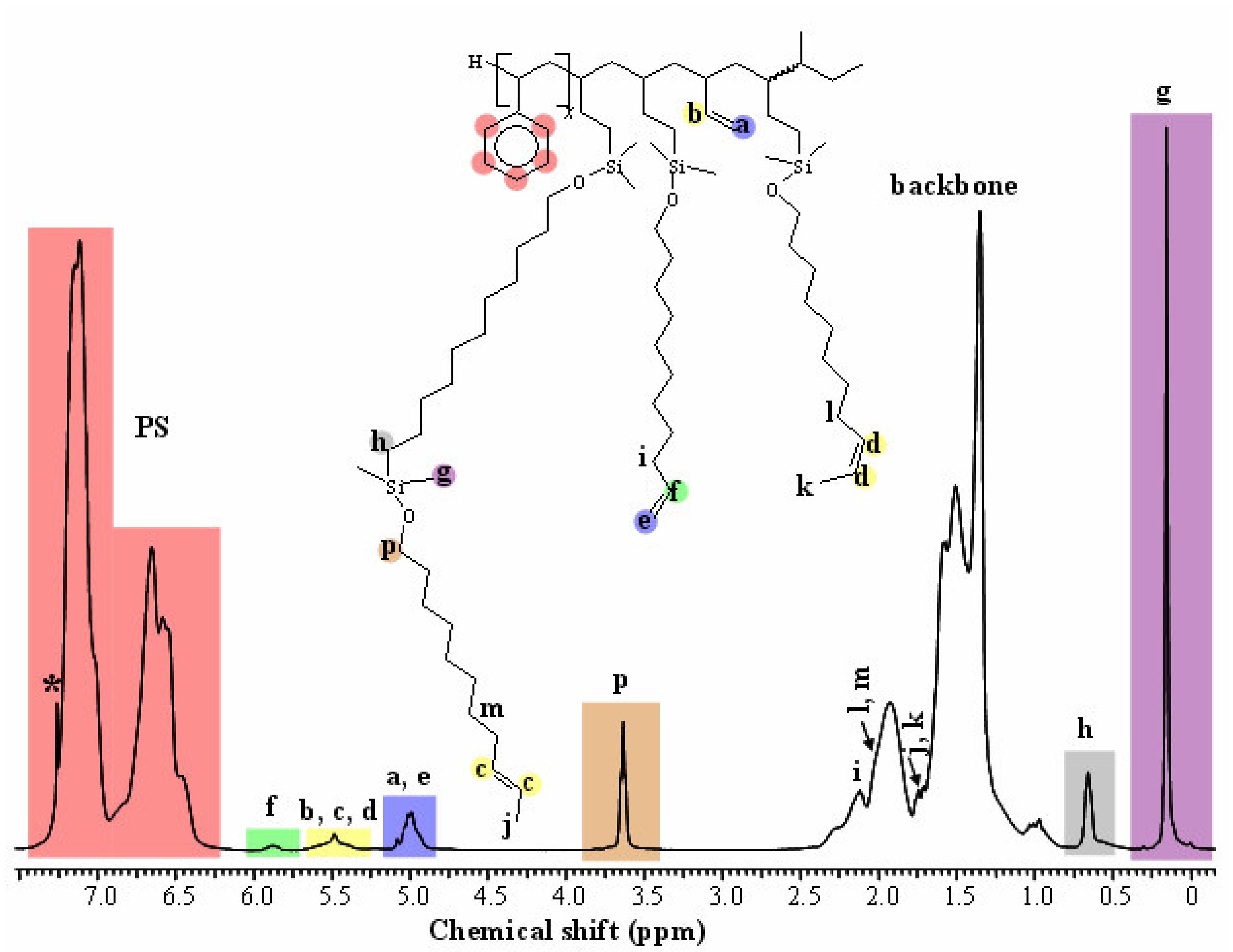

Figure 8.10. ^{1}H NMR spectrum of **P_4LBO_{17}** in $CDCl_3$ (solvent peak denoted by an asterisk).

In general Si-O-alkyl moieties can be easily hydrolyzed in the presence of a protic solvent such as water or methanol. Nucleophiles can then attack alkyl silyl ethers, readily cleaved under acidic or basic conditions.[18] This is shown in Figure 8.11 for the linear brush-like polyalkoxysilanes. To investigate the stability of these polymers, a small amount of deuterated water was added to a linear-hyperbranched polyalkoxysilane sample and a ^{1}H NMR was then recorded immediately and after two weeks to evaluate the stability of these systems upon hydrolysis (Figure 8.12). It is observed that the shape of the peak corresponding to the protons of the alkoxy group and the alkoxy:alkenyl ratio is maintained upon addition of D_2O. This implies that linear-hyperbranched polyalkoxysilanes are reasonably water stable. This is probably related to the more bulky silyl ethers that were employed as branching chains.

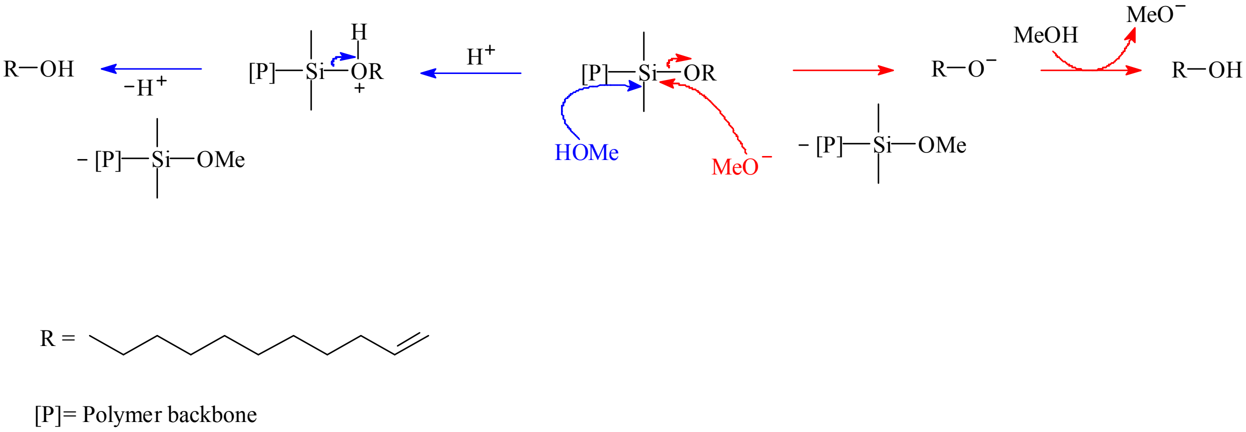

Figure 8.11. Acid- (blue arrows) and base-catalyzed (red arrows) methanolysis on the linear brush-like polyalkoxysilane architectures.

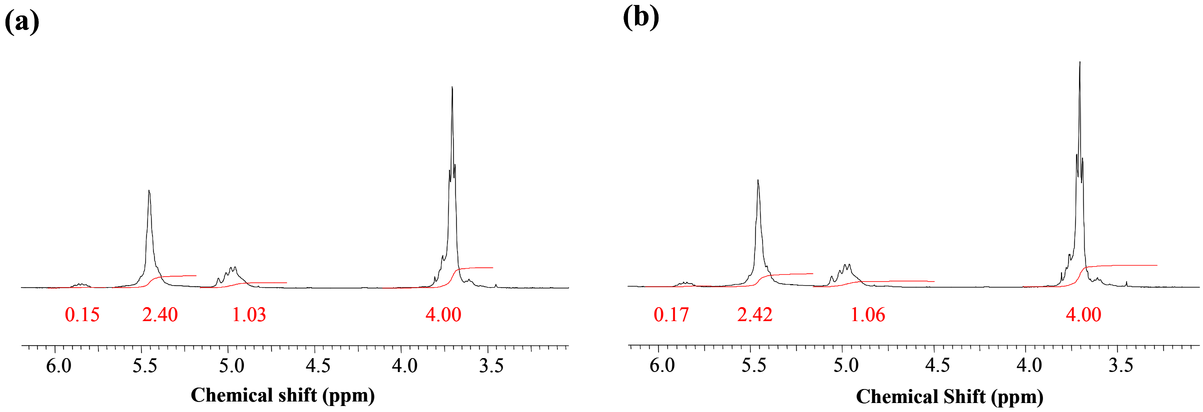

Figure 8.12. ^{1}H NMR of the alkoxy and alkenyl region of a linear-hyperbranched polyalkoxysilane sample in $CDCl_3$: (a) before addition of D_2O and (b) after two weeks in contact with D_2O.

Nonetheless, the linear brush-like polyalkoxysilanes seem to be less stable upon hydrolysis. The ^{1}H NMR of some polymers showed, after fractionated precipitation in diethyl ether/methanol, an additional peak at 3.8 ppm (denoted by an arrow) close to the signal of the Si-O-alkyl moiety (Figure 8.13). It is conceivable that this small peak corresponds to a hydrolyzed Si-O-alkyl group. This lower stability upon hydrolysis would explain, as mentioned before, the lesser than expected reactivity of the AB (DMUOS) alkoxysilane monomer.

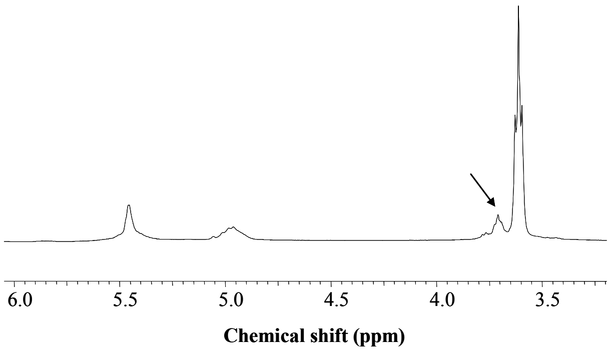

Figure 8.13. ^{1}H NMR of the alkoxy and alkenyl region of a linear brush-like polyalkoxysilane sample in $CDCl_3$ after fractionated precipitation in diethyl ether/methanol (**P_4LBO_{36}**).

The data from the ^{13}C NMR spectra of the linear-hyperbranched and brush-like polyalkoxysilane are consistent with the assignments from the ^{1}H NMR spectra and are presented in Figures 8.14 and 8.15. The carbons from the Si-O-CH_2 groups of both architectures are the characteristic feature and give rise to a peak “p” at 63 ppm. The other assignments for the chemical shift values are comparable to the ones obtained for the linear-hyperbranched and brush-like polycarbosilanes (See Chapters 6 and 7).

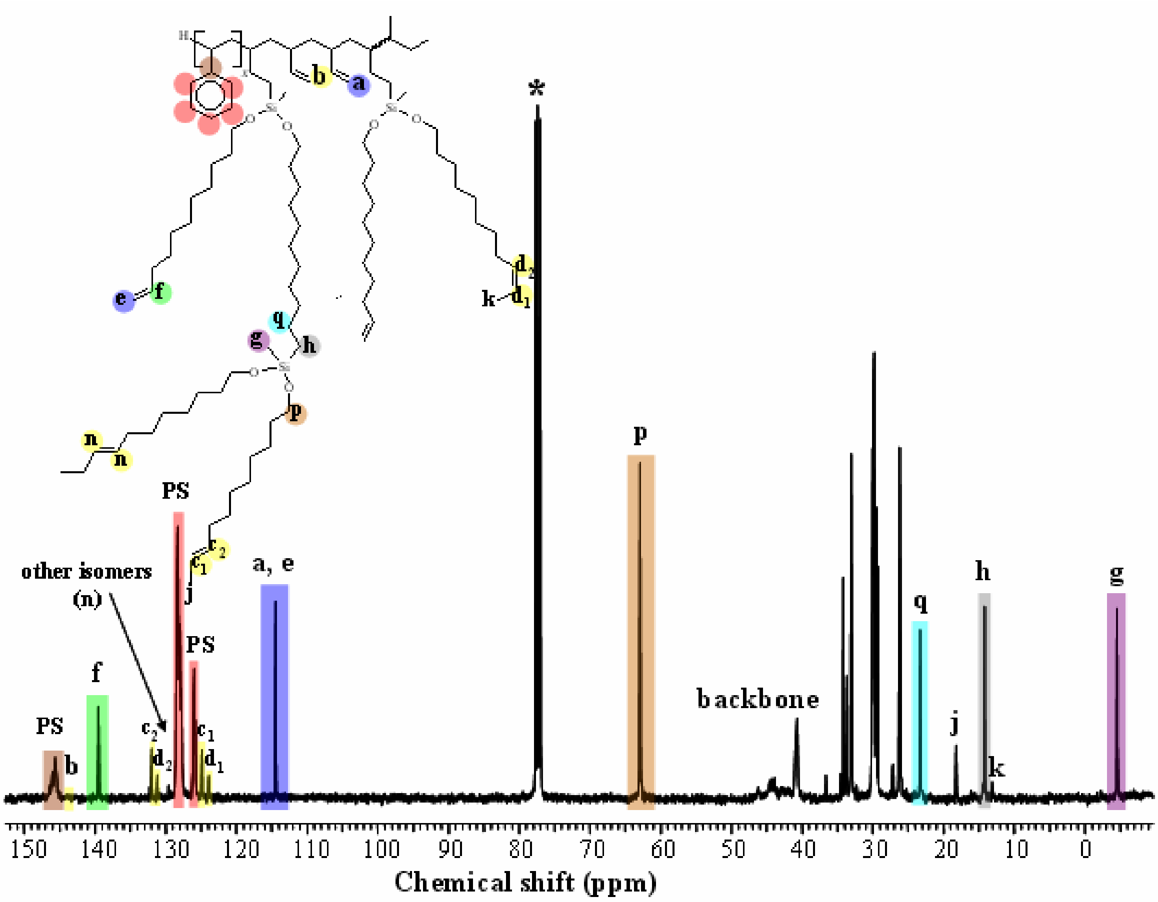

Figure 8.14. ^{13}C NMR spectrum of **P_2LHO_{64}** in $CDCl_3$ (solvent peak denoted by an asterisk).

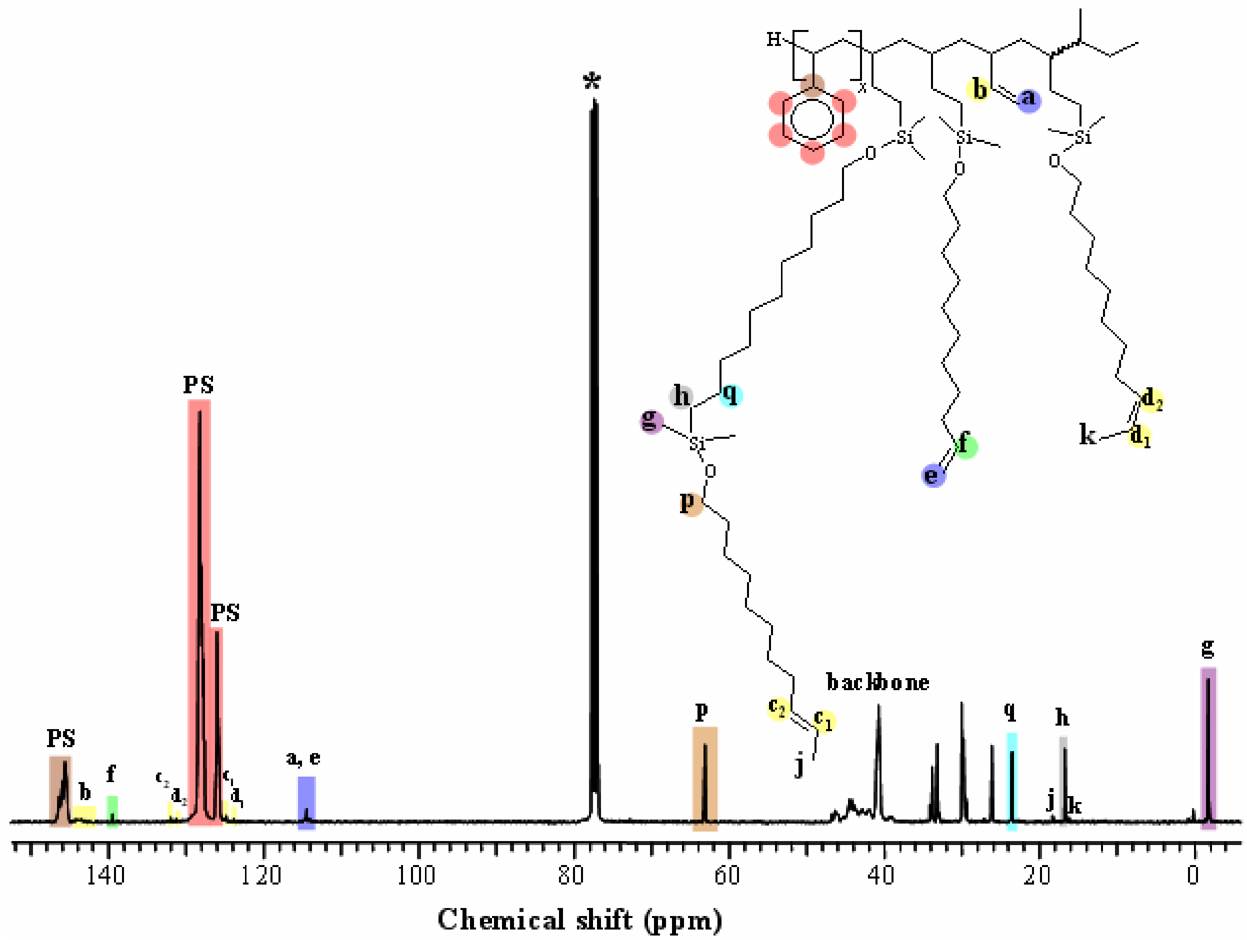

Figure 8.15. ^{13}C NMR spectrum of $\mathbf{P_4LBO_{17}}$ in $CDCl_3$ (solvent peak denoted by an asterisk).

The general trends regarding the microstructure of these linear-hyperbranched and brush-like materials are analogous to those found for the polycarbosilane architectures. These can be recapitulated as follows:

(1) Conversion of the 1,2-units of the PBD core was not complete, as evidenced by ^{1}H NMR spectra. Peaks associated with the double bonds were used for determining the conversion of the 1,2-units of the PBD block. The conversion percentages of the 1,2-butadiene units were estimated from the ^{1}H NMR spectra utilizing the equation 6.1 presented in Chapter 6 and varied between 30 and 65 %. These percentages are only an approximation, as the number of PBD grafting sites from the linear core is small.

(2) ^{1}H and ^{13}C NMR spectroscopy showed that the hydrosilylation reaction yielded exclusively ß-addition products. Further analysis of the spectra showed that hydrosilylation of the double bonds is structurally selective, with the terminal double bonds being attacked and the isomerized internal double bonds remaining unreactive. The percentage of isomerization

can be calculated from the ^{1}H NMR spectra with the help of the Equation 6.3 presented in Chapter 6 and results in values between 30 and 55 %.

(3) The number of vinyl end groups increased as expected after hypergrafting with MDUOS (AB_2) monomer, suggesting that competing side reactions like hydrogenation were suppressed when using the more reactive alkoxysilane branching monomer. On the other hand, the number of double bonds seemed to decrease, instead of remaining constant, when using the less reactive DMUOS (AB) monomer. However, it is more difficult to evaluate the number of end groups in the linear brush-like systems due to the smaller number of vinyl sites.

(4) As expected, there was only one peak in the ^{29}Si NMR spectra of the linear-hyperbranched and brush-like polyalkoxysilanes, which negates the possibility of determining the degree of branching (DB) (Figure 8.16). This is due to the long C_{11} alkyl chains. The silicon signals of both monomers are downfield shifted upon hydrosilylation as shown in Table 8.3. The chemical shift (δ -4.09 ppm) of the silicon with two undecenoxy groups (MDUOS) is similar to the chemical shift (δ -2.2 ppm) reported for $(CH_3)_2Si(OCH_3)_2$ and the chemical shift (δ 17.3 ppm) of the silicon with one undecenoxy group (DMUOS) is in good agreement with that reported for $(CH_3)_3SiOCH_3$ (δ 16.0 ppm).[19]

Table 8.3. ^{29}Si NMR chemical shifts.

Compound	**δ_{Si} (ppm)**
MDUOS	-15.49
P_2LHO_{23}	-4.09
DMUOS	5.1
P_4LBO_{36}	17.3

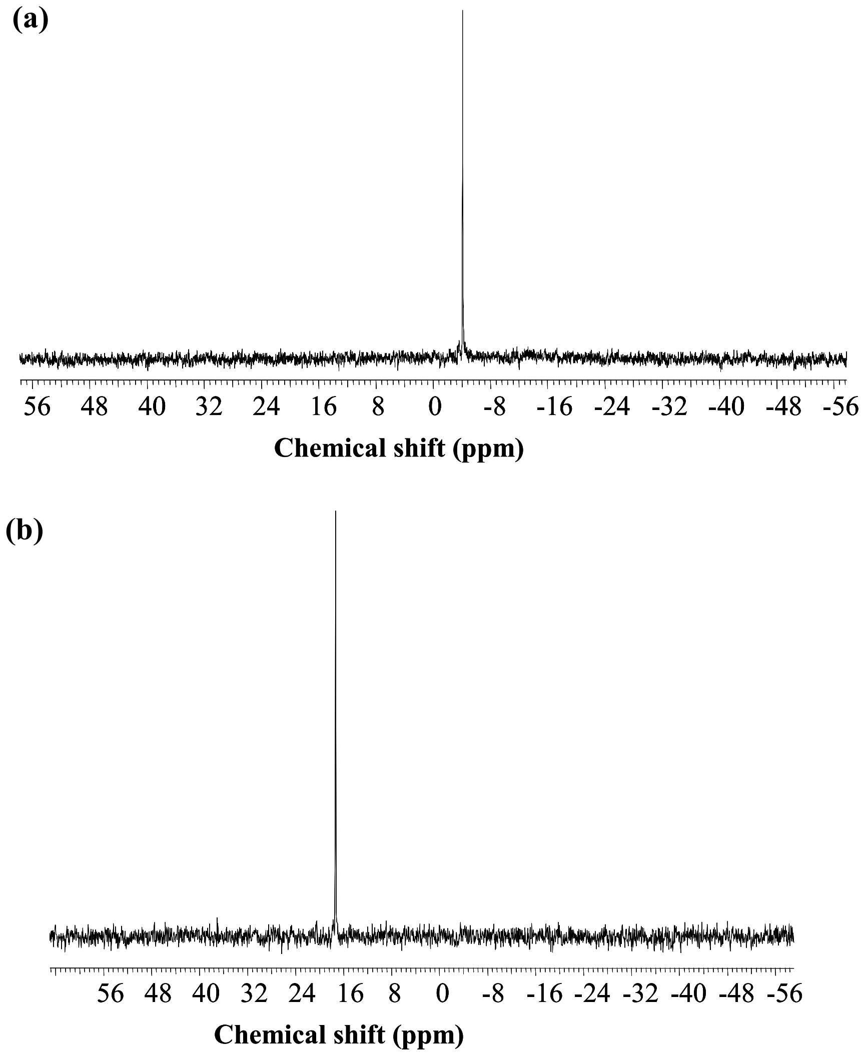

Figure 8.16. Representative ^{29}Si NMR of the linear-hyperbranched and brush-like polyalkoxysilanes: (a) **P_2LHO_{23}** and (b) **P_4LBO_{36}**.

The IR spectra of a linear core and of the linear-hyperbranched and brush-like polyalkoxysilanes are shown in Figure 8.17. After the grafting reaction new stretching bands are seen at 1254 cm^{-1} or 1250 cm^{-1}, reflecting the Si-CH_3 bond, at 1091 cm^{-1} or 1093 cm^{-1}due to the presence of Si-O-CH_2 bonds and at 837 cm^{-1} for the bending vibration of CH_3-Si-CH_3 in the brush-like architecture.

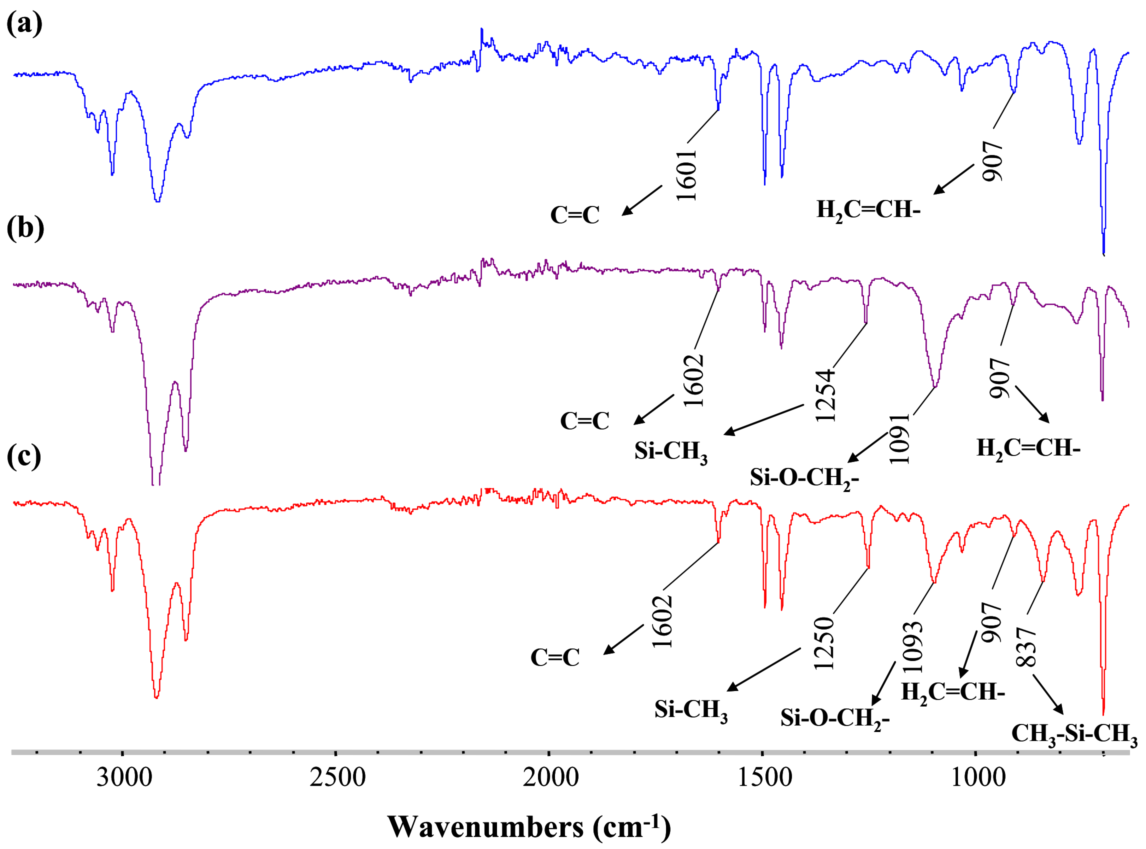

Figure 8.17. IR spectra of (a) **P_2**, (b) **P_2LHO_{64}** and (c) **P_4LBO_{36}**.

8.3.3 Characterization data and thermal properties

The relative molecular weights of the linear-hyperbranched and brush-like samples were determined by GPC analysis with PS standard calibration. The molecular weights of the prepared samples determined by conventional GPC are lower than those determined by membrane osmometry (MO), because of the different hydrodynamic behavior of the studied branched macromolecules and the linear polymer standard.[20] Thus, the characterization data for a series of linear-hyperbranched and brush-like polyalkoxysilanes with the calculated weight fractions for each block by MO are shown in Table 8.4. In general, the polydispersities (PDI) of the modified polymers remained low or slightly larger than those of the starting diblock copolymers. The higher molecular weight peaks evident in the GPC traces were included in the PDI of the polymers. Linear-hyperbranched polyalkoxysilanes with PCSiO fractions between 23 and 76 wt % were synthesized. However, the lower reactivity of the AB alkoxysilane monomer led to the preparation of linear brush-like polyalkoxysilanes with a PCSiO maximum fraction of only 37 wt %.

Table 8.4. Characterization data for the linear PS$_x$-*b*-PBD$_y$ templates (**P$_2$**, **P$_4$**) and for the resulting linear-hyperbranched and brush-like alkoxysilane diblock copolymers.

	GPC^a		**MO**^{b}	
Sample	M$_n$ (10^3 g/mol)	PDI^c	M$_n$ (10^3 g/mol)	wt % PS
P$_2$	40.8	1.03	46.5	95.4
P$_2$LHO$_{23}$	49.4	1.10	58.0	77
P$_2$LHO$_{53}$	56.3	1.19	93.5	47
P$_2$LHO$_{64}$	52.7	1.15	123.8	36
P$_2$LHO$_{66}$	57.4	1.21	130.0	34
P$_2$LHO$_{76}$	77.3	2.41^d	185.0	24
P$_4$	52.6	1.03	63.1	95.7
P$_4$LBO$_{17}$	64.8	1.07	72.3	83
P$_4$LBO$_{33}$	74.8	1.16	90.3	67
P$_4$LBO$_{36}$	75.5	1.16	94.2	64
P$_4$LBO$_{37}$	82.3	1.22	96.0	63

^{a}Gel permeation chromatography (GPC) measured in chloroform at 30 °C with PS standard calibration. ^{b}Membrane osmometry (MO) measured in toluene at 40 °C. ^{c}Polydispersity index $\overline{M}_w/\overline{M}_n$ measured by GPC in chloroform at 30 °C. ^{d}Bimodal distribution.

Thermal characterization of both starting and modified polymers was performed using DSC and TGA. The thermal properties of the materials are summarized on Table 8.5.

Table 8.5. Thermal Properties of the linear PS$_x$-*b*-PBD$_y$ cores and of the linear-hyperbranched and brush-like alkoxysilane diblock copolymers.

Sample	**T$_g$1^a (°C)**	**T$_g$2^a (°C)**	**T$_m$^{a} (°C)**	**T$_c$^{a} (°C)**	**ΔH$_s$ (J/g)**	**ΔH$_c$ (J/g)**	**α$_m$ (%)**	**α$_c$ (%)**
P$_2$	88.1	-30.8	---	---	---	---	---	---
P$_2$LHO$_{23}$	92.5	-61.3	---	---	---	---	---	---
P$_2$LHO$_{53}$	102.7	---	-48.3	-66.3	7.3	-5.4	61	38
P$_2$LHO$_{64}$	101.4	---	-40.0	-58.0	15.9	-16.0	>100	93
P$_2$LHO$_{66}$	103.2	---	-40.0	-58.4	18.4	-15.2	>100	86
P$_2$LHO$_{76}$	73.5	---	-37.5	-55.1	23.8	-20.6	>100	101
P$_4$	97.3	-29.3	---	---	---	---	---	---
P$_4$LBO$_{17}$	99.2	-27.5	---	---	---	---	---	---
P$_4$LBO$_{33}$	103.3	-67.6	---	---	---	---	---	---
P$_4$LBO$_{36}$	85.9	-70.4	---	---	---	---	---	---
P$_4$LBO$_{37}$	108.0	-61.9	---	---	---	---	---	---

T$_m$ = melting endotherm of the PCSiO block
T$_c$ = crystallization exotherm of the PCSiO block
ΔH$_s$ = heat of fusion of the PCSiO block
ΔH$_c$ = heat of crystallization of the PCSiO block
α$_m$ = relative degree of crystallinity of the PCSiO block calculated from **ΔH$_s$**
α$_c$ = relative degree of crystallinity of the PCSiO block calculated from **ΔH$_c$**
^{a}measured at a heating rate of 25 °C/min.

The DSC thermograms for the linear-hyperbranched polyalkoxysilanes show a T$_g$ between 74 and 103 °C and a broad melting peak (T$_m$) with a maximum between -37 and -48 °C. The T$_g$ corresponds to the PS block and the T$_m$ to the PCSiO hyperbranched block. For low weight percentages of the PCSiO hyperbranched block (*i.e.*, sample **P$_2$LHO$_{23}$**), the entanglement of the PS chains suppresses the crystallization of the PCSiO chains, showing a T$_g$ at -61.3 °C instead of a T$_m$ for the PCSiO hyperbranched block. Figure 8.18 presents a typical DSC heating/cooling thermogram for the linear-hyperbranched polyalkoxysilane samples. Data were recorded during the second heating/cooling cycle at a rate of 25 °C/min. The DSC shows an exotherm and an endotherm corresponding to the crystallization (T$_c$) and melting of the PCSiO hyperbranched block, which is the crystallizable component in these materials. The T$_m$ and T$_c$ are defined by the maximum temperature of the endothermic and exothermic peaks respectively. Similar melting behavior was observed at slower heating rates. The T_m and T_c values for the PCSiO hyperbranched block and the T_gs for the PS block of the synthesized samples are summarized in Table 8.5. The DSC heating traces for these samples reveal relatively broad melting endotherms for the PCSiO hyperbranched block, indicating a broad crystallite size distribution.[21] This monomodal but broad endotherm is therefore due to the formation of crystalline domains of different quality as a consequence of the hyperbranched structure. Table 8.5 shows that the melting points exhibited by the PCSiO hyperbranched block increase from -48.3 °C for **P_2LHO_{53}** to -37.5 °C for **P_2LHO_{76}**. This slight increase can be attributed to the higher freedom of the crystalline domains, due to the fact that in the latter samples the PCSiO hyperbranched block forms the matrix, *i.e.* the continuous phase. Additionally, T_m and T_c increase with increasing molecular weight of the PCSiO hyperbranched block.

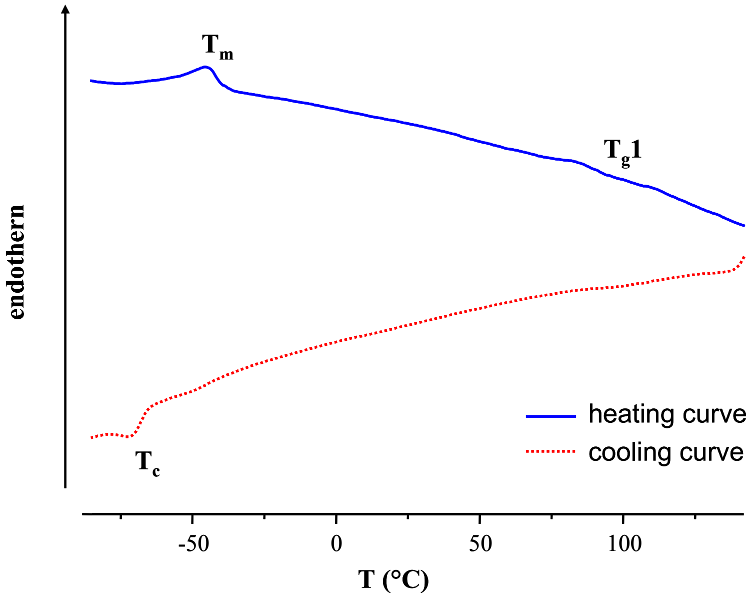

Figure 8.18. Typical DSC for the linear-hyperbranched polyalkoxysilanes (**P_2LHO_{53}**): data shown are recorded during the second heating (blue solid line) and cooling cycle (red dotted line) at a scanning rate of 25 °C/min.

The homopolymer from MDUOS AB_2 alkoxysilane monomer (PMDUOS) was synthesized as a reference for comparing the thermal properties with the linear-hyperbranched materials. The DSC of PMDUOS shows a broad endotherm and exotherm during the heating and cooling cycle at -32.0 and -47.0 °C respectively (Figure 8.19). The observed T_m and T_c of the linear-hyperbranched materials are then slightly lower than those observed for PMDUOS. The broadness of the melting and crystallization peak is again related to the crystallite distribution size of the branched polymer structure. Additionally, T_m and T_c in the homopolymer show a small shoulder. Multiple endotherms arise usually from recrystallization; *i.e.* imperfect crystals melt and recrystallize into more perfect crystals. Such an effect has been reported by Berghmans *et al.* and Booth *et al.* in PEO-*b*-PCL and PEO-*b*-POB block copolymers respectively[22] and in syndiotactic PP homopolymers.[23] Nevertheless, it might also indicate changes in the crystalline state,[24] possibly reflecting a complicated crystallization mechanism of the PCSiO hyperbranched polymer. Therefore, the broad double melting peak observed in our case can arise from less ordered crystallites melting before those with better-ordered domains of chain-folded PCSiO or from melting of crystals with different fold lengths. The broad distribution of the polymer chains in PMDUOS (PDI = 4.6) may be an additional factor contributing to the multimodal melting and crystallization peaks. The observation of a wide melting peak without a shoulder for the linear-hyperbranched samples is possibly a consequence of the increasing heating rates utilized and/or the more defined molecular weight distribution. PDMUOS was heated at a heating rate of 10 °C/min, while the linear-hyperbranched samples were heated at 25 °C/min. In any case, crystallization in homopolymers and in block copolymers must be distinguished, as the equilibrium chain folding in diblocks might be controlled by the size of the non-crystallizable block.[21] Therefore, the absence of a multimodal peak in the linear-hyperbranched samples can be related to the attachment of a branched structure to the PS glassy block, which might change the crystallization process as reported before.[25]

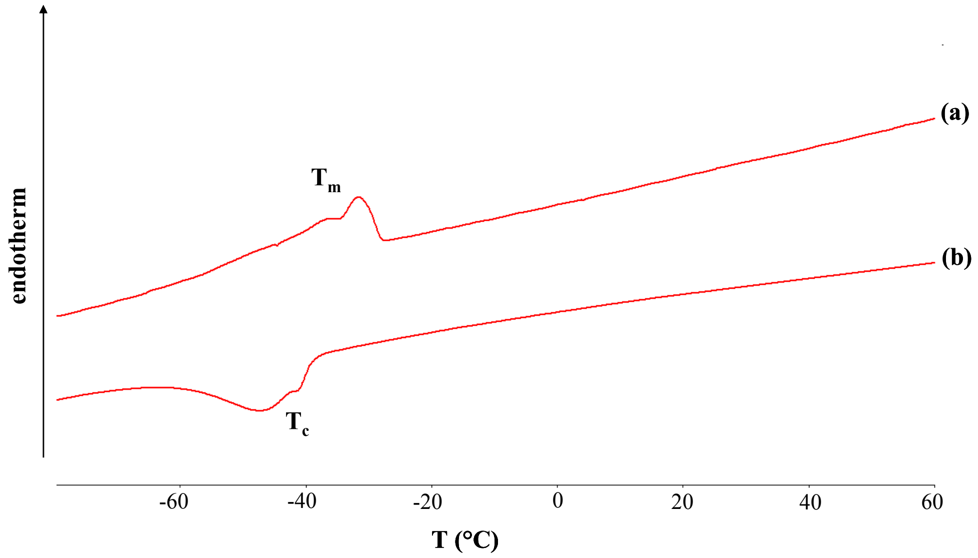

Figure 8.19. DSC (a) heating and (b) cooling scans (scanning rate of 10 °C/min) of PMDUOS hyperbranched homopolymer ($\overline{M}_n$ = 6,000 g/mol; PDI = 4.6).

The fractional degree of crystallization (α) for the PCSiO hyperbranched chains in the linear-hyperbranched samples can be evaluated from DSC measurements.[21] T_m and T_c in the linear-hyperbranched samples are defined by the maximum temperature of the endothermic or exothermic peak respectively and α can be calculated from the corresponding peak area ΔH_{exp} (J/g) according to equation 8.1. f_w is the weight fraction of the PCSiO hyperbranched block in the linear-hyperbranched samples and ΔH_{exp}^* is the experimental heat of fusion or crystallization for PCSiO hyperbranched crystals (22.7 and -26.8 J/g respectively). The calculated α values are presented in Table 8.5. The α values increase with increasing molecular weight of the PCSiO hyperbranched block, which might be attributed to a higher incompatibility between the PS and the PCSiO block due to the increasing values of χN. It is as well noticeable that the α´s obtained from the heating scans are considerably higher than those calculated from the cooling scans. This indicates that annealing of the crystals might take place during heating, especially in the diblock copolymer with 53 wt % of the hyperbranched block. However, the crystalline values for some of the samples, which were obtained using the heats of fusion from the DSC measurements, were higher than 100 %. This indicates that the values obtained by DSC are by no means accurate and provide only a trend of increasing crystallinity with an increasing molecular weight of the PCSiO hyperbranched block.

$$\alpha = \Delta H_{\exp} / (\Delta H_{\exp}{}^{*} f_w) \times 100$$

Equation 8.1. Evaluation of the fractional degrees of crystallinanity (α) for the linear-hyperbranched polyalkoxysilanes.

The linear-hyperbranched polycarbosilanes presented in Chapter 6 exhibited a T_g for the PCSi block and not a melting endotherm. The presence of a T_m for the PCSiO block in the linear-hyperbranched polyalkoxysilanes is explainable by the increased flexibility and therefore higher ability to fold of the undecenoxy chains that have been lengthened in an atom when compared to the undecenyl ones. Nevertheless, it is surprising to note that this subtle difference of the chain structure exits such a significant effect on the macroscopic properties.

On the other hand, the linear brush-like polyalkoxysilanes are completely amorphous, showing no signs of melting or cold crystallization in the DSC. They exhibit a very low T_g between -27.5 and -61.9 °C that reflects the conformational freedom of the alkoxysilane block scaffold and a high T_g corresponding to the PS block. A representative DSC recorded during the second heating and cooling cycle at a rate of 25 °C/min is shown in Figure 8.20. The presence of two glass transitions evidences that the linear brush-like copolymers are microphase-separated. Nonetheless, thermal characterization of the homopolymer from DMUOS AB alkoxysilane monomer (PDMUOS) showed a multiple endotherm and exotherm at -56 and -61 °C, respectively, corresponding to the melting and crystallization of the PCSiO brush-like homopolymer (Figure 8.21). As before, this double melting endotherm indicates that melting is immediately followed by recrystallization and this is more pronounced at slower heating rates.[21,22] The absence of a melting or cold crystallization peak for the PCSiO brush-like block in the linear-brush-like architectures can be tentatively explained by the following description: in the homopolymer, the polymer chains are not attached to a core and upon cooling they can pack close to each other, leading to crystallization. On the contrary, the PCSiO brushes in the linear brush-like architectures have been attached to the vinyl groups of the PBD core. As not all the PBD vinyl grafting sites have been substituted (as demonstrated before), the polymer chains are not able to crystallize upon cooling due to the higher inter-chain separation.

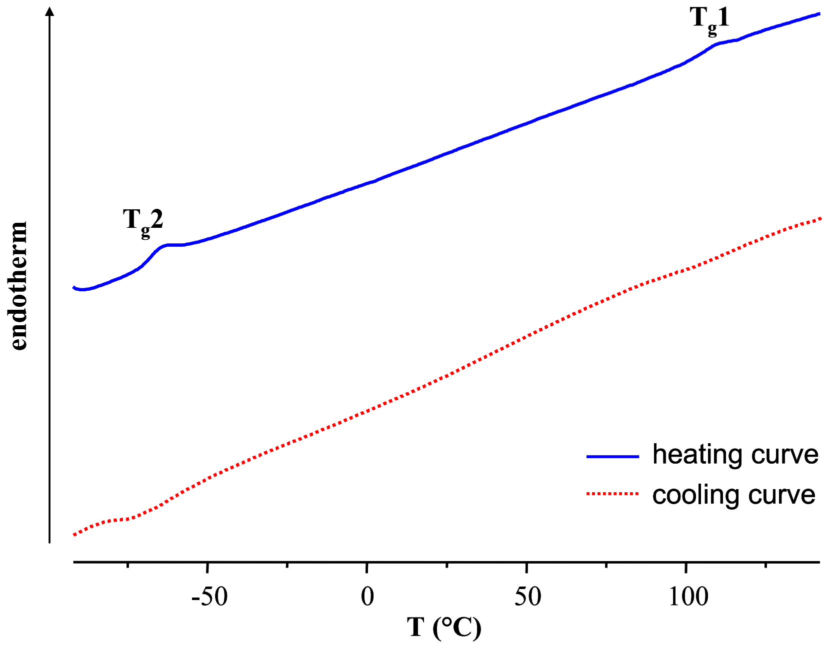

Figure 8.20. Typical DSC for the linear brush-like polyalkoxysilanes (**P$_4$LBO$_{37}$**): data shown are recorded during the second heating (blue solid line) and cooling cycle (red dotted line) at a scanning rate of 25 °C/min.

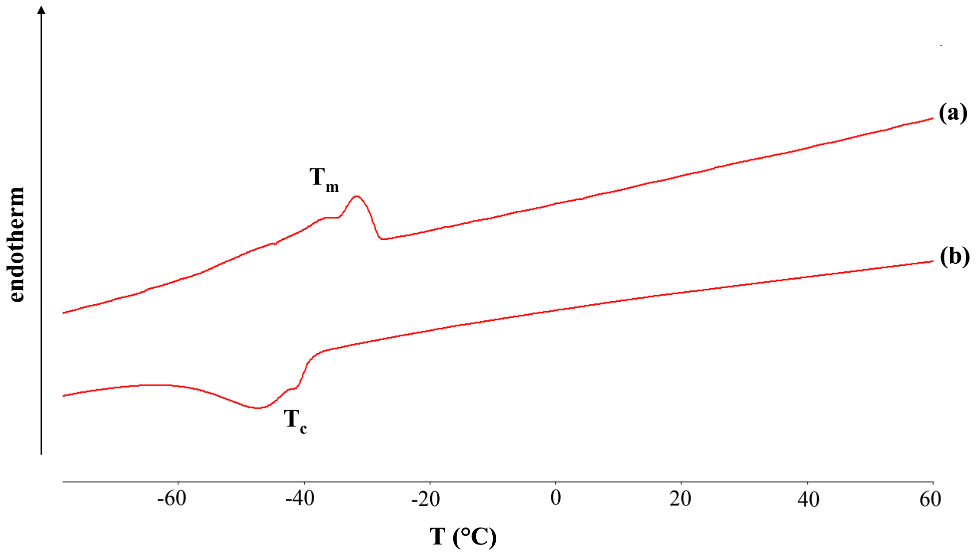

Figure 8.21. DSC (a) heating and (b) cooling scans (scanning rate of 10 °C/min) of PDMUOS brush-like homopolymer ($\overline{M}_n$ = 2,700 g/mol; PDI = 1.65).

The presence of crystallization for the PCSiO block in the linear-hyperbranched samples and the absence of this in the linear brush-like architectures can be similarly explained. Although the PBD vinyl grafting sites of the linear cores have not been entirely substituted in both types of architectures, the branching nature of the MDUOS AB_2 monomeric units in the linear-hyperbranched systems allows for a better packing of the polymer chains.

The modified polymers demonstrated excellent thermal stability. The thermal stabilities were measured by TGA in nitrogen. The linear-hyperbranched and brush-like polyalkoxysilanes start to thermally degrade at temperatures (*i.e.* 422.5 °C for **P_2LHO_{76}** and 452.9 °C for **P_4LBO_{37}**) comparable to the corresponding polycarbosilane architectures (Figure 8.22). In other words, no differences were found on the thermal stability between the polycarbosilanes and polyalkoxysilane hybrid diblock copolymers. This is also an indication of the high thermal stability of the alkoxysilane linkages.

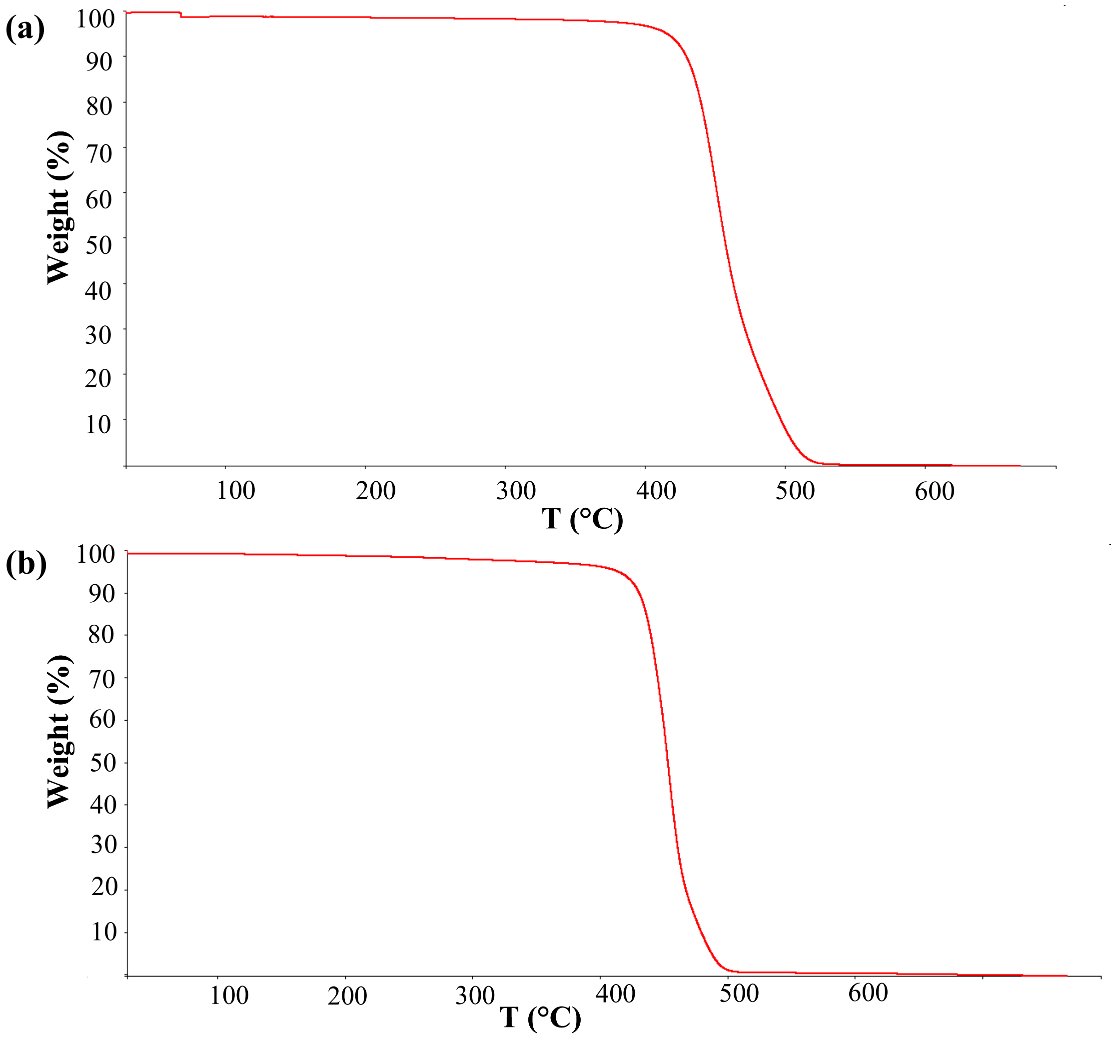

Figure 8.22. Typical TGA of the linear-hyperbranched and brush-like polyalkoxysilanes in N_2, heating rate 10 °C/min: (a) **P_2LHO_{76}** (b) **P_4LBO_{37}**.

8.3.4 Solid state properties

The microphase morphology of the linear-hyperbranched and brush-like samples was studied by Transmission Electron Microscopy (TEM), Atomic Force Microscopy (AFM) and Small Angle X-ray Scattering (SAXS). TEM samples are unstained and so the PS domains appear white and the PCSiO hyperbranched or brush-like domains appear dark.

As the linear-hyperbranched materials showed crystallinity for the PCSiO hyperbranched block, a “conflict” between microphase separation and crystallization is to be expected for the final morphology, especially when the PCSiO hyperbranched content is relatively high. It has been recognized that the microphase morphology in semicrystalline block copolymers is strongly influenced by the competition between crystallization and microphase separation.

This has been extensively investigated by several groups for diblock copolymers in polyethylene (PE),[12g,12k,26] poly(caprolactone) (PCL)[24b,27], poly(ethylene oxide) (PEO)[22a,24b,28] and poly(tetrahydrofuran) (PTHF)[29] containing systems.[22b,25a,30] It has been found from these studies that the interplay between microphase separation and crystallization in semicrystalline diblock copolymers is a complicated function of crystallization temperature, segregation strength and physical state of the non-crystalline block.[25a] On cooling from the melt, structural changes from crystallization compete with those due to microphase separation, which results in a final morphology dependent on whether crystallization is confined or unconfined.[12] When the order-disorder transition of the diblock copolymer occurs at a temperature higher than the temperature of crystallization, as in strongly segregated block copolymers or in block copolymers containing glassy blocks, the ordered microdomain structures may be created prior to crystallization. Further crystallization of the crystallizable block can then occur in the ordered confined boundaries.[12a-f,12g,12h,12j] Depending on the type of microdomain, the chains may be geometrically restricted in three (spheres), two (cylinders) or one (lamellae) dimension. In the case of lamellae this can lead to unexpected chain folding (chains parallel to the interfaces between the block copolymer domains). On the other hand, if crystallization occurs in a weakly segregated block copolymer or directly from a disordered phase, it will control the final microphase morphology, leading to conventional chain folding behavior with the chain folds roughly normal to the lamellar surfaces.[12i,12k-m]

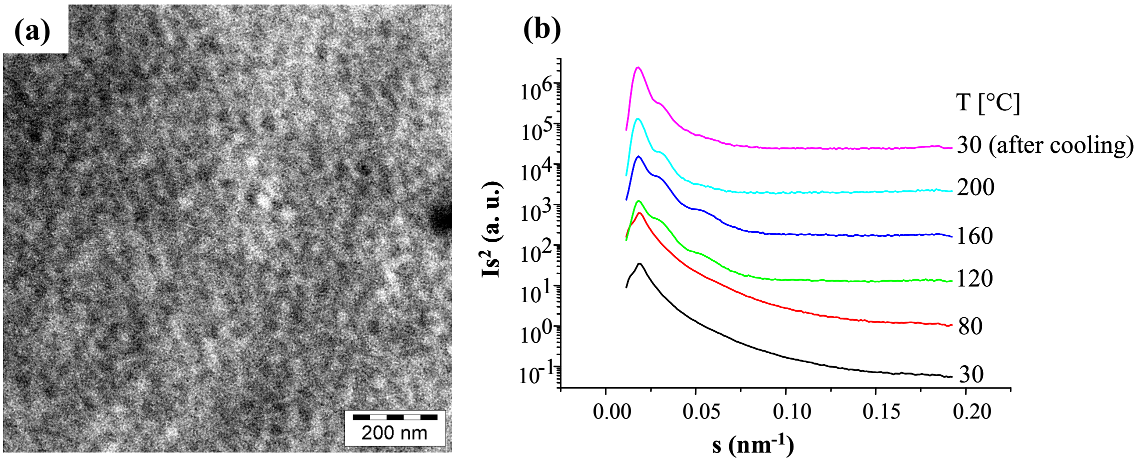

Figure 8.23. (a) Unstained TEM (compression-molded sample) and (b) SAXS diffraction pattern (compression-molded sample) of $\mathbf{P_2LHO_{23}}$.

The amorphous linear-hyperbranched sample **P_2LHO_{23}** (**P_2** = PS_{426}-*b*-PBD_{40}), having 23 wt % of the PCSiO hyperbranched block exhibits a strongly distorted cylindrical structure of the PCSiO domains without showing any long-range order in the TEM image (Figure 8.23a). The rather irregular cylindrical domains are dispersed in the PS matrix with no discernible lattice. A linear diblock copolymer with similar weight fractions would exhibit a hexagonally packed cylindrical morphology or be at the interface between the spherical and the cylindrical morphologies. Although the reflections in SAXS are broad and weak, the formation of a cylindrical structure can be deduced from the position of the two reflections at s^* and $\sqrt{3}s^*$ and $\sqrt{4}s^*$ at high annealing temperatures (Figure 8.23b). A similar type of morphology was observed for the linear-hyperbranched polycarbosilanes with 25 wt % of the PCSi block. As suggested in Chapter 6 the sample might not be at the SSL or the disordered morphology observed is related to the "wormlike micelle" structure found by Gido *et al.* for an $(PI)_2PS$ graft block copolymer having 81 % volume fraction of the styrene block.[31]

All other linear-hyperbranched diblock copolymer samples prepared possess a crystallizable PCSiO block that is covalently linked to a glassy block (PS) at the crystallization temperature. The morphology of these linear-hyperbranched semicrystalline diblocks was characterized using TEM and AFM at r.t. Typical images for the samples **P_2LHO_{64}**, **P_2LHO_{66}** and **P_2LHO_{76}**, which possess the PCSiO hyperbranched block as the majority block, are shown respectively in Figures 8.24, 8.25 and 8.26.

The TEM and AFM images of **P_2LHO_{64}** and **P_2LHO_{66}** show a partially developed layered structure (Figures 8.24a-e and 8.25a-e). The AFM images demonstrate how the lamellar order resulting from the microphase separation of the blocks is partially destroyed (Figures 8.24c-d and 8.25c-d). This is probably caused by the crystallization of the PCSiO hyperbranched block. Striations in the layers are visible in both TEM and AFM images of **P_2LHO_{64}** (Figures 8.24a-b and 8.24e respectively). This might result from a density change upon crystallization of the PCSiO block and the consequent change in the layer thicknesses. The partially developed **P_2LHO_{64}** layered structure shows how the PS and PCSiO layers alternate. As crystallites tend to organize themselves in lamellae,[6a,121] **P_2LHO_{64}** consists probably of a crystallized microdomain structure of lamellar PCSiO crystals and amorphous PS layers. As in all the samples the degree of crystallinity of the hyperbranched block is less than 100 %, the hyperbranched domains probably resemble a semicrystalline homopolymer, with alternating crystalline and amorphous layers. Therefore, the crystalline layers are probably formed by the PCSiO block and the amorphous layers of a mixture of PCSiO and PS.

Crystallization confined within the microphase-separated PCSiO hyperbranched layers with retention of the preformed microphase-separated lamellar morphology should be the case. In other words, the crystallization of the hyperbranched block should occur within the microphase-separated morphology. However, these samples show incompletely developed morphologies, which might have been trapped on cooling at low annealing times (*ca.* 30 minutes at 120 °C).[25a] Moreover, no fine crystal structure for the PCSiO hyperbranched block was observed for the samples under the studied conditions. The observation of crystalline superstructures is known to be dependent on the thickness of the sample (*i.e.* thin film *vs.* bulk sample).[12c,25a] In our case, no thin films of the samples were prepared for the microscope measurements. The formation of different lamellar thicknesses is a consequence of the fractionated crystallization within the morphology,[32] which was already reflected in the DSC by a broad and low crystallization exotherm. Nucleation in semicrystalline polymers in the bulk occurs on existing heterogeneities (*i.e.* impurities). However, if the bulk polymer is subdivided into isolated regions (like microphase-separated domains in block copolymers) whose number is of the same order of magnitude or greater than the number of usually active heterogeneities, a fractionated crystallization phenomenon will develop. In the limit where heterogeneities are completely absent, homogeneous nucleation takes place under conditions of extreme undercooling.

A microphase-separated state between lamellae and inversed cylinders should be expected for a linear diblock copolymer with similar weight fractions. This agrees with the broad exotherm observed in the DSC, which could correspond as well to crystallization in different morphologies that coexist at such crystallization temperature due to metastability in the morphology.[24a] As the weight fraction of the PCSiO block increases from **P_2LHO_{64} to P_2LHO_{66}** the observed lamellae become increasingly disordered, showing not only striations, but also cracks. This is observed in the AFM images of **P_2LHO_{66}**, which resembles “wormlike” PS structures in a PCSiO semicrystalline matrix (Figure 8.25c-e). It is obvious for both samples that crystallization of the PCSiO block causes an increase in the lamellar thickness. The PCSiO hyperbranched domains become feasibly thick enough to accommodate multiple crystallites.[12l,33] The lamellar thickening is probably also controlled by the compromise between the random-coil configuration preferred by the amorphous blocks and the extended chain conformation of the crystallites.[24a]

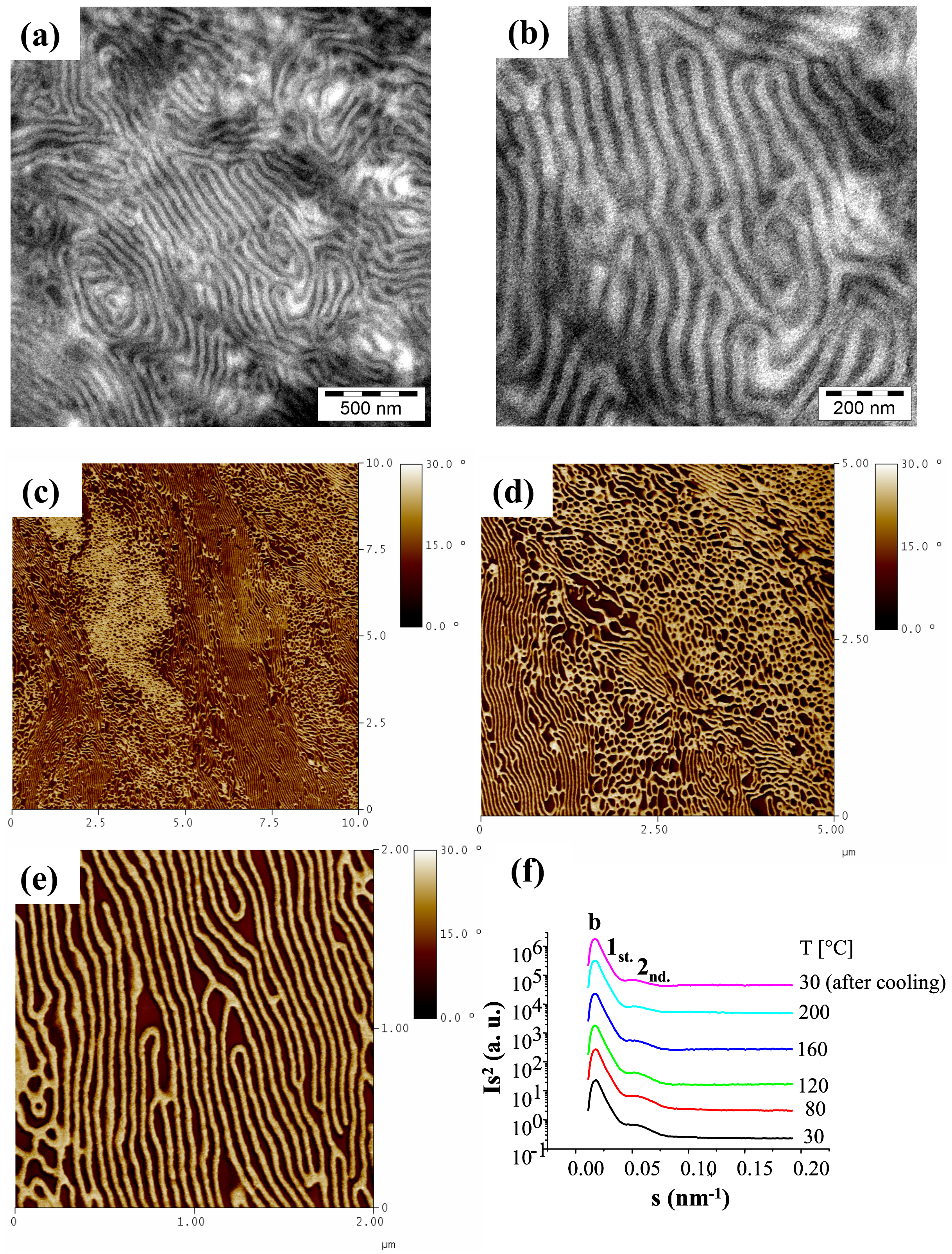

Figure 8.24. (a), (b) Unstained TEMs (compression-molded sample); (c), (d), (e) AFM tapping mode phase images and (f) SAXS diffraction pattern (compression-molded sample) of **P$_2$LHO$_{64}$** (“b” represents the beam stop).

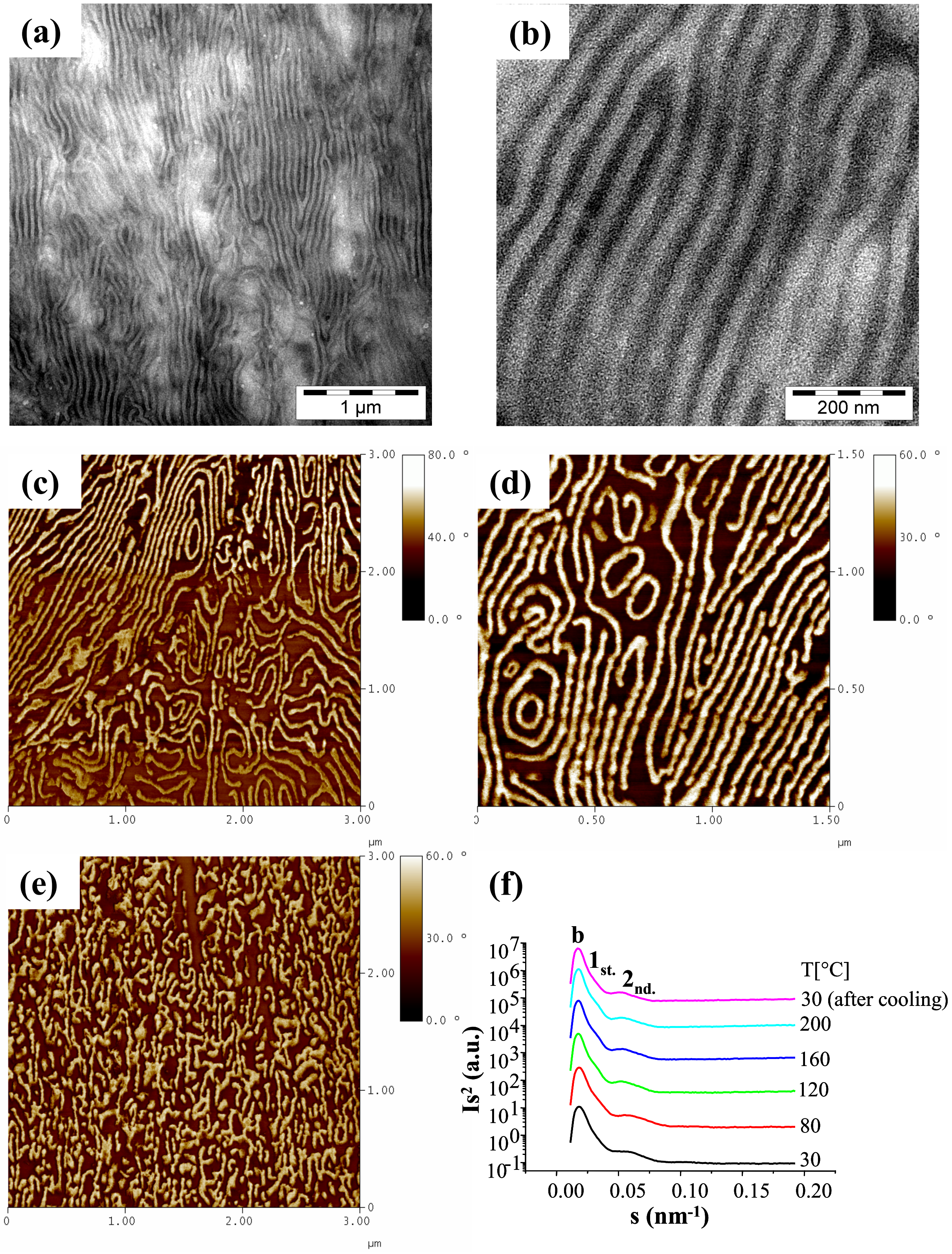

Figure 8.25. (a), (b) Unstained TEMs (compression-molded sample); (c), (d), (e) AFM tapping mode phase images and (f) SAXS diffraction pattern (compression-molded sample) of **P$_2$LHO$_{66}$** (“b” represents the beam stop).

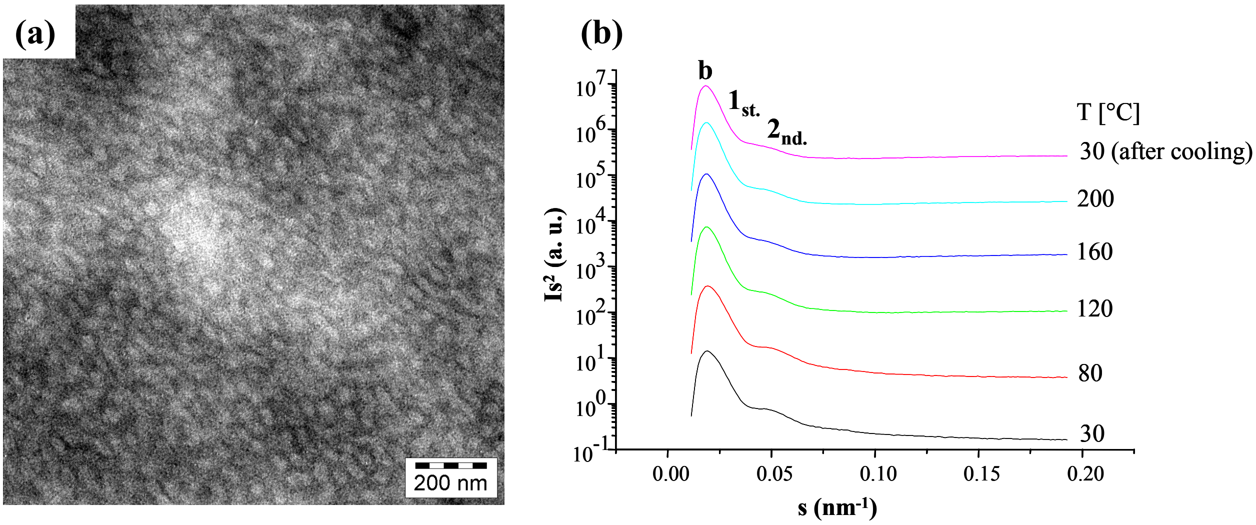

Figure 8.26. (a) Unstained TEM (compression-molded sample) and (b) SAXS diffraction pattern (compression-molded sample) of $\mathbf{P_2LHO_{76}}$ ("b" represents the beam stop).

The unstained TEM micrograph for the linear-hyperbranched sample $\mathbf{P_2LHO_{76}}$ reveals a cylindrical morphology, where the minority PS domains are embedded in a PCSiO semicrystalline matrix (Figure 8.26). However, the PS cylinders are strongly distorted and do not show any long-range order. This deformation of the PS cylinders can be attributed to the presence of a semicrystalline PCSiO matrix.

The structure of semicrystalline diblocks at the nanoscale level is usually probed using X-ray scattering.[21] SAXS would provide information on the crystalline domain spacing, *i.e.* the crystal and amorphous layer thicknesses, while WAXS identifies the structure of the crystalline unit cell. In the SAXS profile for samples $\mathbf{P_2LHO_{64}}$, $\mathbf{P_2LHO_{66}}$ and $\mathbf{P_2LHO_{76}}$, we can see two diffraction peaks (represented by 1st. and 2nd.), confirming microphase separation in the solid-state (Figures 8.24f, 8.25f and 8.26b). However the absence of sharp diffraction peaks and higher order reflections, as the samples are heated from the solid into the melt, agree with the not-well developed morphologies observed by TEM and AFM. The lack of high order reflections in the melt does not allow an unambiguous assignment of the microdomain structure. Moreover, the scattering of the two reflections is broad and vague and the fitting procedure cannot be carried out. Absolute values of the domain periodicities are then unrealistic, in agreement with TEM and AFM. If microphase-separation preceded crystallization, this would cause the appearance of transient sharp diffraction peaks in the SAXS curves. As this is not the case, it is obvious that a degree of crystallization of the PCSiO hyperbranched block occurs already at r.t. Nonetheless, conclusions cannot be made as

SAXS measurements were not performed below the melting temperature of the PCSiO hyperbranched block (between -30 and -50 °C).

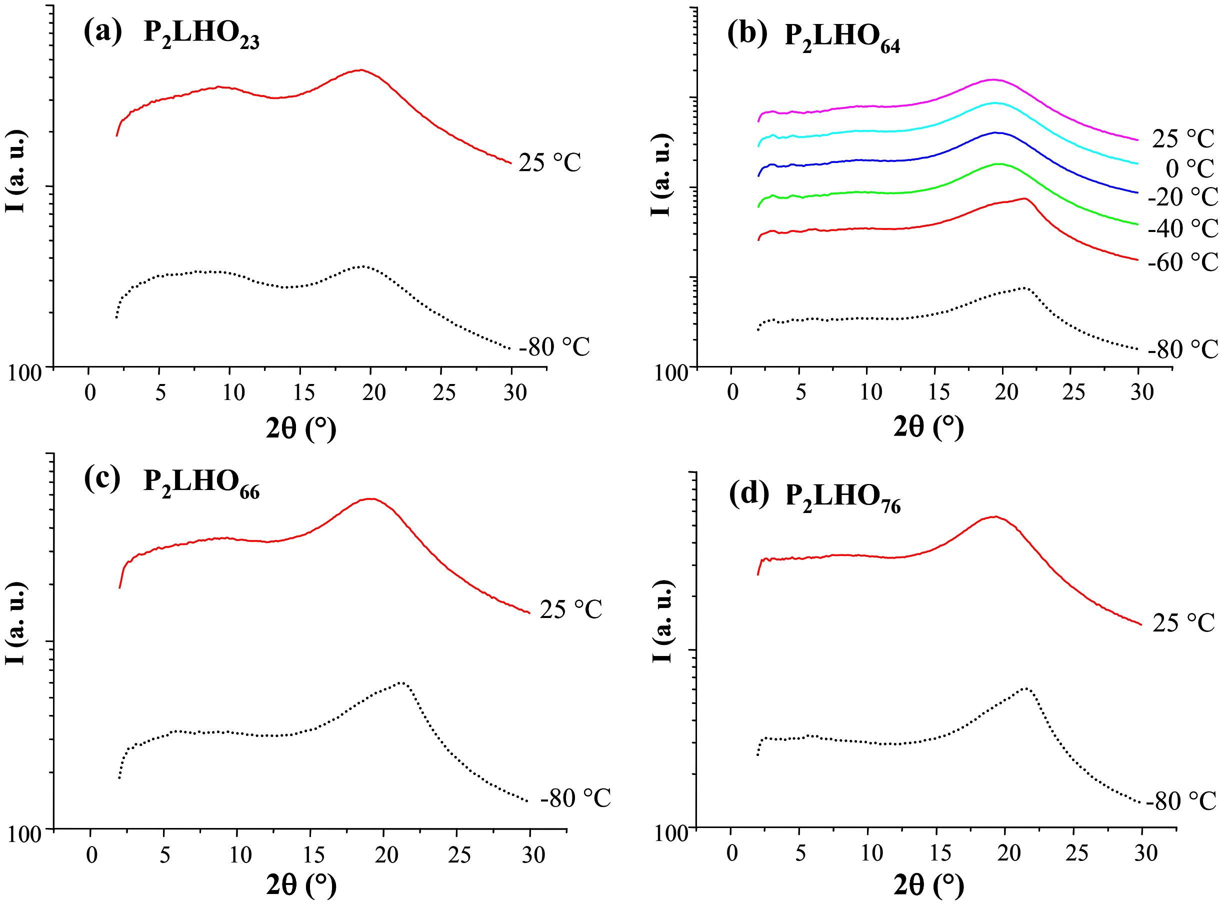

Figure 8.27. Representative WAXS patterns at 25 °C (red solid curve) and -80 °C (dotted black curve) for the linear-hyperbranched polyalkoxysilane samples: (a) **P_2LHO_{23}**, (b) **P_2LHO_{64}**, (c) **P_2LHO_{66}** and (d) **P_2LHO_{76}**.

The crystallization behavior obtained via DSC of the PCSiO hyperbranched block in the linear-hyperbranched samples was confirmed by WAXS patterns. Figure 8.27 shows the XRD profiles at 25 and -80 °C of four linear-hyperbranched samples with an increasing wt % of the crystallizable PCSiO block. The WAXS curve at 25 °C for **P_2LHO_{23}** shows two broad amorphous halos, arising from PS and PCSiO blocks that do not change significantly upon cooling. This is in agreement with the DSC results from this amorphous sample. However, the WAXS scattering patterns for **P_2LHO_{64}**, **P_2LHO_{66}** and **P_2LHO_{76}** show how the first broad amorphous halo decreases in intensity and the second reflection becomes sharper upon cooling (at -80 °C). The decrease in the first amorphous halo at both 25 °C and -80 °C indicates that the amorphous PS block represents the minority block for these samples. The second peak changes from an amorphous halo to a semicrystallographic reflection at -80 °C and this is more pronounced as the weight fraction of the crystallizable PCSiO hyperbranched block becomes higher. This broad crystallite peak probably corresponds to the scattering from the amorphous and crystalline PCSiO hyperbranched block. There is a clear shift and sharpening of the peak corresponding to the semicrystalline PCSiO hyperbranched block as its wt % increases. However, the reflection is still very broad, indicating the presence of many defects in the PCSiO crystallites of the diblock copolymers. The PCSiO crystallites are probably characterized by irregular folds induced by the non-uniform alkoxysilane branches.

The relative degrees of crystallinity can be estimated from the WAXS pattern, using the ratio of the integrated intensity of the crystal peak to that of the total amorphous and crystalline scattering at the melting point temperature.[21] This calculation is, however, not possible due to the amorphous and crystalline character of the PCSiO peak in the linear-hyperbranched samples. Moreover, the relative broad scattering of the PCSiO peak does also not allow the crystalline unit cell orientation to be deduced from the WAXS patterns. The linear-hyperbranched polyalkoxysilanes possess branches with different lengths at irregular intervals along the PBD backbone. Therefore, the lamellar orientations of the PCSiO crystals in the samples **P_2LHO_{64}** and **P_2LHO_{66}** are probably random and no assignment of a preferred chain direction relative to the lamellar morphology is possible using WAXS.

The 2θ value at -80 °C of the semicrystalline peak in the linear-hyperbranched polyalkoxysilanes is very close to that observed for the corresponding PMDUOS homopolymer, indicating that PCSiO probably crystallizes within the nanodomains existing in the melt (Figure 8.28). However, the scattering peak in PMDUOS is sharper, showing that the crystal structure is partially distorted when crystallization occurs between glassy walls in the solidified block copolymer.

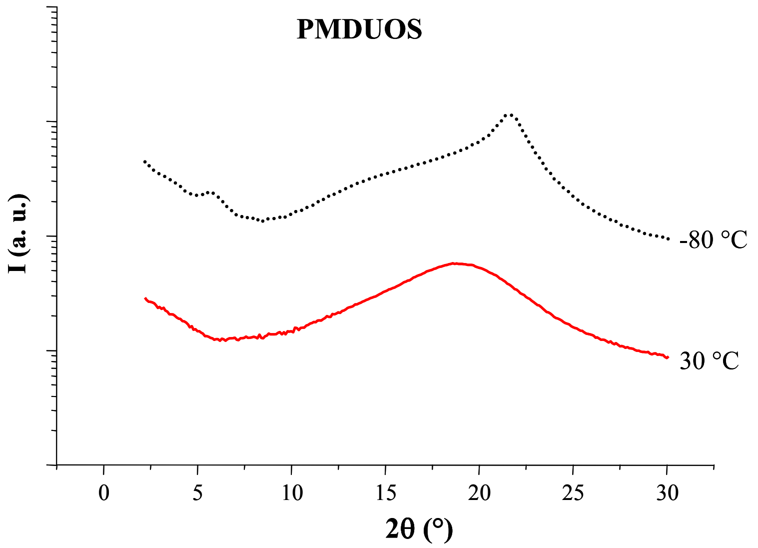

Figure 8.28. WAXS pattern at 30 °C (red solid curve) and -80 °C (dotted black curve) of hyperbranched homopolymer PMDUOS.

A model to describe the morphology of the linear-hyperbranched semicrytalline diblock copolymers is depicted in Figure 8.29. The PCSiO block is the crystallizable block and is represented by the folded-chain lamellae. The chains are irregularly folded, due to the hyperbranched nature of the PCSiO block. As depicted in Figure 8.29, a part of the PCSiO block is non-crystalline and forms a miscible mixture with the PCSiO crystallites at molecular scale. This miscibility was confirmed by the previously presented WAXS measurements.

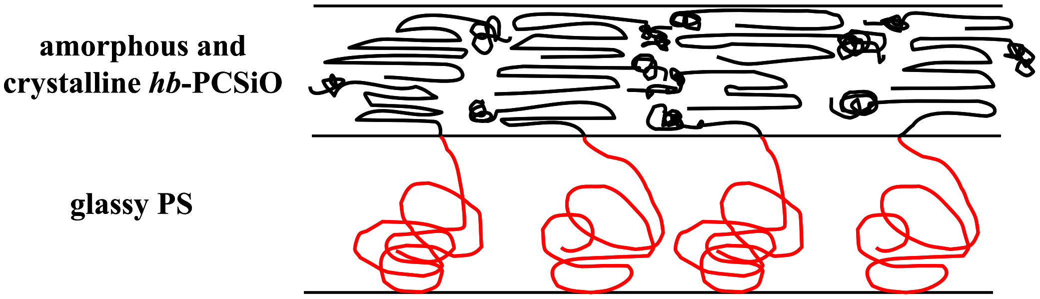

Figure 8.29. Cartoon schematically showing a 2D-model to describe the morphology of the linear-hyperbranched semicrystalline diblock copolymers. The PCSiO chains are irregularly folded, due to the presence of branches with different lengths. For simplicity, the PCSiO stems have been depicted parallel to the lamellar interface, although their orientation has not been determined.

In summary and regardless of the composition, no long-range order was observed for any of the linear-hyperbranched polyalkoxysilanes. This may be related to the competing crystallization. The crystallization of the PCSiO block was confirmed by DSC and WAXS measurements. As the PCSiO hyperbranched block gets larger, this affects the development of the microphase-separated structure due to crystallization of the PCSiO block. Nonetheless, the samples were submitted to short annealing times (*ca.* 30 minutes above the T_g of PS) and this might have caused an irregular development of the morphologies. Partially destroyed layered morphologies were obtained for **P_2LHO_{64}** and **P_2LHO_{66}** as observed by thickening and disruption of the lamellae by TEM and AFM. This is likely to happen when the thermodynamic forces to form the crystalline structure and the ones to maintain the microphase morphology formed in the melt compete. No crystallization within the observed layered morphologies was observed under the studied conditions. The solid-state structures of the semicrystalline diblock copolymers were evaluated below the T_g of PS but not below the melting temperature of the crystallizable block. Crystallization studies were therefore not performed at temperatures below the PCSiO melting point, where the layered morphology formed in the melt might have been preserved. In addition, the presence of a glassy PS block is likely to disturb the crystallization process, inhibiting nucleation and growth of the crystallites. In fact, it has been theoretically predicted by Dobrynin *et al.* that the loss of mobility of monomers in the glassy block results in the elimination of microphase-separation.[34] Concluding, it is obvious that confining of the irregular semicrystalline component to the lamellar morphology (in contrast to confinement of narrowly distributed crystallites) leads to a more pronounced “conflict” between crystallization and microphase separation. No high-order SAXS peaks were observed for the linear-hyperbranched samples, which agrees with the poor long-range order reached.[21] This is possibly due to the deformation of the microdomains caused by the presence of crystallites in the diblock copolymers.

In contrast, clear microphase separation has been found for the linear brush-like polyalkoxysilanes. This was anticipated on the basis of DSC measurements, which gave two distinct T_gs.

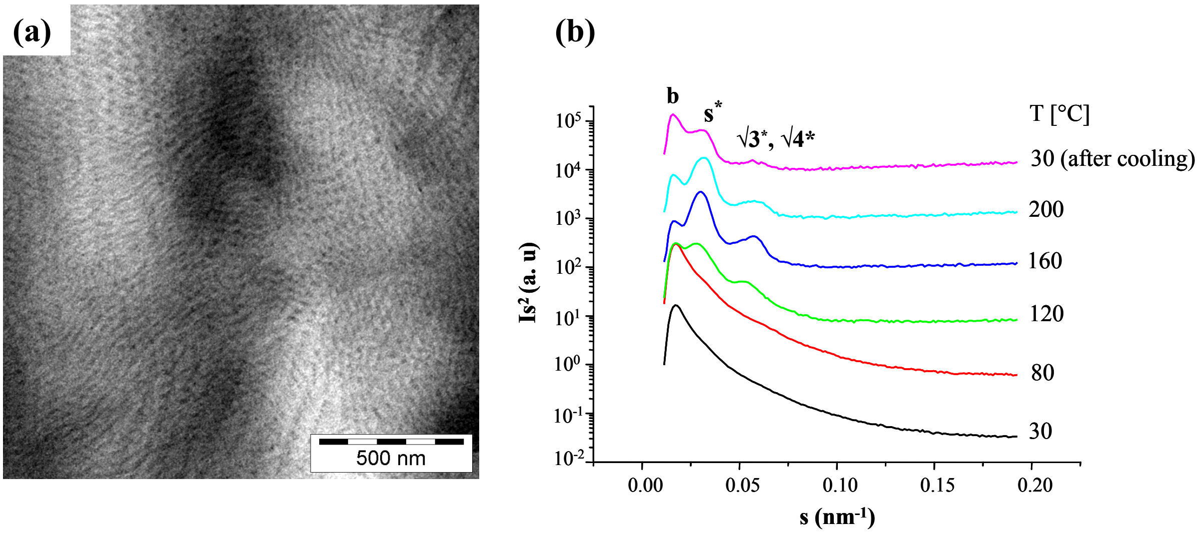

Figure 8.30. (a) Unstained TEM (compression-molded sample) and (b) SAXS diffraction pattern (compression-molded sample) of **P$_4$LBO$_{17}$**.

The linear-brush like sample **P$_4$LBO$_{17}$** (**P$_4$** = PS$_{580}$-*b*-PBD$_{50}$), with 17 wt % fraction of the PCSiO brush-like block, forms, according to TEM, a poorly ordered morphology of hexagonally packed cylinders (Figure 8.30a). In the SAXS data at low temperatures, the scattering value of the primary reflection is obscured by the beam stop (represented by a "b"). However upon increasing the annealing temperature, the first peak at s* becomes distinguishable and a new reflection at √3s* and √4s*appears, indicating cylinders on a hexagonal lattice with a domain periodicity of 38.5 nm (Figure 8.30b). The lack of higher-order reflections agrees with the lack of long-range order observed by TEM and might be related to the short annealing times applied to the sample before performing the measurements. At this weight fraction of the PCSiO block (17 %), the sample should show a spherical morphology or in any case be at the phase border with a cylindrical morphology as it does in the case of linear diblocks. It is evident that the macromolecular architecture of the linear brush-like sample is affecting the domain borders of the classical block copolymer phase diagram. This molecular architecture effect was already observed by Hadjichristidis *et al.* for (PI)$_3$PS miktoarm star copolymers.[35] They observed the formation of locally-ordered and long-range ordered hexagonally packed cylindrical morphologies in samples containing 92 and 85 vol % of the PS block respectively. This was attributed to the curving of the interface towards the PS side due to the overcrowding of the PI chains. Additionally, they predicted and confirmed experimentally that at high PS contents the spherical structure was eliminated from the phase diagram of the miktoarm star copolymers. A cylindrical morphology was also found by Román *et al.* for dendron weight fractions of 13 % in linear-dendritic block copolymers.[6e] Further studies on these hybrid systems by Mackay *et al.* showed a cylindrical structure for a linear-dendritic PS-(sixth generation) PBE diblock at 18 wt % of the dendritic block.[6e] For the same class of linear-dendritic diblocks, Pochan *et al.* found a random phase-separated structure with fractions lower or equal to 12 wt %.[6c] Although they could not demonstrate the presence of a cylindrical morphology between 12 and 22 wt % of the dendrimer block, they concluded that the lack of a well-ordered lattice for the sample containing 12 wt % of the dendrimer block might have been attributed to sample preparation procedures. Mackay *et al.* made use of solution-casting, while Pochan *et al.* of melt-pressing sample preparation. No thin film was prepared for **P_4LBO_{17}**, which could explain the only local-range lattice formation reached or frustration of the lattice in this sample.

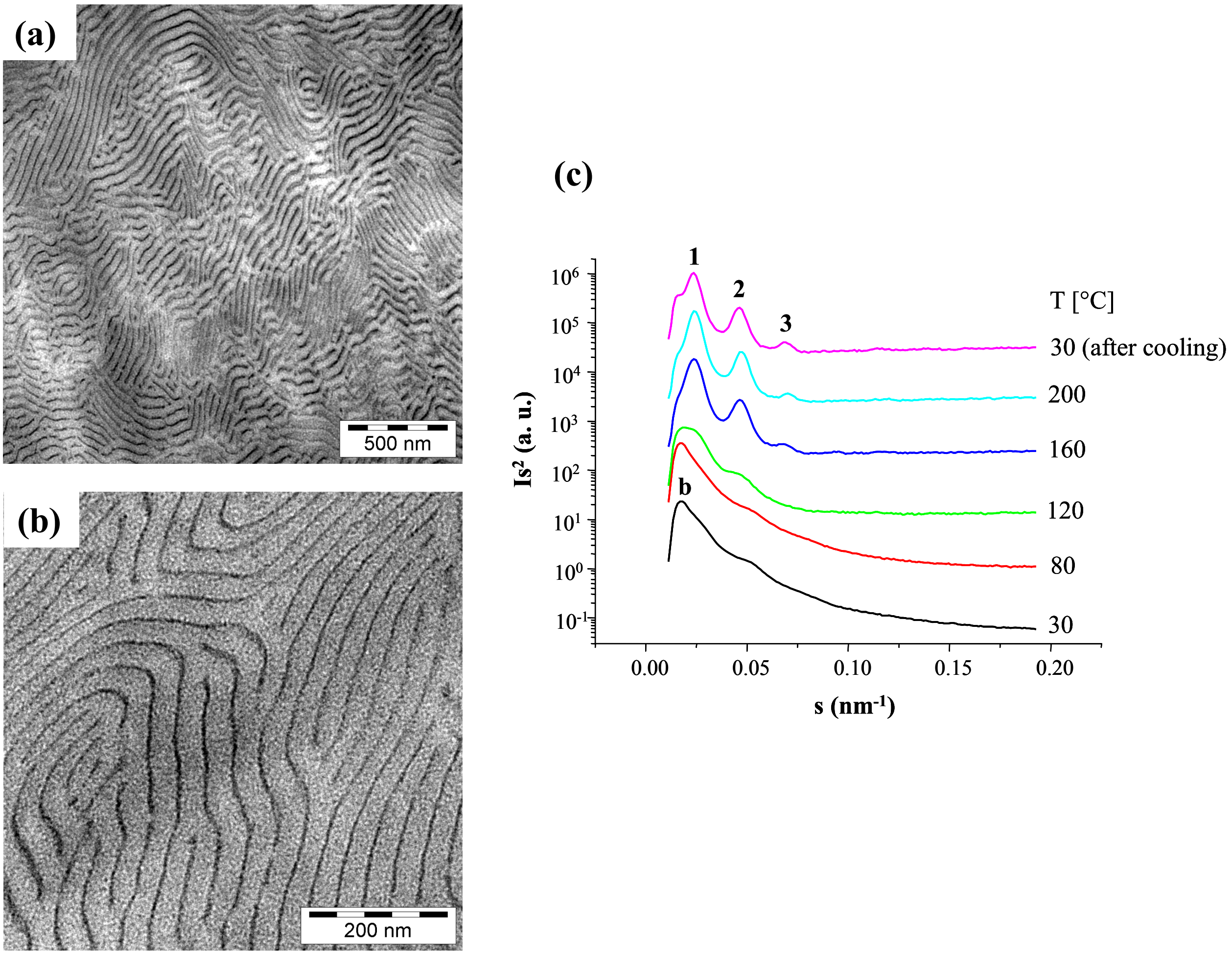

Figure 8.31. (a), (b) Unstained TEMs (compression-molded sample) and (c) SAXS diffraction pattern (compression-molded sample) of **P_4LBO_{22}** ("b" represents the beam stop).

The linear brush-like samples **P_4LBO_{22}** and **P_4LBO_{33}** exhibit a clear lamellar-like morphology (Figures 8.31 and 8.32). There is a significant molecular architecture effect on these samples as linear diblocks with the same relative wt % fractions would display a cylindrical morphology. Unstained TEM micrographs for **P_4LBO_{22}** indicating a lamellar-like morphology, are presented in Figures 8.31a-b. The scattering of **P_4LBO_{22}** (Figure 8.31b) shows two broad and weak diffraction peaks at low temperatures with the location of the first maximum readily visible at 160 °C. Upon annealing the sample, reflections at relative positions of 1:2:3 are distinguishable, confirming a lamellar structure with a lamellar long period of 42 nm. Despite the unambiguous assignment of the morphology, the sample shows a reduced long-range order with the presence in the TEM images of more curved lamellae and defects. A frustrated lamellar structure was as well found by Pochan *et al.* for linear-dendritic PS-(sixth generation) PBE systems in a sample having 22 wt % of the dendrimer block.[6c] In the linear brush-like polycarbosilane architectures presented in Chapter 7, a multi-lamellar onion-like structure was found for a sample containing 28 wt % of the PCSi brush-like block. The presence of curved lamellae was in that case ascribed to the presence of a majority PS block, which is forced to reside on a flat interface characteristic of a lamellar structure, causing then varied defects in the layers. This applies in a similar manner to the defects observed for the lamellar-like morphology of **P_4LBO_{22}**.

Unstained TEMs and AFM height images for **P_4LBO_{33}** demonstrating a lamellar morphology are presented in Figures 8.32a-c and 8.32d-e respectively. The TEM images in Figures 8.31a-b show a lamellar morphology with fingerprint domains and characteristic edge dislocations, respectively. The AFM images in Figures 8.32 d-e are in agreement with the TEM micrographs. The scattering vector ratios at 1:2:3:4:5 found upon annealing the sample, corroborate the formation of a lamellar morphology with a domain periodicity of 41.4 nm (Figure 8.32f). The collected two-dimensional SAXS data illustrate the high degree of long-range order present in this sample (Figure 8.32f). This finding is in accordance with the studies on the linear-brush like polycarbosilanes presented in Chapter 7, where a lamellar morphology with characteristic fingerprint domains was also found for a sample containing 34 wt % of the PCSi brush-like block. Mackay *et al.* also encountered a lamellae structure for linear-dendritic PS-(sixth generation) PBE diblocks containing 31 wt % of the dendrimer block.[6e]

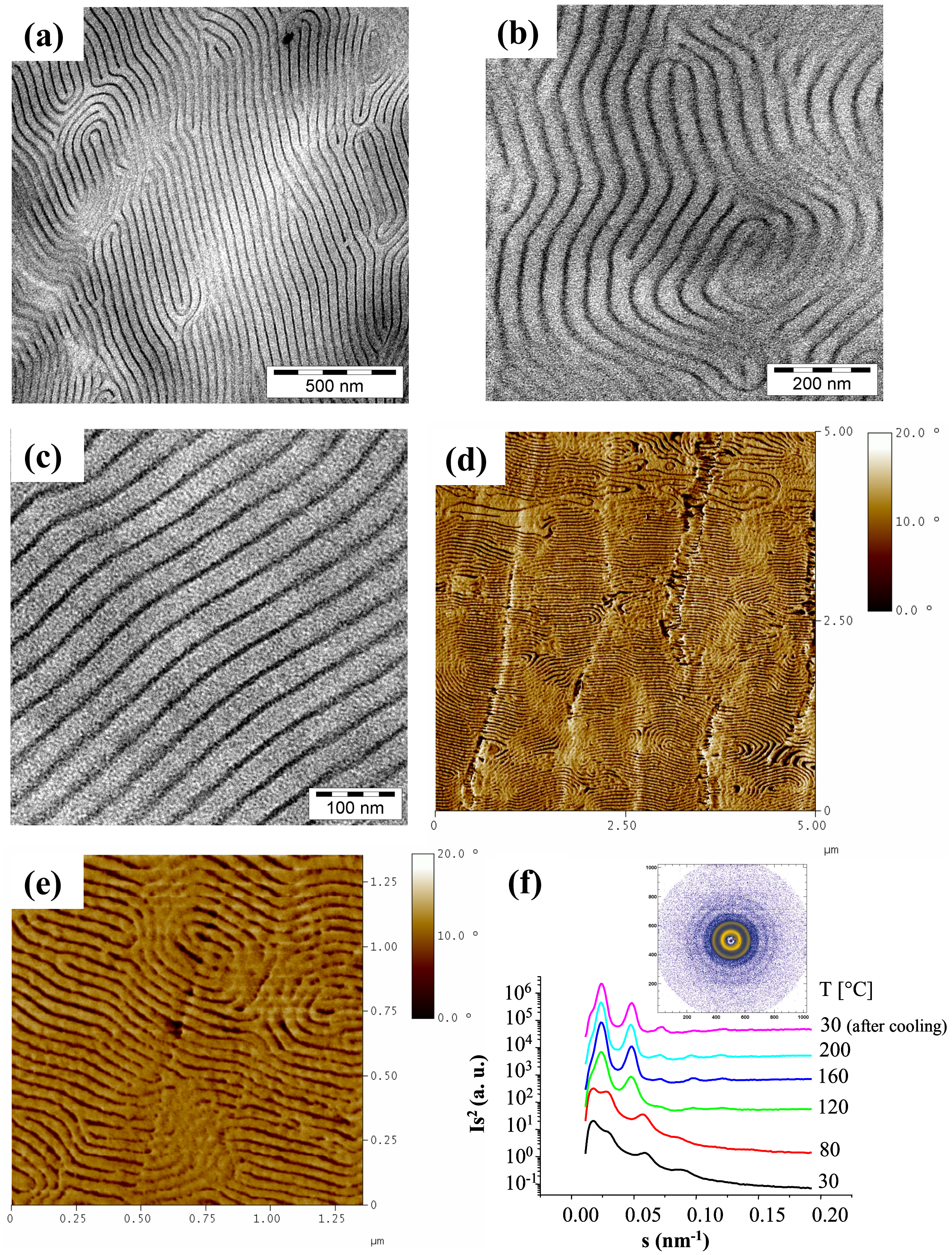

Figure 8.32. (a), (b), (c) Unstained TEMs (compression-molded sample); (d), (e) AFM tapping mode phase images and (f) 2D- and 1D-SAXS diffraction pattern (compression-molded sample) of **P$_4$LBO$_{33}$**.

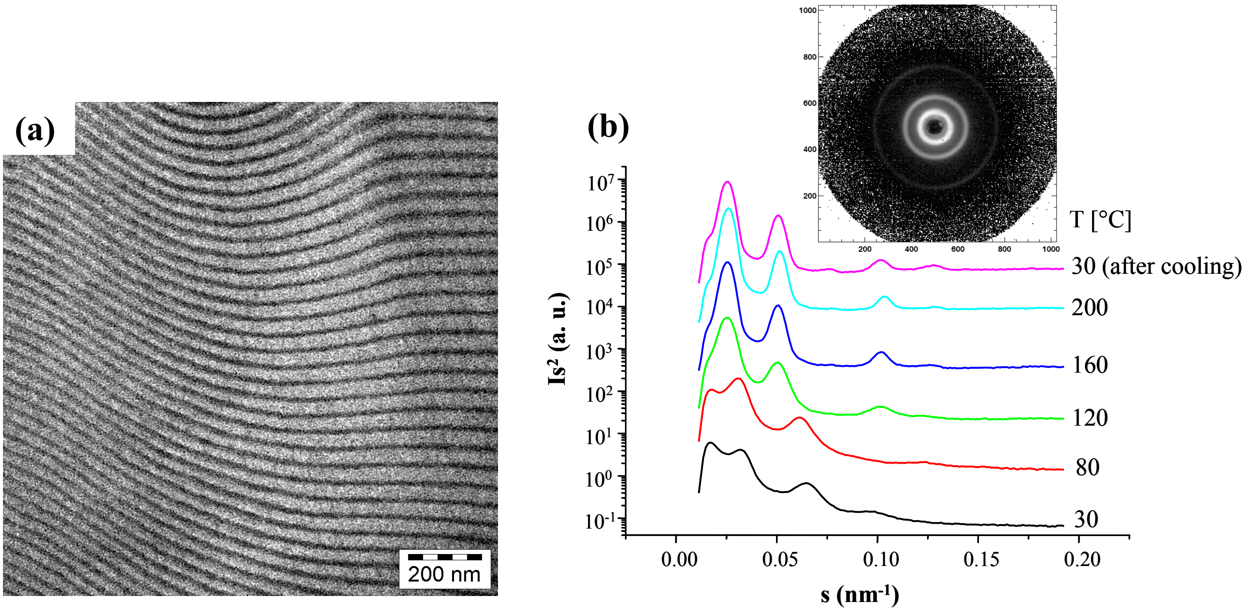

Figure 8.33. (a) Unstained TEM (compression-molded sample) and (b) 2D- and 1D-SAXS diffraction pattern (compression-molded sample) of **P_4LBO_{36}**.

P_4LBO_{36} displays also a clear lamellar morphology, as demonstrated by both TEM and SAXS measurements (Figure 8.33). A linear-linear diblock copolymer having 36 wt % for one of the blocks would be at a phase boundary between lamellar and cylindrical morphologies. This suggests once more a strong contribution of the molecular architecture in shifting the classical phase boundaries. The SAXS pattern of **P_4LBO_{36}** shows depression of the third and sixth scattering peaks and a lamellar long period of 39.2 nm. This is characteristic of systems in which the volume composition of one component is between 30 and 40 %,[36] agreeing with the calculated wt % fraction for the PCSiO block via MO measurements. A similar diffraction pattern has been found for a linear brush-like polycarbosilane sample containing 42 wt % of the PCSi brush-like block (Chapter 7, Figure 7.23).

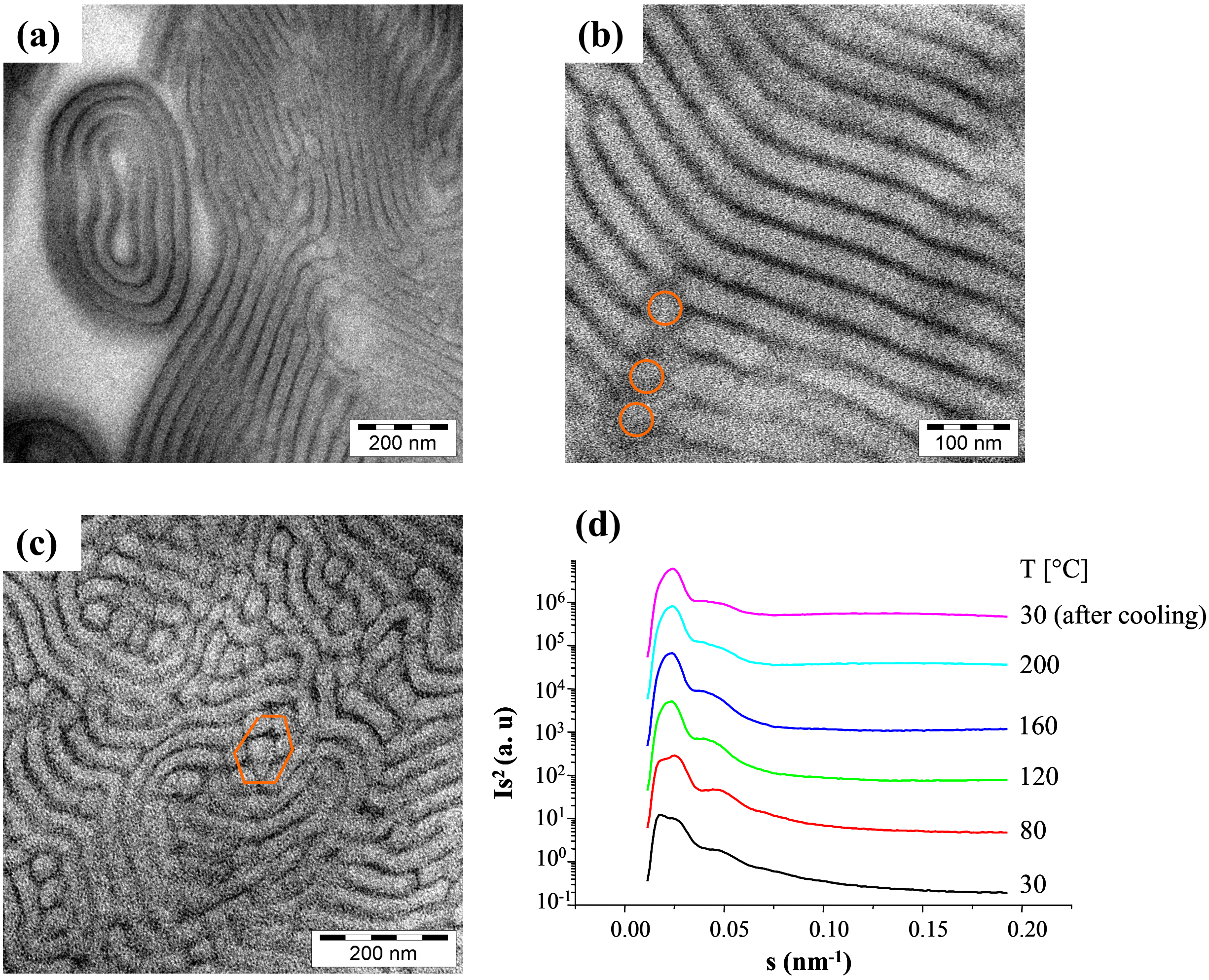

Figure 8.34. (a), (b), (c) Unstained TEMs (compression-molded sample) and (d) SAXS diffraction pattern (compression-molded sample) of **P$_4$LBO$_{37}$**.

An unclear morphology was found for **P$_4$LBO$_{37}$**. The unstained TEMs presented in Figures 8.34a-b seem to show a lamellar morphology. However, occasional chevron grain boundaries represented with an orange circle in Figure 8.34b, are visible in the lamellar morphology. This bending of the lamellae results in broken chevrons (Figure 8.34c). In other words, the continuity of the lamellar layers is partially broken in patches of hexagonally packed PS cylindrical domains. The appearance of chevron gain boundaries in lamellae was already discussed in Chapter 6 and appeared to be a sign of a transition between the lamellae and cylinder stages. Only PS cylinders in poor register are observed. However, long annealing periods that could lead to the transition and to the equilibrium morphology were not applied. In the X-ray diffraction pattern, the lack of high order reflections does not allow for definitive identification of the structure. In conclusion, **P$_4$LBO$_{37}$** appears to be at a phase boundary between lamellae and inversed cylinders. In any case, this result illustrates the influence of molecular architecture on phase behavior when compared to linear block copolymers, as a clear lamellar structure should appear for diblocks possessing 37 wt % for one of the blocks.

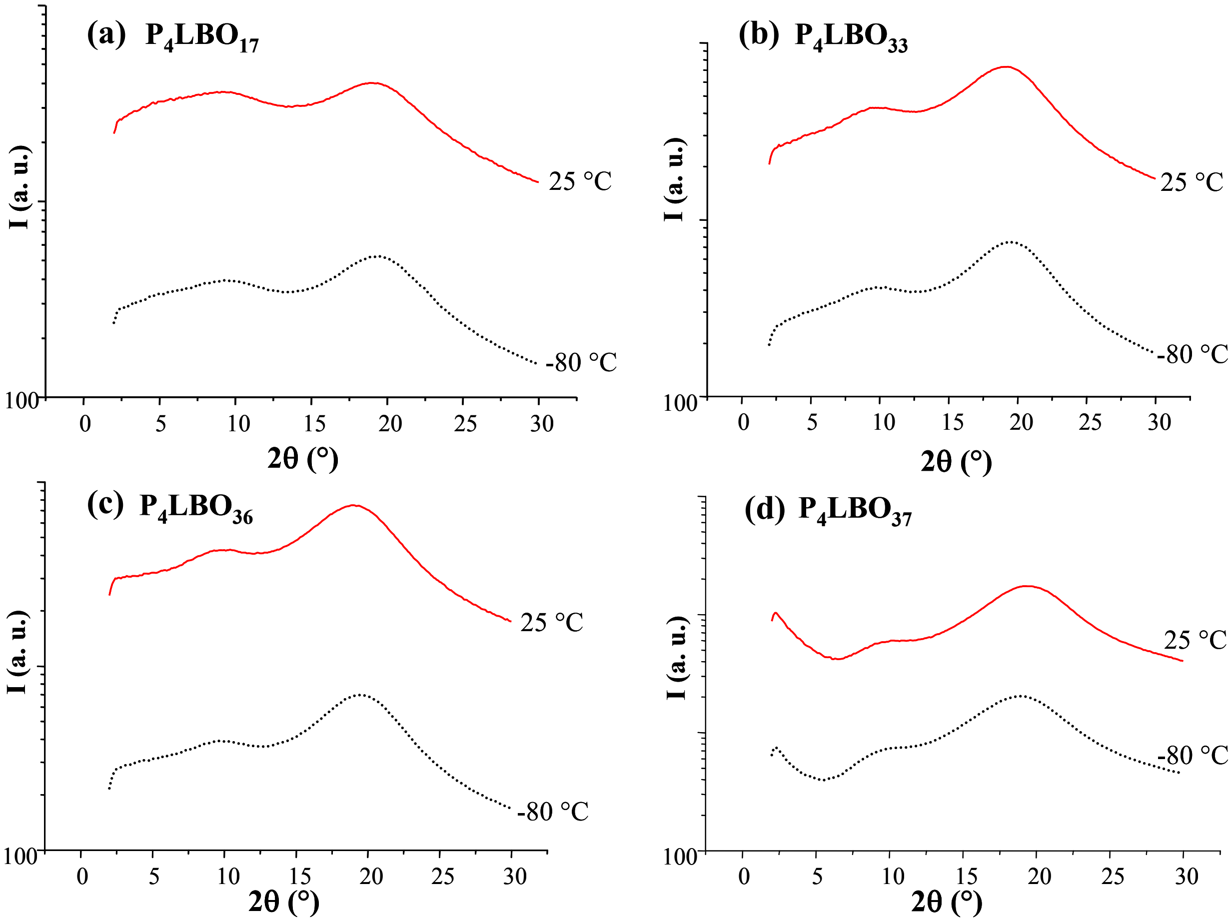

Figure 8.35. Representative WAXS intensity profiles at 25 °C (red solid curve) and -80 °C (dotted black curve) for the linear brush-like polyalkoxysilane samples: (a) **P_4LBO_{17}**, (b) **P_4LBO_{33}**, (c) **P_4LBO_{36}** and (d) **P_4LBO_{37}**.

The WAXS patterns measured at 25 and -80 °C for different samples of the linear brush-like polyalkoxysilanes reveal that the PS and the PCSiO domains are both amorphous; a conclusion which is further supported by the previously presented DSC measurements. In contrast to the results obtained for the linear-hyperbranched systems, Figure 8.35 shows how both amorphous halos, representing the scattering from the PS and the PCSiO block, do not experience shape change either by cooling or by increasing the weight fraction of the PCSiO brush-like block. This demonstrates the non-ability of the PCSiO brushes to crystallize.

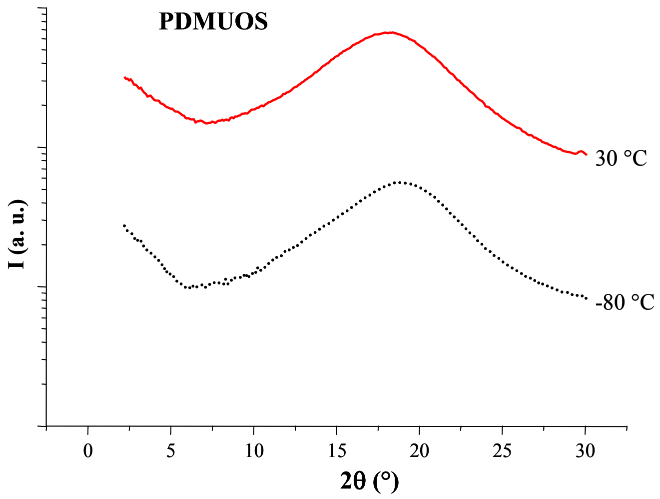

Figure 8.36. WAXS pattern at 30 °C (red solid curve) and -80 °C (dotted black curve) of brush-like homopolymer PDMUOS.

The WAXS curve for the corresponding brush-like homopolymer (PDMUOS) shows a broad halo at 30 and -80 °C, which is nearly the superimposition of the PCSiO amorphous halo from the linear brush-like diblocks (Figure 8.36). This indicates the lack of ability for the brushes to crystallize. This is however, contradictory to the DSC results for PDMUOS, where a T_m and T_c were observed. Crystallization of the homopolymer can therefore not be discarded. In fact, a closer look to the WAXS pattern reveals a slight stretching and shifting of the amorphous halo at -80 °C.

In general and summarizing, well defined ordered morphologies have been found for the linear-brush like polyalkoxysilanes. Likewise, the morphological behavior compared to linear diblock copolymers was altered for all the samples due to changes in molecular packing of the PCSiO brush-like block. The difference in architecture between the two blocks shifted the morphology phase boundaries to significantly higher wt % fractions of the PS block. This morphological behavior is in agreement with the one found for the linear brush-like systems consisting of PS and PCSi brush-like block (Chapter 7).

8.4 CONCLUSIONS

Synthesis and characterization: the synthesis and characterization of linear-hyperbranched and brush-like polyalkoxysilanes, analogous in their structure to the hybrid polycarbosilane systems, is presented. As expected, the presence of electron-withdrawing substituents (*i.e.* undecenoxy *vs.* undecenyl) in the branched AB_2 silane monomer enhanced the hydrosilylation grafting efficiency from the PS-*b*-PBD diblock copolymers. On the contrary, the AB undecenoxysilane monomer gave worse grafting efficiencies than the analogous AB undecenylsilane monomer. The AB undecenoxysilane monomer (DMUOS) presented the greatest downfield silicon chemical shift of the monomers employed. Thus, this unexpected result may be related to the silicon chemical shift of the monomers, which is presumably related to their reactivity.

Phase separation and crystallization of the linear-hyperbranched polyalkoxysilane structures: the linear-hyperbranched polyalkoxysilanes samples contained one crystallizable block. To our best knowledge, there are no experimental studies regarding the morphology of amorphous-crystalline hybrid block copolymers, where the crystalline block is the dendritic block. The crystallization of the PCSiO hyperbranched blocks was confirmed by two methods: (a) observation of an endothermic and an exothermic peak by DSC and (b) detection of characteristic reflections from the PCSiO crystals by WAXS. As expected, very broad melting endotherms were found by DSC indicating melting of crystals with different fold-lengths. Additionally, low crystallization temperatures were encountered, indicating that fractionated crystallization is taking place. The large supercooling necessary for crystallization might be ascribed to the lack of nucleation opportunity.

The linear-hyperbranched alkoxysilane diblock copolymers, which were not submitted for special annealing treatment, were not able to form well-defined superstructures. Indeed, poorly ordered or nearly disordered morphologies were observed. A disrupted lamellar morphology was adopted for compositions of the PCSiO hyperbranched block slightly higher than 60 wt %. The lack of ordering observed in these samples correlates with the low T_m of the PCSiO block. Crystallization confined within the PCSiO lamellar layers was not observed. Nevertheless, no analysis of the samples by polarized optical microscopy was performed and it remains a question if crystallization can occur within the observed lamellar structures below $T_{m.}$ It is also conceivable that the confinement of the non-uniform chains of the crystalline block within the nanodomains hindered their crystallization. The existing microdomain structures might have been then partially destroyed due to PCSiO chain folding upon crystallization, which readily occurred at ambient temperature. The length for the folded chains is probably set by the branch density, although it is possible that an equilibrium degree of chain folding cannot be reached at ambient temperature. If crystallization occurs partially at ambient temperature, the energy barrier to disrupt the microphase-separated morphologies can be overcome, especially if the samples have been annealed for short periods of time.

In conclusion, the increase in the crystalline morphology for the linear-hyperbranched polyalkoxysilanes is accompanied by a decrease in the microphase-separated structure. This could indicate that the decay of the microphase-separated structure occurs cooperatively with crystallization from the beginning of the phase transformation. However, it is difficult to determine if microphase separation preceeds crystallization. If this had been the case, the appearance of transient sharp peak in the SAXS curves would have been evident. Unfortunately, detailed morphology studies by changing the crystallization conditions (time and temperature) and as a function of the annealing time at high temperature have not carried out, due to time limitations.

Phase separation of the linear brush-like polyalkoxysilane structures: a detailed study on the phase separation behavior of the linear brush-like polyalkoxysilanes was performed. An understanding of the factors affecting phase separation and structure (*i.e.* architecture) of the resulting domains was achieved in these hybrid systems, due to the absence of a block having a strong amphiphilic or crystallization force. Well-ordered morphologies were obtained in general, alike for the linear brush-like polycarbosilanes, in spite of the different length of the brushes emanating from the PBD core. Furthermore, packing frustrations of the PCSiO brush-like block led to the formation of lamellar morphologies for extremely low mass fractions (0.22) of the PCSiO block.

8.5 EXPERIMENTAL

Materials. $\mathbf{P_4}$ and $\mathbf{P_2}$ diblock copolymers were prepared in 20 g scales via a *Sänger et al.* simplified procedure of anionic polymerization as described in Chapter 2. The monomers MDUOS and DMUOS were synthesized according to described literature procedures and the details for the synthesis are given in Chapter 3. For the polymer-analogous hydrosilylation grafting reaction, anhydrous *cis,trans*-decahydronaphthalene was used as received, *n*-pentane distilled over sodium before use and platinum-1,3-divinyltetramethyldisiloxane complex in xylene (2.1-2.4 % platinum, Karstedt catalyst) used as the hydrosilylation catalyst.

Equipment. The polymerization via the SMA procedure was carried out in a specially designed apparatus as depicted in Chapter 6 (Figure 6.31).

Synthesis of $\mathbf{P_2LHO_{23}}$. The monomer MDUOS (1.65 g, 4.3 mmol) was dissolved in pentane (300 ml) and slowly added via a dosing pump to a solution of the diblock copolymer $\mathbf{P_2}$ (1 g, 0.85 mmol PBD) in *cis,trans*- decahydronaphthalene (15 mL) containing 0.0095 mmol of Karstedt catalyst (100 µL of the Pt solution) under a stream of argon with stirring at 70 °C. Pentane was removed by distillation during the slow addition of the monomer. After addition of the monomer solution, the mixture was cooled down at room temperature and an aliquot taken for GPC analysis of the crude reaction product. The polymer **P_2LHO_{23}** was purified by fractionating precipitation. This was achieved by diluting the decaline reaction mixture with diethyl ether (*ca.* 150 mL) followed by the drop wise addition of methanol until the polymer precipitated. The supernatant fluid was decanted and the isolated polymer was washed several times with methanol and dried in vacuo at 40 °C. For the synthesis of analogous linear brush-like diblock copolymers the quantity of monomer added was gradually increased, so that the molar quantity of the monomer was at least equal to the molar quantity of the 1,2-PBD core. A polymer (0.8 g, 30 %) with a number-average molecular weight ($\overline{M}_n$) of 58,000 g/mol and with a polydispersity index (PDI) of 1.10 was obtained as determined by MO and GPC measurements respectively. The analogous one pot reaction was carried out by adding the neat monomer directly to a solution of the diblock copolymer in decaline and heating at 70 °C for 24 hours.

^{1}H NMR (400 MHz, $CDCl_3$): δ (ppm) 0.12 (Si-CH_3), 0.63 (-Si-CH_2), 1.05-1.6 (polymer backbone), 1.7 (m, C**H**$_3$-CH=CH-), 1.8-2.05 (m, -C**H**$_2$-CH=CH-CH_3 and polymer backbone), 2.2 (m, -C**H**$_2$-CH=CH_2), 3.7 (m, Si-O-CH_2-), 5.0 (m, -CH=C**H**$_2$, PBD, PCSiO), 5.3-5.6 (m, -C**H**=C**H**-, PCSiO; -C**H**=CH_2, PBD), 5.8 (m, -C**H**=CH_2, PCSiO), 6.3-7.4 (m, C_6H_5); ^{13}C NMR (100 MHz, $CDCl_3$): δ (ppm) -4.57 (Si-CH_3), 13.1 (**C**H_3-CH=CH-, *cis*), 14.2 (Si-CH_2), 18.3 (**C**H_3-CH=CH-, *trans*), 23.2 (Si-CH_2-**C**H_2), 26.2, 29.3, 29.5, 29.78, 29.85, 29.9, 30, 33, 33.7, 34.2, 40-48 (polymer backbone), 62.9 ppm (Si-O-CH_2-), 114.4 (**C**H_2=CH-, PBD, PCSiO), 123.9 (CH_3-**C**H=CH-, *cis*), 124.8 (CH_3-**C**H=CH-, *trans*), 126.0 (C_6H_5), 128.3 (C_6H_5), 131.2 (CH_3-CH=**C**H-, *cis*), 132 (CH_3-CH=**C**H-, *trans*), 139.5 (**C**H_2=CH-, PCSiO), 144.2 (CH_2=**C**H-, PBD), 145.6 (C_6H_5, C_{ipso}); ^{29}Si NMR (80 MHz, $CDCl_3$): δ (ppm) 2.4; IR (characteristic absorption bands): γ(cm^{-1}) 1602 (stretching C=C mode), 1254 (stretching Si-CH_3 mode), 1091 (stretching Si-O-CH_2-), 907 (terminal PBD and PCSi C=C deformation).

Synthesis of P_4LBO_{17}. The polymer was prepared analogously to **P_4LHO_{23}** from DMUOS (0.91 g, 4 mmol) in pentane (300 ml) added slowly to **P_4** (1 g, 0.79 mmol PBD) in *cis,trans*-decahydronaphtalene (15 mL) containing 0.0047 mmol of Karstedt catalyst (52 µL of the Pt solution). A polymer (0.7 g, 37 %) with $\overline{M}_n$ of 72,300 g/mol and with a PDI of 1.07 was obtained as determined by MO and GPC measurements respectively. The analogous one pot reaction was carried out by adding the neat monomer directly to a solution of the diblock copolymer in decaline and heating at 70 °C for 24 hours.

^{1}H NMR (400 MHz, CDCl$_3$): δ (ppm) 0.15 (Si-CH$_3$), 0.66 (-Si-CH$_2$), 1.05-1.6 (polymer backbone), 1.7 (m, C**H**$_3$-CH=CH-), 1.8-2.05 (m, -C**H**$_2$-CH=CH-CH$_3$ and polymer backbone), 2.2 (m, -C**H**$_2$-CH=CH$_2$), 3.7 (m, Si-O-CH$_2$-), 5.0 (m, -CH=C**H**$_2$, PBD, PCSiO), 5.2-5.7 (m, -C**H**=C**H**-, PCSiO; -C**H**=CH$_2$, PBD), 5.9 (m, -C**H**=CH$_2$, PCSiO), 6.2-7.4 (m, C$_6$H$_5$); ^{13}C NMR (100 MHz, CDCl$_3$): δ (ppm) -1.73 (Si-CH$_3$), 13.1 (**C**H$_3$-CH=CH-, *cis*), 16.7 (Si-CH$_2$), 18.3 (**C**H$_3$-CH=CH-, *trans*), 23.6 (Si-CH$_2$-**C**H$_2$), 26.2, 29.71, 29.82, 29.9, 30, 33.1, 33.8, 40-48 (polymer backbone), 63.1 ppm (Si-O-CH$_2$-), 114.4 (**C**H$_2$=CH-, PBD, PCSiO), 123.9 (CH$_3$-**C**H=CH-, *cis*), 124.8 (CH$_3$-**C**H=CH-, *trans*), 125.9 (C$_6$H$_5$), 128.3 (C$_6$H$_5$), 131.2 (CH$_3$-CH=**C**H-, *cis*), 132 (CH$_3$-CH=**C**H-, *trans*), 139.5 (**C**H$_2$=CH-, PCSiO), 144.2 (CH$_2$=**C**H-, PBD), 145.6 (C$_6$H$_5$, C$_{\mathit{ipso}}$); ^{29}Si NMR (80 MHz, CDCl$_3$): δ (ppm) 17.3; IR (characteristic absorption bands): γ(cm^{-1}) 1602 (stretching C=C mode), 1250 (stretching Si-CH$_3$ mode), 1093 (stretching Si-O-CH$_2$-), 907 (terminal PBD and PCSi C=C deformation), 837 (bending CH$_3$-Si-CH$_3$ mode).

Synthesis of PMDUOS. 0.0052 mmol of Karstedt catalyst (56 μL of the Pt solution) were added under argon to a solution of MDUOS (1 g, 2.6 mmol) in toluene (10 ml), and the system was stirred at r.t. for 24 hours. The resulting polymer was isolated by precipitation in methanol to give **PMDUOS** (0.91 g, $\overline{M}_n$ = 6,000 g/mol, PDI = 4.6).

^{1}H NMR (400 MHz, CDCl$_3$): δ (ppm) 0.08 (Si-CH$_3$), 0.6 (-Si-CH$_2$), 1.1-1.4 (polymer backbone), 1.53 (m, Si-O-CH$_2$-C**H**$_2$-), 1.59 (m, -CH$_2$-CH=CH-C**H**$_3$, *cis*), 1.63 (m, -CH$_2$-CH=CH-C**H**$_3$, *trans*), 1.95 (m, -C**H**$_2$-CH=CH-CH$_3$, *cis* and *trans*), 2.03 (m, -C**H**$_2$-CH=CH$_2$), 3.65 (m, Si-O-CH$_2$-), 4.95 (m, -CH=C**H**$_2$), 5.3-5.4 (m, -C**H**=C**H**-), 5.8 (m, -C**H**=CH$_2$); ^{13}C NMR (100 MHz, CDCl$_3$): δ (ppm) -4.57 (Si-CH$_3$), 13.06 (**C**H$_3$-CH=CH-, *cis*), 14.16 (Si-CH$_2$), 18.24 (**C**H$_3$-CH=CH-, *trans*), 23.24, 26.16, 27.17, 29.16, 29.28, 29.77, 29.48, 29.85, 29.95, 30.03, 32.93, 33.01, 33.04, 33.68, 34.14, 62.9 (Si-O-CH$_2$-), 114.4 (**C**H$_2$=CH-), 123.9 (CH$_3$-**C**H=CH-, *cis*), 124.8 (CH$_3$-**C**H=CH-, *trans*), 131.2 (CH$_3$-CH=**C**H-, *cis*), 132 (CH$_3$-CH=**C**H-, *trans*), 139.5 (**C**H$_2$=CH-).

Synthesis of PDMUOS. The polymer was prepared analogously to **PMDUOS** from DMUOS (1 g, 4.4 mmol) in toluene (10 ml) containing 0.0044 mmol of Karstedt catalyst (47 μL of the Pt solution). The resulting polymer was isolated by precipitation in methanol to give

PDMUOS (0.75 g, $\overline{M}_n$ = 2,700 g/mol, PDI = 1.65). Note: The NMR data demonstrate partial hydrolysis of the Si-O-alkyl moiety and complete isomerization of the terminal double bonds. Small signals, not included in the NMR data, indicate several types of isomers along the alkyl chain.

^{1}H NMR (400 MHz, $CDCl_3$): δ (ppm) 0.05 (m, Si-CH_3 from polymer and hydrolyzed backbone), 0.55 (-Si-CH_2), 1.0-1.4 (polymer backbone), 1.50 (m, Si-O-CH_2-C**H**$_2$-), 1.60 (m, -CH_2-CH=CH-C**H**$_3$, *trans* and *cis*), 1.93 (m, -C**H**$_2$-CH=CH-CH_3, *cis* and *trans*), 3.53 (m, Si-O-CH_2-), 3.63 (m, hydrolyzed Si-O-CH_2-), 5.3-5.5 (m, -C**H**=C**H**-); ^{13}C NMR (100 MHz, $CDCl_3$): δ (ppm) -1.7 (m, Si-CH_3 from polymer and hydrolyzed backbone), 13.9 (**C**H_3-CH=CH-, *cis*), 16.7 (Si-CH_2), 18.75 (**C**H_3-CH=CH-, *trans*), 23.55, 23.63, 26.19, 26.26, 29.71, 29.81, 29.93, 30, 32.96, 33.13, 33.82, 63.19, 63.28, 63.1 (Si-O-CH_2-), 62.89 (hydrolyzed Si-O-CH_2-), 123.9 (CH_3-**C**H=CH-, *cis*), 124.8 (CH_3-**C**H=CH-, *trans*), 131.9 (CH_3-CH=**C**H-, *cis*), 132.2 (CH_3-CH=**C**H-, *trans*).

8.6 REFERENCES

[1] Clarson, S. J., Semlyen, J. A. *Siloxane Polymers*; PTR Prentice Hall: Englewood Cliffs, NJ, 1993.

[2] Noll, W. *Chemistry and technology of silicones*; Academic Press: New York, 1968, 437-530.

[3] (a) Lang, H.; Lühmann, B. *Adv. Mater.* **2001**, *13*, 1523. (b) Majoral, J.-P.; Carminade, A.-M. *Chem. Rev.* **1999**, *99*, 845. (c) Cuadrado, I.; Casado, C. M.; Alonso, B.; Moran, M.; Losada, J.; Belsky, V. *J. Am. Chem. Soc.* **1997**, *119*, 7613. (d) Lorenz, K.; Mulhaupt, R.; Frey, H.; Rapp, U.; Mayer-Posner, F. J. *Macromolecules* **1995**, *28*, 6657. (e) Lambert, J. B.; Pflug, J. L.; Stern, C. I. *Angew. Chem., Int. Ed. Engl.* **1995**, *34*, 98. (f) Seyferth, D.; Son, D. Y.; Rheighold, A. L. Ostrander, R. L. *Organometallics* **1994**, *13*, 2682. (g) Knapen, J. W. J.; van der Made, A. W.; de Wilde, J. C.; van Leewven, P. W. N. M.; Wijkens, P.; Grove, D. M.; van Koten, G. *Nature* **1994**, *372*, 659. (h) van der Made, A. W.; van Leewen, P. W. N. M.; Brandes, R. A. C. *Adv. Mater.* **1993**, *5*, 466. (i) Morikawa, A.; Kakimoto, M.; Imai, Y. *Macromolecules* **1992**, *25*, 3247. (j) Morikawa, A.; Kakimoto, M.; Imai, Y. *Polym. J.* **1992**, *24*, 573. (k) Morikawa, A.; Kakimoto, M.; Imai, Y. *Macromolecules* **1991**, *24*, 3469. (l) Uchida, H.; Kabe, Y.; Yoshino, H.; Kawamata, A.; Tsumuraya, T.; Masamune, S. *J. Am. Chem. Soc.* **1990**, *112*, 7077.

[4] (a) Si, Q.-F.; Wang, X.; Fan, X.-D.; Wang, S.-J. *J. Polym. Sci., Part A. Polym. Chem.* **2005**, *43*, 1883. (b) Xiao, Y.; Son, D. Y. *J. Polym. Sci., Part A. Polym. Chem.* **2001**, 39,

3383. (c) Oishi, M.; Minakawa, M.; Imae, I.; Kawakami, Y. *Macromolecules* **2002**, *35*, 4938. (d) Paulasaari, J. K.; Weber, W. P. *Macromolecules* **2000,** *33*, 2005. (e) Paulasaari, J. K.; Weber, W. P. *Macromol. Chem. Phys.* **2000**, *201*, 1585 (f) Gong, C.; Fréchet, J. M. J. *J. Polym. Sci., Part A. Polym. Chem.* **2000**, *38*, 2970. (g) Gong, C.; Miravet, J. F.; Fréchet, J. M. J. *J. Polym. Sci., Part A. Polym. Chem.* **1999**, *37*, 3193. (h) Miravet, J. F.; Fréchet, J. M. J. *Macromolecules* **1998**, *31*, 3461. (i) Muzafarov, A. M.; Rebrov, E. A.; Gorbacevich, O. B.; Golly, M.; Gankema, H.; Möller, M. *Macromol. Symp.* **1996**, *102*, 35. (j) Rubinsztajn, S.; Stein, J. *J. Inorg. Organomet. Polym.* **1995**, *5*, 43. (k) Muzafarov, A. M.; Golly, M.; Möller, M. *Macromolecules* **1995**, *28*, 8444. (l) Rubinsztajn, S. *J. Inorg. Organomet. Polym.* **1994**, *4*, 61. (m) Mathias, L. J.; Carothers, T. W. *J. Am. Chem. Soc.* **1991**, *113*, 4043.

[5] (a) Pyun, J.; Tang, C.; Kowalewski, T.; Fréchet, J. M. J.; Hawker, C. J. *Macromolecules* **2005**, *38*, 2674. (b) Zubarev, E. R.; Stupp, S. I. *J. Am. Chem. Soc.* **2002**, *124*, 5762. (c) Gitsov, I. *Linear-Dendritic Block Copolymers. Synthesis and Characterization*; in *Advances in Dendritic Macromolecules*, Newkome G. R.; Elsevier Science, Amsterdam, 2002, Vol. 5, Chapter 2, 45-87. (d) Zubarev, E. R.; Pralle, M. U.; Sone, E. D.; Stupp, S. I. *J. Am. Chem. Soc.* **2001**, *123*, 4105. (e) Gitsov, I.; Lambrych, K. L.; Ivanova, P. T.; Lewis, S. *Polym. Mater. Sci. Eng.* **2001**, *84*, 926. (f) Chang, Y.; Kwon, Y. C.; Lee, S. C.; Kim, C. *Macromolecules* **2000**, *33*, 4496. (g) Iyer, J; Fleming, K; Hammond, P. T. *Macromolecules* **1998**, *31*, 8757. (h) Leduc, M.; Hayes, W.; Fréchet, J. M. J. *J. Polym. Sci., Part A: Polym. Chem.* **1998**, *36*, 1. (i) van Hest, J. C. M.; Delnoye, D. A. P.; Baars, M. W. P. L.; van Genderen, M. H. P.; Meijer, E. W. *Science* **1995**, *268*, 1592. (j) Chapman, T. M.; Hillyer, G. L.; Mahan, E. J.; Shaffer, K. A. *J. Am. Chem. Soc.* **1994**, *116*, 11195. (k) Gitsov, I; Ivanova, P. T.; Fréchet, J. M. J. *Macromol. Rapid Commun.* **1994**, *15*, 387. (l) Newkome, G. R.; Baker, G. R.; Arai, S.; Saunders, M. J.; Russo, P. S.; Theriot, K. J.; Moorefield, C. N.; Rogers, L. E.; Miller, J. E.; Lieux, T. R.; Murray, M. E.; Phillips, B.; Pascal, L. *J. Am. Chem. Soc.* **1990**, *112*, 8458.

[6] (a) Duan, X. X.; Yuan, F.; Wen, X. J.; Yang, M.; He, B.; Wang, W. *Macromol. Chem. Phys.* **2004**, *205*, 1410. (b) Johnson, M. A.; Iyer, J.; Hammond, P. T. *Macromolecules* **2004**, *37*, 2490. (c) Pochan, D. J.; Pakstis, L.; Huang, E.; Hawker, C.; Vestberg, R.; Pople, J. *Macromolecules* **2002**, *35*, 9239. (d) Mackay, M. E.; Hong, Y.; Jeong, M.; Tande, B. M.; Wagner, N. J.; Hong, S.; Gido, S. P.; Vestberg, R.; Hawker, C. J. *Macromolecules* **2002**, *35*, 8391. (e) Román, C.; Fischer, H. R.; Meijer, E. W. *Macromolecules* **1999**, *32*, 5525. (f) Gitsov, J.; Fréchet, J. M. J. *Macromolecules* **1993**, *26*, 6536.

[7] (a) Gitsov, I.; Wooley, K. L.; Hawker, C. J.; Ivanova, P. T.; Fréchet, J. M. J. *Macromolecules* **1993**, *26*, 5621. (b) Gitsov, I.; Wooley, K. L.; Fréchet, J. M. J. *Angew. Chem., Int. Ed. Engl.* **1992**, *31*, 1200.

[8] Drohmann, C.; Möller, M.; Gorbatsevich, O. B.; Muzafarov, A. M. *J. Polym. Sci., Part A: Polym. Chem.* **2000**, *38*, 741.

[9] (a) Stein, J.; Lewis, L. N.; Smith, K. A.; Lettko, K. X. *J. Inorg. Organomet. Polym.* **1991**, *1*, 325. (b) Uriarte, R. J.; Lewis, L. N. *Organometallics* **1990**, *9*, 621. (c) Lewis, L. N. *J. Am. Chem. Soc.* **1990**, *112*, 5998.

[10] (a) Hanselmann, R.; Hölter, D.; Frey, H. *Macromolecules* **1998**, *31*, 3790. (b) Radke, W.; Litvinenko, G.; Müller, A. H. E. *Macromolecules* **1998**, *31*, 239.

[11] (a) Cohen, R. E.; Cheng, P.L.; Douzinas, K.; Kofinas, P.; Berney, C. V. *Macromolecules* **1990**, *23*, 324. (b) Séguéla, R.; Prud΄homme, J. *Polymer* **1989**, 30, 1446.

[12] (a) Li, L.-B.; Séréro, Y.; Koch, M. H. J.; de Jeu, W. H. *Macromolecules* **2003**, *36*, 529. (b) Zhu, L.; Mimnaugh, B. R.; Ge, Q.; Quirk, R. P.; Cheng, S. Z. D.; Thomas, E. L.; Lotz, B.; Hsiao, B. S.; Yeh, F.; Liu, L. *Polymer* **2001**, *42*, 9121. (c) Kim, G.; Han, C. C.; Libera, M.; Jackson, C. L. *Macromolecules* **2001**, *34*, 7336. (d) Chen, H.-L.; Hsiao, S.-C.; Lin, T.-L.; Yamauchi, K. H.; Hasegawa, T.; Hashimoto, T. *Macromolecules* **2001**, *34*, 671. (e) Loo, Y.-L.; Register, R. A.; Ryan, A. J.; Dee, G. T. *Macromolecules* **2001**, *34*, 8968. (f) Chen, H.-L.; Wu, J.-C.; Lin, T.-L.; Lin, K. J. S. *Macromolecules* **2001**, *34*, 6936. (g) Loo, Y.-L.; Register, R. A.; Ryan, A. *Phys. Rev. Letts.* **2000**, *84*, 4120. (h) Zhu, L.; Chen, Y.; Zhang, A.; Calhoun, B. H.; Chun, M.; Quirk, R. P.; Cheng, S. Z. D.; Hsiao, B. S.; Yeh, F.; Hashimoto, T. *Phys. Rev. B* **1999**, *60*, 10022. (i) Floudas, G.; Tsitsilianis, C. *Macromolecules* **1997**, *30*, 4381. (j) Quiram, D. J.; Register, R. A. Marchand, G. R. *Macromolecules* **1997**, *30*, 4551. (k) Ryan, A. J.; Hamley, I. W.; Bras, W.; Bates, F. S. *Macromolecules* **1995**, *28*, 3860. (l) Rangarajan, P.; Register, R. A.; Fetters, L. J. *Macromolecules* **1993**, *26*, 4640. (m) Douzinas, K. C.; Cohen, R. E.; Halasa, A. F. *Macromolecules* **1991**, *24*, 4457.

[13] Brook, M. A. *Silicon in Organic, Organometallic and Polymer Chemistry*; Wiley: Canada, 2000.

[14] (a) Ashby, B. A.; Modic, F. J. US Patent 4,288,345, 1981. (b) Karstedt, B. D. (General Electric) US Patent 3,715,334, 1973.

[15] Stober, M. R.; Musolf, M. C.; Speier, J. L. *J. Org. Chem.* **1965**, *30*, 1651.

[16] Lee, J. S.; Quirk, R. P.; Foster, M. D.; Wollyung, K. M.; Wesdemiotis, C. *Macromolecules* **2004**, *37*, 6385.

[17] (a) Corey, E. J.; Venkateswarlu, A. *J. Am. Chem. Soc.* **1972**, *94*, 6190. (b) Stork, G.; Hudrlik, P. F. *J. Am. Chem. Soc.* **1968**, *90*, 4462.

[18] Thomas, S. E. *Organic Synthesis: The Roles of Boron and Silicon*; Oxford University Press: New York, 1991.

[19] Smith, A.L. *The Analitical Chemistry of Silicones*; Wiley & Sons: New York, 1992.

[20] (a) Rabek, J. F. *Experimental Methods in Polymer Chemistry*; John Wiley & Sons: New York, 1980, p. 438. (b) Billingham, N. C. *Molar Mass Measurement in Polymer Science*; Kogan Press Ltd.: 1977, p. 220.

[21] Hamley, I. W. *The Physics of Block Copolymers*; Oxford University Press: Oxford, 1998.

[22] (a) Bogdanov, B.; Vidts, A.; Schacht, E.; Berghmans, H. *Macromolecules* **1999**, *32*, 726. (b) Ryan, A. J.; Fairclough, J. P. A.; Hamley, I. W.; Mai, S. M.; Booth, C. *Macromolecules* **1997**, *30*, 1723.

[23] (a) Supaphol, P.; Spruiell, J. E. *J. Appl. Polym. Sci.* **2000**, *75*, 44. (b) Schmidtke, J.; Strobl, G.; Thurn-Albrecht, T. *Macromolecules* **1997**, 30, 5804.

[24] (a) Balsamo, V.; Urbina de Navarro, C.; Gil, G. *Macromolecules* **2003**, *36*, 4507. (b) Gan, Z.; Jiang, B.; Zhang, J. *J. Appl. Polym. Sci.* **1996**, *59*, 961.

[25] (a) Balsamo, V.; Gil, G.;Urbina de Navarro, C.; Hamley, I. W.; von Gyldenfeldt, F.; Abetz, V.; Cañizales, E. *Macromolecules* **2003**, *36*, 4515. (b) Hamley, I. W.; Fairclough, J. P. A.; Bates, F. S.; Ryan, A. J. *Polymer* **1997**, 39, 1429.

[26] (a) Quiram, D. J.; Register, R. A.; Marchand, G. R.; Ryan, A. J. *Macromolecules* **1997**, 30, 8338. (b) Rangarajan, P; Register, R. A.; Adamson, D. H.; Fetters, L. J.; Bras, W.; Naylor, S.; Ryan, A. J. *Macromolecules* **1995**, *28*, 1422. (c) Rangarajan, P; Register, R. A.; Fetters, L. J.; Bras, W.; Naylor, S.; Ryan, A. J. *Macromolecules* **1995**, *23*, 4932.

[27] (a) Nojima, S.; Kikuchi, N.; Rohadi, A.; Tanimoto, S.; Sasaki, S. *Macromolecules* **1999**, *32*, 3727. (b) Nojima, S.; Fujimoto, M.; Kakihira, H.; Sasaki, S. *Polym. J.* **1998**, *30*, 968. (c) Nojima, S.; Nakano, H.; Takahashi, Y.; Ashida, T. *Polymer* **1994**, *35*, 3479. (c) Heuschen, J.; Jerome, R.; Teyssie, P. *J. Polym. Sci., Part B: Polym. Phys.* **1989**, *27*, 523.

[28] (a) Mai, S.; Fairclough, J. P. A.; Viras, K., Gorry, P. A.; Hamley, I. W.; Ryan, A. J.; Booth, C. *Macromolecules* **1997**, *30*, 8392. (b) Nojima, S.; Ono, M.; Ashida, T. *Polym. J.* **1992**, *24*, 1271.

[29] (a) Liu, L.-H.; Yeh, F.; Chu, B. *Macromolecules* **1996**, *29*, 5336. (b) Ishikawa, S.; Ishizu, K.; Fukutomi, T. *Eur. Polym. J.* **1992**, *28*, 1219.

[30] (a) Hamley, I. W.; Fairclough, J. P. A.; Bates, F. S.; Ryan, A. J. *Polymer* **1998**, *39*, 1429. (b) Richardson, P. H.; Richards, R. W.; Blundell, D. J.; Mac-Donald, W. A.; Mills, P. *Polymer* **1995**, *36*, 3059. (c) Gervais, M.; Gallot, B.; Jerome, R.; Teyssie, P. *Makromol. Chem.* **1981**, *182*, 989.

[31] (a) Pochan, D.; Gido, S. P.; Pispas, S.; Mays, J. W.; Ryan, A. J.; Fairclough, J. P. A.; Hamley, I. W.; Terrill, N. J. *Macromolecules* **1996**, *29*, 5091. (b) Pochan, D.; Gido, S. P.; Pispas, S.; Mays, J. W. *Macromolecules* **1996**, *29*, 5099.

[32] (a) Müller, A. J.; Balsamo, V.; Arnal, M. L.; Jakob, T.; Schmalz, H.; Abetz, V. *Macromolecules* **2002**, *35*, 3048. (b) Arnal, M. L.; Balsamo, V.; López-Carrasquero, F.; Contreras, J.; Carrillo, M.; Schmalz, H.; Abetz, V.; Laredo, E.; Müller, A. J. *Macromolecules* **2001**, *34*, 7973 and references therein.

[33] Rangarajan, P; Register, R. A.; Adamson, D. H.; Fetters, L. J.; Bras, W.; Naylor, S.; Ryan, A. J. *Macromolecules* **1995**, *28*, 1422.

[34] Dobrynin, A. V. *Journal de Physique I* **1995**, *5*, 657.

[35] Hadjichristidis, N.; Tselikas, Y.; Iatrou, H.; Efstratiadis, V.; Avgeropoylos, A. *J. Macromol. Sci., Pure Appl. Chem.* **1996**, *A33*, 1447.

[36] Shibayama, M.; Hashimoto, T. *Macromolecules* **1986**, *19*, 740.

Methyldiundec-10-enylsilane (MDUS)

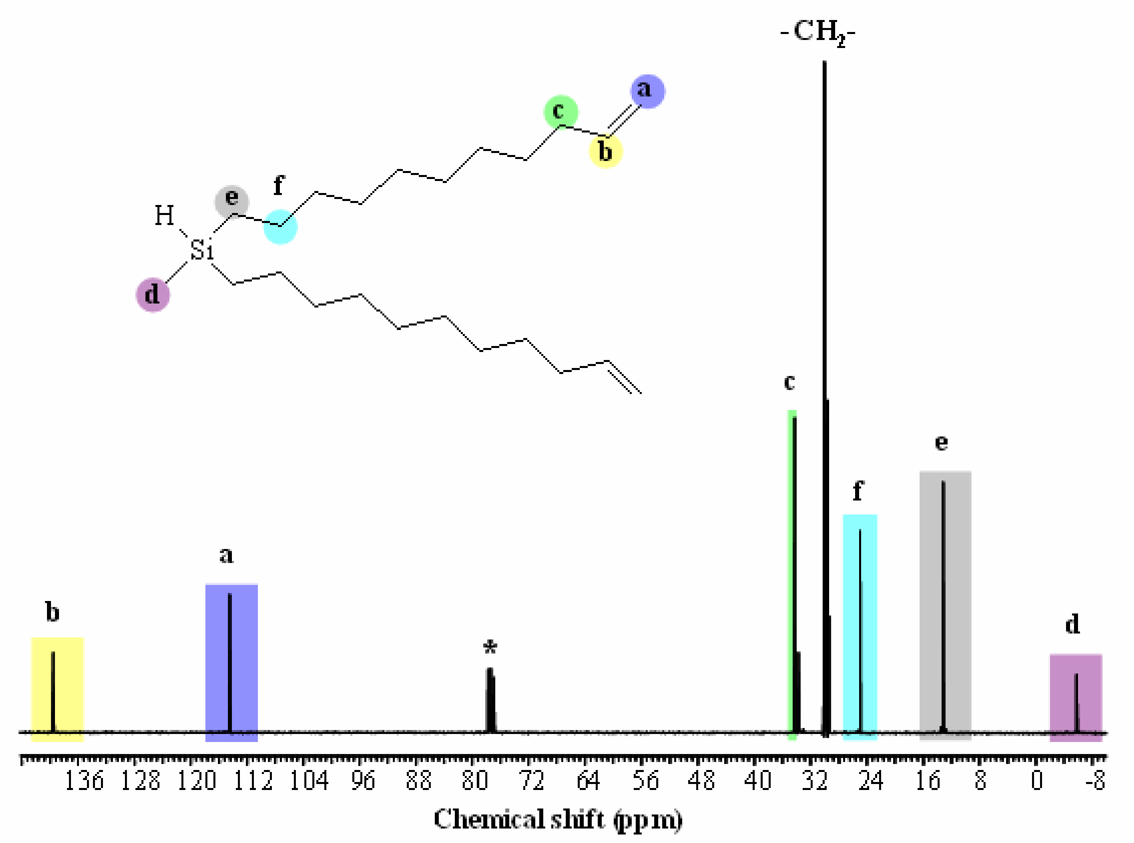

Figure A3.1. ^{13}C NMR spectrum of MDUS in $CDCl_3$ (solvent peak denoted by an asterisk).

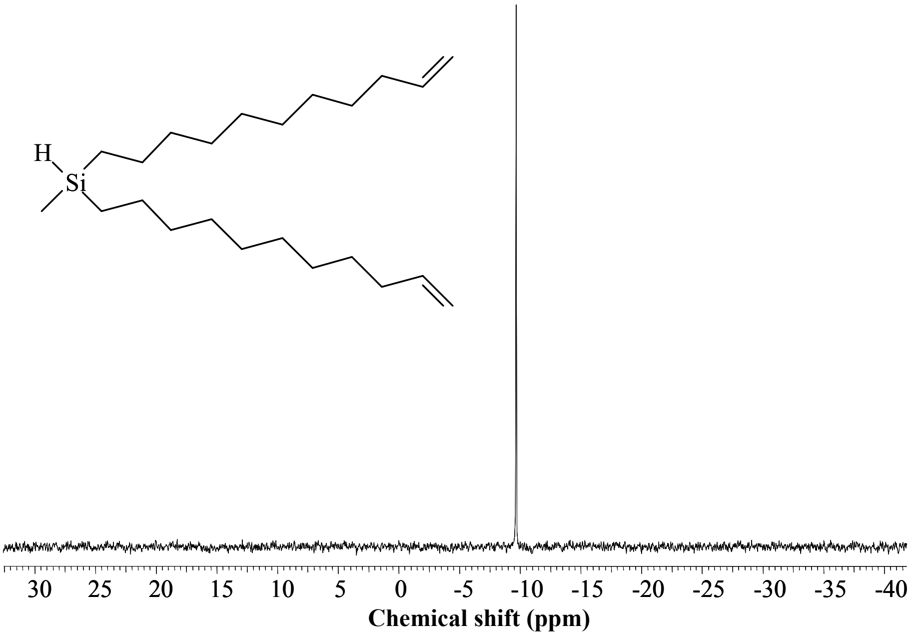

Figure A3.2. ^{29}Si NMR spectrum of MDUS in $CDCl_3$.

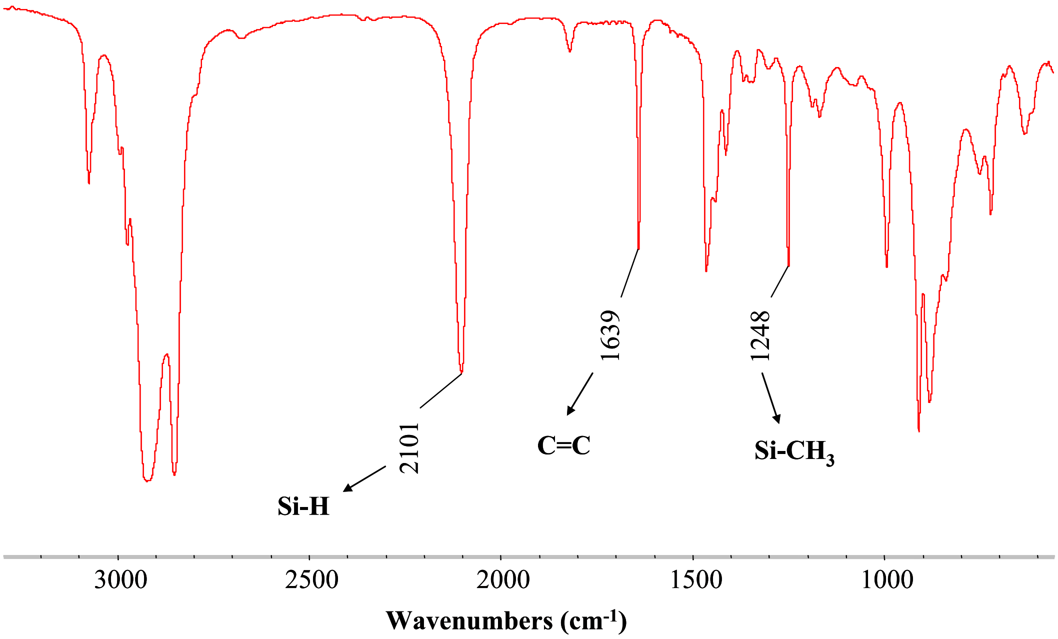

Figure A3.3 IR spectrum of MDUS.

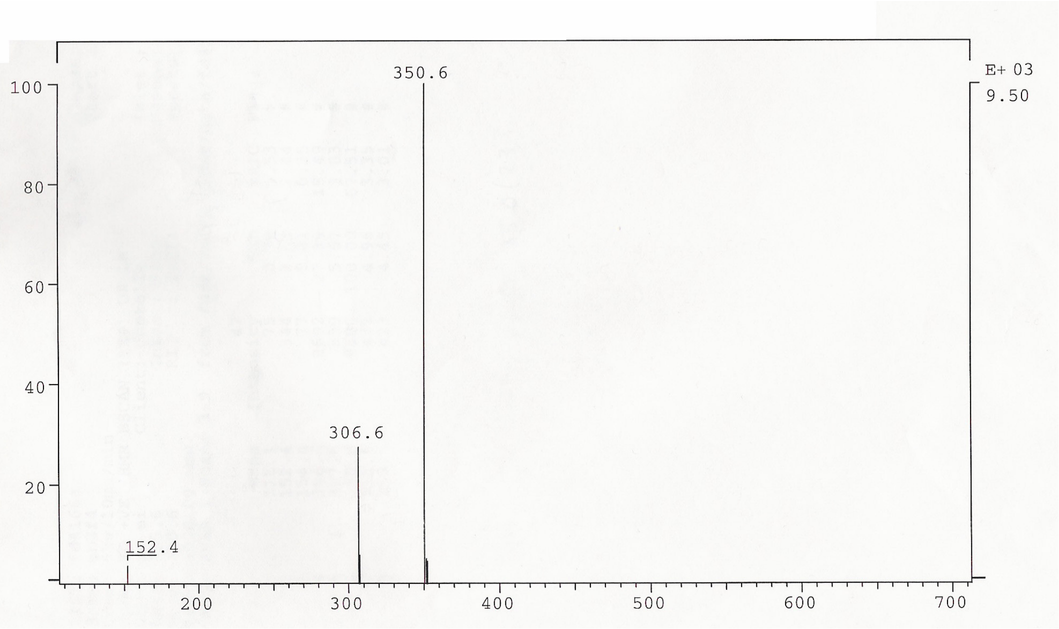

Figure A3.4. FD mass spectrum of MDUS.

Dimethyl(undec-10-enyl)silane (DMUS)

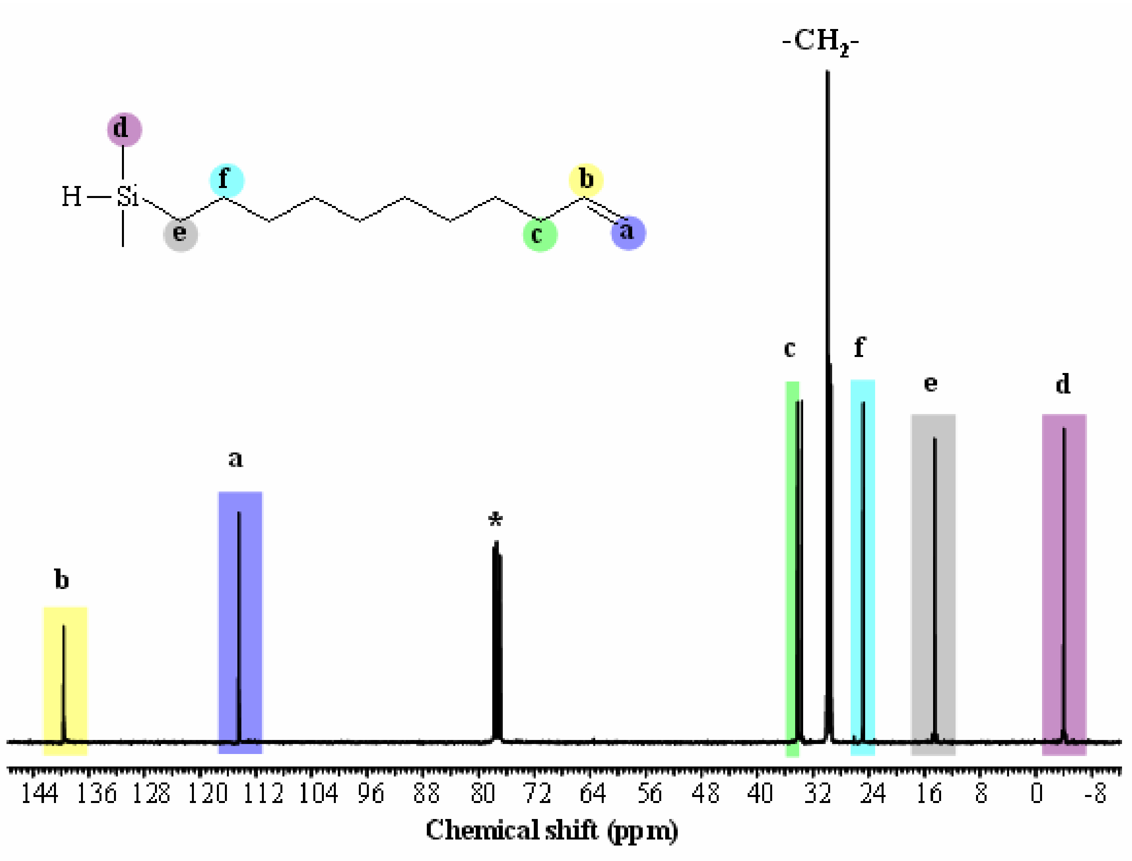

Figure A3.5. ^{13}C NMR spectrum of DMUS in $CDCl_3$ (solvent peak denoted by an asterisk).

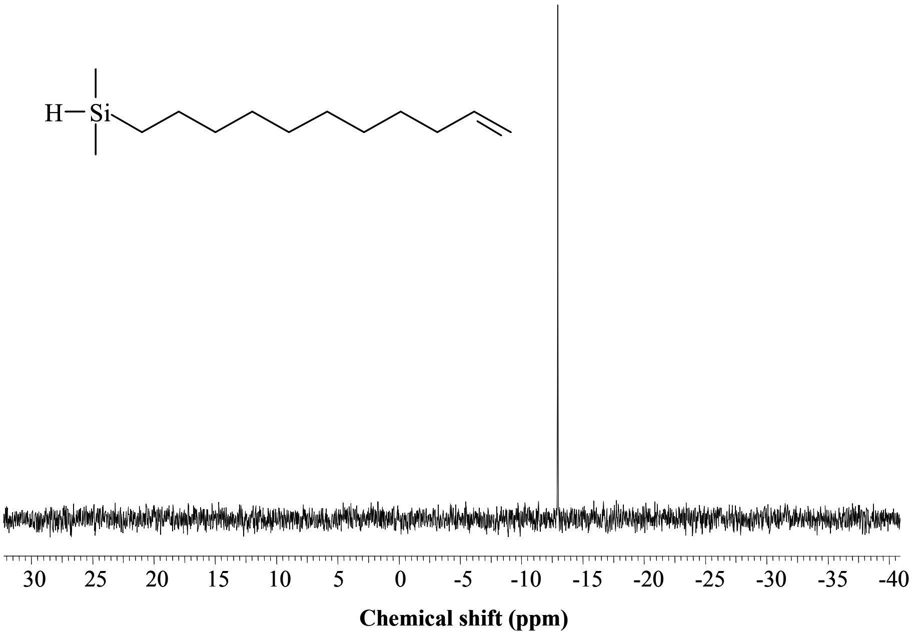

Figure A3.6. ^{29}Si NMR spectrum of DMUS in $CDCl_3$.

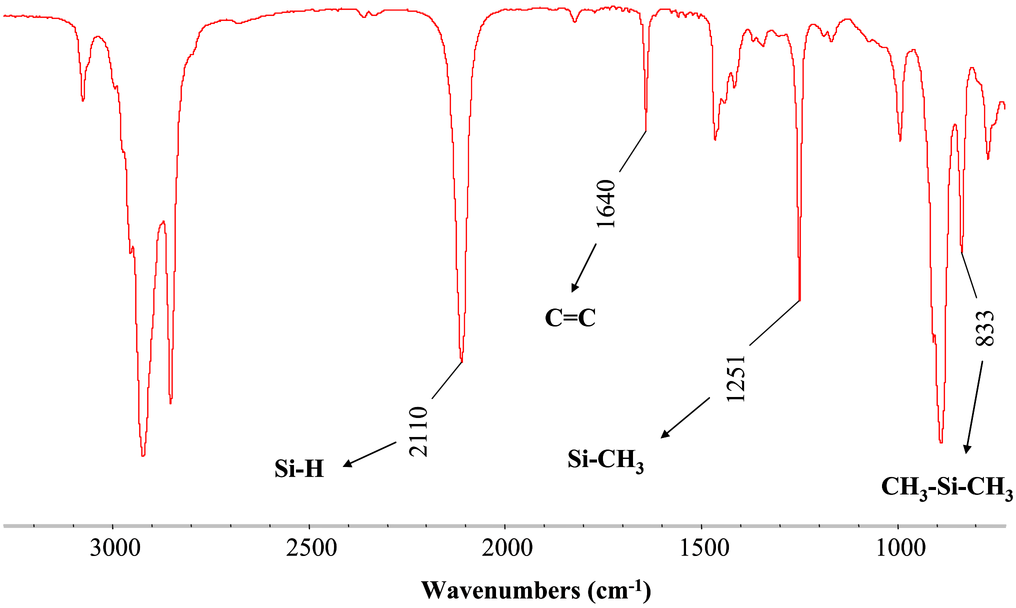

Figure A3.7. IR spectrum of DMUS.

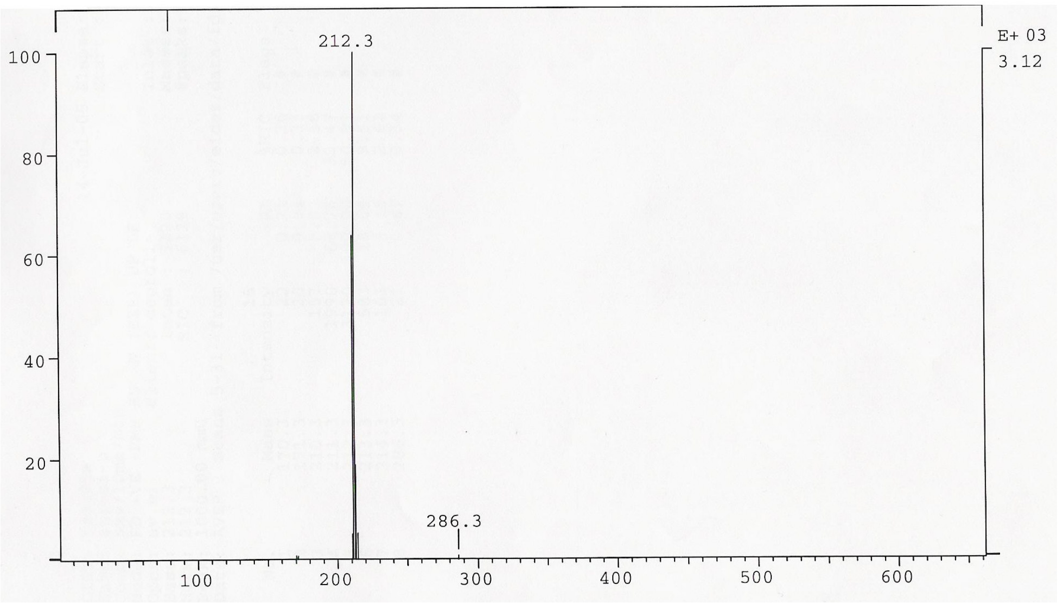

Figure A3.8. FI mass spectrum of DMUS.

Triundec-10-enylsilane (TUS)

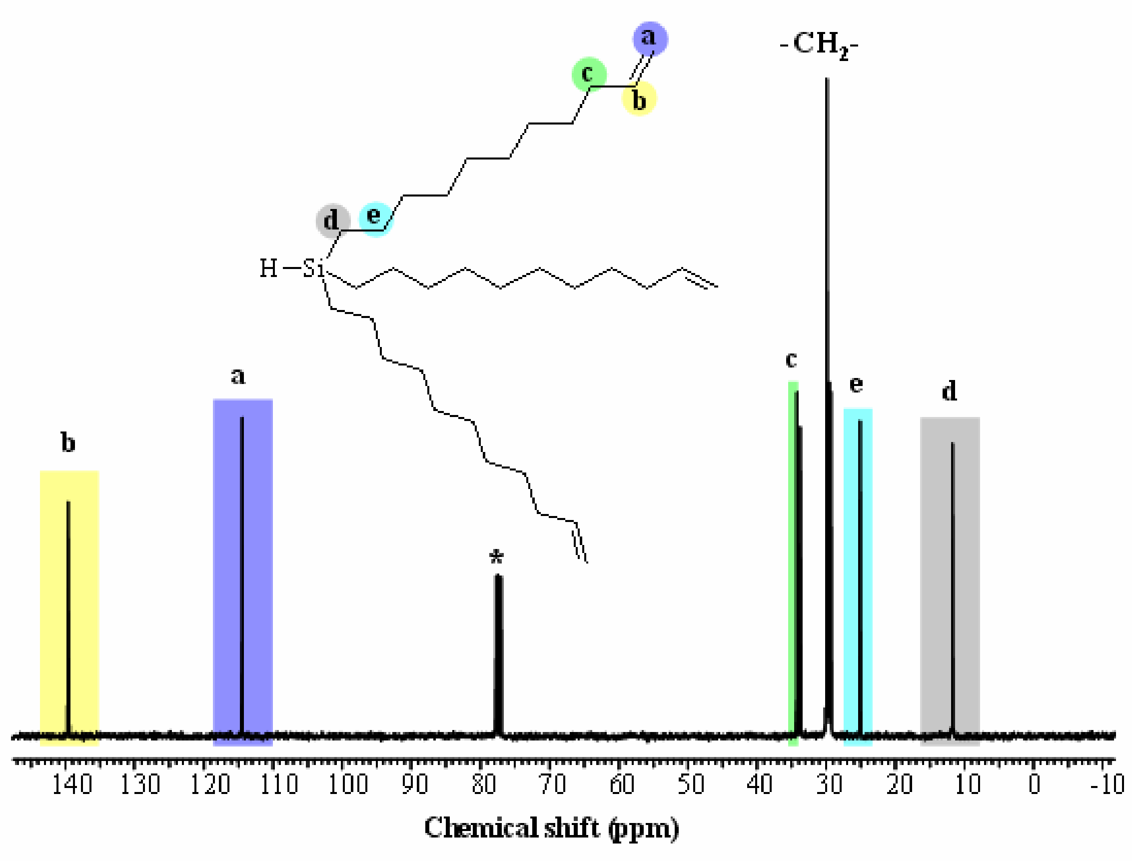

Figure A3.9. ^{13}C NMR spectrum of TUS in CDCl$_3$ (solvent peak denoted by an asterisk).

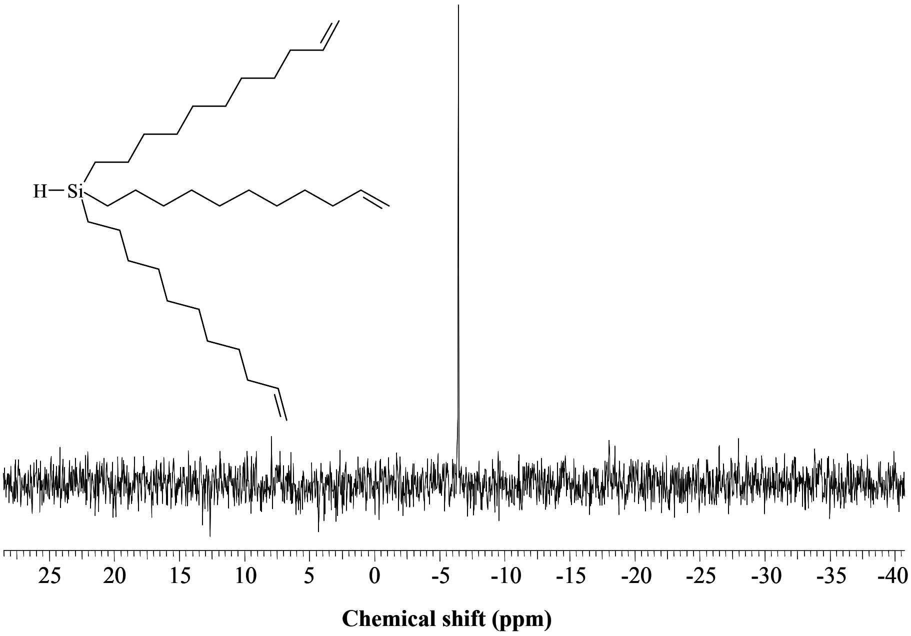

Figure A3.10. ^{29}Si NMR spectrum of TUS in CDCl$_3$.

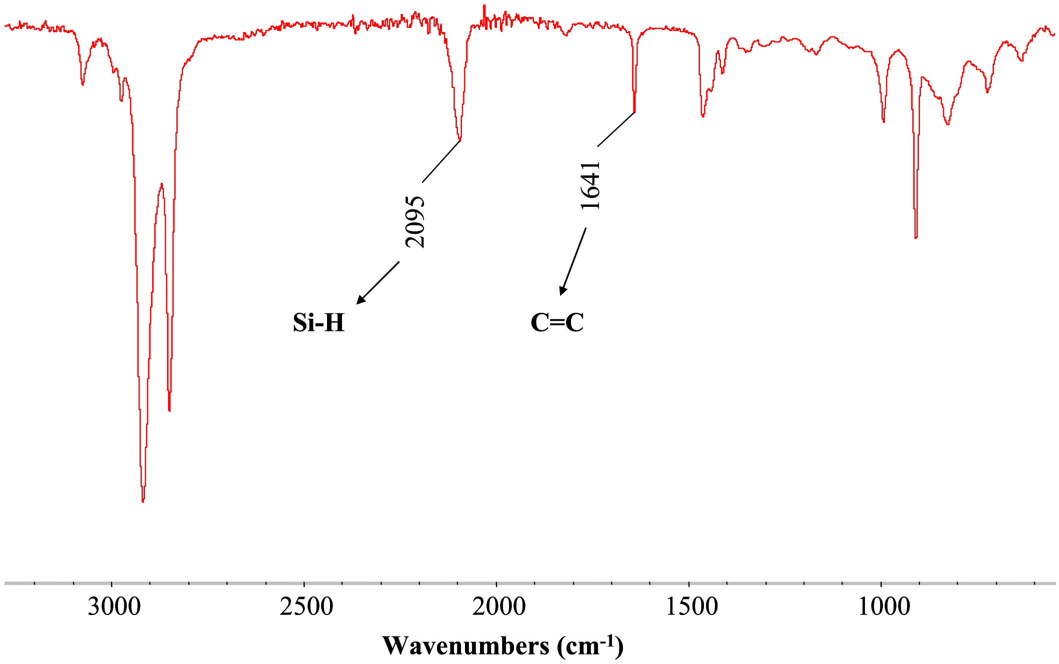

Figure A3.11. IR spectrum of TUS.

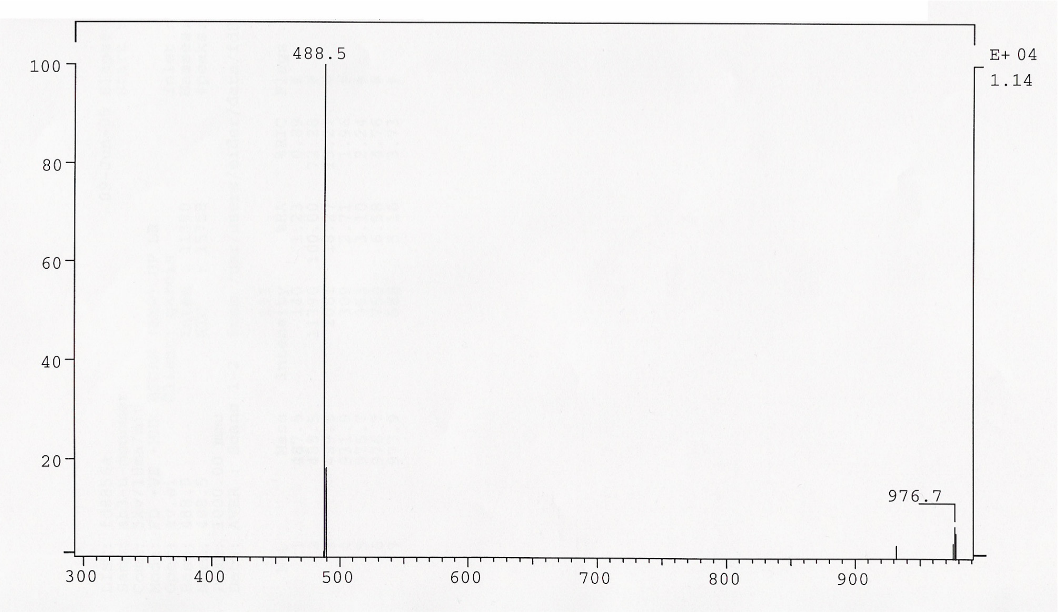

Figure A3.12. FD mass spectrum of TUS.

Diallyl(methyl)silane (MDAS)

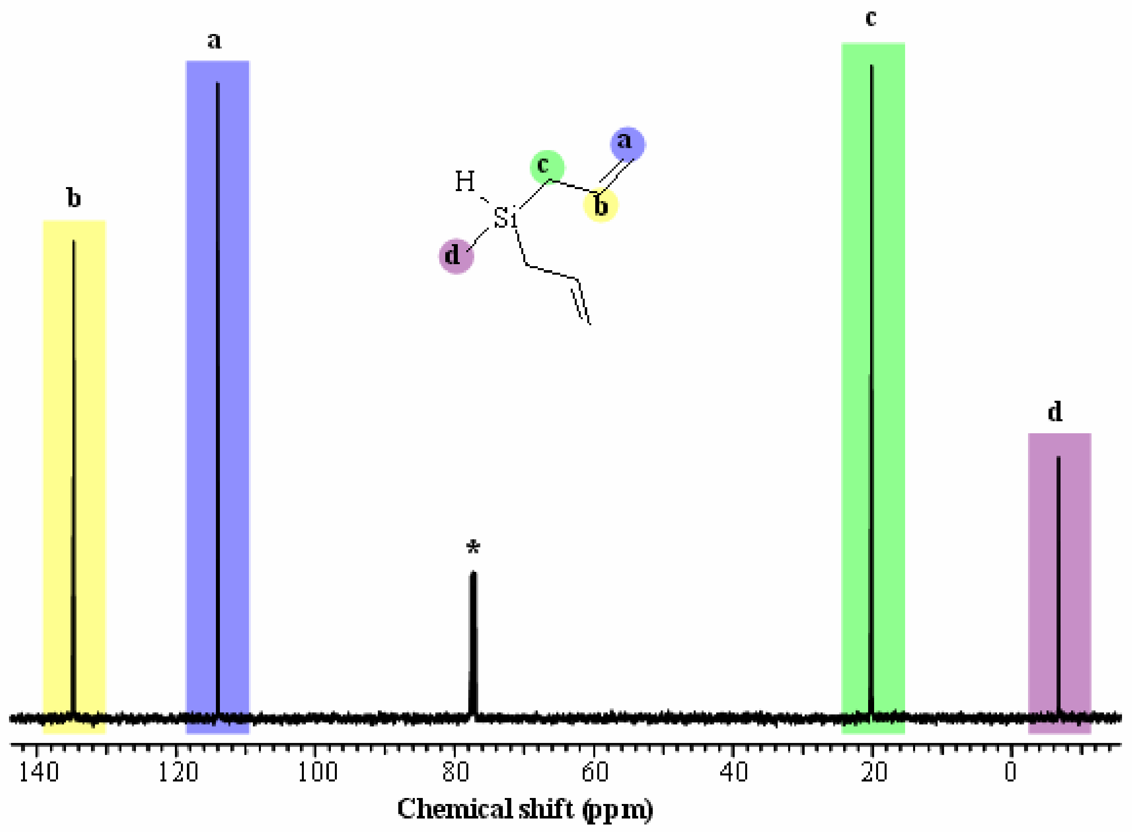

Figure A3.13. ^{13}C NMR spectrum of MDAS in $CDCl_3$ (solvent peak denoted by an asterisk).

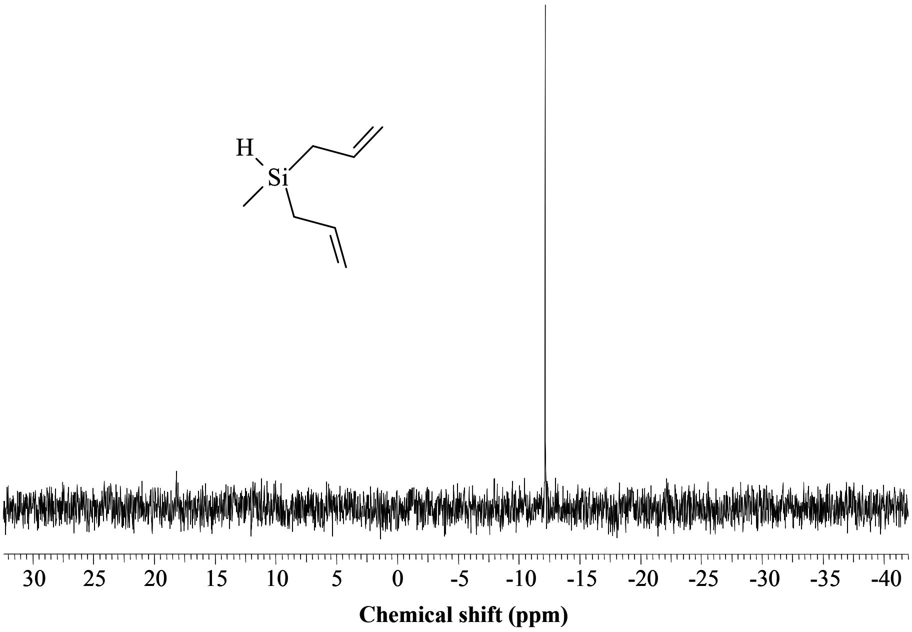

Figure A3.14. ^{29}Si NMR spectrum of MDAS in $CDCl_3$.

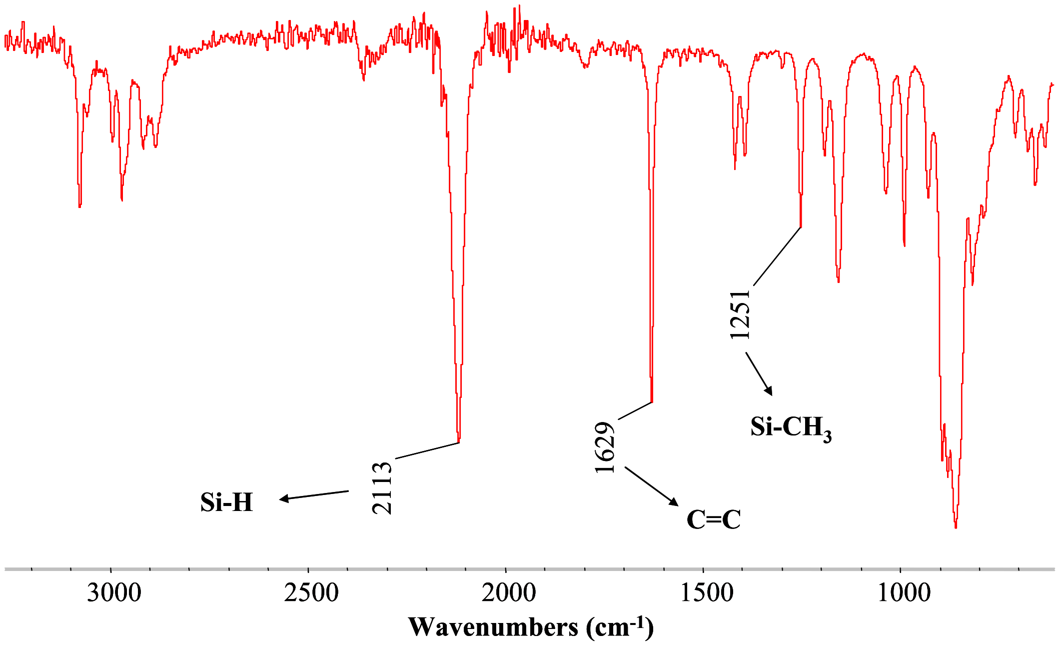

Figure A3.15. IR spectrum of MDAS.

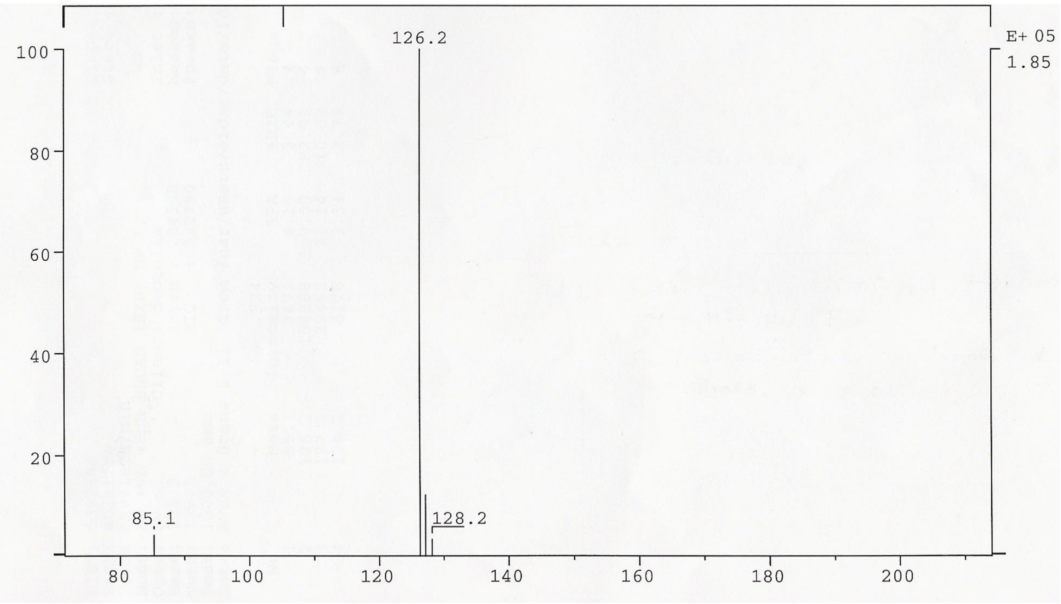

Figure A3.16. FI mass spectrum of MDAS.

Allyldimethylsilane (DMAS)

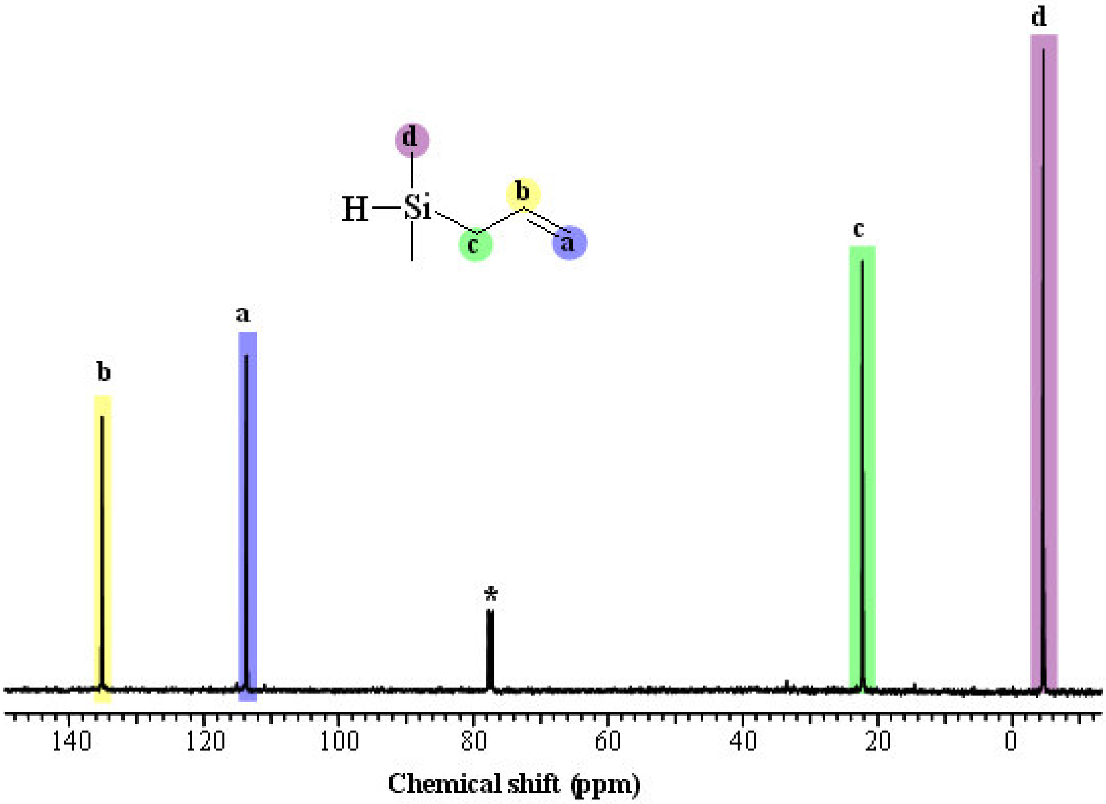

Figure A3.17. ^{13}C NMR spectrum of DMAS in CDCl$_3$ (solvent peak denoted by an asterisk).

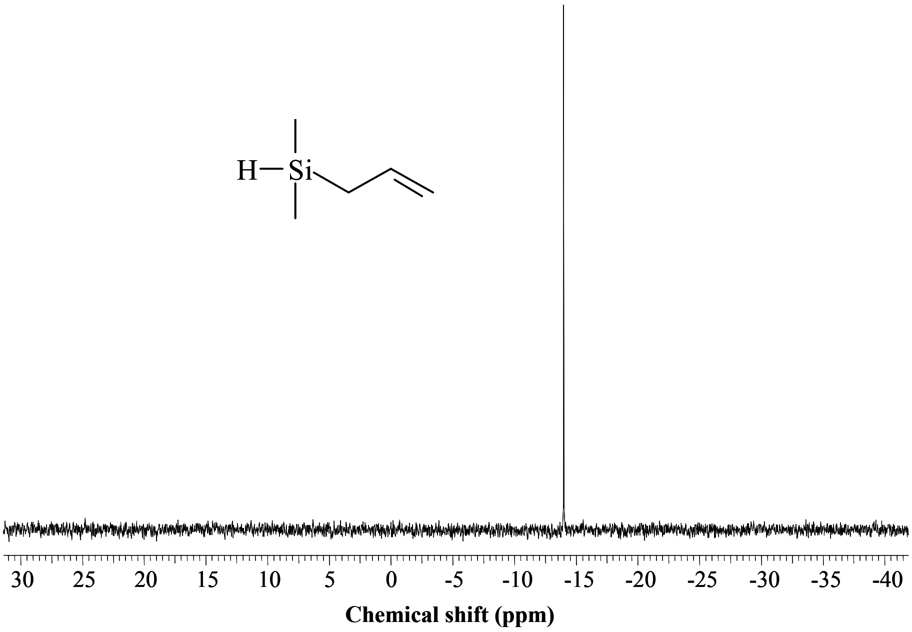

Figure A3.18. ^{29}Si NMR spectrum of DMAS in CDCl$_3$.

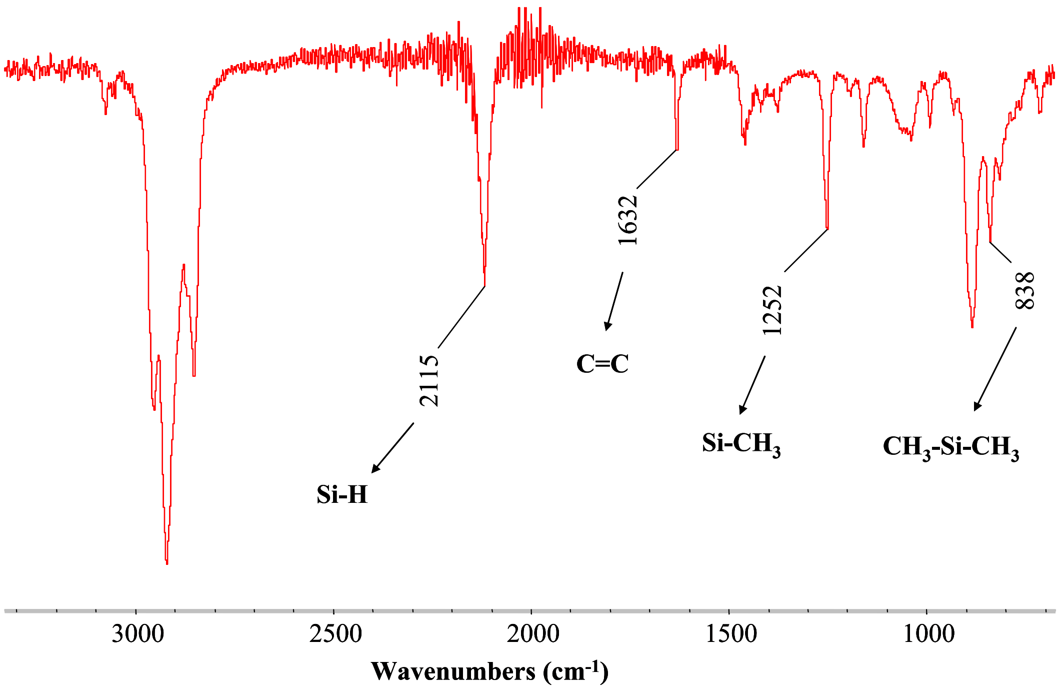

Figure A3.19. IR spectrum of DMAS.

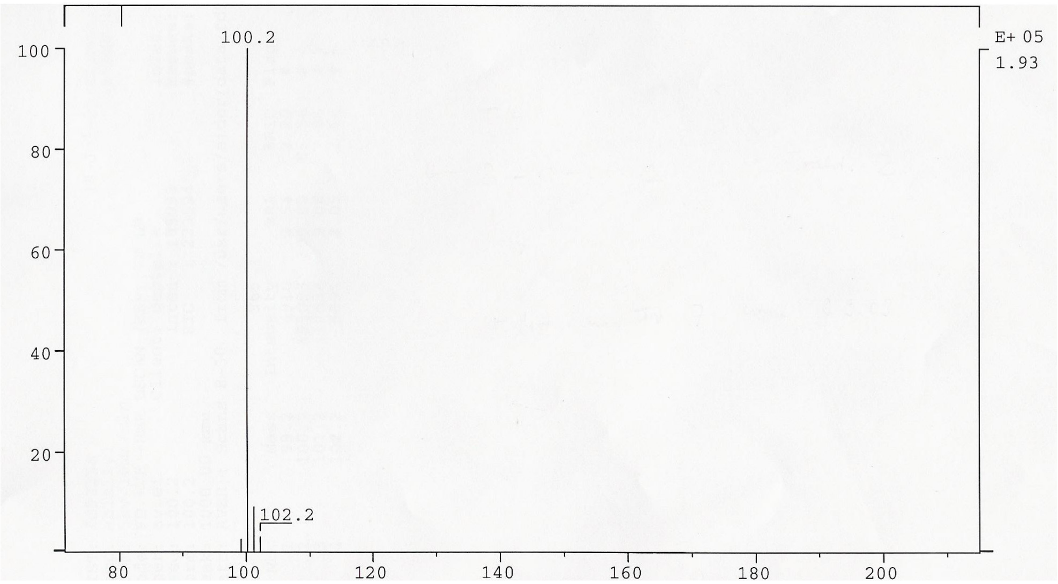

Figure A3.20. FI mass spectrum of DMAS.

Triallylsilane (TAS)

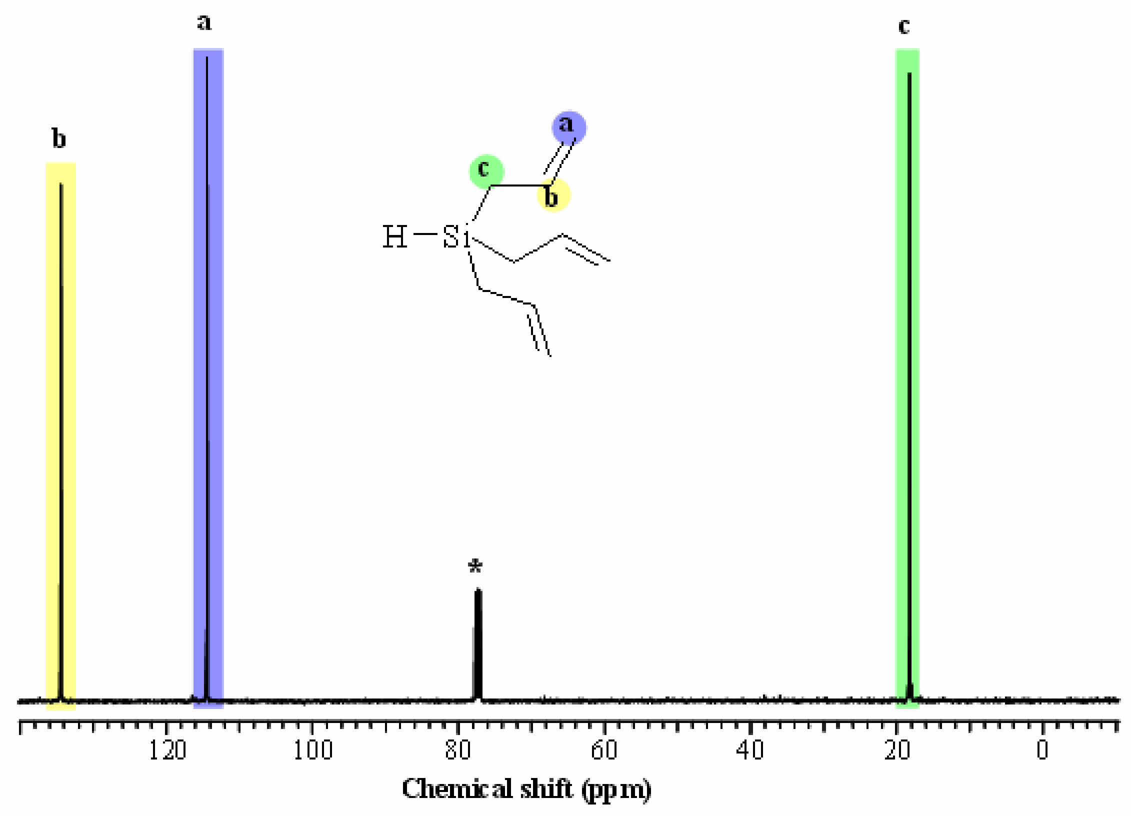

Figure A3.21. ^{13}C NMR spectrum of TAS in $CDCl_3$ (solvent peak denoted by an asterisk).

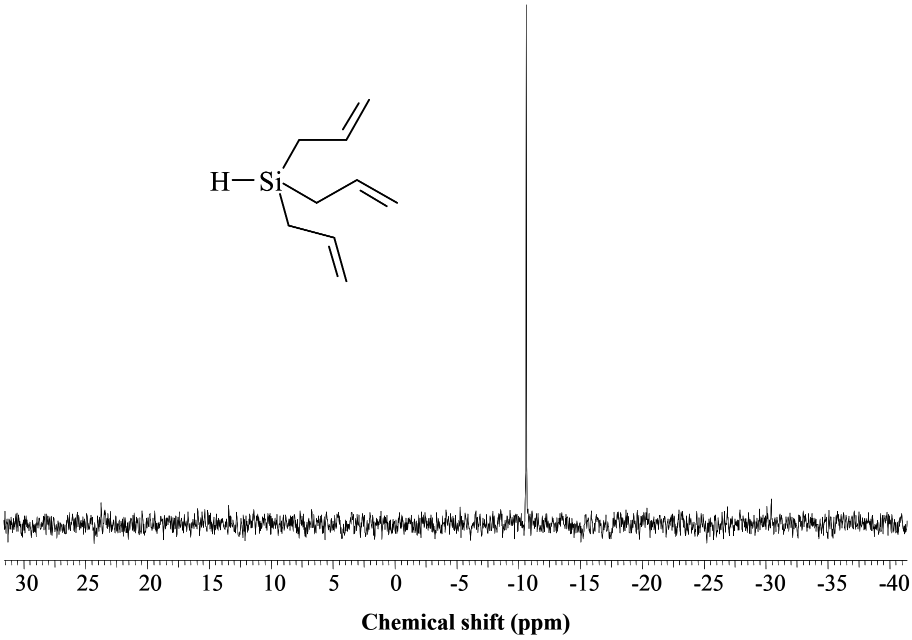

Figure A3.22. ^{29}Si NMR spectrum of TAS in $CDCl_3$.

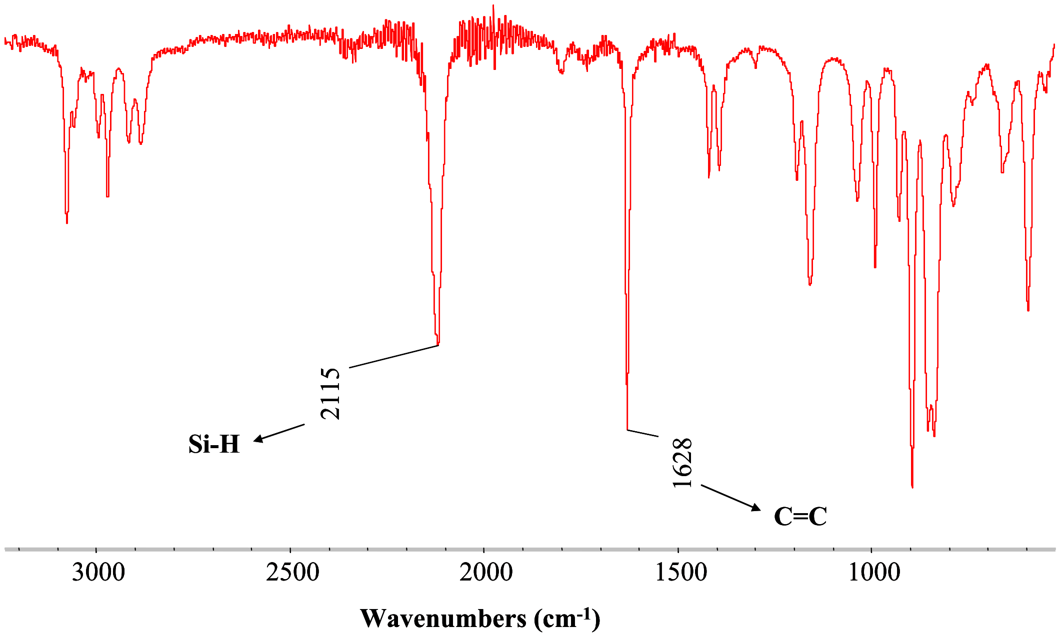

Figure A3.23. IR spectrum of TAS.

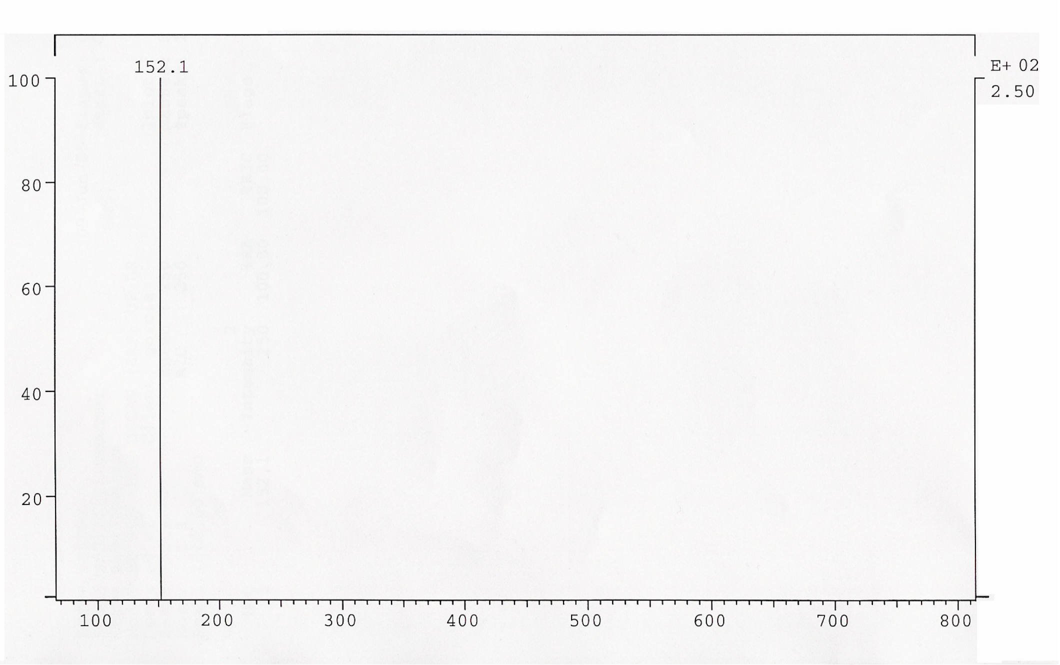

Figure A3.24. FD mass spectrum of TAS.

Methylbis(undec-10-enyloxy)silane (MDUOS)

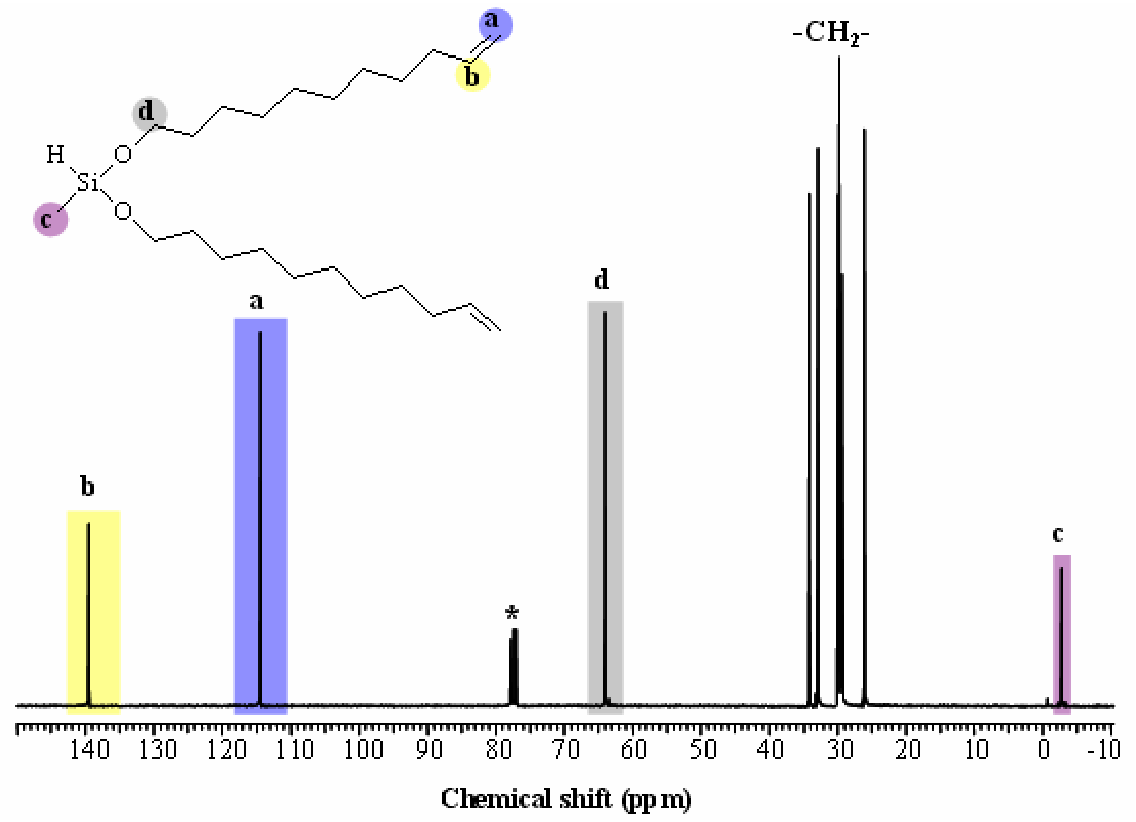

Figure A3.25. ^{13}C NMR spectrum of MDUOS in CDCl$_3$ (solvent peak denoted by an asterisk).

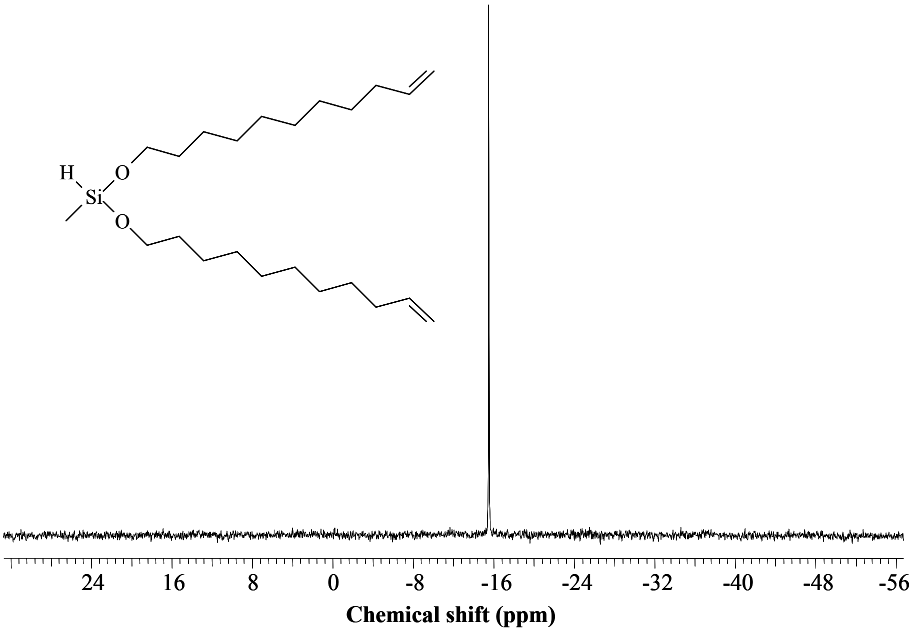

Figure A3.26. ^{29}Si NMR spectrum of MDUOS in CDCl$_3$.

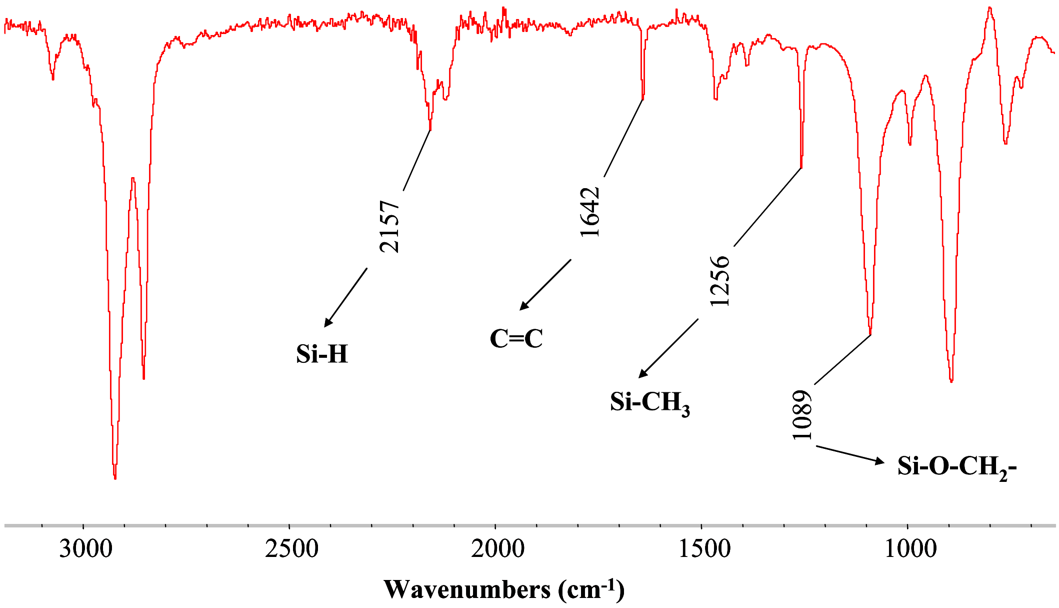

Figure A3.27. IR spectrum of MDUOS.

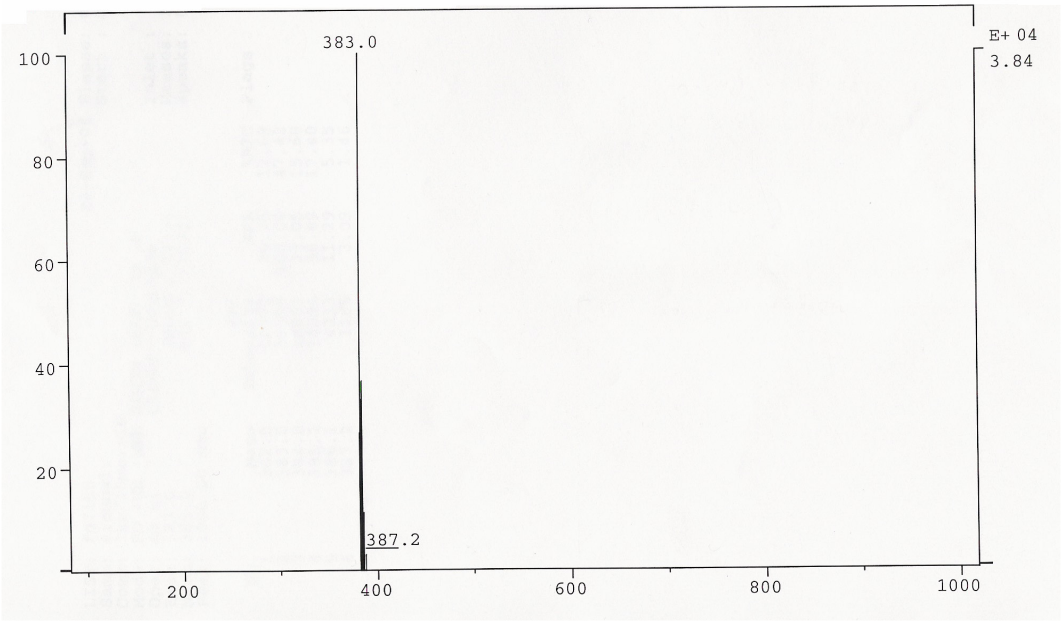

Figure A3.28. FD mass spectrum of MDUOS.

Dimethyl(undec-10-enyloxy)silane (DMUOS)

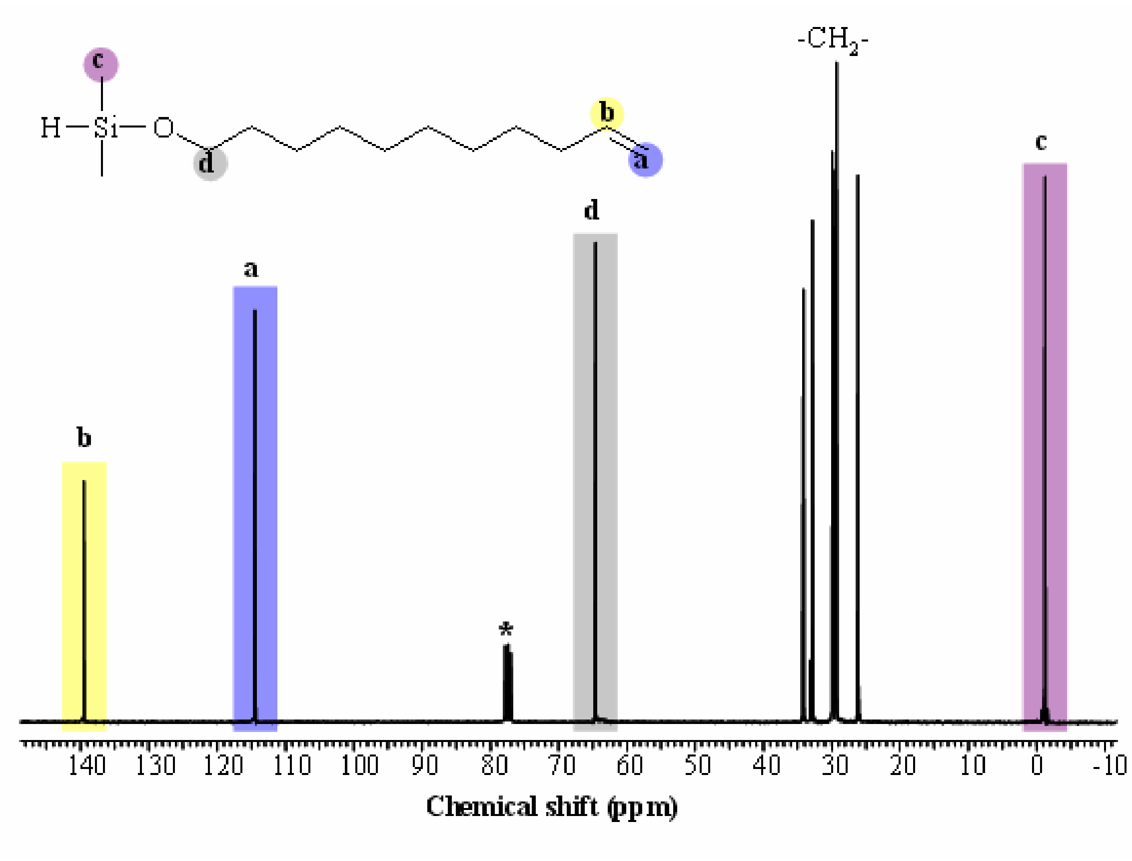

Figure A3.29. ^{13}C NMR spectrum of DMUOS in $CDCl_3$ (solvent peak denoted by an asterisk).

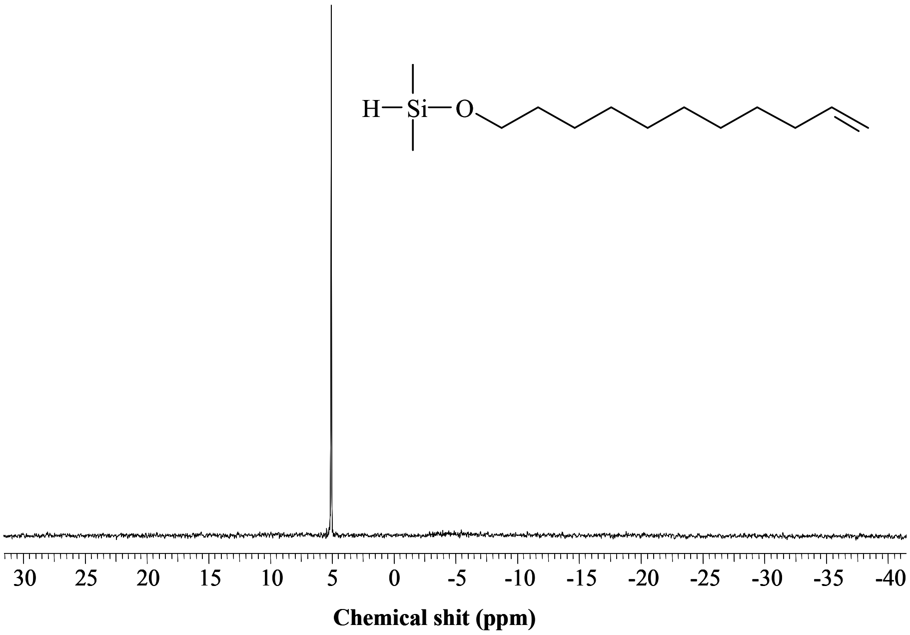

Figure A3.30. ^{29}Si NMR spectrum of DMUOS in $CDCl_3$

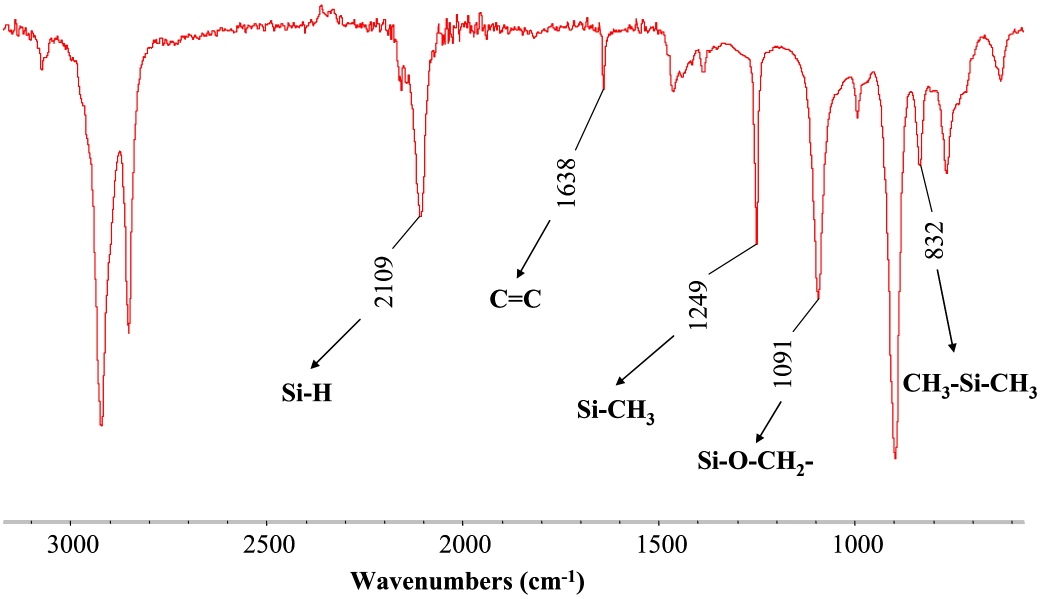

Figure A3.31. IR spectrum of DMUOS.

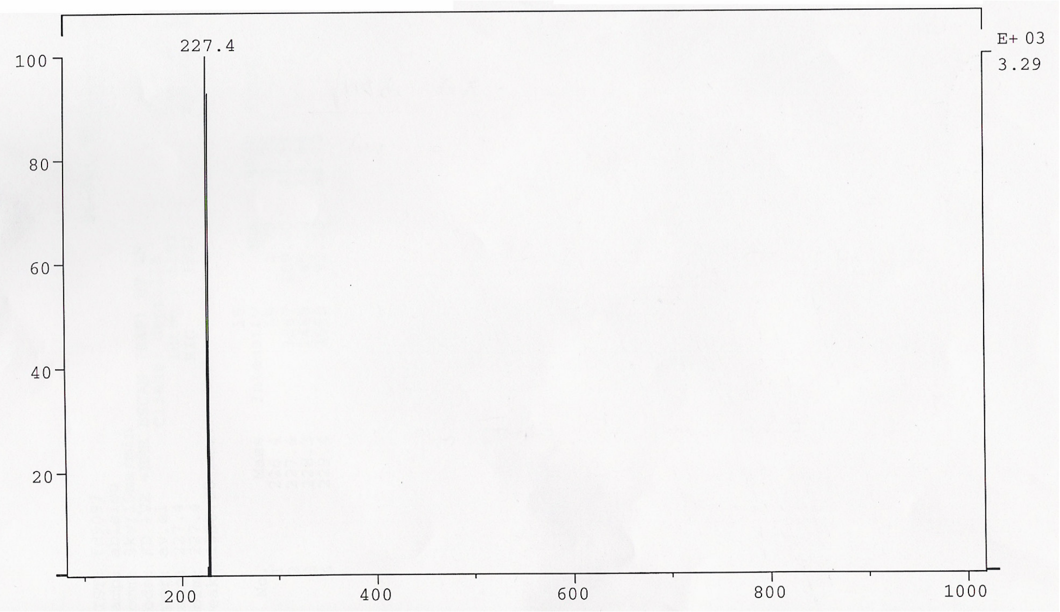

Figure A3.32. FD mass spectrum of DMUOS.

Bis(allyloxy)(methyl)silane (MDAOS)

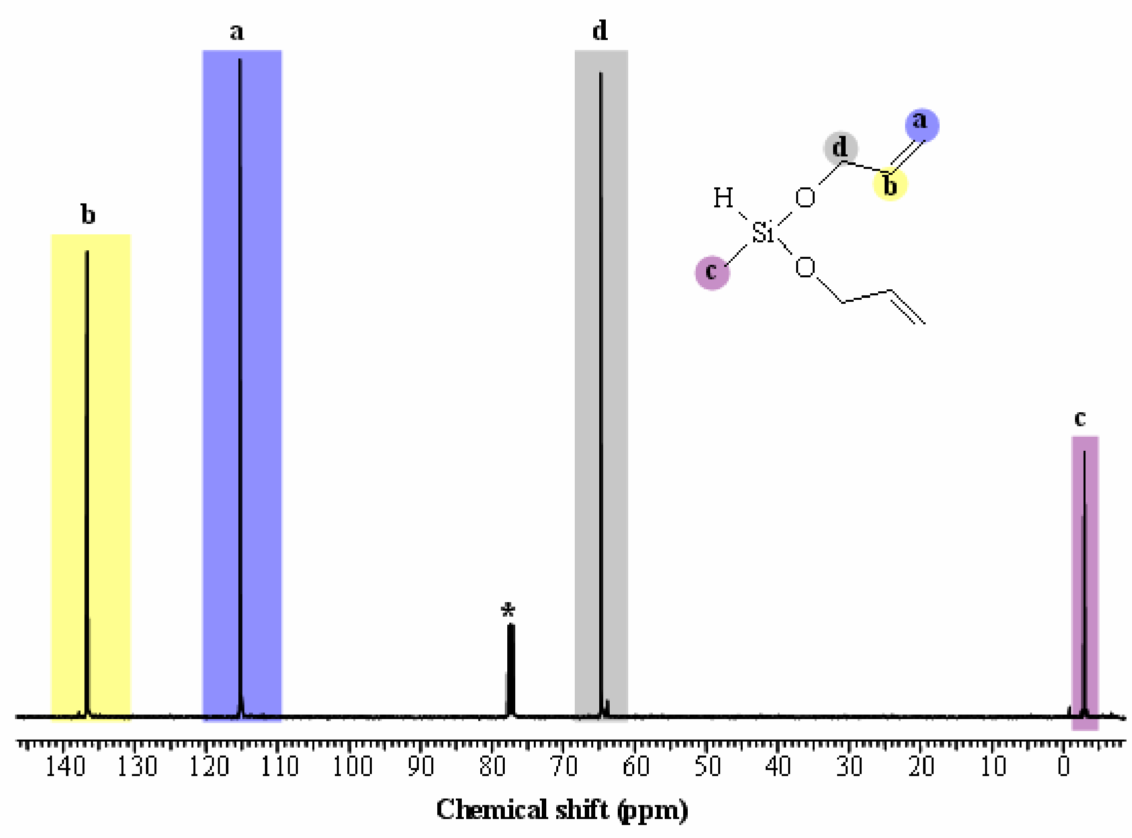

Figure A3.33. ^{13}C NMR spectrum of MDAOS in $CDCl_3$ (solvent peak denoted by an asterisk).

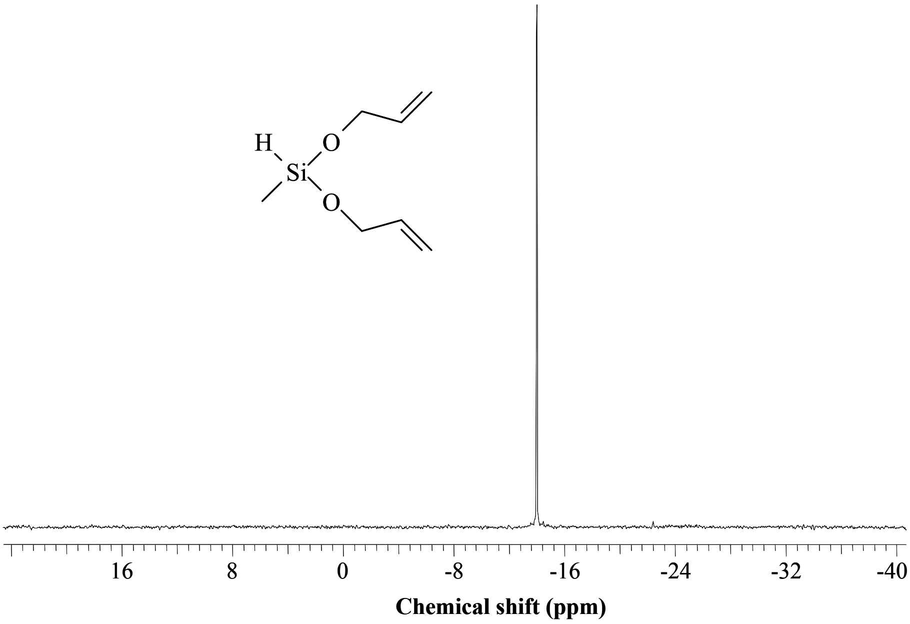

Figure A3.34. ^{29}Si NMR spectrum of MDAOS in $CDCl_3$

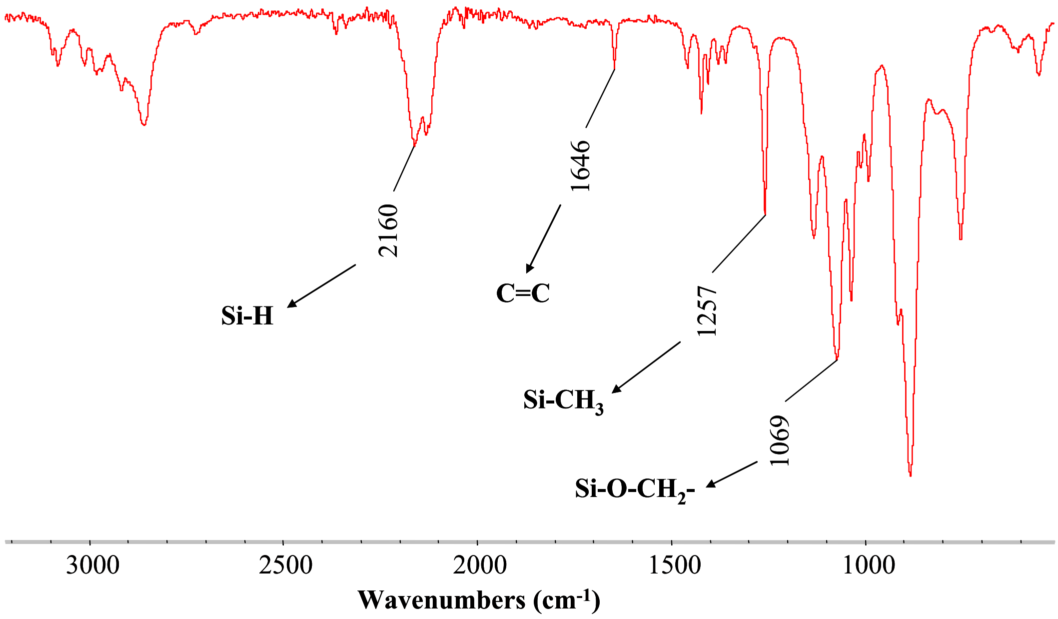

Figure A3.35. IR spectrum of MDAOS.

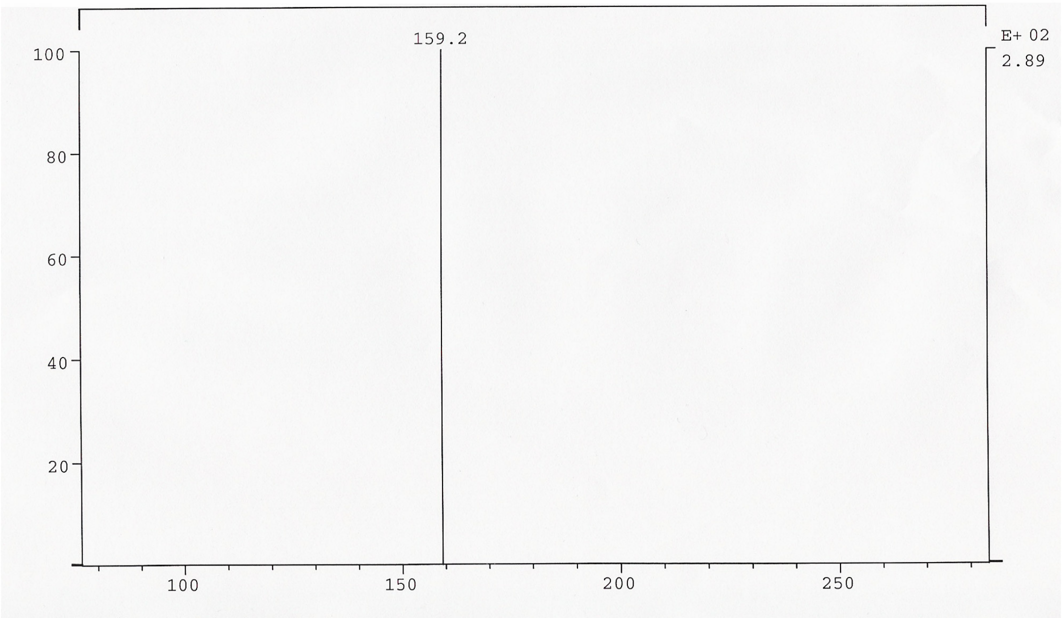

Figure A3.36. FD mass of MDAOS.

Allyloxydimethylsilane (DMAOS)

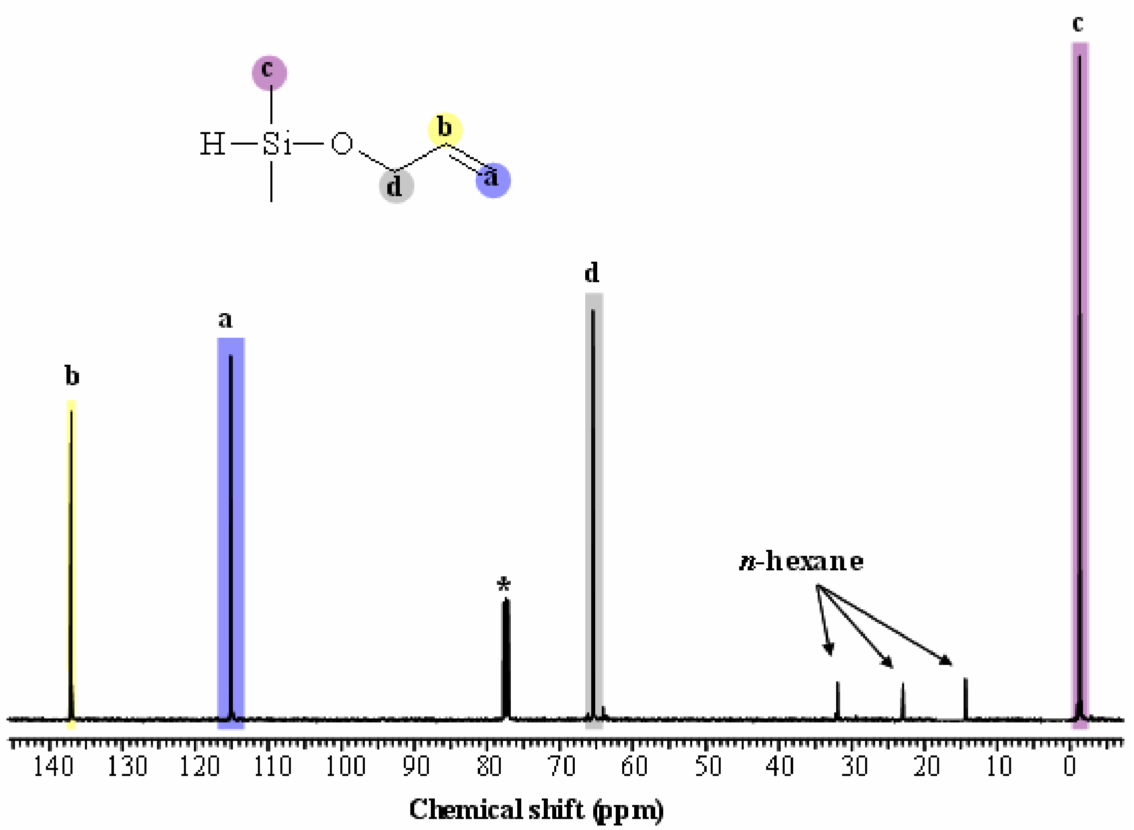

Figure A3.37. ^{13}C NMR spectrum of DMAOS in $CDCl_3$ (solvent peak denoted by an asterisk).

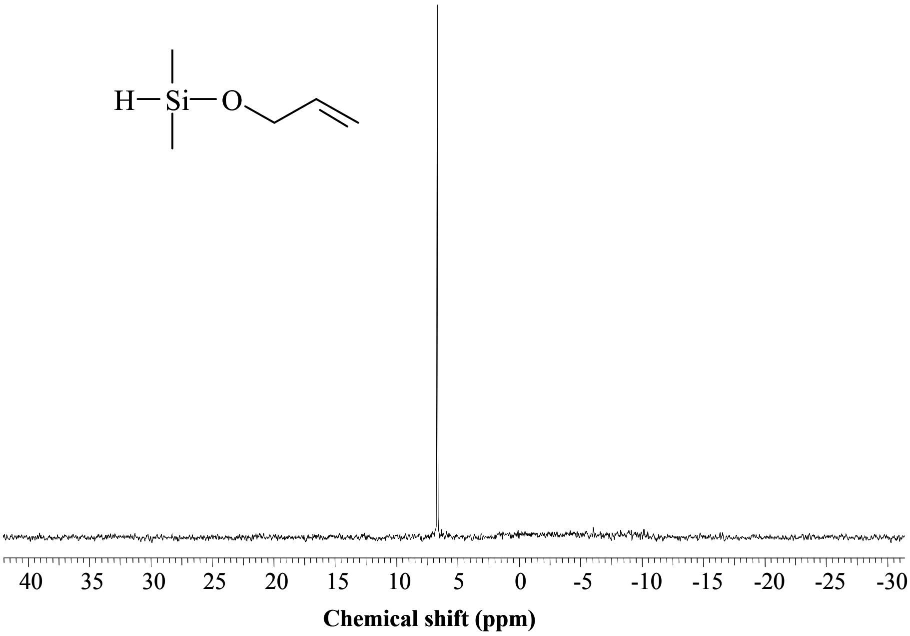

Figure A3.38. ^{29}Si NMR spectrum of DMAOS in $CDCl_3$.

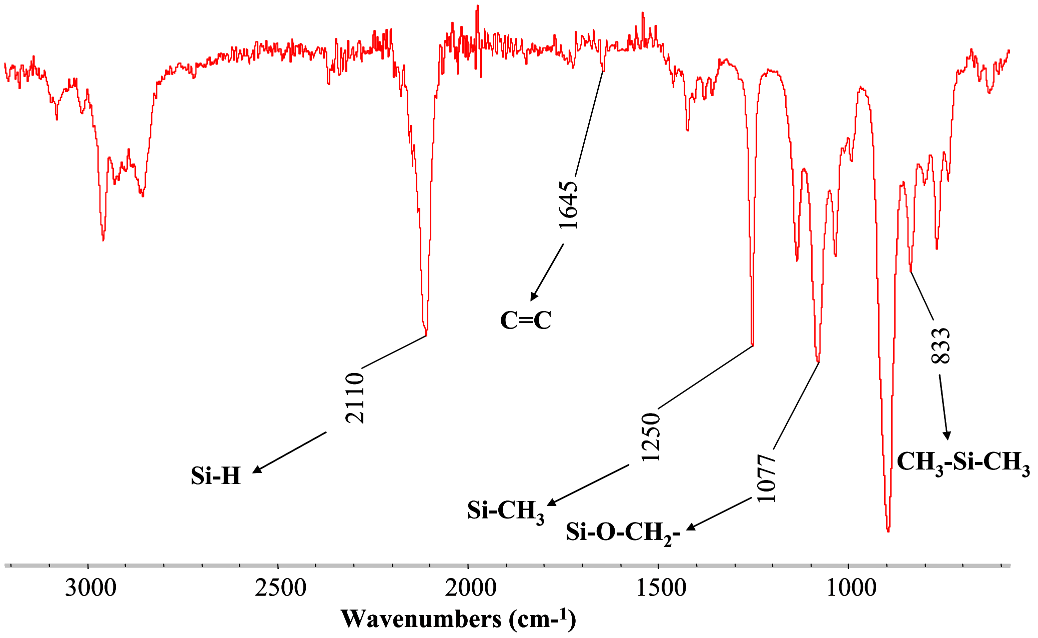

Figure A3.39. IR spectrum of DMAOS.

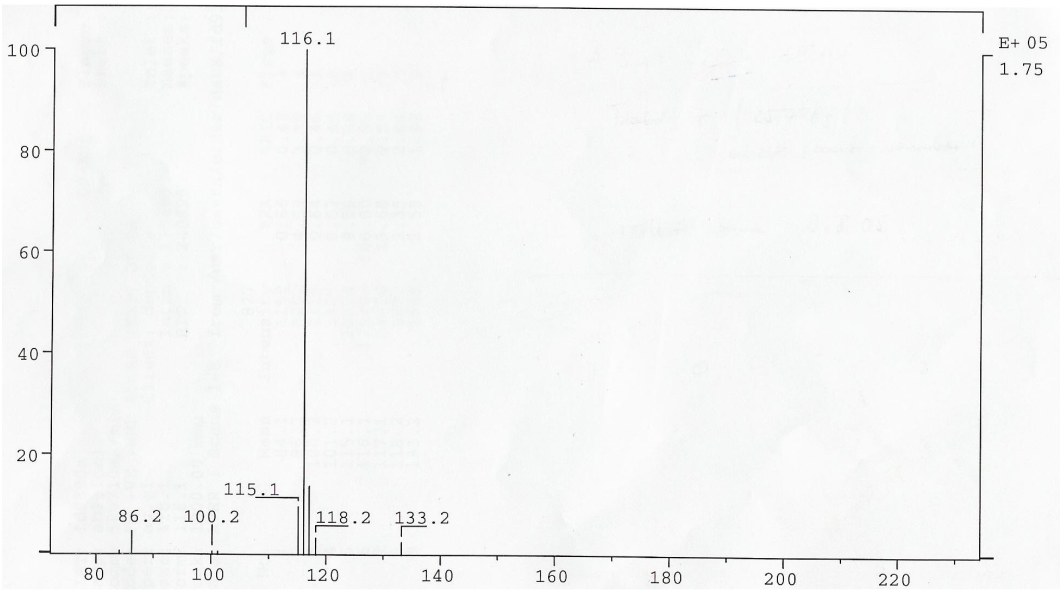

Figure A3.40. FI mass spectrum of DMAOS.

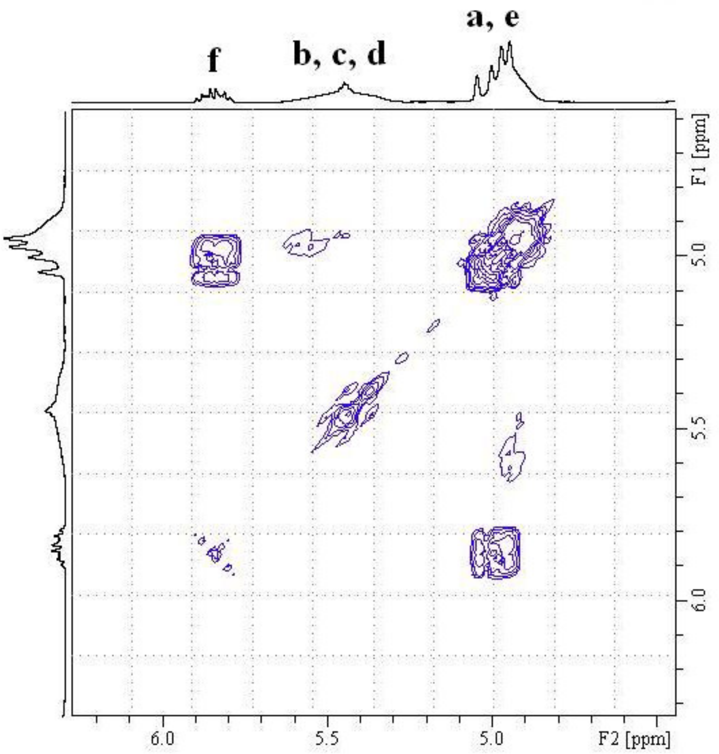

Figure A7.1. ^{1}H-^{1}H COSY spectrum of **P$_1$LB$_{43}$**.

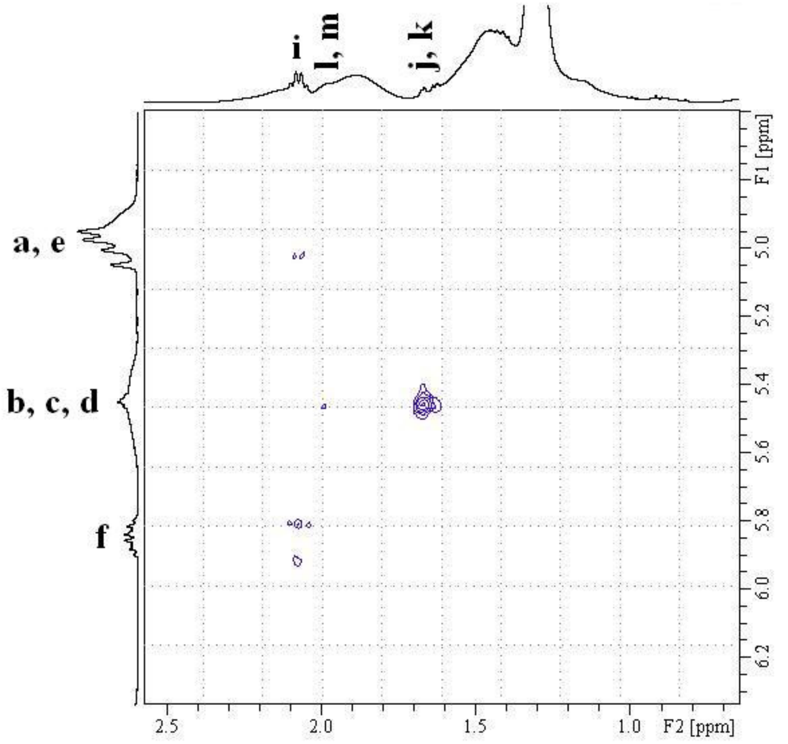

Figure A7.2. ^{1}H-^{1}H COSY spectrum of **P$_1$LB$_{43}$**.

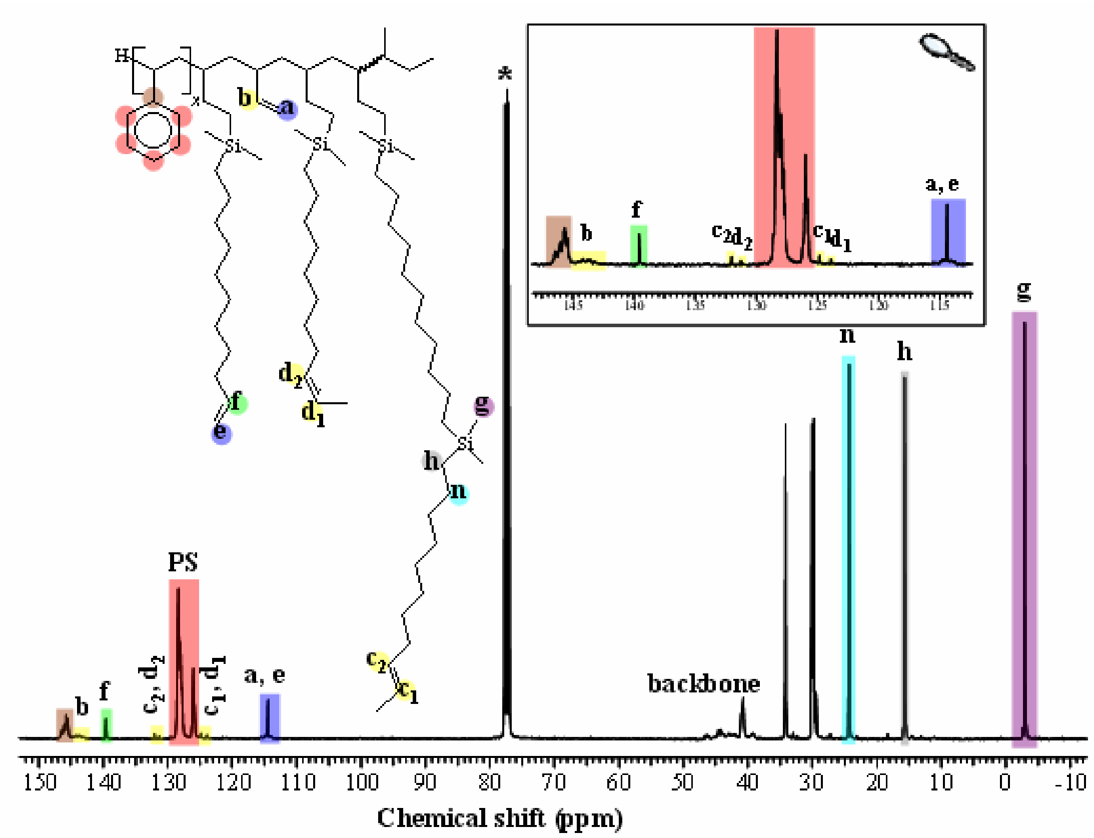

Figure A7.3. ^{13}C NMR spectrum of **P_1LB_{43}** in $CDCl_3$ (solvent peak denoted by an asterisk).

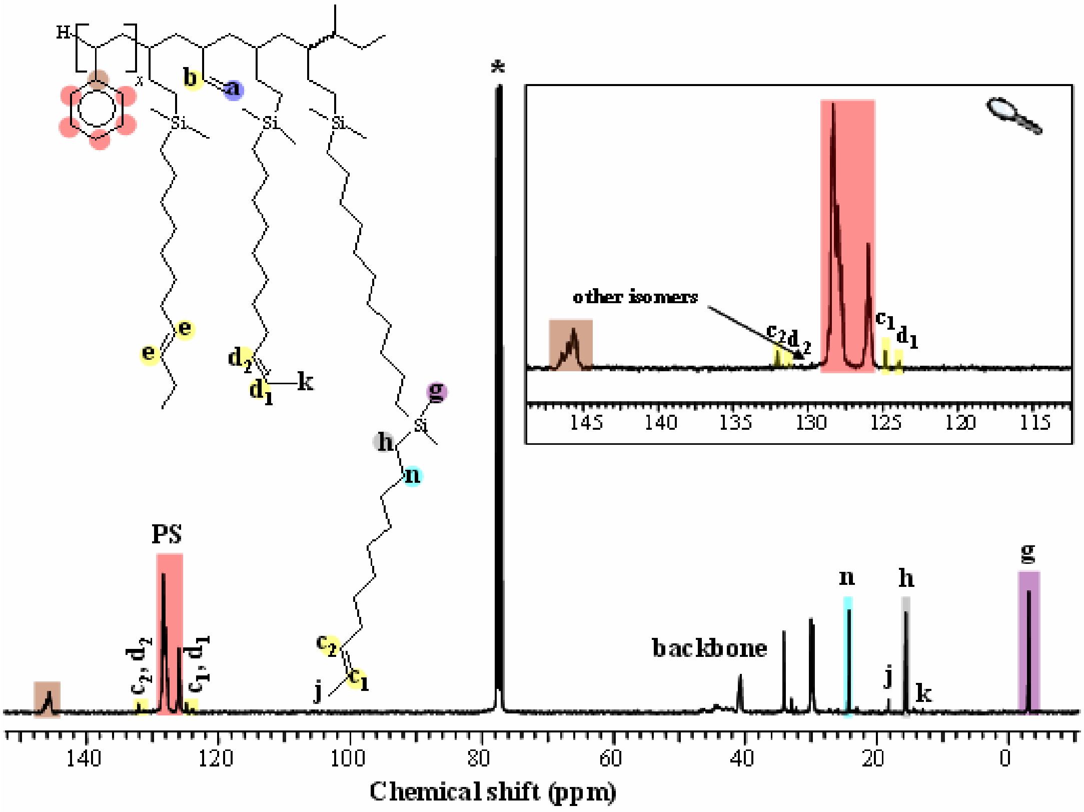

Figure A7.4. ^{13}C NMR spectrum of **P_3LB_{42}**, obtained by using diethyl ether as the monomer solvent of DMUS, in $CDCl_3$ (solvent peak denoted by an asterisk).

Summary

In the past decade, block copolymers (BCPs) have attracted increasing scientific and technological interest because of their inherent capability to spontaneously self-assemble into ordered array of nanostructures. The importance of nanostructures in a number of applications has fostered the need for well-defined, complex macromolecular architectures. With the development of a variety of controlled synthetic techniques, new macromolecular architectures beyond common segmented structures have been realized. Linear-dendritic BCPs are nonlinear block copolymer systems containing cascade-branched blocks. Several groups have focused on block copolymer structures consisting of a linear and a dendrimer block, showing some peculiar properties of such materials. However, the preparation of a perfectly branched dendron block represents a time-consuming multistep synthesis. In addition, the size of the dendrimer block is limited to the respective perfect dendrimer generation.

This thesis has been directed at a study of the influence of macromolecular architecture on the resulting bulk morphologies of silicon-containing linear-hyperbranched and brush-like diblock copolymer structures. The presence of a small amount of silicon atoms permitted in most cases visualization of the branched domains via Transmission Electron Microscopy (TEM) without additional staining procedures.

A general strategy for the preparation of well-defined diblock copolymers combining a random cascade-branched dendritic (*i.e.*, hyperbranched) and a linear block has been developed. The strategy is based on a linear polystyrene-*block*-poly(1,2-butadiene) (PS_x-*b*-PBD_y) diblock copolymer with high molecular weight PS block and short, functional 1,2-PBD, prepared by conventional anionic polymerization. The functional PBD block is used for the grafting of branched AB_2-type carbosilane monomers, resulting in the attachment of a hyperbranched structure to the backbone. Slow monomer addition (SMA) of AB_2 methyldi(undecenyl)silane (MDUS) by means of a hydrosilylation reaction in the presence of the Karstedt catalyst permits control of the molecular weight of the hyperbranched block. High molecular weight linear-hyperbranched diblock copolymers with low polydispersity have been obtained. Morphological studies by TEM, Atomic Force Microscopy (AFM) and Small Angle X-ray Scattering (SAXS) on these systems have demonstrated - for the first time - that various microdomain structures typical for microphase-separated block copolymers can be obtained upon increasing the size of the hyperbranched block with respect to the linear one, despite the strong architectural asymmetry of the linear-hyperbranched macromolecules. However, due to the hyperbranched structure and the crowding at the interface, an asymmetry of the phase diagram has been observed.

The above mentioned innovative strategy has also been employed for the preparation of well-defined linear brush-like diblock copolymers with a linearly-grafted block unit. Better grafting efficiencies have been obtained for these systems, due to the lower cyclization probability and less bulky nature of the AB dimethyl(undec-10-enyl-silane) compared to the branched AB_2 MDUS monomer. Bulk morphological studies using TEM and SAXS have shown well-ordered morphologies despite the non-uniform-length of the brushes on the core. Furthermore, lamellar morphologies for low brush polycarbosilane weight fractions and cylindrical morphologies for nearly symmetric compositions have been observed for several samples. It is concluded that the classical phase boundaries have been shifted to higher PS weight percentage fractions. Interestingly, new morphologies consisting of extremely well-ordered hexagonally packed ellipsoids have also been found. This indicates the dramatic effect that macromolecular architecture can have on the morphology of the BCPs.

In order to improve the grafting efficiencies, the concept has been expanded to linear-hyperbranched and linear brush-like polyalkoxysilanes by employing AB_2 and AB undecenoxysilane type monomers, analogous to the undecenylsilane monomers previously utilized. Differential Scanning Calorimetry (DSC) and Wide-Angle X-ray scattering (WAXS) measurements confirmed the crystallization of the polyalkoxysilane hyperbranched blocks and this conflict between microphase separation and crystallization for the linear-hyperbranched polyalkoxysilanes have resulted in irregular superstructures. In contrast, well-ordered morphologies have been obtained for the linear brush-like polyalkoxysilanes. Furthermore, lamellar morphologies for extremely low mass fractions (0.22) of the polyalkoxysilane block have been observed, confirming the effect of molecular architecture on morphology.